marine drugs

Special Issue Reprint

Bioactive Secondary Metabolites of Marine Fungi

Edited by
Hee Jae Shin

mdpi.com/journal/marinedrugs

MDPI

Bioactive Secondary Metabolites of Marine Fungi

Bioactive Secondary Metabolites of Marine Fungi

Editor

Hee Jae Shin

MDPI

Basel • Beijing • Wuhan • Barcelona • Belgrade • Novi Sad • Cluj • Manchester

Editor
Hee Jae Shin
Korea Institute of
Ocean Science and
Technology (KIOST)
Busan, Republic of Korea

Editorial Office
MDPI
St. Alban-Anlage 66
4052 Basel, Switzerland

This is a reprint of articles from the Special Issue published online in the open access journal *Marine Drugs* (ISSN 1660-3397) (available at: https://www.mdpi.com/journal/marinedrugs/special_issues/MarineFungi2022).

For citation purposes, cite each article independently as indicated on the article page online and as indicated below:

Lastname, A.A.; Lastname, B.B. Article Title. *Journal Name* **Year**, *Volume Number*, Page Range.

ISBN 978-3-0365-9086-8 (Hbk)
ISBN 978-3-0365-9087-5 (PDF)
doi.org/10.3390/books978-3-0365-9087-5

Contents

About the Editor

Hee Jae Shin

Hee Jae Shin is a principal research Scientist at the Department of Marine Biotechnology and Bioresource Research, Korea Institute of Ocean Science and Technology (KIOST) and a professor at the University of Science and Technology. He received his PhD from the University of Tokyo (1997), where he studied the isolation and structure determination of protease inhibitors from cyanobacteria. He undertook two post-doctoral positions at the Marine Biotechnology Institute, Japan (1997–1999) and the center for marine biotechnology and biomedicine, Scripps Institution of Oceanography with Professor William Fenical (1999–2000). He spent 3 years working in the pharmaceutical industry (2000–2003) and then returned to the Korea Ocean Research and Development Institute, which is now KIOST. His research interest is on the isolation and structure determination of bioactive marine natural products from marine microorganisms including fungi, actinomycetes, deep-sea and symbiotic microorganisms, and discovery and development of drug candidates.

Preface

Marine fungi can be isolated from marine animals, plants, sediments, and seawater. Due to the complex marine environments, marine fungal metabolites have novel structures and diverse activities. Over 1,500 species of marine fungi, including about 530 species of obligate marine fungi, are known. Marine fungi are important sources of biologically active natural products due to their ability to produce secondary metabolites with novel structures and pharmacological activities. Over recent decades, pharmaceutical and medical applications of marine fungi have been explored, and new drugs from relatively underexplored sources are essential. Halimide (phenylahistin), a naturally occurring fungal natural product with a diketopiperazine structure isolated from *Aspergillus ustus*, is being studied in a Phase 3 clinical trial for the treatment of non-small-cell lung cancer (NSCLC). Its synthetic analog, plinabulin (NPI 2358), is being developed by BeyondSpring Pharmaceuticals, and a New Drug Application (NDA) has been submitted in the United States and China for its use in the treatment of NSCLC and chemotherapy-induced neutropenia (CIN).

This book provides details about the isolation, structure determination, and bioactivities of marine fungal natural products. Hence, bioactive secondary metabolites from marine fungi are important for academic research, pharmaceutical, nutraceutical, and biomedical industries. I would like to acknowledge *Marine Drugs* for their encouragement and suggestions to get this wonderful compilation related to the special issue "Bioactive Secondary Metabolites of Marine Fungi". I would also like to sincerely thank all the contributors for their high-quality manuscripts, support, and advice.

Hee Jae Shin
Editor

marine drugs

MDPI

Review

Natural Products from Chilean and Antarctic Marine Fungi and Their Biomedical Relevance

Dioni Arrieche [1,†], Jaime R. Cabrera-Pardo [2,†], Aurelio San-Martin [3], Héctor Carrasco [4,*] and Lautaro Taborga [1,*]

[1] Laboratorio de Productos Naturales, Departamento de Química, Universidad Técnica Federico Santa María, Avenida España 1680, Valparaíso 2340000, Chile
[2] Laboratorio de Química Aplicada y Sustentable (LabQAS), Departamento de Química, Universidad del Bio-Bio, Avenida Collao 1202, Concepción 4030000, Chile
[3] Departamento de Ciencias y Recursos Naturales, Facultad de Ciencias Naturales, Universidad de Magallanes, Avenida Bulnes 01855, Punta Arenas 6200112, Chile
[4] Grupo QBAB, Instituto de Ciencias Químicas y Aplicadas, Facultad de Ingeniería, Universidad Autónoma de Chile, Llano Subercaseaux 2801, Santiago 8900000, Chile
* Correspondence: hector.carrasco@uautonoma.cl (H.C.); lautaro.taborga@usm.cl (L.T.)
† These authors contributed equally to this work.

Abstract: Fungi are a prolific source of bioactive molecules. During the past few decades, many bioactive natural products have been isolated from marine fungi. Chile is a country with 6435 Km of coastline along the Pacific Ocean and houses a unique fungal biodiversity. This review summarizes the field of fungal natural products isolated from Antarctic and Chilean marine environments and their biological activities.

Keywords: marine natural products; marine fungi; Chilean marine fungi; biological activities

Citation: Arrieche, D.; Cabrera-Pardo, J.R.; San-Martin, A.; Carrasco, H.; Taborga, L. Natural Products from Chilean and Antarctic Marine Fungi and Their Biomedical Relevance. *Mar. Drugs* **2023**, *21*, 98. https://doi.org/10.3390/md21020098

Academic Editor: Hee Jae Shin

Received: 16 December 2022
Revised: 23 January 2023
Accepted: 26 January 2023
Published: 29 January 2023

1. Introduction

Natural products (NPs) represent a rich and vast biologically relevant chemical space that remains extremely difficult to access with the current arsenal of tools in chemical synthesis [1]. NPs are characterized by enormous scaffold diversity and structural complexity. Nature, via evolution, has optimized secondary metabolites to serve pivotal biological functions, including endogenous defense mechanisms as well as interaction with other organisms [2]. Natural products-based medicines can be traced back thousands of years and still contribute to many approved drugs. Indeed, natural products and their derivatives represented 27% of all therapeutics approved by the FDA between 1981 and 2019 [3,4]. In recent years, this proportion has increased, illustrating the continued importance of NPs. Research programs focused on unveiling new NPs from understudied microorganisms, such as fungi isolated from Chilean marine environments, are crucial to the future drug development pipeline.

Fungi represent one of the largest groups of organisms. They are widely distributed across both mild and extreme ecosystems on our planet [5]. They have developed a unique metabolic plasticity, allowing them to rapidly adapt and survive through the biosynthesis of an array of fascinating natural products [6]. A recent analysis of fungal genomes has revealed many secondary metabolite pathways that can be tuned or modified, producing novel and valuable chemical scaffolds [7]. Fungal-derived natural products are pharmaceutically abundant, with several important biological applications ranging from highly potent toxins to approved drugs [8]. Since the discovery of penicillin, an antibiotic of fungal origin, many efforts around the globe have been devoted to searching for fungal-derived bioactive products. Fungi are a vast yet untapped source to search for pharmaceutically relevant molecules displaying a range of bioactivity, including anticancer, antioxidant, hepatoprotective, antibacterial, antidiabetic, and anti-inflammatory capabilities.

Oceans are the source of a wide variety of natural products with unique structures mainly produced by marine macro-organisms, such as invertebrates (e.g., sponges, soft corals, tunicates) and algae. Additionally, many marine natural products have proved to be pharmacologically relevant [9–11].

Secondary metabolites obtained from marine fungi have been particularly interesting, mainly because of their unique chemical structures and biomedical applications [8,12]. In 1949, cephalosporin C was discovered from a culture of *Cephalosporium* fungus species obtained from the Sardinian coast [13]. Since then, extensive efforts over decades of work have revealed the vast chemical and biological potential of marine fungal natural products. Strains of marine fungi have been obtained from practically every possible marine habitat, including inorganic, marine microbial communities, marine plants, and marine vertebrates [10]. While the number of cultivable marine fungi is extremely low (1% or less) compared to their global biodiversity [8–10], the number of natural products that have been isolated and characterized from marine fungi exceeds 1000 molecules [14]. These include alkaloids, lipids, peptides, polyketides, prenylated polyketides, and terpenoids [14–17].

Chile has 6435 km of coastline and exercises exclusive rights over its maritime space called the Chilean Sea. This comprises four zones: the Territorial Sea (120,827 km^2), the contiguous zone (131,669 km^2), the exclusive economic zone (3,681,989 km^2), and that corresponding to the Continental shelf (161,338 km^2) [18].

The Chilean maritime territory, in the Pacific Ocean, consists of highly structured geographic sections displaying unique features that arise from the interactions of water masses with the seabed, emerged relief, air masses and centers of atmospheric action [19]. These phenomena lead to an environment suitable for a rich biodiversity ranging from microscopic organisms that swarm the waters in incredible numbers to large fish and other organisms [20]. Along the lengthy coastline, Chilean waters also differ in terms of important characteristics, e.g., mineral and saline composition [19].

The cold waters associated with both the Humboldt and Antarctic currents are characterized by a high gas and nitrogen content, unlike in temperate and warm waters. Consequently, phytoplankton is abundant in the Chilean sea and supports the growth of various marine organisms, specifically fungi. Therefore, Chile´s coastline provides a distinct environment for fungal biodiversity to flourish [21].

Despite its importance, there are not many reports about secondary metabolites from marine fungi or marine-derived fungi in Chile. Reports included in this review cover the period from 1996 until present. In this work, we have made a comprehensive review of compounds that have been isolated and chemically characterized during this time. Their biological activities are also reported.

2. Secondary Metabolites Isolated from Chilean Marine Fungi in Continental Coasts

Studies carried out on cultures of *Cladosporium cladosporioides*, a fungus isolated from the marine sponge *Cliona* sp. collected in Region IV of Chile in 2004, led to the identification of *p*-methylbenzoic acid (**1**) and peroxyergosterol (**2**) (Figure 1). This was the first time that **1** had been isolated as a natural product. It was reported that peroxyergosterol from *Inonotus obliquus* inhibited the growth of cancer cells and showed cytotoxic effects on the same cell lines. Additionally, peroxyergosterol displayed potent inhibition of lipid peroxidation and higher antioxidant activity than well-known antioxidants, such as α-tocopherol and thiourea. A recent study also revealed inhibitory effects of peroxyergosterol on inflammation and tumor promotion in mouse skin [22]. In addition, compounds **1** and **2** did not show antimicrobial activity against Gram-positive (*Staphylococcus aureus*, *S. epidermidis*) or Gram-negative bacteria (*Escherichia coli*, *Proteus mirabilis*, *Enterococcus faecalis*) in the agar plate diffusion assay. Both compounds were inactive against *Artemia salina* [23].

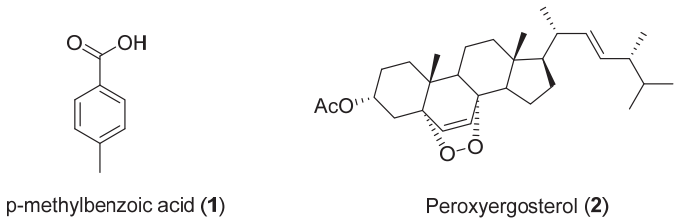

Figure 1. Secondary metabolites isolated from *Cladosporium cladosporioides*.

Four previously reported metabolites (**3**–**6**, Figure 2) were isolated from *Penicillium brevicompactun*, collected in Quintay, Chile (region V). The mycelium and broth were extracted with ethyl acetate, and the solvent was evaporated to provide a crude extract that showed in vitro antibacterial activity against both Gram-positive (*Staphylococcus aureus*, *S. epidermidis*) and Gram-negative bacteria (*Escherichia coli*, *Proteus mirabilis*, *Enterococcus faecalis* and *Pseudomonas aeruginosa*) [24].

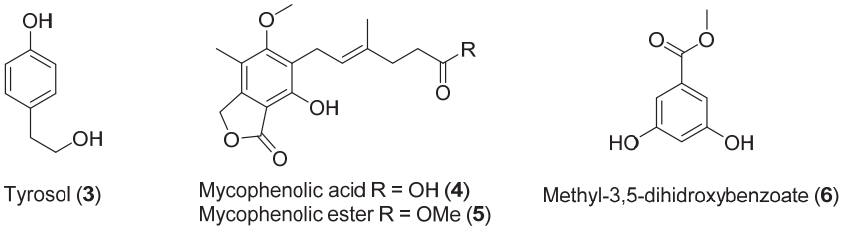

Figure 2. Secondary metabolites isolated from *Penicillium brevicompactun*.

Four steroids (**2**, **7**–**9**) (Figures 1 and 3) were isolated from cultures of *Geotrichum* sp., a fungus obtained from marine sediment collected in Concepción Bay, Chile (Region VIII). Compound **7** is commonly found in fungal extracts since it plays a structural role in the cytoplasmic membrane. Similarly, **2** is a ubiquitous NP present in a variety of lichens, fungi, sponges, and marine organisms. Compound **8** has been isolated from *Lampteromyces japonicus* and a luminous bacterium. Additionally, **8** has been found in non-luminous basidiomycete fungi, including *Fomes officinalis* and *Scleroderma polyrhizum*. It has also been isolated from a marine sponge *Dictyonella incisa* [25]. This is the first time this compound has been identified in a facultative marine fungus [26].

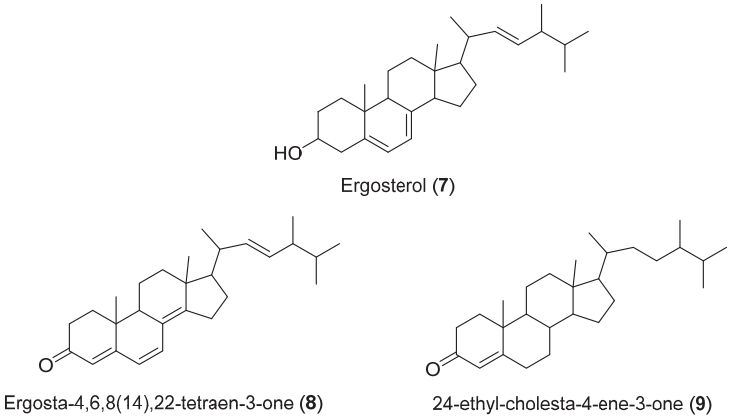

Figure 3. Secondary metabolites isolated from *Geotrichum* sp.

Compound **10** is the first indole derivative isolated from a marine fungus (*Cladosporium cladosorioides)*. The crystal structure of N-methyl-1H-indole-2-carboxamide (**10**) (Figure 4) was determined by single-crystal X-ray diffraction [27].

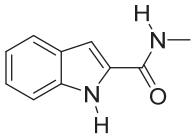

N-methyl-1H-indole-2-carboxamide (**10**)

Figure 4. Secondary metabolite isolated from *Cladosporium cladosorioides*.

Two dibenzylbutyrolactones (**11**,**12**) (Figure 5) and two sesterterpenoids (**13**,**14**) (Figure 5) were obtained from *Aspergillus* sp. (2P-22) isolated from the marine sponge, *Cliona chilensis* collected in Los Molles, Chile (Region IV) [28]. Spectroscopic data highlighted compound **11** as a novel compound named butylrolactone-VI. All four compounds were then tested for antibacterial activity against both Gram-positive (*Clavibacter michiganensis* 807) and Gram-negative bacteria (*Pseudomonas syringae pv syringae, Xanthomonas arboricola pv juglandis* 833, *Erwinia carotovora, Agrobacterium tumefaciens* A348), vasorelaxant effects, and antitumor bioactivities employing a broth culture of *A. tumefaciens* [28].

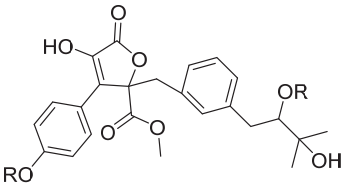

Butyrolactone VI R = H (**11**)
Butyrolactone VI acetate R = Ac (**11a**)

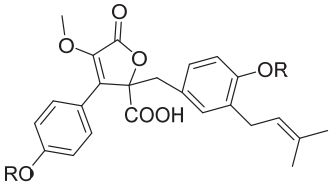

Butyrolactone **I** R = H (**12**)
Butyrolactone **I** acetate R = Ac (**12a**)

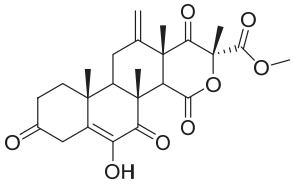

Terretonin A (**13**)

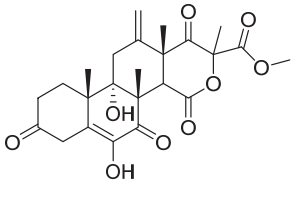

Terretonin B (**14**)

Figure 5. Secondary metabolites isolated from *Aspergillus* sp.

3. Secondary Metabolites Isolated from Antarctic Marine Fungi

The Antarctic continent represents one of the most extreme environments on earth for life to exist [29]. This ecosystem is characterized by high-stress conditions, including low temperatures, scarce availability of nutrients, high acidity, and high levels of ultraviolet radiation [30]. In order to survive under these highly demanding conditions, fungi living in the Antarctic have had to adapt their biochemical machinery and have done so through modifications in gene expression as well as the biosynthesis of secondary metabolites. Thus, Antarctic fungi represent a unique, biologically relevant chemical space with tremendous potential to contribute to the development of effective therapeutics [31]. Indeed, a number of efforts have reported unique NPs isolated from fungi living in Antarctic environments [31] and this emerging field promises a vast capacity for expansion.

In cold marine ecosystems, the presence of fungi has been associated with macroalgae and invertebrates, although some species have also been recorded in seawater and sediments [32,33]. Five new asterric acid derivatives were identified and isolated from the fermentation of the Antarctic ascomycete *Geomyces* sp.: ethyl asterrate (**15**) (Figure 6), n-butyl asterrate (**16**) (Figure 6), and geomycins A–C (**17**–**19**) (Figure 6). These compounds were evaluated for antifungal and antibacterial properties. Geomycin B (**18**) showed significant activity against *Aspergillus fumigatus* ATCC 10894, with IC_{50}/MIC values of 0.86/29.5 μM, indicating much higher antifungal activity than the positive control fluconazole, which showed IC_{50}/MIC values of 7.35/163.4 μM [31,34].

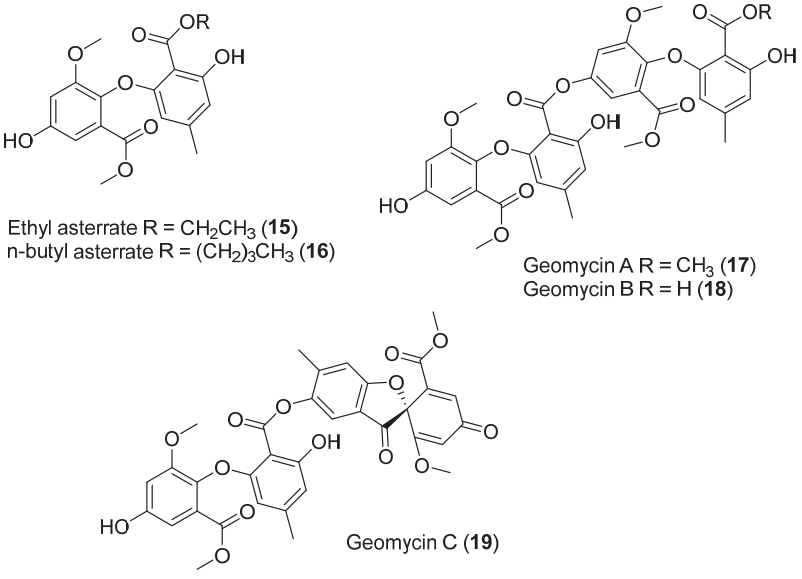

Figure 6. Secondary metabolites isolated from *Geomyces* sp.

Six new peptaibols (linear or cyclic peptides), named asperelines A–F (**20**–**25**) (Figure 7), were characterized from the fermentation of the marine-derived fungus *Tridocherma asperellum* collected from the sediment of the Antarctic Penguin Island. Chemical structures were determined using 1D and 2D NMR techniques as well as ESIMS/MS [35].

Next, two highly oxygenated polyketides, penylactones A and B (**26** and **27**) (Figure 8) were isolated and identified from *Penicillium crustosum* PRB-2. These compounds had a similar chemical structure but opposite absolute stereochemistry. Compounds **26** and **27** were tested for their ability to inhibit nuclear factor-κB (NF-κB) via transient transfection and reporter gene expression assays. Of the two compounds, only **27** showed inhibitory activity with a relatively weak effect of 40% inhibitory rate at a concentration of 10 μM [36]. The authors also proposed a biosynthetic pathway for both compounds, shown in Scheme 1 [36]. These penylactones are characterized by a new carbon skeleton formed from two units of 3,5-dimethyl-2,4-diol-acetophenone and γ-butyrolactone. Six compounds were subsequently synthesized through a novel biomimetic synthesis pathway, as shown in Scheme 2 [37].

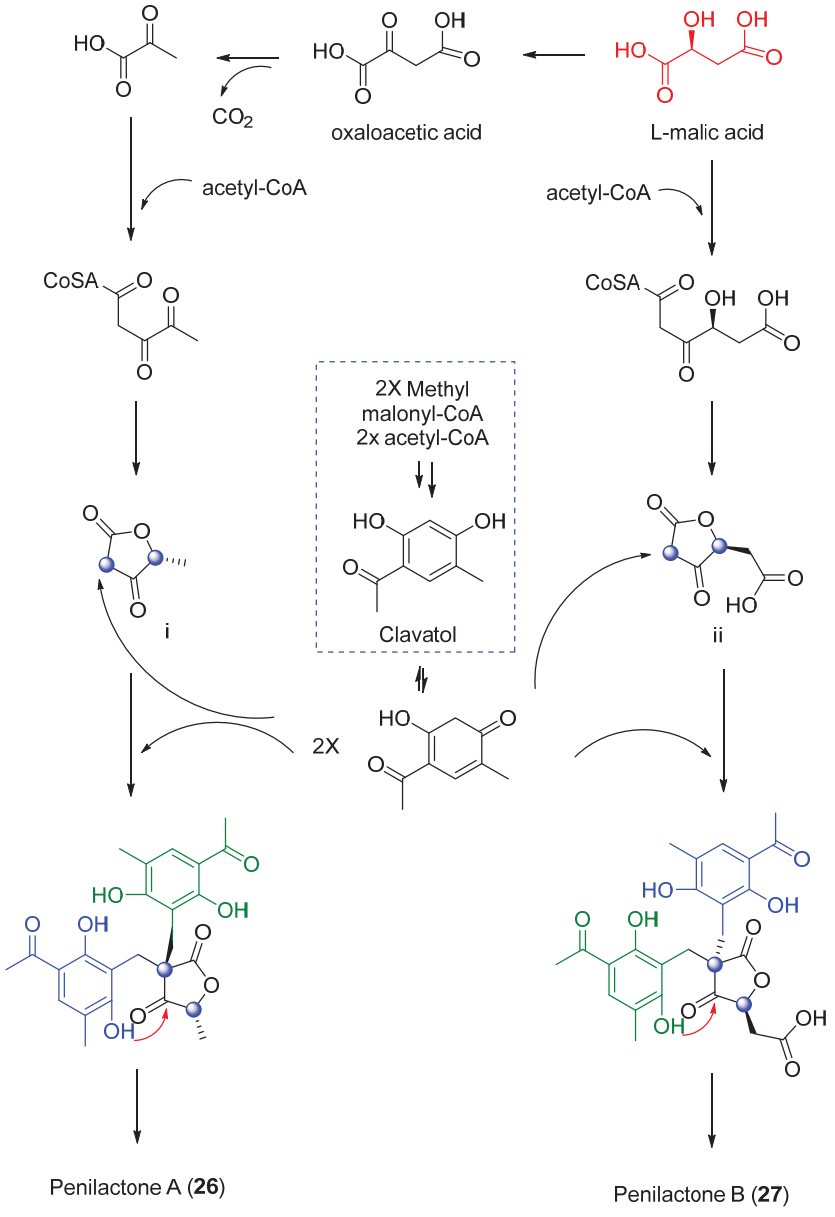

Scheme 1. Proposed biosynthetic pathway to **26** and **27**.

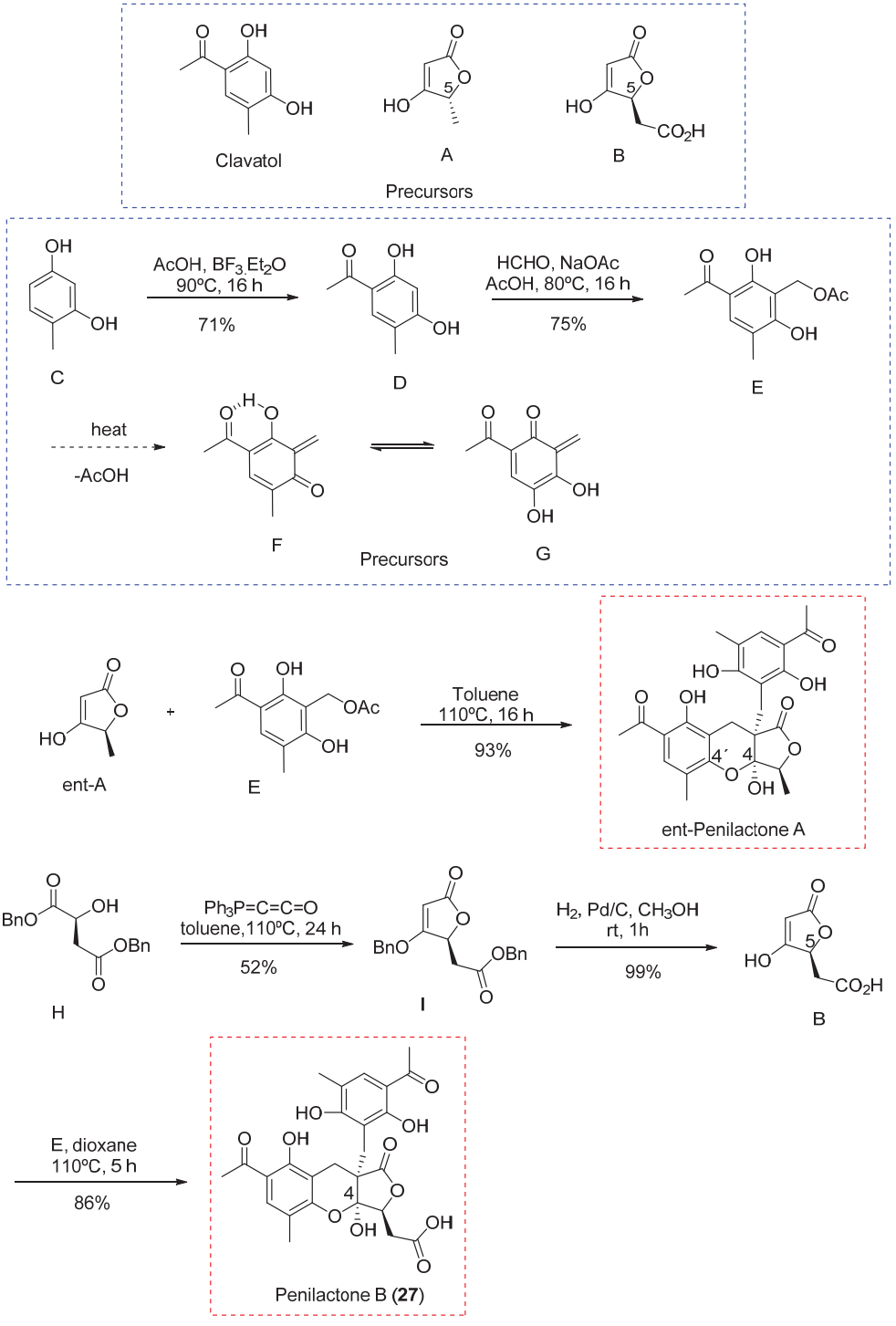

Scheme 2. Biomimetic synthesis of *ent*-Penilactone A and Penilactone B.

A study of the Antarctic fungus *Oidiodendron truncatum* GW3-13 isolated two new epipolythiodioxopiperazines, chetrazins B (**28**) and C (**29**), together with five new diketopiperazines, chetracin D (**30**), and oidiooperazines A–D (**31**–**34**) (Figure 9). In vitro studies using 3-(4,5-dimethylthiazol-2-yl) 2,5-diphenyltetrazolium bromide (MTT) showed that compound **28** exhibits potent biological activity in the nanomolar range against a panel of five human cancer lines (HCT-8, BEL-7402, BGC-823, A-549, and A-2780) [38].

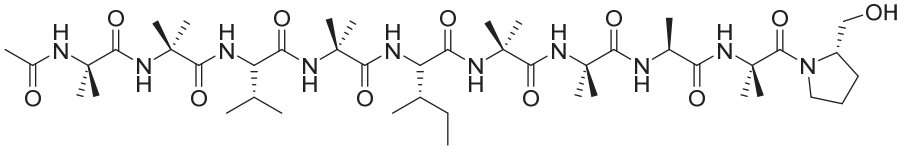

Asperelin A (**20**)

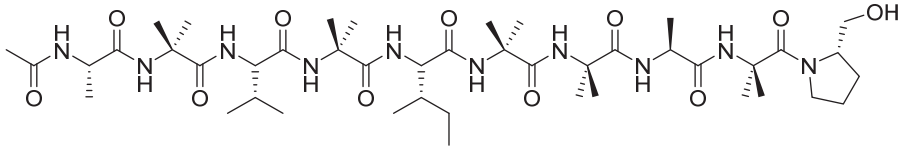

Asperelin B (**21**)

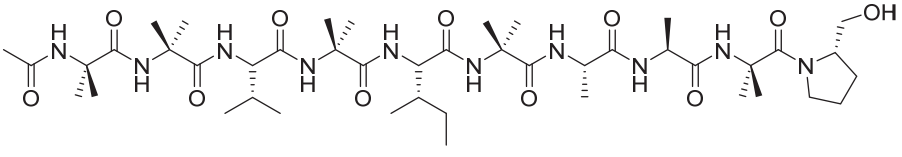

Asperelin C (**22**)

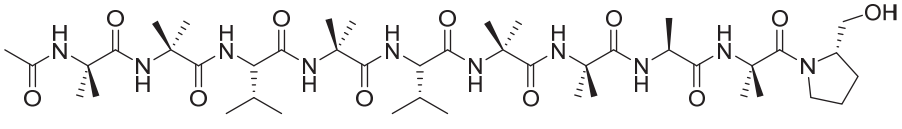

Asperelin D (**23**)

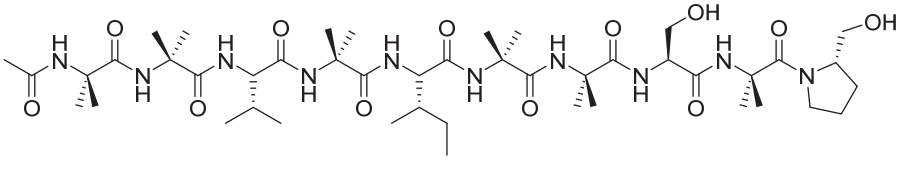

Asperelin E (**24**)

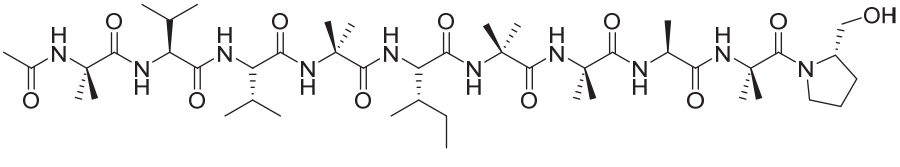

Asperelin F (**25**)

Figure 7. Secondary metabolites isolated from *Tridocherma asperellum*.

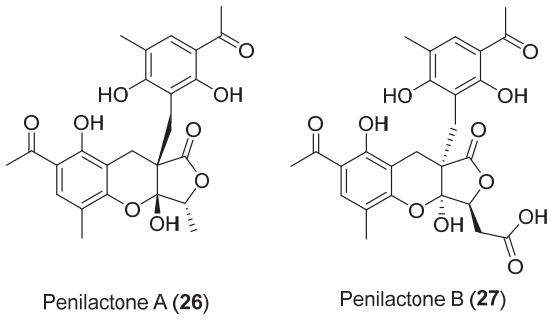

Figure 8. Secondary metabolites isolated from *Penicillium crustosum* PRB-2.

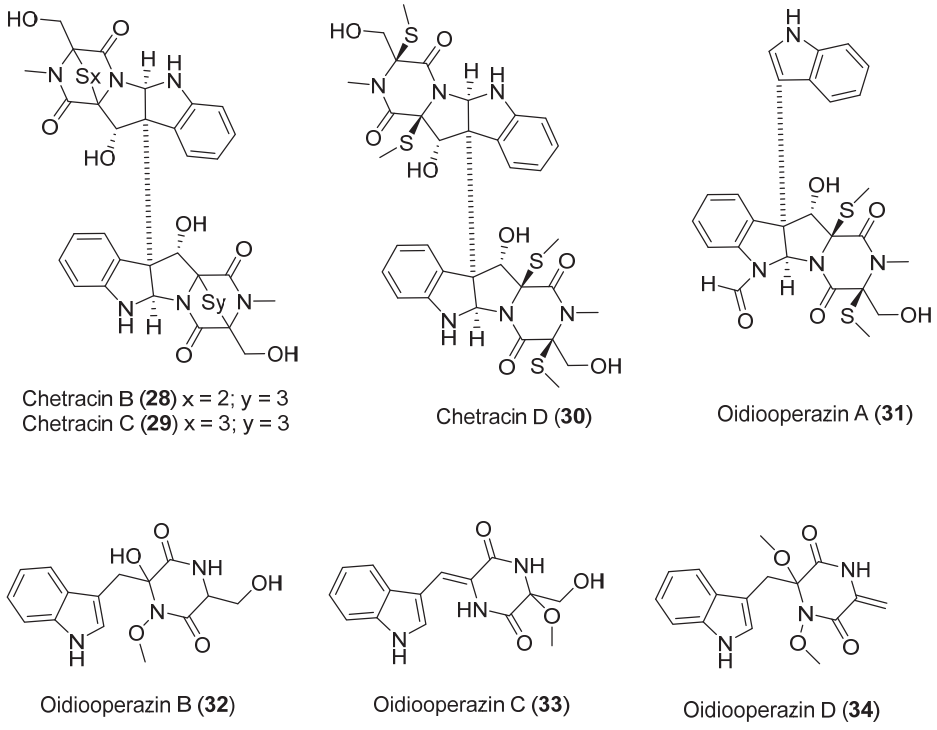

Figure 9. Secondary metabolites isolated from the Antarctic fungus *Oidiodendron truncatum*.

In the same study, compounds **29** and **30** exhibited significant cytotoxicity at micromolar concentration. Finally, it was observed that compounds **31**–**34** did not show cytotoxicity at a concentration of 10 μM. This led to the conclusion that the sulfide bridge was a determining factor in the biological activity presented by these compounds. In contrast, the number of sulfur atoms in the bridge did not seem to influence the bioactivity [38].

Organic extracts of several fungi were isolated from samples of Porifera collected on King George Island. Although pure compounds could not be isolated, the presence of biological activities and potential as antimicrobial agents could be investigated. Antimicrobial activity was tested using strains of *Pseudomonas aeruginosa*, *Staphylococcus aureus* ATCC25922, *Clavibacter michiganensis* 807, and *Xanthomonas campestris* 833. Antitumoral activity was assessed using *Agrobacterium tumefaciens* At348 as a model, and antioxidant activity was determined by comparing the absorbance of ascorbic acid obtained from each

extract. Approximately 50% of the 101 extracts showed antibacterial activity against at least one of the bacteria tested, being more active against Gram-positive bacteria such as *Staphylococcus aureus*. Moreover, 43 extracts showed 50% inhibition of crown gall tumor growth on potato. Antioxidant studies revealed that 97 fungal extracts displayed decent activities varying from very low to mild, and only three isolates showed high antioxidant activities [39].

Four new compounds, namely Pseudogymnoascins A–C (**35**–**37**) and 3-nitroasterric acid (**38**) (Figure 10), were characterized from a culture of *Pseudogymnoascus* sp., obtained from an Antarctic marine sponge of the genus *Hymeniacidon* [40]. Remarkably, these compounds were the first nitro derivatives of asterric acid identified. The antimicrobial activity of compounds **35**–**38** was evaluated against *Pseudomonas aeruginosa* PAO1, *Actinobacter baumannii* CL5973, *Escherichia coli* MB2884, *Staphylococcus aureus* EP1167, and *S. aureus* MB5394. Their antifungal activity was also tested against *Candida albicans* MY1055, *C. albicans* ATCC64124, and *Aspergillus fumigatus* ATCC46645. Cytotoxicity against the tested microorganisms was not observed, suggesting that the presence of the nitro group in the structure may negatively influence the biological activity of these compounds [40].

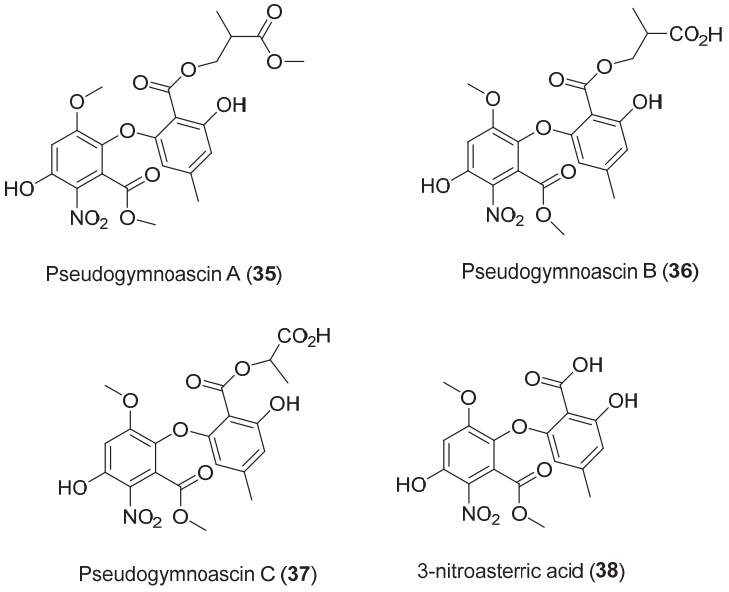

Figure 10. Secondary metabolites isolated from *Pseudogymnoascus* sp.

One hundred fungal strains were isolated from 55 samples of maritime Antarctic and classified into 35 fungal taxa within 20 genera. Extracts from these strains were tested against human tumoral cells, parasitic protozoa (*Leishmania amazonensis*, *Trypanosoma cruzi*), fungi, and bacteria. The extracts from *Purpureocillum lilacinum* displayed high trypanocidal, antibacterial, and antifungal activities with moderate toxicity over normal cells [41].

In recent years the chemical compounds of *Penicillium* sp. S-1-18 isolated from Antarctic seabed sediments has been extensively investigated. Butanolide A (**39**), a new furanone derivative, and guignarderemophilane F (**40**), a new sesquiterpene, together with six known compounds: penicyclone A (**41**), xylarenone A (**42**), callyspongidipeptide A (**43**), cyclo-(L-Phe-4R-hydroxyl-L-Pro) (**44**), cyclo-(L-Pro-L-Phe) (**45**), and N-(2-hydroxypropanoyl)-2-aminobenzoic acid amide (**46**), were isolated (Figure 11). The structures of these metabolites were determined using 1D- and 2D-NMR spectroscopic methods. Inhibitory effects against PTP1B activity were tested for all compounds. Only compound **39**

showed activity against PTP1B, which was moderate compared with the positive control oleanolic acid [42].

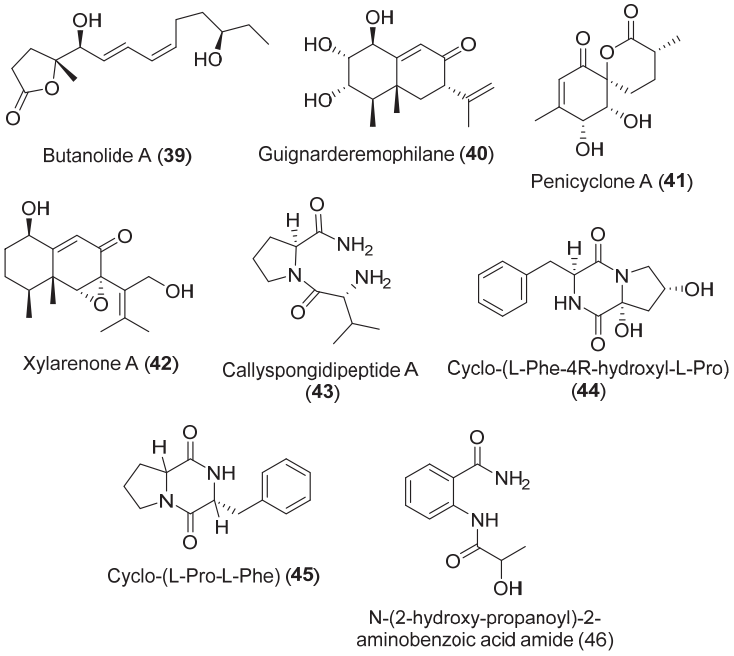

Figure 11. Secondary metabolites isolated from *Penicillium* sp. S-1-18.

An interesting study of the distribution of marine fungi found that *Pseudogymnoascus* sp. and species of the genus *Penicillium* were present in all marine samples. Samples collected at 20 m or more in depth, at temperatures near 0 °C, had higher diversity those from the intertidal zone (superficial samples) [43].

The antibacterial activity was assessed for four new compounds, Penixylarins A–D (**47**–**50**), obtained from a culture of the Antarctic fungus *Penicillium crustosum* PRB-2 and the mangrove-derive fungus *Xylaria* sp. HDN12-249 (Figure 12). Compounds **48** and **49** showed antibacterial activity against *B. subtilis*, *M. phlei*, and *V. parahemolyticus*. Compound **49** additionally displayed potential antituberculosis effects against *Mycobacterium phlei* [44].

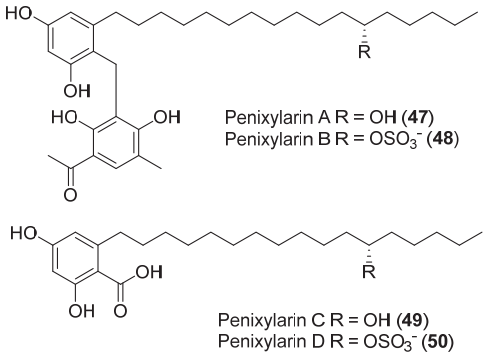

Figure 12. Penixylarins A–D, isolated from *Penicillium crestosum* PRB-2 and the fungus *Xylaria* sp. HDN12-249.

In a 2018 review, Tripathi et al. described more than two hundred natural products isolated from prokaryotes and eukaryotes living in polar regions, including fungi. Their pharmacology, relevant bioactivity, and chemical structures were reported in the review [45]. One year later, anticancer compounds were isolated from seaweed-derived endophytic fungi [46].

Using a different sampling strategy, pieces of excrement from Adelie penguins allowed the isolation of *Penicillium chrysogenum*. Although the sample was not collected from a marine environment per se, the feeding habits of the penguins support the idea that the microorganisms isolated are marine. The exact location of the sample collection site was not stated but is presumably near the Chinese Great Wall Antarctic base. A new compound Chrysonin (**51**) was obtained as a pair of enantiomers 6S- and 6R-chrysonin (**51a** and **51b**) (Figure 13). These compounds display an eight-membered heterocycle fused with a benzene ring. Interestingly, there is no precedent of one natural compound with this structure. Compound 52 was also isolated as a mixture of a new zwitterionic compound chrysomamide (**52a**) and N-[2-trans-(4-hydroxyphenyl) ethenyl] formamide (**52b**) (Figure 13). Compound **53**, shown in Figure 13, contains the unusual isocyanide functional group. This functional group has been found in several marine organisms, such as cyanobacteria, Penicillium fungi, marine sponges, and nudibranchs. Furthermore, there is no precedent of one natural compound with an eight-membered heterocycle fused with a benzene ring. Antibacterial activity of each compound against eight microorganisms was determined. Compound **53** (Figure 13) was active against *Pseudomonas aeruginosa*, *Klebsiella pneumoniae*, and *Acinetobacter baumannii*. The same metabolite and compound **54** (Figure 13) both showed significant cytotoxicity against four cancer cell lines: *A. baumannii* ATCC 19606, *E. coli* ATCC 25922, *M. luteus* SCSIO MLO1, and MRSA, shhs-A1. Compound **55** (Figure 13) displayed the best alpha glucosidase inhibition [47].

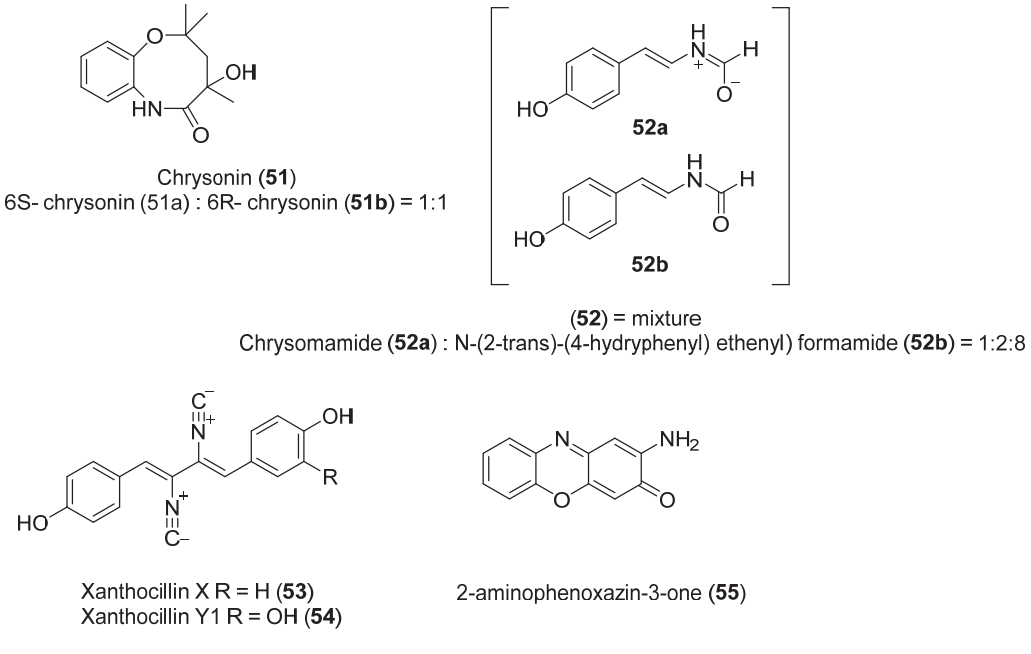

Figure 13. Secondary metabolites isolated from *Penicillium chrysogenum*.

Penicillium echinulatum was isolated from the surface of the alga *Adenocystis utricularis* collected on a beach close to Comandante Ferraz Brazilian station on King George Island. In this study, photosafety was evaluated using photoreactivity (OECD TG 495) and pho-

totoxicity assays performed by 3T3 neutral red uptake (3T3 NRU PT, OECD TG 432) and the RHS model. The purification of four alkaloids was achieved in a bio-guided process. Four known metabolites were identified: (−)-cyclopenin (**56**), dehydrocyclopeptine (**57**), viridicatin (**58**), and viridicatol (**59**) (Figure 14), and their photoprotective and antioxidant activities were shown [48].

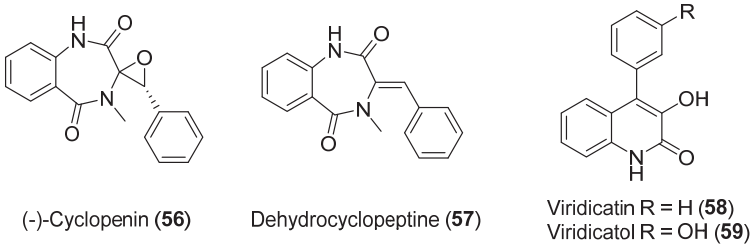

Figure 14. Alkaloids isolated from *Penicillium echinulatum*.

The antibacterial activity of Penicillic acid (**60**) (Figure 15), isolated from *Penicillium* sp. CRM-1540 found in Antarctic marine sediment at King George Island, was evaluated. This compound was obtained as the major bioactive fraction through a bioguided study. Results showed 90% bacterial inhibition in vitro at 25 μg mL^{-1} against *Xanthomonas citri* [49].

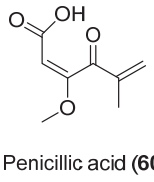

Figure 15. Penicillic acid isolated from *Penicillium* sp. *CRM-1540*.

Talaverrucin A (**61**) (Figure 16), a heterodimeric oxaphenalenone with a rare fused ring system, was isolated from *Talaromyces* sp. HDN151403 (Prydz Bay, Antarctica). The oncogenic Wnt/β-catecin inhibitory effect was tested and showed inhibitory activity in zebrafish embryos in vivo and cultured mammalian cells in vitro [50].

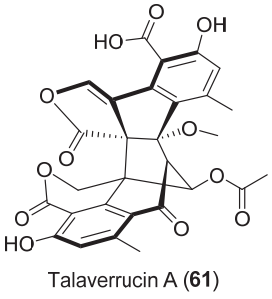

Figure 16. Talaverrucin A isolated from *Penicillium* sp. CRM-1540.

The cytotoxic activity of Citromycin (**62**) (Figure 17) was tested against ovarian cancer SKOV3 and A2780 cells. No cytotoxic activity was observed. The compound **62** was obtained from *Sporothrix* sp. and showed inhibition of extracellular signal-regulated kinase (ERK)-1/1 [51].

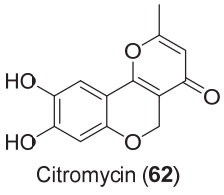

Figure 17. Citromycin isolated from *Sporothrix* sp.

Four new cytotoxic nitrobenzoyl sesquiterpenoids, insulicolides D–G (**63**–**66**) (Figure 18), were isolated from *Aspergillus insulicola* HDN151418, which was obtained from an unidentified Antarctica sponge (Prydz Bay). Compounds **65** and **66** showed selective inhibition against human PDAC cell lines [52].

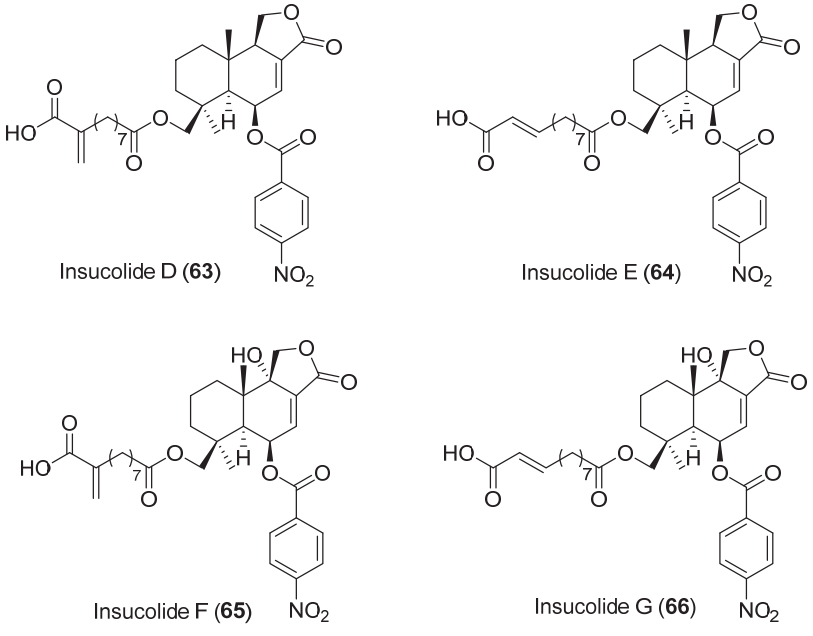

Figure 18. Insucolides (D–G) isolated from *Aspergillus insulicola* HDN151418.

Three new perylenequinone derivatives (Xanalterate A, **67**, Altertoxin VIII, **68** and IX, **69**) together with a known natural product, Stemphyperylenol (**70**) (Figure 19), were isolated from *Alternaria* sp. HDN19-690 associated to an Antarctic sponge. Compound **67** exhibited promising antibacterial activity against methicillin-resistant coagulase negative *Staphylococcus* (MRCNS), *Bacillus subtilis*, *Proteus mirabilis*, *Bacillus cereus*, *Escherichia coli*, and *Mycobacterium phlei* with MIC values ranging from 3.13 to 12.5 μM [53].

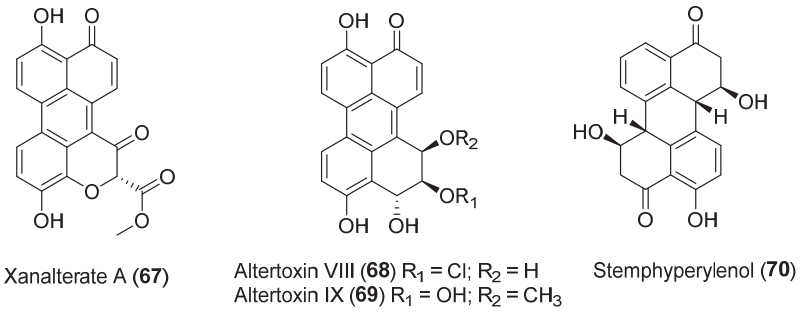

Figure 19. Perylenequinones isolated from *Aspergillus insulicola* HDN151418.

4. Materials and Methods

Scifinder database and the repositories of the Pontificia Universidad Católica de Chile and Universidad Técnica Federico Santa Maria were used to search for reports published from 1996 to date. The search criteria focused on marine fungi obtained from Chilean coasts, the South Shetland Islands, and Antarctic peninsula and reports of novel marine NPs that were spectroscopically characterized and presented biological or pharmaceutical properties. Descriptions involving vegetable extracts or primary metabolites were omitted.

5. Conclusions

Natural products from Chilean marine fungi represent a prolific and yet underexplored source of chemical structures with remarkable biomedical applications (Table 1). Alkaloids, polyketides, terpenoids, isoprenoids, non-isoprenoid compounds, and quinones display the most relevant biological activities. There are few studies on secondary metabolites isolated from marine fungi collected in Chile, highlighting the antimicrobial activity presented by some crude extracts and the antitumor activity of some of the isolated compounds. The dearth of studies may be attributed to the difficulties in cultivating microorganisms, some of which cannot survive under standard laboratory conditions and therefore cannot be cultured using traditional techniques. It is complicated to reproduce the conditions found inside the host marine organisms. The culture medium used is suitable for facultative fungi but probably inadequate for natural marine fungi. Recent advances in chromatographic and spectroscopic techniques now open a world of possibility for isolating secondary metabolites of these organisms that are abundant in Chilean marine ecosystems.

Table 1. Secondary metabolites isolated from Chilean and Antarctic Fungi.

Compounds	Fungi	Region	Bioactivity	References
1	*Cladosporium cladosporioides*	Chilean coasts	Not antimicrobial activity showed	[23]
2	*Inonotus obliquus* *Geotrichum* sp.		Cytotoxic activity, Lipid-peroxidation, Antioxidant activity	[22,23,26]
3	*Penicillium brevicompactum*		Antibacterial activity	[24]
4				
5				
6				
7	*Geotrichum* sp.		Not tested	[26]
8	*Scleroderma polyrizum* *Geotrichum* sp. *Lampteromyces japonicus* *Fomes officinalis*		Not tested	[25,26]

Table 1. *Cont.*

Compounds	Fungi	Region	Bioactivity	References
9	*Geotrichum* sp.	Chilean coasts	Not tested	[26]
10	*Geomyces* sp.		Not tested	[27]
11	Aspergillus sp.		Antibacterial activity	[28]
12			Antitumor activity	
13			Vasorelaxant activity	
14	Aspergillus sp.		Not tested	[28]
15	*Geomyces* sp.		Not antimicrobial, and antifungal activity showed	[31–34]
16			Not antimicrobial, and antifungal activity showed	
17			Not antimicrobial, and antifungal activity showed	
18			Antifungal activity	
19			Antibacterial activity	
20	*Tridocherma asperellum*	Antarctic	Not tested	[35]
21			Not tested	
22			Not tested	
23			Not tested	
24			Not tested	
25			Not tested	
26	*Penicillium crustosum*		Not cytotoxic activity showed	[36,37]
27			Inhibit nuclear factor-κB (NF-κB)	
28	*Oidiodendron truncatum* GW3-13		Cytotoxic activity	[38]
29				
30				
31			No significant cytotoxic activity showed	
32			No significant cytotoxic activity showed	
33			No significant cytotoxic activity showed	
34			No significant cytotoxic activity showed	
35	*Pseudogymnoascus* sp.		Not antimicrobial and antifungal activity showed	[40]
36			Not antimicrobial and antifungal activity showed	
37			Not antimicrobial and antifungal activity showed	
38			Not antimicrobial and antifungal activity showed	
39	*Penicillium* sp.	Antarctic	Antiproliferative effect	[42]
40			Not antiproliferative effect showed	
41			Not antiproliferative effect showed	
42			Not antiproliferative effect showed	
43			Not antiproliferative effect showed	
44			Not antiproliferative effect showed	
45			Not antiproliferative effect showed	
46			Not antiproliferative effect showed	

Table 1. *Cont.*

Compounds	Fungi	Region	Bioactivity	References
47	*Penicillium crestosum* (PRB-2)	Antarctic	No cytotoxic and antibacterial activity showed	[44]
48			Antibacterial activity	
49			Antibacterial activity	
50			No cytotoxic, and antibacterial activity showed	
51	*Penicillium chrysogenum*		Moderate alpha glucosidase inhibition, no cytotoxic and antibacterial activity showed	[47]
51a			Moderate alpha glucosidase inhibition, no cytotoxic and antibacterial activity showed	
51b			Moderate alpha glucosidase inhibition, no cytotoxic and antibacterial activity showed	
52a			Moderate alpha glucosidase inhibition, no cytotoxic and antibacterial activity showed	
52b			Moderate alpha glucosidase inhibition, no cytotoxic and antibacterial activity showed	
53			Antibacterial activity	
54			Cytotoxic activity	
55			Alpha glucosidase inhibition	
56	*Penicillium echinulatum*		Photoprotective and antioxidant activity	[48]
57			No cytotoxic and antibacterial activity showed	
58			Cytotoxic activity	
59			Cytotoxic activity	
60	*Penicillium* sp. *CRM-1540*		Antibacterial activity	[49]
61	*Talaromyces* sp. HDN151403		Cytotoxic activity	[50]
62	*Sporothrix* sp.		Cytotoxic activity	[51]
63	*Aspergillus insulicola* HDN151418		No cytotoxic activity showed	[52]
64			No cytotoxic activity showed	
65			Cytotoxic activity	
66			Cytotoxic activity	
67	*Alternaria* sp. HDN19-690		Antibacterial activity, no cytotoxic activity showed	[53]
68			No cytotoxic and antibacterial activity showed	
69			No cytotoxic and antibacterial activity showed	
70			No cytotoxic and antibacterial activity showed	

Author Contributions: Conceptualization, D.A. and J.R.C.-P.; writing—original draft preparation, D.A.; resources, D.A.; H.C., A.S.-M. and J.R.C.-P.; writing—review and editing, L.T., H.C., J.R.C.-P. and A.S.-M. All authors participated in similar measure in the preparation of this manuscript. All authors have read and agreed to the published version of the manuscript.

Funding: Instituto Antártico Chileno (INACH) RT_16-21.

Acknowledgments: J.R.C.-P thanks Instituto Antártico Chileno (INACH), for grant RT_16-21, D.A express thanks to the Dirección de Postgrado y Programas (DPP), Universidad Técnica Federico Santa María. The authors thank Ellen Leffler for critical reading and suggestions.

Conflicts of Interest: The authors declare that they have no conflicting interest in the publication.

References

1. Tong, Y.; Deng, Z. An Aurora of Natural Products-Based Drug Discovery Is Coming. *Synth. Syst. Biotechnol.* **2020**, *5*, 92–96. [CrossRef]
2. Newman, D.J.; Cragg, G.M. Natural Products as Sources of New Drugs from 1981 to 2014. *J. Nat. Prod.* **2016**, *79*, 629–661. [CrossRef]
3. Newman, D.J.; Cragg, G.M. Natural Products as Sources of New Drugs over the Nearly Four Decades from 01/1981 to 09/2019. *J. Nat. Prod.* **2020**, *83*, 770–803. [CrossRef]
4. Clardy, J.; Walsh, C. Lessons from Natural Molecules. *Nature* **2004**, *432*, 829–837. [CrossRef]
5. Choi, J.; Kim, S.-H. A Genome Tree of Life for the Fungi Kingdom. *Proc. Natl. Acad. Sci. USA* **2017**, *114*, 9391–9396. [CrossRef]
6. Calvo, A.M.; Wilson, R.A.; Bok, J.W.; Keller, N.P. Relationship between Secondary Metabolism and Fungal Development. *Microbiol. Mol. Biol. Rev.* **2002**, *66*, 447–459. [CrossRef]
7. Nielsen, J.C.; Grijseels, S.; Prigent, S.; Ji, B.; Dainat, J.; Nielsen, K.F.; Frisvad, J.C.; Workman, M.; Nielsen, J. Global Analysis of Biosynthetic Gene Clusters Reveals Vast Potential of Secondary Metabolite Production in Penicillium Species. *Nat. Microbiol.* **2017**, *2*, 17044. [CrossRef]
8. Schueffler, A.; Anke, T. Fungal Natural Products in Research and Development. *Nat. Prod. Rep.* **2014**, *31*, 1425–1448. [CrossRef]
9. Carroll, A.R.; Copp, B.R.; Davis, R.A.; Keyzers, R.A.; Prinsep, M.R. Marine Natural Products. *Nat. Prod. Rep.* **2021**, *38*, 362–413. [CrossRef]
10. Carroll, A.R.; Copp, B.R.; Davis, R.A.; Keyzers, R.A.; Prinsep, M.R. Marine Natural Products. *Nat. Prod. Rep.* **2022**, *39*, 1122–1171. [CrossRef]
11. Montuori, E.; De Pascalle, D.; Lauritano, C. Recent Discoveries on Marine Organism Immunomodulatory Activities. *Mar. Drugs.* **2022**, *20*, 422. [CrossRef]
12. Durães, F.; Szemerédi, N.; Kumla, D.; Pinto, M.; Kijjoa, A.; Spengler, G.; Sousa, E. Metabolites from Marine-Derived Fungi as Potential Antimicrobial Adjuvants. *Mar. Drugs.* **2021**, *19*, 475. [CrossRef]
13. De la Calle, F. Fármacos de Origen Marino. *Treballs de la SCB.* **2007**, *58*, 141–155. [CrossRef]
14. Rateb, M.E.; Ebel, R. Secondary Metabolites of Fungi from Marine Habitats. *Nat. Prod. Rep.* **2011**, *28*, 290. [CrossRef]
15. Hafez Ghoran, S.; Kijjoa, A. Marine-Derived Compounds with Anti-Alzheimer's Disease Activities. *Mar. Drugs.* **2021**, *19*, 410. [CrossRef]
16. Jiang, M.; Wu, Z.; Guo, H.; Liu, L.; Chen, S. A Review of Terpenes from Marine-Derived Fungi: 2015–2019. *Mar. Drugs.* **2020**, *18*, 321. [CrossRef]
17. El-Demerdash, A.; Kumla, D.; Kijjoa, A. Chemical Diversity and Biological Activities of Meroterpenoids from Marine Derived-Fungi: A Comprehensive Update. *Mar. Drugs.* **2020**, *18*, 317. [CrossRef]
18. Nuestro País. Available online: https://www.gob.cl/nuestro-pais/ (accessed on 24 October 2022).
19. Masas de Agua En El Mar Chileno. Available online: http://www7.uc.cl/sw_educ/geo_mar/html/h43.html (accessed on 24 October 2022).
20. Biblioteca del Congreso Nacional | SIIT | Chile Nuestro País. Available online: https://www.bcn.cl/siit/nuestropais/index_html (accessed on 24 October 2022).
21. Núñez-Pons, L.; Shilling, A.; Verde, C.; Baker, B.J.; Giordano, D. Marine Terpenoids from Polar Latitudes and Their Potential Applications in Biotechnology. *Mar. Drugs* **2020**, *18*, 401. [CrossRef]
22. Yasukawa, K.; Akihisa, T.; Kanno, H.; Kaminaga, T.; Izumida, M.; Sakoh, T.; Tamura, T.; Takido, M. Inhibitory Effects of Sterols Isolated from Chlorella Vulgaris on 12-O-Tetradecanoylphorbol-13-Acetate-Induced Inflammation and Tumor Promotion in Mouse Skin. *Biol. Pharm. Bull.* **1996**, *19*, 573–576. [CrossRef]
23. San Martin, A.; Painemal, K.; Diaz, Y.; Martinez, C.; Rovirosa, J. Metabolites from the marine fungus *Cladosporium cladosporioides*. *J. Chil. Chem. Soc.* **2005**, *93*, 247–251.
24. Rovirosa, J.; Diaz-Marrero, A.; Darias, J.; Painemal, K.; San Martin, A. Secondary metabolites from the marine *Penicillium brevicompactum*. *J. Chil. Chem. Soc.* **2006**, *51*, 775–778. [CrossRef]
25. Ciminiello, P.; Fattorusso, E.; Magno, S.; Mangoni, A.; Pansini, M. A Novel Conjugated Ketosteroid from the Marine Sponge Dictyonella Incisa. *J. Nat. Prod.* **1989**, *52*, 1331–1333. [CrossRef]
26. San-Martín, A.; Orejarena, S.; Gallardo, C.; Silva, M.; Becerra, J.; Reinoso, R.; Chamy, M.C.; Vergara, K.; Rovirosa, J. Steroids from the marine fungus *Geotrichum* sp. *J. Chil. Chem. Soc.* **2008**, *53*, 1377–1378. [CrossRef]
27. Manríquez, V.; Galdámez, A.; Veliz, B.; Rovirosa, J.; Díaz-Marrero, A.R.; Cueto, M.; Darias, J.; Martínez, C.; San-Martín, A. N-methyl-1H-indole-2-carboxamide from the marine fungus *Cladosporium cladosporioides*. *J. Chil. Chem. Soc.* **2009**, *54*, 314–316. [CrossRef]
28. San-Martín, A.; Rovirosa, J.; Vaca, I.; Vergara, K.; Acevedo, L.; Viña, D.; Orallo, F.; Chamy, M.C. New butyrolactone from a marine-derived fungus *Aspergillus* sp. *J. Chil. Chem. Soc.* **2011**, *56*, 625–627. [CrossRef]
29. Wilson, Z.E.; Brimble, M.A. Molecules Derived from the Extremes of Life. *Nat. Prod. Rep.* **2009**, *26*, 44–71. [CrossRef] [PubMed]
30. Rusman, Y.; Held, B.W.; Blanchette, R.A.; He, Y.; Salomon, C.E. Cadopherone and Colomitide Polyketides from Cadophora Wood-Rot Fungi Associated with Historic Expedition Huts in Antarctica. *Phytochemistry* **2018**, *148*, 1–10. [CrossRef]
31. Tian, Y.; Li, Y.-L.; Zhao, F.-C. Secondary Metabolites from Polar Organisms. *Mar. Drugs.* **2017**, *15*, 28. [CrossRef]

32. *Fungi of Antarctica: Diversity, Ecology and Biotechnological Applications*; Rosa, L.H. (Ed.) Springer International Publishing: Cham, Switzerland, 2019; ISBN 978-3-030-18366-0.
33. Cong, M.; Pang, X.; Zhao, K.; Song, Y.; Liu, Y.; Wang, J. Deep-Sea Natural Products from Extreme Environments: Cold Seeps and Hydrothermal Vents. *Mar. Drugs.* **2022**, *20*, 404. [CrossRef]
34. Li, Y.; Sun, B.; Liu, S.; Jiang, L.; Liu, X.; Zhang, H.; Che, Y. Bioactive Asterric Acid Derivatives from the Antarctic Ascomycete Fungus *Geomyces* Sp. *J. Nat. Prod.* **2008**, *71*, 1643–1646. [CrossRef]
35. Ren, J.; Xue, C.; Tian, L.; Xu, M.; Chen, J.; Deng, Z.; Proksch, P.; Lin, W. Asperelines A−F, Peptaibols from the Marine-Derived Fungus *Trichoderma Asperellum*. *J. Nat. Prod.* **2009**, *72*, 1036–1044. [CrossRef] [PubMed]
36. Wu, G.; Ma, H.; Zhu, T.; Li, J.; Gu, Q.; Li, D. Penilactones A and B, Two Novel Polyketides from Antarctic Deep-Sea Derived Fungus *Penicillium Crustosum* PRB-2. *Tetrahedron.* **2012**, *68*, 9745–9749. [CrossRef]
37. Spence, J.T.J.; George, J.H. Biomimetic Total Synthesis of *ent*-Penilactone A and Penilactone B. *Org. Lett.* **2013**, *15*, 3891–3893. [CrossRef] [PubMed]
38. Li, L.; Li, D.; Luan, Y.; Gu, Q.; Zhu, T. Cytotoxic Metabolites from the Antarctic Psychrophilic Fungus *Oidiodendron Truncatum*. *J. Nat. Prod.* **2012**, *75*, 920–927. [CrossRef]
39. Henríquez, M.; Vergara, K.; Norambuena, J.; Beiza, A.; Maza, F.; Ubilla, P.; Araya, I.; Chávez, R.; San-Martín, A.; Darias, J.; et al. Diversity of Cultivable Fungi Associated with Antarctic Marine Sponges and Screening for Their Antimicrobial, Antitumoral and Antioxidant Potential. *World J. Microbiol. Biotechnol.* **2014**, *30*, 65–76. [CrossRef]
40. Figueroa, L.; Jiménez, C.; Rodríguez, J.; Areche, C.; Chávez, R.; Henríquez, M.; de la Cruz, M.; Díaz, C.; Segade, Y.; Vaca, I. 3-Nitroasterric Acid Derivatives from an Antarctic Sponge-Derived *Pseudogymnoascus* Sp. Fungus. *J. Nat. Prod.* **2015**, *78*, 919–923. [CrossRef]
41. Gonçalves, V.N.; Carvalho, C.R.; Johann, S.; Mendes, G.; Alves, T.M.A.; Zani, C.L.; Junior, P.A.S.; Murta, S.M.F.; Romanha, A.J.; Cantrell, C.L.; et al. Antibacterial, Antifungal and Antiprotozoal Activities of Fungal Communities Present in Different Substrates from Antarctica. *Polar Biol.* **2015**, *38*, 1143–1152. [CrossRef]
42. Zhou, Y.; Li, Y.-H.; Yu, H.-B.; Liu, X.-Y.; Lu, X.-L.; Jiao, B.-H. Furanone Derivative and Sesquiterpene from Antarctic Marine-Derived Fungus *Penicillium* Sp. S-1-18. *J. Asian Nat. Prod. Res.* **2018**, *20*, 1108–1115. [CrossRef]
43. Wentzel, L.C.P.; Inforsato, F.J.; Montoya, Q.V.; Rossin, B.G.; Nascimento, N.R.; Rodrigues, A.; Sette, L.D. Fungi from Admiralty Bay (King George Island, Antarctica) Soils and Marine Sediments. *Microb. Ecol.* **2019**, *77*, 12–24. [CrossRef] [PubMed]
44. Yu, G.; Sun, Z.; Peng, J.; Zhu, M.; Che, Q.; Zhang, G.; Zhu, T.; Gu, Q.; Li, D. Secondary Metabolites Produced by Combined Culture of *Penicillium crustosum* and a *Xylaria* Sp. *J. Nat. Prod.* **2019**, *82*, 2013–2017. [CrossRef]
45. Tripathi, V.C.; Satish, S.; Horam, S.; Raj, S.; lal, A.; Arockiaraj, J.; Pasupuleti, M.; Dikshit, D.K. Natural Products from Polar Organisms: Structural Diversity, Bioactivities and Potential Pharmaceutical Applications. *Polar Sci.* **2018**, *18*, 147–166. [CrossRef]
46. Teixeira, T.R.; Santos, G.S.d.; Armstrong, L.; Colepicolo, P.; Debonsi, H.M. Antitumor Potential of Seaweed Derived-Endophytic Fungi. *Antibiotics.* **2019**, *8*, 205. [CrossRef] [PubMed]
47. Khan, I.; Zhang, H.; Liu, W.; Zhang, L.; Peng, F.; Chen, Y.; Zhang, Q.; Zhang, G.; Zhang, W.; Zhang, C. Identification and Bioactivity Evaluation of Secondary Metabolites from Antarctic-Derived *Penicillium chrysogenum* CCTCC M 2020019. *RSC Adv.* **2020**, *10*, 20738–20744. [CrossRef]
48. Teixeira, T.R.; Rangel, K.C.; Tavares, R.S.N.; Kawakami, C.M.; dos Santos, G.S.; Maria-Engler, S.S.; Colepicolo, P.; Gaspar, L.R.; Debonsi, H.M. *In Vitro* Evaluation of the Photoprotective Potential of Quinolinic Alkaloids Isolated from the Antarctic Marine Fungus *Penicillium echinulatum* for Topical Use. *Mar. Biotechnol.* **2021**, *23*, 357–372. [CrossRef]
49. Vieira, G.; Khalil, Z.G.; Capon, R.J.; Sette, L.D.; Ferreira, H.; Sass, D.C. Isolation and Agricultural Potential of Penicillic Acid against Citrus Canker. *J. Appl. Microbiol.* **2022**, *132*, 3081–3088. [CrossRef] [PubMed]
50. Sun, C.; Liu, Q.; Shah, M.; Che, Q.; Zhang, G.; Zhu, T.; Zhou, J.; Rong, X.; Li, D. Talaverrucin A, Heterodimeric Oxaphenalenone from Antarctica Sponge-Derived Fungus *Talaromyces* Sp. HDN151403, Inhibits Wnt/β-Catenin Signaling Pathway. *Org. Lett.* **2022**, *24*, 3993–3997. [CrossRef]
51. Choi, H.Y.; Ahn, J.-H.; Kwon, H.; Yim, J.H.; Lee, D.; Choi, J.-H. Citromycin Isolated from the Antarctic Marine-Derived Fungi, *Sporothrix* Sp., Inhibits Ovarian Cancer Cell Invasion via Suppression of ERK Signaling. *Mar. Drugs.* **2022**, *20*, 275. [CrossRef]
52. Sun, C.; Liu, X.; Sun, N.; Zhang, X.; Shah, M.; Zhang, G.; Che, Q.; Zhu, T.; Li, J.; Li, D. Cytotoxic Nitrobenzoyl Sesquiterpenoids from an Antarctica Sponge-Derived *Aspergillus Insulicola*. *J. Nat. Prod.* **2022**, *85*, 987–996. [CrossRef]
53. Hou, Z.; Sun, C.; Chen, X.; Zhang, G.; Che, Q.; Li, D.; Zhu, T. Xanalterate A, Altertoxin VIII and IX, Perylenequinone Derivatives from Antarctica-Sponge-Derived Fungus *Alternaria* Sp. HDN19-690. *Tetrahedron Lett.* **2022**, *96*, 153778. [CrossRef]

marine drugs

MDPI

Review

Secondary Metabolites, Biological Activities, and Industrial and Biotechnological Importance of *Aspergillus sydowii*

Sabrin R. M. Ibrahim [1,2,*], Shaimaa G. A. Mohamed [3], Baiaan H. Alsaadi [4], Maryam M. Althubyani [4], Zainab I. Awari [5], Hazem G. A. Hussein [6], Abrar A. Aljohani [7], Jumanah Faisal Albasri [8], Salha Atiah Faraj [9] and Gamal A. Mohamed [10]

[1] Preparatory Year Program, Department of Chemistry, Batterjee Medical College, Jeddah 21442, Saudi Arabia
[2] Department of Pharmacognosy, Faculty of Pharmacy, Assiut University, Assiut 71526, Egypt
[3] Faculty of Dentistry, British University, El Sherouk City, Cairo 11837, Egypt; shaimaag1973@gmail.com
[4] Department of Clinical Service, Pharmaceutical Care Services, King Salman Medical City, MOH, Al Madinah Al Munawwarah 11176, Saudi Arabia; bayanhs@hotmail.com (B.H.A.); ph.maryam91@gmail.com (M.M.A.)
[5] Pharmaceutical Care Services, King Salman Medical City, MOH, Al Madinah Al Munawwarah 11176, Saudi Arabia; zawari.3000@outlook.com
[6] Preparatory Year Program, Batterjee Medical College, Jeddah 21442, Saudi Arabia; hazemgamal2005@gmail.com
[7] Pharmaceutical Care Services, Medina Cardiac Center, MOH, Al Madinah Al Munawwarah 11176, Saudi Arabia; ph1993abrar@gmail.com
[8] Pharmacy Department, Home Health Care, MOH, Al Madinah Al Munawwarah 11176, Saudi Arabia; jumanah.albasri@gmail.com
[9] Pharmacy Department, King Salman Medical City, MOH, Almadinah Almunawarah 11176, Saudi Arabia; salhafaraj66@gmail.com
[10] Department of Natural Products and Alternative Medicine, Faculty of Pharmacy, King Abdulaziz University, Jeddah 21589, Saudi Arabia; gahussein@kau.edu.sa
* Correspondence: sabrin.ibrahim@bmc.edu.sa or sabreen.ibrahim@pharm.aun.edu.eg; Tel.: +966-581-1830-34

Citation: Ibrahim, S.R.M.; Mohamed, S.G.A.; Alsaadi, B.H.; Althubyani, M.M.; Awari, Z.I.; Hussein, H.G.A.; Aljohani, A.A.; Albasri, J.F.; Faraj, S.A.; Mohamed, G.A. Secondary Metabolites, Biological Activities, and Industrial and Biotechnological Importance of *Aspergillus sydowii*. *Mar. Drugs* **2023**, *21*, 441. https://doi.org/10.3390/md21080441

Academic Editor: Hafiz M.N. Iqbal

Received: 11 July 2023
Revised: 29 July 2023
Accepted: 2 August 2023
Published: 5 August 2023

Abstract: Marine-derived fungi are renowned as a source of astonishingly significant and synthetically appealing metabolites that are proven as new lead chemicals for chemical, pharmaceutical, and agricultural fields. *Aspergillus sydowii* is a saprotrophic, ubiquitous, and halophilic fungus that is commonly found in different marine ecosystems. This fungus can cause aspergillosis in sea fan corals leading to sea fan mortality with subsequent changes in coral community structure. Interestingly, *A. sydowi* is a prolific source of distinct and structurally varied metabolites such as alkaloids, xanthones, terpenes, anthraquinones, sterols, diphenyl ethers, pyrones, cyclopentenones, and polyketides with a range of bioactivities. *A. sydowii* has capacity to produce various enzymes with marked industrial and biotechnological potential, including α-amylases, lipases, xylanases, cellulases, keratinases, and tannases. Also, this fungus has the capacity for bioremediation as well as the biocatalysis of various chemical reactions. The current work aimed at focusing on the bright side of this fungus. In this review, published studies on isolated metabolites from *A. sydowii*, including their structures, biological functions, and biosynthesis, as well as the biotechnological and industrial significance of this fungus, were highlighted. More than 245 compounds were described in the current review with 134 references published within the period from 1975 to June 2023.

Keywords: fungi; *Aspergillus sydowii*; metabolites; enzymes; biotechnology; bioremediation; renewable resources; life on land; marine natural products; drug discovery

1. Introduction

Fungi have so far received substantial attention for enhancing value in agricultural, industrial, pharmaceutical, and health fields [1–4]. During the past few decades, there have been some extremely intriguing advances in the utilization of fungi for new processes,

products, and solutions that are crucial for the world. Also, fungi are proven to be a prolific pool of structurally varied bioactive metabolites. Additionally, fungal enzymes have been utilized instead of chemical processes in various industries, including those of textiles, leather, paper, pulp, animal feed, baked goods, beer, wine, and juice, which greatly reduces negative environmental effects [5]. Genus *Aspergillus* (Moniliaceae) is one of the most valuable fungal genera of commercial, biotechnological, and medicinal importance [6–8]. It comprises 400 species and attracts remarkable interest as a wealthy pool of structurally varied metabolites, including terpenoids, alkaloids, peptides, xanthones, and polyketides [7–9]. These metabolites have diverse bioactivities such as antibacterial, cytotoxic, antifungal, and anti-HIV activities.

Aspergillus sydowii is a saprotrophic, ubiquitous, and halophilic fungus and represents one of the widely distributed *Aspergillus* species [10–12]. It is commonly found in different habitats all over the world, including diverse soil and marine ecosystems, and possesses a broad range of salinity tolerance [13]. Interestingly, halophilic *A. sydowii* is employed as a model organism for investigating filamentous fungi's molecular adaptation to hyperosmolarity [13]. *A. sydowii* can survive as a food contaminant, as a soil-decomposing saprotroph, and as an opportunistic human pathogen [14]. It causes onychomycosis and aspergillosis in humans, as well as aspergillosis in sea fan corals, on the basis of Koch's postulate and physiological, morphological, and nucleotide sequence analyses [15–17]. Aspergillosis symptoms involve small necrotic lesions of tissues with purple halos, like the pathology of coral bleaching [18]. This leads to sea fan mortality and subsequent changes in coral community structure [18]. It was reported to cause 20–90% mortality in sea fans in the Florida Keys [18].

In addition to its pathogenic potential, *A. sydowii* has captured a considerable number of researchers' attention due to its capacity to create a variety of biotechnologically and industrially significant enzymes, such as lipases, α-amylases, xylanases, cellulases, tannases, and keratinases [19–23]. Additionally, *A. sydowii* biosynthesizes various classes of metabolites, such as sesquiterpenoids, alkaloids, xanthones, monoterpenes, anthraquinones, sterols, triterpenes, diphenyl ethers, pyrones, cyclopentenones, anthocyanins, and polyketides [11,24–38]. These metabolites have drawn remarkable interest because of their prominent bioactivities, including antioxidant, immunosuppression, antiviral, anti-mycobacterial, antimicrobial, cytotoxic, anti-inflammation, protein tyrosine phosphatase 1B (PTP1B) inhibition, anti-nematode, anti-diabetic, and anti-obesity properties [32,34,37,39–48]. Further, this fungus is employed for the synthesis of different types of nanoparticles that could have beneficial pharmaceutical, biotechnological, and industrial applications [49–52]. Recently, the number of articles on *A. sydowii* metabolites and their biotechnological and industrial relevance has risen substantially. It is noteworthy that a review paper discussing *A. sydowii*, particularly the positive aspects of this commercially useful fungus, was not found. Therefore, the current work provided a comprehensive and close insight into this fungus. The published information on the secondary metabolites identified from this fungus and their bioactivities were compiled. Additionally, the research on *A. sydowii*, including applications in industry, biotechnology, and nanotechnology, has been reviewed. Studies published in the literature within the period from 1975 to 2023 were reported. Additionally, the documented biosynthesis routes of the fungus' major metabolites were illustrated.

Searches were conducted in depth on literature databases, namely PubMed, Web of Science, and Scopus, as well as on various websites of publishers (Wiley Online Library, Taylor & Francis, Springer, JACS, Thieme, and Bentham) and scientific websites (Google Scholar, PubMed, and ScienceDirect). The following phrases and keywords were used for the search: "*Aspergillus sydowii*," "*Aspergillus sydowii* + compounds," "*Aspergillus sydowii* + metabolites," "*Aspergillus sydowii* + NMR," "*Aspergillus sydowii* + biological activity," "*Aspergillus sydowii* + Enzymes," "*Aspergillus sydowii* + biotechnology," "*Aspergillus sydowii* + biotechnological importance," and "*Aspergillus sydowii* + nanoparticles".

2. Secondary Metabolites of *Aspergillus sydowii*

2.1. Sesquiterpenes

Phenolic bisabolane sesquiterpenoids are among the main constituents reported from this fungus. They are a rare class of terpenes that have a p-alkylated benzene connected with 1C and 8C side chains at C-5 and C-2, respectively. Their structural variability is due to cyclization, reduction, or oxidation at various alkyl chain carbons to yield carboxylic acid, alcohol, lactone, double bond, pyran, and furan functionalities. Besides their fascinating skeletons, they show various bioactivities. It is noteworthy that most of the reported bisabolanes were separated from marine-derived *A. sydowii* as discussed below (Table 1).

Table 1. Sesquiterpenoids reported from *Aspergillus sydowii* (molecular weight and formulae, strain, host, and location).

Compound Name	Mol. Wt.	Mol. Formula	Strain, Host, Location	Ref.
(+)-(7*S*)-Sydonic acid (**1**)	266	$C_{15}H_{22}O_4$	Cultured, IFO 7531, Japan	[11]
	-	-	*Acanthophora spicifera* (red alga), Rameswaram, India	[53]
			Marine sediment, Hsinchu, Taiwan	[54]
	-	-	CUGB-F126, seawater, Bohai Sea, Tianjin	[15]
	-	-	C1-S01-A7, seawater sample, West Pacific Ocean	[55]
	-	-	PSU-F154, genus *Annella* sp. (gorgonian sea fan), coastal area, Surat Thani, Thailand	[56]
	-	-	MSX19583, spruce litter, Colorado, USA	[33]
	-	-	ZSDS1-F6, unidentified marine sponge, Xisha Islands, China	[45]
	-	-	C1-S01-A7, seawater sample, West Pacific Ocean	[55]
	-	-	SCSIO 41301, *Phakellia fusca* (marine sponge), Xisha Islands, China	[35]
	-	-	MCCC 3A00324, deep-sea sediment, South Atlantic Ocean	[57]
	-	-	Deep-sea mud, Dalian, China	[58]
	-	-	CPCC 401353, cultured, China	[59]
	-	-	LW09, deep-sea sediment, Southwest Indian Ridge	[47]
(7*S*)-(+)-Hydroxysydonic acid = Aspergoterpenin C (**2**)	282	$C_{15}H_{22}O_5$	Cultured, IFO 7531, Japan	[11]
	-	-	*Acanthophora spicifera* (red alga), Rameswaram, India	[53]
	-	-	SP-1, marine sediment sample, Antarctic Great Wall Station	[40]
	-	-	EN-434, *Symphyocladia latiuscula* (red alga), Qingdao coastline, China	[32]
	-	-	MCCC 3A00324, deep-sea sediment, South Atlantic Ocean	[57]
	-	-	Piece of deep-sea mud, Dalian, China	[58]
	-	-	CPCC 401353, cultured, China	[59]
	-	-	LW09, deep-sea sediment, Southwest Indian Ridge	[47]
(7*S*)-(−)-10-Hydroxysydonic acid (**3**)	282	$C_{15}H_{22}O_5$	Piece of deep-sea mud, Dalian, China	[58]
	-	-	MCCC 3A00324, deep-sea sediment, South Atlantic Ocean	[57]
	-	-	CPCC 401353, cultured, China	[59]
(+)-(7*S*)-7-O-Methylsydonic acid (**4**)	280	$C_{16}H_{24}O_4$	PSU-F154, genus *Annella* sp. (marine gorgonian sea fan), coastal area, Surat Thani, Thailand	[56]
(7*S*,11*S*)-(+)-12-Hydroxysydonic acid (**5**)	282	$C_{15}H_{22}O_5$	Marine sediment, Hsinchu, Taiwan	[54]
	-	-	SP-1, marine sediment, Antarctic Great Wall Station	[40]
	-	-	SCSIO 41301, *Phakellia fusca* (marine sponge), Xisha Islands, China	[35]
	-	-	LW09, deep-sea sediment, Southwest Indian Ridge	[47]

Table 1. *Cont.*

Compound Name	Mol. Wt.	Mol. Formula	Strain, Host, Location	Ref.
(7*S*,11*S*)-(+)-12-Acetoxysydonic acid (**6**)	324	$C_{17}H_{24}O_6$	ZSDS1-F6, unidentified marine sponge, Xisha Islands, China	[45]
(S)-(+)-Dehydrosydonic acid (**7**)	264	$C_{15}H_{20}O_4$	ZSDS1-F6, unidentified marine sponge, Xisha Islands, China	[45]
7-Deoxy-7,14-didehydrosydonic acid (**8**)	248	$C_{15}H_{20}O_3$	CUGB-F126, seawater, Bohai Sea, Tianjin	[15]
	-	-	SCSIO 41301, *Phakellia fusca* (marine sponge), Xisha Islands, China	[35]
(E)-7-deoxy-7,8-didehydrosydonic acid (**9**)	248	$C_{15}H_{20}O_3$	SCSIO 41301, *Phakellia fusca* (marine sponge), Xisha Islands, China	[35]
(Z)-7-deoxy-7,8-didehydrosydonic acid (**10**)	248	$C_{15}H_{20}O_3$	SCSIO 41301, marine sponge *Phakellia fusca*, Xisha Islands, China	[35]
(−)-(R)-Cyclohydroxysydonic acid (**11**)	280	$C_{15}H_{20}O_5$	LW09, deep-sea sediment, Southwest Indian Ridge	[47]
Penicibisabolane G (**12**)	264	$C_{15}H_{20}O_4$	LW09, deep-sea sediment, Southwest Indian Ridge	[47]
11,12-Dihydroxysydonic acid (**13**)	298	$C_{15}H_{22}O_6$	LW09, deep-sea sediment, Southwest Indian Ridge	[47]
Expansol G (**14**)	324	$C_{17}H_{24}O_6$	LW09, deep-sea sediment, Southwest Indian Ridge	[47]
Aspergillusene C (**15**)	264	$C_{15}H_{20}O_4$	ZSDS1-F6, unidentified marine sponge, Xisha Islands, China	[45]
Aspergillusene D (**16**)	250	$C_{15}H_{22}O_3$	SCSIO 41301, *Phakellia fusca* (marine sponge), Xisha Islands, China	[35]
Methyl (S)-(3-Hydroxy-4-(2-hydroxy-6-methylheptan-2-yl)benzoyl)glycinate = (+)-(7*S*)-Sydonic acid glycinate (**17**)	337	$C_{18}H_{27}NO_5$	CUGB-F126, seawater, Bohai Sea, Tianjin	[15]
Serine sydonate (**18**)	353	$C_{18}H_{27}NO_6$	Deep-sea mud, Dalian, China	[58]
	-	-	Cultured, CPCC 401353, China	[59]
4′-Alkenyl serine sydonate (**19**)	351	$C_{18}H_{25}NO_6$	Deep-sea mud, Dalian, China	[58]
4′-Hydroxyl serine sydonate (**20**)	369	$C_{18}H_{27}NO_7$	Deep-sea mud, Dalian, China	[58]
5′-Hydroxyl serine sydonate (**21**)	369	$C_{18}H_{27}NO_7$	Deep-sea mud, Dalian, China	[58]
cyclo-12-Hydroxysydonic acid (**22**)	264	$C_{15}H_{20}O_4$	SCSIO 41301, *Phakellia fusca* (marine sponge), Xisha Islands, China	[35]
Sydowic acid (**23**)	264	$C_{15}H_{20}O_4$	Cultured, Japan	[27,29,30]
	-	-	IFO 4284, cultured, Japan	[29,30]
	-	-	*Acanthophora spicifera* (red alga), Rameswaram, India	[53]
	-	-	CUGB-F126, seawater, Bohai Sea, Tianjin	[15]
	-	-	C1-S01-A7, seawater sample, West Pacific Ocean	[55]
	-	-	EN-434, *Symphyocladia latiuscula* (red alga), Qingdao coastline, China	[32]
	-	-	*Rhododendron mole* (leaves), Xing'an, Guangxi, China	[26]

Table 1. *Cont.*

Compound Name	Mol. Wt.	Mol. Formula	Strain, Host, Location	Ref.
(7*S*,8*S*)-8-Hydroxysydowic acid (**24**)	280	$C_{15}H_{20}O_5$	EN-434, *Symphyocladia latiuscula* (red alga), Qingdao coastline, China	[32]
(±)-(7*R**,10*R**)-10-Hydroxysydowic acid (**25**)	280	$C_{15}H_{20}O_5$	EN-434, *Symphyocladia latiuscula* (red alga), Qingdao coastline, China	[32]
(−)-(7*R*,10*S*)-10-Hydroxysydowic acid (**26**)	280	$C_{15}H_{20}O_5$	MCCC 3A00324, deep-sea sediment, South Atlantic Ocean	[57]
	-	-	*Rhododendron mole* (leaves), Xing'an, Guangxi, China	[26]
(−)-(7*R*,10*R*)-iso-10-Hydroxysydowic acid (**27**)	280	$C_{15}H_{20}O_5$	MCCC 3A00324, deep-sea sediment, South Atlantic Ocean	[57]
Asperbisabolane A (**28**)	278	$C_{15}H_{18}O_5$	MCCC 3A00324, deep-sea sediment, South Atlantic Ocean	[57]
Asperbisabolane B (**29**)	292	$C_{15}H_{16}O_6$	MCCC 3A00324, deep-sea sediment, South Atlantic Ocean	[57]
Asperbisabolane C (**30**)	280	$C_{15}H_{20}O_5$	MCCC 3A00324, deep-sea sediment, South Atlantic Ocean	[57]
Asperbisabolane D (**31**)	278	$C_{15}H_{18}O_5$	MCCC 3A00324, deep-sea sediment, South Atlantic Ocean	[57]
Asperbisabolane E (**32**)	280	$C_{15}H_{20}O_5$	MCCC 3A00324, deep-sea sediment, South Atlantic Ocean	[57]
Asperbisabolane F (**33**)	278	$C_{15}H_{18}O_5$	MCCC 3A00324, deep-sea sediment, South Atlantic Ocean	[57]
Asperbisabolane G (**34**)	280	$C_{15}H_{20}O_5$	MCCC 3A00324, deep-sea sediment, South Atlantic Ocean	[57]
Asperbisabolane H (**35**)	280	$C_{15}H_{20}O_5$	MCCC 3A00324, deep-sea sediment, South Atlantic Ocean	[57]
Asperbisabolane I (**36**)	280	$C_{15}H_{20}O_5$	MCCC 3A00324, deep-sea sediment, South Atlantic Ocean	[57]
Asperbisabolane J (**37**)	264	$C_{14}H_{16}O_5$	MCCC 3A00324, deep-sea sediment, South Atlantic Ocean	[57]
Asperbisabolane K (**38**)	284	$C_{13}H_{16}O_5S$	MCCC 3A00324, deep-sea sediment, South Atlantic Ocean	[57]
Asperbisabolane L (**39**)	206	$C_{12}H_{14}O_3$	MCCC 3A00324, deep-sea sediment, South Atlantic Ocean	[57]
Asperbisabolane M (**40**)	280	$C_{15}H_{20}O_5$	MCCC 3A00324, deep-sea sediment, South Atlantic Ocean	[57]
Asperbisabolane N (**41**)	340	$C_{17}H_{24}O_7$	MCCC 3A00324, deep-sea sediment, South Atlantic Ocean	[57]
Aspergillusene A = (E)-5-(Hydroxymethyl)-2-(6′-methylhept-2′-en-2′-yl)phenol (**42**)	234	$C_{15}H_{22}O_2$	PSU-F154, marine gorgonian sea fan of the genus *Annella* sp., coastal area, Surat Thani, Thailand	[56]
	-	-	Marine sediment, Hsinchu, Taiwan	[54]
	-	-	ZSDS1-F6, unidentified marine sponge, Xisha Islands, China	[45]
	-	-	MCCC 3A00324, deep-sea sediment, South Atlantic Ocean	[57]
	-	-	LW09, deep-sea sediment, Southwest Indian Ridge	[47]

Table 1. *Cont.*

Compound Name	Mol. Wt.	Mol. Formula	Strain, Host, Location	Ref.
Aspergillusene B (**43**)	246	$C_{15}H_{18}O_3$	PSU-F154, genus *Annella* sp. (gorgonian sea fan), coastal area, Surat Thani, Thailand	[56]
	-	-	LW09, deep-sea sediment, Southwest Indian Ridge	[47]
β-D-Glucopyranosyl aspergillusene A (**44**)	396	$C_{21}H_{32}O_7$	J05B-7F-4, *Stelletta* sp. (marine sponge), South Korea	[36]
(+)-(7*S*)-Sydonol (**45**)	252	$C_{15}H_{24}O_3$	MSX19583, spruce litter, Colorado, USA	[33]
	-	-	Marine sediment, Hsinchu, Taiwan	[54]
	-	-	MCCC 3A00324, deep-sea sediment, South Atlantic Ocean	[57]
(+)-(7*S*)-7-O-Methylsydonol (**46**)	266	$C_{16}H_{26}O_3$	Marine sediment, Hsinchu, Taiwan	[54]
7-Deoxy-7,14-didehydrosydonol (**47**)	234	$C_{15}H_{22}O_2$	Marine sediment, Hsinchu, Taiwan	[54]
	-	-	MCCC 3A00324, deep-sea sediment, South Atlantic Ocean	[57]
(−)-5-(hydroxymethyl)-2-(2′,6′,6′-trimethyltetrahydro-2H-pyran-2-yl)phenol (**48**)	250	$C_{15}H_{22}O_3$	*Rhododendron mole* (leaves), Xing'an, Guangxi, China	[26]
Anhydrowaraterpol B (**49**)	250	$C_{15}H_{22}O_3$	Marine sediment, Hsinchu, Taiwan	[54]
	-	-	ZSDS1-F6, unidentified marine sponge, Xisha Islands, China	[45]
(Z)-5-(Hydroxymenthyl)-2-(6′)-methylhept-2′-en-2′-yl)-phenol (**50**)	234	$C_{15}H_{22}O_2$	ZSDS1-F6, unidentified marine sponge, Xisha Islands, China	[45]
	-	-	MCCC 3A00324, deep-sea sediment, South Atlantic Ocean	[57]
Methyl(R,E)-6-(2,3-dihydroxy-4-methylpenyl)-2-methylhept-5-enoate (**51**)	278	$C_{16}H_{22}O_4$	SW9, seawater sample, Yangma Island, Yantai, China	[41]
Cyclowaraterpol A (**52**)	250	$C_{15}H_{22}O_3$	ZSDS1-F6, unidentified marine sponge, Xisha Islands, China	[45]
(7*S*)-Flavilane A (**53**)	298	$C_{16}H_{26}O_3S$	10–31, deep-sea sediments, cold seep off southwestern Taiwan	[38]
(7*S*)-4-Iodo-flavilane A (**54**)	424	$C_{16}H_{25}IO_3S$	10–31, deep-sea sediments, cold seep off southwestern Taiwan	[38]
Aspersydosulfoxide A (**55**)	280	$C_{16}H_{24}O_2S$	LW09, deep-sea sediment, Southwest Indian Ridge	[47]
Aspercuparene A (**56**)	262	$C_{15}H_{18}O_4$	MCCC 3A00324, deep-sea sediment, South Atlantic Ocean	[57]
Aspercuparene B (**57**)	264	$C_{15}H_{20}O_4$	MCCC 3A00324, deep-sea sediment, South Atlantic Ocean	[57]
Aspercuparene C (**58**)	260	$C_{15}H_{16}O_4$	MCCC 3A00324, deep-sea sediment, South Atlantic Ocean	[57]

In 1978, Hamasaki and his group separated and characterized compounds **1** and **2** as optically inactive metabolites from *A. sydowii* acetone extract by spectral and chemical means. These compounds were soluble in saturated $NaHCO_3$ and positively reacted with bromophenol blue [11] (Figure 1).

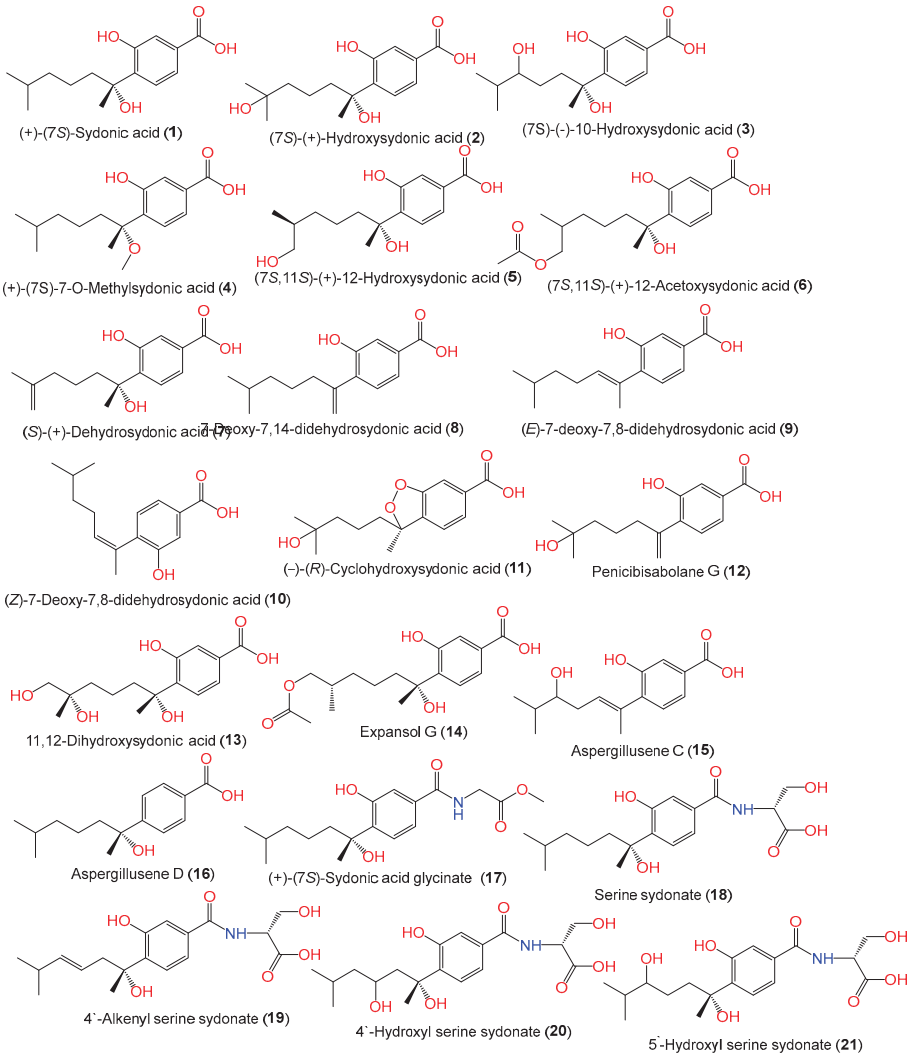

Figure 1. Structures of sesquiterpenoids (**1**–**21**) reported from *A. sydowii.*

Aspergillusene D (**16**) with a 7*S*-configuration was reported as a new sesquiterpenoid from *Phakellia fusca*-associated *A. sydowii* SCSIO-41301 by Liu et al., along with compounds **1**, **5** **8**, **9**, **10**, and **22** that were characterized based on spectral and ECD (electronic circular dichroism) analyses [35]. Xu et al. separated compound **17**, along with compounds **1**, **8**, and **23**, from *A. sydowii* CUGB-F126 isolated from the Bohai Sea, Tianjin, using SiO_2 (silica gel)/Sephadex LH-20/HPLC (high-performance liquid chromatography). Compound **17** is a new sydonic acid analog with a glycinate moiety [15].

Sun et al. developed a new approach that integrated computational programs (MS (mass spectrometry)-DIAL and MS-FINDER) and web-based tools (MetaboAnalyst and GNPS) for the identification of *A. sydowii*–*Bacillus subtilis* coculture metabolites, wherein 25 biosynthesized metabolites were detected and purified by SiO_2/ODS CC/HPLC. Among them, compounds **1**, **2**, **3**, and **18**–**21** were characterized by spectral and CD (circular dichroism) analyses [58]. Further, Hu et al. separated and characterized new bisabolene-type sesquiterpenoids **24** and **25** as well as the known analogs **2** and **23** from *A. sydowii* EN-434 ob-

tained from *Symphyocladia latiuscula* marine red alga using RP-18 (reversed phase-18)/SiO_2 CC (silica gel column chromatography) and spectral and ECD data. Compounds **24** and **25** have 7*S*/8*S* and 7*R**/10*R** configurations, respectively [32]. Fourteen new phenolic bisabolanes with varied structures, labeled **28**–**41**, were separated and characterized by Niu et al. from the deep-sea sediment-derived *A. sydowii* MCCC-3A00324 (Figure 2).

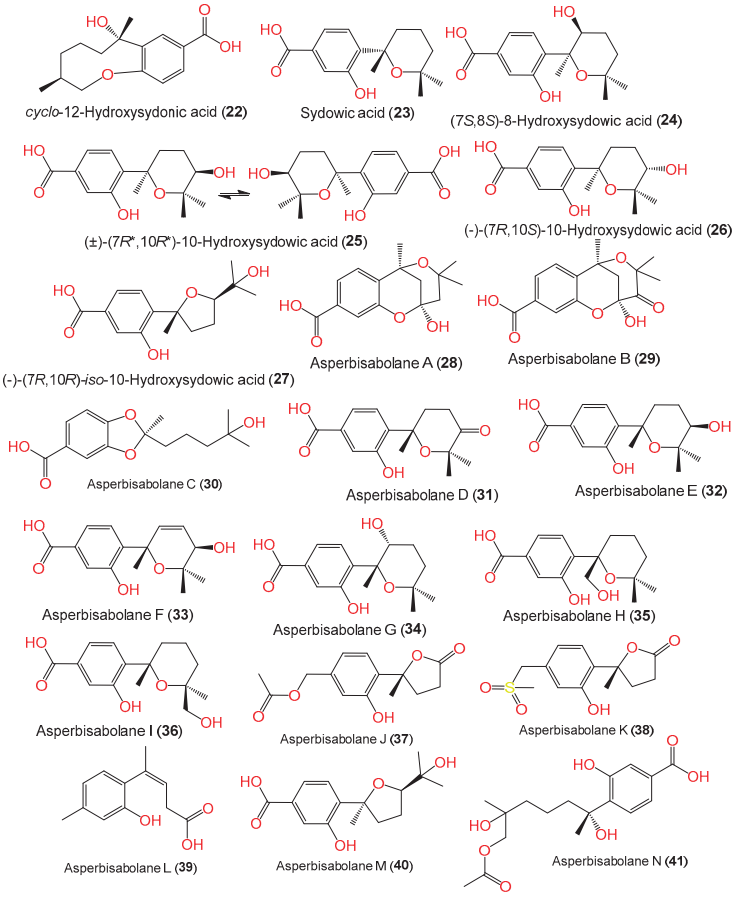

Figure 2. Structures of sesquiterpenoids (**22**–**41**) reported from *A. sydowii*.

Compounds **28** and 29 are the first bisabolanes with a 6/6/6 tricyclic skeleton, whereas compound **30** features a novel *seco*-bisabolane with a rare dioxolane moiety, and compound **38** has an unusual methylsulfonyl moiety [57]. Trisuwan et al. purified—from *A. sydowii* PSUF154 isolated from gorgonian sea fan of genus *Annella*—new bisabolane-type sesquiterpenes **4**, **42**, and **43**, along with **1**. Compound **42** has 2-substituted 6-methyl-2-heptenyl and 1,2,4-trisubstituted benzene. Compound **43**'s benzofuran moiety results from the ether linkage of C-1 OH of the tri-substituted phenyl and 2-substituted 6-methyl-2-heptenyl moieties. Compound **4** is a methyl ether of compound **1** with a 7*S* configuration [56]. The first phenolic bisabolane sesquiterpene glycoside, *β*-D-glucopyranosyl aspergillusene A (**44**), was purified from sponge-derived *A. sydowii* [36] and assigned using spectral and chemical methods [36].

Chung et al. stated that the addition of 5-azacytidine (a DNA methyltransferase inhibitor) to the culture of marine sediment-derived *A. sydowii* obtained from Hsinchu, Taiwan, significantly promoted the production of various metabolites [54]. Investigation

of the EtOAc (ethyl acetate) extract of 5-azacytidine-treated culture broth by SiO_2 CC and HPLC yielded new bisabolane sesquiterpenoids **5**, **46**, and **47**, along with **1**, **42**, **45**, and **49**, that were assigned based on spectral analyses. The S-configuration of compounds **5** and **46** was assigned using optical rotation comparison, whereas compound **46** ([α]D +1.87) is a methyl derivative of compound **45** ([α]D +7.2) and compound **5** ([α]D +3.9) is C-12 hydroxy analog of compound **1** ([α]D +23) (Figure 3). On the other hand, compound **47** is closely similar to the previously reported compound **8** except for the absence of the C-3 carboxylic group in compound **47** [54]. Compounds **5**, **46**, and **47** were proposed to be biosynthesized from farnesyl diphosphate (FPP) created from the addition of an IPP (isopentenyl diphosphate) unit to a GPP (geranyl diphosphate) (Scheme 1). Then, cyclization and folding of the carbon chain through an electrophilic attack on double bonds produced the bisabolane nucleus that then underwent a series of carboxylation, hydration, oxidation, and reduction to give compounds **5**, **46**, and **47** [54].

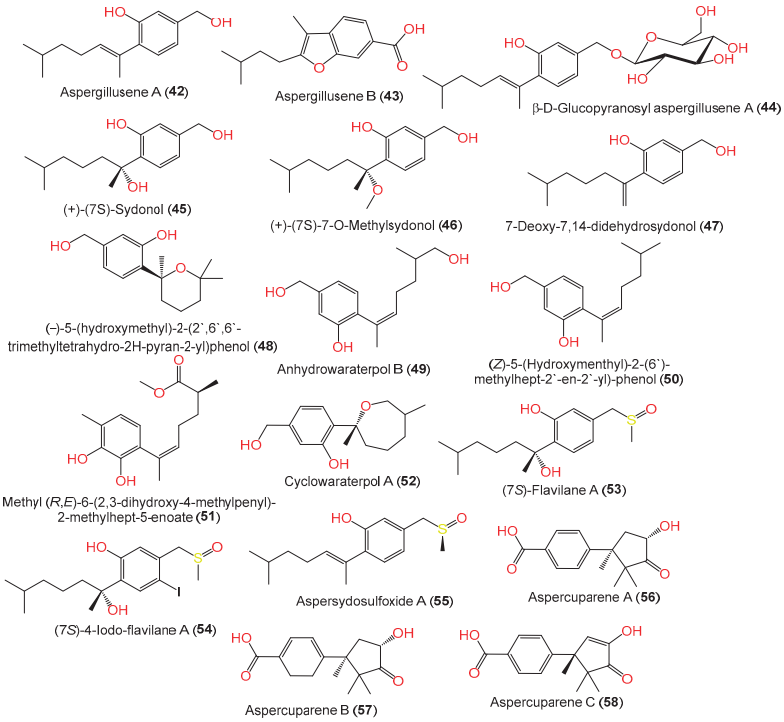

Figure 3. Structures of sesquiterpenoids (**42**–**58**) reported from *A. sydowii*.

A new bisabolane sesquiterpenoid, compound **15**, in addition to compounds **1**, **7**, **6**, **42**, **47**, **49**, **50**, and **52**, were purified from *A. sydowii* ZSDS1-F6 EtOAc extract using SiO_2/Sephadex LH-20/RP-HPLC by Wang et al. [45]. Compound **51** is a new aromatic bisabolene-type sesquiterpenoid with 11S-configuration purified and characterized from the sea-derived *A. sydowii* SW9 [41]. In 2022, Liu et al. purified a rare iodine- and sulfur-containing derivative (7*S*)- 4-iodo-flavilane A (**54**) along with compound **53**. Compound **54** is 4-iodinated analog of compound **53** and its absolute S-configuration was proven by ECD analysis [38]. Furthermore, three undescribed cuparene-type sesquiterpenes, labeled **56**–**58**, were isolated from fermented cultured EtOAc extract of the sea sediment-derived *A. sydowii* MCCC-3A00324 using SiO_2/RP-18/Sephadex LH-20 CC/HPLC and assigned using spectral and ECD analyses. They represent rare cuparene-type sesquiterpenoids having a C-10 keto group and were discovered for the first time from filamentous fungi [57].

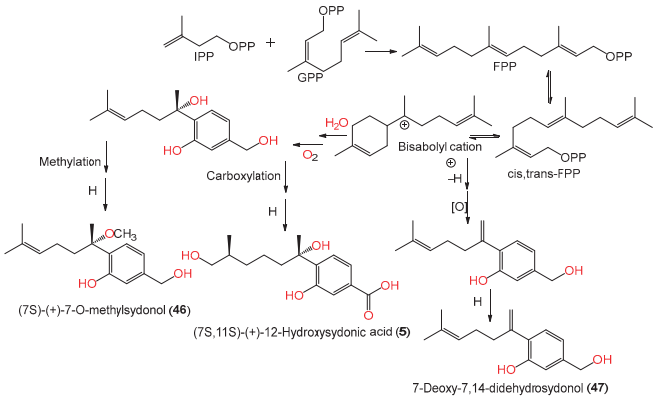

Scheme 1. Biosynthetic pathway of compounds **5**, **46**, and **47**: GPP: Geranyl diphosphate; FPP: Farnesyl diphosphate; IPP: Isopentenyl diphosphate [54].

2.2. Mono- and Triterpenoids and Sterols

In 2020, the chemical investigation of deep-sea sediment-isolated *A. sydowii* MCCC-3A00324 by Niu et al. led to the separation of new osmane-type monoterpenoids aspermonoterpenoids A (**59**) and B (**60**) by SiO_2 CC/HPLC and their structures were determined by spectral, ECD, and specific rotation analyses (Table 2, Figure 4). Compounds **59** and **60** are the first osmane monoterpenes reported from fungi, whereas compound **59** features a novel skeleton, which is possibly derived after the cleavage of the cyclopentane ring and oxidation reaction of the osmane monoterpenoid. They have 4*S* and 4*S*/5*R*/6*S* configurations, respectively [60].

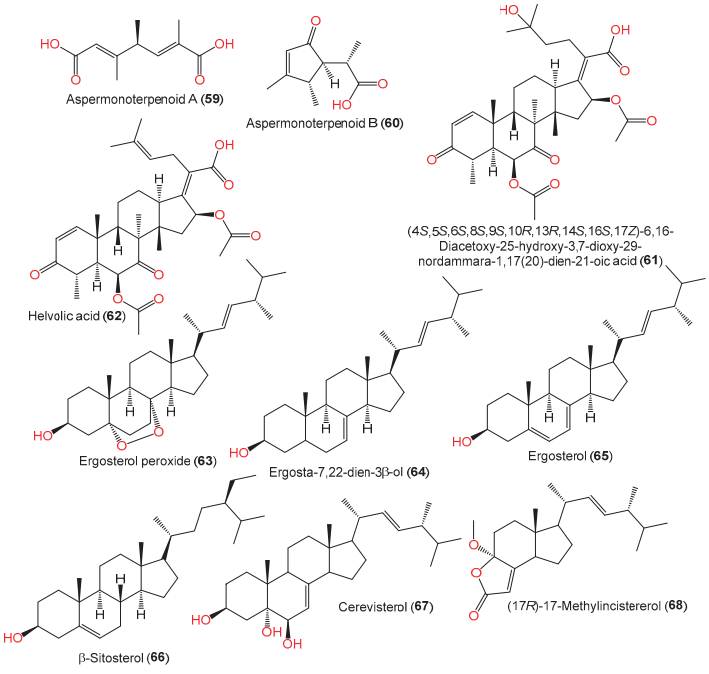

Figure 4. Structures of mono- (**59** and **60**) and triterpenoids (**61** and **62**) and sterols (**63**–**68**) reported from *A. sydowii.*

Table 2. Mono- and triterpenoids and sterols reported from *A. sydowii* (molecular weight and formulae, strain, host, and location).

Compound Name	Mol. Wt.	Mol. Formula	Strain, Host, Location	Ref.
Monoterpenoids				
Aspermonoterpenoid A (**59**)	198	$C_{10}H_{14}O_4$	MCCC 3A00324, deep-sea sediment, South Atlantic Ocean	[60]
Aspermonoterpenoid B (**60**)	182	$C_{10}H_{14}O_3$	MCCC 3A00324, deep-sea sediment, South Atlantic Ocean	[60]
Triterpenoids				
(4*S*,5*S*,6*S*,8*S*,9*S*,10*R*,13*R*,14*S*,16*S*,17*Z*)-6,16-Diacetoxy-25-hydroxy-3,7-dioxy-29-nordammara-1,17(20)-dien-21-oic acid (**61**)	572	$C_{32}H_{44}O_9$	PFW1-13, driftwood, beach of Baishamen, Hainan, China	[48]
Helvolic acid (**62**)	554	$C_{32}H_{42}O_8$	PFW1-13, driftwood, beach of Baishamen, Hainan, China	[48]
Sterols				
Ergosterol peroxide (**63**)	430	$C_{28}H_{46}O_3$	C1-S01-A7, seawater, West Pacific Ocean	[55]
Ergosta-7,22-dien-3β-ol (**64**)	398	$C_{28}H_{46}O$	C1-S01-A7, seawater, West Pacific Ocean	[55]
Ergosterol (**65**)	396	$C_{28}H_{44}O$	C1-S01-A7, seawater, West Pacific Ocean	[55]
β-Sitosterol (**66**)	414	$C_{29}H_{50}O$	C1-S01-A7, seawater, West Pacific Ocean	[55]
Cerevisterol (**67**)	430	$C_{28}H_{46}O_3$	YH11-2, deep-sea fungus, Guam, South Japan	[44]
(17*R*)-17-Methylincistererol (**68**)	346	$C_{22}H_{34}O_3$	YH11-2, deep-sea fungus, Guam, South Japan	[44]

These metabolites were proposed to be biosynthesized from a GPP that underwent subsequent hydrolysis/oxygenation/cyclization to yield the monocyclic osmane monoterpenoid ring. Then, carbon–carbon bond cleavage of osmane gives intermediate **I** and its further oxygenation yields compound **59**, whilst the osmane oxygenation forms compound **60** [60] (Scheme 2).

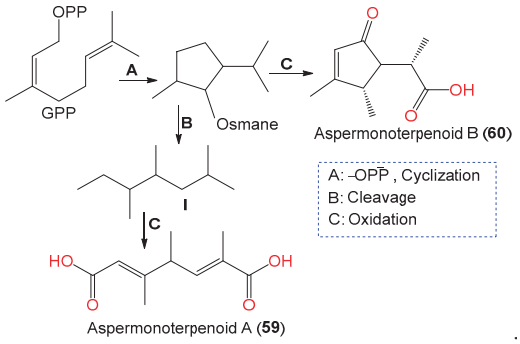

Scheme 2. Biosynthetic pathway of compounds **59** and **60** [60].

Zhang et al. purified and characterized compound **61**, a new 29-nordammarane-type triterpenoid, in addition to its known analog, compound **62**, from the marine-derived *A. sydowii* PFW1-13 [48]. Compound **61** is structurally similar to compound **62** with a 1,1,2-trisubstituted ethanol unit instead of a trisubstituted ethenyl unit, suggesting that compound **61** is a C_{24}–C_{25} hydrated derivative of compound **62** [48]. Its configuration

was assigned as 4*S*/5*S*/6*S*/8*S*/9*S*/10*R*/13*R*/14*S*/16*S*/17*Z* based on comparing its optical rotation (−118.9) with that of compound **62** (optical rotation −105.1) [48].

Wang et al., in 2019, reported the separation of ergosterol derivatives **63**–**66** from deep-sea water-isolated *A. sydowii* [55], while compounds **68** and **69** were separated by Li et al.; compound **69** was assumed to be a sterol degradation product [44].

2.3. Xanthone and Anthraquinone Derivatives

Xanthones are commonly found in lichen, fungi, plants, and bacteria [61]. In fungi, xanthones are mostly derived from acetyl-CoA through a series of polyketide synthase-catalyzed chemical transformations [62]. These metabolites were found to demonstrate diverse bioactivities.

Compounds **69** and **71** were reported from the EtOAc extract of 5-azacytidine-treated *A. sydowii* culture broth [54]. Additionally, from liverwort *Scapania ciliate*-accompanied *A. sydowii*, new xanthone derivatives, labeled **72**, **76**, and **77**, and known compounds **74** and **78** were isolated by SiO_2/Sephadex LH-20 CC/HPLC and assigned by spectral data. Compounds **76** and **77** are examples of sulfur-containing xanthones; compound **77** has an additional acetyl group at C-13 and compound **72** features C-2-OH instead of the methylthio moiety as in compound **76** [63]. New hydrogenated xanthones, aspergillusones A (**86**) and B (**87**), along with compounds **69**, **71**, **73**, **88**, and **90**, were purified from a strain associated with the gorgonian sea fan of the genus *Annella* by Trisuwan et al. Compound **86** is a 11-deoxy derivative of compound **88** with an optical rotation of −1.6 and the same C-7 and C-8 absolute configuration, whereas compound **87** is a 1-hydroxy analog of compound **90** with 7R/8R and −46.3 optical rotation (Figure 5) [56].

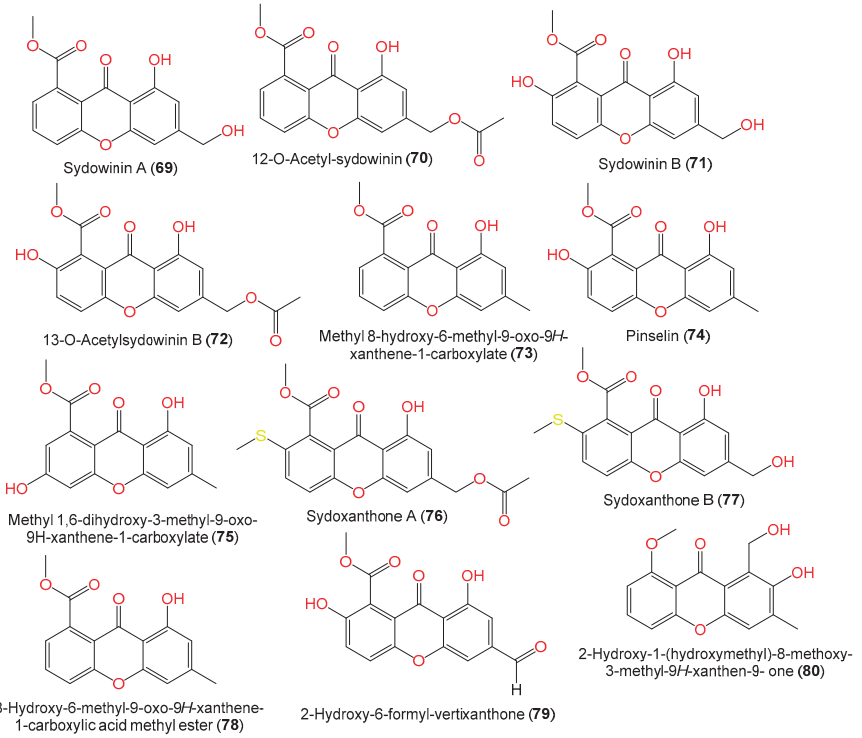

Figure 5. Structures of xanthones (**69**–**80**) reported from *A. sydowii*.

In 2019, Wang et al. purified two novel xanthones, labeled **70** and **79**, along with the known xanthones **71**, **72**, **74**, **86**, **88**, and **89** and quinones **91**, **94**, and **96**, from seawater-

derived *A. sydowii* C1-S01-A7 using SiO_2/Sephadex LH-20/RP-18/HPLC; the compounds were elucidated by spectral analyses (Table 3). Compound **79** is similar to previously reported 2-hydroxyvertixanthone with an additional formyl moiety at C-6, whereas compound **70** is similar to compound **69** with one more acetyl group at C-12 [55].

Table 3. Xanthones and quinones reported from *Aspergillus sydowii* (molecular weight and formulae, strain, host, and location).

Compound Name/Chemical Class	Mol. Wt.	Mol. Formula	Strain, Host, and Location	Ref.
Xanthones				
Sydowinin A (**69**)	300	$C_{16}H_{12}O_6$	Cultured, IFO 4284, Japan	[29]
	-	-	PSU-F154, genus *Annella* sp. (gorgonian sea fan), coastal area, Surat Thani, Thailand	[56]
12-O-Acetyl-sydowinin A (**70**)	342	$C_{18}H_{14}O_7$	C1-S01-A7, seawater, West Pacific Ocean	[55]
Sydowinin B (**71**)	316	$C_{16}H_{12}O_7$	Cultured, IFO 4284, Japan	[29]
	-	-	Marine sediment, Hsinchu, Taiwan	[54]
	-	-	PSU-F154, genus *Annella* sp. (gorgonian sea fan), coastal area, Surat Thani, Thailand	[56]
	-	-	Marine sediment, Hsinchu, Taiwan	[54]
	-	-	C1-S01-A7, seawater, West Pacific Ocean	[55]
13-O-Acetylsydowinin B (**72**)	358	$C_{18}H_{14}O_8$	*Scapania ciliata* (Chinese liverwort), Maoer Mountain, Guangxi, China	[63]
	-	-	J05B-7F-4, *Stelletta* sp. (marine sponge), South Korea	[36]
	-	-	C1-S01-A7, seawater, West Pacific Ocean	[55]
Methyl 8-hydroxy-6-methyl-9-oxo-9*H*-xanthene-1-carboxylate (**73**)	284	$C_{16}H_{12}O_5$	PSU-F154, genus *Annella* sp. (gorgonian sea fan), coastal area, Surat Thani, Thailand	[56]
Pinselin (**74**)	300	$C_{16}H_{12}O_6$	PSU-F154, genus *Annella* sp. (gorgonian sea fan), coastal area, Surat Thani, Thailand	[56]
	-	-	*Scapania ciliata* (Chinese liverwort), Maoer Mountain, Guangxi, China	[63]
	-	-	C1-S01-A7, seawater, West Pacific Ocean	[55]
Methyl 1,6-dihydroxy-3-methyl-9-oxo-9*H*-xanthene-1-carboxylate (**75**)	300	$C_{16}H_{12}O_6$	*Scapania ciliata* (Chinese liverwort), Maoer Mountain, Guangxi, China	[56]
Sydoxanthone A (**76**)	388	$C_{19}H_{16}O_7S$	*Scapania ciliata* (Chinese liverwort), Maoer Mountain, Guangxi, China	[63]
Sydoxanthone B (**77**)	346	$C_{17}H_{14}O_6S$	*Scapania ciliata* (Chinese liverwort), Maoer Mountain, Guangxi, China	[63]
8-Hydroxy-6-methyl-9-oxo-9*H*-xanthene-1-carboxylic acid methyl ester (**78**)	284	$C_{16}H_{12}O_5$	*Scapania ciliata* (Chinese liverwort), Maoer Mountain, Guangxi, China	[63]
2-Hydroxy-6-formyl-vertixanthone (**79**)	314	$C_{16}H_{10}O_7$	C1-S01-A7, seawater, West Pacific Ocean	[55]
2-Hydroxy-1-(hydroxymethyl)-8-methoxy-3-methyl-9*H*-xanthen-9-one (**80**)	286	$C_{16}H_{14}O_5$	SCSIO 41301, *Phakellia fusca* (marine sponge), Xisha Islands, China	[35]
2-Hydroxy-1-(hydroxymethyl)-7,8-dimethoxy-3-methyl-9*H*-xanthen-9-one (**81**)	316	$C_{17}H_{16}O_6$	SCSIO 41301, *Phakellia fusca* (marine sponge), Xisha Islands, China	[35]
Austocystin A (**82**)	372	$C_{19}H_{13}ClO_6$	SCSIO 00305, *Verrucella unbracculum* (gorgonian), South China Sea, Sanya, Hainan, China	[24]

Table 3. *Cont.*

Compound Name/Chemical Class	Mol. Wt.	Mol. Formula	Strain, Host, and Location	Ref.
6-Methoxyl austocystin A (**83**)	402	$C_{20}H_{15}ClO_7$	SCSIO 00305, *Verrucella unbracculum* (gorgonian), South China Sea, Sanya, Hainan, China	[24]
Sterigmatocystin (**84**)	324	$C_{18}H_{12}O_6$	DC08, *Dachtylospongia* sp. (marine sponge), South Coast, West Sumatra, Indonesia	[39]
Sydowinol (**85**)	318	$C_{16}H_{14}O_7$	IFO 4284, Cultured, Japan	[29]
Aspergillusone A (**86**)	304	$C_{16}H_{16}O_6$	PSU-F154, genus *Annella* sp. (gorgonian sea fan), coastal area, Surat Thani, Thailand	[56]
	-	-	C1-S01-A7, seawater, West Pacific Ocean	[55]
Aspergillusone B (**87**)	338	$C_{16}H_{18}O_8$	PSU-F154, genus *Annella* sp. (gorgonian sea fan), coastal area, Surat Thani, Thailand	[56]
(7*R*,8*R*)-AGI-B4 (**88**)	320	$C_{16}H_{16}O_7$	PSU-F154, genus *Annella* sp. (gorgonian sea fan), coastal area, Surat Thani, Thailand	[56]
	-	-	Marine sediment, Hsinchu, Taiwan	[54]
	-	-	C1-S01-A7, seawater, West Pacific Ocean	[55]
12-O-Acetyl (7*R*,8*R*)-AGI-B4 (**89**)	362	$C_{18}H_{18}O_8$	C1-S01-A7, seawater, West Pacific Ocean	[55]
(7*R*,8*R*)-α-Diversonolic ester (**90**)	322	$C_{16}H_{18}O_7$	PSU-F154, genus *Annella* sp. (gorgonian sea fan), coastal area, Surat Thani, Thailand	[56]
Quinones				
Emodin (**91**)	270	$C_{15}H_{10}O_5$	*Scapania ciliata* (Chinese liverwort), Maoer Mountain, Guangxi, China	[63]
	-	-	C1-S01-A7, seawater, West Pacific Ocean	[55]
Emodic acid (**92**)	300	$C_{15}H_8O_7$	SCSIO 41301, *Phakellia fusca* (marine sponge), Xisha Islands, China	[35]
Parietinic acid (**93**)	314	$C_{16}H_{10}O_7$	SCSIO 41301, *Phakellia fusca* (marine sponge), Xisha Islands, China	[35]
Questin (**94**)	284	$C_{16}H_{12}O_5$	*Scapania ciliata* (Chinese liverwort), Maoer Mountain, Guangxi, China	[63]
	-	-	C1-S01-A7, seawater, West Pacific Ocean	[55]
	-	-	SCSIO 41301, marine sponge *Phakellia fusca*, Xisha Islands, China	[35]
1,6,8-Trihydroxy-3-methylanthraquinone (**95**)	270	$C_{15}H_{10}O_5$	SCSIO 41301, marine sponge *Phakellia fusca*, Xisha Islands, China	[35]
Yicathin C (**96**)	312	$C_{17}H_{12}O_6$	C1-S01-A7, seawater sample, West Pacific Ocean	[55]
1-Hydroxy-6,8-dimethoxy-3-methylanthraquinone (**97**)	298	$C_{17}H_{14}O_5$	*Scapania ciliata* (Chinese liverwort), Maoer Mountain, Guangxi, China	[63]
(+)-3,3′,7,7′,8,8′-hexahydroxy-5,5′-dimethyl-bianthra-quinone (**98**)	538	$C_{30}H_{18}O_{10}$	#2B, leaves, *Aricennia marina*, Yangjiang, Guangdong, China	[64]
Xanthoradone A (**99**)	490	$C_{27}H_{22}O_9$	#2B, leaves, *Aricennia marina*, Yangjiang, Guangdong, China	[64]

The cultured EtOAc extract of *A. sydowii* SCSIO-41301 associated with *Phakellia fusca* provided new xanthones **80** and **81**. Compound **80** is related to versicone A with 3-OH instead of the isopentene group in versicone A, while compound **81** has an additional 6-OCH_3 group compared to compound **80** [35]. The new mycotoxin 6-methoxyl austocystin A (**83**) and the related known compound **82** were isolated from *Verrucella umbraculum*-associated *A. sydowii* SCSIO-00305 (Figure 6). Compound **83** is similar to compound **82** except for the presence of an additional C6-OCH_3. Their 1′R/2S configuration was assigned based on X-ray analysis [24].

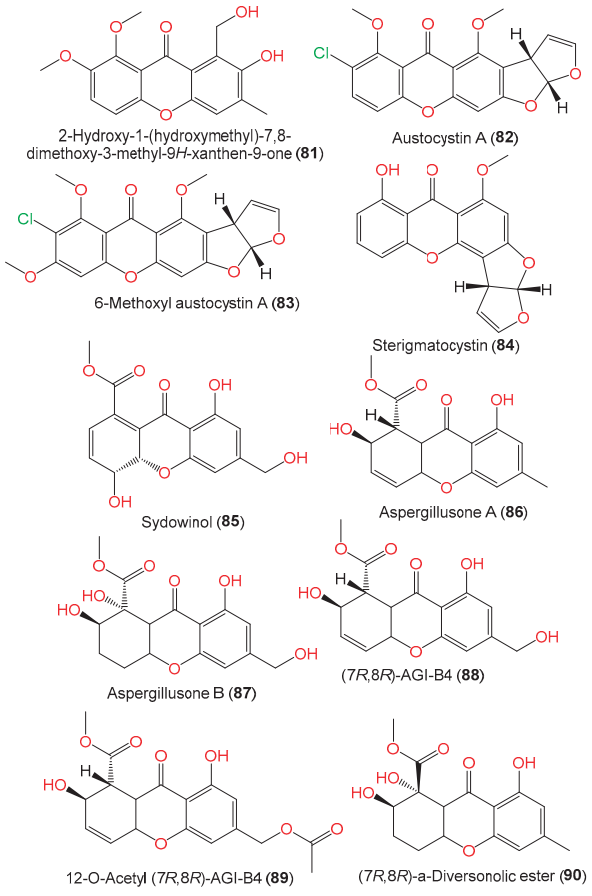

Figure 6. Structures of xanthones (**81**–**90**) reported from *A. sydowii.*

Additionally, compounds **92**–**95** are anthraquinones reported by Liu et al. from a *Phakellia fusca*-associated fungal strain [35] (Figure 7). Compounds **98** and **99** are quinone derivatives separated from *A. sydowii* #2B associated with *Aricennia marina* by Wang et al. [64].

2.4. Alkaloids

Alkaloids have drawn considerable attention because of their unique structural features and varied bioactivities. Interestingly, alkaloids belonging to various classes were reported from *A. sydowii*.

From the culture broth of coral *Verrucella umbraculum*-accompanied *A. sydowii* SCSIO-00305, using bio-guided fractionation, a new indole diketopiperazine member, cyclotryprostatin E (**101**), and compounds **100**, **102**, and **117**–**123** were purified using RP-18 CC/HPLC and characterized by spectral data interpretation [31] (Figure 8). Compound **101** is similar to compound **100** bar the replacement of the tri-substituted double bond in compound **100** with an oxygen-bonded quaternary carbon; compound **117** possesses indolyl, piperazinyl, and 1,2-disubstituted phenyl groups [31].

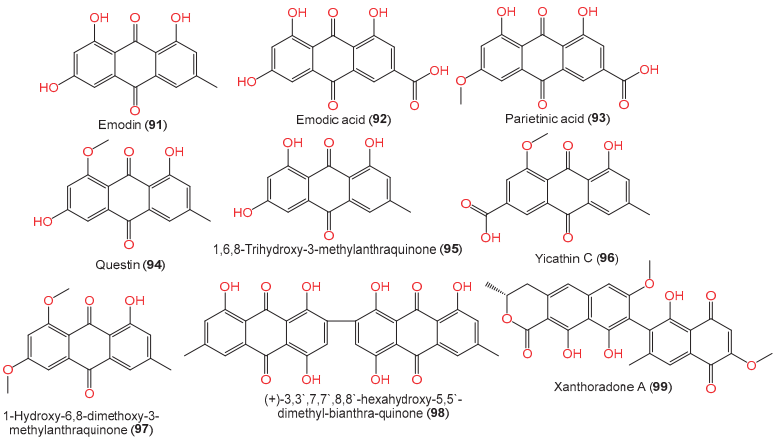

Figure 7. Structures of quinones (**91–99**) reported from *A. sydowii*.

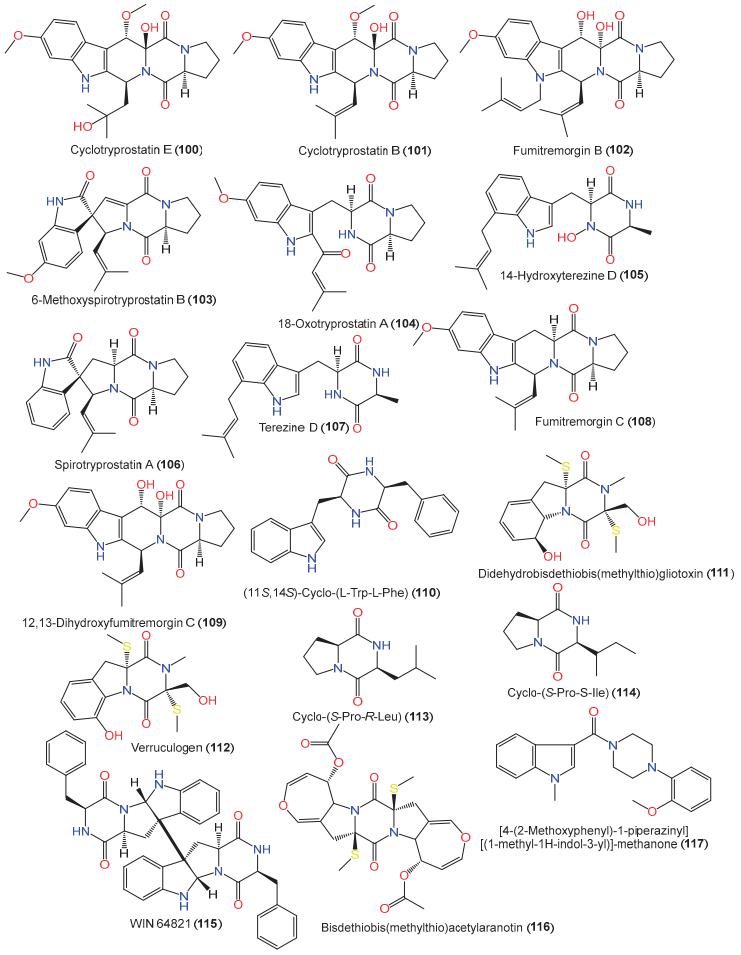

Figure 8. Structures of alkaloids (**100–117**) reported from *A. sydowii*.

In 2008, Zheng et al. purified new diketopiperazines **103**–**105** and a new oxaspiro [4.4]lactam-containing alkaloid, labeled **131**, along with compounds **106**–**109**, **111**, **112**, **130**, and **140**–**143** from the EtOAc extract of *A. sydowii* PFW1-13 isolated from driftwood sourced from Baishamen beach, Hainan, China, using SiO_2/Sephadex LH-20 CC/HPLC [48]. The configurations of compounds **103**–**105** and **131** were assigned based on NMR (nuclear magnetic resonance) and CD spectral analyses, and the specific rotation was 3*S*/12*S*/18*S* for compound **103** and 9*S*/12*S* for compounds **104** and **105**, while compound **131** was identified as a 14-nor-derivative of compound **130** with 5*S*/8*S*/9*R*/10*S*/11*S*/12*Z* configuration [48].

Biosynthetically, compounds **103**–**105** were postulated to be generated through a mixed mevalonic acid/amino acid pathway. Compound **105** is generated from the oxidation of compound **107**, which results from mevalonic acid, tryptophan, and alanine. A cyclo(Trp-Pro) is formed from proline and tryptophan and is further oxidized and methylated to produce ethoxylated cyclo(Trp-Pro). Then, the latter reacts with mevalonic acid to yield compound **104** and intermediate **I**. An intramolecular aldol reaction of intermediate **I** yields intermediate **III**, which is deoxygenated to produce compound **106**. Additionally, the dehydrogenation of compound **106** gives compound **103** (Scheme 3).

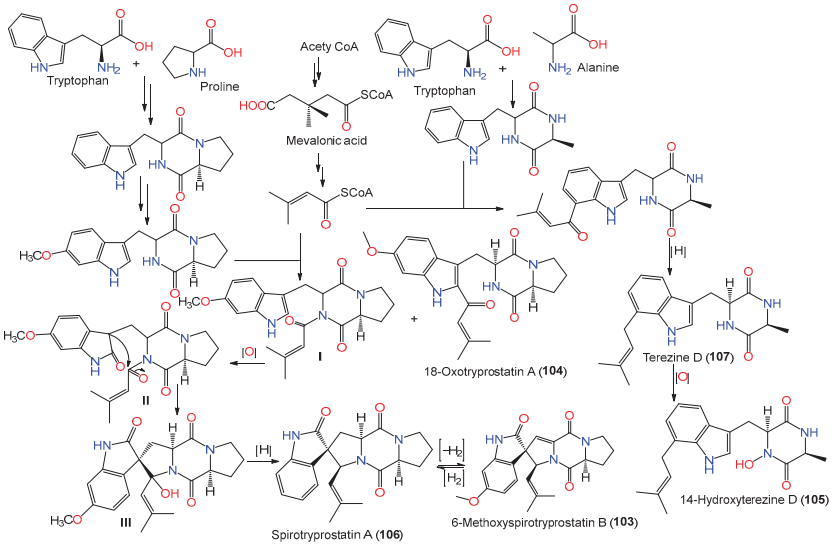

Scheme 3. Biosynthetic pathway of compounds **103**–**106** [48].

Kaur et al. separated a new diketopiperazine dimer WIN 64821 (**115**) and the known compound **110** using SiO_2 CC and RP-HPLC from the CH_3OH/CH_3CN extract of *A. sydowii* MSX-19583 obtained from spruce litter; the compounds were assigned by spectral and ECD analyses and Marfey's Method (Table 4). Compound **115** is structurally similar to the ditryptophenaline reported in various *Aspergillus* species and derived from tryptophan and phenylalanine subunits [33].

Table 4. Alkaloids reported from *Aspergillus sydowii* (molecular weight and formulae, strain, host, and location).

Compound Name	Mol. Wt.	Mol. Formula	Strain, Host, and Location	Ref.
Cyclotryprostatin B (**100**)	425	$C_{23}H_{27}N_3O_5$	SCSIO 00305, *Verrucella umbraculum* (gorgonian), Sanya, Hainan, China	[31]
Cyclotryprostatin E (**101**)	443	$C_{23}H_{29}N_3O_6$	SCSIO 00305, *Verrucella umbraculum* (gorgonian), Sanya, Hainan, China	[31]
Fumitremorgin B (**102**)	479	$C_{27}H_{33}N_3O_5$	SCSIO 00305, *Verrucella umbraculum* (gorgonian), Sanya, Hainan, China	[31]
6-Methoxyspirotryprostatin B (**103**)	393	$C_{22}H_{23}N_3O_4$	PFW1-13, driftwood, Baishamen beach, Hainan, China	[48]
18-Oxotryprostatin A (**104**)	395	$C_{22}H_{25}N_3O_4$	PFW1-13, driftwood, Baishamen beach, Hainan, China	[48]
14-Hydroxyterezine D (**105**)	341	$C_{19}H_{23}N_3O_3$	PFW1-13, driftwood, Baishamen beach, Hainan, China	[48]
Spirotryprostatin A (**106**)	365	$C_{21}H_{23}N_3O_2$	PFW1-13, driftwood, Baishamen beach, Hainan, China	[48]
Terezine D (**107**)	325	$C_{19}H_{23}N_3O_2$	PFW1-13, driftwood, Baishamen beach, Hainan, China	[48]
Fumitremorgin C (**108**)	379	$C_{22}H_{25}N_3O_3$	PFW1-13, driftwood, Baishamen beach, Hainan, China	[48]
12,13-Dihydroxyfumitremorgin C (**109**)	411	$C_{22}H_{25}N_3O_5$	PFW1-13, driftwood, Baishamen beach, Hainan, China	[48]
(11*S*,14*S*)-Cyclo-(L-Trp-L-Phe) (**110**)	333	$C_{20}H_{19}N_3O_2$	PSU-F154, genus *Annella* sp. (gorgonian sea fan), coastal area, Surat Thani, Thailand	[56]
	-	-	MSX19583, spruce litter, Colorado, USA	[33]
	-	-	J05B-7F-4, *Stelletta* sp. (marine sponge), South Korea	[36]
	-	-	ZSDS1-F6, unidentified marine sponge, Xisha Islands, China	[45]
	-	-	SP-1, marine sediment, Antarctic Great Wall Station	[40]
	-	-	MCCC 3A00324, deep-sea sediment, South Atlantic Ocean	[65]
Didehydrobisdethiobis(methylthio) gliotoxin (**111**)	356	$C_{15}H_{20}N_2O_4S_2$	PFW1-13, driftwood, Baishamen beach, Hainan, China	[48]
Verruculogen (**112**)	354	$C_{15}H_{18}N_2O_4S_2$	PFW1-13, driftwood, Baishamen beach, Hainan, China	[48]
Cyclo-(S-Pro-S-Ile) (**114**)	210	$C_{11}H_{18}N_2O_2$	Cultured, China	[28]
Cyclo-(S-Pro-R-Leu) (**113**)	210	$C_{11}H_{18}N_2O_2$	Cultured, China	[28]
WIN 64821 (**115**)	664	$C_{40}H_{36}N_6O_4$	MSX19583, spruce litter, Colorado, USA	[33]
	-	-	C1-S01-A7, seawater, West Pacific Ocean	[55]
Bisdethiobis(methylthio)-acetylaranotin (**116**)	534	$C_{24}H_{26}N_2O_8S_2$	Cultured, China	[28]
[4-(2-Methoxyphenyl)-1-piperazinyl][(1-methyl-1*H*-indol-3-yl)]-methanone (**117**)	349	$C_{21}H_{23}N_3O_2$	SCSIO 00305, *Verrucella umbraculum* (gorgonian), Sanya, Hainan, China	[31]
Fumiquinazoline A (**118**)	445	$C_{24}H_{23}N_5O_4$	SCSIO 00305, *Verrucella umbraculum* (gorgonian), Sanya, Hainan, China	[31]
Fumiquinazoline B (**119**)	445	$C_{24}H_{23}N_5O_4$	SCSIO 00305, *Verrucella umbraculum* (gorgonian), Sanya, Hainan, China	[31]

Table 4. *Cont.*

Compound Name	Mol. Wt.	Mol. Formula	Strain, Host, and Location	Ref.
Fumiquinazoline C (**120**)	443	$C_{24}H_{21}N_5O_4$	SCSIO 00305, *Verrucella umbraculum* (gorgonian), Sanya, Hainan, China	[31]
Fumiquinazoline D (**121**)	443	$C_{24}H_{21}N_5O_4$	SCSIO 00305, *Verrucella umbraculum* (gorgonian), Sanya, Hainan, China	[31]
Fumiquinazoline F (**122**)	358	$C_{21}H_{18}N_4O_2$	SCSIO 00305, *Verrucella umbraculum* (gorgonian), Sanya, Hainan, China	[31]
Fumiquinazoline G (**123**)	358	$C_{21}H_{18}N_4O_2$	SCSIO 00305, *Verrucella umbraculum* (gorgonian), Sanya, Hainan, China	[31]
2-(4-Hydroxybenzyl)-4-(3-acetyl)quinazolin-one (**124**)	294	$C_{17}H_{14}N_2O_3$	SW9, seawater, Yangma Island, Yantai, China	[41]
2-(4-Hydroxybenzoyl)-4(3*H*)-quinazolinone (**125**)	252	$C_{15}H_{12}N_2O_2$	SW9, seawater, Yangma Island, Yantai, China	[41]
2-(4-Oxo-3,4-dihydroquinazolin-2-yl)benzoic acid (**126**)	266	$C_{15}H_{10}N_2O_3$	MCCC 3A00324, deep-sea sediment, South Atlantic Ocean	[65]
Acremolin (**127**)	231	$C_{11}H_{13}N_5O$	MCCC 3A00324, deep-sea sediment, South Atlantic Ocean	[65]
Acremolin C (**128**)	245	$C_{12}H_{15}N_5O$	SP-1, marine sediment, Antarctic Great Wall Station	[40]
Acremolin D (**129**)	289	$C_{13}H_{15}N_5O_3$	MCCC 3A00324, deep-sea sediment, South Atlantic Ocean	[65]
Pseustin A (**130**)	431	$C_{22}H_{25}NO_8$	PFW1-13, driftwood, Baishamen beach, Hainan, China	[48]
14-Norpseurotin A (**131**)	417	$C_{21}H_{23}NO_8$	PFW1-13, driftwood, Baishamen beach, Hainan, China	[48]
Azaspirofurans A (**132**)	411	$C_{21}H_{19}NO_7$	D2-6, Marine sediment, Jiaozhou Bay, China	[43]
Azaspirofurans B (**133**)		$C_{22}H_{21}NO_7$	D2-6, Marine sediment, Jiaozhou Bay, China	[43]
Chrysotriazole A (**134**)	311	$C_{17}H_{17}N_3O_3$	SW9, seawater, Yangma Island, Yantai, China	[41]
Indoleacetic acid (**135**)	175	$C_{10}H_9NO_2$	MCCC 3A00324, deep-sea sediment, South Atlantic Ocean	[65]
Pyrrole-2-carboxylic acid (**136**)	111	$C_5H_5NO_2$	MCCC 3A00324, deep-sea sediment, South Atlantic Ocean	[65]
2-Acetylaminobenzamide (**137**)	178	$C_9H_{10}N_2O_2$	C1-S01-A7, seawater, West Pacific Ocean	[55]
1,4-Dioxa-9,12-diazacyclohexadecane-5,8,13,16-tetraone (**138**)	286	$C_{12}H_{18}N_2O_6$	Cultured, China	[28]
N-Acetyltyramine (**139**)	179	$C_{10}H_{13}NO_2$	Cultured, China	[28]
Fumigaclavine B (**140**)	366	$C_{23}H_{30}N_2O_2$	PFW1-13, driftwood, Baishamen beach, Hainan, China	[48]
Fumigaclavine C (**141**)	298	$C_{18}H_{22}N_2O_2$	PFW1-13, driftwood, Baishamen beach, Hainan, China	[48]
Pyripyropene A (**142**)	525	$C_{29}H_{35}NO_8$	PFW1-13, driftwood, Baishamen beach, Hainan, China	[48]
Pyripyropene E (**143**)	569	$C_{30}H_{35}NO_{10}$	PFW1-13, driftwood, Baishamen beach, Hainan, China	[48]

A new quinazolinone alkaloid, labeled **124**, as well as related alkaloid **125** and triazole analog **134** were separated and characterized from the mycelia EtOAc extract of seawater-derived *A. sydowii* SW9 using SiO_2/Rp-18/Sephadex LH-20 CC and spectral analyses (Figure 9). Compound **124** is an acetyl derivative of 2-(4-hydroxybenzyl)quinazolin-4(3*H*)-one, previously reported from *Cordyceps*-associated *Isaria farinose* [41,66].

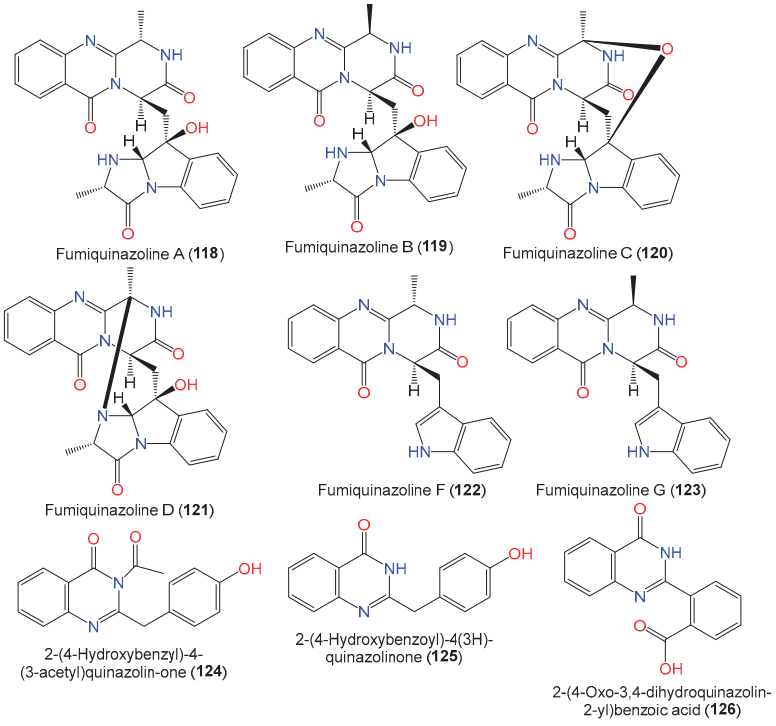

Figure 9. Structures of quinazoline alkaloids (**118**–**126**) reported from *A. sydowii*.

Acremolins are rare alkaloids with a 5/6/5 tricyclic core, possessing an imidazole moiety fused with a methyl guanine moiety. Interestingly, acremolins were reported from *Aspergillus* species *Aspergillus* sp. S-3-75 and SCSIO-Ind09F01 and *A. sydowii* SP-1 [40,67]. From the Antarctic *A. sydowii* SP-1, a new alkaloid acremolin C (**128**) along with compound **110** were separated using SiO_2 CC/ODS/HPLC and characterized by spectral methods. Compound **128** is a regio-isomer of acremolin B previously reported by Tian et al. from the deep-sea-derived fungus *Aspergillus sp.* SCSIO and has a isopropyl group at C-2′ instead of C-1′ (Figure 10) [40,67]. In 2022, Niu et al. purified and characterized, from the deep-sea-derived *A. sydowii* MCCC-3A00324, a new acremolin alkaloid acremolin D (**129**) along with compounds **110**, **126**, **127**, **135**, and **136** using SiO_2 CC/HPLC and spectral and ECD data. Compound **129** is closely related to compound **127** in that one CH_3 group in **127** has been replaced by an acetoxy methylene group [65].

New hetero-spirocyclic γ-lactam analogs azaspirofurans A (**132**) and B (**133**) were separated from the marine sediment-derived *A. sydowii* D2-6 using SiO_2/Sephadex LH-20 CC and were characterized based on spectral and chemical evidence (Figure 10). These compounds featured an ethyl furan ring linked to 1-oxa-7-azaspiro[4,4]non2-ene-4,6-dione core [43].

2.5. Phenyl Ether Derivatives

Phenyl ethers are a group of simple polyketides that are widely reported in various *Aspergillus* species and have shown significant bioactivities (Table 5).

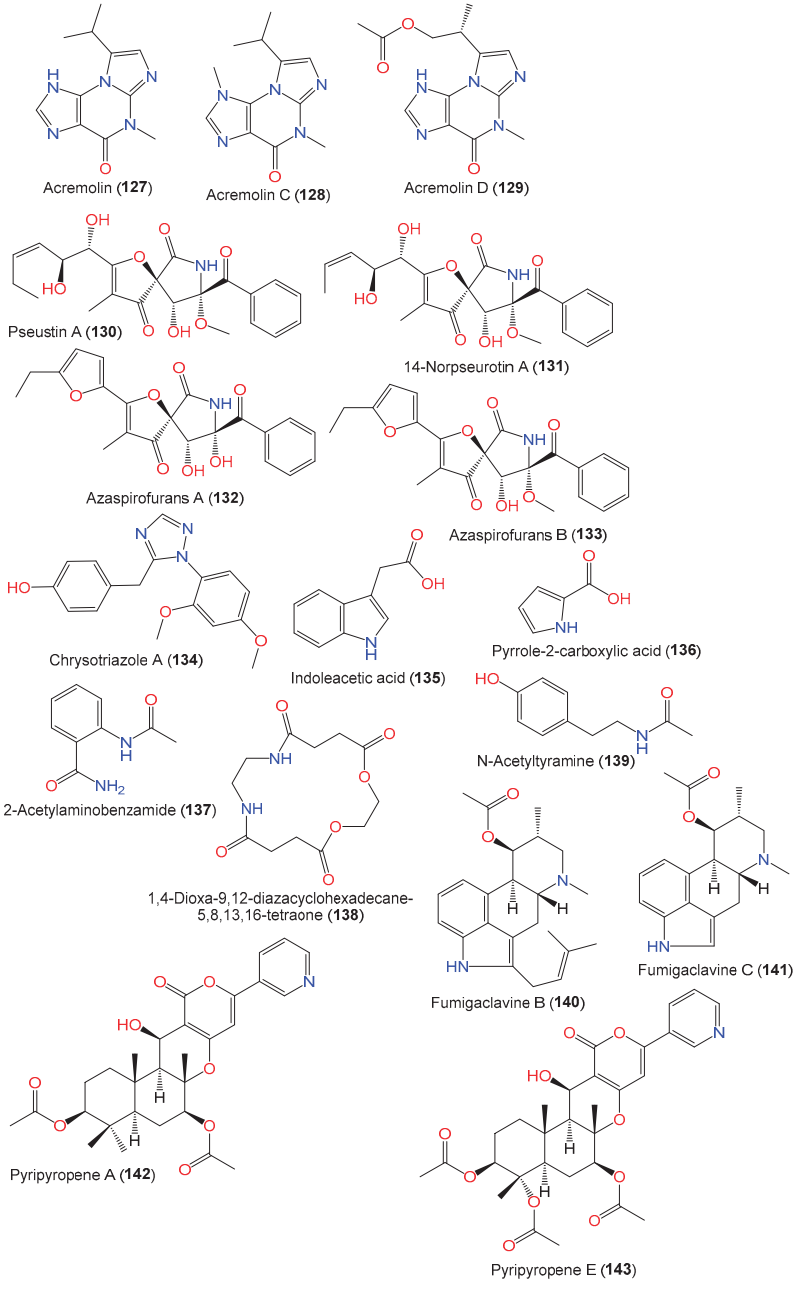

Figure 10. Structures of alkaloids (**127–143**) reported from *A. sydowii*.

Table 5. Phenyl ether derivatives reported from *Aspergillus sydowii* (molecular weight and formulae, strain, host, and location).

Compound Name	Mol. Wt.	Mol. Formula	Strain, Host, Location	Ref.
Violaceol I (**144**)	262	$C_{14}H_{14}O_5$	MF357, sea sediment, East China Sea, China	[37]
	-	-	J05B-7F-4, *Stelletta* sp. (marine sponge), South Korea	[36]
Violaceol II (**145**)	248	$C_{13}H_{12}O_5$	MF357, sea sediment, East China Sea, China	[37]
	-	-	J05B-7F-4, *Stelletta* sp. (marine sponge), South Korea	[36]
Diorcinol (**146**)	230	$C_{14}H_{14}O_3$	Marine sediment, Hsinchu, Taiwan	[54]
	-	-	J05B-7F-4, *Stelletta* sp. (marine sponge), South Korea	[36]
	-	-	FNA026, seawater, Xiamen, China	[9]
	-	-	MCCC 3A00324, deep-sea sediment, South Atlantic Ocean	[60]
4-Carboxydiorcinal (**147**)	274	$C_{15}H_{14}O_5$	J05B-7F-4, *Stelletta* sp. (marine sponge), South Korea	[36]
			FNA026, seawater, Xiamen, China	[9]
Diorcinolic acid (**148**)	318	$C_{16}H_{14}O_7$	J05B-7F-4, *Stelletta* sp. (marine sponge), South Korea	[36]
Glyceryl diorcinolic acid (**149**)	392	$C_{19}H_{20}O_9$	FNA026, seawater, Xiamen, China	[9]
4-Methoxycarbonyl diorcinol (**150**)	288	$C_{16}H_{16}O_5$	FNA026, seawater, Xiamen, China	[9]
10-Deoxygerfelin (**151**)	274	$C_{15}H_{14}O_5$	CPCC 401353, cultured, China	[59]
Cordyol C (**152**)	246	$C_{14}H_{14}O_4$	J05B-7F-4, *Stelletta* sp. (marine sponge), South Korea	[36]
	-	-	FNA026, seawater, Xiamen, China	[9]
	-	-	MCCC 3A00324, deep-sea sediment, South Atlantic Ocean	[60]
Cordyol E (**153**)	244	$C_{15}H_{16}O_3$	J05B-7F-4, *Stelletta* sp. (marine sponge), South Korea	[36]
Cordyol F (**154**)	276	$C_{15}H_{16}O_5$	FNA026, seawater, Xiamen, China	[9]
Cordyol C-3-O-α-D-ribofuranoside (**155**)	378	$C_{19}H_{22}O_8$	FNA026, seawater, Xiamen, China	[9]
Diorcinol-3-O-α-D-ribofuranoside (**156**)	362	$C_{19}H_{22}O_7$	FNA026, seawater, Xiamen, China	[9]
4-Methoxycarbonyl diorcinol-3-O-α-D-glucoside (**157**)	450	$C_{22}H_{26}O_{10}$	FNA026, seawater, Xiamen, China	[9]
Disydonol B (**158**)	486	$C_{30}H_{46}O_5$	FNA026, seawater, Xiamen, China	[55]
2-(Ethoxycarbonyl)-4′-carboxydiorcinal (**159**)	348	$C_{17}H_{16}O_8$	FNA026, seawater, Xiamen, China	[9]
7-Ethyldiorcinol (**160**)	244	$C_{15}H_{16}O_3$	FNA026, seawater, Xiamen, China	[9]
3-Hydroxydiorcinol (**161**)	246	$C_{14}H_{14}O_4$	FNA026, seawater, Xiamen, China	[9]
Aspergilol E (**162**)	304	$C_{16}H_{16}O_6$	FNA026, seawater, Xiamen, China	[9]
4-Hydroxy-2-(3′-hydroxy-4-methoxycarbonyl-5′-methylphenoxy)-6-methylbenzoic acid (**163**)	332	$C_{17}H_{16}O_7$	FNA026, seawater, Xiamen, China	[9]

Table 5. *Cont.*

Compound Name	Mol. Wt.	Mol. Formula	Strain, Host, Location	Ref.
Aspermutarubrol (**164**)	262	$C_{14}H_{14}O_5$	FNA026, seawater, Xiamen, China	[9]
Bisviolaceol II (**165**)	506	$C_{28}H_{26}O_9$	10–31, sediments, deep-sea, cold seep off southwestern Taiwan	[38]
Sydowiol A (**166**)	370	$C_{20}H_{18}O_7$	MF357, sea sediment, East China Sea, China	[37]
Sydowiol B (**167**)	384	$C_{21}H_{20}O_7$	MF357, sea sediment, East China Sea, China	[37]
Sydowiol C (**168**)	384	$C_{21}H_{20}O_7$	MF357, sea sediment, East China Sea, China	[37]

A new biphenyl ether derivative diorcinolic acid (**148**) together with compounds **144**–**147**, **152**, and **153** were separated from marine sponge *Stelletta* sp.-associated *A. sydowii* (Figure 11). Compound **149** featured two ether-linked 1,3-dioxy-6-carboxy-5-methylphenyl units. It was assigned as dicarboxylated diorcinol (carboxylated orcinol's ether-linked dimer) [36]. Bioassay-guided separation of the East China Sea sediment-derived *A. sydowii* MF357 yielded new tris-pyrogallol ethers sydowiols A–C (**166**–**168**) and related bis-pyrogall ol ethers **144** and **145** that were characterized based on detailed spectral analysis and symmetry considerations [37]. On the other hand, the LC–UV–MS-guided separation of EtOAc extract of China Sea-derived *A. sydowii* resulted in new diphenyl ethers **155**–**157** and **159**–**161** along with compounds **146**, **147**, **149**, **150**, **152**, and **162**–**164** using SiO_2/Sephadex LH-20 CC/HPLC; the compounds were assigned using spectral and chemical methods. Compounds **155** and **156** are rare glycosides, possessing a D-ribose moiety, whereas compound **157** has a D-glucose moiety [9].

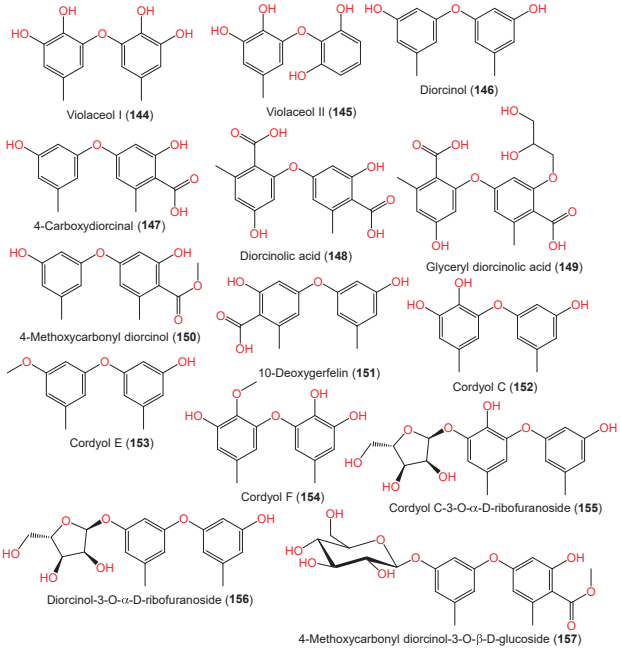

Figure 11. Structures of phenyl ether derivatives (**144**–**157**) reported from *A. sydowii*.

From cold seep-derived *A. sydowii* 10–31, bisviolaceol II (**165**), a new tetraphenyl ether derivative, was isolated and characterized by Liu et al. using SiO_2/Sephadex LH-20 CC/HPLC and spectral tools, respectively [38] (Figure 12).

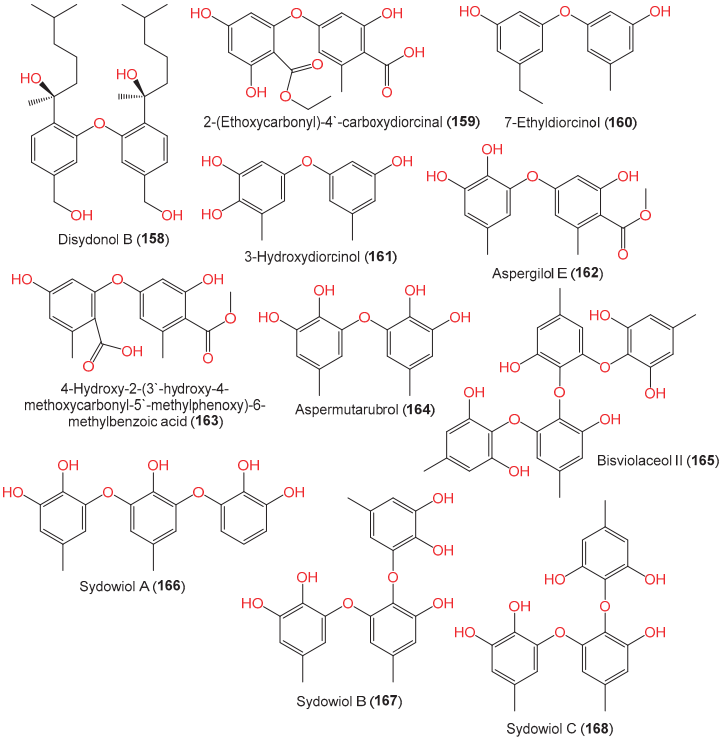

Figure 12. Structures of phenyl ether derivatives (**158**–**168**) reported from *A. sydowii.*

2.6. Chromane and Coumarin Derivatives

Citrinin is a polyketide-derived mycotoxin that was first reported in *Penicillium citrinum* as lemon-yellow particles. Also, other species of *Monascus*, *Penicillium*, and *Aspergillus* genera are found to be capable of producing this toxin [68].

The coculture of two or more different microbes is a useful approach for activating silent biosynthetic genes to accumulate cryptic compounds. In this regard, an investigation on the EtOAc extract of a coculture of *A. sydowii* EN-534 and *P. citrinum* EN-535 obtained from the marine red alga *Laurencia okamurai* using SiO_2/Sephadex LH-20/RP-18 CC/preparative TLC (thin-layer chromatography) resulted in the separation of new citrinin analogs **171** and **172**, in addition to compounds **169**, **170**, and **173**–**176**, that were characterized by spectral, optical rotation, ECD, and X-ray analyses (Table 6, Figure 13). Compounds **171** and **172** are a citrinin dimer and citrinin monomer, respectively. The configurations of compounds **171**–**173** were assigned as 3*R*/4*S*/2′*R*/3′*S*, 3*R*/4*S*/2′*R*, and 3′*S*/1*S*/3*R*/4*S* by X-ray and ECD analyses [69]. Further, asperentin B (**178**), a new asperentin analog, was obtained from the Mediterranean sea sediment-derived *A. sydowii* EN50, which is closely related to compound **177** but with an additional OH at C-6 [46]; it was proposed to be derived from the hydroxylation of PKS (polyketide synthase) precursor at the aromatic ring [46].

Table 6. Chromane and coumarin derivatives reported from *Aspergillus sydowii* (molecular weight and formulae, strain, host, and location).

Compound Name	Mol. Wt.	Mol. Formula	Strain, Host, Location	Ref.
Citrinin (**169**)	250	$C_{13}H_{14}O_5$	EN-534, *Laurencia okamurai* (red alga), Qingdao, China	[69]
Penicitrinol A (**170**)	382	$C_{23}H_{26}O_5$	EN-534, *Laurencia okamurai* (red alga), Qingdao, China	[[6]
seco-Penicitrinol A (**171**)	398	$C_{23}H_{26}O_6$	EN-534, *Laurencia okamurai* (red alga), Qingdao, China	[69]
Penicitrinol L (**172**)	266	$C_{14}H_{18}O_5$	EN-534, *Laurencia okamurai* (red alga), Qingdao, China	[69]
Penicitrinone A (**173**)	380	$C_{23}H_{24}O_5$	EN-534, *Laurencia okamurai* (red alga), Qingdao, China	[69]
Penicitrinone F (**174**)	394	$C_{24}H_{26}O_5$	EN-534, *Laurencia okamurai* (red alga), Qingdao, China	[69]
Dihydrocitrinone (**175**)	266	$C_{13}H_{14}O_6$	EN-534, *Laurencia okamurai* (red alga), Qingdao, China	[69]
Decarboxydihydrocitrinone (**176**)	222	$C_{12}H_{14}O_4$	EN-534, *Laurencia okamurai* (red alga), Qingdao, China	[69]
(−)-Asperentin (**177**)	292	$C_{16}H_{20}O_5$	F00785, *Enteromorpha prolifera* (green alga), Jinjiang Saltern, Fujian province, China LF660, sea sediment, Mediterranean Sea, Levantine Basin SE of Crete	[70] [46]
Asperentin B (**178**)	308	$C_{16}H_{20}O_6$	LF660, sea sediment, Mediterranean Sea, Levantine Basin SE of Crete	[46]
5-*O*-Methyl-asperentin B = 5-Hydroxyl-6-*O*-methylasperentin (**179**)	322	$C_{17}H_{22}O_6$	F00785, *Enteromorpha prolifera* (green alga), Jinjiang Saltern, Fujian province, China LF660, sea sediment, Mediterranean Sea, Levantine Basin SE of Crete	[70] [46]
6-*O*-α-D-Ribosylasperentin (**180**)	424	$C_{21}H_{28}O_9$	F00785, *Enteromorpha prolifera* (green alga), Jinjiang Saltern, Fujian province, China	[70]
6-*O*-α-D-Ribosyl-8-*O*-methylasperentin (**181**)	438	$C_{22}H_{30}O_9$	F00785, *Enteromorpha prolifera* (green alga), Jinjiang Saltern, Fujian province, China	[70]
5′-Hydroxyasperentin (**182**)	308	$C_{16}H_{20}O_6$	F00785, *Enteromorpha prolifera* (green alga), Jinjiang Saltern, Fujian province, China	[70]
4′-Hydroxyasperentin (**183**)	308	$C_{16}H_{20}O_6$	F00785, *Enteromorpha prolifera* (green alga), Jinjiang Saltern, Fujian province, China	[70]
Asperentin-8-methyl ether (**184**)	306	$C_{17}H_{22}O_5$	F00785, *Enteromorpha prolifera* (green alga), Jinjiang Saltern, Fujian province, China	[70]
5′-Hydroxyasperentin-8-methyl ether (**185**)	322	$C_{17}H_{22}O_6$	F00785, *Enteromorpha prolifera* (green alga), Jinjiang Saltern, Fujian province, China	[70]
4′-Hydroxyasperentin-6-methyl ether (**186**)	322	$C_{17}H_{22}O_6$	F00785, *Enteromorpha prolifera* (green alga), Jinjiang Saltern, Fujian province, China	[70]
(3*R*,4*S*)-3,4,5-Trimethyl-isochroman-6,8-diol (**187**)	208	$C_{12}H_{16}O_3$	YH11-2, deep-sea fungus, Guam, South Japan	[44]
(3*R*,4*S*)-6,8-dihydroxy-3,4,5-trimethylisochroman-1-one (**188**)	222	$C_{12}H_{14}O_4$	YH11-2, deep-sea fungus, Guam, South Japan	[44]

Table 6. *Cont.*

Compound Name	Mol. Wt.	Mol. Formula	Strain, Host, Location	Ref.
2-(12*S*-Hydroxypropyl)-3-hydroxymethyl-6-hydroxy-7-methoxychromone (**189**)	280	$C_{14}H_{16}O_6$	#2B, *Aricennia marina* (leaves), Yangjiang, Guangdong, China	[64]
7-Hydroxy-2-(2-hydroxypropyl)-5-methyl chromone (**190**)	234	$C_{13}H_{14}O_4$	J05B-7F-4, *Stelletta* sp. (marine sponge), South Korea	[36]
Aspercoumarine acid (**191**)	206	$C_{10}H_6O_5$	MCCC 3A00324, deep-sea sediment, South Atlantic Ocean	[60]
(2*R*)-2,3-Dihydro-7-hydroxy-6,8-dimethyl-2-[(E)-prop-1-enyl]chromen-4-one (**192**)	232	$C_{14}H_{16}O_3$	YH11-2, deep-sea fungus, Guam, South Japan	[44]

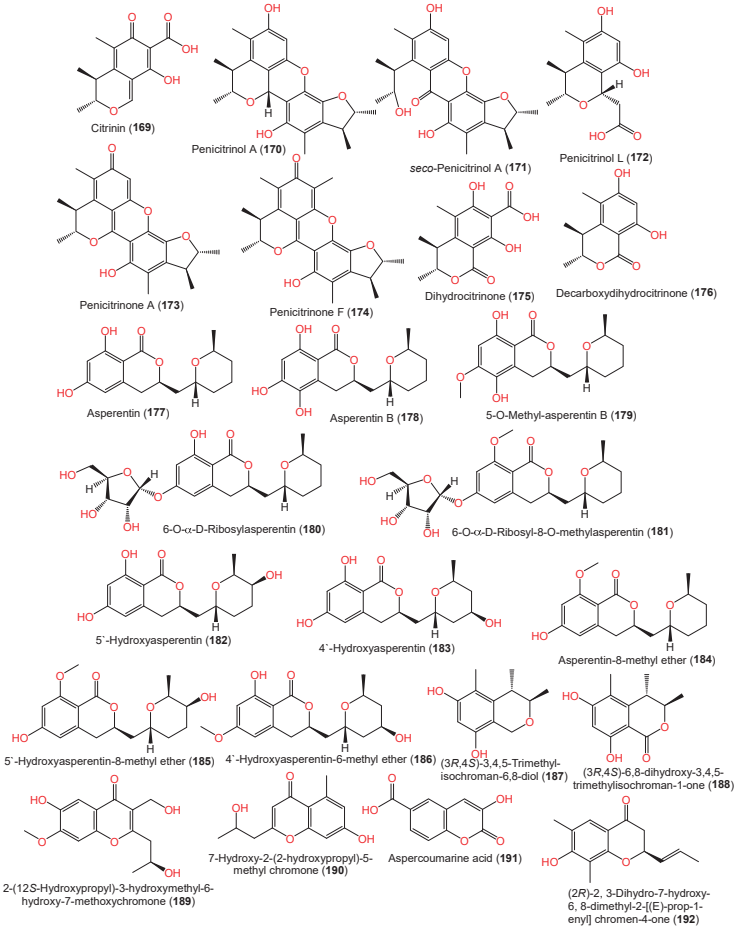

Figure 13. Structures of chromane and coumarin derivatives (**169**–**192**) reported from *A. sydowii.*

2.7. Pyrane, Cyclopentene, Cyclopropane, and Lactone Derivatives

Two new 2-pyrone derivatives **195** and **196** and a new cyclopentenone derivative **208** along with known analog **197** were isolated from the South China Sea gorgonian

Verrucella umbraculum-derived *A. sydowii* SCSIO-00305 utilizing SiO_2/RP-10/Sephadex LH-20 CC/HPLC (Figure 14). The 8*R*/8*S*/5*S* absolute configuration of compounds **195**, **196**, and **208** was established using Mosher's method and ECD spectra [24]. Liu et al. separated pryan analogs **194** and **193** from *A. sydowii* SCSIO-41301 (Table 7) [35]. Two new pyrone derivatives, labeled **189** and **198**, together with compounds **199** and **200** were separated from *Aricennia marina*-inhabiting *A. sydowii* #2B by SiO_2/Sephadex LH-20 CC/HPLC. Based on X-ray analysis and optical rotation measurement, compound **189** has 1S-configuration, while compounds **198** and **200** are racemic mixtures. Compounds **198** and **200** are alpha-pyrone derivatives; however, compound **189** is γ-pyrone [64]. Further, two undescribed α-pyrone derivatives **191** and **201** were separated and characterized from deep-sea-derived *A. sydowii* MCCC-3A00324. Compound **201** bears two phenyl moieties at C-3 and C-5 [60].

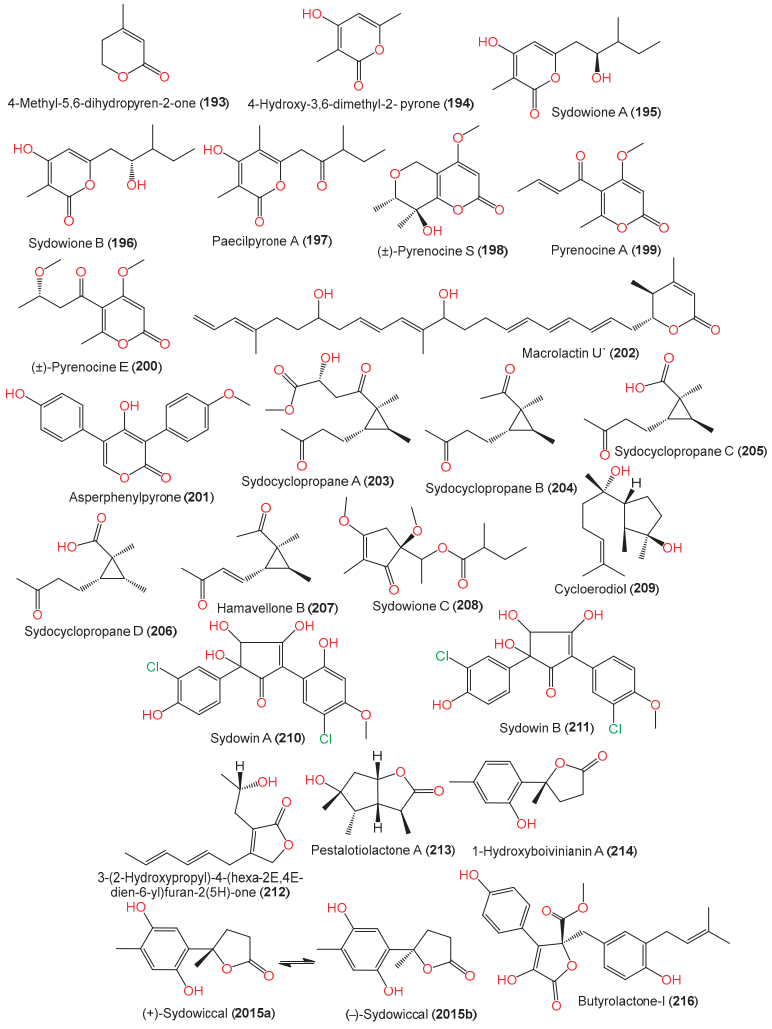

Figure 14. Structures of pyrane, cyclopentene, cyclopropane, and lactone derivatives (**193–216**) reported from *A. sydowii*.

Table 7. Chromane and coumarin derivatives reported from *Aspergillus sydowii* (molecular weight and formulae, strain, host, and location).

Compound Name	Mol. Wt.	Mol. Formula	Strain, Host, Location	Ref.
4-Hydroxy-3,6-dimethyl-2-pyrone (**194**)	140	$C_7H_8O_3$	SCSIO 41301, *Phakellia fusca* (marine sponge), Xisha Islands, China	[35]
4-Methyl-5,6-dihydropyren-2-one (**193**)	112	$C_6H_8O_2$	SCSIO 41301, *Phakellia fusca* (marine sponge), Xisha Islands, China	[35]
Sydowione A (**195**)	226	$C_{12}H_{18}O_4$	SCSIO 00305, *Verrucella unbracculum* (gorgonian), South China Sea, Sanya, Hainan, China	[24]
Sydowione B (**196**)	226	$C_{12}H_{18}O_4$	SCSIO 00305, *Verrucella unbracculum* (gorgonian), South China Sea, Sanya, Hainan, China	[24]
Paecilpyrone A (**197**)	238	$C_{13}H_{18}O_4$	SCSIO 00305, *Verrucella unbracculum* (gorgonian), South China Sea, Sanya, Hainan, China	[24]
(±)-Pyrenocine S (**198**)	226	$C_{11}H_{14}O_5$	#2B, *Aricennia marina* (leaves), Yangjiang, Guangdong, China	[64]
Pyrenocine A (**199**)	208	$C_{11}H_{12}O_4$	#2B, *Aricennia marina* (leaves), Yangjiang, Guangdong, China	[64]
(±)-Pyrenocine E (**200**)	240	$C_{12}H_{16}O_5$	#2B, *Aricennia marina* (leaves), Yangjiang, Guangdong, China	[64]
Asperphenylpyrone (**201**)	310	$C_{18}H_{14}O_5$	MCCC 3A00324, deep-sea sediment, South Atlantic Ocean	[60]
Macrolactin U′ (**202**)	480	$C_{31}H_{44}O_4$	Deep-sea mud, Dalian, China	[58]
Sydocyclopropane A (**203**)	270	$C_{14}H_{22}O_5$	MCCC 3A00324, deep-sea sediment, South Atlantic Ocean	[42]
Sydocyclopropane B (**204**)	182	$C_{11}H_{18}O_2$	MCCC 3A00324, deep-sea sediment, South Atlantic Ocean	[42]
Sydocyclopropane C (**205**)	184	$C_{10}H_{16}O_3$	MCCC 3A00324, deep-sea sediment, South Atlantic Ocean	[42]
Sydocyclopropane D (**206**)	184	$C_{10}H_{16}O_3$	MCCC 3A00324, deep-sea sediment, South Atlantic Ocean	[42]
Hamavellone B (**207**)	180	$C_{11}H_{16}O_2$	MCCC 3A00324, deep-sea sediment, South Atlantic Ocean	[42]
Sydowione C (**208**)	284	$C_{15}H_{24}O_5$	SCSIO 00305, *Verrucella unbracculum* (gorgonian), South China Sea, Sanya, Hainan, China	[24]
Cycloerodiol (**209**)	240	$C_{15}H_{28}O_2$	Cultured, China	[28]
Sydowin A (**210**)	412	$C_{18}H_{14}Cl_2O_7$	*Acanthophora spicifera* (red alga), Rameswaram, India	[53]
Sydowin B (**211**)	396	$C_{18}H_{14}Cl_2O_6$	*Acanthophora spicifera* (red alga), Rameswaram, India	[53]
3-(2-Hydroxypropyl)-4-(hexa-2*E*,4*E*-dien-6-yl)furan-2(5*H*)-one (**212**)	222	$C_{13}H_{18}O_3$	Cultured, China	[28]
Pestalotiolactone A (**213**)	184	$C_{10}H_{16}O_3$	MCCC 3A00324, deep-sea sediment, South Atlantic Ocean	[60]

Table 7. *Cont.*

Compound Name	Mol. Wt.	Mol. Formula	Strain, Host, Location	Ref.
1-Hydroxyboivinianin A (**214**)	206	$C_{12}H_{14}O_3$	MCCC 3A00324, deep-sea sediment, South Atlantic Ocean	[57]
(±)-Sydowiccal (**215**)	222	$C_{12}H_{14}O_4$	*Rhododendron mole* (leaves), Xing'an, Guangxi, China	[26]
Butyrolactone-I (**216**)	424	$C_{24}H_{24}O_7$	#2B, *Aricennia marina* (leaves), Yangjiang, Guangdong, China	[64]

The cyclopropyl moiety is the smallest cycloalkane moiety. It is a strained moiety that usually occurs as a structural subunit of various natural metabolites, particularly alkaloids, steroids, and terpenoids [71,72]. Many polycyclic natural metabolites bearing this ring were reported in higher plants, archaea, fungi, and bacteria, while monocyclic molecules are rarely found [73]. In 1920, the first monocyclic cyclopropane (+)-trans-chrysanthemic acid was reported [42]. In 2022, sydocyclopropanes A–D (**203**–**206**), novel monocyclic cyclopropane acids, along with compound **207** were separated from the deep-sea sediment-associated *A. sydowii* MCCC-3A00324 using SiO_2 CC/Sephadex LH-20/HPLC and were characterized by spectral, ECD, and $DP4^+$ probability analyses by Niu et al. [42]. These metabolites feature a 1,1,2,3-tetrasubstituted cyclopropane moiety with different alkyl side chains. Their established configurations were 1*S*/2*S*/3*S*/12*R* for compound **203**, 1*S*/2*S*/3*S* for compounds **204** and **205**, and 1*S*/2*R*/3*S* for compound **206**, which was identified as a C-2 epimer of compound **205** [42].

In 2006, Teuscher et al. separated and characterized new hydroxylated, chlorinated diaryl cyclopentenone derivatives **210** and **211** from red alga *Acanthophora spicifera*-associated *A. sydowii* using Sephadex LH-20/HPLC and NMR/CD analyses, respectively. These kinds of metabolites were related to diaryl cyclopentenones reported in order Boletales basidiomycetic fungi and involved in conspicuous bluing reactions of fruiting bodies and reported for the first time from ascomycetes [53]. Compound **215** was isolated as enantiomers, involving (+)-(**215a**) and (−)-(**215b**), using SiO_2/RP-18 CC/HPLC from *Rhododendron mole*-accompanied *A. sydowii* and elucidated by spectral and CD analyses. They were purified by chiral HPLC and identified to have 7*S* and 7*R* configurations, respectively [26].

2.8. Other Metabolites

New catechol derivatives **223** and **224** were separated as racemic by Liu et al. and could not be separated into their enantiomers. Compound **224** resembles compound **223**, except for the presence of the C-2 COOH group and a 2-methylpentan-1-ol unit, instead of the 2-CH_3 and propionic acid moiety in compound **223** [35] (Table 8, Figure 15). A new chorismic acid analog, labeled **217**, was reported by Liu et al. and its 3*R*/4*S*/5*R*/1′*S* configuration was assigned based on ECD analysis [41]. The same group separated a dibenzofuran derivative, labeled **234**, from *A. sydowii* SCSIO-41301 [35]. Compounds **228**–**230** and **234** were separated by Niu et al. from the deep-sea sediment-associated *A. sydowii* MCCC-3A00324 [60].

Anthocyanins belong to the flavonoids family and are generally reported from plant sources. These metabolites have various applications in agro-food industries such as in natural dyes; additionally, their substantial therapeutic human health in treating obesity and improving cardiovascular function are of note [74]. In 2020, Bu et al. reported the capacity of *A. sydowii* H-1 to produce anthocyanins using metabolomic and transcriptomic analyses [25]. Compounds **242**–**246** were characterized; compounds **242** and **244** were the most abundant of the identified anthocyanins [25]. Interestingly, cinnamate-4-hydroxylase and chalcone synthase genes were identified as the key genes involved in anthocyanin biosynthesis [25]. This expanded the knowledge of natural anthocyanin biosynthesis by fungi for the first time.

Table 8. Other metabolites reported from *Aspergillus sydowii* (molecular weight and formulae, strain, host, and location).

Compound Name	Mol. Wt.	Mol. Formula	Strain, Host, Location	Ref.
Sydowether (**217**)	354	$C_{18}H_{26}O_7$	SW9, seawater, Yangma Island, Yantai, China	[41]
1,9-Dihydroxy-3-(hydroxymethyl)-10-methoxydibenzo[b,e]oxepine-6,11-dione (**218**)	316	$C_{16}H_{12}O_7$	*Scapania ciliata* (Chinese liverwort), Maoer Mountain, Guangxi, China	[63]
8-Demethoxy-10-methoxy-wentiquinone C (**219**)	300	$C_{16}H_{12}O_6$	C1-S01-A7, seawater, West Pacific Ocean	[55]
Moniliphenone (**220**)	286	$C_{16}H_{14}O_5$	*Scapania ciliata* (Chinese liverwort), Maoer Mountain, Guangxi, China	[63]
Phenol A acid (**221**)	240	$C_{12}H_{16}O_5$	EN-534, *Laurencia okamurai* (red alga), Qingdao, China	[69]
Phenol A (**222**)	196	$C_{11}H_{16}O_3$	EN-534, *Laurencia okamurai* (red alga), Qingdao, China	[69]
3-(2,5-Dimethylbenzo[d][1,3]dioxol-2-yl)propanoic acid (**223**)	222	$C_{12}H_{14}O_4$	SCSIO 41301, *Phakellia fusca* (marine sponge), Xisha Islands, China	[35]
2-(5-Hydroxy-4-methylpentyl)-2-methylbenzo[d][1,3]dioxole-5-carboxylic acid (**224**)	280	$C_{15}H_{20}O_5$	SCSIO 41301, *Phakellia fusca* (marine sponge), Xisha Islands, China	[35]
4-Hydroxyphenylacetic acid (**225**)	152	$C_8H_8O_3$	SP-1, marine sediment, Antarctic Great Wall Station	[40]
Orcinol (**226**)	124	$C_7H_8O_2$	PSU-F154, genus *Annella* sp. (gorgonian sea fan), coastal area, Surat Thani, Thailand	[56]
3-Hydroxybenzoic acid (**227**)	138	$C_7H_6O_3$	CPCC 401353, cultured, China	[59]
4-Hydroxybenzoic acid (**228**)	138	$C_7H_6O_3$	MCCC 3A00324, deep-sea sediment, South Atlantic Ocean	[60]
3,4,5-Trimethoxybenzoic acid (**229**)	212	$C_{10}H_{12}O_5$	MCCC 3A00324, deep-sea sediment, South Atlantic Ocean	[60]
4-(3′,4′-Dihydroxyphenyl)-2-butanone (**230**)	180	$C_{10}H_{12}O_3$	MCCC 3A00324, deep-sea sediment, South Atlantic Ocean	[60]
4-Hydroxybenzaldehyde (**231**)	122	$C_7H_6O_2$	C1-S01-A7, seawater, West Pacific Ocean	[55]
Benzoic acid (**232**)	122	$C_7H_6O_2$	CPCC 401353, cultured, China	[59]
Gibellulin B (**233**)	260	$C_{14}H_{12}O_5$	FNA026, seawater, Xiamen, China	[9]
3,7-Dihydroxy-1,9-dimethyldibenzofuran (**234**)	228	$C_{14}H_{12}O_3$	FNA026, seawater, Xiamen, China	[9]
	-	-	SCSIO 41301, *Phakellia fusca* (marine sponge), Xisha Islands, China	[35]
	-	-	MCCC 3A00324, deep-sea sediment, South Atlantic Ocean	[60]
Orsellinic acid (**235**)	168	$C_8H_8O_4$	Deep-sea mud, Dalian, China	[58]
	-	-	CPCC 401353, cultured, China	[59]
2-Methoxy-5-methyl-3-(methylsulfonyl)phenol (**236**)	216	$C_9H_{12}O_4S$	*Rhododendron mole* (leaves), Xing'an, Guangxi, China	[26]
2,3,5-Trimethyl-6-(3-oxobutan-2-yl)-4H-pyran-4-one (**237**)	208	$C_{12}H_{16}O_3$	YH11-2, deep-sea fungus, Guam, South Japan	[44]
5-[(2*S*,3*R*)-3-Hydroxybutan-2-yl]-4-methylbenzene-1,3-diol (**238**)	196	$C_{11}H_{16}O_3$	YH11-2, deep-sea fungus, Guam, South Japan	[44]
2,4-Dihydroxy-3,5,6-trimethylbenzaldehyde (**239**)	180	$C_{10}H_{12}O_3$	YH11-2, deep-sea fungus, Guam, South Japan	[44]

Table 8. *Cont.*

Compound Name	Mol. Wt.	Mol. Formula	Strain, Host, Location	Ref.
Macrolactin A (**240**)	402	$C_{24}H_{34}O_5$	Piece of deep-sea mud, Dalian, China	[58]
(*Z*)-6-Tridecenoic acid (**241**)	212	$C_{13}H_{24}O_2$	Cultured, China	[28]
Malvidin 3-O-glucoside (**242**)	479	$C_{22}H_{23}O_{12}^{+}$\	H-1, bacterial wilt-affected ginger humus, Chengdu, China	[25]
Malvidin 3-O-galactoside (**243**)	449	$C_{21}H_{21}O_{11}^{+}$	H-1, bacterial wilt-affected ginger humus, Chengdu, China	[25]
Cyanidin 3-O-glucoside (**244**)	493	$C_{23}H_{25}O_{12}^{+}$	H-1, bacterial wilt-affected ginger humus, Chengdu, China	[25]
Peonidin O-malonylhexoside (**245**)	549	$C_{25}H_{25}O_{14}^{+}$	H-1, bacterial wilt-affected ginger humus, Chengdu, China	[25]
Cyanidin (**246**)	287	$C_{15}H_{11}O_6^{+}$	H-1, bacterial wilt-affected ginger humus, Chengdu, China	[25]

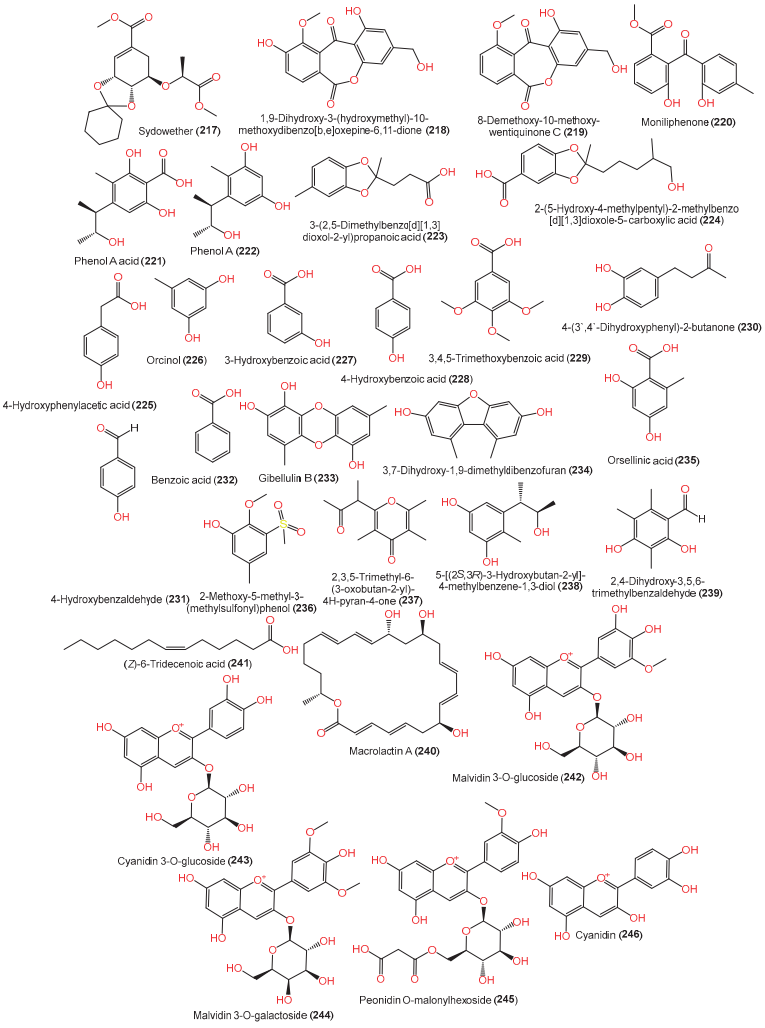

Figure 15. Other metabolites (**217**–**246**) reported from *A. sydowii.*

3. Biological Activities of *A. sydowii* Extracts and Its Metabolites

3.1. Cytotoxic Activity

A. sydowii MSX19583 extract (%cell viability: 54%, conc.: 20 µg/mL) had moderate cytotoxic capacity against MDA-MB-435 (human melanoma cell line) in an MTT assay [33], while a cultured EtOAc extract displayed a marked toxic effect (LD_{50} (lethal dose 50) 36 µg/mL) in a brine shrimp assay [36].

Vascular endothelial cell growth factor (VEGF) is a tumor-secreted protein that stimulates both the migration and growth of vascular endothelial cells; thus, interference with VEGF signaling suppresses tumor growth or blocks angiogenesis [34].

Compound **88** was found to suppress HUVEC (human umbilical vein endothelial cell) proliferation caused by VEGF, bFGF (basic fibroblast growth factor), or ECGS (endothelial cell growth supplement) (IC_{50}s: 1.4, 2.8 µM, and 6.2 µM, respectively) compared to SU5416 (a tyrosine kinase inhibitor, IC_{50}s: 0.05, 5.3, and 30.5 µM, respectively) [34] and demonstrated selective cytotoxic capacity versus A549 (human lung adenocarcinoma epithelial cell line) (IC_{50} < 10 µM) [55].

In an MTT assay, compounds **101** and **117** demonstrated a notable cytotoxic capacity toward A375 (human melanoma cell line) (IC_{50}: 5.7 µM), whereas compound **101** had no cytotoxicity towards adenocarcinoma cells A549, A375, and Hela (human cervical epitheloid carcinoma cell line) compared to cis-platin [31] and compounds **1**, **45**, **110**, and **115** were inactive against MDA-MB-435 and HT-29 (human colon cancer cell lin) [33] (Table 9).

Table 9. Cytotoxic metabolites reported from *A. sydowii*.

Compound Name	Assay/Cell Line	Biological Results (IC_{50}) *		Ref.
		Compound	Positive Control	
Cerevisterol (**67**)	P388/SRB	0.12 µM	CDDP 0.039 µM	[44]
6-Methoxyl austocystin A (**83**)	*Artemia salina*	2.9 µM	Toosendanin 2.2 µM	[24]
[4-(2-Methoxyphenyl)-1-piperazinyl][(1-methyl-1*H*-indol-3-yl)]-methanone (**117**)	MTT/A375	5.7 µM	-	[31]
(3*R*,4*S*)-3,4,5-Trimethylisochroman-6,8-diol (**187**)	P388/SRB	1.95 µM	CDDP 0.039 µM	[44]
(2*R*)-2,3-Dihydro-7-hydroxy-6,8-dimethyl-2-[(*E*)-prop-1-enyl] chromen-4-one (**192**)	P388/SRB	0.14 µM	CDDP 0.039 µM	[44]
Sydowione A (**195**)	*Artemia salina*	19.5 µM	Toosendanin 2.2 µM	[24]
Sydowione B (**196**)	*Artemia salina*	14.3 µM	Toosendanin 2.2 µM	[24]
Sydowione C (**208**)	*Artemia salina*	8.3 µM	Toosendanin 2.2 µM	[24]
2,4-Dihydroxy-3,5,6-trimethylbenzaldehyde (**239**)	P388/SRB	0.59 µM	CDDP 0.039 µM	[44]

* IC50, Half maximal inhibitory concentration.

Acremolin D (**129**) had cytotoxic efficacy versus K562 (human erythroleukemic) and Hela-S3 (human cervix adenocarcinoma) cell lines with % inhibition equal to 25.1 and 30.6%, respectively, while compound **127** displayed activity (% inhibition: 20.9–35.5%) versus HepG2 (human hepatocellular liver carcinoma cell line), A549, and K562 in an MTT (3-(4,5-dimethylthiazol-2-yl)-2,5-diphenyltetrazolium bromide) assay [65]. Azaspirofurans A (**132**) displayed moderate cytotoxic potential versus A549 cell proliferation (IC_{50}: 10 µM) in the MTT method [43] and compounds **103–105** (IC_{50}s: 8.29, 1.28, and 7.31 µM, respectively) demonstrated weak capacities [48].

Compounds **44** and **149** were mildly active versus KB (human oral epidermoid carcinoma cell line), HepG2, and HCT-116 (human colon cancer cell line) cells (IC_{50}s: 50–70 µM) compared to doxorubicin (IC_{50}s: 5–6 µM) [36]. Wang et al. reported that compounds **146**, **149**, **152, 155**, **160**, and **161** were found to exhibit cytotoxic potential versus A549, U937 (promonocytic, human myeloid leukaemia cell line), HL-60 (human promyelocytic leukemia cell line), and K562 cells (IC_{50}: 3.36–23.03 µM) [9]. Wang et al. stated that compounds **98**, **99**,

199, **200**, and **216** possessed cytotoxic capacities versus VCaP (human prostate cancer cell line) (IC_{50}s: 1.92–33.36 μM), but compound **189** was inactive in comparison with docetaxel (IC_{50}: 4.95 nM) in the MTT method [64]. Compounds **83**, **195**, **196**, and **208** possessed toxicity towards brine shrine nauplii (LC_{50}s: 2.9–19.5 μM), whereas compound **83** had a potent efficacy (LC_{50}: 2.9 μM) compared to toosendanin (LC_{50}: 2.2 μM) [24]. On the other hand, compounds **192** and **239** revealed powerful cytotoxic potential versus P388 (menogaril-resistant mouse leukaemia cell line) (IC_{50}s: 0.14 and 0.59 μM, respectively) in a SRB (sulforhodamine B) assay; however, compound **237** was inactive [44].

3.2. Antioxidant and Immunosuppression Activities

Compound **24** was found to have DPPH (1,1-diphenyl-2-picrylhydrazyl) scavenging activity (IC_{50}: 113.5 μM/L), while compound **25** was inactive (IC_{50} value > 300 μM/L) compared to BHT (butylated hydroxytoluene) (IC_{50}: 30.8 μM/L) in a DPPH assay, suggesting that the OH position and racemization influenced the activity [32]. Also, compound **88** demonstrated antioxidant capacity (IC_{50}: 17.0 μM) compared to butylated hydroxyanisole (IC_{50}: 0.13 μM). Compound **88** differed from compound **71** in lacking C_7–C_8 double bonds, revealing that the planar structure of compound **71** might reduce its activity [56]. On the other hand, compounds **195** and **196** had more potent antioxidant activity (IC_{50}s: 46.0 and 46.6 μM, respectively) than L-ascorbic acid (IC_{50}: 61.0 μM); however, compounds **83** and **208** were weakly active (IC_{50}s: 98.0 and 86.3 μM, respectively) [24].

Compounds **72**, **74**, **76–78**, **91, 94**, **97**, **218**, and **220** were evaluated in vitro for immunosuppression capacity against Con-A (concanavalin A)- and LPS (lipopolysaccharide)-induced mouse splenic lymphocyte proliferation. It was noted that compounds **91** and **94** displayed moderate potential (IC_{50}s: 8.45 and 10.10 μg/mL and 10.25 and 14.10 μg/mL, respectively), compared to cyclosporin A (IC_{50}: 0.62 μg/mL for Con-A and 0.53 μg/mL for LPS). Other compounds showed weak or no activity [63].

3.3. Anti-Mycobacterial, Anti-Microalgal, and Antimicrobial Activities

Infectious illnesses seriously threaten human health worldwide [75,76]. Recently, the increasing recurrence of pathogens' resistance to antimicrobials represents an alarming trend in infectious diseases that results from misuse or overuse of existing antimicrobials and has become a universal health concern [75,76].

A. sydowii ethyl acetate extract (conc.: 500 μg/disk) had selective activity against *B. subtilis* and *E. coli* (inhibition zone diameters (IZDs) 12 and 15 mm, respectively); however, it was inactive against *S. aureus*, *C. albicans*, *Cladosporium herbarum*, and *C. cucumerinum* [53]. In another study, the EtOAc extract of *Dactylospongia* sp.-associated *A. sydowii* DC08 revealed antibacterial potential versus *E. coli* and *S. aureus* (IZDs 12.31 and 14.25 mm, respectively) [77]. Wang et al. reported that *A. sydowii* ZSDS1-F6 EtOAc extract displayed significant antimicrobial capacity versus *Aeromonas hydrophila* and *Klebsiella pneumonia* [45].

The antibacterial effectiveness of compounds **1**, **2**, **5**, **11–14**, **42**, **43**, and **55** versus phytopathogenic bacteria *Ralstonia solanacarum* and *Pseudomonas syringae* utilizing a broth microdilution method revealed that compound **5** had inhibition potential versus *P. syringae* (MIC (minimum inhibitory concentration): 32 μg/mL), whereas compounds **1**, **14**, and **43** were active versus *R. solanacarum* (MICs: 32 μg/mL) using the broth microdilution method [47] (Table 10). Further, compounds **11** and **14** inhibited *Fusarium oxysporum* spore germination (EC_{50}s: 54.55 and 77.16 μg/mL, respectively), while compounds **1**, **11**, **14**, and **43** inhibited *Alternaria alternata* spore germination (EC_{50}s: 26.02–46.15 μg/mL), suggesting the possible use of bisabolane sesquiterpenoids as anti-phytopathogens [47]. Also, compound **44** revealed antibacterial efficacy versus the human pathogen *S. aureus* and fish pathogens *S. iniae* and *V. ichthyoenteri* [36]. Compounds **71**, **88**, and **91** showed weak potential against *Vibrio rotiferianus* (MICs: 16–33 μg/mL); however, compounds **69**, **79**, **86**, **88**, **91**, and **219** were weakly active versus MRSA (methicillin-resistant *Staphylococcus aureus*) (MICs: 15–32 μg/mL) compared to erythromycin and chloramphenicol [55].

Table 10. Anti-mycobacterial, antimicrobial, and anti-microalgal metabolites reported from *A. sydowii*.

Compound Name	Assay/Organism	Biological Results		Ref.
		Compound	Positive Control	
Antibacterial (MIC)				
(7*S*)-(+)-hydroxysydonic acid (**2**)	Broth microdilution/*S. aureus*	0.5 µg/mL	Tigecycline 0.06 µg/mL	[40]
	Broth microdilution/ MRSA	1 µg/mL	Tigecycline 0.25 µg/mL	[40]
	Broth microdilution/*S. epidermidis*	0.25 µg/mL	Tigecycline 0.03 µg/mL	[40]
	Broth microdilution/ MRAE	0.5 µg/mL	Tigecycline 0.12 µg/mL	[40]
(7*S*,11*S*)-(+)-12-Hydroxysydonic acid (**5**)	Broth microdilution/*S. aureus*	0.5 µg/mL	Tigecycline 0.06 µg/mL	[40]
	Broth microdilution/ MRSA	1 µg/mL	Tigecycline 0.25 µg/mL	[40]
	Broth microdilution/*S. epidermidis*	0.25 µg/mL	Tigecycline 0.03 µg/mL	[40]
	Broth microdilution/ MRAE	0.5 µg/mL	Tigecycline 0.12 µg/mL	[40]
(11*S*,14*S*)-Cyclo-(L-Trp-L-Phe) (**110**)	Broth microdilution/*S. aureus*	0.25 µg/mL	Tigecycline 0.06 µg/mL	[40]
	Broth microdilution/ MRSA	1 µg/mL	Tigecycline 0.25 µg/mL	[40]
	Broth microdilution/*S. epidermidis*	0.12 µg/mL	Tigecycline 0.03 µg/mL	[40]
	Broth microdilution/ MRAE	0.5 µg/mL	Tigecycline 0.12 µg/mL	[40]
Citrinin (**169**)	Microplate assay/*E. coli*	8 µg/mL	Chloramphenicol 1 µg/mL	[69]
	Microplate assay/*Micrococcus luteus*	16 µg/mL	Chloramphenicol 2 µg/mL	[69]
	Microplate assay/*Vibrio parahaemolyticus*	8 µg/mL	Chloramphenicol 2 µg/mL	[69]
Penicitrinol A (**170**)	Microplate assay/*E. coli*	8 µg/mL	Chloramphenicol 1 µg/mL	[69]
	Microplate assay/*Micrococcus luteus*	4 µg/mL	Chloramphenicol 2 µg/mL	[69]
	Microplate assay/*Vibrio parahaemolyticus*	8 µg/mL	Chloramphenicol 2 µg/mL	[69]
Antituberculosis (IC_{50})				
Sydowiol A (**166**)	*M. tuberculosis* protein tyrosine phosphatase inhibitor	14.0 µg/mL	-	[37]
Sydowiol B (**167**)		24.0 µg/mL	-	[37]
Anti-microalgae (IC_{50})				
(7*S*)-Flavilane A (**53**)	Broth microdilution/ *Prorocentrum micans*	4.6 µg/mL	$CuSO_4$ 2.7 µg/mL	[38]
	Broth microdilution/ *Prorocentrum minimum*	2.4 µg/mL	$CuSO_4$ 2.2 µg/mL	[38]
(7*S*)- 4-Iodo-flavilane A (**54**)	Broth microdilution/ *Prorocentrum micans*	11.0 µg/mL	$CuSO_4$ 2.7 µg/mL	[38]
	Broth microdilution/ *Prorocentrum minimum*	1.3 µg/mL	$CuSO_4$ 2.2 µg/mL	[38]
Bisviolaceol II (**165**)	Broth microdilution/ *Prorocentrum minimum*	5.2 µg/mL	$CuSO_4$ 2.2 µg/mL	[38]

Compounds **2**, **3**, and **110** demonstrated notable antibacterial efficacy versus *S. aureus*, MRSA, *S. epidermidis*, and MRSE (MICs: 0.25–1.0 µg/mL) compared to trigecycline (MICs: 0.06–0.12 µg/mL); however, compound **128** displayed moderate-to-weak activity (MICs: 4–32 µg/mL) [40]. Compounds **42**, **50,** and **146** had moderate effectiveness versus *K. pneumonia* (MICs: 21.4, 10.7, and 21.7 µM, respectively); also, compounds **1** and **42** exhibited moderate

activity against *E. faecalis* (MIC: 18.8 μM) and *A. hydrophila* (MIC: 4.3 μM), respectively, using an agar dilution method [45].

Compounds **53**, **54**, and **165** (conc.: 20 μg/disc) were found to prohibit the growth of bacteria (*V. anguillarum*, *V. harveyi*, *V. parahaemolyticus*, and *V. splendidus)* and harmful microalgae (*P. micans* and *P. minimum*) in a disc diffusion assay [38]. Pathogenic bacteria and harmful algal blooms pose substantial threats to marine aquaculture. Compounds **53** and **54** inhibited *P. micans* and *P. minimum* (IC_{50} ranging from 1.3 to 11 μg/mL), while compound **165** only had inhibitory efficacy against *P. minimum* (IC_{50}: 5.2 μg/mL). Additionally, these compounds showed inhibition against *Vibrio* species (*V. anguillarum*, *V. harveyi*, *V. parahaemolyticus*, and *V. splendidus)* with IZDs ranging from 6.4 to 8.7 mm. The MICs for compounds **53** and **54** were 8 μg/mL against *V. anguillarum* and *V. parahaemolyticus* and 16 μg/mL against *V. harveyi* [38].

Compounds **61**, **62**, **130**, and **131** displayed notable growth inhibition potential versus *E. coli*, *B. subtilis*, and *M. lysoleikticus* (MICs: 3.74–87.92 μM); compounds **131** and **61** were more powerful than compounds **62** and **130** [48]. Antibacterial testing of compounds **51**, **124**, **125**, and **134** against human pathogenic bacterial strains *E. coli*, *S. aureus*, *S. pneumoniae*, and *S epidermidis* revealed that compounds **51, 124**, and **125** demonstrated selective inhibitory capacities (MICs ranging from 2.0–16 μg/mL), whereas compound **51** had significant activity against *E. coli* (MIC: 2.0 μg/mL) that was comparable to chloramphenicol (MIC: 2.0 μg/mL) [41].

Among the pyrogallol ethers, i.e., compounds **144**, **145**, and **166**–**168** reported by Liu et al. in 2013, compounds **166** and **168** (IC_{50}: 14.0 and 24.0 μg/mL, respectively) demonstrated Mt PtpA (protein tyrosine phosphatase A) (*Mycobacterium tuberculosis* protein tyrosine phosphatase A)-inhibitory activity and compound **168** moderately inhibited *S. aureus* (MIC: 12.5 μg/mL) [37]. *M. tuberculosis* secretes PtpA into the infected macrophages' cytosol to avoid devastation by macrophage phagocytosis. Inhibition of PtpA remarkably attenuates *M. tuberculosis* growth in human macrophages; therefore, Mt PtpA is a target for developing anti-tuberculosis drugs [37].

Liu et al. stated that compounds **144**–**146**, **152**, and **153** were moderately effective versus fish pathogens *S. iniae* FP3187, and *V. ichthyoenteri* (Vi0917-1 and Vi099-7) and human pathogen *S. aureus* (SG 511 and SG 503) [36]. Compounds **147** and **149** were inactive, suggesting that methoxy groups increased the antibacterial potential; however, the carboxyl group reduced the activity of diphenyl ether derivatives [36]. Additionally, compounds **138**, **139**, **144**, **209**, and **210** possessed moderate antibacterial effectiveness (MICs: 6.3–25.0 μM) versus series of bacterial strains [28] and compound **84** was moderately active (MICs: 64, 128, 16, 32, and 32 μg/mL, respectively) versus MRSA, MDRPA (multi-drug-resistant *Pseudomonas aeruginosa*), *E. coli*, *S. aureus*, and *P. aeruginosa* in an agar diffusion assay [39].

Compounds **137**, **169**–**172**, **174**–**176**, **221**, and **222** reported from *A. sydowii* EN-534 and *Penicillium citrinum* EN-535 coculture were examined for antibacterial potential versus strains of human and aquatic bacteria. Compounds **137**, **169**, and **170** showed antibacterial capacity against bacteria *E. coli*, *E. ictaluri*, *M. luteus*, *V. parahaemolyticus*, and *V. alginolyticus* (MICs ranged from 4 to 64 μg/mL), while compounds **137**, **171**, **172**, and **174** were active against *V. alginolyticus* and *E. ictaluri* (MICs: 32–64 μg/mL). Additionally, compound **170** had marked activity against *M. luteus* (MIC: 4 μg/mL) compared to chloramphenicol (MIC: 2 μg/mL) [69].

3.4. Anti-Influenza Virus Activity

The influenza pandemic remains a threat to public health because of its elevated rates of mortality and morbidity. Although vaccination is the primary means for preventing this illness, antiviral medications are an essential adjunct to vaccines for influenza control and prevention [78,79]. In the last several decades, natural products have been subjected to intensive investigations as a possible alternative therapy for the recovery and treatment of influenza. Various reports have demonstrated that developing natural bioactive metabolites has remarkable advantages [78,79]. It is noteworthy that the renowned anti-

influenza oseltamivir was synthesized using natural shikimic and quinic acids as starting materials [78,79]. Some reports assessed the anti-influenza potential of *A. sydowii*-isolated metabolites; these are highlighted below (Table 11).

Table 11. Anti-influenza virus metabolites reported from *Aspergillus sydowii.*

Compound Name	Virus/Assay	Biological Results (IC_{50})		Ref.
		Compound	Positive Control	
7-Deoxy-7,14-didehydrosydonic acid (**8**)	Puerto Rico/8/34 (H1N1)/Pseudovirus neutralization and MTT	7.07 μM	Ribavirin 2.53 μM	[35]
cyclo-12-Hydroxysydonic acid (**22**)	Puerto Rico/8/34 (H1N1)/Pseudovirus neutralization and MTT	8.89 μM	Ribavirin 2.53 μM	[35]
	Aichi/2/68 (H3N2)/Pseudovirus neutralization and MTT	36.41 μM	Ribavirin 6.23 μM	[35]
	FM-1/1/47(H1N1)/Pseudovirus neutralization and MTT	24.46 μM	Ribavirin 3.97 μM	[35]
2-Hydroxy-1-(hydroxymethyl)-8-methoxy-3-methyl-9*H*-xanthen-9-one (**80**)	Puerto Rico/8/34 (H1N1)/Pseudovirus neutralization and MTT	4.70 μM	Ribavirin 2.53 μM	[35]
	FM-1/1/47 (H1N1)/Pseudovirus neutralization and MTT	4.04 μM	Ribavirin 3.97 μM	[35]
2-Hydroxy-1-(hydroxymethyl)-7,8-dimethoxy-3-methyl-9*H*-xanthen-9-one (**81**)	Puerto Rico/8/34 (H1N1)/Pseudovirus neutralization and MTT	2.17 μM	Ribavirin 2.53 μM	[35]
Emodic acid (**92**)	Puerto Rico/8/34 (H1N1)/Pseudovirus neutralization and MTT	2.00 μM	Ribavirin 2.53 μM	[35]
	Aichi/2/68 (H3N2)/Pseudovirus neutralization and MTT	17.53 μM	Ribavirin 6.23 μM	[35]
	FM-1/1/47(H1N1)/Pseudovirus neutralization and MTT	5.37 μM	Ribavirin 3.97 μM	[35]
Parietinic acid (**93**)	Puerto Rico/8/34 (H1N1)/Pseudovirus neutralization and MTT	7.88 μM	Ribavirin 2.53 μM	[35]
	Aichi/2/68 (H3N2)/Pseudovirus neutralization and MTT	30.09 μM	Ribavirin 6.23 μM	[35]
	FM-1/1/47(H1N1)/Pseudovirus neutralization and MTT	39.60 μM	Ribavirin 3.97 μM	[35]
Questin (**94**)	Puerto Rico/8/34 (H1N1)/Pseudovirus neutralization and MTT	1.92 μM	Ribavirin 2.53 μM	[35]
	Aichi/2/68 (H3N2)/Pseudovirus neutralization and MTT	9.62 μM	Ribavirin 6.23 μM	[35]
	FM-1/1/47(H1N1)/Pseudovirus neutralization and MTT	11.1 μM	Ribavirin 3.97 μM	[35]
1,6,8-Trihydroxy-3-methylanthraquinone (**95**)	Aichi/2/68 (H3N2)/Pseudovirus neutralization and MTT	9.72 μM	Ribavirin 6.23 μM	[35]
	FM-1/1/47(H1N1)/Pseudovirus neutralization and MTT	18.48 μM	Ribavirin 3.97 μM	[35]

Table 11. *Cont.*

Compound Name	Virus/Assay	Biological Results (IC_{50})		Ref.
		Compound	Positive Control	
Bisdethiobis(methylthio)-acetylaranotin (**116**)	Puerto Rico/8/34 (H1N1)/Pseudovirus neutralization and MTT	34.60 μM	Ribavirin 2.53 μM	[35]
	Aichi/2/68 (H3N2)/Pseudovirus neutralization and MTT	24.56 μM	Ribavirin 6.23 μM	[35]
	FM-1/1/47(H1N1)/Pseudovirus neutralization and MTT	44.08 μM	Ribavirin 3.97 μM	[35]
Citrinin (**169**)	H_5N_1/Influenza neuraminidase inhibition screen kit	45.6 nM	Oseltamivir 3.6 nM	[69]
Penicitrinol A (**170**)	H_5N_1/Influenza neuraminidase inhibition screen kit	21.2 nM	Oseltamivir 3.6 nM	[69]
seco-Penicitrinol A (**171**)	H_5N_1/Influenza neuraminidase inhibition screen kit	24.7 nM	Oseltamivir 3.6 nM	[69]
Penicitrinol L (**172**)	H_5N_1/Influenza neuraminidase inhibition screen kit	41.5 nM	Oseltamivir 3.6 nM	[69]
Penicitrinone A (**173**)	H_5N_1/Influenza neuraminidase inhibition screen kit	12.9 nM	Oseltamivir 3.6 nM	[69]
Penicitrinone F (**174**)	H_5N_1/Influenza neuraminidase inhibition screen kit	18.5 nM	Oseltamivir 3.6 nM	[69]
Sydocyclopropane A (**203**)	WSN/33 (H1N1)/Cytopathic effect reduction/A/WSN/33 (H1N1)	26.7 μM	Oseltamivir 18.1 μM	[42]
Sydocyclopropane B (**204**)	Cytopathic effect reduction/A/WSN/33 (H1N1)	29.5 μM	Oseltamivir 18.1 μM	[42]
Hamavellone B (**207**)	Cytopathic effect reduction/A/WSN/33 (H1N1)	35.8 μM	Oseltamivir 18.1 μM	[42]
3,7-Dihydroxy-1,9-dimethyldibenzofuran (**234**)	Puerto Rico/8/34 (H1N1)/Pseudovirus neutralization and MTT	1.31 μM	Ribavirin 2.53 μM	[35]
	Aichi/2/68 (H3N2)/Pseudovirus neutralization and MTT	1.24 μM	Ribavirin 6.23 μM	[35]
	FM-1/1/47(H1N1)/Pseudovirus neutralization and MTT	2.84 μM	Ribavirin 3.97 μM	[35]

Interestingly, compounds **80** and **81** possessed notable selective inhibition versus two influenza A virus subtypes, including A/Puerto Rico/8/34 (H1N1) and A/FM-1/1/47 (H1N1) (IC_{50}s: 2.17–4.70 μM), compared to ribavirin (IC_{50}s: 2.53 to 6.23 μM). Additionally, compounds **92** and **94** had potent efficacy on A/Puerto Rico/8/34 (H1N1) (IC_{50}s: 1.92 and 2.0 μM, respectively). Furthermore, compound **234** demonstrated broad inhibitory potential against A/Puerto Rico/8/34 (H1N1), A/Aichi/2/68 (H3N2), and A/FM-1/1/47 (H1N1) (IC_{50}s: 1.31, 1.24, and 2.84 μM, respectively) compared to ribavirin (IC_{50}s: 2.53, 6.23, and 3.97 μM, respectively) [35]. Compounds **50**, **146,** and **152** demonstrated weak anti-H3N2 potential (IC_{50}s: 57.4, 66.5, and 78.5 μM, respectively) in a CPE (cytopathic effect) inhibition assay compared to Tamiflu (IC_{50}: 0.95 μM) [45]. Further, Yang et al. stated that compounds **137**, **169**–**172**, and **174** demonstrated anti-influenza NA (neuraminidase) activity, with compounds **137** and **174** displaying better efficacy (IC_{50}s: 12.9 nM and 18.5 nM, respectively) compared to oseltamivir (IC_{50}: 3.6 nM) [69]. Additionally, compounds **203**–**207** demonstrated antiviral potential versus the A/WSN/33 virus (H1N1) (IC_{50}s ranged from 26.7 to 77.2 μM), compared to oseltamivir (IC_{50}: 18.1 μM); compounds **203**, **204**, and **207** were the most active (IC_{50}s: 26.7, 29.5, and 35.8 μM, respectively). It was found that the C-1 methyl 2-hydroxy-4-oxobutanoate side chain significantly enhanced the antiviral activity (e.g., compound **203** vs. compound **205**) and C-3 configuration had less influence on activity (e.g., compound **205** vs. compound **206**) [42].

3.5. Anti-Diabetic and Anti-Obesity Activities

A close relation among between diabetes and obesity has been proven [80]. Insulin-triggered cellular glucose uptake is a crucial step in glucose regulation and any defect in this mechanism results in insulin resistance [81]. Enhancement of insulin sensitivity is one of the significant hallmarks of anti-diabetic agents. Lipid accumulation in diabetic patients can result in serious effects such as diabetic cardiomyopathy [82]. Hence, efficient anti-diabetics should decrease adipocytes' lipid accumulation and facilitate lipid metabolism and burning [54].

In an anti-diabetic assay, compounds **1**, **5**, **42, 45**, **46**, **47**, **49**, **69**, **71**, and **88** were found to increase differentiated 3T3-L1 (fibroblast embryo mouse cell line) adipocytes' medium glucose consumption. Among them, compound **45** significantly reduced culture medium glucose concentration (324.6 mg/dL) by 24% compared to control (glucose: 427.4 mg/dL). It was noted that the presence of a methylene alcohol and a hydroxy group on C-3 and C-7, respectively, in bisabolane sesquiterpenes is substantial in promoting 3T3-L1 adipocytes' glucose uptake [54]. Additionally, their efficacy on differentiated 3T3-L1 adipocytes' lipid accumulation utilizing oil-red O stain revealed that compound **45** notably prohibited lipid accumulation up to 48% in a 3T3-L1 adipocyte culture medium, indicating the compound **45** promoted glucose consumption and suppressed lipid accumulation in adipocytes [54].

3.6. Protein Tyrosine Phosphatase Inhibition

Protein tyrosine phosphatases (PTPs) are proven to be substantial new targets for new anti-diabetes [58]. For example, PTP1B (protein tyrosine phosphatase 1B) negatively regulates insulin action in the insulin receptor signaling pathway, SHP1 (SH2-containing protein tyrosine phosphatase 1) negatively controls signaling pathways, which streamlines glucose homeostasis through modulating insulin signaling in muscles and the liver, and CD45 (leukocyte common antigen) is a receptor for some ligands and regulates SHP-1 recruitment [58]. Also, PTP1B has a substantial role in cancer development, inflammation processes, and insulin signaling cascade. Therefore, PTP1B inhibitors are considered drug candidates for treating cancer, diabetes, inflammation processes, and sleeping sickness [46].

Asperentin B (**178**) had potent PTP1B inhibition capacity (IC_{50}: 2.05 μM) compared to suramin (IC_{50}: 11.85 μM). It was sixfold more potent than suramin, suggesting its possible application in anti-diabetes and anti-sleeping sickness therapeutic agents [46]. Furthermore, compounds **1**, **3**, and **18** displayed significant PTP1B-inhibitory potential (IC_{50}s: 7.97, 15.88, and 14.18 μM, respectively), while compounds **1**, **2**, **18**, and **240** had potent activity towards SHP1 (IC_{50}s: 8.35, 15.72, 11.68, and 14.61 μM, respectively). The PTP1B data indicated that the side chains influenced activities [58].

3.7. Anti-Inflammation Activity

Compounds **42**, **45**, and **88** markedly inhibited fMLP (tripeptide N-formyl-L-methionyl-L-leucyl-L-phenylalanine)/CB (cytochalasin B)-caused superoxide anion generation (IC_{50}s: 5.23, 6.11, and 6.00 μM, respectively) and elastase release (IC_{50}s: 16.39, 8.80, and 6.60 μM, respectively) by neutrophils [54]. It is noteworthy that compounds **1**, **5**, **46**, and **49** had selective inhibition versus fMLP/CB-caused superoxide anion generation [54]. These results demonstrated the importance of C-7 OH (compound **45** vs. compound **46**) and C-3 methylene alcohol (compounds **46**, **45**, and **49** vs. compounds **1** and **5**) on activity (Table 12). On the other hand, compound **71** also revealed a significant superoxide anion generation inhibition capacity (IC_{50}: 21.20 μM) compared to compound **69** [54]. The isolated metabolites, compounds **1**–**3**, **26**–**42**, **45**, **47**, **50**, **56**–**58**, and **214**, showed a dose-dependent inhibition of LPS-induced NO (nitric oxide) secretion (conc.: 10 and 5 μM) in BV-2 microglia cells using a CCK-8 (cell counting kit-8) assay. Compounds **33**, **39**, **42**, **47**, **50**, and **57** revealed an inhibition rate >45% (conc.: 10 μM). The structure–activity relation indicated that the $\Delta^{7,8}$ double bond in sydowic acid derivatives enhanced NO secretion inhibition (e.g., compound **33** vs. compound **26**). Compound **39**, with a 56.8% inhibition rate, was found to exert its

anti-inflammation activity by prohibiting the NF-κB (nuclear factor kappa B)-activated pathway [57].

Table 12. Anti-inflammatory metabolites reported from *Aspergillus sydowii.*

Compound Name	Assay	Biological Results		Ref.
		Compound	Positive Control	
(S)-(+)-Sydonic acid (**1**)	Inhibition of superoxide anion	17.82 μM (IC_{50})	Sorafenib 1.27 μM (IC_{50})	[54]
(7*S*,11*S*)-(+)-12-Hydroxysydonic acid (**5**)	Inhibition of superoxide anion	31.95 μM (IC_{50})	Sorafenib 1.27 μM (IC_{50})	[54]
Aspergillusene A (**42**)	Inhibition of superoxide anion	6.11 μM (IC_{50})	Sorafenib 1.27 μM (IC_{50})	[54]
	Inhibition of elastase release	8.80 μM (IC_{50})	Sorafenib 1.27 μM (IC_{50})	[54]
(+)-(7*S*)-Sydonol (**45**)	Inhibition of superoxide anion	5.23 μM (IC_{50})	Sorafenib 1.27 μM (IC_{50})	[54]
	Inhibition of elastase release	16.39 μM (IC_{50})	Sorafenib 1.27 μM (IC_{50})	[54]
(7*S*)-(+)-7-O-Methylsydonol (**46**)	Inhibition of superoxide anion	13.80 μM (IC_{50})	Sorafenib 1.27 μM (IC_{50})	[54]
Anhydrowaraterpol B (**49**)	Inhibition of superoxide anion	21.52 μM (IC_{50})	Sorafenib 1.27 μM (IC_{50})	[54]
Sydowinin B (**71**)	Inhibition of superoxide anion	21.20 μM (IC_{50})	Sorafenib 1.27 μM (IC_{50})	[54]
	Inhibition of elastase release	12.62 μM (IC_{50})	Sorafenib 1.27 μM (IC_{50})	[54]
(7*R*,8*R*)-AGI-B4 (**88**)	Inhibition of superoxide anion	6.00 μM (IC_{50})	Sorafenib 1.27 μM (IC_{50})	[54]
	Inhibition of elastase release	6.60 μM (IC_{50})	Sorafenib 1.27 μM (IC_{50})	[54]

It was found that compounds **145** and **153** mildly suppressed NO production induced by LPS-NO in RAW 264.7 cells (IC_{50}: 73 μM) compared to dexamethasone (IC_{50}: 18 μM) [36]. Additionally, compounds **59**, **60**, **146**, **152**, **191**, **201**, **213**, **228**–**230**, and **234** demonstrated an inhibitory capacity of NO production induced by LPS in BV-2 microglia cells without toxicity according to a CCK-8 assay. Interestingly, compound **234** (10 μM) was the most potent (inhibition rate: 94.4%) among these tested compounds (inhibition rate: 10.2–35.4%) [60].

Compounds **98**, **189**, **199**, and **200** possessed inhibitory effectiveness on LPS-boosted NO production in RAW264.7 cells (IC_{50}s: 25.25–43.08 μM), compared to dexamethasone (IC_{50}: 35.17 uM) [64]. Recently, Chen et al. reported that compounds **215** and **236** exhibited weak inhibition of LPS-induced NO production (20.1, 21.5, and 18.1%, respectively), compared to dexamethasone (% inhibition: 99.9%) in RAW 264.7 cells using a Griess reaction assay [26].

3.8. Anti-Nematode Activity

Globally, parasitic nematodes cause diseases of major socio-economic significance to humans and animals. They have a long-term impact on human health, especially in children [83]. Indeed, nematodes' resistances to available anti-nematode agents are widespread all over the world [84]. Thus, there is an insistent demand to discover new agents for the effective and sustained control of nematodes.

Sun et al. evaluated the anti-nematode activity of compounds **1**–**3**, **18**–**21**, **202, 235**, and **240**. It is noteworthy that only compound **3** showed anti-nematode potential (IC_{50}: 50 μM) [58]. A study by Yang et al. revealed that compounds **1**, **11**, and **14** possessed nematicidal potential versus second-stage juvenile *Meloidogyne incognita* (J2s); compound **1** had the strongest activity (% mortality: 80% at 60 and LC_{50}: 192.40 μg/mL). Furthermore, compounds **1, 11**, and **14** paralyzed the nematode and then impaired its pathogenicity [47].

4. Industrial and Biotechnological Applications

The discovery and development of effective enzymes for the use of renewable resources as raw materials is a requirement for the transition to a biobased economy. Many enzymes are crucial in efficiently hydrolyzing raw materials by enzymatic means. Exploring the potential of untapped natural habitats is a potent method for overcoming the limited enzymatic toolkit.

A. sydowii was found to be a rich source of enzymes with marked industrial and biotechnological potential, including α-amylases, lipases, xylanases, cellulases, keratinase, and tannases, which are discussed here.

4.1. α-Amylase, Tannases, and Lipase Enzymes

Amylases (AAs) are utilized in multiple manufacturing processes, including fermentation, textile, detergent, paper, and pharmaceutical sectors [85]. Given the low cost and wide availability of the starch feedstock used to make food, bioethanol, textile, paper, detergent, and chemicals, there is a significant demand for α-amylase [86]. However, because of advancements in biotechnology, the use of AAs has increased in a variety of sectors such as those of clinical, pharmaceutical, and analytical chemistry, as well as in the food, textile, and brewing industries [85]. The huge industrial demand for AAs to support economically competitive manufacturing processes is still being severely hampered by the cost and effectiveness of AA cocktails [19]. In this regard, it is imperative to generate effective and affordable AAs by using inexpensive sources such as agricultural wastes.

Adegoke and Odibo produced AAs from *A. sydowii* IMI-502692 utilizing the solid-state fermentation of buffered cassava root fiber. It was found that this activity was enhanced by Ca^{2+}, Cu^{2+}, and Zn^{2+}; however, it was prohibited by Fe^{2+}, Sr^{2+}, Ni^{2+}, and Mn^{2+} [19].

A study by Elwan et al. reported that *A. sydowii* had a potential for lipase production (lipase yield of 90 μ/mL) in optimum culture conditions, specifically 5.4 pH; 2.0% sucrose, 0.2% corn oil, 0.23% $(NH_4)_2SO_4$, 0.1% KH_2PO_4, 0.05% $MgSO_4 \cdot 7H_2O$, 0.05%KCl, and using 0.1 M phosphate–citrate buffer and incubating at 30°C for 20 h [22].

Tannase, an extracellular enzyme belonging to the hydrolase family, is derived from various species of the *Aspergillus* genus [8,87]. It catalyzes the breakdown of depsides and tannins. Tannase lessens tannins' unwanted effects (astringent and bitter taste), enhancing the flavor qualities of products such as animal feeds and foodstuffs. It is used in various applications, including polyphenolic compound structural elucidation, bioremediating tannin-contaminated wastewaters, gallic acid production, and coffee-flavored soft drink, fruit juice, and instant tea production [20].

In 2020, Albuquerque et al. purified and characterized tannase-acyl hydrolase from *A. sydowii* SIS-25 derived from Caatinga soil (Serra Talhada, Pernambuco, Brazil) utilizing a polyethylene glycol-citrate aqueous two-phase system. This enzyme removed phenolic components and enhanced the sensory qualities of green tea and produced gallic acid [20].

4.2. Bioremediation and Biodegradation

Sustainable development goals (SDGs) target various concerns in our planet such as food security, health, environmental sustainability, bioremediation, climate change, alternative eco-friendly fuel, improving water quality, sustainable food production, and discovering new drugs [88]. Treatment and measurement of various contaminants in water, soil, and air are complicated issues and are linked to the nature of contaminants and their environmental interactions. Reusing wastewater offers a substitute supply for the irrigation of agricultural land that has been used for decades in many nations. Recycling wastewater adheres to circular economy principles by reducing waste and encouraging ongoing resource reuse [89] which potentially assists various national initiatives in promoting sustainable agriculture methods. Creating agricultural systems with minimal required inputs and zero waste contributes to SDG 2 (End hunger) (via sustainable food production), SDG 12 (Responsible consumption and production), SDG 13 (Climate action), and SDG 15 (Sustainable use of terrestrial ecosystems) [90]. Various researches have focused on

biologically based methods, relying on natural processes to remove contaminants such as the utilization of microorganisms (bioremediation) such as fungi to remarkably contribute to achieving the SDGs [88].

4.2.1. Polycyclic Aromatic Hydrocarbons

PAHs (polycyclic aromatic hydrocarbons) are a heterogeneous class of hydrocarbons having two or more fused aromatic rings. In nature, they are formed as a result of organic matter's incomplete decomposition and human activities such as petroleum spilling, waste incineration, home heaters, and the burning of carbon, oil, gas, or wood [91]. Additionally, PhCs (pharmaceutical compounds), a second class of contaminants, have become more significant in recent years as a result of their durability and abundance in surface water bodies and the ineffectiveness of treatment facilities eliminating them [92]. According to Olicón-Hernández et al., these contaminants are hazardous to aquatic life and contribute to microbial resistance's emergence [93]. Numerous studies have focused on the microbial biodegradation of these contaminants, particularly by fungi [93,94], because these pollutants are known for their high toxicity and persistence [94]. It is noteworthy that halophilic fungi are useful in xenobiotic mycoremediation under high-salinity conditions [94].

González-Abradelo et al. studied the potential of *A. sydowii* EXF-12860 toward the bioremediation of saline wastewaters, containing toxic and persistent PAHs and PhCs. It was stated that *A. sydowii* may be helpful in lowering the amounts of harmful PAHs and PhCs under high-salinity conditions (>1 M NaCl) during the biotechnological downstream processing of diverse industrial wastewater. It removed 100% of fifteen complex PAHs at 500 ppm in biorefinery wastewater at high salt concentrations. Additionally, it has ecotoxic activity as it demonstrated the same capability to eliminate PhCs. This supported its capabilities for xenobiotic biodegradation in low-water activity [94]. A novel piezo-tolerant and hydrocarbon-oclastic deep-sea sediment-derived *A. sydowii* BOBA1 demonstrated a marked degradation potential for PAHs in spent engine oil hydrocarbon fractions (71.2 and 82.5% of spent engine oil, respectively) under high-pressure (0.1 and 10 MPa, respectively) culture conditions with a 21-day retention period. This provided insights into the bioremediation of hydrocarbon-contaminated deep-sea environments [95].

Additionally, Birolli et al. stated that *A. sydowii* CBMAI-935 isolated from a non-contaminated site on the coast of São Sebastião (Brazil) biodegraded anthracene [96]. To biodegrade dieldrin, one of the most widely employed organo-chlorine pesticides, banned due to its long persistence and high toxicity to the environment, Birolli et al. found that *A. sydowii* CBMAI-935 and *A. sydowii* CBMAI-933 were capable of growing in the presence of dieldrin, suggesting its high tolerance. It is noteworthy that no biodegradation byproducts were found in the GCMS, revealing that dieldrin could be converted into polar molecules or mineralized, prohibiting the emergence of harmful or durable derivatives [97].

4.2.2. Heavy Metals and Insecticides

Cadmium (Cd) is often used in the electroplating and metallurgical industries and is found in several pesticides, fertilizers, and fungicides [98]. Upon its absorption by both animals and humans, it accumulates in the kidneys and liver, severely harming the renal tubules and resulting in a variety of symptoms such as proteinuria and hyperglycemia [99]. Trichlorfon (TCF) is a broad-spectrum organic phosphorus pesticide that is utilized for controlling pests on a variety of crops [100]. It is an inhibitor of cholinesterase that causes delayed neuropathy in both animals' and humans' nervous systems [98].

Zhang et al. reported that by inoculating *A. sydowii* into Cd-TCF co-contaminated soil, TCF breakdown was accelerated, and soil enzyme activity was raised. When *Brassica juncea* (Indian mustard) was planted along with *A. sydowii* inoculation, maximum TCF degradation and Cd removal efficacy were noted. *Brassica juncea* is among those hyperaccumulator plant species that are frequently employed for heavy metal phytoextraction from contaminated soil. Thus, using *B. juncea* and *A. sydowii* together is a promising strategy to bioremediate soil that has been contaminated with both TCF and Cd [98]. Tian et al. isolated PAF-2,

a new strain of *A. sydowii* from pesticide-contaminated soils, that had potential for the biodegradation of TCF and its degradation [100].

Esfenvalerate (S,S-fenvalerate), is a pyrethroid insecticide that deposits in marine sediments and is extremely harmful to aquatic creatures. Birolli et al. examined its biodegradation by marine-associated *A. sydowii* CBMAI-935. This strain metabolized esfenvalerate into 3-phenoxybenzoic acid, 2-(4-chlorophenyl)-3-methylbutyric acid, and its dihydroxylated derivatives [101].

Alvarenga et al. assessed the biodegradation of a commercial formulation of chlorpyrifos (Lorsban 480 BR), which is one of the most widely utilized organophosphate pesticides, by marine-derived *A. sydowii* CBMAI-935 associated with *C. erecta*. The fungus degraded ≈ 63% of the chlorpyrifos and decreased the concentration of its hydrolysis product 3,5,6-trichloropyridin-2-ol after 30 days [102]. In 2021, Soares et al. reported that this fungus also metabolized chlorpyrifos and profenofos to 3,5,6-trichloro-1-methylpyridin-2(1H)-one/2,3,5-trichloro-6-methoxypyridine/tetraethyl dithiodiphosphate/3,5,6-trichloropyridin-2-ol and 4-bromo-2-chlorophenol/4-bromo-2-chloro-1-methoxybenzene/O,O-diethyl S-propylphosphorothioate, respectively [103].

Methyl parathion is an efficient organophosphate acaricide and insecticide that is widely utilized for pest control on a wide variety of crops, but it is extremely toxic. Alvarenga et al. reported the ability of *A. sydowii* CBMAI-935 to biodegrade this pesticide completely after 20 days. This fungus metabolized this pesticide to its more toxic isomerization and oxidation products isoparathion and methyl paraoxon, which were subsequently metabolized to the less toxic product 1-methoxy-4-nitrobenzene/p-nitrophenol/O,O,O-trimethyl phosphorothioate/O,O,S-trimethyl phosphorothioate/trimethyl phosphate, suggesting *A. sydowii* CBMAI-935's efficiency in the bioremediation of this pesticide and its toxic forms [103,104].

4.2.3. Lignocellulosic Biomasses

Due to the acute energy crisis and increased demand for fossil fuels, lignocellulose is widely considered a potential cost-effective, renewable resource for bioethanol production [105,106]. Lignocellulose consists of cellulose, hemicellulose, and lignin. Lignin, which together with hemicellulose and cellulose makes up the majority of a plant's skeleton, is the second-most abundant organic renewable resource on Earth after cellulose [105,106]. The ligninolytic enzymes Lac (laccase), LiP (lignin peroxidase), VP (versatile peroxidase), and Mnp (manganese peroxidase) play a major role in the breakdown of lignin [105,106] and are found among the extracellular enzymes in filamentous fungi. These enzymes play a significant role in bioremediation, as they neutralize or degrade contaminants in the environment [6]. They also have a wide range of uses in the paper, textile, cosmetic, food, chemical, agricultural, and energy industries.

A thermostable, low-molecular-weight xylanase belonging to the glycosyl hydrolase 11 family was purified from *A. sydowii* MG49 by Ghosh et al. and demonstrated specific efficacy only in the presence of xylan and had no activity in the presence of cellulose or carboxymethyl cellulose [23].

A. sydowii MS-19 isolated from the Antarctic region produced low-temperature lignin-degrading enzymes LiP and Mnp. These results suggested that *A. sydowii* MS-19 could be used as a source of lignocellulosic enzymes [107].

Xylan is the prime constituent of hemicellulose. Its backbone consists of a linear chain of 1,4-linked β-D-xylopyranosyl units, which are substituted with α-L-arabinofuranosyl, 4-O-methyl-α-D-glucuronopyranosyl, or acetyl units. It is degraded by β-D-xylosidases, endo-1,4-β-xylanases, α-glucuronidases, α-l-arabinofuranosidases, acetyl xylan esterases, and ferulic acid esterases [108].

Brandt et al. stated that *A. sydowii* Fsh102 isolated from shrimp shells showed notable xylanase-producing capacity [109]. Two xylanases I and II belonging to GH-11 (glycoside hydrolases) and GH-10 families, respectively, were characterized and expressed in *E. coli*. These enzymes can function in a wide pH range and are tolerant of mesophilic

temperatures. Both xylanases can be characterized as being extremely interesting for the enzymatic breakdown of xylan-containing biomasses in industrial bioprocesses based on their activity and stability [109]. In another study on *A. sydowii* SBS-45 culture filtrate, two xylanases (I and II) were purified. They showed optimum activity at 50 °C and 10.0 pH. This activity was boosted by certain metal ions and L-tryptophan [110].

Cellulose breakdown is carried out by cellulases, including β-glucosidase, endoglucanase, and cellobiohydrolase [108,111,112]. Cellulase has wide applications in various fields like oil extraction, agricultural industries, food processing, waste management, carotenoid extraction, animal feed, brewery, textile, bio-stoning, color clarification, paper, laundry, pulp, detergent industry, and deinking [108,111,112].

A. sydowii isolated from Indore, India, had the potential to produce cellulases under submerged fermentation. It was found that β-glucosidase, exoglucanase, and endoglucanase were produced at a ratio of 64:27:9, whereas lactose was the best carbon source for inducing cellulase production [113].

4.2.4. Keratinous Wastes

Keratins are components of hooves, wool, horns, nails, hair, and feathers [8,114]. They are insoluble proteins with highly stable polypeptide chains, containing many disulfide bonds [115,116]. According to estimates, the United States, China, and Brazil produce 40 million tons of keratinous waste each year [117]. Also, keratinous waste is produced in millions of tons annually in meat industry slaughterhouses worldwide [115,116]. Normal enzymes such as papain and pepsin that break down proteins cannot break them down. Keratinous waste management utilizing a low-cost solution is needed particularly in underdeveloped nations. These wastes can be broken down by microbial keratinases which are extracellular enzymes secreted by various bacterial and fungal genera [8,114]. They are widely used in different pharmaceutical industries, in treating keratinized skin, calluses, acne, and psoriasis, and in cosmetic products manufacture (e.g., nutritional lotions, anti-dandruff shampoos, and creams) [21,115,116]. Also, they are usually employed in nitrogen fertilizers, feed formulas, and the leather industry, as well as in treating keratin waste-contaminated wastewater [21].

Alwakeel et al. studied the capability of keratinase produced by *A. sydowii* AUMC-10935 isolated from male scalp hair to degrade keratinous materials from chicken feathers. The enzyme had optimal activity (120 IU/mg) at 50 °C and pH 8.0, which was notably prohibited by EDTA and certain metal ions [21].

4.3. Biocatalysis

The pharmaceutical sector is continually looking for new approaches to new therapeutic agent syntheses, which has increased the demand for biocatalytic techniques [118]. Whole microorganism cells are effectively used as catalysts in the stereoselective biotransformation of a variety of chemical molecules. Also, many chemical reactions such as carbonyl ketone reduction, sulfide oxidation, secondary alcohol deracemization, and Baeyer–Villiger reactions were all catalyzed by enzymes from various microorganisms [6]. The whole cell of *A. sydowii* was investigated as a biocatalyst for various chemical reactions. This was highlighted in the current work.

Whole cells of the marine sponge-derived *A. sydowii* Gc12 obtained from the South Atlantic Ocean catalyzed the hydrolysis of (R,S)-benzyl glycidyl ether to produce (R)-benzyl glycidyl ether. Derivatives of glycidyl ether are potentially beneficial intermediates in the manufacture of β-adrenergic blockers. *A. sydowii* Gc12 hydrolases showed regioselectivity in opening the epoxide ring of racemic oxirane [119].

Sponge-associated *A. sydowii* CBMAI-934 derived from *Chelonaplysilla erecta* produced oxidoreductase that catalyzed regioselective mono-hydroxylation of (−)-ambrox® to 1β-hydroxy-ambrox. (−)-Ambrox®, a naturally occurring terpene, was separated from ambergris, a pathological substance formed in the blue whale's intestine. This compound is of great commercial value in the perfume industry as a fixative or fragrant agent [120]. de

Paula and Porto investigated progesterone biotransformation by *A. sydowii* CBMAI-935 associated with marine sponge *Geodia corticostylifera*. In a good yield, this fungus was able to oxidize progesterone at the C17-site, resulting in the two major products testololactone and testosterone. Additionally, this Baeyer–Villiger reaction-based bio-oxidation revealed the existence of crucial enzymes in this fungus that can aid in related steroid biotransformation [121]. *A. sydowii* CBMAI-935 only produced 2′,4-dihydroxy-dihydrochalcone with a yield of 26% from 2′,4-dihydroxy-dihydrochalcone [122].

Further research was conducted by de Oliveira et al. to assess the potential of *A. sydowii* CBMAI-934 isolated from the marine sponge *Chelonaplysilla erecta* in converting a number of methylphenylacetonitriles into corresponding acids at a high yield. It was found that aryl aliphatic nitrilases were induced by phenyl acetonitrile. Thus, *A. sydowii* CBMAI-934 might serve as a biocatalyst for the production of carboxylic acids from nitriles [123]. Zhou et al. reported that *A. sydowii* PT-2 isolated from Pu-erh tea degraded theobromine to 3-methylxanthine in a liquid culture through N-7 demethylation [124]. Also, Jimenez et al. reported that *A. sydowii* CBMAI 935 associated with *C. erecta* sponge collected from Sao Sebastiao, São Paulo, Brazil, enantioselectively reduced ene of E-2-cyano-3-(furan-2-yl)acrylamide to (R)-2-cyano-3-(furan-2-yl)propanamide with a high yield [125]. In 2018, Morais et al. studied the reduction of α-chloroacetophenones to (S)-alcohols using whole cells of marine-derived *A. sydowii* CBMAI 935 [126]. α-bromoacetophenones' biotransformation by the marine-derived *A. sydowii* Ce19 was studied by Rocha et al. in 2010 [127]. This fungus accelerated α-bromoacetophenones' bioconversion into (R)-2-bromo-1-phenylethanol (56%), in addition to acetophenone (4%), 1-phenylethan-1,2-diol (26%), phenylethanol (5%) and α-chlorohydrin (9%). The substituted p-nitro- and p-bromoacetophenone's biotransformation produced a low-concentration complex combination of breakdown products [127]. In 2017, Alvarenga and Porto tested the biocatalytic ability of *A. sydowii* CBMAI-935 of marine origin to convert 2-azido-1-phenylethanone and some derivatives to related alcohols for use in the synthesis of enantiomerically bioactive β-hydroxy-1,2,3-triazoles. *A. sydowii* CBMAI 935 displayed extremely high stereoselectivity and conversion values for the bio-reduction of 2-azido-1-phenylethanones to (S)-2-azido-1-phenylethanols [128]. Further, the marine-derived *A. sydowii* Ce15 converted 1-(4-methoxyphenyl)ethenone to (R)-1-(4-methoxyphenyl)ethanol [129].

5. Nanoparticle Synthesis

Nanoparticles (NP) have attracted great interest recently because of their apparent applications in different fields such as biosensors, biomedicine, cosmetics, drugs, photocatalysis, animal dietary supplements, biolabeling, etc. [130]. Conventional NP synthesis approaches are not environment-friendly and are cost-intensive. Therefore, the development of biocompatible, environment-friendly, and non-toxic protocols in nanostructure biosynthesis is a wealthy area for scientific research, wherein the use of microbes could be an auspicious alternative [131,132]. Fungi are more effective organisms for these purposes than other microbes because of their special features, including their greater growth capacity, greater potential to produce a variety of enzymes, richness in mycelial branching, ability to accumulate different metals, and capacity to grow in harsh environments [133].

A. sydowii derived from Bhavnagar coast water (Gulf of Khambhat, India) had a remarkable intra/extracellular capacity to biosynthesize gold nanoparticles with variable sizes depending on gold ion concentration [52]. Additionally, silver NPs were biosynthesized by Wang et al. using soil-derived *A. sydowii* culture supernatants. These NPs revealed an in vitro antiproliferative capacity against MCF-7 (human breast adenocarcinoma cell line) and HeLa cells and efficient antifungal potential versus various clinical pathogenic fungi [134].

Zhang et al. prepared magnetic chitosan microsphere-immobilized *A. sydowii* by utilizing the cross-linking of γ-Fe_2O_3 magnetic chitosan nanocomposites with *A. sydowii* through the instant gelation method. This microsphere demonstrated marked Cu adsorp-

tion capacity (19.21 mg/g) and good regeneration properties after four cycles, suggesting its potential application as a biosorbent for treating heavy metal-contaminated water [51].

The AgNPs synthesized by Nayak and Anitha from dune-associated *A. sydowii* had significant antimicrobial potential versus selected bacterial stains; its combination with vancomycin and ampicillin showed enhanced activity (by sevenfold against *Shigella* sp. and by sixfold against *B. cereus* and *S. aureus* [50]).

Organic waste and heavy metal removal from wastewater have always been a major concern for the environment. In order to simultaneously remove trichlorfon and cadmium from an aqueous solution, Zhang et al., in 2020, created magnetic chitosan beads-immobilized *A. sydowii* [49]. The beads demonstrated considerable trichlorfon and cadmium removal capabilities, as well as outstanding four-cycle recyclability. As a result, the beads are appropriate and efficient for removing cadmium and trichlorfon simultaneously from wastewater [49].

6. Conclusions

Fungi have been subjected to much research due to their significance as wealth generators for various enzymes and bio-metabolites, as well as being intriguing for applications in agricultural, industrial, and pharmaceuticals fields.

A. sydowii is a globally distributed fungus that was found to have the capacity to biosynthesize diverse classes of metabolites. In the current work, 246 metabolites were separated from *A. sydowii* in the period from 1975 to 2023 (Figure 16). Most of these metabolites were reported from 2017 to 2022.

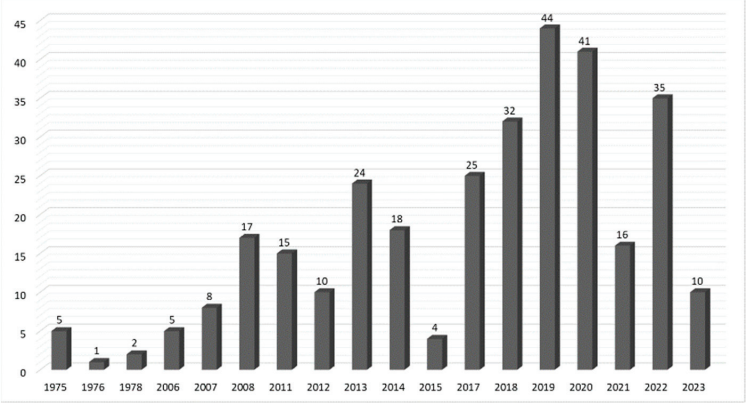

Figure 16. Number of metabolites reported from *A. sydowii* per year.

These metabolites include sesquiterpenoids, alkaloids, xanthones, monoterpenes, anthraquinones, sterols, triterpenes, phenyl ethers, pyrones, cyclopentenones, anthocyanins, coumarins, chromanes, acids, phenols, and other metabolites. Sesquiterpenoids (58 compounds, 24%), phenyl ethers (25 compounds, 10%), alkaloids (44 compounds, 18%), and xanthones (22 compounds, 9%) are the major constituents reported from this fungus (Figure 17).

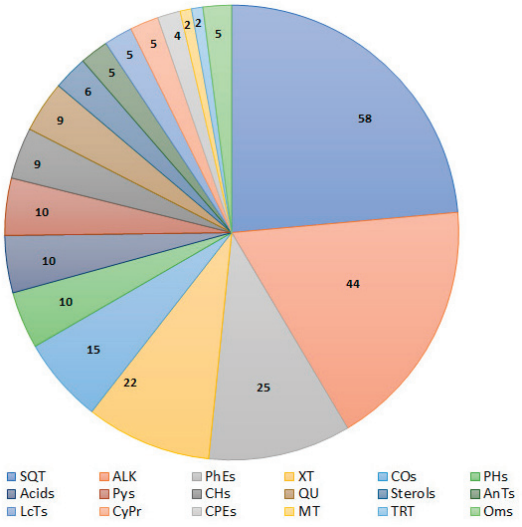

Figure 17. Different classes of metabolites reported from *A. sydowii*. AnTs: anthocyanins; SQT: sesquiterpenes; MT: monoterpenes; OMs: other metabolites; PHs: phenols; TRT: triterpens; ST: sterols: XT: xanthones; QU: quinones; ALK: alkaloids; PhEs: phenyl ethers; CHs: chromanes; COs: coumarins; Pys: pyranes; CPEs cyclopentenes; CyPr: cyclopropane, and lactone derivatives.

This fungus was collected from different sources such as cultures, plants, marine environments (water, sea mud, sediment, gorgonian sea fans, algae, sponge, and driftwood), and liverworts. Most of the reported studies were carried out on *A. sydowii* isolated from marine sources. It is remarkable that this fungus has many enzymatic systems, which may help to explain why its metabolites are so diverse. Future studies will be useful in understanding the enzymes and genes responsible for the manufacture of these metabolites.

It was found that the coculture of this fungus with other microbes, as well as the modification of the culture media, significantly promoted the production of structurally varied metabolites, suggesting avenues of further research using these approaches for activating *A. sydowii*'s silent biosynthetic genes toward the accumulation of various substantial compounds.

These metabolites were assessed for different bioactivities, including cytotoxic, antimicrobial, antioxidant, antiviral, anti-obesity, anti-inflammation, immunosuppression, anti-diabetic, protein tyrosine phosphatase 1B (PTP1B) inhibition, and anti-nematode activities (Figure 18).

Compounds **195** and **196** displayed potent antioxidant activity. Compounds **67**, **187**, **192**, and **239** demonstrated powerful cytotoxic potential. Compounds **2**, **3**, and **110** had notable antibacterial efficacy. Compounds **80**, **81**, **92**, **94**, and **234** displayed potent anti-influenza virus activity. Furthermore, compound **45** was found to possess anti-diabetic and anti-obesity capacities through promoting glucose consumption and suppressing lipid accumulation, whereas compound **178** had a potent PTP1B inhibition capacity compared to suramin, suggesting its possible application in anti-diabetic and anti-sleeping sickness therapeutic agents.

Despite the large number of metabolites, biological evaluation has only been conducted for a limited number of them, mainly in vitro, and there is a lack of pharmacological investigations that focus on studying the possible action mechanisms of the active metabolites. Therefore, mechanistic and in vivo studies are recommended to clarify and validate potential mechanisms for the active metabolites. Moreover, studies on the structure–activity relationships of these metabolites should be carried out.

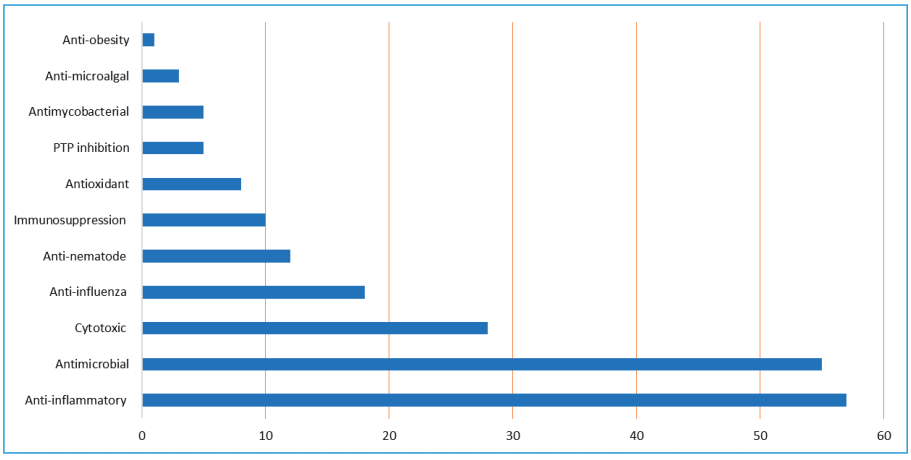

Figure 18. Number of metabolites evaluated for each bioactivity.

Additionally, molecular dynamic and docking studies could be employed to investigate the possible bioactivities of the untested metabolites.

On the other side, many of the tested metabolites displayed no notable effectiveness in some of the tested activities. Therefore, estimation of other possible bioactivities and molecular dynamic and docking studies, as well as derivatization of these metabolites, should clearly be the target of future research.

For further production of structurally varied metabolites by this fungus, cocultivation techniques should be considered an area for future investigation. In addition, exploring the biosynthetic pathways of these bio-metabolites is required and could enable the rational engineering or refactoring of these pathways for industrial purposes. Further, identification of the biosynthetic genes responsible for these metabolites may provide the opportunity to discover *A. sydowii*'s genetic potential for discovering novel metabolites by metabolic engineering, which could lead to more affordable and novel pharmaceutics.

According to the published reports, *A. sydowii* can produce diverse types of enzymes with potential biotechnological and industrial applications. Research that focuses on engineering enzymes in such a way for maximum activity and stability under appropriate conditions is desirable. Recombinant DNA technology and engineering of proteins are required to improve the industrial production of these enzymes. *A. sydowii* can withstand high-salinity conditions, pointing to its biotechnological and industrial relevance. It was proven that this fungus adsorbed heavy metals and degraded pesticides, agrochemicals, and contaminants. As a result, *A. sydowii* might serve as an environmentally safe tool for bioremediation and for converting hazardous materials into useful products. The minor reports described NP synthesis utilizing this fungus. These biosynthesized NPs possessed antiproliferative and antimicrobial potential as well as biosorbent capacity for treating heavy metal- and pesticide-contaminated water. However, the synthesized NPs using *A. sydowii* are limited to silver, γ-Fe_2O_3 magnetic chitosan nanocomposites, and chitosan beads-immobilized *A. sydowii*. Therefore, future research should focus on developing protocols for implementing the biosynthesis of other types of NPs such as carbides, metal oxides, and nitrides using this fungus and their bio-evaluation, which could be a promising area for more anticipated beneficial effects.

Despite the large number of published studies on *A. sydowii*, mycologists, biologists, and chemists still need to conduct more extensive research to fully understand the potential of this fungus and its secondary metabolites.

Author Contributions: Conceptualization, S.R.M.I., H.G.A.H. and G.A.M.; resources, B.H.A., M.M.A., Z.I.A., A.A.A., J.F.A., S.A.F., and S.G.A.M.; data curation, B.H.A., M.M.A., Z.I.A., A.A.A., J.F.A. and S.A.F.; writing—original draft preparation, S.R.M.I., S.G.A.M., H.G.A.H. and G.A.M.; writing—review and editing, B.H.A., M.M.A., Z.I.A., A.A.A., J.F.A. and S.A.F. All authors have read and agreed to the published version of the manuscript.

Funding: This research received no external funding.

Institutional Review Board Statement: Not applicable.

Informed Consent Statement: Not applicable.

Data Availability Statement: Not applicable.

Conflicts of Interest: The authors declare no conflict of interest.

References

1. Ibrahim, S.R.; Mohamed, S.G.; Altyar, A.E.; Mohamed, G.A. Natural Products of the Fungal Genus Humicola: Diversity, Biological Activity, and Industrial Importance. *Curr. Microbiol.* **2021**, *78*, 2488–2509. [CrossRef] [PubMed]
2. Ibrahim, S.R.; Altyar, A.E.; Mohamed, S.G.; Mohamed, G.A. Genus Thielavia: Phytochemicals, Industrial Importance and Biological Relevance. *Nat. Prod. Res.* **2022**, *36*, 5108–5123. [CrossRef] [PubMed]
3. Ibrahim, S.R.; Mohamed, G.A.; Al Haidari, R.A.; El-Kholy, A.A.; Zayed, M.F.; Khayat, M.T. Biologically Active Fungal Depsidones: Chemistry, Biosynthesis, Structural Characterization, and Bioactivities. *Fitoterapia* **2018**, *129*, 317–365. [PubMed]
4. Ibrahim, S.R.; Mohamed, G.A.; Khedr, A.I. γ-Butyrolactones from Aspergillus Species: Structures, Biosynthesis, and Biological Activities. *Nat. Prod. Commun.* **2017**, *12*, 791–800. [CrossRef]
5. Lange, L. The Importance of Fungi and Mycology for Addressing Major Global Challenges. *IMA Fungus* **2014**, *5*, 463–471. [CrossRef]
6. Ibrahim, S.R.; Abdallah, H.M.; Mohamed, G.A.; Deshmukh, S.K. Exploring Potential of Aspergillus Sclerotiorum: Secondary Metabolites and Biotechnological Relevance. *Mycol. Prog.* **2023**, *22*, 8.
7. Ibrahim, S.R.M.; Fadil, S.A.; Fadil, H.A.; Eshmawi, B.A.; Mohamed, S.G.A.; Mohamed, G.A. Fungal Naphthalenones; Promising Metabolites for Drug Discovery: Structures, Biosynthesis, Sources, and Pharmacological Potential. *Toxins* **2022**, *14*, 154. [CrossRef]
8. Ghazawi, K.F.; Fatani, S.A.; Mohamed, S.G.; Mohamed, G.A.; Ibrahim, S.R. Aspergillus nidulans—Natural Metabolites Powerhouse: Structures, Biosynthesis, Bioactivities, and Biotechnological Potential. *Fermentation* **2023**, *9*, 325. [CrossRef]
9. Wang, Y.; Mou, Y.; Dong, Y.; Wu, Y.; Liu, B.; Bai, J.; Yan, D.; Zhang, L.; Feng, D.; Pei, Y. Diphenyl Ethers from a Marine-Derived *Aspergillus sydowii*. *Mar. Drugs* **2018**, *16*, 451.
10. Hamasaki, T.; Nakajima, H.; Yokota, T.; Kimura, Y. A New Metabolite, 3-Carboxy-2, 4-Diphenyl-but-2-Enoic Anhydride, Produced by *Aspergillus nidulans*. *Agric. Biol. Chem.* **1983**, *47*, 891–892. [CrossRef]
11. Hamasaki, T.; Nagayama, K.; Hatsuda, Y. Two New Metabolites, Sydonic Acid and Hydroxysydonic Acid, from Aspergillus Sydowi. *Agric. Biol. Chem.* **1978**, *42*, 37–40.
12. Ishida, M.; Hamasaki, T.; Hatsuda, Y. The Structure of Two New Metabolites, Emerin and Emericellin, from *Aspergillus nidulans*. *Agric. Biol. Chem.* **1975**, *39*, 2181–2184. [CrossRef]
13. Jiménez-Gómez, I.; Valdés-Muñoz, G.; Moreno-Ulloa, A.; Pérez-Llano, Y.; Moreno-Perlín, T.; Silva-Jiménez, H.; Barreto-Curiel, F.; Sanchez-Carbente, M.d.R.; Folch-Mallol, J.L.; Gunde-Cimerman, N. Surviving in the Brine: A Multi-Omics Approach for Understanding the Physiology of the Halophile Fungus *Aspergillus sydowii* at Saturated NaCl Concentration. *Front. Microbiol.* **2022**, *13*, 1520.
14. Alker, A.P.; Smith, G.W.; Kim, K. Characterization of *Aspergillus sydowii* (Thom Et Church), a Fungal Pathogen of Caribbean Sea Fan Corals. *Hydrobiologia* **2001**, *460*, 105–111. [CrossRef]
15. Xu, X.; Zhao, S.; Yin, L.; Yu, Y.; Chen, Z.; Shen, H.; Zhou, L. A New Sydonic Acid Derivative from a Marine Derived-Fungus *Aspergillus sydowii*. *Chem. Nat. Compd.* **2017**, *53*, 1056–1058. [CrossRef]
16. Toledo-Hernández, C.; Zuluaga-Montero, A.; Bones-González, A.; Rodríguez, J.A.; Sabat, A.M.; Bayman, P. Fungi in Healthy and Diseased Sea Fans (Gorgonia Ventalina): Is *Aspergillus sydowii* always the Pathogen? *Coral Reefs* **2008**, *27*, 707–714. [CrossRef]
17. Takahata, Y.; Hiruma, M.; Sugita, T.; Muto, M. A Case of Onychomycosis due to *Aspergillus sydowii* Diagnosed using DNA Sequence Analysis. *Mycoses* **2008**, *51*, 170–173. [CrossRef]
18. Hayashi, A.; Crombie, A.; Lacey, E.; Richardson, A.J.; Vuong, D.; Piggott, A.M.; Hallegraeff, G. *Aspergillus sydowii* Marine Fungal Bloom in Australian Coastal Waters, its Metabolites and Potential Impact on Symbiodinium Dinoflagellates. *Mar. Drugs* **2016**, *14*, 59. [CrossRef]
19. Adegoke, S.A.; Odibo, F. Production, Purification and Characterization of A-Amylase of *Aspergillus sydowii* IMI 502692. *Plant Cell Biotechnol. Mol. Biol.* **2019**, *20*, 1050–1058.
20. Albuquerque, K.K.; Albuquerque, W.W.; Costa, R.M.; Batista, J.M.S.; Marques, D.A.; Bezerra, R.P.; Herculano, P.N.; Porto, A.L. Biotechnological Potential of a Novel Tannase-Acyl Hydrolase from *Aspergillus sydowii* using Waste Coir Residue: Aqueous Two-Phase System and Chromatographic Techniques. *Biocatal. Agric. Biotechnol.* **2020**, *23*, 101453. [CrossRef]

21. Alwakeel, S.S.; Ameen, F.; Al Gwaiz, H.; Sonbol, H.; Alghamdi, S.; Moharram, A.M.; Al-Bedak, O.A. Keratinases Produced by Aspergillus Stelliformis, *Aspergillus sydowii*, and Fusarium Brachygibbosum Isolated from Human Hair: Yield and Activity. *J. Fungi* **2021**, *7*, 471.
22. Elwan, S.H.; Ammar, M.S.; Mohawed, S.M. Lipases from Aspergillus Sydowi. *Zent. Für Mikrobiol.* **1986**, *141*, 233–239.
23. Ghosh, M.; Nanda, G. Purification and some Properties of a Xylanase from *Aspergillus sydowii* MG49. *Appl. Environ. Microbiol.* **1994**, *60*, 4620–4623. [CrossRef]
24. Amin, M.; Liang, X.; Ma, X.; Dong, J.; Qi, S. New Pyrone and Cyclopentenone Derivatives from Marine-Derived Fungus *Aspergillus sydowii* SCSIO 00305. *Nat. Prod. Res.* **2021**, *35*, 318–326.
25. Bu, C.; Zhang, Q.; Zeng, J.; Cao, X.; Hao, Z.; Qiao, D.; Cao, Y.; Xu, H. Identification of a Novel Anthocyanin Synthesis Pathway in the Fungus *Aspergillus sydowii* H-1. *BMC Genom.* **2020**, *21*, 29.
26. Chen, K.; Sun, S.; Cao, H.; Yi, C.; Yang, C.; Liu, Y. Two Sydowic Acid Derivatives and a Sulfonyl Metabolite from the Endophytic Fungus *Aspergillus sydowii*. *J. Asian Nat. Prod. Res.* **2022**, *24*, 1128–1133.
27. Fukuyama, K.; Tsukihara, T.; Katsube, Y.; Hamasaki, T.; Hatsuda, Y. Structural Analysis of Sydowic Acid by X-Ray Diffraction. *Agric. Biol. Chem.* **1976**, *40*, 1053–1054.
28. Gao, T.; Cao, F.; Yu, H.; Zhu, H. Secondary Metabolites from the Marine Fungus *Aspergillus sydowii*. *Chem. Nat. Compd.* **2017**, *53*, 1204–1207.
29. Hamasaki, T.; Sato, Y.; Hatsuda, Y. Isolation of New Metabolites from Aspergillus Sydowi and Structure of Sydowic Acid. *Agric. Biol. Chem.* **1975**, *39*, 2337–2340. [CrossRef]
30. Hamasaki, T. Sydowic Acid, a New Metabolite from Aspergillus Sydowi. *Tetrahedron Lett.* **1975**, *16*, 659–660. [CrossRef]
31. He, F.; Sun, Y.; Liu, K.; Zhang, X.; Qian, P.; Wang, Y.; Qi, S. Indole Alkaloids from Marine-Derived Fungus *Aspergillus sydowii* SCSIO 00305. *J. Antibiot.* **2012**, *65*, 109–111. [CrossRef] [PubMed]
32. Hu, X.; Li, X.; Meng, L.; Wang, B. Antioxidant Bisabolane-Type Sesquiterpenoids from Algal-Derived Fungus *Aspergillus sydowii* EN-434. *J. Oceanol. Limnol.* **2020**, *38*, 1532–1536.
33. Kaur, A.; Raja, H.A.; Darveaux, B.A.; Chen, W.; Swanson, S.M.; Pearce, C.J.; Oberlies, N.H. New Diketopiperazine Dimer from a Filamentous Fungal Isolate of *Aspergillus sydowii*. *Magn. Reson. Chem. MRC* **2015**, *53*, 616.
34. Kim, H.S.; Park, I.Y.; Park, Y.J.; Lee, J.H.; Hong, Y.S.; Lee, J.J. A Novel Dihydroxanthenone, AGI-B4 with Inhibition of VEGF-Induced Endothelial Cell Growth. *J. Antibiot.* **2002**, *55*, 669–672. [CrossRef] [PubMed]
35. Liu, N.; Peng, S.; Yang, J.; Cong, Z.; Lin, X.; Liao, S.; Yang, B.; Zhou, X.; Zhou, X.; Liu, Y. Structurally Diverse Sesquiterpenoids and Polyketides from a Sponge-Associated Fungus *Aspergillus sydowii* SCSIO41301. *Fitoterapia* **2019**, *135*, 27–32.
36. Liu, S.; Wang, H.; Su, M.; Hwang, G.J.; Hong, J.; Jung, J.H. New Metabolites from the Sponge-Derived Fungus *Aspergillus sydowii* J05B-7F-4. *Nat. Prod. Res.* **2017**, *31*, 1682–1686. [CrossRef]
37. Liu, X.; Song, F.; Ma, L.; Chen, C.; Xiao, X.; Ren, B.; Liu, X.; Dai, H.; Piggott, A.M.; Av-Gay, Y. Sydowiols A–C: Mycobacterium Tuberculosis Protein Tyrosine Phosphatase Inhibitors from an East China Sea Marine-Derived Fungus, *Aspergillus sydowii*. *Tetrahedron Lett.* **2013**, *54*, 6081–6083. [CrossRef]
38. Liu, Y.; Fang, S.; Wang, B.; Ji, N. Phenol Derivatives from the Cold-Seep Fungus *Aspergillus sydowii* 10–31. *Phytochem. Lett.* **2022**, *52*, 63–66. [CrossRef]
39. Handayani, D.; Dwinatrana, K.; Rustini, R. Antibacterial Compound from Marine Sponge Derived Fungus *Aspergillus sydowii* DC08. *Rasayan J. Chem.* **2022**, *15*, 2485–2492. [CrossRef]
40. Li, W.; Luo, D.; Huang, J.; Wang, L.; Zhang, F.; Xi, T.; Liao, J.; Lu, Y. Antibacterial Constituents from Antarctic Fungus, *Aspergillus sydowii* SP-1. *Nat. Prod. Res.* **2018**, *32*, 662–667. [CrossRef]
41. Liu, Y.; Zhang, J.; Li, C.; Mu, X.; Liu, X.; Wang, L.; Zhao, Y.; Zhang, P.; Li, X.; Zhang, X. Antimicrobial Secondary Metabolites from the Seawater-Derived Fungus *Aspergillus sydowii* SW9. *Molecules* **2019**, *24*, 4596. [CrossRef] [PubMed]
42. Niu, S.; Huang, S.; Hong, B.; Huang, Q.; Liu, X.; Shao, Z.; Zhang, G. Antiviral Cyclopropane Acids from Deep-Sea-Derived Fungus *Aspergillus sydowii*. *Mar. Drugs* **2022**, *20*, 410. [PubMed]
43. Ren, H.; Liu, R.; Chen, L.; Zhu, T.; Zhu, W.M.; Gu, Q.Q. Two New Hetero-Spirocyclic Γ-Lactam Derivatives from Marine Sediment-Derived Fungus Aspergillus Sydowi D2–6. *Arch. Pharm. Res.* **2010**, *33*, 499–502. [CrossRef]
44. Tian, L.; Cai, S.; Li, D.; Lin, Z.; Zhu, T.; Fang, Y.; Liu, P.; Gu, Q.; Zhu, W. Two New Metabolites with Cytotoxicities from Deep-Sea Fungus, Aspergillus Sydowi YH11-2. *Arch. Pharm. Res.* **2007**, *30*, 1051–1054. [CrossRef]
45. Wang, J.; Lin, X.; Qin, C.; Liao, S.; Wan, J.; Zhang, T.; Liu, J.; Fredimoses, M.; Chen, H.; Yang, B. Antimicrobial and Antiviral Sesquiterpenoids from Sponge-Associated Fungus, *Aspergillus sydowii* ZSDS1-F6. *J. Antibiot.* **2014**, *67*, 581–583. [CrossRef]
46. Wiese, J.; Aldemir, H.; Schmaljohann, R.; Gulder, T.A.; Imhoff, J.F. Asperentin B, a New Inhibitor of the Protein Tyrosine Phosphatase 1B. *Mar. Drugs* **2017**, *15*, 191.
47. Yang, X.; Yu, H.; Ren, J.; Cai, L.; Xu, L.; Liu, L. Sulfoxide-Containing Bisabolane Sesquiterpenoids with Antimicrobial and Nematicidal Activities from the Marine-Derived Fungus *Aspergillus sydowii* LW09. *J. Fungi* **2023**, *9*, 347. [CrossRef]
48. Zhang, M.; Wang, W.; Fang, Y.; Zhu, T.; Gu, Q.; Zhu, W. Cytotoxic Alkaloids and Antibiotic Nordammarane Triterpenoids from the Marine-Derived Fungus Aspergillus Sydowi. *J. Nat. Prod.* **2008**, *71*, 985–989.
49. Zhang, C.; Chen, Z.; Tao, Y.; Ke, T.; Li, S.; Wang, P.; Chen, L. Enhanced Removal of Trichlorfon and Cd (II) from Aqueous Solution by Magnetically Separable Chitosan Beads Immobilized *Aspergillus sydowii*. *Int. J. Biol. Macromol.* **2020**, *148*, 457–465. [PubMed]

50. Nayak, B.K.; Anitha, K. Amplified Antibiotic Potency of Two Different Drugs Combined with Biosynthesized AgNPs from *Aspergillus sydowii* Isolated from Sand Dunes. *Int. J. Pharm. Tech. Res.* **2014**, *6*, 1751–1755.
51. Zhang, C.; Liu, S.; Li, S.; Tao, Y.; Wang, P.; Ma, X.; Chen, L. Enahanced Biosorption of Cu (II) by Magnetic Chitosan Microspheres Immobilized *Aspergillus sydowii* (MCMAs) from Aqueous Solution. *Colloids Surf. Physicochem. Eng. Asp.* **2019**, *581*, 123813. [CrossRef]
52. Vala, A.K. Exploration on Green Synthesis of Gold Nanoparticles by a Marine-derived Fungus *Aspergillus sydowii*. *Environ. Prog. Sustain. Energy* **2015**, *34*, 194–197. [CrossRef]
53. Teuscher, F.; Lin, W.; Wray, V.; Edrada, R.; Padmakumar, K.; Proksch, P.; Ebel, R. Two New Cyclopentanoids from the Endophytic Fungus *Aspergillus sydowii* Associated with the Marine Alga Acanthophora Spicifera. *Nat. Prod. Commun.* **2006**, *1*, 927–933.
54. Chung, Y.; Wei, C.; Chuang, D.; El-Shazly, M.; Hsieh, C.; Asai, T.; Oshima, Y.; Hsieh, T.; Hwang, T.; Wu, Y. An Epigenetic Modifier Enhances the Production of Anti-Diabetic and Anti-Inflammatory Sesquiterpenoids from *Aspergillus sydowii*. *Bioorg. Med. Chem.* **2013**, *21*, 3866–3872. [CrossRef] [PubMed]
55. Wang, W.; Gao, M.; Luo, Z.; Liao, Y.; Zhang, B.; Ke, W.; Shao, Z.; Li, F.; Chen, J. Secondary Metabolites Isolated from the Deep Sea-Derived Fungus *Aspergillus sydowii* C1-S01-A7. *Nat. Prod. Res.* **2019**, *33*, 3077–3082. [CrossRef] [PubMed]
56. Trisuwan, K.; Rukachaisirikul, V.; Kaewpet, M.; Phongpaichit, S.; Hutadilok-Towatana, N.; Preedanon, S.; Sakayaroj, J. Sesquiterpene and Xanthone Derivatives from the Sea Fan-Derived Fungus *Aspergillus sydowii* PSU-F154. *J. Nat. Prod.* **2011**, *74*, 1663–1667. [CrossRef]
57. Niu, S.; Yang, L.; Zhang, G.; Chen, T.; Hong, B.; Pei, S.; Shao, Z. Phenolic Bisabolane and Cuparene Sesquiterpenoids with Anti-Inflammatory Activities from the Deep-Sea-Derived *Aspergillus sydowii* MCCC 3A00324 Fungus. *Bioorg. Chem.* **2020**, *105*, 104420. [CrossRef] [PubMed]
58. Sun, Y.; Liu, W.; Shi, X.; Zheng, H.; Zheng, Z.; Lu, X.; Xing, Y.; Ji, K.; Liu, M.; Dong, Y. Inducing Secondary Metabolite Production of *Aspergillus sydowii* through Microbial Co-Culture with Bacillus Subtilis. *Microb. Cell Factories* **2021**, *20*, 42. [CrossRef]
59. Sun, Y.; Shi, X.; He, L.; Xing, Y.; Guo, Q.; Xiu, Z.; Dong, Y. Biosynthetic Profile in the Co-Culture of *Aspergillus sydowii* and Bacillus Subtilis to Produce Novel Benzoic Derivatives. *Microb. Ecol.* **2022**, *85*, 1288–1299. [CrossRef]
60. Niu, S.; Yang, L.; Chen, T.; Hong, B.; Pei, S.; Shao, Z.; Zhang, G. New Monoterpenoids and Polyketides from the Deep-Sea Sediment-Derived Fungus *Aspergillus sydowii* MCCC 3A00324. *Mar. Drugs* **2020**, *18*, 561. [CrossRef]
61. Huang, Q.; Wang, Y.; Wu, H.; Yuan, M.; Zheng, C.; Xu, H. Xanthone Glucosides: Isolation, Bioactivity and Synthesis. *Molecules* **2021**, *26*, 5575. [CrossRef]
62. Badiali, C.; Petruccelli, V.; Brasili, E.; Pasqua, G. Xanthones: Biosynthesis and Trafficking in Plants, Fungi and Lichens. *Plants* **2023**, *12*, 694. [CrossRef]
63. Song, X.; Zhang, X.; Han, Q.; Li, X.; Li, G.; Li, R.; Jiao, Y.; Zhou, J.; Lou, H. Xanthone Derivatives from *Aspergillus sydowii*, an Endophytic Fungus from the Liverwort Scapania Ciliata S. Lac and their Immunosuppressive Activities. *Phytochem. Lett.* **2013**, *6*, 318–321. [CrossRef]
64. Wang, Y.; Zhong, Z.; Zhao, F.; Zheng, J.; Zheng, X.; Zhang, K.; Huang, H. Two New Pyrone Derivatives from the Mangrove-Derived Endophytic Fungus *Aspergillus sydowii*# 2B. *Nat. Prod. Res.* **2022**, *36*, 3872–3878.
65. Niu, S.; Chen, Z.; Pei, S.; Shao, Z.; Zhang, G.; Hong, B. Acremolin D, a New Acremolin Alkaloid from the Deep-Sea Sediment Derived *Aspergillus sydowii* Fungus. *Nat. Prod. Res.* **2022**, *36*, 4936–4942. [CrossRef]
66. Ma, C.; Li, Y.; Niu, S.; Zhang, H.; Liu, X.; Che, Y. N-Hydroxypyridones, Phenylhydrazones, and a Quinazolinone from Isaria Farinosa. *J. Nat. Prod.* **2011**, *74*, 32–37. [CrossRef]
67. Tian, Y.; Qin, X.; Lin, X.; Kaliyaperumal, K.; Zhou, X.; Liu, J.; Ju, Z.; Tu, Z.; Liu, Y. Sydoxanthone C and Acremolin B Produced by Deep-Sea-Derived Fungus Aspergillus Sp. SCSIO Ind09F01. *J. Antibiot.* **2015**, *68*, 703–706. [CrossRef]
68. Gupta, R.C. Chapter 55-Aflatoxins, Ochratoxins and Citrinin. In *Reproductive and Developmental Toxicology*; CRC Press: Boca Raton, FL, USA, 2011. [CrossRef]
69. Yang, S.; Li, X.; Li, X.; Li, H.; Meng, L.; Wang, B. New Citrinin Analogues Produced by Coculture of the Marine Algal-Derived Endophytic Fungal Strains *Aspergillus sydowii* EN-534 and Penicillium Citrinum EN-535. *Phytochem. Lett.* **2018**, *25*, 191–195. [CrossRef]
70. Tang, Q.; Guo, K.; Li, X.; Zheng, X.; Kong, X.; Zheng, Z.; Xu, Q.; Deng, X. Three New Asperentin Derivatives from the Algicolous Fungus *Aspergillus* Sp. F00785. *Mar. Drugs* **2014**, *12*, 5993–6002. [CrossRef]
71. Fan, Y.; Gao, X.; Yue, J. Attractive Natural Products with Strained Cyclopropane and/Or Cyclobutane Ring Systems. *Sci. China Chem.* **2016**, *59*, 1126–1141. [CrossRef]
72. Burmudžija, A.Z.; Muškinja, J.M.; Kosanić, M.M.; Ranković, B.R.; Novaković, S.B.; Đorđević, S.B.; Stanojković, T.P.; Baskić, D.D.; Ratković, Z.R. Cytotoxic and Antimicrobial Activity of Dehydrozingerone based Cyclopropyl Derivatives. *Chem. Biodiver.* **2017**, *14*. [CrossRef]
73. Ma, S.; Mandalapu, D.; Wang, S.; Zhang, Q. Biosynthesis of Cyclopropane in Natural Products. *Nat. Prod. Rep.* **2022**, *39*, 926–945. [CrossRef] [PubMed]
74. Lee, Y.; Yoon, Y.; Yoon, H.; Park, H.; Song, S.; Yeum, K. Dietary Anthocyanins Against Obesity and Inflammation. *Nutrients* **2017**, *9*, 1089. [CrossRef] [PubMed]

75. Majumder, M.A.A.; Rahman, S.; Cohall, D.; Bharatha, A.; Singh, K.; Haque, M.; Gittens-St Hilaire, M. Antimicrobial Stewardship: Fighting Antimicrobial Resistance and Protecting Global Public Health. *Infect. Drug Resist.* **2020**, *13*, 4713–4738. [CrossRef] [PubMed]
76. Coque, T.M.; Cantón, R.; Pérez-Cobas, A.E.; Fernández-de-Bobadilla, M.D.; Baquero, F. Antimicrobial Resistance in the Global Health Network: Known Unknowns and Challenges for Efficient Responses in the 21st Century. *Microorganisms* **2023**, *11*, 1050. [CrossRef] [PubMed]
77. Sandrawati, N.; Hati, S.P.; Yunita, F.; Putra, A.E.; Ismed, F.; Tallei, T.E.; Hertiani, T.; Handayani, D. Antimicrobial and Cytotoxic Activities of Marine Sponge-Derived Fungal Extracts Isolated from *Dactylospongia* sp. *J. Appl. Pharm. Sci.* **2020**, *10*, 28.
78. Sarker, A.; Gu, Z.; Mao, L.; Ge, Y.; Hou, D.; Fang, J.; Wei, Z.; Wang, Z. Influenza-Existing Drugs and Treatment Prospects. *Eur. J. Med. Chem.* **2022**, *232*, 114189. [CrossRef]
79. Zhang, Z.; Morris-Natschke, S.L.; Cheng, Y.; Lee, K.; Li, R. Development of Anti-influenza Agents from Natural Products. *Med. Res. Rev.* **2020**, *40*, 2290–2338. [CrossRef]
80. Kahn, S.E.; Hull, R.L.; Utzschneider, K.M. Mechanisms Linking Obesity to Insulin Resistance and Type 2 Diabetes. *Nature* **2006**, *444*, 840–846. [CrossRef]
81. Ducluzeau, P.H.; Fletcher, L.M.; Vidal, H.; Laville, M.; Tavare, J.M. Molecular Mechanisms of Insulin-Stimulated Glucose Uptake in Adipocytes. *Diabetes Metab.* **2002**, *28*, 85–92.
82. Ruberg, F.L. Myocardial Lipid Accumulation in the Diabetic Heart. *Circulation* **2007**, *116*, 1110–1112. [CrossRef] [PubMed]
83. Krecek, R.C. Nematode Parasites of Vertebrates: Their Development and Transmission, RC Anderson: Book Review. *J. S. Afr. Vet. Assoc.* **2000**, *71*, 239. [CrossRef]
84. Garcia-Bustos, J.F.; Sleebs, B.E.; Gasser, R.B. An Appraisal of Natural Products Active Against Parasitic Nematodes of Animals. *Parasites Vectors* **2019**, *12*, 306. [CrossRef] [PubMed]
85. Souza, P.M.d.; Magalhães, P.d.O. Application of Microbial A-Amylase in Industry-A Review. *Braz. J. Microbiol.* **2010**, *41*, 850–861. [CrossRef]
86. Castro, A.M.d.; Carvalho, D.F.; Freire, D.M.G.; Castilho, L.d.R. Economic Analysis of the Production of Amylases and Other Hydrolases by Aspergillus Awamori in Solid-State Fermentation of Babassu Cake. *Enzym. Res.* **2010**, *2010*, 576872. [CrossRef]
87. Hareeri, R.H.; Aldurdunji, M.M.; Abdallah, H.M.; Alqarni, A.A.; Mohamed, S.G.; Mohamed, G.A.; Ibrahim, S.R. Aspergillus Ochraceus: Metabolites, Bioactivities, Biosynthesis, and Biotechnological Potential. *Molecules* **2022**, *27*, 6759. [CrossRef]
88. Fagunwa, O.E.; Olanbiwoninu, A.A. Accelerating the Sustainable Development Goals through Microbiology: Some Efforts and Opportunities. *Access Microbiol.* **2020**, *2*, acmi000112.
89. Toop, T.A.; Ward, S.; Oldfield, T.; Hull, M.; Kirby, M.E.; Theodorou, M.K. AgroCycle–developing a Circular Economy in Agriculture. *Energy Procedia* **2017**, *123*, 76–80. [CrossRef]
90. Sallach, J.B.; Thirkell, T.J.; Field, K.J.; Carter, L.J. The Emerging Threat of Human-use Antifungals in Sustainable and Circular Agriculture Schemes. *Plants People Planet* **2021**, *3*, 685–693. [CrossRef]
91. Kadri, T.; Rouissi, T.; Brar, S.K.; Cledon, M.; Sarma, S.; Verma, M. Biodegradation of Polycyclic Aromatic Hydrocarbons (PAHs) by Fungal Enzymes: A Review. *J. Environ. Sci.* **2017**, *51*, 52–74. [CrossRef]
92. Haroune, L.; Saibi, S.; Bellenger, J.; Cabana, H. Evaluation of the Efficiency of Trametes Hirsuta for the Removal of Multiple Pharmaceutical Compounds Under Low Concentrations Relevant to the Environment. *Bioresour. Technol.* **2014**, *171*, 199–202. [CrossRef] [PubMed]
93. Olicón-Hernández, D.R.; González-López, J.; Aranda, E. Overview on the Biochemical Potential of Filamentous Fungi to Degrade Pharmaceutical Compounds. *Front. Microbiol.* **2017**, *8*, 1792. [CrossRef] [PubMed]
94. González-Abradelo, D.; Pérez-Llano, Y.; Peidro-Guzmán, H.; del Rayo Sánchez-Carbente, M.; Folch-Mallol, J.L.; Aranda, E.; Vaidyanathan, V.K.; Cabana, H.; Gunde-Cimerman, N.; Batista-García, R.A. First Demonstration that Ascomycetous Halophilic Fungi (*Aspergillus sydowii* and *Aspergillus destruens*) are Useful in Xenobiotic Mycoremediation Under High Salinity Conditions. *Bioresour. Technol.* **2019**, *279*, 287–296. [CrossRef]
95. Ganesh Kumar, A.; Manisha, D.; Sujitha, K.; Magesh Peter, D.; Kirubagaran, R.; Dharani, G. Genome Sequence Analysis of Deep Sea *Aspergillus sydowii* BOBA1 and Effect of High Pressure on Biodegradation of Spent Engine Oil. *Sci. Rep.* **2021**, *11*, 9347. [CrossRef]
96. Birolli, W.G.; Santos, D.d.A.; Alvarenga, N.; Garcia, A.C.; Romão, L.P.; Porto, A.L. Biodegradation of Anthracene and several PAHs by the Marine-Derived Fungus *Cladosporium* Sp. CBMAI 1237. *Mar. Pollut. Bull.* **2018**, *129*, 525–533. [CrossRef]
97. Birolli, W.G.; Yamamoto, K.Y.; de Oliveira, J.R.; Nitschke, M.; Seleghim, M.H.; Porto, A.L. Biotransformation of Dieldrin by the Marine Fungus Penicillium Miczynskii CBMAI 930. *Biocatal. Agric. Biotechnol.* **2015**, *4*, 39–43. [CrossRef]
98. Zhang, C.; Tao, Y.; Li, S.; Ke, T.; Wang, P.; Wei, S.; Chen, L. Bioremediation of Cadmium-Trichlorfon Co-Contaminated Soil by Indian Mustard (Brassica Juncea) Associated with the Trichlorfon-Degrading Microbe *Aspergillus sydowii*: Related Physiological Responses and Soil Enzyme Activities. Ecotoxicol. *Environ. Saf.* **2020**, *188*, 109756. [CrossRef]
99. Olszowski, T.; Baranowska-Bosiacka, I.; Rębacz-Maron, E.; Gutowska, I.; Jamioł, D.; Prokopowicz, A.; Goschorska, M.; Chlubek, D. Cadmium Concentration in Mother's Blood, Milk, and Newborn's Blood and its Correlation with Fatty Acids, Anthropometric Characteristics, and Mother's Smoking Status. *Biol. Trace Elem. Res.* **2016**, *174*, 8–20. [CrossRef]
100. Tian, J.; Dong, Q.; Yu, C.; Zhao, R.; Wang, J.; Chen, L. Biodegradation of the Organophosphate Trichlorfon and its Major Degradation Products by a Novel *Aspergillus sydowii* PA F-2. *J. Agric. Food Chem.* **2016**, *64*, 4280–4287. [CrossRef] [PubMed]

101. Birolli, W.G.; Alvarenga, N.; Vacondio, B.; Seleghim, M.H.R.; Porto, A.L.M. Growth Assessment of Marine-Derived Fungi in the Presence of Esfenvalerate and its Main Metabolites. *J. Microb. Biochem. Technol.* **2014**, *6*, 260–267. [CrossRef]
102. Alvarenga, N.; Birolli, W.G.; Nitschke, M.; Rezende, M.O.; Seleghim, M.H.; Porto, A.L. Biodegradation of Chlorpyrifos by Whole Cells of Marine-Derived Fungi *Aspergillus sydowii* and *Trichoderma* sp. *J. Microb. Biochem. Technol.* **2015**, *7*, 133–139.
103. Soares, P.R.S.; Birolli, W.G.; Ferreira, I.M.; Porto, A.L.M. Biodegradation Pathway of the Organophosphate Pesticides Chlorpyrifos, Methyl Parathion and Profenofos by the Marine-Derived Fungus *Aspergillus sydowii* CBMAI 935 and its Potential for Methylation Reactions of Phenolic Compounds. *Mar. Pollut. Bull.* **2021**, *166*, 112185. [CrossRef] [PubMed]
104. Alvarenga, N.; Birolli, W.G.; Seleghim, M.H.; Porto, A.L. Biodegradation of Methyl Parathion by Whole Cells of Marine-Derived Fungi *Aspergillus sydowii* and Penicillium Decaturense. *Chemosphere* **2014**, *117*, 47–52. [CrossRef]
105. Mohamed, G.A.; Ibrahim, S.R.M. Untapped Potential of Marine-Associated *Cladosporium* Species: An Overview on Secondary Metabolites, Biotechnological Relevance, and Biological Activities. *Mar Drugs* **2021**, *19*, 645. [CrossRef]
106. Ibrahim, S.R.; Mohamed, S.G.; Sindi, I.A.; Mohamed, G.A. Biologically Active Secondary Metabolites and Biotechnological Applications of Species of the Family Chaetomiaceae (Sordariales): An Updated Review from 2016 to 2021. *Mycol. Prog.* **2021**, *20*, 595–639. [CrossRef]
107. Cong, B.; Wang, N.; Liu, S.; Liu, F.; Yin, X.; Shen, J. Isolation, Characterization and Transcriptome Analysis of a Novel Antarctic *Aspergillus sydowii* Strain MS-19 as a Potential Lignocellulosic Enzyme Source. *BMC Microbiol.* **2017**, *17*, 129. [CrossRef]
108. Ibrahim, S.R.; Choudhry, H.; Asseri, A.H.; Elfaky, M.A.; Mohamed, S.G.; Mohamed, G.A. *Stachybotrys Chartarum*—A Hidden Treasure: Secondary Metabolites, Bioactivities, and Biotechnological Relevance. *J. Fungi* **2022**, *8*, 504. [CrossRef]
109. Brandt, S.C.; Ellinger, B.; Van Nguyen, T.; Harder, S.; Schlüter, H.; Hahnke, R.L.; Rühl, M.; Schäfer, W.; Gand, M. *Aspergillus sydowii*: Genome Analysis and Characterization of Two Heterologous Expressed, Non-Redundant Xylanases. *Front. Microbiol.* **2020**, *11*, 2154. [CrossRef]
110. Nair, S.G.; Sindhu, R.; Shashidhar, S. Purification and Biochemical Characterization of Two Xylanases from *Aspergillus sydowii* SBS 45. *Appl. Biochem. Biotechnol.* **2008**, *149*, 229–243. [CrossRef]
111. Bhardwaj, N.; Kumar, B.; Agrawal, K.; Verma, P. Current Perspective on Production and Applications of Microbial Cellulases: A Review. *Bioresour. Bioprocess.* **2021**, *8*, 95. [CrossRef]
112. Ejaz, U.; Sohail, M.; Ghanemi, A. Cellulases: From Bioactivity to a Variety of Industrial Applications. *Biomimetics* **2021**, *6*, 44. [CrossRef]
113. Matkar, K.; Chapla, D.; Divecha, J.; Nighojkar, A.; Madamwar, D. Production of Cellulase by a Newly Isolated Strain of *Aspergillus sydowii* and its Optimization Under Submerged Fermentation. *Int. Biodeterior. Biodegrad.* **2013**, *78*, 24–33. [CrossRef]
114. Ibrahim, S.R.M.; Sirwi, A.; Eid, B.G.; Mohamed, S.G.A.; Mohamed, G.A. Bright Side of *Fusarium Oxysporum*: Secondary Metabolites Bioactivities and Industrial Relevance in Biotechnology and Nanotechnology. *J. Fungi* **2021**, *7*, 943. [CrossRef] [PubMed]
115. Hassan, M.A.; Abol-Fotouh, D.; Omer, A.M.; Tamer, T.M.; Abbas, E. Comprehensive Insights into Microbial Keratinases and their Implication in various Biotechnological and Industrial Sectors: A Review. *Int. J. Biol. Macromol.* **2020**, *154*, 567–583. [CrossRef]
116. Verma, A.; Singh, H.; Anwar, S.; Chattopadhyay, A.; Tiwari, K.K.; Kaur, S.; Dhilon, G.S. Microbial Keratinases: Industrial Enzymes with Waste Management Potential. *Crit. Rev. Biotechnol.* **2017**, *37*, 476–491. [CrossRef] [PubMed]
117. Sharma, S.; Gupta, A. Sustainable Management of Keratin Waste Biomass: Applications and Future Perspectives. *Braz. Arch. Biol. Technol.* **2016**, *59*, e16150684. [CrossRef]
118. Wu, S.; Snajdrova, R.; Moore, J.C.; Baldenius, K.; Bornscheuer, U.T. Biocatalysis: Enzymatic Synthesis for Industrial Applications. *Angew. Chem. Int. Ed.* **2021**, *60*, 88–119. [CrossRef] [PubMed]
119. Martins, M.P.; Mouad, A.M.; Boschini, L.; Regali Seleghim, M.H.; Sette, L.D.; Meleiro Porto, A.L. Marine Fungi *Aspergillus sydowii* and Trichoderma Sp. Catalyze the Hydrolysis of Benzyl Glycidyl Ether. *Mar. Biotechnol.* **2011**, *13*, 314–320. [CrossRef]
120. Martins, M.P.; Ouazzani, J.; Arcile, G.; Jeller, A.H.; de Lima, J.P.; Seleghim, M.H.; Oliveira, A.L.L.; Debonsi, H.M.; Venâncio, T.; Yokoya, N.S. Biohydroxylation of (-)-ambrox®, (-)-sclareol, and (+)-sclareolide by whole cells of Brazilian marine-derived fungi. *Mar. Biotechnol.* **2015**, *17*, 211–218. [CrossRef]
121. de Paula, S.F.C.; Porto, A.L.M. Cascate Reactions of Progesterone by Mycelia and Culture Broth from Marine-Derived Fungus *Aspergillus sydowii* CBMAI 935. *Biocatal. Agric. Biotechnol.* **2020**, *25*, 101546. [CrossRef]
122. de Matos, I.L.; Nitschke, M.; Porto, A.L.M. Regioselective and Chemoselective Biotransformation of 2′-Hydroxychalcone Derivatives by Marine-Derived Fungi. *Biocatal. Biotransform.* **2023**, *41*, 46–56. [CrossRef]
123. de Oliveira, J.R.; Seleghim, M.H.R.; Porto, A.L.M. Biotransformation of Methylphenylacetonitriles by Brazilian Marine Fungal Strain *Aspergillus sydowii* CBMAI 934: Eco-Friendly Reactions. *Mar. Biotechnol.* **2014**, *16*, 156–160. [CrossRef] [PubMed]
124. Zhou, B.; Ma, C.; Zheng, C.; Xia, T.; Ma, B.; Liu, X. 3-Methylxanthine Production through Biodegradation of Theobromine by *Aspergillus sydowii* PT-2. *BMC Microbiol.* **2020**, *20*, 269. [CrossRef] [PubMed]
125. Jimenez, D.E.; Barreiro, J.C.; dos Santos, F.M., Jr.; de Vasconcellos, S.P.; Porto, A.L.; Batista, J.M., Jr. Enantioselective Ene-reduction of E-2-cyano-3-(Furan-2-yl) Acrylamide by Marine and Terrestrial Fungi and Absolute Configuration of (R)-2-cyano-3-(Furan-2-yl) Propanamide Determined by Calculations of Electronic Circular Dichroism (ECD) Spectra. *Chirality* **2019**, *31*, 534–542. [CrossRef]
126. Morais, A.T.d.B.; Ferreira, I.M.; Jimenez, D.E.; Porto, A.L. Synthesis of A-Chloroacetophenones with NH4Cl/Oxone® in Situ Followed by Bioreduction with Whole Cells of Marine-Derived Fungi. *Biocatal. Agric. Biotechnol.* **2018**, *16*, 314–319. [CrossRef]

127. Rocha, L.C.; Ferreira, H.V.; Pimenta, E.F.; Berlinck, R.G.S.; Rezende, M.O.O.; Landgraf, M.D.; Seleghim, M.H.R.; Sette, L.D.; Porto, A.L.M. Biotransformation of A-Bromoacetophenones by the Marine Fungus *Aspergillus sydowii*. *Mar. Biotechnol.* **2010**, *12*, 552–557. [CrossRef]
128. Alvarenga, N.; Porto, A.L. Stereoselective Reduction of 2-Azido-1-Phenylethanone Derivatives by Whole Cells of Marine-Derived Fungi Applied to Synthesis of Enantioenriched B-Hydroxy-1, 2, 3-Triazoles. *Biocatal. Biotransform.* **2017**, *35*, 388–396. [CrossRef]
129. Rocha, L.C.; Ferreira, H.V.; Luiz, R.F.; Sette, L.D.; Porto, A.L. Stereoselective Bioreduction of 1-(4-Methoxyphenyl) Ethanone by Whole Cells of Marine-Derived Fungi. *Mar. Biotechnol.* **2012**, *14*, 358–362. [CrossRef]
130. Prasad, R.; Pandey, R.; Barman, I. Engineering Tailored Nanoparticles with Microbes: Quo Vadis? *Wiley Interdiscip. Rev. Nanomed. Nanobiotechnol.* **2016**, *8*, 316–330. [CrossRef]
131. Fariq, A.; Khan, T.; Yasmin, A. Microbial Synthesis of Nanoparticles and their Potential Applications in Biomedicine. *J. Appl. Biomed.* **2017**, *15*, 241–248. [CrossRef]
132. Singh, C.R.; Kathiresan, K.; Anandhan, S. A Review on Marine Based Nanoparticles and their Potential Applications. *Afr. J. Biotechnol.* **2015**, *14*, 1525–1532.
133. Hulkoti, N.I.; Taranath, T.C. Biosynthesis of Nanoparticles using Microbes—A Review. *Colloids Surf. B Biointerfaces* **2014**, *121*, 474–483. [CrossRef] [PubMed]
134. Wang, D.; Xue, B.; Wang, L.; Zhang, Y.; Liu, L.; Zhou, Y. Fungus-Mediated Green Synthesis of Nano-Silver using *Aspergillus sydowii* and its Antifungal/Antiproliferative Activities. *Sci. Rep.* **2021**, *11*, 10356. [CrossRef] [PubMed]

marine drugs

MDPI

Article

Discovery of Anti-MRSA Secondary Metabolites from a Marine-Derived Fungus *Aspergillus fumigatus*

Rui Zhang [1,2], Haifeng Wang [1], Baosong Chen [2], Huanqin Dai [2], Jingzu Sun [2], Junjie Han [2,*] and Hongwei Liu [1,2,*]

[1] Key Laboratory of Structure-Based Drug Design & Discovery of Education, College of Traditional Chinese Materia Medica, Shenyang Pharmaceutical University, Shenyang 110016, China; zhangrui950714@163.com (R.Z.); wanghaifeng0310@163.com (H.W.)

[2] State Key Laboratory of Mycology, Institute of Microbiology, Chinese Academy of Sciences, Beijing 100101, China; chenbs@im.ac.cn (B.C.); daihq@im.ac.cn (H.D.); sunjz@im.ac.cn (J.S.)

* Correspondence: hanjj@im.ac.cn (J.H.); liuhw@im.ac.cn (H.L.); Tel.: +86-10-64806074 (H.L.)

Abstract: Methicillin-resistant *Staphylococcus aureus* (MRSA), a WHO high-priority pathogen that can cause great harm to living beings, is a primary cause of death from antibiotic-resistant infections. In the present study, six new compounds, including fumindoline A–C (**1**–**3**), 12β, 13β-hydroxy-asperfumigatin (**4**), 2-*epi*-tryptoquivaline F (**17**) and penibenzophenone E (**37**), and thirty-nine known ones were isolated from the marine-derived fungus *Aspergillus fumigatus* H22. The structures and the absolute configurations of the new compounds were unambiguously assigned by spectroscopic data, mass spectrometry (MS), electronic circular dichroism (ECD) spectroscopic analyses, quantum NMR and ECD calculations, and chemical derivatizations. Bioactivity screening indicated that nearly half of the compounds exhibit antibacterial activity, especially compounds **8** and **11**, and **33**–**38** showed excellent antimicrobial activities against MRSA, with minimum inhibitory concentration (MIC) values ranging from 1.25 to 2.5 μM. In addition, compound **8** showed moderate inhibitory activity against *Mycobacterium bovis* (MIC: 25 μM), compound **10** showed moderate inhibitory activity against *Candida albicans* (MIC: 50 μM), and compound **13** showed strong inhibitory activity against the hatching of a *Caenorhabditis elegans* egg (IC_{50}: 2.5 μM).

Keywords: methicillin-resistant *Staphylococcus aureus*; *Aspergillus fumigatus*; chemical diversity; chemical ecology

Citation: Zhang, R.; Wang, H.; Chen, B.; Dai, H.; Sun, J.; Han, J.; Liu, H. Discovery of Anti-MRSA Secondary Metabolites from a Marine-Derived Fungus *Aspergillus fumigatus*. *Mar. Drugs* **2022**, *20*, 302. https://doi.org/10.3390/md20050302

Academic Editor: Hee Jae Shin

Received: 11 April 2022
Accepted: 25 April 2022
Published: 28 April 2022

1. Introduction

Methicillin-resistant *Staphylococcus aureus* (MRSA) is recognized as one of the most common bacteria in both community and hospital-acquired infections, causing significant morbidity and mortality [1]. Compared to non-resistant *Staphylococcus aureus* infections, the mortality rate of MRSA infections increases by 64% [2]. Vancomycin is a last-resort treatment for MRSA infections. However, strains that are less susceptible to vancomycin are emerging in clinics [3,4]. As a result, new antibiotics to treat MRSA infections are desperately needed. In 2017, the development of new antibiotics for the treatment of MRSA infections is listed as a high urgency level by the WHO (World Health Organization) [5].

The marine environment is one of the most complex atmospheres on the earth, due to the huge variations in predation, temperature, pressure, light, and nutrient circumstances, etc. [6]. The organisms that thrive in marine environments could produce extremely diverse and complicated functional secondary metabolites that differ from those observed in terrestrial environments [6–8]. In recent decades, an increasing number of bioactive marine natural products (MNPs) have piqued the interest of chemists and pharmacologists for their medicinal values [9,10], such as the earliest marine sponge-derived anticancer drug cytarabine (Cytosar-U®), the marine sponge-derived antiviral drug vidarabine (Arasena A®), the mollusk-derived ziconotide (Prialt®) for the treatment of neuropathic pain, the famous sponge-derived anticancer drugs trabectedin (Yondelis®) and eribulin mesylate

(Halaven®), and the marine cyanobacterium-derived anticancer drug disitamab vedotin (Aidixi™) and tisotumab vedotintftv (TIVDAK™), etc. [11–17].

Marine fungi have been shown to produce a variety of secondary metabolites with a variety of structures and bioactivities [18], including antibacterial, antiviral, anticancer, and anti-inflammatory characteristics, and have already provided a number of promising leads against MRSA [19,20]. Pestalone is a well-known anti-MRSA compound that was discovered by Fenical and colleagues, after co-culturing a fungus of the genus *Pestalotia* with a unicellular marine bacteria (strain CNJ-328) [21,22].

In our search for new anti-MRSA agents from marine-derived fungi, the EtOAc extract of the fungus *Aspergillus fumigatus* H22 was found to show strong anti-MRSA activity by in vitro anti-MRSA assay. A chemical investigation on its extract led to the identification of 45 secondary metabolites (Figure 1), including six new novel compounds, including fumindoline A–C (**1**–**3**), 12β,13β-hydroxy-asperfumigatin (**4**), 2-*epi*-tryptoquivaline F (**17**), and penibenzophenone E (**37**). The isolation and structure characterization of the new compounds, as well as the antibacterial activity of all the compounds, are described in this work.

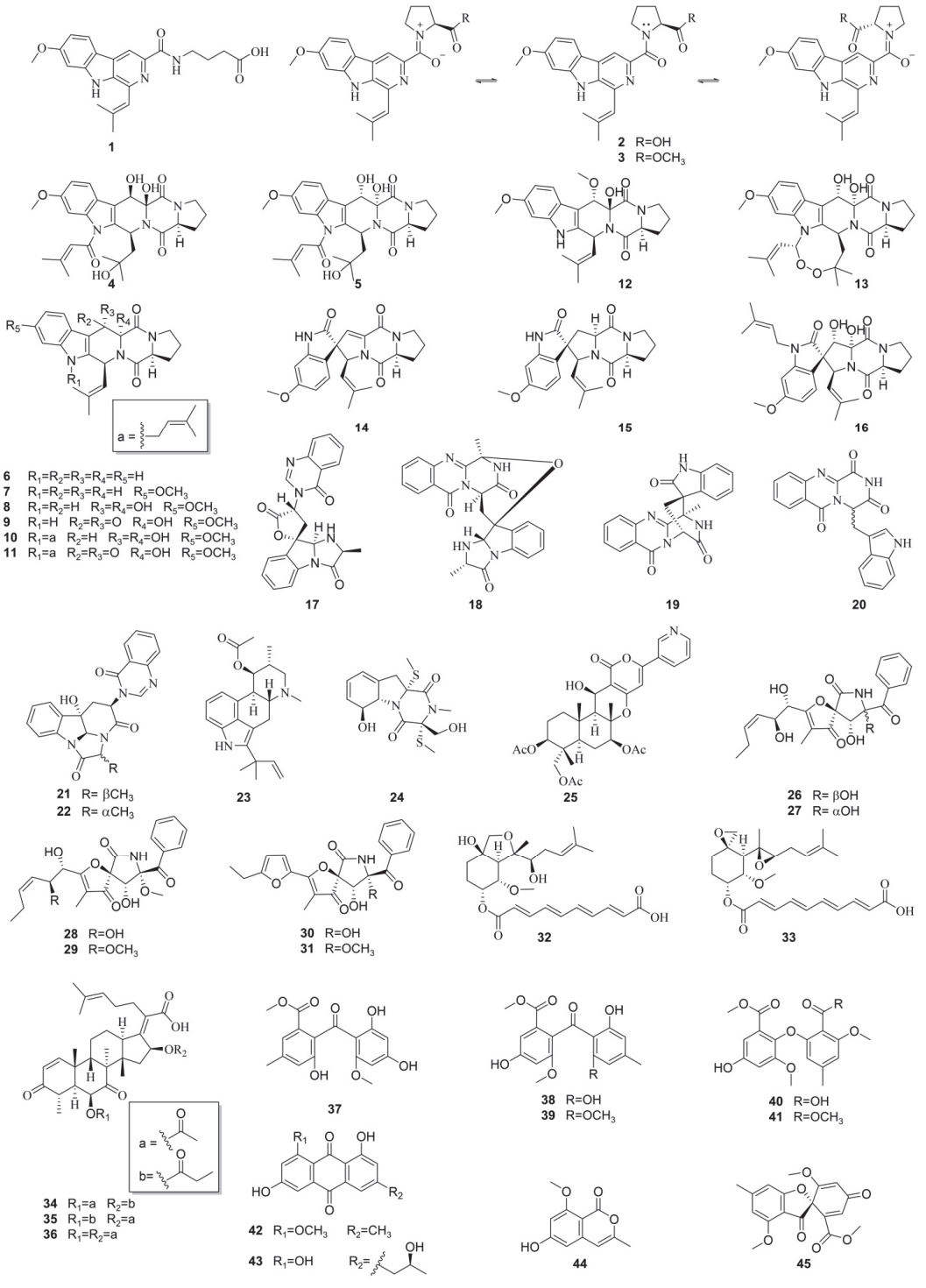

Figure 1. Structures of compounds **1**–**45**.

2. Results

Structure Elucidation of the Isolated Compounds

Fumindoline A (**1**) was obtained as a chartreuse powder and had the molecular formula of $C_{21}H_{23}N_3O_4$, based on HRESIMS data (Figure S8), corresponding to 12 indices of hydrogen deficiency. This molecular formula was corroborated by ^{1}H NMR and ^{13}C NMR spectroscopic data. The ^{1}H NMR data (Table 1) showed characteristic signals for a 1,2,4-trisubstituted benzene ring (δ 8.21 (d, J = 8.7 Hz), 6.91 (dd, J = 8.7 and 2.3 Hz), and 7.05 (d, J = 2.3 Hz)), two singlet olefinic protons (δ_H 8.59 (s) and 6.79 (s)), three singlet methyl groups (δ_H 2.08 (s), 2.17 (s), and 3.89 (s)), and two exchangeable (δ 8.42 (br. s) and 11.85 (br. s)). The ^{13}C NMR and HSQC data of **1** revealed the presence of twenty-one carbon resonances, including three methyls (δ_C 20.6, 27.3, and 55.4), three methylenes (δ_C 24.9, 31.2, and 38.3), five sp^2 methines (δ_C 94.8, 110.2, 111.1, 118.5, and 123.1), and ten nonprotonated carbons (eight sp^2 carbons at δ_C 115.0, 128.9, 135.1, 138.7, 142.4, 142.8, 158.3, and 160.7; one amide carbonyl carbon at δ_C 164.7, and one carboxyl carbon at δ_C 174.2).

Table 1. ^{1}H (500 MHz) and ^{13}C NMR (125 MHz) data of compounds **1**–**3** in DMSO-d_6.

Positions	**1**		**2a**		**2b**		**3a**		**3b**	
	δ_C	δ_H, Mult., (J in Hz)	δ_C	δ_H, Mult., (J in Hz)	δ_C	δ_H, Mult., (J in Hz)	δ_C	δ_H, Mult., (J in Hz)	δ_C	δ_H, Mult., (J in Hz)
1		11.85 br. s		11.83 br. s		11.64 br. s		11.92 br. s		11.60 br. s
2	135.1		134.4		134.2		134.3		134.3	
3	142.4		142.5		141.9		143.4		141.4	
5	158.3		158.2		159.7		158.4		158.1	
6	111.1	8.59 s	113.4	8.41 s	113.3	8.37 s	113.6	8.47 s	113.5	8.45 s
7	128.9		129.0		128.7		129.1		128.7	
8	115.0		114.8		114.9		114.8		114.9	
9	123.1	8.21 d (8.7)	123.2	8.22 d (8.7)	123.1	8.18 d (8.7)	123.4	8.25 d (8.7)	123.1	8.19 d (8.7)
10	110.2	6.91 dd (8.7, 2.3)	110.2	6.91 dd (8.7, 2.2)	110.0	6.89 dd (8.7, 2.2)	110.5	6.93 dd (8.7, 2.2)	110.0	6.89 dd (8.7, 2.2)
11	160.7		160.6		160.8		161.0		160.7	
12	94.8	7.05 d (2.3)	94.7	7.05 d (2.2)	94.7	7.04 d (2.2)	94.7	7.06 d (2.2)	94.8	7.04 d (2.2)
13	142.8		142.9		142.8		143.2		142.8	
14	164.7		166.0		166.6		165.5		165.8	
15		8.42 br. s								
16	38.3	3.39 q (7.4)	49.6	3.96 m 3.88 m	47.5	3.67 m	49.6	3.98 m 3.91 m	47.9	3.70 m
17	24.9	1.80 p (7.4)	25.2	1.94 m 1.90 m	21.9	1.92 m 1.82 m	25.2	1.96 m 1.93 m	21.8	1.92 m 1.83 m
18	31.2	2.30 t (7.4)	28.6	2.26 m 1.89 m	31.2	2.29 m 2.02 m	28.6	2.28 m 1.91 m	31.3	2.29 m 1.98 m
19	174.2		59.8	4.48 dd (8.8, 4.4)	60.4	5.30 dd (8.5, 3.6)	59.7	4.57 dd (8.6, 4.0)	60.8	5.18 dd (8.6, 4.5)
20	118.5	6.79 s	173.5		173.8		172.5		172.9	
21	138.7		118.5	6.76 s	119.0	6.66 s	118.0	6.75 s	119.5	6.59 s
22	27.3	2.08 s	138.1		138.0		138.1		138	
23	20.6	2.17 s	27.1	2.07 s	26.9	2.04 s	27.0	2.07 s	26.5	2.04 s
24	55.4	3.89 s	20.4	2.13 s	20.2	2.01 s	20.4	2.10 s	20.1	1.90 s
25			55.4	3.89 s	55.4	3.88 s	55.5	3.89 s	55.4	3.88 s
26							51.8	3.68 s	51.6	3.45 s

"m" means multiplet or overlapped with other signals.

The planar structure of **1** was defined by the 2D NMR spectra, particularly the ^{1}H–^{1}H COSY and HMBC data (Figures S5 and S7). The HMBC correlations from H-9 to C-8, C-11, C-12, and C-13, from H-10 to C-8, and C-11, and from H-12 to C-8, C-10, C-11, and C-13, together with the ^{1}H–^{1}H COSY correlations of H-9/H-10/H-12, which indicated a 1,2,4-trisubstituted benzene. The ^{1}H–^{1}H COSY correlations of *N*H-15/H_2-16/H_2-17/H_2-18, as well as the HMBC correlations from H_2-16 to C-14, C17, and C18, from H_2-17 to

C-16, C-18, and C-19, from H_2-18 to C-16, C-17, and C-19, led to the identification of the γ-aminobutyric acid residue. The HMBC correlations from H-6 to C-2, C-7, C-8, and C-14, H-9 to C-7, and H_2-16 to C-14, as well as the chemical shifts of C-2 (δ 135.1), C-3 (δ 142.4), C-5 (δ 158.3), C-6 (δ 111.1), and C-14 (δ 164.7), supported a 2-pyridinecarboxylic acid moiety that was connected with a γ-aminobutyric acid moiety through C-14 and linked with a 1,2,4-trisubstituted benzene moiety through C-7, and completed the assignment of the moiety. The HMBC correlations from H-20 to C-2, C-3, and C-21, together with the ^{1}H–^{1}H COSY correlations of H-20/H_3-22/H_3-23, suggested that the isobutenyl group was located at C-3 of the 2-pyridinecarboxylic acid moiety. The key HMBC correlations from H_3-24 to C-11 indicated that the methoxy group was located at C-11. Furthermore, these data accounted for 11 of the 12 degrees of unsaturation, implying the presence of an additional cycle, attributed to the *N*H bridging between C-2 and C-13 to establish the indole-pyridinecarboxylic acid skeleton (Figure 2). Therefore, the 2D structure of **1** was determined as shown below.

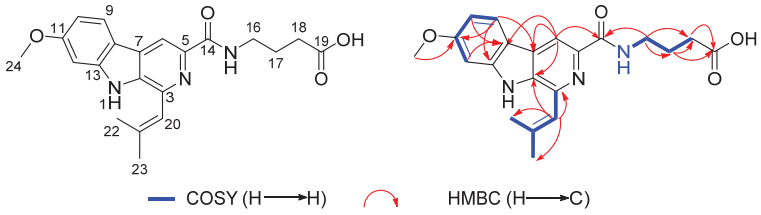

Figure 2. Key ^{1}H–^{1}H COSY and HMBC correlations of **1**.

Fumindoline B (**2**) was obtained as a chartreuse powder. Its molecular formula, $C_{22}H_{23}N_3O_4$, with 14 degrees of unsaturation, was established on the basis of the HRESIMS data (Figure S15). The UV spectrum showed absorptions at 282 nm and 343 nm, which were similar to those of **1**, indicating that **2** might have the same conjugation system as **1**. The IR spectrum indicated the presence of a secondary amine *N*-H signal (2980 cm^{-1}) and an amide carbonyl signal (1628 cm^{-1}). The ^{1}H NMR and ^{13}C NMR spectra indicated the presence of two sets of very similar signals, with the same number of carbons (Figures S9 and S10). The spectra of the two sets of signals are well resolved in pairs at 313K and 298K in DMSO-d_6, indicating the presence of two relatively stable isomers. From the integrals of the completely resolved signals, a ratio of 1:0.7 was calculated for the two stable isomers. To be better distinguished, we assigned the major isomer as **2a** and the minor one as **2b**, respectively (Figure 3).

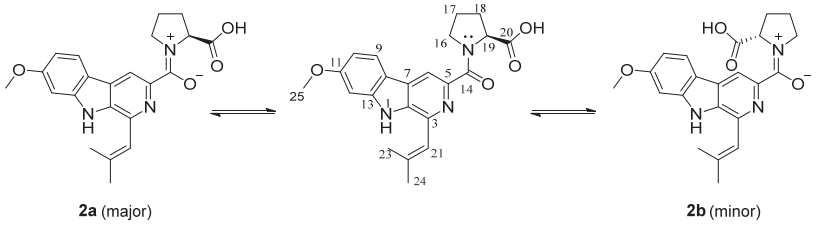

Figure 3. Scheme of the resonance structure of **2** and the chemical equilibrium between **2a** and **2b**.

The ^{1}H NMR and ^{13}C NMR spectra data of **2** showed close similarity to those of **1**, with the biggest difference in the methine (CH-19). A detailed analysis of the 2D NMR data, including HSQC, HMBC, and ^{1}H–^{1}H COSY spectra, revealed that **2** contained the same indole-pyridinecarboxylic acid skeleton as that of **1** (Figures 4 and S11–S13). The HMBC correlations from H_2-16 to C-17 and C-18, H_2-17 to C-16, C-18, and C-19, H_2-18 to C-17, C-19, and C-20, and the ^{1}H–^{1}H COSY correlations of H_2-16/H_2-17/H_2-18/H-19, together with the molecular formula, indicated the presence of a proline moiety, and this conclusion

was also confirmed by the 14 degrees of unsaturation and the chemical shifts of C-16 (δ_C 49.6 (**2a**); δ_C 47.5 (**2b**)) and C-19 (δ_C 59.8 (**2a**); δ_C 60.4 (**2b**)).

The *E*/*Z* isomer exists in the tertiary amide. In the solution at room temperature, the slow rotation of the C–*N* bond in NMR makes it possess the characteristics of a partial double bond [23]. A comparison of the ^{1}H NMR signals and ^{13}C NMR signals of **2a** and **2b** revealed differences in the proline moiety, including variations in the H-19 (δ_H 4.48 (**2a**); δ_H 5.3 (**2b**)), C-16 (δ_C 49.6 (**2a**); δ_C 47.5 (**2b**)), C-17 (δ_C 25.2 (**2a**); δ_C 21.9 (**2b**)), and C-18 (δ_C 28.6 (**2a**); δ_C 31.2 (**2b**)). As shown in Figure 4, strong NOE effects between H-6 and H-16 for **2a** and between H-6 and H-19 for **2b** were observed in the ROSEY spectrum (Figure S14).

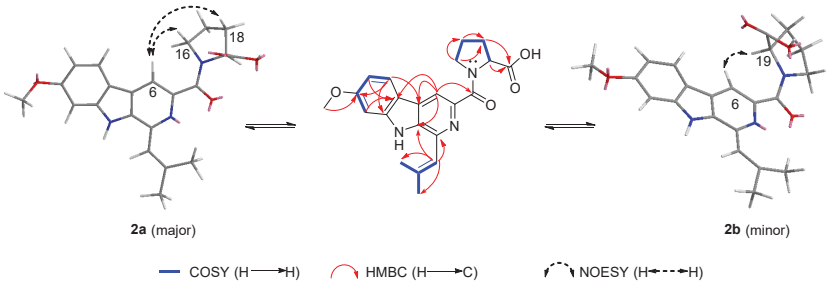

Figure 4. Key ^{1}H-^{1}H COSY, HMBC, and ROESY correlations of **2a** and **2b**.

The absolute configuration of the amino acids from compound **2** was determined by the advanced Marfey's method [24]. The mixture obtained after hydrolyzing compound **2** and further derivatization with L-FDAA was analyzed by HPLC-DAD. The HPLC analyses of the mixture of hydrolysates and appropriate amino acid standards confirmed the L configurations for proline in **2** (Figure 5). Consequently, the absolute configuration of **2** was elucidated to be 19*S*.

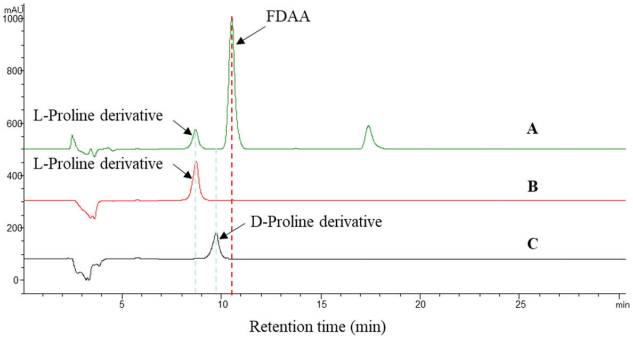

Figure 5. Advanced Marfey's analysis of compound **2**. (**A**): The FDAA derivatives of the hydrolysate of **2**. (**B**,**C**): The retention times for the FDAA derivatives of L-proline and D-proline. The derivatives of the acid hydrolysate and the standard amino acids were subjected to RP HPLC analysis (Kromasil C18 column; 5 μM, 4.6 × 250 mm; 1.0 mL/min; UV detection at 340 nm) with a linear gradient of acetonitrile (30–40%) in water (TFA, 0.01%) over 30 min.

Fumindoline C (**3**) was obtained as a chartreuse powder. The molecular formula of **3** was established to be $C_{23}H_{25}N_3O_4$ from its HREIMS data (Figure S22). The ^{1}H and ^{13}C NMR spectra of **3** were similar to those of **2**, possessing two sets of signals (Figures S16 and S17), except for the presence of an additional methoxyl group. The substitution of the methoxyl group was further confirmed by the HMBC correlations from H_3-26 to C-20. A further comprehensive analysis of its ^{1}H–^{1}H COSY, HSQC, and HMBC spectra assigned the planar structure of **3** (Figures S18–S20). The relative configuration of **3** was determined to be

the same as that of **2** by their similar structure and ROESY data (Figures S14 and S21). Accordingly, **3** was determined to be a methyl ester of **2**.

12β,13β-hydroxy-asperfumigatin (**4**) was obtained as a white amorphous solid. Its molecular formula was determined as $C_{27}H_{33}N_3O_7$ by HRESIMS data (Figure S31). The ^{1}H NMR spectrum of **4** (Figure S25) displayed four singlet methyl groups (δ_H 1.17, 1.25, 2.11, and 2.21), one methoxyl group (δ_H 3.85) and four olefinic/aromatic protons (δ_H 6.40, 6.90, 7.27, and 7.45). The ^{13}C-NMR spectrum (Figure S26) exhibited 27 carbon resonances accounted for the functional groups described above and three amide carbonyl carbons (δ_C 164.7, 165.5, and 165.9). A comprehensive analysis of its 2D NMR spectra, including ^{1}H-^{1}H COSY, HSQC, and HMBC experiments, confirmed the planar structure of **4** (Table 2, Figures S27–S29), revealing the presence of the indole moiety and the diketopiperazine moiety in **4** (Figure 6). The planar structure of **4** was determined to be the same as that of asperfumigatin (**5**), by detailed interpretation of the 2D NMR spectra and NMR data comparison between **4** and **5**. Considering the same biosynthesis origin, compound **4** was deduced to share the same absolute configuration at C-3 and C-6 as those of **5**–**13**.

Table 2. ^{1}H (500 MHz) and ^{13}C NMR (125 MHz) data for **4** in chloroform-*d*.

Positions	δ_C	δ_H, Mult., (*J* in Hz)	Positions	δ_C	δ_H, Mult., (*J* in Hz)
2	137.0		17	111.2	6.90 dd (8.6, 2.2)
3	43.3	6.37 dd (9.5, 1.2)	18	157.7	
5	164.7		19	100.8	7.27 d (2.2)
6	59.8	4.32 dd (10.8, 6.0)	20	136.1	
7	29.6	2.51 m	21	39.5	2.29 dd (14.0, 9.5)
		1.95 m			2.14 dd (14.0, 1.2)
8	22.0	2.08 m	22	74.6	
		1.98 m	23	29.3	1.25 s
9	45.7	3.76 m	24	32.2	1.17 s
		3.65 m	25	165.5	
11	165.9		26	119.8	6.40 br. s
12	86.2		27	158.2	
13	68.4	5.13 s	28	27.4	2.11 s
14	114.3		29	21.2	2.21 s
15	122.3		18-OCH_3	55.9	3.85 s
16	119.4	7.45 d (8.6)			

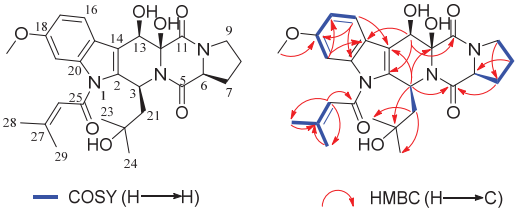

Figure 6. Key ^{1}H-^{1}H COSY, and HMBC correlations of **4**.

Owing to a lack of sufficient ROESY correlations, the relative configurations of C-12 and C-13 were not determined (Figure S30). The relative configurations of **4** were determined by the DP4+ probability, based on a theoretical NMR calculation that has been proven to be a very powerful tool in natural product structure elucidation [25,26]. The NMR shifts of eight possible relative orientation isomers were calculated with the GIAO method at the MPW1PW91/6-31+G(d,p), and the DP4+ probabilities of each configuration were evaluated based on Boltzmann-averaged theoretical NMR shielding tensors, which provided a 91.55% confidence for the relative configuration 3*S**, 6*S**, 12*S**, 13*R** (Tables S1 and S2).

To determine the absolute configurations of **4**, a ECD calculation method was applied. The two configurations (3*S*, 6*S*, 12*S*, 13*R*)-**4** and (3*R*, 6*R*, 12*R*, 13*S*)-**4** were calculated using

time-dependent density functional theory (TDDFT) at PBE1PBE/6-311 G* level, with the PCM model in methanol, and corrected with a 2 nm blue shift according to UV data. A comparison of the experimental ECD spectrum of **4** and the calculated ECD spectra of (3*S*, 6*S*, 12*S*, 13*R*)-**4** and (3*R*, 6*R*, 12*R*, 13*S*)-**4** showed that the experimental ECD spectrum of **4** is consistent with the calculated ECD spectrum of (3*S*, 6*S*, 12*S*, and 13*R*)-**4** (Figure 7). Thus, the absolute configuration of **4** was assigned as 3*S*, 6*S*, 12*S*, and 13*R*, and named as 12*β*,13*β*-hydroxy-asperfumigatin. The only difference between compound **4** and compound **5** is the orientation of the two hydroxyl groups (12-OH, 13-OH).

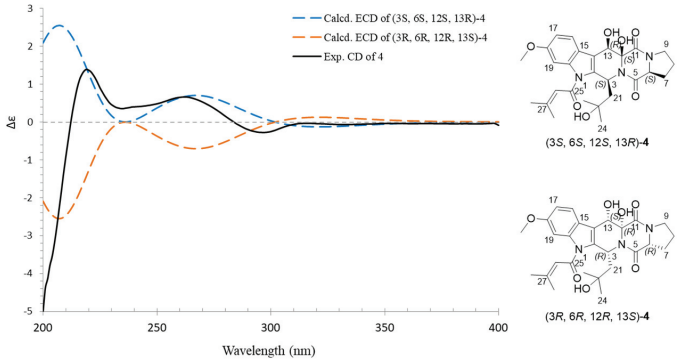

Figure 7. Experimental ECD spectra of compound **4** and the calculated ECD spectra of (3*S*, 6*S*, 12*S*, 13*R*)-**4** and (3*R*, 6*R*, 12*R*, 13*S*)-**4**.

2-*epi*-tryptoquivaline F (**17**), which was isolated as a white amorphous solid, exhibited the $[M + H]^+$ peak at *m*/*z* 403.1399 (HRESIMS), corresponding to $C_{22}H_{18}N_4O_4$, as well as sixteen degrees of unsaturations (Figure S37). The ^{1}H NMR, ^{13}C NMR and HSQC spectra (Table 3, Figures S32–S34) of **17** revealed the presence of two 1, 2-disubstituted benzene rings (δ_H/δ_C 7.31 (d, *J* = 7.5 Hz)/124.4, 7.22 (dd, *J* = 8.0 and 7.5 Hz)/125.8, 7.43 (dd, *J* = 8.0 and 7.5 Hz)/131.3, 7.65 (d, *J* = 8.0 Hz)/115.8; δ_H/δ_C 8.29 (d, *J* = 8.1 Hz)/126.8, 7.58 (dd, *J* = 8.1 and 7.5 Hz)/128.2, 7.85 (dd, *J* = 8.1 and 7.5 Hz)/135.4, 7.78 (d, *J* = 8.1 Hz)/128.0), one methyl (δ_H/δ_C 1.28 (3H, d, *J* = 6.5 Hz)/17.9), one methylene (δ_H 2.61 (dd, *J* = 13.4 and 10.5 Hz), 3.68 (dd, *J* = 13.4 and 4.3 Hz), δ_C 33.4), four nitrogenated methines (δ_H/δ_C 4.26 (d, *J* = 6.5 Hz)/58.5, 5.03 (dd, *J* = 4.3 and 10.5 Hz)/58.3, 5.82 (s)/82.6, 8.11 (s)/145.6), eight quaternary carbons including three carbonyls (δ_C 172.4, 170.9, and 161.0), four aromatic or olefinic carbon atoms (δ_C 121.9, 134.4, 138.9, and 148.1), and one oxygenated one (δ_C 91.3). The NMR data of compound **17** were similar to those of tryptoquivaline F [27], indicating the presence of one 6-5-5 gem-methyl imidazoindolone ring and one quinazoline-4-one moiety.

Table 3. ^{1}H (500 MHz) and ^{13}C NMR (125 MHz) data of compound **17** in chloroform-*d*.

Positions	δ_C	δ_H, Mult., (*J* in Hz)	Positions	δ_C, Type	δ_H, Mult., (*J* in Hz)
2	82.6	5.82 s	14	172.4	
3	91.3		15	58.5	4.26 q (6.5)
4	134.4		18	161.0	
5	124.4	7.31 d (7.5)	19	121.9	
6	125.8	7.22 dd (8.0, 7.5)	20	126.8	8.29 d (8.1)
7	131.3	7.43 dd (8.0, 7.5)	21	128.2	7.58 dd (8.1, 7.5)
8	115.8	7.65 d (8.0)	22	135.4	7.85 dd (8.1, 7.5)
9	138.9		23	128.0	7.78 d (8.1)
11	170.9		24	148.1	
12	58.3	5.03 dd (10.5, 4.3)	26	145.6	8.11 s
13	33.4	3.68 dd (13.4, 4.3) 2.61 dd (13.4, 10.5)	27	17.9	1.28 d (6.5)

The partial relative configuration of **17** was confirmed by a ROESY experiment (Figure S36). The ROESY correlations of H-2 (δ_H 5.82, s) with H-15 (δ_H 4.26, q, J = 6.5 Hz) indicated that H-2 and H-15 were on the same face, while H_3-27 (δ_H 1.28, d, J = 6.5 Hz) were on the opposite face (Figure 8). The relative configurations of C-2 and C-15 were assigned as 2*S* and 15*S*. However, owing to a lack of sufficient ROESY correlations, neither the orientation of C-3 nor C-12 could be determined.

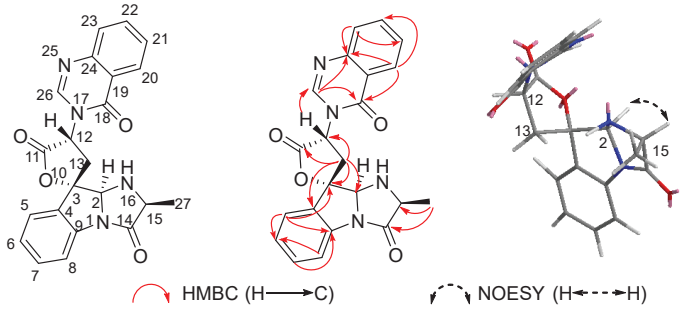

Figure 8. Key HMBC and NOESY correlations of compound **17**.

Similar to compound **4**, the NMR shifts of four relative configuration isomers (2*S*, 3*S*, 12*R*, 15*S*; 2*S*, 3*R*, 12*S*, 15*S*; 2*S*, 3*R*, 12*R*, 15*S*; 2*S*, 3*S*, 12*S*, 15*S*) were calculated and the DP4+ probability, based on a theoretical NMR calculation, was applied. The 100% DP4+ probability for **17a** revealed that the relative configuration of **17** was 2*S**, 3*S**, 12*R** and 15*S** (Tables S3 and S4).

The absolute configurations of **17** were deduced by the comparison of the experimental and simulated ECD spectra generated by TDDFT at B3LYP/6-311+G(2d,p) level with the PCM model in methanol and corrected -5 nm according to the UV data. A comparison of the observed ECD spectra for **17,** with the calculated ECD spectra for the (2*S*, 3*S*, 12*R*, 15*S*)-**17** and (2*R*, 3*R*, 12*S*, 15*R*)-**17** enantiomers, is shown in Figure 9. The overall ECD spectra for (2*S*, 3*S*, 12*R*, 15*S*)-**17** are in good accordance with the experimental ECD for **17**. Thus, compound **17** was determined to be 2*S*, 3*S*, 12*R*, and 15*S*. The differences between **17** and tryptoquivaline F are the configuration of C-2. Therefore, compound **17** was identified as 2-*epi*-tryptoquivaline F.

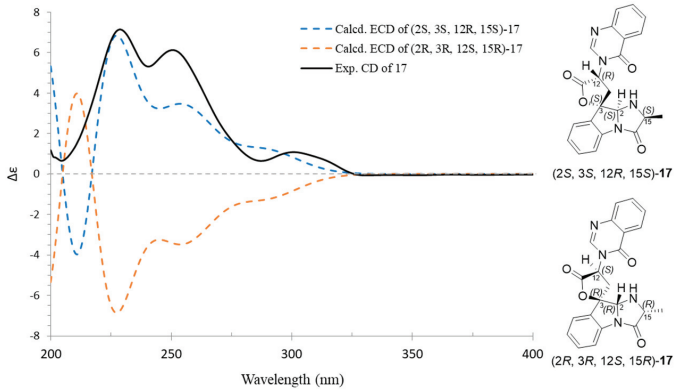

Figure 9. Experimental ECD spectra of compound **17** and the calculated ECD spectra of (2*S*, 3*S*, 12*R*, 15*S*)-**17** and (2*R*, 3*R*, 12*S*, 15*R*)-**17**.

Compound **37** was isolated as a yellowish powder. Its molecular formula was determined as $C_{17}H_{16}O_7$ based on the HRESIMS (Figure S42), implying ten degrees of unsaturation. The ^{1}H NMR spectrum (Figure S38) of **37** showed one hydrogen-bonded phenol

moiety at δ_H 13.55 (s, 6′-OH), four aromatic methine protons at δ_H 7.19 (br. s, H-5), 6.88 (br. s, H-3), 5.90 (d, J = 2.2 Hz, H-5′) and 5.80 (d, J = 2.2 Hz, H-3′) for two sets of AB meta-coupling, two methoxy groups at δ_H 3.64 (s, 8-OMe) and 3.26 (s, 2′-OMe), and a methyl group at δ_H 2.30 (s, 4-Me). A comparison of its ^{1}H NMR and ^{13}C NMR spectra (Table 4) with those of sulochrin (**38**) suggested the same benzophenone skeleton between them [28]. The HMBC correlations from the proton of 6′-OH to C-6′, C-1′ and C-5′ indicate that 6′-OH was located at C-6′. The HMBC correlations from 2′-OCH_3 to C-2′, 4-CH_3 to C-3, C-4, C-5, and 8-CH_3 to C-7 indicate that the two methoxy groups and one methyl group were located at C-2′, C-7 and C-4, respectively. In addition, the HMBC correlations from H-3 to C-1, C-2, C-5, from H-3′ to C-1′, C-2′, C-4′, C-5′, from H-5 to C-1, C-3, C-6 and C-7, and from H-5′ to C-1′, C-3′ and C-6′ confirmed the proposed structure (Figure 10). Therefore, compound **37** was determined as penibenzophenone E.

Table 4. ^{1}H (500 MHz) and ^{13}C NMR (125 MHz) data of compound **37** in DMSO-d_6.

Positions	δ_C	δ_H, Mult., (J in Hz)	Positions	δ_C	δ_H, Mult., (J in Hz)
1	127.2		1′	105.9	
2	153.1		2′	163.0	
3	120.1	6.88 s	3′	91.4	5.80 d (2.2)
4	138.1		4′	165.2	
5	120.2	7.19 s	5′	95.5	5.90 d (2.2)
6	130.3		6′	166.0	
7	166.0		4-CH_3	20.8	2.30 s
8	51.9	3.64 s	2′-OCH_3	55.7	3.26 s
9	198.1		6′-OH		13.55 s

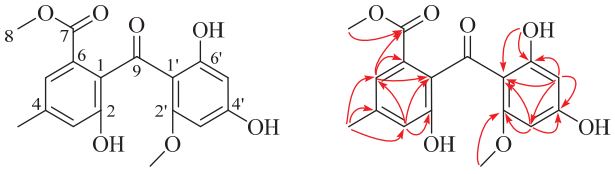

Figure 10. Key HMBC correlations of compound **37**.

Other known compounds were identified as asperfumigatin (**5**) [29], demethoxyfumitremorgin C (**6**) [30], fumitremorgin C (**7**) [30], 12,13-dihydroxyfumitremorgin C (**8**) [31], 12α-hydroxy-13-oxofumitremorgin C (**9**) [32], fumitremorgin B (**10**) [33], 13-oxofumitremorgin B (**11**) [34], cyclotryprostatin B (**12**) [35], verruculogen (**13**) [36], 6-methoxyspirotryprostatin B (**14**) [37], (−)-spirotryprostatin A (**15**) [38], spirotryprostatin C (**16**) [39], fumiquinazoline C (**18**) [40], (+)-alantrypinone (**19**) [41,42], oxoglyantrypine (**20**) [43], (−)-chaetominine (**21**) [44], 11-epi-chaetominine (**22**) [29], fumigaclavine C (**23**) [45,46], bisdethiobis(methylthio)gliotoxin (**24**) [47], pyripyropene A (**25**) [48], pseurotin F1 (**26**) [49], pseurotin F2 (**27**) [49], pseurotin A (**28**) [50], 11-O-methylpseurotin A (**29**) [51], azaspirofuran B (**30**) [52], azaspirofuran A (**31**) [52], fumagiringillin (**32**) [53], fumagillin (**33**) [54], helvolic acid (**34**) [55], 6-O-propionyl-16-O-deacetylhelvolic acid (**35**) [55], 16-O-propionyl-6-O-deacetylhelvolic acid (**36**) [55], sulochrin (**38**) [28], monomethylsulochrin (**39**) [56], 8′-O-methylasterric acid (**40**) [29], dimethyl 2,3′-dimethylosoate (**41**) [56], questin (**42**) [57], (+)-2′*S*-isorhodoptilometrin (**43**) [58], 6-hydroxy-8-methoxy-3-methylisocoumarin (**44**) [59], and trypacidin (**45**) [60], based on the spectroscopic analyses and in comparison with the literature data.

The antibacterial activities of the isolated compounds were determined against methicillin-resistant *Staphylococcus aureus* (MRSA) (clinical isolate strain), vancomycin-resistant enterococci *E. faecalis* (VRE), *Candida albicans* SC5314, *Mycobacterium bovis* ATCC35743 constitutive GFP expression (pUV3583c-GFP), and *Escherichia coli* O57:H7, within 100 µM. The results showed that nearly half of the compounds exhibit antibacterial activity (Table 5), especially compounds **5**, **8**, **10**, **11**, **16**, **21**, **23**, **29**–**38**, and **41** exhibited antimicrobial activities against

MRSA, with minimum inhibitory concentration (MIC) values ranging from 1.25 to 25 μM. Furthermore, compound **8** also exhibited strong activity against *M. bovis* with a MIC of 25 μM, compound **10** showed moderate activity against *C. albicans* with a MIC of 50 μM. Moreover, compound **13** inhibited the egg hatching of *Caenorhabditis elegans* with a IC_{50} of 2.5 μM.

Table 5. Antibacterial assay results of monomeric compounds.

MIC (μM)			
Compound	**MRSA [a]**	**Compound**	**MRSA [a]**
5	5.00	**31**	5.00
8	2.50	**32**	25.0
10	20.0	**33**	2.50
11	1.25	**34**	1.25
16	10.00	**35**	1.25
21	25.00	**36**	1.25
23	12.50	**37**	1.25
29	10.00	**38**	1.25
30	5.00	**41**	5.00
Positive control	Vancomycin (1.00)		

[a] MRSA: methicillin-resistant *Staphylococcus aureus*.

3. Discussion

The marine environmental stress conditions induce many faunae and symbiont microorganisms to synthesize and release secondary metabolites of unique structures and interesting biological activities [61]. These bioactive compounds can serve as an important source for drug discovery. Marine-derived fungi are important sources for the discovery of new antibacterial natural products. Wang et al. isolated the *Chaetomium* sp. strain NA-S01-R1 from a deep-sea (4050 m) fungus that produced novel chlorinated azaphilone polyketides with antibacterial activity against MRSA [62]. The *Emericellopsis minima* strain A11, isolated from Talcahuano Bay (Chile), produced an antibiotic called emerimicin IV, with moderate activity against clinical isolates of MDR vancomycin-resistant strains of *E. faecalis* and MRSA with MIC of 12.5 μg/mL and 100 μg/mL, respectively [63].

A. fumigatus belongs to the filamentous fungi family that is widely distributed in all environments and can cause many diseases and life-threatening conditions in immunocompromised patients [64]. *A. fumigatus* can produce a wide array of secondary metabolites due to its remarkable adaptability to different environmental conditions, such as fumitremorgins, fumagillins, pseurotins, fumigaclavines, gliotoxins, and helvolic acid derivatives.

Inspired by chemical ecology, we found a marine fungus *A. fumigatus* H22 with strong antibacterial activities from the marine fungi library. Through in-depth chemical mining, we found 45 compounds, including 6 new compounds, from the culture of this fungus. A evaluation of biological activity showed that nearly half of the compounds exhibit antimicrobial activity. Fumitremorgins derivatives (**4**-**11**) have very similar structures, but only a few have strong anti-MRSA activity. Compounds **5**, **8** and **11** with strong anti-MRSA activity contain hydroxyl group at C-13, while compounds **6** and **7** without anti-MRSA activity have no hydroxyl group at C-13. In addition, compounds **4** and **5** have the same planar structure, but the 13-OH of compound **4** without anti MRSA activity was α-oriented, while compound **5** and other strongly active compounds were *β*-oriented. Therefore, it is preliminarily speculated that there is a certain correlation between the substituents and stereoconfiguration in C-12 and C-13 and their anti MRSA activity. Fumitremorgin B (**10**) was reported with antifungal activity against a variety of phytopathogenic fungi, but it showed weak activity against vancomycin-resistant *E. faecalis* (VRE), *M. bovis*, and *E. coli* in our in vitro assay, which could be involved in fighting against invasion by other pathogens [65].

Pseurotins, with a unique heterospirocyclic furanone-lactam structure, exhibit a broad range of biological activities. In addition to antifungal and antibiotic activities [66,67],

pseurotins were also shown to regulate enzymes of cellular metabolism [68], to possess anti-angiogenic activity, to modulate cell differentiation [69], and to inhibit endothelial cell migration [70–72]. Fumagillin (**33**) have been demonstrated to have antitumor, antibacterial and antiparasitic effects [73]. Previous studies revealed that helvolic acid (**34**) exhibited in vitro antimalarial activity against multidrug resistant *Plasmodium falciparum* [74], antitrypanosomal activity against *Trypanosoma brucei* [75], and antimycobacterial activity against *M. tuberculosis* H37Ra [76]. Our current research showed the strong activities of oxofumitremorgin B (**11**), helvolic acid (**34**), 6-O-propionyl-16-O-deacetylhelvolic acid (**35**), 16-O-propionyl-6-O-deacetylhelvolic acid (**36**), sulochrin (**38**) and 8′-O-methylasterric acid (**40**) against MRSA, with a MIC of 1.25 μM.

From our current findings, it can be found that *A. fumigatus* from marine sources can produce rich bioactive secondary metabolites, especially in anti-MRSA.

4. Materials and Methods

4.1. General

UV data, optical rotation, and IR data were recorded on Genesys-10S UV–Vis spectrophotometer (Thermo Fisher Scientific, Waltham, MA, USA), MCP 200 automatic polarimeter (Anton Paar, Graz, Austria), and IS5 FT-IR spectrophotometer (Thermo Fisher Scientific, Waltham, MA, USA), respectively. NMR spectral data were obtained with a Bruker AVANCE-500 spectrometer (Bruker, Bremen, Germany) (DMSO-d_6, δ_H 2.50/δ_C 39.52, and $CDCl_3$, δ_H 7.26/δ_C 77.16). High-resolution electrospray ionization mass spectrometry (HRESIMS) data were obtained on an Agilent Accurate-Mass-Q-TOF LC/MS 6520 instrument (Agilent Technologies, Santa Clara, CA, USA). The CD spectra were measured by JASCO J-815 spectropolarimeter (JASCO, Tsukuba, Japan). Silica gel (Qingdao Haiyang Chemical Co., Ltd., Qingdao, China, 200–300 mesh), ODS (octadecylsilyl, 50 μM, YMC Co., Ltd., Kyoto, Japan), and Sephadex LH-20 (GE Healthcare, Uppsala, Sweden) were used for column chromatography. Semi-preparative HPLC was performed on an Agilent 1200 HPLC system equipped with an Agilent DAD UV–vis spectrometric detector (Agilent Technologies Inc., CA, USA), using a reversed-phase Eclipse XDB-C18 column (5 μM, 9.4 × 250 mm; Agilent, MA, USA), with a flow rate of 2.0 mL/min. The biological reagents, chemicals and media were purchased from standard commercial sources, unless stated.

4.2. Fungal Material

The fungus H22 was isolated from middle seawater from the Western Pacific. The sample (1 mL) was diluted with sterile H_2O, 100 μL of which was deposited on a PDA (200 g of potato, 20 g of glucose, 20 g of agar per liter of seawater collected in the Western Pacific) plate containing chloramphenicol (100 μg/mL) and streptomycin (100 μg/mL) as a bacterial inhibitor. A single colony was transferred onto another PDA plate and was identified according to its morphological characteristics and 18*S* rRNA gene sequences. The phylogenetic tree (Figure S1), constructed from the ITS gene sequence, indicated that H22 belonged to the genus of *Aspergillus*, with the highest similarity to *A. fumigatus* (99.86%, accession number NRRL 163 s). In consideration of the morphological features and phylogeny (Figure S2), this fungus was identified as *A. fumigatus*. A reference culture of *A. fumigatus* H22 maintained at −80 °C was deposited in our laboratory.

4.3. Fermentation and Extraction

The isolate was grown for 7 days at 28 °C, on slants of a PDA medium. The spores of the strain on the plate were collected using 0.01% sterile Tween 80 (BTL, Warsaw, Poland) and adjusted to 1×10^6 CFU/mL to make inoculum. A large-scale fermentation was carried out in 50 × 500 mL Fernbach culture flasks, holding 100 g of rice in 110 mL of distilled water (each with 0.5 mL of spore suspension) and incubated for 4 weeks at 28 °C. With the help of ultrasonication, the fermented rice substrates were extracted with ethyl acetate (3 × 5 L), and the organic solvent was filtered and evaporated to dryness under a vacuum to obtain the crude extract (78.0 g).

4.4. Isolation and Characterization Data

The ethyl acetate (EtOAc) fraction was subjected to silica gel column chromatography (CC), eluted with dichloromethane/acetone (D/A, *v*/*v*, 100:0, 100:1, 50:1, 30:1, 25:1, 20:1, 10:1, 5:1) and dichloromethane/methanol (D/M, *v*/*v*, 5:1, 2:1, 0:100) to give 10 fractions (HS.1–HS.10).

HS.3 (4.94 g eluted with D/A, *v*/*v*, 50:1) was purified by RP-HPLC, using 37% acetonitrile in acidic water (0.01% TFA) to obtain compounds **45** (9.0 mg, t_R = 37.5 min), **42** (103.0 mg, t_R = 44.5 min) and **39** (19.2 mg, t_R = 47.6 min).

Fraction HS.4 (5.98 g from D/A, *v*/*v*, 30:1) was separated by ODS, using a gradient from 20% to 100% methanol in water to afford 12 subfractions (HS.4-1–HS.4-12). HS.4-3 (203.0 mg) was further purified using C8-RP-HPLC on a Agilent Eclipse XDB-C8 (5 μM, 250 × 9.4 mm), with a gradient elution from 30% to 40% acetonitrile in 60 min to give compounds **21** (102.1 mg, t_R = 22.5 min), **18** (12.0 mg, t_R = 30.6 min), **17** (7.0 mg, t_R = 39.6 min) and **41** (2.0 mg, t_R = 50.2 min). HS.4-4 (77 mg) was further purified using C8-RP-HPLC with 35% acetonitrile to give compounds **8** (3.5 mg, t_R = 33.6 min), **7** (3.5 mg, t_R = 41.5 min) and **31** (3.0 mg, t_R = 66.2 min). Compounds **13** (79.0 mg, t_R = 17.4 min), **10** (7.0 mg, t_R = 23.6 min) and **33** (5.0 mg, t_R = 25.8 min) were obtained from HS.4-9 (252 mg) by RP-HPLC, using 55% acetonitrile in acidic water.

Fraction HS.5 (5.43 g, from D/A, *v*/*v*, 25:1) was first separated by ODS, using a gradient from 30% to 100% methanol in water to afford HS.5-1–HS.5-11. Subfraction HS.5-4 (30 mg) was purified using RP-HPLC on a Agilent Eclipse XDB-C8 column (5 μM, 250 × 9.4 mm) with 40% acetonitrile in 20 min to give compounds **23** (5.0 mg, t_R = 4.1 min) and **39** (4.2 mg, t_R = 7.5 min). Compound **24** (5.0 mg, t_R = 24.8 min) was obtained from subfraction HS.5-4-5 (32 mg) by RP-HPLC, using 28% acetonitrile in acidic water (0.01% TFA). Compounds **22** (2.2 mg, t_R = 28.1 min) and **21** (3.0 mg, t_R = 29.7 min) were obtained from HS.5-4-8 (144 mg) by RP-HPLC, using 29% acetonitrile in acidic water (0.01% TFA).

Fraction HS.6 (6.72 g, from D/A, *v*/*v*, 20:1) was first separated by ODS, using a gradient from 20% to 100% methanol in water to afford HS.6-1–HS.6-17. HS.6-2 (289 mg) was purified using C8-RP-HPLC eluting with 50% to provide compound **44** (2.0 mg, t_R = 16.3 min). Compounds **37** (3.0 mg, t_R = 19.1 min) and **38** (1.5 mg, t_R = 20.2 min) were obtained from HS.6-4 (326.0 mg) by RP-HPLC, using 45% acetonitrile in acidic water. HS.6-5 (522 mg) was purified using RP-HPLC eluting with 50% acetonitrile to give compounds **15** (9.0 mg, t_R = 10.2 min), **9** (15.0 mg, t_R = 13.2 min), and **12** (100.0 mg, t_R = 14.6 min). Compound **16** (3.0 mg, t_R = 25.2 min) was obtained from subfraction HS.6-9 (17.5mg) by RP-HPLC, using 60% acetonitrile in acidic water. Compounds **33** (19.8 mg, t_R = 10.7 min), **34** (2.0 mg, t_R = 12.3 min) and **35** (2.0 mg, t_R = 13.2 min) were obtained from HS.6-17 (365 mg) by RP-HPLC, using 70% acetonitrile in acidic water.

Fraction HS.7 (10.63 g, D/A, *v*/*v*, 10:1) was first separated by ODS, using a gradient from 35% to 100% methanol in water to afford HS.7-1–HS.7-13. Compounds **40** (6.0 mg) and **29** (2.0 mg) were obtained from HS.7-2 and HS.7-3 by recrystallization in methanol, respectively. Compounds **30** (2.0 mg, t_R = 9.1 min), **20** (2.0 mg, t_R = 11.1 min) and **6** (2.1 mg, t_R = 11.9 min) were obtained from HS.7-4 (11.2 mg) by RP-HPLC, using 65% acetonitrile in acidic water. Compounds **4** (3.2 mg, t_R = 14.9 min) and **5** (2.8 mg, t_R = 16.1 min) were purified from HS.7-7, using RP-HPLC with 50% acetonitrile. HS.7-9 (420.0 mg) was purified using C8-RP-HPLC with 65% methanol to give compounds **43** (2.0 mg, t_R = 12.5 min), **32** (20.2 mg, t_R = 16.2 min) and **19** (37.3 mg, t_R = 18.1 min).

Fraction HS.8 (8.82 g, D/A, *v*/*v*, 5:1) was first separated by ODS, using a gradient from 20% to 100% methanol in water to afford 22 subfractions (HS.8-1–HS.8-22). HS.8-3 (100.0 mg) was further purified on C8-RP-HPLC eluting with 35% acetonitrile in acidic water to give compounds **28** (11.8 mg, t_R = 19.3 min), **27** (3.1 mg, t_R = 22.4 min), and **26** (2.8 mg, t_R = 24.3 min). HS.8-18 (124.0 mg) was purified on a C8-RP-HPLC eluting with a gradient elution from 70% methanol to give compounds **3** (15.0 mg, t_R = 12.5 min), **2** (5.0 mg, t_R = 15.2 min), **11** (20.0 mg, t_R = 18.4 min), **1** (5.0 mg, t_R = 19.2 min) and **25** (8.0 mg, t_R = 22.5 min).

Fumindoline A (**1**). UV (MeOH) λ_{max} (log ε) 286 (1.62), 345 (0.48). ^{1}H NMR and ^{13}C NMR, see Table 1, 2D NMR spectra, see Supplementary Figures S3–S7. Positive HRESIMS: *m/z* 382.1768 $[M + H]^+$ (calcd for $C_{21}H_{24}N_3O_4$, 382.1761, Figure S8).

Fumindoline B (**2**). Chartreuse powder; $(\alpha)_D^{25}$ −34.99 (*c* 0.1, MeOH); UV (MeOH) λ_{max} (log ε) 282 (2.82), 343 (0.82); ^{1}H NMR and ^{13}C NMR, see Table 1, 2D NMR spectra, see Supplementary Figures S9–S14; Positive HRESIMS: *m/z* 394.1765 $[M + H]^+$ (calcd for $C_{22}H_{24}N_3O_4$, 394.1761, Figure S15).

Fumindoline C (**3**). Chartreuse powder; $(\alpha)_D^{25}$ −21.00 (*c* 0.1, MeOH); UV (MeOH) λ_{max} (log ε) 286 (1.62), 345 (0.50); ^{1}H NMR and ^{13}C NMR, see Table 1, 2D NMR spectra, see Supplementary Figures S16–S24; Positive HRESIMS: *m/z* 408.1916 $[M + H]^+$ (calcd for $C_{23}H_{26}N_3O_4$, 408.1918, Figure S22).

12*β*,13*β*-hydroxy-asperfumigatin (**4**). White amorphous solid; $(\alpha)_D^{25}$ +26.00 (*c* 0.1, MeOH); UV (MeOH) λ_{max} (log ε) 222 (1.51), 270 (0.60); ^{1}H NMR and ^{13}C NMR, see Table 2, 2D NMR spectra, see Supplementary Figures S25–S30; Positive HRESIMS: *m/z* 494.2720 $[M + H - H_2O]^+$ (calcd for $C_{27}H_{32}N_3O_6$, 494.2726, Figure S31).

2-*epi*-tryptoquivaline F (**17**). White amorphous solid; $(\alpha)_D^{25}$ +221.96 (*c* 0.1, CH_2Cl_2); UV (CH_2Cl_2) λ_{max} (log ε) 212 (2.21), 233 (1.69); ^{1}H NMR and ^{13}C NMR, see Table 3, 2D NMR spectra, see Supplementary Figures S32–S36; Positive HRESIMS: *m/z* 403.1399 $[M + H]^+$ (calcd for $C_{22}H_{19}N_4O_4$, 403.1401, Figure S37).

Penibenzophenone E (**37**). Yellowish powder; UV (MeOH) λ_{max} (log ε) 205 (3.28), 303 (1.63); ^{1}H NMR and ^{13}C NMR, see Table 4, 2D NMR spectra, see Supplementary Figures S38–S41; Positive HRESIMS: *m/z* 355.0789 $[M + Na]^+$ (calcd for $C_{17}H_{16}O_7Na$, 355.0788, Figure S42).

4.5. Marfey's Analysis of Compound **2**

Compound **2** (2.0 mg) was dissolved in 6 *N* HCl (2.0 mL) and heated at 100 °C for 24 h. The solutions were then evaporated to dryness and placed in a 4 mL reaction vial and treated with a 10 mg/mL solution of FDAA (200 µL) in acetone, followed by 1 M $NaHCO_3$ (40 µL). The reaction mixtures were heated at 45 °C for 90 min, and the reactions were quenched by the addition of HCl (1 *N*, 40 *µ*L). In a similar fashion, the standard L-proline and D-proline were derivatized separately. The derivatives of the acid hydrolysate and the standard amino acids were subjected to RP HPLC analysis (Kromasil C18 column; 5 µM, 4.6 × 250 mm; 1.0 mL/min; UV detection at 340 nm), with a linear gradient of acetonitrile (30–40%) in water (TFA, 0.01%) over 30 min. The retention times for the authentic standards were as follows: L-proline derivative (8.91 min) and D-proline derivative (9.88 min). The absolute configuration of the chiral amino acid in **2** was determined by comparing the retention times.

4.6. Computational Details for NMR and ECD

The GMMX software tool was used to undertake the systematic conformational evaluations for **4** and **17,** utilizing the MMFF94 molecular mechanics force field. Gaussian 16 software was used to further improve the MMFF94 conformers, utilizing the M062X/6-31G(d) basis set level in gas for NMR calculations and B3LYP/6-31+G(d,p) basis set level in methanol, with a PCM model for ECD calculations. The shielding constants were calculated using the GIAO technique in chloroform, using the SMD solvent model and Gaussian function at mPW1PW91/6-31+G(d,p). A previously documented approach was used to calculate the ^{1}H and ^{13}C chemical shifts for the DP4+ probability analysis [77]. ECD spectra were stimulated in methanol with a Gaussian function at the B3LYP/6-311+G(2d,p) level using the PCM model, and 60 NStates were calculated. Boltzmann statistics were used to compute the equilibrium populations of the conformers at 298.15 K, based on their respective free energies (**Δ**G). The Boltzmann weighting of the key conformers was then used to construct the overall ECD spectra. UV correlation was used to correct the systematic mistakes in predicting the wavelength and excited-state energy [78].

4.7. Antimicrobial Assay

An antimicrobial assay was performed according to the Antimicrobial Susceptibility Testing Standards, outlined by the Clinical and Laboratory Standards Institute against MRSA (clinical strain from Chaoyang Hospital, Beijing, China), *Pseudomonas aeruginosa* (ATCC 15692), *Escherichia coli* (O57:H7), *Mycobacterium bovis* (ATCC35743), vancomycin-resistant *Enterococci faecalis* (VRE) (clinical strain from 309 Hospital, Beijing, China), and pathogen fungi *Candida albicans* SC5314. The protocol was performed as previously reported [58,59]. The positive controls were vancomycin against MRSA, *E. faecalis*, ciprofloxacin against *P. aeruginosa* and *E. coli*, amphotericin B for *C. albicans*, and rifampicin for *M. bovis*. All the experiments were performed in triplicate.

5. Conclusions

In summary, we isolated forty-five compounds from *A. fumigatus* H22, including six new compounds **1–4**, **17**, and **37**. The stereochemistry of the new compounds was determined by quantum calculations of NMR, ECD calculations and chemical derivatizations. Bioactivity screening indicated that compounds **5**, **8**, **10**, **11**, **16**, **21**, **23**, **29**–**38**, and **41** exhibited antimicrobial activities against MRSA, with MIC values ranging from 1.25 to 25 μM. Compound **8** also exhibited strong activity against *M. bovis*, with a MIC of 25 μM. To the best of our knowledge, this is the first report for the antimicrobial activities of compounds **5**, **10**, **11**, **16**, **30**, **31**, and **37**. The strains of *A. fumigatus* from ocean environments are a good source of antibacterial natural products, deserving further exploitation.

Supplementary Materials: The following supporting information can be downloaded at: https://www.mdpi.com/article/10.3390/md20050302/s1. Table S1: NMR calculation of **4**; Table S2: sDP4+, uDP4+ and DP4+ probabilities (%) for **4**; Table S3: NMR calculation of **17**; Table S4: sDP4+, uDP4+ and DP4+ probabilities (%) for **17**; Figures S1 and S2: phylogenetic tree and morphology of *A. fumigatus* H22; Figures S3–S8: 1D, 2D NMR, and HRESIMS of **1**; Figures S9–S15: 1D, 2D NMR, and HRESIMS of **2**; Figures S16–S24: 1D, 2D NMR, and HRESIMS of **3**; Figures S25–S31: 1D, 2D NMR, and HRESIMS of **4**; Figures S32–S37: 1D, 2D NMR, and HRESIMS of **17**; Figures S38–S42: 1D, 2D NMR, and HRESIMS of **37**; Figure S43: eight possible stereoisomers of **4** (**4a**–**4h**); Figure S44: four possible stereoisomers of **17** (**17a**–**17d**).

Author Contributions: Conceptualization, R.Z., H.W. and J.H.; methodology, J.H. and B.C.; validation and data curation, R.Z., J.S. and H.D.; formal analysis, R.Z. and J.H.; investigation, J.H. and H.L.; resources, H.D.; writing—original draft preparation, R.Z. and J.H.; writing—review and editing, J.H. and H.L.; supervision and project administration, J.H. and H.L.; funding acquisition, H.L. All authors have read and agreed to the published version of the manuscript.

Funding: This project was supported by the National Natural Science Foundation (Grant No. 82073723).

Institutional Review Board Statement: Not applicable.

Informed Consent Statement: Not applicable.

Data Availability Statement: Not applicable.

Conflicts of Interest: The authors declare no conflict of interest.

References

1. Kuok, C.F.; Hoi, S.O.; Hoi, C.F.; Chan, C.H.; Fong, I.H.; Ngok, C.K.; Meng, L.R.; Fong, P. Synergistic antibacterial effects of herbal extracts and antibiotics on methicillin-resistant *Staphylococcus aureus*: A computational and experimental study. *Exp. Biol. Med.* **2017**, *242*, 731–743. [CrossRef] [PubMed]
2. Asghar, M.A.; Yousuf, R.I.; Shoaib, M.H.; Asghar, M.A.; Ansar, S.; Zehravi, M.; Abdul Rehman, A. Synergistic nanocomposites of different antibiotics coupled with green synthesized chitosan-based silver nanoparticles: Characterization, antibacterial, in vivo toxicological and biodistribution studies. *Int. J. Nanomed.* **2020**, *15*, 7841–7859. [CrossRef] [PubMed]
3. Bezar, I.F.; Mashruwala, A.A.; Boyd, J.M.; Stock, A.M. Drug-like fragments inhibit *agr*-mediated virulence expression in *Staphylococcus aureus*. *Sci. Rep.* **2019**, *9*, 6786. [CrossRef]
4. Rodvold, K.A.; McConeghy, K.W. Methicillin-resistant *Staphylococcus aureus* therapy: Past, present, and future. *Clin. Infect. Dis.* **2014**, *58*, S20–S27. [CrossRef] [PubMed]

5. World Health Organization. *Prioritization of Pathogens to Guide Discovery, Research and Development of New Antibiotics for Drug-Resistant Bacterial Infections, Including Tuberculosis*, 9789240026438 (electronic version); World Health Organization: Geneva, Switzerland, 2017.
6. Althagbi, H.I.; Alarif, W.M.; Al-Footy, K.O. Abdel-Lateff, A Marine-derived macrocyclic alkaloids (MDMAS): Chemical and Biological Diversity. *Mar. Drugs* **2020**, *18*, 368. [CrossRef]
7. Pereira, F.; Aires-de-Sousa, J. Computational methodologies in the exploration of marine natural product leads. *Mar. Drugs* **2018**, *16*, 236. [CrossRef]
8. Hagestad, O.C.; Andersen, J.H.; Altermark, B.; Hansen, E.; Rämä, T. Cultivable marine fungi from the arctic archipelago of svalbard and their antibacterial activity. *Mycology* **2020**, *11*, 230–242. [CrossRef]
9. Pereira, R.B.; Andrade, P.B.; Valentao, P. Chemical diversity and biological properties of secondary metabolites from sea hares of *aplysia* genus. *Mar. Drugs* **2016**, *14*, 39. [CrossRef]
10. Sun, L.; Li, D.; Tao, M.; Chen, Y.; Dan, F.; Zhang, W. Scopararanes C-G: New oxygenated pimarane diterpenes from the marine sediment-derived fungus *Eutypella scoparia* FS26. *Mar. Drugs* **2012**, *10*, 539–550. [CrossRef]
11. Choudhary, A.; Naughton, L.M.; Montanchez, I.; Dobson, A.D.W.; Rai, D.K. Current status and future prospects of marine natural products (MNPs) as antimicrobials. *Mar. Drugs* **2017**, *15*, 272. [CrossRef]
12. Blunt, J.W.; Carroll, A.R.; Copp, B.R.; Davis, R.A.; Keyzers, R.A.; Prinsep, M.R. Marine natural products. *Nat. Prod. Rep.* **2018**, *35*, 8–53. [CrossRef]
13. Blunt, J.W.; Copp, B.R.; Keyzers, R.A.; Munro, M.H.; Prinsep, M.R. Marine natural products. *Nat. Prod. Rep.* **2016**, *33*, 382–431. [CrossRef] [PubMed]
14. Blunt, J.W.; Copp, B.R.; Keyzers, R.A.; Munro, M.H.G.; Prinsep, M.R. Marine natural products. *Nat. Prod. Rep.* **2017**, *34*, 235–294. [CrossRef] [PubMed]
15. Hanif, N.; Murni, A.; Tanaka, C.; Tanaka, J. Marine natural products from indonesian waters. *Mar. Drugs* **2019**, *17*, 364. [CrossRef] [PubMed]
16. Mayer, A.M.; Rodriguez, A.D.; Taglialatela-Scafati, O.; Fusetani, N. Marine pharmacology in 2016–2017: Marine compounds with antibacterial, antidiabetic, antifungal, anti-inflammatory, antiprotozoal, antituberculosis and antiviral activities; affecting the immune and nervous systems, and other miscellaneous mechanisms of action. *Mar. Drugs* **2021**, *19*, 49.
17. Wahab, H.A.; Pham, N.B.; Muhammad, T.S.; Hooper, J.N.; Quinn, R.J. Merosesquiterpene congeners from the australian sponge *Hyrtios digitatus* as potential drug leads for atherosclerosis disease. *Mar. Drugs* **2017**, *15*, 6. [CrossRef] [PubMed]
18. Wong Chin, J.M.; Puchooa, D.; Bahorun, T.; Jeewon, R. Antimicrobial properties of marine fungi from sponges and brown algae of Mauritius. *Mycology* **2021**, *12*, 231–244. [CrossRef] [PubMed]
19. Wu, B.; Wiese, J.; Labes, A.; Kramer, A.; Schmaljohann, R.; Imhoff, J.F. Lindgomycin, an unusual antibiotic polyketide from a marine fungus of the lindgomycetaceae. *Mar. Drugs* **2015**, *13*, 4617–4632. [CrossRef]
20. Niu, S.; Liu, D.; Hu, X.; Proksch, P.; Shao, Z.; Lin, W. Spiromastixones A-O, antibacterial chlorodepsidones from a deep-sea-derived *Spiromastix* sp. fungus. *J. Nat. Prod.* **2014**, *77*, 1021–1030. [CrossRef]
21. Augner, D.; Krut, O.; Slavov, N.; Gerbino, D.C.; Sahl, H.G.; Benting, J.; Nising, C.F.; Hillebrand, S.; Kronke, M.; Schmalz, H.G. On the antibiotic and antifungal activity of pestalone, pestalachloride A, and structurally related compounds. *J. Nat. Prod.* **2013**, *76*, 1519–1522. [CrossRef]
22. Cueto, M.; Jensen, P.R.; Kauffman, C.; Fenical, W.; Lobkovsky, E.; Clardy, J. Pestalone, a new antibiotic produced by a marine fungus in response to bacterial challenge. *J. Nat. Prod.* **2001**, *64*, 1444–1446. [CrossRef] [PubMed]
23. Xie, X.; Wallwey, C.; Matuschek, M.; Steinbach, K.; Li, S.M. Formyl migration product of chanoclavine-I aldehyde in the presence of the old yellow enzyme FgaOx3 from Aspergillus fumigatus: A NMR structure elucidation. *Magn. Reson. Chem.* **2011**, *49*, 678–681. [CrossRef] [PubMed]
24. Wu, W.; Dai, H.Q.; Bao, L.; Ren, B.A.; Lu, J.C.; Luo, Y.M.; Guo, L.D.; Zhang, L.X.; Liu, H.W. Isolation and structural elucidation of proline-containing cyclopentapeptides from an endolichenic *Xylaria* sp. *J. Nat. Prod.* **2011**, *74*, 1303–1308. [CrossRef] [PubMed]
25. Smith, S.G.; Goodman, J.M. Assigning stereochemistry to single diastereoisomers by GIAO NMR calculation: The DP4 probability. *J. Am. Chem. Soc.* **2010**, *132*, 12946–12959. [CrossRef] [PubMed]
26. Rodriguez, I.; Genta-Jouve, G.; Alfonso, C.; Calabro, K.; Alonso, E.; Sanchez, J.A.; Alfonso, A.; Thomas, O.P.; Botana, L.M. Gambierone, a ladder-shaped polyether from the dinoflagellate *Gambierdiscus belizeanus*. *Org. Lett.* **2015**, *17*, 2392–2395. [CrossRef]
27. Buttachon, S.; Chandrapatya, A.; Manoch, L.; Silva, A.; Gales, L.; Bruyere, C.; Kiss, R.; Kijjoa, A. Sartorymensin, a new indole alkaloid, and new analogues of tryptoquivaline and fiscalins produced by *Neosartorya siamensis* (KUFC 6349). *Tetrahedron* **2012**, *68*, 3253–3262. [CrossRef]
28. Pang, X.; Zhao, J.Y.; Fang, X.M.; Zhang, T.; Zhang, D.W.; Liu, H.Y.; Su, J.; Cen, S.; Yu, L.Y. Metabolites from the plant endophytic fungus *Aspergillus* sp. CPCC 400735 and their anti-hiv activities. *J. Nat. Prod.* **2017**, *80*, 2595–2601. [CrossRef]
29. Xie, F.; Li, X.B.; Zhou, J.C.; Xu, Q.Q.; Wang, X.N.; Yuan, H.Q.; Lou, H.X. Secondary metabolites from *Aspergillus fumigatus*, an endophytic fungus from the liverwort *Heteroscyphus tener* (Steph.) Schiffn. *Chem. Biodivers.* **2015**, *12*, 1954. [CrossRef]
30. Cui, C.B.; Kakeya, H.; Osada, H. Novel mammalian cell cycle inhibitors, tryprostatins A, B and other diketopiperazines produced by *Aspergillus fumigatus*. II. Physico-chemical properties and structures. *J. Antibiot.* **1996**, *49*, 534–540. [CrossRef]
31. Abraham, W.R.; Arfmann, H.A. 12,13-Dihydroxy-Fumitremorgin C from *Aspergillus fumigatus*. *Phytochemistry* **1990**, *29*, 1025–1026. [CrossRef]

32. Yan, W.; Song, H.; Song, F.; Guo, Y.; Wu, C.H.; Her, A.S.; Pu, Y.; Wang, S.; Naowarojna, N.; Weitz, A.; et al. Endoperoxide formation by an alpha-ketoglutarate-dependent mononuclear non-haem iron enzyme. *Nature* **2015**, *527*, 539–543. [CrossRef] [PubMed]
33. Zhou, F.; Zhang, H.C.; Liu, R.; Zhang, D.X. Isolation and biological evaluation of secondary metabolites of the endophytic fungus *Aspergillus fumigatus* from *Astragalus membranaceus*. *Chem. Nat. Compd.* **2013**, *49*, 568–570. [CrossRef]
34. Fujimoto, H.; Fujimaki, T.; Okuyama, E.; Yamazaki, M. Immunosuppressive constituents from an Ascomycete, *Sordaria gondaensis*. *Mycotoxins* **2000**, *50*, 93–99. [CrossRef]
35. Cui, C.B.; Kakeya, H.; Osada, H. Novel mammalian cell cycle inhibitors, cyclotryprostatins A-D, produced by Aspergillus fumigatus, which inhibit mammalian cell cycle at G2/M phase. *Tetrahedron* **1997**, *53*, 59–72. [CrossRef]
36. Yu, F.; Holte, D.; Zoller, J.; Umemiya, S.; Simke, L.R.; Baran, P.S. Total synthesis of verruculogen and fumitremorgin a enabled by ligand-controlled *C*–H borylation. *J. Am. Chem. Soc.* **2015**, *137*, 10160–10163.
37. Zhang, M.; Wang, W.L.; Fang, Y.C.; Zhu, T.J.; Gu, Q.Q.; Zhu, W.M. Cytotoxic alkaloids and antibiotic nordammarane triterpenoids from the marine-derived fungus *Aspergillus sydowi*. *J. Nat. Prod.* **2008**, *71*, 985–989. [CrossRef]
38. Cui, C.B.; Kakeya, H.; Osada, H. Novel mammalian cell cycle inhibitors, spirotryprostatins A and B, produced by *Aspergillus fumigatus*, which inhibit mammalian cell cycle at G2/M phase. *Tetrahedron* **1996**, *52*, 12651–12666. [CrossRef]
39. Wang, F.Z.; Fang, Y.C.; Zhu, T.J.; Zhang, M.; Lin, A.Q.; Gu, Q.Q.; Zhu, W.M. Seven new prenylated indole diketopiperazine alkaloids from holothurian-derived fungus *Aspergillus fumigatus*. *Tetrahedron* **2008**, *64*, 7986–7991. [CrossRef]
40. Takahashi, C.; Matsushita, T.; Doi, M.; Minoura, K.; Shingu, T.; Kumeda, Y.; Numata, A. Fumiquinazolines A-G, novel metabolites of a fungus separated from a *Pseudolabrus* marine fish. *J. Chem. Soc. Perkin Trans. 1* **1995**, *18*, 2345–2353. [CrossRef]
41. Ren-Yi, G.; Lei, X.; Yi, K.; Iii-Ming, C.; Jian-Chun, Q.; Li, L.; Sheng-Xiang, Y.; Li-Chun, Z. Chaetominine, (+)-alantrypinone, questin, isorhodoptilometrin, and 4-hydroxybenzaldehyde produced by the endophytic fungus *Aspergillus* sp. YL-6 inhibit wheat (*Triticum aestivum*) and radish (*Raphanus sativus*) germination. *J. Plant. Interact.* **2015**, *10*, 87–92. [CrossRef]
42. Larsen, T.O.; Frydenvang, K.; Frisvad, J.C.; Christophersen, C. UV-guided isolation of alantrypinone, a novel *Penicillium* alkaloid. *J. Nat. Prod.* **1998**, *61*, 1154–1157. [CrossRef] [PubMed]
43. Peng, J.; Lin, T.; Wang, W.; Xin, Z.; Zhu, T.; Gu, Q.; Li, D. Antiviral alkaloids produced by the mangrove-derived fungus *Cladosporium* sp. PJX-41. *J. Nat. Prod.* **2013**, *76*, 1133–1140. [CrossRef] [PubMed]
44. Jiao, R.H.; Xu, S.; Liu, J.Y.; Ge, H.M.; Ding, H.; Xu, C.; Zhu, H.L.; Tan, R.X. Chaetominine, a cytotoxic alkaloid produced by endophytic *Chaetomium* sp. IFB-E015. *Org. Lett.* **2006**, *8*, 5709–5712. [CrossRef] [PubMed]
45. Hui, M.G.; Yu, Z.G.; Jie, Z.; Wu, J.H.; Tan, R.X. Bioactive alkaloids from endophytic *Aspergillus fumigatus*. *J. Nat. Prod.* **2009**, *72*, 753–755.
46. Cole, R.J.; Kirksey, J.W.; Dorner, J.W.; Wilson, D.M.; Johnson, J.C., Jr.; Johnson, A.N.; Bedell, D.M.; Springer, J.P.; Chexal, K.K.; Clardy, J.C.; et al. Mycotoxins produced by *Aspergillus fumigatus* species isolated from molded silage. *J. Agric. Food. Chem.* **1977**, *25*, 826–830. [CrossRef]
47. Okamoto, M.; Yoshida, K.; Uchida, I.; Nishikawa, M.; Kohsaka, M.; Aoki, H. Studies of platelet activating factor (PAF) antagonists from microbial products. I. Bisdethiobis(methylthio)gliotoxin and its derivatives. *Chem. Pharm. Bull.* **1986**, *34*, 340–344. [CrossRef]
48. Liang, W.L.; Le, X.; Li, H.J.; Yang, X.L.; Chen, J.X.; Xu, J.; Liu, H.L.; Wang, L.Y.; Wang, K.T.; Hu, K.C.; et al. Exploring the chemodiversity and biological activities of the secondary metabolites from the marine fungus *Neosartorya pseudofischeri*. *Mar. Drugs* **2014**, *12*, 5657–5676. [CrossRef]
49. Joachim, W.; Susanne, G.; Manfred, G.; Ralf, T.; Reinhard, K. Pseurotin F1/F2, New Metabolites from *Aspergillus fumigatus*, Process for Their Preparation and Their Use as Apomorphine Antagonists. EP19920120724, 4 December 1992.
50. Tsunematsu, Y.; Fukutomi, M.; Saruwatari, T.; Noguchi, H.; Hotta, K.; Tang, Y.; Watanabe, K. Elucidation of pseurotin biosynthetic pathway points to trans-acting *C*-methyltransferase: Generation of chemical diversity. *Angew. Chem. Int. Ed. Engl.* **2014**, *53*, 8475–8479. [CrossRef]
51. Boot, C.M.; Gassner, N.C.; Compton, J.E.; Tenney, K.; Tamble, C.M.; Lokey, R.S.; Holman, T.R.; Crews, P. Pinpointing pseurotins from a marine-derived *Aspergillus* as tools for chemical genetics using a synthetic lethality yeast screen. *J. Nat. Prod.* **2007**, *70*, 1672–1675. [CrossRef]
52. Ren, H.; Liu, R.; Chen, L.; Zhu, T.J.; Zhu, W.M.; Gu, Q.Q. Two new hetero-spirocyclic gamma-lactam derivatives from marine sediment-derived fungus *Aspergillus sydowi* D2-6. *Arch. Pharm. Res.* **2010**, *33*, 499–502. [CrossRef]
53. Jiao, W.X.; Blunt, J.W.; Cole, A.L.J.; Munro, M.H.G. Fumagiringillin, a new fumagillin derivative from a strain of the fungus *Aspergillus fumigatus*. *J. Nat. Prod* **2004**, *67*, 1434–1437. [CrossRef] [PubMed]
54. Chu, M.; Mierzwa, R.; He, L.; Xu, L.; Patel, M.; Patel, D.; Chan, T.M. Structure of sch 528647: A new antitumor antibiotic related to fumagillin. *J. Antibiot.* **2001**, *54*, 1096–1099. [CrossRef] [PubMed]
55. Kong, F.D.; Huang, X.L.; Ma, Q.Y.; Xie, Q.Y.; Wang, P.; Chen, P.W.; Zhou, L.M.; Yuan, J.Z.; Dai, H.F.; Luo, D.Q.; et al. Helvolic acid derivatives with antibacterial activities against *Streptococcus agalactiae* from the marine-derived fungus *Aspergillus fumigatus* HNMF0047. *J. Nat. Prod.* **2018**, *81*, 1869–1876. [CrossRef] [PubMed]
56. Liu, R.; Zhu, W.M.; Zhang, Y.P.; Zhu, T.J.; Liu, H.B.; Fang, Y.C.; Gu, Q.Q. A new diphenyl ether from marine-derived fungus *Aspergillus* sp B-F-2. *J. Antibiot* **2006**, *59*, 362–365. [CrossRef] [PubMed]
57. Fujimoto, K.; Fujimaki, T.; Okuyama, E.; Yamazaki, M. Immunomodulatory constituents from an ascomycete, Microascus tardifaciens. *Chem. Pharm. Bull.* **1999**, *47*, 1426–1432. [CrossRef]

58. Qin, S.; Wang, Y.; Wang, W.; Zhu, W. Anti-H1N1-virus secondary metabolites from mangrove-derived aciduric fungus *Penicillium* sp. OUCMDZ-4736. *Chin. J. Mar. Drugs* **2016**, *35*, 21–28.
59. Wu, J.S.; Shi, X.H.; Zhang, Y.H.; Yu, J.Y.; Fu, X.M.; Li, X.; Chen, K.X.; Guo, Y.W.; Shao, C.L.; Wang, C.Y. Co-cultivation with 5-azacytidine induced new metabolites from the zoanthid-derived fungus *Cochliobolus lunatus*. *Front. Chem.* **2019**, *7*, 763. [CrossRef]
60. Yong, K.; Kaleem, S.; Wu, B.; Zhang, Z.Z. New antiproliferative compounds against glioma cells from the marine-sourced fungus *Penicillium* sp. ZZ1750. *Mar. Drugs* **2021**, *19*, 483. [CrossRef]
61. Abuhijjleh, R.K.; Shabbir, S.; Al-Abd, A.M.; Jiaan, N.H.; Alshamil, S.; El-labbad, E.M.; Khalifa, S.I. Bioactive marine metabolites derived from the Persian Gulf compared to the Red Sea: Similar environments and wide gap in drug discovery. *Peerj* **2021**, *9*, 11778. [CrossRef]
62. Wang, W.Y.; Liao, Y.Y.; Chen, R.X.; Hou, Y.P.; Ke, W.Q.; Zhang, B.B.; Gao, M.L.; Shao, Z.Z.; Chen, J.M.; Li, F. Chlorinated azaphilone pigments with antimicrobial and cytotoxic activities isolated from the deep sea derived fungus *Chaetomium* sp. NA-S01-R1. *Mar. Drugs* **2018**, *16*, 61. [CrossRef]
63. Inostroza, A.; Lara, L.; Paz, C.; Perez, A.; Galleguillos, F.; Hernandez, V.; Becerra, J.; Gonzalez-Rocha, G.; Silva, M. Antibiotic activity of Emerimicin IV isolated from *Emericellopsis minima* from Talcahuano Bay, Chile. *Nat. Prod. Res.* **2018**, *32*, 1361–1364. [CrossRef] [PubMed]
64. Van de Veerdonk, F.L.; Gresnigt, M.S.; Romani, L.; Netea, M.G.; Latgé, J.-P. *Aspergillus fumigatus* morphology and dynamic host interactions. *Nat. Rev. Microbiol.* **2017**, *15*, 661–674. [CrossRef] [PubMed]
65. Li, X.J.; Zhang, Q.; Zhang, A.L.; Gao, J.M. Metabolites from *Aspergillus fumigatus*, an endophytic fungus associated with *Melia azedarach*, and their antifungal, antifeedant, and toxic activities. *J. Agric. Food Chem.* **2012**, *60*, 3424–3431. [CrossRef] [PubMed]
66. Ando, O.; Satake, H.; Nakajima, M.; Sato, A.; Nakamura, T.; Kinoshita, T.; Furuya, K.; Haneishi, T. Synerazol, a New Antifungal Antibiotic. *J. Antibiot.* **1991**, *44*, 382–389. [CrossRef]
67. Pinheiro, E.A.A.; Carvalho, J.M.; dos Santos, D.C.P.; Feitosa, A.D.O.; Marinho, P.S.B.; Guilhon, G.M.S.P.; de Souza, A.D.L.; da Silva, F.M.A.; Marinho, A.M.D.R. Antibacterial activity of alkaloids produced by endophytic fungus *Aspergillus* sp. EJC08 isolated from medical plant *Bauhinia guianensis*. *Nat. Prod. Res.* **2013**, *27*, 1633–1638. [CrossRef]
68. Anjum, K.; Bi, H.; Chai, W.; Lian, X.Y.; Zhang, Z. Antiglioma pseurotin A from marine *Bacillus* sp. FS8D regulating tumour metabolic enzymes. *Nat. Prod. Res.* **2017**, *32*, 1–4. [CrossRef]
69. Komagata, D.; Fujita, S.; Yamashita, N.; Saito, S.; Morino, T. Novel neuritogenic activities of pseurotin A and penicillic acid. *J. Antibiot.* **1996**, *49*, 958–959. [CrossRef]
70. Asami, Y.; Kakeya, H.; Komi, Y.; Kojima, S.; Nishikawa, K.; Beebe, K.; Neckers, L.; Osada, H. Azaspirene, a fungal product, inhibits angiogenesis by blocking Raf-1 activation. *Cancer Sci.* **2008**, *99*, 1853–1858. [CrossRef]
71. Igarashi, Y.; Yabuta, Y.; Sekine, A.; Fujii, K.; Harada, K.; Oikawa, T.; Sato, M.; Furumai, T.; Oki, T. Directed biosynthesis of fluorinated pseurotin A, synerazol and gliotoxin. *J. Antibiot.* **2004**, *57*, 748–754. [CrossRef]
72. Asami, Y.; Kakeya, H.; Onose, R.; Yoshida, A.; Matsuzaki, H.; Osada, H. Azaspirene: A novel angiogenesis inhibitor containing a 1-oxa-7-azaspiro[4.4]non-2-ene-4,6-dione skeleton produced by the fungus *Neosartotya* sp. *Organ. Lett.* **2002**, *4*, 2845–2848. [CrossRef]
73. Guruceaga, X.; Perez-Cuesta, U.; de Cerio, A.A.D.; Gonzalez, O.; Alonso, R.M.; Hernando, F.L.; Ramirez-Garcia, A.; Rementeria, A. Fumagillin, a mycotoxin of *Aspergillus fumigatus*: Biosynthesis, biological activities, detection, and applications. *Toxins* **2020**, *12*, 7. [CrossRef] [PubMed]
74. Sawadsitang, S.; Mongkolthanaruk, W.; Suwannasai, N.; Sodngam, S. Antimalarial and cytotoxic constituents of *Xylaria* cf. *cubensis* PK108. *Nat. Prod. Res.* **2015**, *29*, 2033–2036. [CrossRef] [PubMed]
75. Ganaha, M.; Yoshii, K.; Otsuki, Y.; Iguchi, M.; Okamoto, Y.; Iseki, K.; Ban, S.; Ishiyama, A.; Hokari, R.; Iwatsuki, M.; et al. *In Vitro* antitrypanosomal activity of the secondary metabolites from the mutant strain IU-3 of the insect pathogenic fungus *Ophiocordyceps coccidiicola* NBRC 100683. *Chem. Pharm. Bull.* **2016**, *64*, 988–990. [CrossRef]
76. Sanmanoch, W.; Mongkolthanaruk, W.; Kanokmedhakul, S.; Aimi, T.; Boonlue, S. Helvolic acid, a secondary metabolite produced by *Neosartorya spinosa* KKU-1NK1 and its biological activities. *Chiang Mai J. Sci.* **2016**, *43*, 484–494.
77. Grimblat, N.; Zanardi, M.M.; Sarotti, A.M. Beyond DP4: An improved probability for the stereochemical assignment of isomeric compounds using quantum chemical calculations of NMR shifts. *J. Org. Chem.* **2015**, *80*, 12526–12534. [CrossRef] [PubMed]
78. Han, J.J.; Liu, C.C.; Li, L.; Zhou, H.; Liu, L.; Bao, L.; Chen, Q.; Song, F.H.; Zhang, L.X.; Li, E.W.; et al. Decalin-containing tetramic acids and 4-Hydroxy-2-pyridones with antimicrobial and cytotoxic activity from the fungus *Coniochaeta cephalothecoides* collected in Tibetan Plateau (Medog). *J. Org. Chem.* **2017**, *82*, 11474–11486. [CrossRef] [PubMed]

marine drugs

MDPI

Article

Exophilone, a Tetrahydrocarbazol-1-one Analogue with Anti-Pulmonary Fibrosis Activity from the Deep-Sea Fungus *Exophiala oligosperma* MCCC 3A01264

Ming-Jun Hong [1,†], Meng-Jiao Hao [1,†], Guang-Yu Zhang [1], Hou-Jin Li [2], Zong-Ze Shao [3], Xiu-Pian Liu [3], Wen-Zhe Ma [4], Jun Xu [1], Taifo Mahmud [5] and Wen-Jian Lan [1,*]

1 School of Pharmaceutical Sciences, Sun Yat-sen University, Guangzhou 510006, China; hongmj5@mail2.sysu.edu.cn (M.-J.H.); haomj@mail2.sysu.edu.cn (M.-J.H.); zhanggy39@mail2.sysu.edu.cn (G.-Y.Z.); xujun9@mail.sysu.edu.cn (J.X.)
2 School of Chemistry, Sun Yat-sen University, Guangzhou 510006, China; ceslhj@mail.sysu.edu.cn
3 Key Laboratory of Marine Biogenetic Resources, Third Institute of Oceanography, Ministry of Natural Resources, Xiamen 361005, China; shaozz@163.com (Z.-Z.S.); mccc5177@163.com (X.-P.L.)
4 State Key Laboratory of Quality Research in Chinese Medicine, Macau University of Science and Technology, Taipa 519020, Macau, China; wzma@must.edu.mo
5 Department of Pharmaceutical Sciences, Oregon State University, Corvallis, OR 97331, USA; Taifo.Mahmud@oregonstate.edu
* Correspondence: lanwj@mail.sysu.edu.cn; Tel.: +86-20-399-43-042
† These authors contributed equally to this work.

Abstract: A new compound, exophilone (**1**), together with nine known compounds (**2**–**10**), were isolated from a deep-sea-derived fungus, *Exophiala oligosperma*. Their chemical structures, including the absolute configuration of **1,** were elucidated using nuclear magnetic resonance (NMR) spectroscopy, high-resolution electrospray ionization mass spectroscopy (HRESIMS), and electronic circular dichroism (ECD) calculation. Compounds were preliminarily screened for their ability to inhibit collagen accumulation. Compounds **1**, **4**, and **7** showed weaker inhibition of TGF-β1-induced total collagen accumulation in compared with pirfenidone (73.14% inhibition rate). However, pirfenidone exhibited cytotoxicity (77.57% survival rate), while compounds **1**, **4**, and **7** showed low cytotoxicity against the HFL1 cell line. Particularly, exophilone (**1**) showed moderate collagen deposition inhibition effect (60.44% inhibition rate) and low toxicity in HFL1 cells (98.14% survival rate) at a concentration of 10 μM. A molecular docking study suggests that exophilone (**1**) binds to both TGF-β1 and its receptor through hydrogen bonding interactions. Thus, exophilone (**1**) was identified as a promising anti-pulmonary fibrosis agent. It has the potential to be developed as a drug candidate for pulmonary fibrosis.

Keywords: *Exophiala oligosperma*; marine fungus; pulmonary fibrosis (PF); molecular docking

Citation: Hong, M.-J.; Hao, M.-J.; Zhang, G.-Y.; Li, H.-J.; Shao, Z.-Z.; Liu, X.-P.; Ma, W.-Z.; Xu, J.; Mahmud, T.; Lan, W.-J. Exophilone, a Tetrahydrocarbazol-1-one Analogue with Anti-Pulmonary Fibrosis Activity from the Deep-Sea Fungus *Exophiala oligosperma* MCCC 3A01264. *Mar. Drugs* **2022**, *20*, 448. https://doi.org/10.3390/md20070448

Academic Editor: Hee Jae Shin

Received: 10 June 2022
Accepted: 4 July 2022
Published: 9 July 2022

1. Introduction

Deep-sea is one of the extreme ecological environments on earth, with high salinity, high pressure, low temperature, low oxygen concentration, darkness, and other characteristics [1]. Therefore, organisms, including microbes, that live in deep-sea are normally equipped with certain physical and biochemical traits that help them survive that extreme environment [2]. In addition, many of them have the ability to produce specialized metabolites which are different from those produced by terrestrial organisms. Recent studies have shown that fungi from extreme environments have great potential as a source of clinically important compounds [1,3].

Tetrahydro carbazole derivatives have been isolated from microorganisms of terrestrial and marine origin and exhibit a variety of activities, including anti-*Candida albicans* activity [4], anti-*Bacillus subtilis* activity, and anti-*Micrococcus luteus* activity [5], etc. In

particular, sorazolons D2, E, and E2 from *Sorangium cellulosum* strain Soce375 exhibited anti-fibrosis activity [5]. Pulmonary fibrosis (PF) is a lung disease in which scarring of the lungs increases over time [6]. The progression of PF is related to environmental pollution, certain drug use, connective tissue diseases, infections (including COVID-19 and the related SARS virus), and/or interstitial lung disease [7]. To date, only two drugs, nintedanib and pirfenidone, have been approved by the FDA for the treatment of idiopathic pulmonary fibrosis (IPF). Nintedanib can significantly slow disease progression compared to placebo in IPF patients [8,9]. However, its clinical applications are somewhat limited due to poor oral bioavailability, metabolic instability, and off-target side effects [10]. Clinical trials have shown that pirfenidone alleviates the decline in lung function in patients with IPF, but 24.3% of patients stopped pirfenidone treatment due to adverse drug reactions in Japan [11]. Although lung transplantation is considered the most effective treatment for PF, it is limited by the lack of suitable donor organs [12]. Therefore, there is still an urgent need to identify and discover new agents to treat PF. PF is characterized by excessive collagen deposition in the lung; therefore, an in vitro cell screening assay that is based on deposition of collagen in cells has been established [13].

As part of an effort to discover anti-PF compounds from extremophilic fungi, we investigated the metabolites of the fungus *Exophiala oligosperma* MCCC 3A01264, a "black-yeast" isolated from seawater collected at a depth of 3300 m in the northern basin of the South China Sea. While *E. oligosperma* has been reported to cause infections in humans, particularly in immunocompromised patients [3], little is known about its secondary metabolism or production of natural products. In this study, we focused our effort on bioactive compounds that have potential to be developed as drugs for the treatment of pulmonary fibrosis (PF). Here, we report the isolation, structure characterization, and collagen accumulation inhibitory activity of a new compound, exophilone (**1**), together with eleven known compounds (**2**–**10**) from *E. oligosperma* (Figure 1).

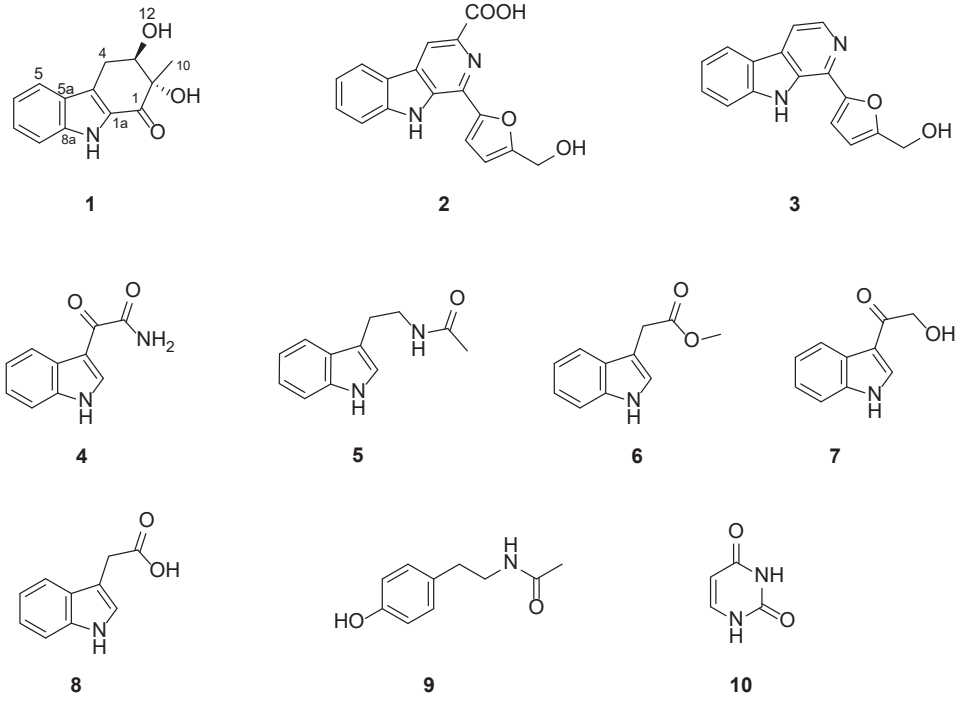

Figure 1. Chemical structures of compounds **1**–**10**.

2. Results and Discussion

2.1. Structural Elucidation

Exophilone (**1**) was isolated as a pale yellow solid, and its molecular formula was established to be $C_{13}H_{13}NO_3$ by HRESIMS (*m/z* 232.0967 $[M + H]^+$, calcd. 232.0968) (Supplementary Figure S1), suggesting eight degrees of unsaturation. Analyses of its ^1H, ^{13}C, and HMQC NMR spectra (Table 1 and Supplementary Figures S2–S5) revealed the presence of one carbonyl (C-1), two aromatic quaternary (C-4a, C-5a), two tertiary amines (C-8a, C-1a), and four aromatic methines (C-5 to C-8), as well as one tertiary alcohol (C-2), one secondary alcohol (C-3), one methylene (C-4), and one methyl (C-10). The carbonyl and four double bonds accounted for five out of the eight degrees of unsaturation required by the molecular formula, and the remaining three suggested a structure with three rings in **1**. Based on the COSY correlations between H-5 (δ_H 7.66, d, *J* = 7.8 Hz) and H-6 (δ_H 7.08, ddd, *J* = 7.8, 7.2, 1.2 Hz), between H-6 and H-7 (δ_H 7.30, ddd, *J* = 7.8, 7.2, 1.2 Hz), between H-7 and H-8 (δ_H 7.38, d, *J* = 7.8 Hz), as well as HMBC correlations between H-5 and C-5a (δ_C 125.3), C-8a (δ_C 138.9), and C-4a (δ_C 123.6), between H-8 and C-5a (δ_C 125.3) and C-8a (δ_C 138.9), between H-9 (δ_H 11.59, s) and C-4a (δ_C 123.6), C-5a (δ_C 125.3), C-8a (δ_C 138.9), and C-1a (δ_C 129.5), the presence of 2,3-substituted indole moiety was confirmed (Figure 2 and Supplementary Figure S6–S7). The third ring was confirmed by C-1 (δ_C 192.4) to C-4 (δ_C 27.5), where C-1 attaches to C-1a and C-4 attaches to C-4a. This was supported by the HMBC correlation between C-4 methylene protons and C-4a, C-1a, C-2, and C-3, between the methylene protons and the carbonyl C-1, between the methyl protons CH_3-10 (δ_H 1.24, s) and C-2, C-1, and between H-3 (δ_H 4.03, m) and C-4a suggested that C-1 is connected to C-2 and C-2 is connected to C-3 and C-10. Further, the HMBC spectrum allowed the assignment of the position of the OH groups (δ_H 5.25 and 5.16 ppm) to C-11 and C-12 from their correlations with C-1 and C-10 as well as C-2 and C-4, respectively (Figure 2 and Supplementary Figure S7). Hence, the structure of **1** was elucidated as shown (Figure 1).

Table 1. ^1H (400 Hz) and ^{13}C (100 Hz) NMR data for compound **1** in DMSO-*d*6.

Position	δ_C, Type	δ_H, Mult. (*J* in Hz)
1	192.4, CO	
2	77.3, C	
3	74.2, CH	4.03, m
4	27.5, CH_2	2.76, m 3.28, m
4a	123.6, C	
5a	125.3, C	
5	121.2, CH	7.66, d (7.8)
6	119.7, CH	7.08, ddd (7.8, 7.2, 1.2)
7	126.2, CH	7.30, ddd (7.8, 7.2, 1.2)
8	112.8, CH	7.38, d (7.8)
8a	138.9, C	
9	NH	11.59, brs
1a	129.5, C	
10	18.6, CH_3	1.24, s
11	OH	5.25, brs
12	OH	5.16, d (3.6)

Since the NOESY spectrum of **1** (Supplementary Figure S8) did not provide enough information to determine its configuration, the absolute configuration of **1** was elucidated to be 2*S*, 3*R* by comparisons of the experimental and calculated electronic circular dichroism (ECD) spectra (Figure 3). Since the structure of **1** has not been reported previously, it is named exophilone (**1**).

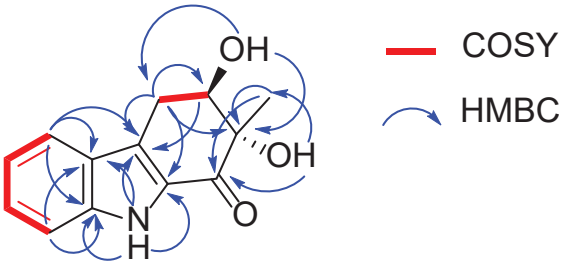

Figure 2. ^{1}H-^{1}H COSY and key HMBC correlations of compound **1**.

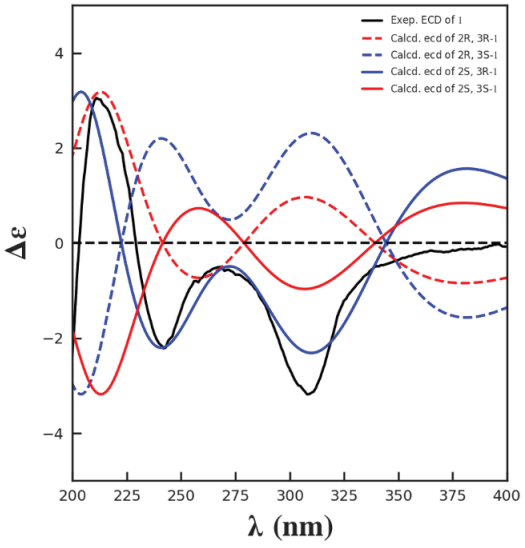

Figure 3. Comparisons of the experimental and calculated ECD spectra of **1**.

The other eleven compounds were determined to be flazine (**2**) [14], perlolyrine (**3**) [15], (1H-indol-3-yl) oxoacetamide (**4**) [16], N-acetyl tryptamine (**5**) [17], indole-3-methylethanoate (**6**) [18], 3-(hydroxyacetyl)-indole (**7**) [19], indole-3-acetic acid (**8**) [20], N-acetyl-tyramine (**9**) [21], and uracil (**10**) [22] by comparing their NMR data (Supplementary Figures S9–S26) with those reported in the literature.

2.2. Effect of Compounds **1–10** *on HFL1 Cell Viability*

To assess the cytotoxicity of compounds **1–10**, we performed cell viability assay with the HFL1 cell line. The cells were treated with compounds **1–10** as well as with pirfenidone as a positive control for 48 h, and the cell viability was measured and compared with the untreated control group (control) (Figure 4A and Table 2). Among the compounds tested, compound **8** and pirfenidone are somewhat toxic to HFL1 cells at 10 μM, with cell survival rates of 78.49% and 77.57%, respectively. On the other hand, compounds **1**, **2–7**, **9**, and **10** did not significantly affect cell viability at the same concentration. Particularly, compounds **1**, **4**, and **7** had no cytotoxicity at 10 μM, with the cell survival rates of above 98%.

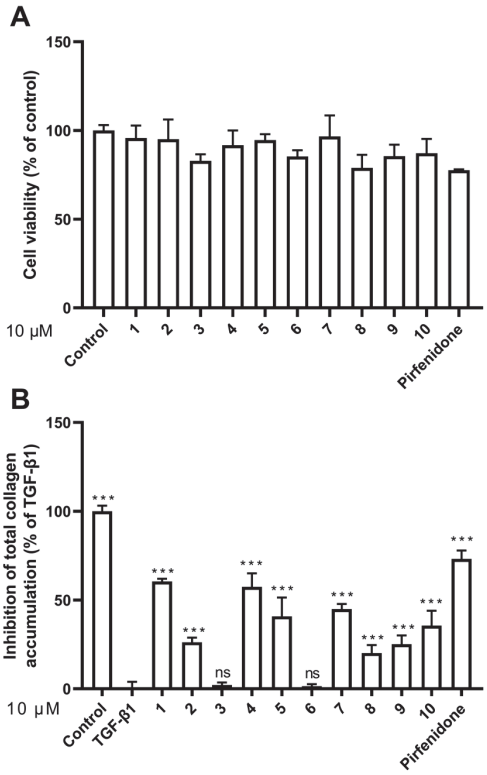

Figure 4. Effects of compounds **1–10** on cell viability and collagen accumulation. (**A**) Cell viability was calculated by CCK8 assay at a concentration of 10 μM; (**B**) Inhibitory activity against TGF-β1-induced total collagen accumulation in HFL1 cells at a concentration of 10 μM. The results are the means ± SD of at least three independent experiments. *** $p < 0.001$ compared with the TGF-β1 group. ns: no statistical difference.

Table 2. Collagen accumulation inhibition rate (IR) and cell survival rate (SR) of **1**-**10**.

Compound	Inhibition (%)	Survival Rate (%)
1	60.44 ± 1.54	98.14 ± 6.20
2	26.28 ± 2.53	98.28 ± 11.15
3	2.19 ± 1.34	81.69 ± 3.36
4	57.37 ± 7.65	91.56 ± 10.17
5	40.88 ± 10.52	96.11 ± 1.80
6	1.46 ± 1.16	87.01 ± 1.13
7	44.96 ± 2.82	99.25 ± 12.96
8	20.15 ± 4.49	78.49 ± 8.92
9	25.11 ± 4.97	84.93 ± 7.86
10	35.62 ± 8.39	86.96 ± 9.81
pirfenidone	73.14 ± 4.72	77.57 ± 0.52

Inhibitory effect against TGF-β1 induced total collagen accumulation in HFL1 cells at a concentration of 10 μM. Cell survival rate is calculated by CCK8 assay. The results are the mean ± SD of at least three independent experiments.

2.3. Effect of Compounds **1–10** *on HFL1 Cell Collagen Accumulation*

To evaluate the compounds' inhibitory activity on TGF-β1-induced total collagen accumulation, the Sirius red dye staining, which has been accepted to be an effective and convenient method for the anti-fibrotic screening model in vitro [13,23], was used. Among the compounds tested, compounds **1**, **4**, and **7** showed good inhibition of collagen

accumulation (60.44%, 57.37%, and 44.96%) in HFL1 cells (Table 2 and Figure 4B). While they are somewhat less active than pirfenidone, their toxicity profiles are less than pirfenidone (77.57% survival rate) toward HFL1 cells. More significantly, exophilone (**1**) showed a respectable collagen deposition inhibition effect (60.44% inhibition rate) and low toxicity toward HFL1 cells (98.14% survival rate) at a concentration of 10 μM. The cells were observed with Picro-Sirius Red staining and visualized (Figure 5).

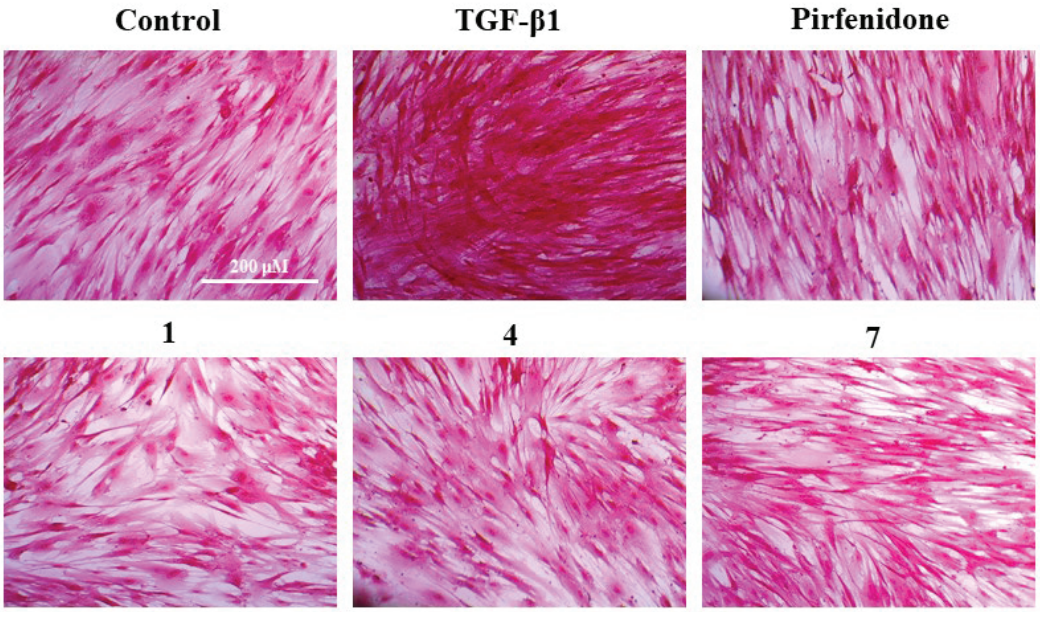

Figure 5. Picro-Sirius Red (PSR) staining for the total collagen accumulation induced by TGF-β1 in HFL1 cells. The representative images are the cells induced by TGF-β1 and treated with 10 μM of compounds **1**, **4**, **7**, pirfenidone, and the control group (untreated normal cells). Scale bar: 200 μM.

2.4. Molecular Docking Study

The inhibitory effect of compound **1** on TGF-β1-induced total collagen accumulation in HFL1 cells might be due to its competitive binding with TGF-β1 (PDBID: 1KLS) or with its receptors (PDBID: 3KFD). In order to investigate the binding mode of compound **1,** molecular docking experiments were performed using Autodock software 1.56 [24]. The results are shown in Figure 6.

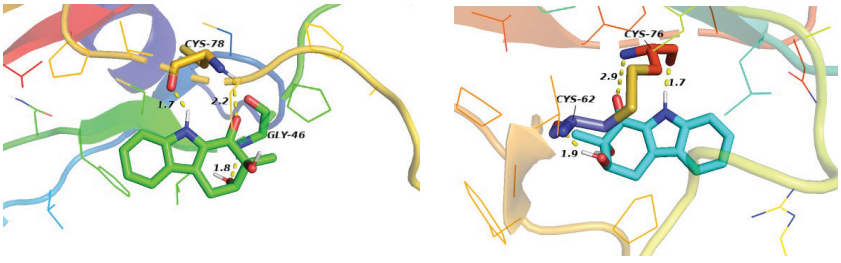

(**A**) (**B**)

Figure 6. Molecular docking studies of compound **1**. (**A**) Docking mode of compound **1** to 1KLS; (**B**) Docking mode of compound **1** to 3KFD (Yellow dotted lines represent hydrogen bonds, and numbers represent bond distances).

The docking study showed three hydrogen bonds between compound **1** and the active site residues of TGF-β1 (1KLS) (Figure 6A); a strong hydrogen bond (distance: 1.7 Å) between the indole nitrogen atom and the Cys-78 residue of TGF-β1, and two hydrogen bonds (distance: 2.2, 1.8 Å) between the two hydroxyl groups and Cys-78 and Gly-46, respectively. The data suggest that compound **1** may inhibit TGF-β1-induced total collagen accumulation in HFL1 cells by directly binding to TGF-β1. However, the study also showed three hydrogen bonds between compound **1** and the TGF-β1 receptor (3KFD) (Figure 6B); one hydrogen bond (distance: 1.7 Å) between the indole nitrogen atom and Cys-76, a hydrogen bond (distance: 2.9 Å) between the C-1 ketone and Cys-76, and another hydrogen bond between the C-3 hydroxyl group and Cys-62 (distance: 1.9 Å). The results suggest that compound **1** may bind to the active site of the TGF-β1 as well as to its receptor by hydrogen bonding interactions. These may preliminarily explain why compound **1** inhibits the accumulation of collagen induced by TGF-β1 similar to pirfenidone in HFL1 cells. The interactions of compound **1** with TGF-β1 and its receptor will be a subject of our future investigations.

3. Discussion

Exophilone (**1**) is a tetrahydro carbazole derivative that is structurally very similar to Sorazolon A [5], which was previously found in soil-derived *Sorangium cellulosum* strain soce375 and thus presumably has a similar biosynthetic pathway. The main differences between exophilone (**1**) and Sorazolon A are the carbonyl C-1 and the secondary alcohol C-3 replacing the tertiary alcohol and carbonyl. Natural tetrahydro carbazole derivatives, including 3-hydroxy-1,2-dimethyl-1,2,3,9-tetrahydrocarbazol-4-one isolated from *Streptomyces ehimensis* strain JB201 [4] and carbazomycin dimers and 3-hydroxy-1,2-dimethyl-2,3-dihydro-1*H*-carbazol-4-one isolated from *Streptomyces* sp. BCC26924 [25], showed antifungal activity and antituberculosis activity. Furthermore, synthetic tetrahydro carbazole protects DNA against oxidative stress [26]. Natural products are a rich source of lead molecules for anti-fibrosis drug discovery. Current pulmonary fibrosis treatment drugs (e.g., colchicine, cyclophosphamide, cyclosporine A, pirfenidone, and nitinol) have therapeutic effects but also significant side effects. Therefore, it is crucial to screen drugs with progressive therapeutic effects to treat pulmonary fibrosis [27].

In this study, a new compound, exophilone (**1**), together with nine known compounds (**2**–**10**), were isolated from a deep-sea-derived fungus, *Exophiala oligosperma*. Among them, exophilone (**1**) showed the best anti-pulmonary fibrosis activity, with low toxicity in HFL1 cells (98.14% survival rate) at a concentration of 10 μM. Exophilone (**1**) has the potential of anti-pulmonary fibrosis and may bind to both TGF-β1 and its receptor through hydrogen bonding interactions.

4. Materials and Methods

4.1. General Procedures

The PerkinElmer Spectrum Two spectrometer (PerkinElmer, Waltham, MA, USA) was used for IR spectra measurement. ECD spectra were measured on a Chirascan circular dichroism spectrometer (Applied Photophysics Ltd., Leatherhead, UK). UV spectra were obtained on a Shimadzu UV-vis-NIR spectrophotometer (Shimadzu Corporation, Nakagyo-ku, Kyoto, Japan). 1D and 2D NMR spectra were recorded in $CDCl_3$ or DMSO-*d*6 on Bruker Avance II 400, Bruker Avance IIIT 500HD, Bruker Avance IIIT 600AV spectrometers (Bruker Bio Spin AG, Industriestrasse 26, Fällanden, Switzerland). The chemical shifts are relative to the residual solvent signals ($CDCl_3$: δ_H 7.260 and δ_C 77.160; DMSO-*d*6: δ_H 2.500, δ_C 39.520). The high-resolution ESI-MS spectra were obtained on a Thermo Fisher LTQ Orbitrap Elite High-Resolution liquid chromatography-mass spectrometer (Thermo Fisher Scientific Inc., Waltham, MA, USA). Preparative HPLC was performed using a Shimadzu LC-15C HPLC pump (Shimadzu Corporation, Nakagyo-ku, Kyoto, Japan) supplied with an SPD-15C dual λ absorbance detector (Shimadzu Corporation, Nakagyo-ku, Kyoto, Japan), and a Shim-pack PRC-ODS HPLC column I (250 × 20 mm i.d., 5 μm, Shimadzu Corporation,

Nakagyo-ku, Kyoto, Japan). Silica gel (SiO_2, 200–300 mesh, Qingdao Puke parting Materials Co., Ltd. Qingdao, China) and Sephadex LH-20 (green herbs, Beijing, China) were used for column chromatography.

4.2. Fungal Strain and Culture Method

The marine fugus *Exophiala oligosperma* MCCC 3A01264 was obtained from Marine Culture Collection of China (MCCC). It was originally isolated from seawater collected at a depth of 3300 m in northern basin of the South China Sea. A voucher specimen was stored in the School of Pharmaceutical Sciences, Sun Yat-sen University, Guangzhou, P.R. China. Analysis of the internal transcribed spacer (ITS) rDNA by BLAST database screening provided a 99.9% match to *Exophiala oligosperma*.

The fermentation medium contained glucose (15 g/L), peptone (10 g/L), yeast extract (2 g/L), L-tryptophan (2 g/L), L-phenylalanine (2 g/L), L-methionine (2 g/L), L-threonine (2 g/L), sea salt (25 g/L), and H_2O (1 L), and was adjusted to pH 7.5. Fungal mycelia were cut uniformly and transferred aseptically to 1 L Erlenmeyer flasks with each containing 600 mL liquid medium sterilized at 120 °C for 30 min. The flasks were incubated at 28 °C for 60 days.

4.3. Extraction and Isolation

Two hundred liters of culture broth were filtered through the cheesecloth. The culture broth was extracted three times using EtOAc and then concentrated under reduced pressure to afford an EtOAc extract (31.68 g).

The EtOAc extract was chromatographed on a silica gel column (diameter: 80 mm, length: 610 mm, silica gel: 400 g) with a gradient of petroleum ether–EtOAc (10:0–0:10, v/v) followed by EtOAc–MeOH (10:0–0:10, v/v) to afford 10 fractions (coded Fr.1–Fr.10). Compound **8** (320 mg) was crystallized from Fr.6 severally. Fr.7 (1.2 g) was subjected to a silica gel column (7 g) eluted with petroleum ether-EtOAc (100:0−0:100) (total volume 2 L) with increasing polarity to obtain ten subfractions (Fr.7-1−Fr.7-10) after pooling the similar fractions as monitored by TLC (petroleum ether−EtOAc = 4:1). Compound **6** (4.2 mg) was obtained from Fr.7-4 directly. Fraction 8 (143 mg) was chromatographed on Sephadex LH-20 (10 g) and eluted with MeOH (total volume 500 mL) to give five subfractions (Fr.8-1−Fr.8-5). Fr.8-4 was further fractionated by preparative HPLC (MeOH–H_2O, 55:45, v/v, column I) to yield compound **1** (2.1 mg, TR = 22 min), compound **7** (3.0 mg, TR = 16.5 min), and compound **4** (4.2 mg, TR = 25 min). Compound **2** was filtered from Fr.10 directly. The rest of Fr.10 was separated by silica gel column using a step gradient elution with petroleum ether–EtOAc (10:0–0:10) to get 5 subfractions (Fr.10-1–Fr.10-5). Compound **5** (RT = 40.2 min, 3 mg), compound **3** (RT = 23 min, 8 mg), and compound **9** (RT = 36 min, 6 mg) were obtained from Fr.10-2 by preparative HPLC (MeOH–H_2O, 80:20, v/v, column I). Compound **10** (RT = 15 min, 2 mg) was isolated by preparative HPLC (MeOH–H_2O, 80:20, v/v, column I).

Exophilone (**1**). UV (MeOH) λmax (logε) 307 (1.20), 233 (1.29), 206 (2.02). ECD (0.3 mM, MeOH) λmax ($\Delta\varepsilon$) 211 (+3.05) nm. IR υ_{max} 3287, 2922, 2852, 1716, 1651, 1456, 1374, 1330, 1237, 1152, 1097, 1070, 1044, 998, 920, 744, 554 cm^{-1}. ^1H and ^{13}C NMR data, shown in Table 1; HR-ESI-MS *m/z* 232.0967 $[M + H]^+$ (calcd. for $C_{13}H_{13}NO_3$, 232.0968).

4.4. Cell Culture and Cytotoxicity Assay

The human fetal lung fibroblasts (HFL1) were purchased from Procell Life Science & Technology Co., Ltd. (Cat. No.: CL-0106 Wuhan, China). Cells were cultured in Ham's F-12K medium (PM150910, Procell Life Science & Technology, Wuhan, China) supplemented with 10% fetal bovine serum (FBS) (#10270-106, GIBCO, Invitrogen, Carlsbad, CA, USA) and 1% penicillin-streptomycin in an incubator at 37 °C with 5% CO_2. The cell viability was assayed using the Cell Counting Kit-8 (CCK8) according to the manufacturer's protocol. The cells were treated with 10 μM compounds **1**-**10**, or pirfenidone (TargetMol, Wellesley Hills, MA, USA) for 48 h. The absorbance of the solution was

then measured at 450 nm using a microplate reader (Thermo Fisher, Waltham, MA, USA). Survival rate = (Administration A value − Blank A value)/(Control A value − Blank A value) × 100%. All assays were repeated in triplicate.

4.5. Collagen Accumulation Inhibition In Vitro

The anti-fibrosis activities of the compounds were tested in HFL1 cells. The cells were treated with medium containing TGF-β1 (5 ng/mL) and 10 μM compounds **1**-**10**, and pirfenidone for 48 h. Subsequently, the supernatant was removed, and 4% paraformaldehyde was added to fix for 30 min at room temperature. Next, the cells were washed with PBS twice and then were added the 0.1% Sirius red dye with saturated picric acid. After 4 h of staining protected from light, the collagenous fiber was dyed red. Then, the cells were washed three times with 0.1% acetic acid and visualized under a cell imaging system (EVOS FL Auto, Life Technologies, Carlsbad, CA, USA). For the quantitative determinations of the accumulated collagen, the stained cells were destained with 0.1 M NaOH (100 μL/well) for 10 min. Then, the absorbance was measured at 540 nm with a spectrophotometer. Total collagen accumulation inhibition = 1 − (Administration A value − control A value)/(model A value − control A value) × 100%. All assays were repeated in triplicate.

4.6. Molecular Docking

Protein structure was obtained from the Protein Data Bank (https://www.pdbus.org/, accessed on 29 May 2022). The X-ray crystal structure of TGF-β1 (PDB ID: 1LKS) and its receptor (PDB ID: 3KFD) were chosen for the molecular docking analysis in this study. Compound **1** was prepared with Avogadro 1.1.1, with a 5000 steps Steepest Descent as well as 1000 steps Conjugate Gradients geometry optimization using MMFF94 force field. Docking experiments were performed using AutoDock 1.56 Vina and Pymol 2.4.

4.7. Statistical Analysis

The data are represented as the mean ± SD. Statistical analysis was performed using the GraphPad Prism 8.0 software (San Diego, CA, USA). The significant differences between groups were statistically analyzed using the one-way analysis of variance (ANOVA) followed by a post hoc test (LSD). All differences were considered statistically significant at $p < 0.05$.

5. Conclusions

A new tetrahydrocarbazol-1-one analogue, exophilone (**1**), together with nine known compounds (**2**–**10**), were isolated from a deep-see-derived fungus *Exophiala oligosperma*. Among all compounds, exophilone (**1**) showed the most significant inhibition of collagen accumulation with low toxicity in HFL1 cells. Further molecular docking experiments showed that exophilone (**1**) may act through hydrogen bonding to the stimulation site of TGF-β1 and its receptor. Given the limitations of the available anti-pulmonary fibrosis drugs, exophilone (**1**) and its analogs could be developed as candidates for the treatment of pulmonary fibrosis.

Supplementary Materials: The following are available online at https://www.mdpi.com/article/10.3390/md20070448/s1. Figures S1–S26: The HR-(+)ESI-MS and NMR spectra of compounds **1**–**10**; Figures S27–S30: NMR spectra of Compounds **11** and **12**.

Author Contributions: Conceived and designed the experiments: W.-J.L. Performed the experiments: M.-J.H. (Ming-Jun Hong), M.-J.H. (Meng-Jiao Hao) and G.-Y.Z. Wrote the paper: M.-J.H. (Ming-Jun Hong), M.-J.H. (Meng-Jiao Hao) and G.-Y.Z. Revised the paper: W.-J.L., T.M. Guided experiments: W.-J.L., H.-J.L., Z.-Z.S., X.-P.L., W.-Z.M. and J.X. All authors have read and agreed to the published version of the manuscript.

Funding: This work was financially supported by the National Science Foundation of China (No. 81872795), Guangdong Basic and Applied Basic Research Foundation (Nos. 2021A1515011761, 2018A030313157), and the Key Research and Development Program of Guangdong Province (No. 2020B1111110003).

Data Availability Statement: All relevant data are available from the corresponding author upon reasonable request.

Conflicts of Interest: The authors declare no conflict of interest.

References

1. Ul Arifeen, Z.M.; Ma, Y.-N.; Xue, Y.-R.; Liu, C.-H. Deep-sea fungi could be the new arsenal for bioactive molecules. *Mar. Drugs* **2019**, *18*, 9. [CrossRef]
2. Ibrar, M.; Ullah, M.W.; Manan, S.; Farooq, U.; Rafiq, M.; Hasan, F. Fungi from the extremes of life: An untapped treasure for bioactive compounds. *Appl. Microbiol. Biotechnol.* **2020**, *104*, 2777–2801. [CrossRef] [PubMed]
3. Rimawi, B.H.; Rimawi, R.H.; Mirdamadi, M.; Steed, L.L.; Marchell, R.; Sutton, D.A.; Thompson, E.H.; Wiederhold, N.P.; Lindner, J.R.; Boger, M.S. A case of *Exophiala oligosperma* successfully treated with voriconazole. *Med. Mycol. Case Rep.* **2013**, *2*, 144–147. [CrossRef] [PubMed]
4. Hwang, B.-S.; Kim, H.-J.; Jeong, G.-S.; Oh, J.-S.; Rho, J.-R. Isolation and structure determination of two new carbazoles from *Streptomyces ehimensis* JB201. *Bull. Korean Chem. Soc.* **2010**, *31*, 3457–3459. [CrossRef]
5. Karwehl, S.; Jansen, R.; Huch, V.; Stadler, M. Sorazolons, carbazole alkaloids from *Sorangium cellulosum* strain soce375. *J. Nat. Prod.* **2016**, *79*, 369–375. [CrossRef] [PubMed]
6. Wu, X.; Huang, J.; Wang, J.; Xu, Y.; Yang, X.; Sun, M.; Shi, J. Multi-pharmaceutical activities of chinese herbal polysaccharides in the treatment of pulmonary fibrosis: Concept and future prospects. *Front. Pharmacol.* **2021**, *12*, 707491. [CrossRef] [PubMed]
7. Ahmad Alhiyari, M.; Ata, F.; Islam Alghizzawi, M.; Bint, I.B.A.; Salih Abdulhadi, A.; Yousaf, Z. Post COVID-19 fibrosis, an emerging complicationof SARS-CoV-2 infection. *IDCases* **2021**, *23*, e01041. [CrossRef] [PubMed]
8. Dimitroulis, I.A. Nintedanib: A novel therapeutic approach for idiopathic pulmonary fibrosis. *Respir. Care* **2014**, *59*, 1450–1455. [CrossRef]
9. Richeldi, L.; du Bois, R.M.; Raghu, G.; Azuma, A.; Brown, K.K.; Costabel, U.; Cottin, V.; Flaherty, K.R.; Hansell, D.M.; Inoue, Y.; et al. Efficacy and safety of nintedanib in idiopathic pulmonary fibrosis. *N. Engl. J. Med.* **2014**, *370*, 2071–2082. [CrossRef]
10. Roth, G.J.; Binder, R.; Colbatzky, F.; Dallinger, C.; Schlenker-Herceg, R.; Hilberg, F.; Wollin, S.-L.; Kaiser, R. Nintedanib: From discovery to the clinic. *J. Med. Chem.* **2015**, *58*, 1053–1063. [CrossRef]
11. Ogura, T.; Azuma, A.; Inoue, Y.; Taniguchi, H.; Chida, K.; Bando, M.; Niimi, Y.; Kakutani, S.; Suga, M.; Sugiyama, Y.; et al. All-case post-marketing surveillance of 1371 patients treated with pirfenidone for idiopathic pulmonary fibrosis. *Respir. Investig.* **2015**, *53*, 232–241. [CrossRef] [PubMed]
12. George, P.M.; Patterson, C.M.; Reed, A.K.; Thillai, M. Lung transplantation for idiopathic pulmonary fibrosis. *Lancet Respir. Med.* **2019**, *7*, 271–282. [CrossRef]
13. Xue, L.; Deng, D.; Zheng, S.; Tang, M.; Yang, Z.; Pei, H.; Chen, Y.; Yang, T.; Liu, K.; Ye, H.; et al. Design, synthesis and discovery of 2(1H)-quinolone derivatives for the treatment of pulmonary fibrosis through inhibition of TGF-β/smad dependent and independent pathway. *Eur. J. Med. Chem.* **2020**, *197*, 112259. [CrossRef] [PubMed]
14. Su, B.N.; Chang, L.C.; Park, E.J.; Cuendet, M.; Santarsiero, B.D.; Mesecar, A.D.; Mehta, R.G.; Fong, H.H.; Pezzuto, J.M.; Kinghorn, A.D. Bioactive constituents of the seeds of *Brucea javanica*. *Planta Med.* **2002**, *68*, 730–733. [CrossRef]
15. Chen, P.-N.; Hao, M.-J.; Li, H.-J.; Xu, J.; Mahmud, T.; Lan, W.-J. Biotransformations of anthranilic acid and phthalimide to potent antihyperlipidemic alkaloids by the marine-derived fungus *Scedosporium apiospermum* F41–1. *Bioorg. Chem.* **2021**, *116*, 105375. [CrossRef]
16. Bao, B.; Zhang, P.; Lee, Y.; Hong, J.; Lee, C.-O.; Jung, J.H. Monoindole alkaloids from a marine sponge *Spongosorites* sp. *Mar. Drugs* **2007**, *5*, 31–39. [CrossRef]
17. Vaca, J.; Salazar, F.; Ortiz, A.; Sansinenea, E. Indole alkaloid derivatives as building blocks of natural products from *Bacillus thuringiensis* and *Bacillus velezensis* and their antibacterial and antifungal activity study. *J. Antibiot.* **2020**, *73*, 798–802. [CrossRef]
18. Liu, Y.; Jung, J.H.; Zhang, S. Indole alkaloids from a sponge *Sarcotragus* species. *Biochem. Syst. Ecol.* **2006**, *34*, 453–456. [CrossRef]
19. Tang, M.; Zhou, X.; Cai, J.; Chen, G. Chemical constituents from the fresh flower buds of *Musa nana* and their chemotaxonomic significance. *Biochem. Syst. Ecol.* **2021**, *99*, 104348. [CrossRef]
20. Evidente, A.; Iacobellis, N.S.; Sisto, A. Isolation of indole-3-acetic acid methyl ester, a metabolite of indole-3-acetic acid from *Pseudomonas amygdali*. *Experientia* **1993**, *49*, 182–183. [CrossRef]
21. Sobolevskaya, M.P.; Denisenko, V.A.; Moiseenko, A.S.; Shevchenko, L.S.; Menzorova, N.I.; Sibirtsev, Y.T.; Kim, N.Y.; Kuznetsova, T.A. Bioactive metabolites of the marine actinobacterium *Streptomyces* sp. KMM 7210. *Russ. Chem. Bull.* **2007**, *56*, 838–840. [CrossRef]
22. Kan, S.; Chen, G.; Han, C.; Chen, Z.; Song, X.; Ren, M.; Jiang, H. Chemical constituents from the roots of *Xanthium sibiricum*. *Nat. Prod. Res.* **2011**, *25*, 1243–1249. [CrossRef] [PubMed]

23. Deng, D.; Pei, H.; Lan, T.; Zhu, J.; Tang, M.; Xue, L.; Yang, Z.; Zheng, S.; Ye, H.; Chen, L. Synthesis and discovery of new compounds bearing coumarin scaffold for the treatment of pulmonary fibrosis. *Eur. J. Med. Chem.* **2020**, *185*, 111790. [CrossRef] [PubMed]
24. Mnafgui, K.; Ghazouani, L.; Hajji, R.; Tlili, A.; Derbali, F.; da Silva, F.I.; Araújo, J.L.; de Oliveira Schinoff, B.; Bachega, J.F.R.; da Silva Santos, A.L.; et al. Oleuropein protects against cerebral ischemia injury in rats: Molecular docking, biochemical and histological findings. *Neurochem. Res.* **2021**, *46*, 2131–2142. [CrossRef] [PubMed]
25. Intaraudom, C.; Rachtawee, P.; Suvannakad, R.; Pittayakhajonwut, P. Antimalarial and antituberculosis substances from *Streptomyces* sp. BCC26924. *Tetrahedron* **2011**, *67*, 7593–7597. [CrossRef]
26. Zhao, F.; Liu, Z.-Q. Indole and its alkyl-substituted derivatives protect erythrocyte and DNA against radical-induced oxidation. *J. Biochem. Mol. Toxicol.* **2009**, *23*, 273–279. [CrossRef]
27. Dudala, S.S.; Venkateswarulu, T.C.; Kancharla, S.C.; Kodali, V.P.; Babu, D.J. A review on importance of bioactive compounds of medicinal plants in treating idiopathic pulmonary fibrosis (special emphasis on isoquinoline alkaloids). *Future J. Pharm. Sci.* **2021**, *7*, 156. [CrossRef]

marine drugs

MDPI

Article

Anti-inflammatory Polyketides from the Marine-Derived Fungus *Eutypella scoparia*

Ya-Hui Zhang [1,2,3], Hui-Fang Du [2], Wen-Bin Gao [4], Wan Li [2], Fei Cao [2,*] and Chang-Yun Wang [1,3,*]

[1] Key Laboratory of Marine Drugs, the Ministry of Education of China, School of Medicine and Pharmacy, Institute of Evolution & Marine Biodiversity, Ocean University of China, Qingdao 266003, China; 15689932652@163.com
[2] College of Pharmaceutical Sciences, Key Laboratory of Pharmaceutical Quality Control of Hebei Province, Key Laboratory of Medicinal Chemistry and Molecular Diagnostics of Education Ministry of China, Hebei University, Baoding 071002, China; dhf12031203@163.com (H.-F.D.); liwanjingmin@163.com (W.L.)
[3] Laboratory for Marine Drugs and Bioproducts, Qingdao National Laboratory for Marine Science and Technology, Qingdao 266237, China
[4] College of Life Sciences, Cangzhou Normal University, Cangzhou 061000, China; wenbinxing@yeah.net
* Correspondence: caofei542927001@163.com (F.C.); changyun@ouc.edu.cn (C.-Y.W.)

Abstract: Three new polyketides, eutyketides A and B (**1** and **2**) and cytosporin X (**3**), along with four known compounds (**4**–**7**), were obtained from the marine-derived fungus *Eutypella scoparia*. The planar structures of **1** and **2** were elucidated by extensive HRMS and 1D and 2D NMR analyses. Their relative configurations of C-13 and C-14 were determined with chemical conversions by introducing an acetonylidene group. The absolute configurations of **1**–**3** were determined by comparing their experimental electronic circular dichroism (ECD) data with their computed ECD results. All of the isolated compounds were tested for their anti-inflammatory activities on lipopolysaccharide-induced nitric oxide production in RAW 264.7 macrophages. Compounds **5** and **6** showed stronger anti-inflammatory activities than the other compounds, with the inhibition of 49.0% and 54.9% at a concentration of 50.0 μg/mL, respectively.

Keywords: marine-derived fungus; *Eutypella scoparia*; polyketide; absolute configuration; anti-inflammatory activity

Citation: Zhang, Y.-H.; Du, H.-F.; Gao, W.-B.; Li, W.; Cao, F.; Wang, C.-Y. Anti-inflammatory Polyketides from the Marine-Derived Fungus *Eutypella scoparia*. *Mar. Drugs* **2022**, *20*, 486. https://doi.org/10.3390/md20080486

Academic Editor: Hee Jae Shin

Received: 8 July 2022
Accepted: 27 July 2022
Published: 28 July 2022

1. Introduction

Eutypella species, which are one genus of the ubiquitous fungi, are widely distributed in many extreme environments, including Antarctica, tropical forests, and marine organisms [1–3]. Chemical investigations of *Eutypella* species have resulted in diverse metabolites, including γ-lactones, benzopyrans, cysporins, terpenoids, and nitrogen-containing compounds [4,5]. Among them, many bioactive secondary metabolites were obtained, such as antibacterial scoparasin B [5], cytotoxic phenochalasin B [6], and antitumor diaporthein B [7]. The *Eutypella* genus has become an attractive target for discovering leading compounds due to its remarkable biological activity and novel complex structures. In recent years, a lot of work has been carried out on the isolation, total synthesis, pharmacological research, and drug development for the genus *Eutypella* [8–10].

As part of our ongoing investigation of bioactive natural products from marine-derived fungi [11–16], the strain *Eutypella scoparia* HBU-91 attracted our attention because the EtOAc extract of the culture showed anti-inflammatory activity. As a result, the new eutyketides A and B (**1** and **2**) and cytosporin X (**3**), together with four known compounds (**4**–**7**) (Figure 1), were obtained by using silica gel and LH-20 column chromatography and semipreparative HPLC. Structurally, compounds **1** and **2** were a pair of epimers with *vic*-diol unit on their side chain, while **3** exhibited a skeleton characterized by a polyketide moiety and a terpenoid part. All of the isolated compounds were tested for their anti-inflammatory activities. Herein, we report their isolation, structure elucidation, and biological activities.

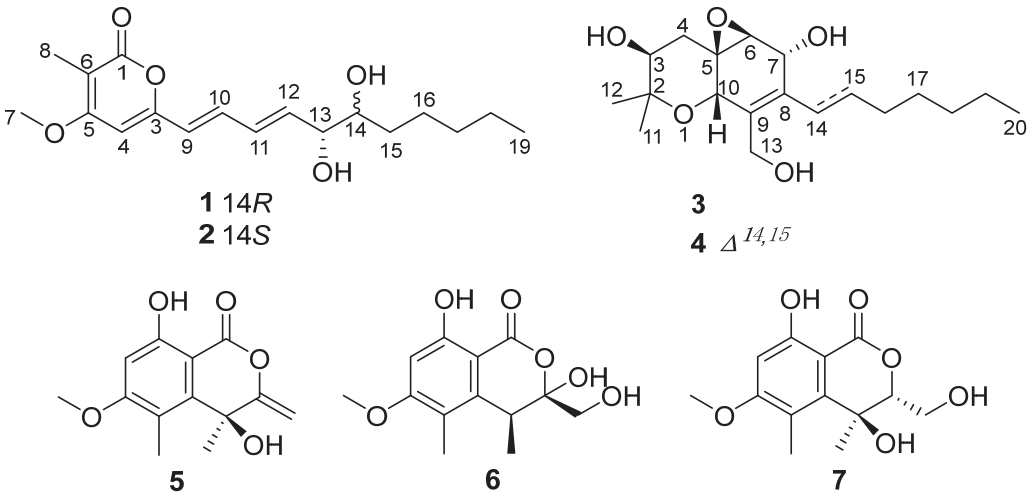

Figure 1. Chemical structures of compounds **1**−**7**.

2. Results and Discussion

2.1. Structural Elucidation

Eutyketide A (**1**) was obtained as a pale yellow oil. The molecular formula of **1** was determined to be $C_{18}H_{26}O_5$ based on the HRESIMS of the pseudomolecular ion (*m*/*z* 345.1669 $[M + Na]^+$, calcd for $C_{18}H_{26}O_5Na$, 345.1672), indicating six degrees of unsaturation. The IR spectrum suggested the presence of hydroxy (3385 cm^{-1}), double bond (1558 cm^{-1}), and ester carbonyl (1683 cm^{-1}) functionalities. The ^1H NMR spectrum (Table 1) showed resonances for five olefinic protons [δ_H 7.13 (dd, *J* = 15.0, 11.5 Hz), 6.42 (dd, *J* = 15.0, 11.5 Hz), 6.08 (d, *J* = 15.0 Hz), 6.07 (s), and 6.05 (dd, *J* = 15.0, 6.0 Hz)], two oxymethines [δ_H 4.23 (dd, *J* = 6.0, 4.2 Hz) and 3.72 (m)], a methoxy [δ_H 3.87 (s)], and two methyls [δ_H 1.93 (s) and 0.88 (t, *J* = 6.6 Hz)]. ^{13}C NMR combined with HSQC spectra (Table 1) of **1** displayed 18 carbon resonances that could be assignable to 9 sp^2 deshielded carbons, including a *α*,*β*-unsaturated carbonyl [δ_C 165.0, (C-1)] and 8 olefinic carbons [δ_C 157.3 (C-3), 96.1 (C-4), 165.8 (C-5), 103.2 (C-6), 122.8 (C-9), 134.8 (C-10), 130.8 (C-11), and 137.5 (C-12)], and 9 sp^3 deshielded carbons, including a methoxy [δ_C 56.4, (C-7)], 2 oxymethines [δ_C 75.2 (C-13) and 74.6 (C-14)], 4 methylenes [δ_C 32.2 (C-15), 31.9 (C-17), 25.7 (C-16), and 22.7 (C-18)], and 2 methyls [δ_C 8.9 (C-8) and 14.1 (C-19)]. The ^1H and ^{13}C NMR data revealed that **1** shares the same carbon framework as graphostrin I, a polyketide obtained from the Atlantic hydrothermal fungus *Graphostroma* sp. MCCC 3A00421 [17]. The main differences between them were the presence of a methyl at C-6 and a *vic*-diol [−OHCH−CHOH−] substructure at C-13/14 in **1** instead of the group [$-CH_2-CH_2-$] and the absence of the hydroxy group at C-18 in graphostrin I. The above differences were confirmed by the COSY cross-peaks of H-12/H-13/H-14/H_2-15 and H_2-17/H_2-18/H_3-19 and the HMBC correlations from H-8 to C-1, C-5, and C-6, from H-13 to C-11 and C-15, and from H-14 to C-12 and C-16, respectively (Figure 2). In addition, *trans* geometries at C-9−C-10 and C-11−C-12 double bonds were assigned by the large coupling constants ($J_{9,10}$ = 15.0 Hz and $J_{11,12}$ = 15.0 Hz) [17]. By detailed analysis of its 2D NMR spectra, the planar structure of **1** was assigned.

Eutyketide B (**2**) was also obtained as a pale yellow oil. It exhibited the same molecular formula as **1**, $C_{18}H_{26}O_5$, according to the pseudomolecular ion at *m*/*z* 345.1669 $[M + Na]^+$ in the HRESIMS spectrum. Detailed analysis of the ^1H and ^{13}C NMR spectra of **2** (Table 1) revealed that its 1D NMR data were similar to those of **1**. The differences were attributable to the signals [δ_H 4.05 (m, H-13) and 3.51 (m, H-14); δ_C 138.7 (C-12), 74.4 (C-13), and 33.2 (C-15) in **2** vs. δ_H 4.23 (dd, *J* = 6.0, 4.2 Hz, H-13) and 3.72 (m, H-14); δ_C 137.5 (C-12), 75.2 (C-13), and 32.2 (C-15) in **1**], indicating that the structural differences between them

should be located in this part of the structure (C-13 and C-14). Thus, it was deduced that **1** and **2** were either C-13 or C-14 epimers.

Table 1. ^{1}H (600 MHz) and ^{13}C (150 MHz) NMR Data of **1** and **2** in $CDCl_3$.

No.	1		2	
	δ_C, Type	δ_H (*J* in Hz)	δ_C, Type	δ_H (*J* in Hz)
1	165.0, C	-	165.0, C	-
3	157.3, C	-	157.2, C	-
4	96.1, CH	6.07, s	96.2, CH	6.06, s
5	165.8, C	-	165.8, C	-
6	103.2, C	-	103.3, C	-
7	56.4, CH_3	3.87, s	56.4, CH_3	3.87, s
8	8.9, CH_3	1.93, s	9.0, CH_3	1.93, s
9	122.8, CH	6.08, d (15.0)	123.0, CH	6.07, d (15.2)
10	134.8, CH	7.13, dd (15.0, 11.5)	134.7, CH	7.13, dd (15.2, 11.1)
11	130.8, CH	6.42, dd (15.0, 11.5)	130.7, CH	6.44, dd (15.2, 11.1)
12	137.5, CH	6.05, dd (15.0, 6.0)	138.7, CH	6.01, dd (15.2, 6.2)
13	75.2, CH	4.23, dd (6.0, 4.2)	74.4, CH	4.05, m
14	74.6, CH	3.72, m	74.7, CH	3.51, m
15	32.2, CH_2	1.42, m	33.2, CH_2	1.47, m
16	25.7, CH_2	1.31, m; 1.50, m	25.4, CH_2	1.48, m
17	31.9, CH_2	1.29, m	31.9, CH_2	1.30, m
18	22.7, CH_2	1.30, m	22.7, CH_2	1.29, m
19	14.1, CH_3	0.88, t (6.6)	14.1, CH_3	0.88, t (6.6)

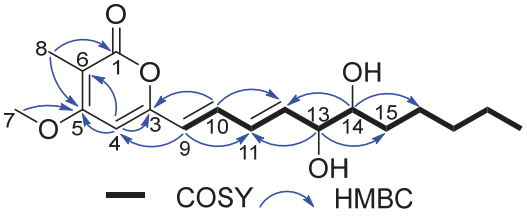

Figure 2. COSY and key HMBC correlations of compounds **1** and **2**.

The structural differences between **1** and **2** and their relative configurations were elucidated on the basis of chemical conversions and 1D NOE experiments. Treatment of **1** and **2** with 2,2-dimethoxypropane in the presence of TsOH afforded **1a** and **2a** as the acetonide products. In the selective NOE of **1a** (Figure 3), irradiation of H-13 at δ_H 4.59 and H-14 at δ_H 4.17 resulted in the enhancement of H_3-21, indicating that H-13 and H-14 should be placed on the same face of **1**. In the selective NOE of **2a** (Figure 3), irradiation of H-13 at δ_H 4.09 led to the enhancement of H_3-21, while irradiation of H-14 at δ_H 3.70 caused the enhancement of H_3-22, suggesting that H-13 and H-14 should be placed on the opposite side of **2**.

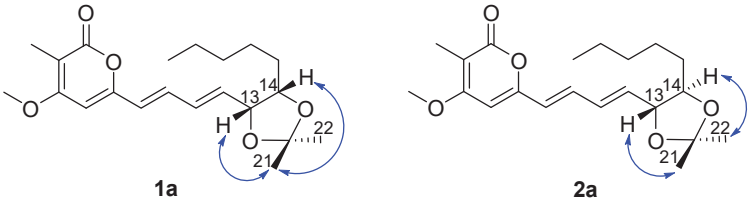

Figure 3. Structures and 1D NOE correlations of the acetonide products of **1a** and **2a**.

The calculation of the solution conformers is the most time-demanding part of the ECD calculation in conformationally flexible molecules and may be aided by simplifying the input geometry to reduce the number of conformers and save computational time [18]. For example, alkyl side chains and unsaturated side chains with isolated chromophores in an achiral environment could be simplified by truncation [18]. The absolute configuration of the hydroxyl group at C-13 was affected by the conjugate system, which can be determined by ECD calculation [19]. For **1** and **2**, the absolute configurations of C-13 and C-14 were determined by comparing their experimental electronic circular dichroism (ECD) results with the computed results of their simplified model compounds. The group of C-15 to C-19 was a saturated alkyl side chain with no chromophore and had a negligible effect on the ECD spectrum. Thus, the C-15 to C-19 alkyl substituent was truncated to a methyl group as model compound **1b** (Figure 4)**.** Molecules of (13*S*,14*S*)-**1b**, (13*R*,14*R*)-**1b**, (13*R*,14*S*)-**1b**, and (13*S*,14*R*)-**1b** were chosen for ECD calculations, which were carried out at the B3LYP/6-311+G(d,p) level in MeOH using the PCM model. The predicted ECD spectrum of (13*R*,14*R*)-**1b** matched well with the experimental ECD curve of **1**, and the predicted ECD spectrum of (13*R*,14*S*)-**1b** was in good agreement with the experimental ECD data of **2** (Figure 4). Therefore, the absolute configurations of **1** and **2** could be defined as 13*R*,14*R* and 13*R*,14*S*, respectively.

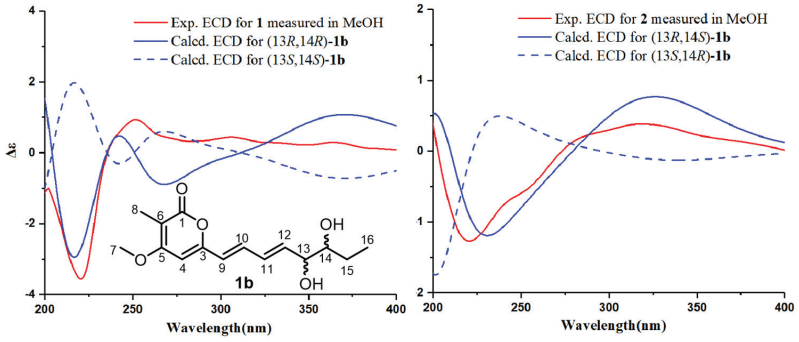

Figure 4. Calculated ECD spectra of (13*R*,14*R*)-**1b**, (13*S*,14*S*)-**1b**, (13*R*,14*S*)-**1b**, and (13*S*,14*R*)-**1b** and the experimental ECD spectra of **1** and **2**.

To the best of our knowledge, compounds **1** and **2** are very similar to prosolanapyrones and their congeners [20]. They share the same pyranone framework with long alkyl side chains. In addition to the conjugate double bonds, compounds **1** and **2** also contain a *vic*-diol unit on their side chains, while prosolanapyrones just possess double bonds on their side chains.

Cytosporin X (**3**) was obtained as a colorless oil. The molecular formula $C_{19}H_{32}O_5$ was determined for **3** from the pseudomolecular ion peak at *m*/*z* 363.2132 $[M + Na]^+$ (calcd 363.2142 for $C_{19}H_{32}O_5Na$), which is consistent with four degrees of unsaturation. The IR spectrum of **3** at 3402 and 1652 cm^{-1} suggested the presence of hydroxyl and double bond groups. The ^1H NMR spectrum of **3** displayed resonances for four oxygenated methine protons [δ_H 4.40 (s), 4.26 (d, *J* = 3.6 Hz), 3.67 (d, *J* = 12.0 Hz), and 3.24 (d, *J* = 3.6 Hz)], an oxygenated methylene proton [δ_H 4.24 (d, *J* = 12.0 Hz) and 4.04 (d, *J* = 12.0 Hz)], two singlet methyl protons [δ_H 1.32 (s) and 1.30 (s)], a terminal methyl proton [δ_H 0.87 (t, *J* = 6.6 Hz)], and a series of multiplet signals (Table 2). The ^{13}C NMR spectrum of **3** revealed 19 resonances, including 2 olefinic carbons [δ_C 128.3 (C-8) and 138.1 (C-9)], 2 oxygenated quaternary carbons [δ_C 56.1 (C-5) and 77.2 (C-2)], 4 oxygenated methine carbons [δ_C 60.1 (C-6), 67.2 (C-7), 68.6 (C-10), and 73.5 (C-3)], an oxygenated methylene carbon [δ_C 62.2 (C-13)], 7 methylene carbons [δ_C 22.7 (C-19), 29.0 (C-15), 29.2 (C-17), 29.8 (C-16), 30.6 (C-14), 31.9 (C-18), and 35.6 (C-4)], and 3 methy carbons [δ_C 28.0 (C-12), 16.3 (C-11), and 14.2 (C-20)] (Table 2). The NMR data revealed that **3** belongs to the family of hexahydrobenzopyrane

skeletons and is characterized by a polyketide moiety and a terpenoid part (the red part in Figure 5) with a tricyclic structure containing a hexahydrobenzopyrane moiety fused with an oxirane ring [1]. Careful comparison of the NMR data of **3** with those of the known hexahydrobenzopyrane cytosporin D (**4**) indicated that the structure of **3** is closely related to **4**. The notable difference between them lay in the presence of two methylene signals [δ_H 2.27 and 2.16 (H-14), 1.33 and 1.42 (H-15); δ_C 30.6 (C-14) and 29.0 (C-15) in **3**] and the absence of two olefinic methine signals [δ_H 6.48 (H-14), 6.15 (H-15); δ_C 124.8 (C-14) and 135.9 (C-15) in **4**]. The COSY cross-peaks of H-14/15/16 and the key HMBC correlations from H-14 to C-7/C-9 and from H-15 to C-8/C-17 (Figure 5) confirmed the above difference. Therefore, the planar structure of **3** was established.

Table 2. ^{1}H (600 MHz) and ^{13}C (150 MHz) NMR Data of **3** in $CDCl_3$.

No.	δ_C, Type	δ_H (*J* in Hz)
2	77.2, C	-
3	73.5, CH	3.67, d (12.0)
4	35.6, CH_2	2.23, dd (13.2, 5.4); 1.67, dd (13.2, 5.4)
5	56.1, C	-
6	60.1, CH	3.24, d (3.6)
7	67.2, CH	4.26, d (3.6)
8	128.3, C	-
9	138.1, C	-
10	68.6, CH	4.40, s
11	16.3, CH_3	1.32, s
12	28.0, CH_3	1.30, s
13	62.2, CH_2	4.24, d (12.0); 4.04, d (12.0)
14	30.6, CH_2	2.27, m; 2.16, m
15	29.0, CH_2	1.33, m; 1.42, m
16	29.8, CH_2	1.25, m
17	29.2, CH_2	1.26, m
18	31.9, CH_2	1.24, m
19	22.7, CH_2	1.27, m
20	14.2, CH_3	0.87, t (6.6)

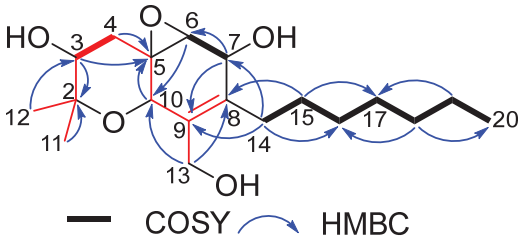

Figure 5. COSY and key HMBC correlations of **3**.

The relative configuration of **3** was determined by analysis of the NOESY data (Figure 6). The NOESY correlations of H-3/H_3-12, H_3-11/H-10, H-10/H-7, H-10/H-4β, and H-4α/H-6 indicated that H-3 and H-6 were situated on the same side of the molecule with an α-orientation, while C-5, C-6, H-7, and H-10 were accordingly assigned to be β-configured. In addition, the observed NOEs are consistent with the structure and relative configuration of **4**.

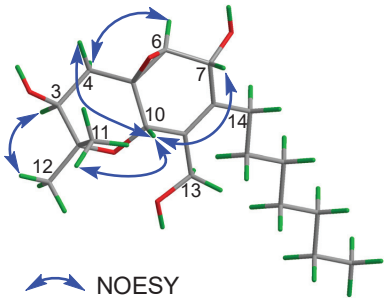

Figure 6. Key NOESY correlations of **3**.

The absolute configuration of **3** was determined on the basis of ECD calculations. Compound **3** had a long flexible side chain with no chromophore. Thus, the side chain was truncated to two methyl groups attached at C-8, and model compound **3a** was used for ECD calculations. The calculations were carried out for (3*S*,5*R*,6*S*,7*R*,10*S*)-**3a** and (3*R*,5*S*,6*R*,7*S*,10*R*)-**3a** at the B3LYP/6-311+G(d,p) level using the PCM model (MeOH). The calculated ECD curve of (3*S*,5*R*,6*S*,7*R*,10*S*)-**3a** matched well with the experimental ECD data of **3** (Figure 7). Therefore, the absolute configuration of **3** was defined as 3*S*,5*R*,6*S*,7*R*,10*S*.

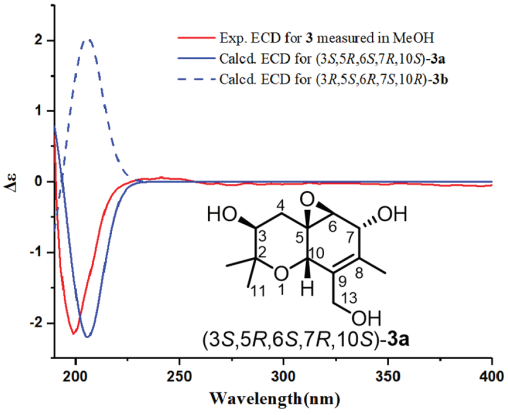

Figure 7. Calculated ECD spectra of (3*S*,5*R*,6*S*,7*R*,10*S*)-**3a** and (3*R*,5*S*,6*R*,7*S*,10*R*)-**3a** and the experimental ECD spectrum of **3**.

The known compounds **4**−**7** were identified as cytosporin D (**4**) [1], 4,8-dihydroxy-6-methoxy-4,5-dimethyl-3-methyleneisochroman-1-one (**5**) [21], banksialactone A (**6**) [22], and 4,8-dihydroxy-3-(hydr-oxymethyl)-6-methoxy-4,5-dimethylisochroman-1-one (**7**) [23], respectively, by comparing their NMR and MS data with reported values.

2.2. Anti-Inflammatory Activity

The anti-inflammatory activities of **1**−**7** were tested by evaluating their influence on nitric oxide (NO) production in RAW264.7 cells induced by lipopolysaccharide (LPS). Compounds **5** and **6** showed stronger anti-inflammatory activities than other compounds, with inhibition rates of 49.0%, 32.1%, and 27.4% for **5** and 54.9%, 35.9%, and 21.1% for **6** at concentrations of 50.0, 25.0, and 12.5 μg/mL, respectively. Moreover, **5** was also active at 6.25 μg/mL with 24.1% inhibition. In addition, **1** exhibited 20.3% inhibition when tested at 6.25 μg/mL (Table S2).

3. Materials and Methods

3.1. General Experimental Procedures

The OR data were recorded on a JASCO P-2000 spectrometer (Jasco Corp., Tokyo, Japan) in MeOH. ECD and UV spectra were measured by MOS450-SFM300 (Biologic, Grenoble, France) and a Perkin-Elmer model 241 spectrophotometers (Perkin-Elmer Corp., Waltham, MA, USA), respectively, with samples dissolved in MeOH. IR spectra were acquired on an FTIR-8400 spectrometer (Shimadzu, Kyoto, Japan) using KBr pellets. NMR data were recorded on a Bruker AV-600 spectrometer (Bruker Corp., Rheinstetten, Germany) with TMS as the internal standard. HRESIMS spectra were obtained from a Bruker apex-ultra 7.0T spectrometer (Bruker Corp., Rheinstetten, Germany). HPLC separation was performed on the Shimadzu LC-20AT system (Shimadzu, Kyoto, Japan) using an RP-18 HPLC column (Waters, Worcester, MA, USA, 10 × 250 mm, 5 μm).

3.2. Isolation of Fungal Material

3.2.1. Fungal Material

The fungal strain *Eutypella scoparia* HBU-91 (GenBank, OM892669) was collected from the Bohai Sea (Huanghua, China, Apr. 2017). The strain was deposited in the College of Pharmaceutical Sciences, Hebei University, Baoding, China.

3.2.2. Fermentation and Purification

Fermentation was carried out for the fungus *E. scoparia* using rice medium (170 mL water and 200 g rice in 1 L Erlenmeyer flasks, 200 flasks) at 28 °C for 40 days. After cultivation, the fermented rice substrate was extracted with a mixture of CH_2Cl_2/MeOH (1:1, 500 mL for each flask) five times and EtOAc five times successively to produce a residue (40.0 g), which was further subjected to silica gel column chromatography (CC), eluting with EtOAc−petroleum ether (PE) stepped gradient elution (0%–100%), to afford six fractions, Fr.1−Fr.6. Fr.2 was separated by Sephadex LH-20 CC (PE−CH_2Cl_2−MeOH (*v*/*v*, 2:1:1)) to afford four subfractions, Fr.2-1−Fr.2-4. Then, Fr.2-2 was fractionated by silica gel CC (PE−EtOAc, 5:1) and further purified by semipreparative HPLC (MeOH−H_2O, 70:30, 2.0 mL/min) to afford **6** (2.3 mg) and **5** (3.9 mg). Fr.4 was separated by Sephadex LH-20 CC (MeOH−CH_2Cl_2 (*v*/*v*, 1:1)) to give subfractions Fr.4-1−Fr.4-3. Fr.4-1 was fractionated by silica gel CC (PE−Acetone, 3:1) and further purified by semipreparative HPLC (MeOH−H_2O, 70:30, 2.0 mL/min) to give **4** (15.9 mg). Compound **3** (15.5 mg) was obtained from Fr.4-2 under the same conditions as **4.** Fr.4-3 was fractionated by semipreparative HPLC (MeOH−H_2O, 60:40, 2 mL/min) to provide **1** (4.0 mg) and **2** (3.2 mg). Fr.5 was separated by Sephadex LH-20 CC (MeOH−CH_2Cl_2 (*v*/*v*, 1:1)) to give subfractions Fr.5-1 and Fr.5-2. Fr.5-2 was fractionated by silica gel CC (CH_2Cl_2/MeOH, 80:1) and further purified by semipreparative HPLC (MeOH−H_2O, 50:50, 2.0 mL/min) to afford **7** (4.8 mg).

Eutylactone A (**1**): pale yellow oil; $[\alpha]_{20}^{D}$ +105.8 (*c* 0.1, MeOH); UV (MeOH) λ_{max} (log ε) 225 (2.85), 396 (2.36) nm; ECD (1.04 mM, MeOH) λ_{max} ($\Delta\varepsilon$) 221 (−3.5), 251 (+0.9) nm; IR (KBr) v_{max} 3385, 2932, 2341, 1683, 1558, 1027 cm^{-1}; ^1H and ^{13}C NMR data see Table 1; HRESIMS *m*/*z* 345.1669 $[M + Na]^+$ (calcd for $C_{18}H_{26}O_5Na$, 345.1672 $[M + Na]^+$).

Eutylactone B (**2**); pale yellow oil; $[\alpha]_{20}^{D}$ +9.5 (*c* 0.1, MeOH); UV (MeOH) λ_{max} (log ε) 223 (2.85), 392 (2.39) nm; ECD (1.04 mM, MeOH) λ_{max} ($\Delta\varepsilon$) 221 (−1.3), 319 (+0.4) nm; IR (KBr) v_{max} 3300, 2929, 2359,1679, 1556, 1027 cm^{-1}; ^1H and ^{13}C NMR data see Table 1; HRESIMS *m*/*z* 345.1669 $[M + Na]^+$ (calcd for $C_{18}H_{26}O_5Na$, 345.1672 $[M + Na]^+$).

Cytosporin X (**3**); pale yellow oil; $[\alpha]_{20}^{D}$ −314.5 (*c* 0.1, MeOH); UV (MeOH) λ_{max} (log ε) 254 (2.64), 335 (2.04) nm; ECD (0.98 mM, MeOH) λ_{max} ($\Delta\varepsilon$) 199 (−2.15) nm; IR (KBr) v_{max} 3402, 2918, 2351, 1652, 1018 cm^{-1}; ^1H and ^{13}C NMR data see Table 2; HRESIMS *m*/*z* 363.2132 $[M + Na]^+$ (calcd for $C_{19}H_{32}O_5Na$, 363.2142 $[M + Na]^+$); 379.1871 $[M + K]^+$ (calcd for $C_{19}H_{32}O_5K$, 379.1881 $[M + K]^+$).

3.2.3. Acetonide Formation of **1** and **2**

A mixture of **1** (1.0 mg), 2,2-dimethoxypropane (2.0 mL), and *p*-TsOH (0.2 mg) was stirred at room temperature for 0.5 h. Saturated aqueous $NaHCO_3$ (6.0 mL) was then added, and the reaction mixture was extracted with EtOAc (24 mL × 3). The organic solvents were removed with a high-vacuum pump, and the crude mixture was subjected to preparative HPLC to obtain acetonide product **1a** (0.96 mg). Acetonide product **2a** (0.91 mg) was obtained from **2** under the same conditions as **1a.**

Compound **1a**: ^{1}H NMR (600 MHz, $CDCl_3$) δ 7.17 (1H, dd, *J* = 15.1, 10.9 Hz, H-10), 6.74 (1H, dd, *J* = 15.0, 5.6 Hz, H-11), 6.37 (1H, dd, *J* = 15.0, 10.9 Hz, H-9), 6.06 (1H, s, H-4), 5.96 (1H, dd, *J* = 15.0, 7.2 Hz, H-12), 4.59 (1H, m, H-13), 4.35 (1H, s, H-14), 3.88 (3H, m, H-7), 1.94 (3H, s, H-8), 1.38 (3H, s, H-21), 1.34 (3H, s, H-22), 1.30-1.50 (8H, m, H-15/16/17/18), 0.88 (3H, t, *J* = 6.6 Hz, H-19).

Compound **2a**: ^{1}H NMR (600 MHz, $CDCl_3$) δ 7.15 (1H, dd, *J* = 15.0, 11.1 Hz, H-10), 6.43 (1H, dd, *J* = 15.0, 11.1 Hz, H-11), 6.09 (1H, d, *J* = 15.0 Hz, H-9), 6.06 (1H, s, H-4), 5.94 (1H, dd, *J* = 15.0, 7.2 Hz, H-12), 4.09 (1H, m, H-13), 3.88 (3H, s, H-8), 3.70 (1H, m, H-14), 1.95 (3H, s, H-8), 1.26 (3H, s, H-21), 1.25 (3H, s, H-22), 1.30-1.50 (8H, m, H-15/16/17/18), 0.89 (3H, t, *J* = 6.6 Hz, H-19).

3.3. Computational Section

A conformational search for the molecules was carried out using the MMFF94S force field and Compute VOA software, with relative energies ranging from 0−10.0 kcal/mol energy, respectively. The conformers were optimized at the B3LYP/6-31G(d)//B3LYP/6-311+G(d) levels with Gaussian 09 software [24]. Then, stable conformers with relative energy within a 2.5 kcal/mol energy window were chosen for ECD calculations at the B3LYP/6-311+G(d,p) level in methanol using the PCM model, with a total of 60 excited states. A standard deviation of 0.3 eV was used for ECD simulations. Boltzmann statistics were applied for the final simulations of the ECD spectra by the software SpecDis 1.64 [25].

3.4. Cell Culture and Viability Assay

Compounds **1**−**7** were first tested for their cytotoxic effects on RAW264.7 cells at 3.13, 6.25, 12.5, 25.0, and 50.0 μg/mL. Murine monocytic RAW264.7 macrophages were cultivated at 37 °C with 5% CO_2 in Dulbecco's modified Eagle's medium (DMEM), which was added with 10% (*v*/*v*) fetal bovine serum (FBS) as well as 1% (*v*/*v*) penicillin/streptomycin. RAW264.7 cells were grown in 96-well plates and then incubated with the tested compounds for 24 h. A solution of 3-(4,5-dimethylthiazol-2-yl)-2,5-diphenyl tetrazolium bromide (MTT) at a concentration of 5.0 mg/mL was substituted for the culture medium. After incubation at 37 °C for 4 h, the MTT solution was removed, and DMSO was chosen for the dissolution of the formazan crystals. The absorbance was measured at 540 nm with a microplate reader [26]. Compounds **3**−**7** exhibited no toxicity at a concentration of 50.0 μg/mL, **1** showed no toxicity at a concentration of 25.0 μg/mL, and **2** displayed no toxicity at a concentration of 6.25 μg/mL.

3.5. Inhibition of NO Production Assay

The Griess assay was applied to evaluate the production of NO through the level of nitrite (NO_2) in the medium [27]. RAW264.7 cells were inoculated into 96-well plates, and then LPS at a concentration of 1.0 μg/mL was added to induce inflammation. The tested compounds at different concentrations were added to the above mixture. The Griess reaction was used for the quantification of NO production in the supernatant. The absorbance was measured at 540 nm with a microplate reader. All of the experiments were carried out in triplicate.

4. Conclusions

In summary, three new polyketides (**1**−**3**), together with four known compounds (**4**−**7**), were isolated from the marine-derived fungus *Eutypella scoparia*. Chemical conver-

sions and TDDFT ECD calculations were used to determine the absolute configurations of **1**−**3**. Compounds **1**, **5**, and **6** exhibited certain anti-inflammatory activities on nitric oxide (NO) production in RAW264.7 cells induced by lipopolysaccharide (LPS). Our findings will contribute to the diversity of these fungal metabolites.

Supplementary Materials: The following supporting information can be downloaded at: https://www.mdpi.com/article/10.3390/md20080486/s1. Figures S1−S29: 1D and 2D NMR, HRESIMS, and IR and UV spectra of compounds **1**−**3** and 1D NOE of **1a** and **2a**; Table S1: Cytotoxic activity data of compounds **1**−**7**; Table S2: Anti-inflammatory activity data of compounds **1**−**7**; Tables S3−S8: The coordinates for the lowest-energy conformers of **1b** and **3a** in ECD calculations.

Author Contributions: Conceptualization, Y.-H.Z. and F.C.; methodology, Y.-H.Z.; software, H.-F.D.; validation, Y.-H.Z. and H.-F.D.; formal analysis, Y.-H.Z. and W.-B.G.; investigation, Y.-H.Z.; resources, F.C.; data curation, Y.-H.Z. and W.L.; writing—original draft preparation, Y.-H.Z.; writing—review and editing, F.C. and C.-Y.W., visualization, F.C.; supervision, F.C. and C.-Y.W.; project administration, F.C. and C.-Y.W.; funding acquisition, F.C. and C.-Y.W. All authors have read and agreed to the published version of the manuscript.

Funding: This research was funded by the National Natural Science Foundation of China (No. 41830535), Shandong Provincial Natural Science Foundation (Major Basic Research Projects) (ZR2019ZD18), the Program of Open Studio for Druggability Research of Marine Natural Products, Pilot National Laboratory for Marine Science and Technology (Qingdao, China) directed by Kai-Xian Chen and Yue-Wei Guo, and the Taishan Scholars Program, China, Natural Science Foundation of Hebei Province of China (No. H2021201059).

Institutional Review Board Statement: Not applicable.

Data Availability Statement: Data are contained within the article or Supplementary Material.

Acknowledgments: We would like to thank the High Performance Computer Center of Hebei University for providing computational services.

Conflicts of Interest: The authors declare no conflict of interest.

References

1. Ciavatta, M.L.; Lopez-Gresa, M.P.; Gavagnin, M.; Nicoletti, R.; Manzo, E.; Mollo, E.; Guo, Y.W.; Cimino, G. Cytosporin-related compounds from the marine-derived fungus *Eutypella scoparia*. *Tetrahedron* **2008**, *64*, 5365–5369. [CrossRef]
2. Bergero, R.; Girlanda, M.; Varese, G.C.; Intili, D.; Luppi, A.M. Psychrooligotrophic fungi from arctic soils of Franz Joseph Land. *Polar Biol.* **1999**, *21*, 361–368. [CrossRef]
3. Yuan, Z.Q. Fungi and associated tree diseases in Melville Island, Northern Territory, Australia. *Aust. Syst. Bot.* **1996**, *9*, 337–360. [CrossRef]
4. Isaka, M.; Palasarn, S.; Lapanun, S.; Chanthaket, R.; Boonyuen, N.; Lumyong, S. γ-Lactones and *ent*-eudesmane sesquiterpenes from the endophytic fungus *Eutypella* sp. BCC 13199. *J. Nat. Prod.* **2009**, *72*, 1720–1722. [CrossRef]
5. Pongcharoen, W.; Rukachaisirikul, V.; Phongpaichit, S.; Rungjindamai, N.; Sakayaroj, J. Pimarane diterpene and cytochalasin derivatives from the endophytic fungus *Eutypella scoparia* PSU-D44. *J. Nat. Prod.* **2006**, *69*, 856–858. [CrossRef] [PubMed]
6. Kongprapan, T.; Rukachaisirikul, V.; Saithong, S.; Phongpaichit, S.; Poonsuwan, W.; Sakayaroj, J. Cytotoxic cytochalasins from the endophytic fungus *Eutypella scoparia* PSU-H267. *Phytochem. Lett.* **2015**, *13*, 171–176. [CrossRef]
7. Li, D.; Sun, L.; Chen, Y.; Zhang, W.; Zhang, Q.; Wang., L. Manufacture Method and Application of Diaporthein B in Antitumor agents. CN Patent 102168119A, 31 August 2011.
8. Liu, H.; Zhang, L.; Chen, Y.; Li, S.; Tan, G.; Sun, Z.; Pan, Q.; Ye, W.; Li, H.; Zhang, W. Cytotoxic pimarane-type diterpenes from the marine sediment-derived fungus *Eutypella* sp. FS46. *Nat. Prod. Res.* **2017**, *31*, 404–410. [CrossRef]
9. Sun, L.; Li, D.; Tao, M.; Chen, Y.; Zhang, Q.; Dan, F.; Zhang, W. Two new polyketides from a marine sediment-derived fungus *Eutypella scoparia* FS26. *Nat. Prod. Res.* **2013**, *27*, 1298–1304. [CrossRef]
10. Sun, L.; Li, D.; Tao, M.; Chen, Y.; Dan, F.; Zhang, W. Scopararanes C–G: New oxygenated pimarane diterpenes from the marine sediment-derived fungus *Eutypella scoparia* FS26. *Mar. Drugs* **2012**, *10*, 539–550. [CrossRef] [PubMed]
11. Cao, F.; Meng, Z.H.; Mu, X.; Yue, Y.F.; Zhu, H.J. Absolute configuration of bioactive azaphilones from the marine-derived fungus *Pleosporales* sp. CF09-1. *J. Nat. Prod.* **2019**, *82*, 386–392. [CrossRef] [PubMed]
12. Cao, F.; Meng, Z.H.; Wang, P.; Luo, D.Q.; Zhu, H.J. Dipleosporalones A and B, dimeric azaphilones from a marine-derived *Pleosporales* sp. fungus. *J. Nat. Prod.* **2020**, *83*, 1283–1287. [CrossRef]
13. Liu, Y.F.; Yue, Y.F.; Feng, L.X.; Zhu, H.J.; Cao, F. Asperienes A–D, bioactive sesquiterpenes from the marine-derived fungus *Aspergillus flavus*. *Mar. Drugs* **2019**, *17*, 550–559. [CrossRef] [PubMed]

14. Guo, X.C.; Xu, L.L.; Yang, R.Y.; Yang, M.Y.; Hu, L.D.; Zhu, H.J.; Cao, F. Anti-*vibrio* indole-diterpenoids and C-25 epimeric steroids from the marine-derived fungus *Penicillium janthinellum*. *Front. Chem.* **2019**, *7*, 80. [CrossRef]
15. Meng, Z.H.; Sun, T.T.; Zhao, G.Z.; Yue, Y.F.; Chang, Q.H.; Zhu, H.J.; Cao, F. Marine-derived fungi as a source of bioactive indole alkaloids with diversified structures. *Mar. Life Sci. Technol.* **2021**, *3*, 44–61. [CrossRef]
16. Hai, Y.; Wei, M.Y.; Wang, C.Y.; Gu, Y.C.; Shao, C.L. The intriguing chemistry and biology of sulfur-containing natural products from marine microorganisms (1987–2020). *Mar. Life Sci. Technol.* **2021**, *3*, 488–518. [CrossRef]
17. Niu, S.; Liu, Q.; Xia, J.M.; Xie, C.L.; Luo, Z.H.; Shao, Z.; Liu, G.; Yang, X.W. Polyketides from the deep-sea-derived fungus *Graphostroma* sp. MCCC 3A00421 showed potent antifood allergic activities. *J. Agric. Food Chem.* **2018**, *66*, 1369–1376. [CrossRef]
18. Mándi, A.; Kurtán, T. Applications of OR/ECD/VCD to the structure elucidation of natural products. *Nat. Prod. Rep.* **2019**, *36*, 889–918. [CrossRef]
19. Ren, J.; Ding, S.S.; Zhu, A.; Cao, F.; Zhu, H.J. Bioactive azaphilone derivatives from the fungus *Talaromyces aculeatus*. *J. Nat. Prod.* **2017**, *80*, 2199–2203. [CrossRef]
20. Oikawa, H.; Kobayashi, T.; Katayama, K.; Suzuki, Y.; Ichihara, A. Total synthesis of (−)-solanapyrone a via enzymatic Diels−Alder reaction of prosolanapyrone. *J. Org. Chem.* **1998**, *63*, 8748–8756. [CrossRef]
21. Tayone, W.C.; Honma, M.; Kanamaru, S.; Noguchi, S.; Tanaka, K.; Nehira, T.; Hashimoto, M. Stereochemical investigations of isochromenones and isobenzofuranones isolated from *Leptosphaeria* sp. KTC 727. *J. Nat. Prod.* **2011**, *74*, 425–429. [CrossRef] [PubMed]
22. Tayone, W.C.; Kanamaru, S.; Honma, M.; Tanaka, K.; Nehira, T.; Hashimoto, M. Absolute stereochemistry of novel isochromanone derivatives from *Leptosphaeria* sp. KTC 727. *Biosci. Biotechnol. Biochem.* **2011**, *75*, 2390–2393. [CrossRef] [PubMed]
23. El-Elimat, T.; Raja, H.A.; Figueroa, M.; Falkinham, J.O., III.; Oberlies, N.H. Isochromenones, isobenzofuranone, and tetrahydronaphthalenes produced by *Paraphoma radicina*, a fungus isolated from a freshwater habitat. *Phytochemistry* **2014**, *104*, 114–120. [CrossRef] [PubMed]
24. Frisch, M.J.; Trucks, G.W.; Schlegel, H.B.; Scuseria, G.E.; Robb, M.A.; Cheeseman, J.R.; Scalmani, G.; Barone, V.; Mennucci, B.; Petersson, G.A.; et al. *Gaussian 09*; Gaussian Inc.: Wallingford, CT, USA, 2009.
25. Bruhn, T.; Schaumlöffel, A.; Hemberger, Y.; Bringmann, G. SpecDis: Quantifying the comparison of calculated and experimental electronic circular dichroism spectra. *Chirality* **2013**, *25*, 243–249. [CrossRef] [PubMed]
26. Mosmann, T. Rapid colorimetric assay for cellular growth and survival: Application to proliferation and cytotoxicity assays. *J. Immunol. Methods* **1983**, *65*, 55–63. [CrossRef] [PubMed]
27. Griess, L.C.; Wagner, D.A.; Glogowski, J.; Skipper, P.L.; Wishnok, J.S.; Tannenbaum, S.R. Analysis of nitrate, nitrite and [^{15}N] in biological fluids. *Anal. Biochem.* **1982**, *126*, 131–138. [CrossRef]

marine drugs

MDPI

Article

New Alkylpyridinium Anthraquinone, Isocoumarin, C-Glucosyl Resorcinol Derivative and Prenylated Pyranoxanthones from the Culture of a Marine Sponge-Associated Fungus, *Aspergillus stellatus* KUFA 2017

Fátima P. Machado [1,2], Inês C. Rodrigues [1], Luís Gales [1,3], José A. Pereira [1,2], Paulo M. Costa [1,2], Tida Dethoup [4], Sharad Mistry [5], Artur M. S. Silva [6], Vitor Vasconcelos [2,7] and Anake Kijjoa [1,2,*]

[1] ICBAS-Instituto de Ciências Biomédicas Abel Salazar, Rua de Jorge Viterbo Ferreira, 228, 4050-313 Porto, Portugal
[2] Interdisciplinary Centre of Marine and Environmental Research (CIIMAR), Terminal de Cruzeiros do Porto de Leixões, Av. General Norton de Matos s/n, 4450-208 Matosinhos, Portugal
[3] Instituto de Biologia Molecular e Celular (i3S-IBMC), Universidade do Porto, Rua de Jorge Viterbo Ferreira, 228, 4050-313 Porto, Portugal
[4] Department of Plant Pathology, Faculty of Agriculture, Kasetsart University, Bangkok 10240, Thailand
[5] Department of Chemistry, University of Leicester, University Road, Leicester LE 7 RH, UK
[6] Departamento de Química & QOPNA, Universidade de Aveiro, 3810-193 Aveiro, Portugal
[7] FCUP-Faculty of Sciences, University of Porto, Rua do Campo Alegre, s/n, 4169-007 Porto, Portugal
* Correspondence: ankijjoa@icbas.up.pt; Tel.: +351-962712474; Fax: +351-22-206-2232

Citation: Machado, F.P.; Rodrigues, I.C.; Gales, L.; Pereira, J.A.; Costa, P.M.; Dethoup, T.; Mistry, S.; Silva, A.M.S.; Vasconcelos, V.; Kijjoa, A. New Alkylpyridinium Anthraquinone, Isocoumarin, C-Glucosyl Resorcinol Derivative and Prenylated Pyranoxanthones from the Culture of a Marine Sponge-Associated Fungus, *Aspergillus stellatus* KUFA 2017. *Mar. Drugs* **2022**, *20*, 672. https://doi.org/10.3390/md20110672

Academic Editor: Hee Jae Shin

Received: 22 September 2022
Accepted: 26 October 2022
Published: 27 October 2022

Abstract: An unreported isocoumarin, (*3S*,*4R*)-4-hydroxy-6-methoxymellein (**2**), an undescribed propylpyridinium anthraquinone (**4**), and an unreported C-glucosyl resorcinol derivative, acetyl carnemycin E (**5c**), were isolated, together with eight previously reported metabolites including *p*-hydroxybenzaldehyde (**1**), 1,3-dimethoxy-8-hydroxy-6-methylanthraquinone (**3a**), 1,3-dimethoxy-2,8-dihydroxy-6-methylanthraquinone (**3b**), emodin (**3c**), 5[(*3E*,*5E*)-nona-3,5-dien-1-yl]benzene (**5a**), carnemycin E (**5b**), tajixanthone hydrate (**6a**) and 15-acetyl tajixanthone hydrate (**6b**), from the ethyl acetate extract of the culture of a marine sponge-derived fungus, *Aspergillus stellatus* KUFA 2017. The structures of the undescribed compounds were elucidated by 1D and 2D NMR and high resolution mass spectral analyses. In the case of **2**, the absolute configurations of the stereogenic carbons were determined by comparison of their calculated and experimental electronic circular dichroism (ECD) spectra. The absolute configurations of the stereogenic carbons in **6a** and **6b** were also determined, for the first time, by X-ray crystallographic analysis. Compounds **2**, **3a**, **3b**, **4**, **5a**, **5b**, **5c**, **6a**, and **6b** were assayed for antibacterial activity against four reference strains, viz. two Gram-positive (*Staphylococcus aureus* ATCC 29213, *Enterococcus faecalis* ATCC 29212) and two Gram-negative (*Escherichia coli* ATCC 25922, *Pseudomonas aeruginosa* ATCC 27853), as well as three multidrug-resistant strains. However, only **5a** exhibited significant antibacterial activity against both reference and multidrug-resistant strains. Compound **5a** also showed antibiofilm activity against both reference strains of Gram-positive bacteria.

Keywords: *Aspergillus stellatus*; Trichocomaceae; marine sponge-associated fungus; anthraquinones; isocoumarin; C-glucosyl resorcinols; antibacterial activity; antibiofilm activity

1. Introduction

The genus *Aspergillus* (family Aspergillaceae) is one of the most extensively studied genera of filamentous fungi, mainly due to the medical relevance, food spoilage, and industrial application of some of its species. Aspergilli can grow in a wide range of niches, mainly in soils and on dead matter, but some are also capable of colonizing living animal or plant hosts. However, the increasing numbers of *Aspergillus* species have been found in

different niches in the marine environment, from tropical waters [1] to the Arctic [2], and from shallow waters [3] to the deep-sea [4]. In total, approximately 350 *Aspergillus* species have been identified [5].

In the last two decades, marine-derived *Aspergillus* species have attracted tremendous attention from researchers working on marine natural products since they were responsible for a production of the highest numbers of marine fungal metabolites as demonstrated by two review articles, one covering the period of January 1992 to December 2014, reporting 512 metabolites, and another covering the period of 2015 to December 2020, which reported 361 compounds, isolated from marine-derived *Aspergillus* species [6]. It is also worth mentioning that the specialized metabolites produced by marine-derived *Aspergillus* species possess not only structural diversity such as indole alkaloids, diketopiperazine derivatives, meroterpenoids, anthraquinones, isocoumarins, xanthones, *p*-terphenyl derivatives, and peptides, but also a myriad of biological activities [6].

In our pursuit of antibiotic and antibiofilm compounds from marine-derived fungi from tropical seas, we focused our attention on the marine sponge-associated *Aspergillus stellatus* since this fungus has not been extensively investigated. A literature search revealed that a mycotoxin, asteltoxin, was isolated from toxic maize meal cultures of *A. stellatus* Curzi (MRC 277) [7]. In another work, Kamal et al. reported the isolation of tajixanthone, shamixanthone, ajamxanthone, shahenxanthone, najamxanthone, radixanthone, and mannitol from the mycelium of *A. stellatus* Curzi [8]. For this reason, we investigated secondary metabolites from the culture of *A. stellatus* KUFA 2017, isolated from a marine sponge, *Mycale* sp., which was collected from the coral reef at the Samaesan Island, in the Gulf of Thailand.

Fractionation of the ethyl acetate (EtOAc) extract of the culture *A. stellatus* KUFA 2017 by column chromatography of silica gel, followed by purification by preparative TLC, Sephadex LH-20 column and crystallization, led to the isolation of undescribed (*3S*,*4R*)-4-hydroxy-6-methoxymellein (**2**), stellatanthraquinone (**4**), and acetyl carnemycin E (**5c**), as well as the previously reported *p*-hydroxybenzaldehyde (**1**) [9], 1,3-dimethoxy-8-hydroxy-6-methylanthraquinone (**3a**) [10], 1,3-dimethoxy-2,8-dihydroxy-6-methylanthraquinone (**3b**) [11], emodin (**3c**) [12] and 5[(3*E*,5*E*)-nona-3,5-dien-1-yl]benzene (**5a**) [13], carnemycin E (**5b**) [13], tajixanthone hydrate (**6a**) [14,15], and 15-acetyl tajixanthone hydrate (**6b**) [16]. (Figure 1). The structures of the undescribed compounds were established on the basis of an extensive analysis of their 1D and 2D NMR as well as HRMS spectra. In the case of **2**, the absolute configurations of their stereogenic carbons were established by comparison of their experimental and calculated electronic circular dichroism (ECD) spectra. Additionally, the absolute structures of tajixanthone hydrate (**6a**), and 15-acetyl tajixanthone hydrate (**6b**) were also unambiguously determined by X-ray analysis for the first time.

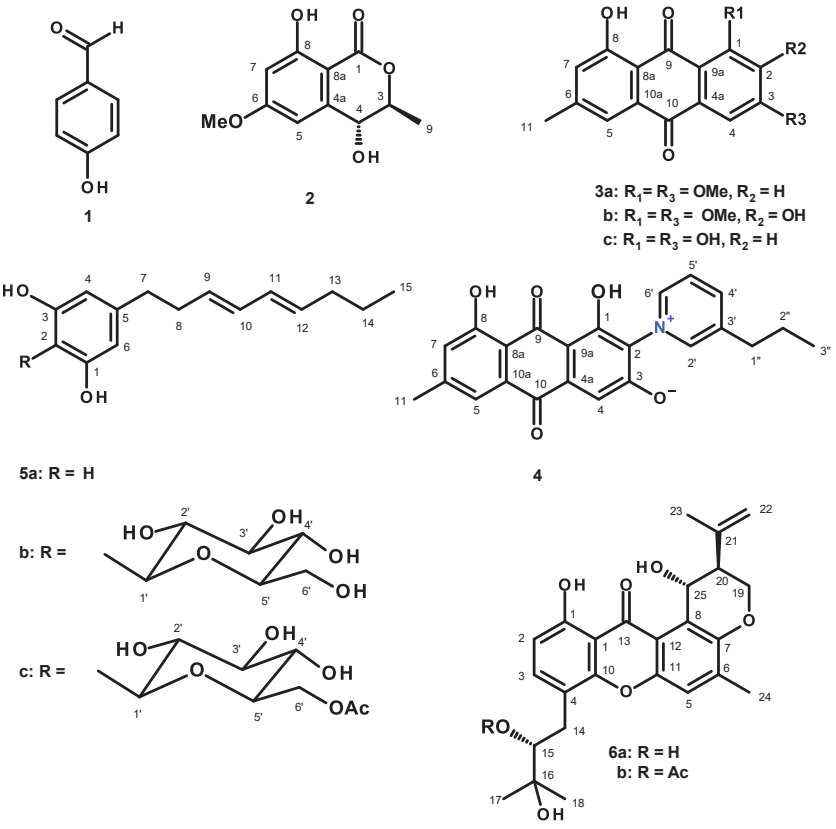

Figure 1. Structures of *p*-hydroxybenzaldehyde (**1**), (3*S*,4*R*)-4-hydroxy-6-methoxymellein (**2**), 1,3-dimethoxy-8-hydroxy-6-methylanthraquinone (**3a**), 1,3-dimethoxy-2,8-dihydroxy-6-methylanthraquinone (**3b**), emodin (**3c**), stellatanthraquinone (**4**), 5[(3*E*,5*E*)-nona-3,5-dien-1-yl]benzene-1,3-diol (**5a**), carnemycin E (**5b**), acetyl carnemycin E (**5c**), tajixanthone hydrate (**6a**), 15-acetyl tajixanthone hydrate (**6b**).

2. Results and Discussion

The structures of *p*-hydroxybenzaldehyde (**1**) [9], 1,3-dimethoxy-8-hydroxy-6-methylanthraquinone (**3a**) [10], 1,3-dimethoxy-2,8-dihydroxy-6-methylanthraquinone (**3b**) [11], emodin (**3c**) [12], 5[(3*E*,5*E*)-nona-3,5-dien-1-yl]benzene-1,3-diol (**5a**) [13], carnemycin E (**5b**) [13], tajixanthone hydrate (**6a**) [14,15], and 15-acetyl tajixanthone hydrate (**6b**) [16] were elucidated by the analysis of their 1D and 2D NMR spectra as well as HRMS data (Figures S1, S2, S9–23, S29–S38, S47–S56, S59 and S60, Tables S1–S3) and by the comparison of their NMR spectral data with those reported in the literature.

Compound **2** was isolated as white crystals (mp 116–118 °C), and its molecular formula $C_{11}H_{12}O_5$ was established based on the (+)-HRESIMS *m/z* 225.0765 $[M + H]^+$ (calculated for $C_{11}H_{13}O_5$, 225.0763) (Figure S57), requiring six degrees of unsaturation. The ^{13}C NMR spectrum (Table 1, Figure S4), exhibited eleven carbon signals, which in combination with DEPT and HSQC spectra (Figure S6), can be categorized as one conjugated ester carbonyl (δ_C 169.1), two oxygen-bearing non-protonated sp^2 (δ_C 166.2 and 164.5), two non-protonated sp^2 (δ_C 142.1 and 100.0), two protonated sp^2 (δ_C 106.8 and 101.3), two oxymethine sp^3 (δ_C 77.8 and 67.5), one methoxy (δ_C 55.8) and one methyl (δ_C 15.9) carbon, respectively. The ^1H NMR spectrum (Table 1, Figure S3), in combination with the HSQC spectrum (Figure S6), displayed a singlet of the hydrogen-bonded hydroxyl proton at δ_H 11.20 (OH-8), a multiplet of a hydroxyl proton at δ_H 2.28 (OH-4), two doublets of meta-

coupled aromatic protons at δ_H 6.48 (J = 2.3 Hz, H-5/δ_C 106.8) and δ_H 6.45 (J = 2.3 Hz, H-7/δ_C 101.3), a double quartet at δ_H 4.63 (J = 6.6, 2 Hz, H-3/δ_C 77.8), which was coupled with a double doublet at δ_H 4.50 (J = 5.6, 1.5 Hz, H-4/δ_C 67.5), a methoxy singlet at δ_H 3.85 (δ_C 55.8) and a methyl doublet at δ_H 1.55 (J = 6.6 Hz, Me-9/δ_C 15.9). The HMBC spectrum (Table 1, Figure S7) exhibited correlations from OH-8 to the carbons at δ_C 164.5 (C-8), 101.3 (C-7) and 100.0 (C-8a), H-5 to the carbons at δ_C 166.2 (C-6), C-7, C-8a, C-4, H-7 to C-5, C-6, C-8a, H-3 to Me-9, H-4 to C-4a (δ_C 142.1), C-5, C-8a, OMe-6 to C-6, Me-9 to C-3, C-4, and a weak correlation from OH-4 to C-3 and C-4.

Table 1. ^{1}H and ^{13}C NMR data ($CDCl_3$, 300 and 75 MHz), COSY, HMBC, and NOESY for **2**.

Position	δ_C, Type	δ_H, (J in Hz)	COSY	HMBC	NOESY
1	169.1, CO	-			
3	77.8, CH	4.63, dq (6.6, 2.0)	CH_3-9	CH_3-9	CH_3-9
4	67.5, CH	4.50, dd (5.6, 1.5)	OH-4	C-4a, 5, 8a	H-5, CH_3-9
4a	142.1, C	-	-		
5	106.8, CH	6.48, d (2.3)	H-7	C-4, 6, 7, 8a	H-4, OCH_3-6
6	166.2, C	-			
7	101.3, CH	6.45, d (2.3)	H-5,	C-5, 6, 8a	OCH_3-6
8	164.5, C	-			
8a	100.0, C	-			
9	15.9, CH_3	1.55, d (1.6)	H-3	C-3, 4	H-3, 4
OCH_3-6	55.8, CH_3	3.85, s		C-6	
OH-4	-	2.28, m		C-3, 4	
OH-8	-	11.20, s		C-7, 8, 8a	

The ^{1}H and ^{13}C NMR chemical shift values, together with COSY and HMBC correlations, revealed that the planar structure of **2** is the same as that of the enantiomeric mixture of (3*R*,4*R*)- and (3*S*,4*S*)-4-hydroxy-6-methoxymellein, previously isolated from the culture extract of the mycobionts of *Graphis* sp. Since the mixture showed a negative sign of Cotton effect at 267 nm, the authors proposed that the (3*R*,4*R*)-enantiomer was predominant [17]. Surprisingly, the NOESY spectrum (Table 1, Figure S8) of **2** exhibited a strong correlation from H-4 to Me-9, but not from H-3 to H-4, suggesting that H-4 and Me-9 are on the same face, which is contrary to (3*R*,4*R*)- and (3*S*,4*S*)-4-hydroxy-6-methoxymellein where H-3 and H-4 are on the same face.

The absolute configurations of C-3 and C-4 were thus determined by comparison of the experimental ECD spectrum with a quantum-mechanically simulated spectrum derived from the most significant conformations of the computational models of (3*S*,4*R*)-**2** and (3*R*,4*S*)-**2** (Figure 2). Figure 3 shows a very good match between the experimental ECD spectrum and the calculated ECD spectrum for (3*S*,4*R*)-**2**, thus confirming that **2** is (3*S*,4*R*)-4-hydroxy-6-methoxymellein. Compound **2** is, therefore, a diastereomer of (3*R*,4*R*)- and (3*S*,4*S*)-4-hydroxy-6-methoxymellein [17] and has never been previously reported.

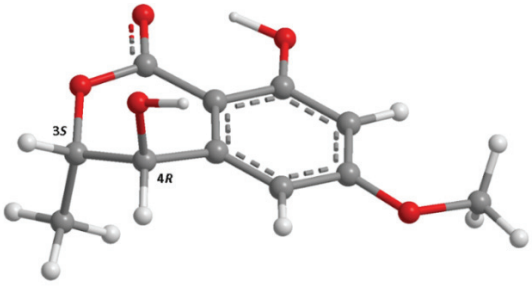

Figure 2. Model of the most abundant conformation of **2** (lowest APFD/6-311+G(2d,p)/acetonitrile energy conformer), accounting for 25% of conformer population, in its ECD-assigned (3*S*,4*R*) configuration.

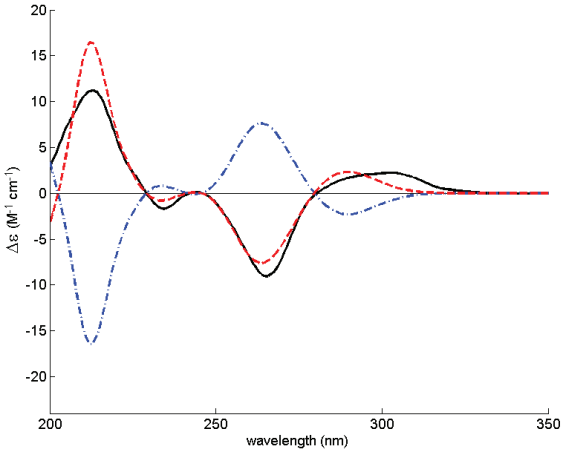

Figure 3. Experimental acetonitrile ECD spectrum of **2** (solid black line) and theoretical ECD spectra of its (3*R*,4*S*) (dot-dashed blue line) and (3*S*,4*R*) (dashed red line) computational models. Of the two theoretical spectra, the (3*R*,4*S*) was the one actually simulated and the (3*S*4,*R*) was obtained by changing the sign of every point of the (3*R*,4*S*) spectrum.

Compound **4** was isolated as a red solid (mp. 228–229 °C), and its molecular formula $C_{23}H_{19}NO_5$ was established on the basis of (+)-HRESIMS *m/z* 390.1340 $[M + H]^+$ (calculated for $C_{23}H_{20}NO_5$, 390.1341) (Figure S58), requiring fifteen degrees of unsaturation. The ^{13}C NMR spectrum (Table 2, Figure S25) displayed 23 carbon signals which, in combination with DEPT and HSQC spectra (Figure S27), can be classified as two conjugated ketone carbonyls (δ_C 184.5 and 183.3), three oxygen-bearing non-protonated sp^2 (δ_C 171.9, 161.2, 159.5), seven non-protonated sp^2 (δ_C 146.7, 142.8, 134.4, 133.2, 123.2, 114.6, 100.0), seven protonated sp^2 (δ_C 147.2, 146.2, 145.6, 127.5, 124.4, 120.4, and 118.6), two methylene sp^3 (δ_C 33.8 and 23.7), and two methyl (δ_C 21.9 and 13.7) carbons. The ^1H NMR spectrum (Table 2, Figure S24) showed two singlets of hydrogen-bonded phenolic hydroxyls at δ_H 12.50 and 13.44, seven aromatic protons appearing as a broad singlet at δ_H 8.91, two singlets at δ_H 7.11 and 6.80, three doublets at δ_H 8.57 (J = 8.0 Hz), 8.85 (J = 6.1 Hz), 7.46 (J = 1.0 Hz), one double doublet at δ_H 8.16 (J = 8.0, 6.1 Hz), one methylene triplet at δ_H 2.83 (J = 7.4 Hz), one methylene sextet at δ_H 1.70 (J = 7.4 Hz), one methyl singlet at δ_H 2.40, and one methyl triplet at δ_H 0.94 (J = 7.3 Hz). The presence of the 1,8-dihydroxy-6-methyl-1,2,3,6,8-pentasubstitututed anthraquinone scaffold was supported by COSY correlations (Table 2, Figures 4 and S26) from H-7 (δ_H 7.11, s/δ_C 124.4) to H-5 (7.46, d, J = 1.0 Hz)/δ_C 120.4) and Me-11 (2.40, s/δ_C 21.9), as well as by HMBC correlations (Table 2, Figures 4 and S28) from OH-1 (δ_H 13.44, s) to C-1 (δ_C 159.5), C-2 (δ_C 123.2), C-9a (δ_C 100.0), OH-8 (δ_H 12.50, s) to C-7 (δ_C 124.4), C-8

(δ_C 161.2), C-8a (δ_C 114.6), H-5 (δ_H 7.46, d, J = 1.0 Hz) to C-10 (δ_C 183.3), C-7, C-8a, Me-11 (δ_C 21.9), H-7 (δ_H 7.11, s) to C-8, C-5 (δ_C 120.4), C-8a, Me-11, H-4 (δ_H 6.80,s) to C-10, C-2 (δ_C 123.2), and C-9a. That another portion of the molecule is 3-propylpyridinium was corroborated by COSY correlations (Table 2, Figures 4 and S26) from H-4′ (δ_H 8.57, d, J = 8.0 Hz) to H-5′ (δ_H 8.16, dd, J = 8.0, 6.1 Hz) and H-2′ (δ_H 8.91, brs), H-5′ to H-4′ and H-6′ (8.85, d, J = 6.1 Hz), which was confirmed by HMBC correlations (Table 2, Figures 4 and S28) from H-2′ to C-3′ (δ_C 142.8), C-4′ (δ_C 146.2) and C-1″ (δ_C 33.8), H-4′ to C-2′ (δ_C 147.2), C-6′ (δ_C 145.6) and C-1″, H-5′ to C-3′, and C-6′ and H-6′ to C-4′ and C-5′ [18]. That the propyl group was on C-3′ of the pyridinium ring was supported by the spin system from H_2-1″ (δ_H 2.83, t, J = 7.4 Hz/δ_C 33.8) through H_2-2″ (δ_H 1.70, sex, J = 7.4 Hz/δ_C 23.7) to H_3-3″ (δ_H 0.94, t, J = 7.4 Hz/δ_C 13.7) as well as by HMBC correlations from H-3″ to C-1″ and C-2″, H-2″ to C-1″, and C-3″ and C-2′. Since H-2′ and H-6′ showed strong and weak cross peaks, respectively, to C-2 (Table 2, Figures 4 and S28), the 3-propylpyridinium moiety is linked to the anthraquinone scaffold through the nitrogen atom for the former and C-2 of the latter.

Table 2. ^{1}H and ^{13}C NMR data (DMSO-d_6, 500 and 125 MHz), COSY and HMBC assignment for **4**.

Position	δ_C, Type	δ_H, (J in Hz)	COSY	HMBC
1	159.5, C			
2	123.2, C			
3	171.9, C			
4	118.6, CH	6.80, s		C-2, 9a, 10
4a	133.2, C			
5	120.4, CH	7.46, d (1.0)	H-7	C-7, 8a, 10, CH_3-11
6	146.7, C			
7	124.4, CH	7.11, s	H-5, CH_3-11	C-5, 8, 8a, CH_3-11
8	161.2, C			
8a	114.6, C			
9	184.5, CO			
9a	100.0, C			
10	183.3, CO			
10a	134.4, C			
11	21.9, CH_3	2.40, s	H-7	C-5, 6,7
2′	147.2, CH	8.91, brs	H-4′	C-2, 3′, 4′, 1″
3′	142.8, C			
4′	146.2, CH	8.57, d (8.0)	H-2′,5′	C-2′, 6′, 1″
5′	127.5, CH	8.16, dd (8.0, 6.1)	H-4′, 6′	C-3′, 6′
6′	145.6, CH	8.85, d (6.1)	H-5′	C-2, 4′, 5′
1″	33.8, CH_2	2.83, t (7.4)	H-2″	C-2′, 2″, 3′, 3″
2″	23.7, CH_2	1.70, sex (7.4)	H-1″, 3″	C-1″, 3′, 3″
3″	13.7, CH_3	0.94, t (7.3)	H-2″	C-1″, 3″
OH-1		13.44, s		C-1, 2, 9a
OH-8		12.50, s		C-7, 8, 8a

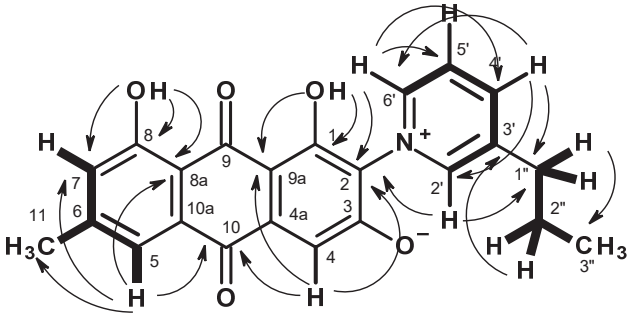

Figure 4. Key COSY (——) and HMBC (⌒) correlations in **4**.

Since 1,8-dihydroxy-6-methyl anthraquinone and the 3-propylpyridinium moiety account for $C_{23}H_{19}NO_4$, the only oxygen atom left must be on C-3 of the anthraquinone nucleus to produce a molecular formula $C_{23}H_{19}NO_5$. Therefore, the oxygen atom on C-3 should bear a negative charge (**4**). This was supported by a high chemical shift value of C-3 (δ_C 171.9). This phenoxide ion can establish an ionic interaction with the positive-charged nitrogen of the pyridinium ring. Interestingly, although alkyl pyridinium-containing compounds have never been reported from marine-derived fungi, cyclic 3-alkylpyridinium alkaloids are common secondary metabolites from sponges of the order Haplosclerida [19,20]. Therefore, **4** is the first 3-alkylpyridinium anthraquinone reported from nature, and it was named stellatanthraquinone.

Compound **5b** was isolated as a pale-yellow viscous mass, and its molecular formula $C_{21}H_{30}O_7$ was established on the basis of the (+)-HRESIMS *m/z* 395.2076 $[M + H]^+$ (calculated for $C_{21}H_{31}O_7$, 395.2070 (Figure S60), requiring seven degrees of unsaturation. Analysis of its ^{1}H, ^{13}C NMR, DEPT, COSY, HSQC, and HMBC spectra (Table 3, Figures S34–S38) revealed the presence of a 5 [(3*E*,5*E*)-nona-3,5-dien-1-yl]benzene-1,3-diol moiety, identical to **5a**, with a substitution on C-2. The presence of five oxymethine sp^3 (δ_C 81.5, 79.1, 75.0, 72.1, 70.3), one oxymethylene sp^3 (δ_C 61.2) carbons, two hydroxyl groups at δ_H 4.90 dd (*J* = 10.7, 2.9 Hz) and 4.59 d (*J* = 5.5 Hz), and the molecular formula $C_6H_{11}O_5$ of the substituent on C-2 revealed the presence of a pyranosyl moiety. However, since four oxymethine protons of the sugar moiety appeared as complex multiplets at δ_H 3.20–3.22 and 3.74, it was not possible to identify the sugar moiety of **5b**. Although Wen et al. [13] identified the sugar moiety in carnemycin E as glucopyranosyl, it was not possible to compare its ^{1}H and ^{13}C chemical shift values with those of the sugar moiety **5b** since the ^{1}H and ^{13}C NMR spectra of carnemycin E were obtained in pyridine-*d5*, while those of **5b** were obtained in DMSO-*d6*. Moreover, carnemycin E was obtained as an amorphous reddish gum, while **5b** was obtained as a pale-yellow viscous mass. In order to unravel the identity of the sugar moiety in **5b**, we tried to compare its carbon chemical shift values with those of the C-glycosides from the ^{13}C NMR spectra obtained in DMSO-*d6*. The chemical shift values of C-1′, C-2′, C-3′, C-4′, C-5′ and C-6′ of the sugar moiety of **5b** (Table 3, Figure S36) were nearly identical to those of C-glucosyl moiety of tricetin 6,8-di-C-glucoside [21]. Moreover, the chemical shift value and coupling constant of H-1′ were also identical with those of the corresponding proton in tricetin 6,8-di-C-glucoside [21]. The value of the coupling constant of H-1′ (*J* = 9.6 Hz) confirmed the presence of a β-D-glucopyranosyl moiety. Therefore, **5a** was elucidated as carnemycin E, previously isolated from the culture extract of *Aspergillus* sp., which was isolated from superficial mycobiota of the brown alga, *Saccharina cichorioides* f. *sachalinensis*, collected from the South China Sea [13].

Table 3. ^{1}H and ^{13}C NMR data (DMSO-d_6, 300 and 75 MHz), COSY, and HMBC assignment for **5b**.

Position	δ_C, Type	δ_H, (*J* in Hz)	COSY	HMBC
1	157.1, C			
2	110.2, C			
3	157.1, C			
4	107.6, CH	6.11, s		C-1′, 3, 6, 7
5	142.5, C			
6	107.6, CH	6.11, s		C-1′, 2, 4, 7
7	35.5, CH_2	2.45, t (6.8)	H-8	C-4, 5, 6, 8, 9
8	34.0, CH_2	2.27, dd (14.3, 6.6)	H-7, H-9	C-5, 7, 9, 10
9	131.8, CH	5.62, m	H-8, 10	C-10, 11
10	130.9, CH	5.91, m	H-9, 11	C-8, 9, 12
11	131.1, CH	6.04, m	H-10, 12	C-9, 13
12	132.6, CH	5.55, m	H-11, 13	C-10, 13, 14
13	34.5, CH_2	2.00, dd (14.3, 7.2)	H-12, 14	C-11, 12, 14, 15
14	22.5, CH_2	1.36, sext (7.2)	H-13, 15	C-12, 13, 15
15	14.0, CH_3	0.87, t (7.2)	H-14	C-13, 14
1′	75.0, CH	4.62, d (9.6)	H-2′	C-1, 2, 2′, 3, 3′
2′	72.1, CH	3.74, m		
3′	79.1, CH	3.22, m		
4′	70.3, CH	3.22, m	OH-4′	
5′	81.5, CH	3.20, m		
6′a b	61.2, CH_2	3.50, dd (11.0, 5.5) 3.65, dd (11.0, 5.2)	H-5′, 6′b, OH-6′ H-5′, 6′a, OH-6′	
OH-3		8.67, s		C-2, 3, 4
OH-4′		4.90, dd (10.7, 2.9)	H-4′	C-4′, 5′
OH-6′		4.59, d (5.5)	H_2-6′	C-6′

Compound **5c** was also isolated as a pale-yellow viscous mass and its molecular formula $C_{23}H_{32}O_8$ was established on the basis of the (+)-HRESIMS *m/z* at 437.2175 $[M + H]^+$ (calculated for $C_{23}H_{33}O_8$, 437.2175), and *m/z* 459.1989 $[M + Na]^+$ (calculated for $C_{23}H_{32}O_8Na$, 459.1995) (Figure S61).The ^{1}H and ^{13}C NMR spectra of **5c** (Table 4; Figures S39 and S40) resembled those of **5b** (Table S2 and Figures S34 and S35) except for CH_2-6′, which appeared at higher frequencies (δ_H 4.32 d, *J* = 11.6 Hz, and 3.98 dd, *J* = 11.6, 3.9 Hz/δ_C 64.8) than those of **5b** (δ_H 3.50, dd, *J* = 11.0, 5.5 Hz, and 3.65, dd, *J* = 11.0, 5.2 Hz)/δ_C 61.2) as well as the appearance of an acetyl group (δ_H 2.00, s/δ_C 21.2, CH_3; δ_C 170.9, CO), suggesting that **5c** is a C-21 acetate of **5b**.

Contrary to other proton signals, the signals of OH-3, OH-3′, and OH-4′ appeared as broad signals in the ^{1}H NMR spectrum at 500 MHz (Figure S39). Moreover, they did not show any COSY and HMBC correlations with any protons (Table 4, Figures S41 and S43), which made it impossible to assign them. Interestingly, in the ^{1}H NMR spectrum at 300 MHz (Figure S44), the signal of OH-3 appeared as a sharp singlet at δ_H 8.70, whereas those of OH-3′ and OH-4′ appeared as two well-resolved doublets at δ_H 4.59, d (*J* = 6.5 Hz) and 5.15, d (*J* = 4.4 Hz), respectively. Furthermore, in the 300 MHz spectra, OH-3 displayed HMBC correlations to C-2 (δ_C 109.9) and C-3 (δ_C 157.2) (Figure S46), while OH-3′ and OH-4′ showed COSY correlations to H-3′ (δ_H 3.20) and H-4′ (δ_H 3.18) (Figure S45), respectively.

The coupling constant of H-1′ (J = 9.8 Hz) confirmed the β-anomer of the glucosyl moiety. Since **5c** has never been previously reported, it was named acetyl carnemycin E.

Table 4. ^{1}H and ^{13}C NMR data (DMSO-d_6, 500 and 125 MHz), COSY, and HMBC assignment for **5c**.

Position	δ_C, Type	δ_H, (J in Hz)	COSY	HMBC
1	157.3, C			
2	109.9, C			
3	157.3, C			
4	107.5, CH	6.11, s		C-1′, 2, 3, 6, 7
5	142.5, C			
6	107.5, CH	6.11, s		C-1′, 2, 3, 4, 7
7	35.5, CH_2	2.44, t (7.2)	H-8	C-4, 5, 6, 8, 9
8	34.0, CH_2	2.26, dd (14.7, 7.2)	H-7, 9	C-7, 9, 10
9	131.8, CH	5.59, ddd (14.6, 7.2, 7.2)	H-8, 10	C-11
10	130.9, CH	5.97, m	H-9, 11	
11	131.1, CH	6.04, m	H-10, 12	C-9 (w), 13
12	132.6, CH	5.57, ddd (14.5, 7.7, 7.1)	H-11, 13	C-10, 13, 14
13	34.5, CH_2	2.01, m	H-12, 14	C-11, 12, 14, 15
14	22.5, CH_2	1.36, sex (7.4)	H-13, 15	12, 13, 15
15	14.0, CH_3	0.86, t (7.4)	H-14	C-13, 14
1′	74.9, CH	4.60, d (9.8)	H-2′	C-1, 2, 2′ 3, 3′
2′	71.5, CH	3.83, t (9.2)	H-1′, 3′	C-1′, 3′
3′	79.0, CH	3.21, t (8.7)	H-4′	C-4′
4′	70.6, CH	3.18, t (8.7)	H-3′	C-3′
5′	78.4, CH	3.36 (under water peak)	H-6′b	C-4′ (w)
6′a b	64.8, CH_2	4.32, d (11.6) 3.98, dd (11.6, 3.9)	H-6′b H-5′, 6′a	C-4′, CO (OAc) C-5′, 6′
OAc	170.9, CO	-		
OAc	21.2, CH_3	2.00, s		C-6′
OH-3		8.74, brs		
OH-3′		4.95, br		
OH-4′		5.15, br		

The ^{1}H and ^{13}C NMR spectra of **6a** and **6b** (Table S3. Figures S47, S48, S52 and S53) are in agreement with those reported for tajixanthone hydrate [14] and 15-acetyl tajixanthone hydrate [16]. However, Pornpakakul et al. [14] assigned the configurations of C-15, C-20 and C-25 of tajixanthone hydrate, based on the coupling constant between H-14 and H-15 and NOESY correlations of the protons in tajixanthone methanoate, and also referred its stereochemistry to the previous study by Chexal et al. [22], who elegantly determined the absolute configurations of C-15 and C-25 of tajixanthone as 15*S* and 25*R* by chemical transformation (the method of Boar and Damps) while the relative configuration of C-20 was suggested by the preferred axial conformation of the isopropyl substituent in the hydrogenated derivatives [22]. Later on, the same group [23], described the isolation of tajixanthone hydrate which they obtained in a small quantity. The structure and stereochemistry of tajixanthone hydrate were identified on the basis of the same optical rotation of the acid-catalyzed hydrolysis product of tajixanthone and of the natural product. On the other hand, the absolute stereochemistry of 15-acetyl tajixanthone hydrate was concluded

to be the same as that of tajixanthone hydrate, which was obtained by hydrolysis of 15-acetyl tajixanthone hydrate. However, neither optical rotation nor absolute configurations of their stereogenic carbons were provided [16].

Literature search revealed that the absolute configurations of C-15, C-20, and C-25 of both tajixanthone hydrate and 15-acetyl tajixanthone hydrate have never been established by either X-ray crystallographic or chiroptical methods. Fortunately, we were able to obtain suitable crystals of both **6a** and **6b** for X-ray analysis using an X-ray diffractometer equipped with CuKα radiation. The Ortep views of **6a** and **6b** are shown in Figures 5A and 5B, respectively, revealing that the absolute configurations of C-15, C-20, and C-25 in both compounds are 15*S*, 20*S*, and 25*R*. Moreover, both compounds are levorotatory.

(**A**)

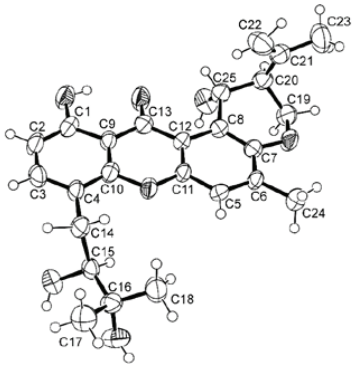

(**B**)

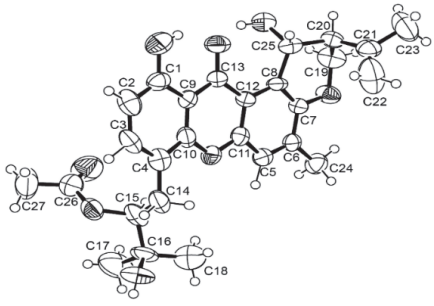

Figure 5. Ortep views of **6a** (**A**) and **6b** (**B**).

The antimicrobial activity of **2**, **3a**, **3b**, **4**, **5a**, **5b**, **5c**, **6a**, and **6b** was evaluated against four reference bacterial species and three multidrug-resistant strains. However, only **5a** exhibited antibacterial activity against all Gram-positive strains, viz. *E. faecalis* ATCC 29212, vancomycin-resistant *E. faecalis* B3/101, and methicillin-resistant *S. aureus* 74/24, with a MIC value of 16 μg/mL, and *S. aureus* ATCC 29213, with a MIC value of 32 μg/mL (Table 5). The minimal bactericidal concentration (MBC) for **5a** was equal to or one-fold higher than the MIC, indicating its bactericidal effect towards *E. faecalis* ATCC 29212, *S. aureus* 74/24, and *S. aureus* ATCC 29213. For *E. faecalis* B3/101, its MBC was more than two-fold higher than the MIC, suggesting its bacteriostatic effect.

Table 5. Antibacterial activity of **2**, **3a**, **3b**, **4**, **5a**, **5b**, **5c**, **6a**, and **6b** against Gram-positive reference and multidrug-resistant strains. MIC and MBC are expressed in μg/mL.

Compound	*E. faecalis* ATCC 29212		*E. faecalis* B3/101 (VRE)		*S. aureus* ATCC 29213		*S. aureus* 74/24 (MRSA)	
	MIC	MBC	MIC	MBC	MIC	MBC	MIC	MBC
2	>64	>64	>64	>64	>64	>64	>64	>64
3a	>32	>32	>32	>32	>32	>32	>32	>32
3b	>64	>64	>64	>64	>64	>64	>64	>64
4	>32	>32	>32	>32	>32	>32	>32	>32
5a	16	32	16	64	32	32	16	32
5b	>64	>64	>64	>64	>64	>64	>64	>64
5c	>64	>64	>64	>64	>64	>64	>64	>64
6a	>64	>64	>64	>64	>64	>64	>64	>64
6b	>32	>32	>32	>32	>32	>32	>32	>32
VAN	4	-	-	-	-	-	-	-
OXA	-	-	-	-	0.2	-	-	-

MIC, minimal inhibitory concentration; MBC, minimal bactericidal concentration; VAN, vancomycin; OXA, oxacillin.

Although **5a** was found to significantly inhibit NO production in lipopolysaccharide (LPS)-induced murine macrophage RAW264.7 cells [13], this compound has never been tested for antibacterial acivity. Interestingly, some alkenylresorcinols, such as 9-(3,5-dihydroxy-4-methylphenyl)nona-3(*Z*)-enoic acid, isolated from the methanolic extract of fruits of *Hakea sericea*, significantly inhibited the growth of *E. faecalis*, *Listeria monocytogenes* and *Bacillus cereus*, and showed good MIC values against *S. aureus* strains, including the clinical isolates and MRSA strains [24]. Intriguingly, **5b** and **5c**, analogs of **5a** which possess a β-glucosyl moiety on C-2 of the benzene ring, were void of antibacterial activity in our assays. We speculate that the polar and bulky glucosyl moiety might have negatively affected the antibacterial activity, possibly by preventing the compounds from penetrating the bacterial cell wall.

Another interesting aspect is that even though there were several reports on the antibaterial activity of anthraquinones from marine-derived fungi [25], neither of the three anthraquinones tested, i.e., **3a**, **3b**, and **4**, showed antibacterial activity in our assays. This is not surprising since we also found in our previous report that the anthraquinone purnipurdin A, isolated from the culture extract of the marine sponge-associated fungus, *Neosartorya spinosa* KUFA 1047, did not exhibit any antibacterial activity against the same bacterial strains tested [26].

Compounds **2**, **3a**, **3b**, **4**, **5a**, **5b**, **5c**, **6a,** and **6b** were also investigated for their potential synergy with clinically relevant antibiotics on multidrug-resistant strains, by both disk diffusion method and checkerboard assay; however, no interactions were found with cefotaxime (ESBL *E. coli*), methicillin (MRSA *S. aureus*), and vancomycin (VRE *E. faecalis*).

The inhibitory effect of **2**, **3a**, **3b**, **4**, **5a**, **5b**, **5c**, **6a**, and **6b** on biofilm production was also evaluated in all reference strains. However, only **5a** showed an extensive ability to significantly inhibit biofilm formation in two of the four reference strains used in this study (Table 6). Indeed, **5a** was able to completely inhibit biofilm formation in *S. aureus* ATCC 29213 and *E. faecalis* ATCC 29212, at both MIC and 2xMIC concentrations.

Table 6. Percentage of biofilm formation in the presence of **5a** after 24 h incubation.

Compound	Concentration	Biofilm Biomass (% of Control)	
		***E. faecalis* ATCC 29212**	***S. aureus* ATCC 29213**
5a	64 µg/mL	-	0.00 ± 0.06 ***
	32 µg/mL	0.01 ± 0.01 ***	0.04 ± 0.12 ***
	16 µg/mL	0.02 ± 0.01 ***	-
DMSO	1% (*v*/*v*)	1.00 ± 0.03 ***	1.00 ± 0.01 ***

Data are shown as mean ± SD of three independent experiments. One-sample *t*-test: * $p < 0.05$, ** $p < 0.01$, *** $p < 0.001$ significantly different from 100%.

3. Experimental Sections

3.1. General Experimental Procedures

The melting points were determined on a Stuart Melting Point Apparatus SMP3 (Bibby Sterilin, Stone, Staffordshire, UK) and are uncorrected. Optical rotations were measured on an ADP410 Polarimeter (Bellingham + Stanley Ltd., Tunbridge Wells, Kent, UK). ^{1}H and ^{13}C NMR spectra were recorded at ambient temperature on a Bruker AMC instrument (Bruker Biosciences Corporation, Billerica, MA, USA) operating at 300 or 500 and 75 or 125 MHz, respectively. High resolution mass spectra were measured with a Waters Xevo QToF mass spectrometer (Waters Corporations, Milford, MA, USA) coupled to a Waters Aquity UPLC system. A Merck (Darmstadt, Germany) silica gel GF_{254} was used for preparative TLC, and a Merck Si gel 60 (0.2–0.5 mm) was used for column chromatography. LiChroprep silica gel and Sephadex LH 20 were used for column chromatography.

3.2. Fungal Material

The fungus was isolated from the marine sponge *Mycale* sp., which was collected by scuba diving at a depth of 5–10 m, from the coral reef at Samaesan Island (12°34′36.64″ N 100°56′59.69″ E), in the Gulf of Thailand, Chonburi province, in May 2015. The sponge was washed with 0.01% sodium hypochlorite solution for 1 min, followed by sterilized seawater three times, and then dried on a sterile filter paper under a sterile aseptic condition. The sponge was cut into small pieces (*ca*. 5 × 5 mm) and placed on Petri dish plates containing 15 mL potato dextrose agar (PDA) medium mixed with 300 mg/L of streptomycin sulfate and incubated at 28 °C for 7 days. The hyphal tips emerging from sponge pieces were individually transferred onto a PDA slant and maintained as pure cultures at Kasetsart University Fungal Collection, Department of Plant Pathology, Faculty of Agriculture, Kasetsart University, Bangkok, Thailand. The fungal strain KUFA 2017 was identified as *Aspergillus stellatus*, based on morphological characteristics such as colony growth rate and growth pattern on standard media, namely Czapek's agar, Czapek yeast autolysate agar, and malt extract agar. Microscopic characteristics including size, shape, and ornamentation of conidiophores and spores were examined under light microscope. This identification was confirmed by molecular techniques using internal transcribed spacer (ITS) primers. DNA was extracted from young mycelia following a modified Murray and Thompson method [27]. Primer pairs ITS1 and ITS4 were used for ITS gene amplification [28]. PCR reactions were conducted on Thermal Cycler and the amplification process consisted of initial denaturation at 95 °C for 5 min, 34 cycles at 95 °C for 1 min (denaturation), at 55 °C for 1 min (annealing), and at 72 °C for 1.5 min (extension), followed by final extension at 72 °C for 10 min. PCR products were examined by Agarose gel electrophoresis (1% agarose with 1× Tris-Borate-EDTA (TBE) buffer) and visualized under UV light after staining with ethidium bromide. DNA sequencing analyses were performed using the dideoxyribonucleotide chain termination method [29] by Macrogen Inc. (Seoul, South Korea). The DNA sequences were edited using FinchTV software and submitted to the BLAST program for alignment and compared with that of fungal species in the NCBI database (http://www.ncbi.nlm.nih.gov/, accessed on 18 May 2021). Its gene sequences were deposited in GenBank with the accession number MZ331807.

3.3. Extraction and Isolation

The fungus was cultured in five Petri dishes (i.d. 90 mm) containing 20 mL of PDA per dish at 28 °C for one week. The mycelial plugs (5 mm in diameter) were transferred to two 500 mL Erlenmeyer flasks containing 200 mL of potato dextrose broth (PDB), and incubated on a rotary shaker at 120 rpm at 28 °C for one week. Thirty 1000 mL Erlenmeyer flasks, each containing 300 g of cooked rice, were autoclaved at 121 °C for 15 min. After cooling to room temperature, 20 mL of mycelial suspension of the fungus was inoculated per flask and incubated at 28 °C for 30 days, after which 500 mL of EtOAc was added to each flask of the moldy rice and macerated for 7 days, and then filtered with Whatman No. 1 filter paper.

The EtOAc solutions were combined and concentrated under reduced pressure to yield 280.4 g of a crude EtOAc extract, which was dissolved in 300 mL of $CHCl_3$, washed with H_2O (3 × 500 mL) and dried with anhydrous Na_2SO_4, and filtered and evaporated under reduced pressure to obtain 134.9 g of a crude $CHCl_3$ extract. The crude $CHCl_3$ extract (57.1 g) was applied on a silica gel column (385 g) and eluted with mixtures of petrol-$CHCl_3$ and $CHCl_3$-Me_2CO, wherein 250 mL fractions (frs) were collected as follows: frs 1–61 (petrol-$CHCl_3$, 1:1), 62–129 (petrol-$CHCl_3$, 3:7), 130–231 (petrol-$CHCl_3$, 1:9), 232–397 ($CHCl_3$-Me_2CO, 9:1), 398–524 ($CHCl_3$-Me_2CO, 7:3). Frs 40–45 were combined (241.9 mg) and applied over a Sephadex LH-20 column (15 g), and eluted with MeOH, wherein 37 subfractions (sfrs) of 2 mL were collected. Sfrs 30–35 were combined (102.9 mg) and precipitated in MeOH to produce 13.6 mg of **3a**. Frs 74–77 were combined (851.6 mg) and precipitated in Me_2CO to produce 20.3 mg of **3b**. Frs 78–89 were combined (396.5 mg) and applied over a Sephadex LH-20 column (15 g), and eluted with MeOH, wherein 28 sfrs of 2 mL were collected. Sfrs 21–25 were combined to produce 11.4 mg of **3c**. Frs 95–118 were combined (535.5 mg) and applied over a Sephadex LH-20 column (15 g), and eluted with MeOH, wherein 47 sfrs of 2 mL were collected. Sfrs 16–33 were combined (231.4 mg) and applied over another Sephadex LH-20 column (5 g), and eluted with $CHCl_3$, wherein 22 sub-subfractions (ssfrs) of 1 mL were collected. Ssfrs 9–10 were combined to produce 69.4 mg of **2**, while ssfrs 20–22 were combined to produce 45.0 mg of **1**. Frs 126–140 were combined (274.9 mg) and applied over a Sephadex LH-20 column (15 g), and eluted with MeOH, wherein 31 sfrs of 2 mL were collected. Sfrs 4–15 were combined (108.4 mg) and precipitated in Me_2CO to produce 26.7 mg of **6b**. Frs 149-173 were combined (1.02 g) and applied over a Sephadex LH-20 column (15 g), and eluted with MeOH, wherein 49 sfrs of 1 mL were collected. Sfrs 20–28 were combined (305.2 mg) and applied over another Sephadex LH-20 column (5 g), and eluted with $CHCl_3$, wherein 20 ssfrs of 0.5 mL were collected. Ssfrs 15–19 were combined to produce 153.0 mg of **5a**. Frs 178–206 were combined (509.4 mg) and precipitated in MeOH to produce 46.8 mg of **6a**. Frs 237–238 were combined (209.3 mg) and applied over a Sephadex LH-20 column (15 g), and eluted with MeOH, wherein 20 sfrs of 2 mL were collected. Sfrs14-20 were combined (182.4 g) and applied over another Sephadex LH-20 column (5 g), and eluted with $CHCl_3$, wherein 13 ssfrs of 1 mL were collected. Ssfrs 8–9 were combined to produce 7.3 mg of **5c**. Frs 437-455 were combined (323.3 mg) and applied over a Sephadex LH-20 column (15 g), and eluted with MeOH, wherein 24 sfrs of 2 mL were collected. Sfrs 11–15 were combined (211.9 mg) and applied over another Sephadex LH-20 column (5 g), and eluted with $CHCl_3$, wherein 18 ssfrs of 0.5 mL were collected. Ssfrs 17–18 were combined to produce 141.7 mg of **5b**. Frs 460–513 were combined (297.3 mg) and applied over a Sephadex LH-20 column (15g), and eluted with MeOH, wherein 25 sfrs of 2 mL were collected. Sfrs 15–18 were combined (20.9 mg) and applied over another Sephadex LH-20 column (5 g), and eluted with $CHCl_3$, wherein 13 ssfrs of 0.5 mL were collected. Ssfrs 4–7 were combined to produce 5.6 mg of **4**.

3.3.1. (3*S*,4*R*)-4-Hydroxy-6-Methoxymellein (**2**)

White crystal. Mp 116–118 °C. $[\alpha]_D^{23}$ −200 (*c* 0.05, MeOH); For ^1H and ^{13}C spectroscopic data ($CDCl_3$, 300 and 75 MHz), see Table 1; (+)-HRESIMS *m/z* 225.0765 $[M + H]^+$ (calculated for $C_{11}H_{13}O_5$, 225.0763).

3.3.2. Stellatanthraquinone (**4**)

Red solid. Mp. 228–229 °C. For ^{1}H and ^{13}C spectroscopic data (DMSO-*d6*, 500 and 125 MHz), see Table 2; (+)-HRESIMS *m/z* 390.1340 $[M + H]^+$ (calculated for $C_{23}H_{20}NO_5$, 390.1341).

3.3.3. Carnemycin E (**5b**)

Pale-yellow viscous mass. $[\alpha]^{20}_D$ +60 (*c* 0.05, MeOH). ^{1}H and ^{13}C spectroscopic data (DMSO-*d6*, 300 and 75 MHz), see Table 3; (+)-HRESIMS *m/z* 395.2076 $[M + H]^+$ (calculated for $C_{21}H_{331}O_7$, 395.2070).

3.3.4. Acetyl Carnemycin E (**5c**)

Pale-yellow viscous mass. $[\alpha]^{20}_D$ +260 (*c* 0.05, MeOH). ^{1}H and ^{13}C spectroscopic data (DMSO-*d6*, 500 and 125 MHz), see Table 4; (+)-HRESIMS *m/z* 437.2175 $[M + H]^+$, (calculated for $C_{23}H_{33}O_8$, 437.2175); *m/z* 459.1989 $[M + Na]^+$ (calculated for $C_{23}H_{32}O_8Na$, 459.1995).

3.4. X-ray Crystal Structures

Single crystals were mounted on cryoloops using paratone. X-ray diffraction data were collected at 290 K with a Gemini PX Ultra equipped with CuK_α radiation (λ = 1.54184 Å). The structures were solved by direct methods using SHELXS-97 and refined with SHELXL-97 [30]. Non-hydrogen atoms were refined anisotropically. Hydrogen atoms were either placed at their idealized positions using appropriate HFIX instructions in SHELXL and included in subsequent refinement cycles or were directly found from difference Fourier maps and were refined freely with isotropic displacement parameters.

3.4.1. X-ray Crystal Structure of **6a**

Crystal was orthorhombic, space group $P2_12_12_1$, cell volume 2178.1(4) $Å^3$ and unit cell dimensions *a* = 6.2933(5) Å, *b* = 17.9862(18) Å and *c* = 19.243(3) Å (uncertainties in parentheses). Flack *x* [31] was refined parameter by means of TWIN and BASF in SHELXL to 0.0(5). The refinement converged to R (all data) = 8.88% and wR2 (all data) = 17.80%. Full details of the data collection and refinement and tables of atomic coordinates, bond lengths and angles, and torsion angles have been deposited with the Cambridge Crystallographic Data Centre (CCDC 2206108).

3.4.2. X-ray Crystal Structure of **6b**

The crystal was orthorhombic, space group $P2_12_12_1$, cell volume 2454.0(4) $Å^3$, and unit cell dimensions *a* = 5.9772(6) Å, *b* = 13.8321(13) Å and *c* = 29.682(2) Å (uncertainties in parentheses). Calculated crystal density was 1.306 g/cm^{-3}. The structure was solved by direct methods using SHELXS-97 and refined with SHELXL-97 [30]. The refinement converged to R (all data) = 8.45% and wR2 (all data) = 12.84% and Flack parameter = 0.0(3). Full details of the data collection and refinement and tables of atomic coordinates, bond lengths and angles, and torsion angles have been deposited with the Cambridge Crystallographic Data Centre (CCDC 2204631).

3.5. Electronic Circular Dichroism (ECD)

The experimental ECD spectrum of **2** (*ca.* 2 mg/mL in acetonitrile) was obtained in a Jasco J-815 CD spectropolarimeter (Jasco Europe S.R.L., Cremella, Italy) with a 0.1 mm cuvette and 6 accumulations. The simulated ECD spectra were obtained by first determining all the relevant conformers of the computational model. Its conformational space was developed by rotating all the single, non-ring, bonds for each of the two possible bends of the non-aromatic ring. The resulting 24 molecular mechanics conformers were minimized using the quantum mechanical DFT method B3LYP/6-31G with Gaussian 16W (Gaussian Inc., Wallingford, USA). The lowest 95% of the conformer Boltzmann populations (11 models) were subjected to a final minimization round using the method APFD/6-311+G(2d,p)/acetonitrile method (Gaussian 16W), which was also used, coupled with a TD method, to calculate its first 50 ECD transitions. The line spectrum for each one of the

11 models was built by applying a Gaussian line broadening of 0.15 eV to each computed transition with a constant UV-shift of 5 nm. The final ECD spectrum was obtained by the Boltzmann-weighted sum of the 11 line spectra [32].

3.6. Antibacterial Activity Bioassays

3.6.1. Bacterial Strains and Testing Conditions

Four reference strains, obtained from the American Type Culture Collection (ATCC), viz. two Gram-positive (*Staphylococcus aureus* ATCC 29213, *Enterococcus faecalis* ATCC 29212), and two Gram-negative (*Escherichia coli* ATCC 25922, *Pseudomonas aeruginosa* ATCC 27853), were included in this study. Additionally, three multidrug-resistant strains including an extended-spectrum β-lactamase (ESBL)-producing *E. coli* (clinical isolate SA/2), and two environmental isolates, i.e., a methicillin-resistant isolate (MRSA) *S. aureus* 74/24 [33], and a vancomycin-resistant (VRE) isolate *E. faecalis* B3/101 [34]. All bacterial strains were cultured in MH agar (MH-BioKar Diagnostics, Allone, France) and incubated overnight at 37 °C before each assay. Stock solutions of each compound (4 mg/mL for the less soluble compounds, **3a** and **4**, and 10 mg/mL for the others) were prepared in dimethyl sulfoxide (DMSO-Alfa Aesar, Kandel, Germany), kept at −20 °C, and freshly diluted in the appropriate culture media before each assay. In all experiments, in-test concentrations of DMSO were kept below 1%, as recommended by the Clinical and Laboratory Standards Institute [35].

3.6.2. Antimicrobial Susceptibility Testing

The Kirby–Bauer method was performed to screen the antimicrobial activity of the compounds according to CLSI recommendations [36]. Briefly, sterile blank paper discs with 6 mm diameter (Oxoid/Thermo Fisher Scientific, Basingstoke, UK) were impregnated with 15 μg of each compound and placed on MH plates, previously inoculated with a bacterial inoculum equal to 0.5 McFarland turbidity. After 18–20 h incubation at 37 °C, the diameter of the inhibition zones was measured in mm. Blank paper discs impregnated with DMSO were used as a negative control. Minimal inhibitory concentrations (MIC) were determined by the broth microdilution method, as recommended by the CLSI [37]. Two-fold serial dilutions of the compounds were prepared in cation-adjusted Mueller–Hinton broth (CAMHB-Sigma-Aldrich, St. Louis, MO, USA). With the exception of **3a** and **4**, the tested concentrations ranging from 1 to 64 μg/mL were used to keep in-test concentrations of DMSO below 1% to avoid bacterial growth inhibition. For **3a** and **4**, the highest concentration tested was 32 μg/mL. Colony forming unit (CFU) counts of the inoculum were conducted to ensure that the final inoculum size closely approximated the 5×10^5 CFU/mL. The 96-well U-shaped untreated polystyrene plates were incubated for 16–20 h at 37 °C, and the MIC was determined as the lowest concentration of the compound that prevented visible growth. During the essays, vancomycin (VAN-Oxoid/Thermo Fisher Scientific, Basingstoke, UK) and oxacillin sodium salt monosulfate (OXA-Sigma-Aldrich, St. Louis, MO, USA) were used as positive controls for *E. faecalis* ATCC 29212 and *S. aureus* ATCC 29213, respectively. The minimal bactericidal concentration (MBC) was determined by spreading 10 μL of the content of the wells with no visible growth on MH plates. The MBC was defined as the lowest concentration to effectively reduce 99.9% of the bacterial growth after overnight incubation at 37 °C [38]. At least three independent assays were conducted for reference and multidrug-resistant strains.

3.6.3. Antibiotic Synergy Testing

The Kirby–Bauer method was also used to evaluate the combined effect of the tested compounds with clinically relevant antibacterial drugs, as previously described [39]. A set of antibiotic discs (Oxoid/Thermo Fisher Scientific, Basingstoke, UK), to which the isolates were resistant, was selected: cefotaxime (CTX, 30 μg) for *E. coli* SA/2, vancomycin (VAN, 30 μg) for *E. faecalis* B3/101, and oxacillin (OXA, 1 μg) for *S. aureus* 74/24. Antibiotic discs impregnated with 15 μg of each compound were placed on seeded MH plates. The

controls used included antibiotic discs alone, blank paper discs impregnated with 15 µg of each compound alone, and blank discs impregnated with DMSO. Plates with CTX were incubated for 18–20 h and plates with VAN and OXA were incubated for 24 h at 37 °C [35]. Potential synergy was considered when the inhibition halo of the antibiotic disc impregnated with compound was greater than the inhibition halo of the antibiotic or compound-impregnated blank disc alone.

The MIC method was also performed in order to evaluate the combined effect of the compounds and clinically relevant antimicrobial drugs. Briefly, when it was not possible to determine a MIC value for the tested compound, the MIC of CTX (Duchefa Biochemie, Haarlem, The Netherlands), VAN (Oxoid, Basingstoke, England), and OXA (Sigma-Aldrich, St. Louis, MO, USA) for the respective multidrug-resistant strains was determined in the presence of the highest concentration of each compound tested in previous assays (64 µg/mL or 32 µg/mL for compounds **3a** and **4**). The tested antibiotic was serially diluted whereas the concentration of each compound was kept fixed. Antibiotic MICs were determined as described above. Potential synergy was considered when the antibiotic MIC was lower in the presence of compound [40]. Fractional inhibitory concentrations (FIC) were calculated as follows: FIC of the compound = MIC of the compound combined with antibiotic/MIC of the compound alone, and FIC antibiotic = MIC of antibiotic combined with compound/MIC of antibiotic alone. The FIC index (FICI) was calculated as the sum of each FIC and interpreted as follows: FICI $\leq$ 0.5, 'synergy'; 0.5 < FICI $\leq$ 4, 'no interaction'; 4 < FICI, 'antagonism' [41].

3.6.4. Biofilm Formation Inhibition Assay

In order to evaluate the antibiofilm activity of the compounds, the crystal violet method was used to quantify the total biomass produced [39,42]. Briefly, the highest concentration of the compound tested in the MIC assay was added to bacterial suspensions of 1×10^6 CFU/mL prepared in unsupplemented Tryptone Soy broth (TSB-Biokar Diagnostics, Allone, Beauvais, France) or TSB supplemented with 1% (*w/v*) glucose (D-(+)-glucose anhydrous for molecular biology, PanReac AppliChem, Barcelona, Spain) for Gram-positive strains. When it was possible to determine the MIC, concentrations between 2× MIC and 1/4 MIC were tested, while keeping in-test concentrations of DMSO below 1%. When it was not possible to determine the MIC value, the concentration tested was 64 µg/mL (or 32 µg/mL for compounds **3a** and **4**). Controls with appropriate concentration of DMSO, as well as a negative control (TSB or TSB + 1% glucose alone) were included. Sterile 96-well flat-bottomed untreated polystyrene microtiter plates were used. After a 24 h incubation at 37 °C, the biofilms were heat-fixed for 1 h at 60 °C and stained with 0.5% (*v/v*) crystal violet (Química Clínica Aplicada, Amposta, Spain) for 5 min. The stain was resolubilized with 33% (*v/v*) acetic acid (Acetic acid 100%, AppliChem, Darmstadt, Germany) and the biofilm biomass was quantified by measuring the absorbance of each sample at 570 nm in a microplate reader (Thermo Scientific Multiskan® FC, Thermo Fisher Scientific, Waltham, MA, USA). The background absorbance (TSB or TSB + 1% glucose without inoculum) was subtracted from the absorbance of each sample and the data are presented as percentage of control. Three independent assays were performed for reference strains, with triplicates for each experimental condition.

4. Conclusions

The EtOAc extract of the culture of a marine-derived fungus, *Aspergillus stellatus* KUFA 2017, isolated from a marine sponge *Mycale* sp., which was collected in the Gulf of Thailand, furnished three previously unreported secondary metabolites viz. (3*S*,4*R*)-4-hydroxy-6-methoxymellein (**2**), a structurally unique propylpyridinium anthraquinone, stellatanthraquinone (**4**), and acetyl carnemycin E (**5c**), in addition to eight previously reported compounds, including *p*-hydroxybenzaldehyde (**1**), 1,3-dimethoxy-8-hydroxy-6-methylanthraquinone (**3a**), 1,3-dimethoxy-2,8-dihydroxy-6-methylanthraquinone (**3b**), emodin (**3c**), 5[(3*E*,5*E*)-nona-3,5-dien-1-yl]benzene (**5a**), carnemycin E (**5b**), tajixanthone

hydrate (**6a**), and 15-acetyl tajixanthone hydrate (**6b**). While the absolute configurations of the stereogenic carbons in **2** were established unambiguously by a combination of NOESY correlations and a comparison of experimental and calculated ECD spectra, the stereostructures of **6a** and **6b** were established by X-ray analysis for the first time.

All the compounds, except **1** and **3c**, were evaluated for their antibacterial activity against four reference strains: two Gram-positive (*Staphylococcus aureus* ATCC 29213, *Enterococcus faecalis* ATCC 29212) and two Gram-negative (*Escherichia coli* ATCC 25922, *Pseudomonas aeruginosa* ATCC 27853), as well as three multidrug-resistant strains including an extended-spectrum β-lactamase (ESBL)-producing *E. coli* (clinical isolate SA/2), a methicillin-resistant isolate (MRSA) *S. aureus* 74/24 and a vancomycin-resistant (VRE) isolate *E. faecalis* B3/101. However, only **5c** exhibited antibacterial activity against all Gram-positive strains with a MIC value of 16 μg/mL toward *E. faecalis* ATCC 29212, vancomycin-resistant *E. faecalis* B3/101, and methicillin-resistant *S. aureus* 74/24, but with a higher MIC value (32 μg/mL) toward *S. aureus* ATCC 29213. Since **5a** displayed the minimal bactericidal concentration (MBC) equal to or one-fold higher than the MIC, it was suggested that **5a** exerted a bactericidal effect towards *E. faecalis* ATCC 29212, *S. aureus* 74/24, and *S. aureus* ATCC 29213. On the contrary, the MBC of **5a** was more than two-fold higher than the MIC toward *E. faecalis* B3/101; therefore, this compound was suggested to have a bacteriostatic effect against this multidrug-resistant species. Interestingly, **5b** and **5c**, which are C-glucosylated **5a**, were void of antibacterial activity against all the tested organisms. These results lead to a conclusion that the polar and bulky glucosyl substituent on the benzene ring can negatively affect the antibacterial activity of this series of compounds. Finally, **5a** was also able to completely inhibit biofilm formation in *S. aureus* ATCC 29213 and *E. faecalis* ATCC 29212 at both MIC and 2× MIC concentrations. Since **5a** possesses interesting antibacterial and potent antibiofilm activities, this compound can be considered as an interesting model for the development of a new type of antibiotics.

Supplementary Materials: The following are available online at https://www.mdpi.com/article/10.3390/md20110672/s1. Figures S1–S56: 1D and 2D NMR spectra of compounds **1**, **2**, **3a**, **3b**, **3c**, **4**, **5a**, **5b**, **5c**, **6a**, **6b**. Figures S57–S61: HRMS data for compounds **2**, **4**, **5a**, **5b**, and **5c**. Table S1: ^{1}H and ^{13}C NMR data ($CDCl_3$, 300 and 75 MHz) of compounds **3a** and **3b**. Table S2: ^{1}H and ^{13}C NMR data of **5b** (DMSO-$_{d6}$, 300 and 75 MHz), **5c** (DMSO-$_{d6}$, 500 and 125 MHz), and **5a** ($CDCl_3$, 300 and 75 MHz). Table S3: ^{1}H and ^{13}C NMR data of **6a** and **6b** ($CDCl_3$, 300 and 75 MHz).

Author Contributions: A.K. conceived, designed the experiments, and elaborated the manuscript; F.P.M. performed isolation, purification, and part of structure elucidation of the compounds; T.D. collected, isolated, identified, and cultured the fungus; J.A.P. performed calculations and measurement of ECD spectra and interpretation of the results; L.G. performed X-ray analysis; I.C.R. and P.M.C. performed antibacterial and antibiofilm assays; S.M. provided HRMS; A.M.S.S. provided NMR spectra; V.V. assisted in the preparation of a manuscript. All authors have read and agreed to the published version of the manuscript.

Funding: This work is partially supported by the national infrastructure PT-OPENSCREEN (NORTE-01-0145-FEDER-085468) and the national funds through the FCT-Foundation for Science and Technology with the scope of UIDB/04423/2020 and UIDP/04423/2020.

Institutional Review Board Statement: Not applicable.

Data Availability Statement: Data sharing is not applicable.

Acknowledgments: The authors acknowledge the support of the Biochemical and Biophysical Technologies i3S Scientific Platform with the assistance of Frederico Silva and Maria de Fátima Fonseca for the access of the Jasco J-815 CD spectropolarimeter.

Conflicts of Interest: The authors declare no conflict of interest.

References

1. Wang, X.-C.; Zhuang, W.-Y. New species of *Aspergillus* (Aspergillaceae) from tropical islands of China. *J. Fungi* **2022**, *8*, 225. [CrossRef] [PubMed]
2. Hagestad, O.C.; Andersen, J.H.; Altermark, B.E.; Rämä, T. Cultivable marine fungi from the Arctic Archipelago of Svalbard and their antibacterial activity. *Mycology* **2020**, *11*, 230–242. [CrossRef] [PubMed]
3. Machado, F.P.; Kumla, D.; Pereira, J.A.; Sousa, E.; Dethoup, T.; Freitas-Silva, J.; Costa, P.M.; Mistry, S.; Silva, A.M.S.; Kijjoa, A. Prenylated phenylbutyrolactones from cultures of a marine sponge-associated fungus *Aspergillus flavipes* KUFA1152. *Phytochemistry* **2021**, *185*, 112709. [CrossRef] [PubMed]
4. Wang, Y.-T.; Xue, Y.-R.; Liu, C.-H. A brief review of bioactive metabolites derived from deep-sea fungi. *Mar. Drugs* **2015**, *13*, 4594–4616. [CrossRef]
5. Samson, R.; Visagie, C.M.; Houbraken, J.; Hong, S.B.; Hubka, V.; Klaassen, C.H.W.; Perrone, G.; Seifert, K.A.; Susca, A.; Tanney, J.B.; et al. Phylogeny, identification and nomenclature of the genus *Aspergillus*. *Stud. Mycol.* **2014**, *78*, 141–173. [CrossRef] [PubMed]
6. Orfali, R.; Aboseada, M.A.; Abdel-Wahab, N.M.; Hassan, H.M.; Perveen, S.; Ameen, F.; Alturki, E.; Abdelmohsen, U.R. Recent updates on the bioactive compounds of the marine-derived genus *Aspergillus*. *RSC Adv.* **2021**, *11*, 17116–17150. [CrossRef]
7. Kruger, G.J.; Steyn, P.S.; Vleggaar, R.; Rabie, C.J. X-ray crystal structure of astelotoxin, a novel mycotoxin from *Aspergillus stellatus* Curzi. *J. Chem. Soc. Chem. Comm.* **1979**, *10*, 441–442. [CrossRef]
8. Kamal, A.; Husain, S.A.; Noorani, R.; Murtaza, N.; Qureshi, I.H.; Quershi, A.A. Studies in the biochemistry of microorganisms. XI. Isolation of tajixanthone, shamixanthone, ajamxanthone, shahenxanthone, najamxanthone, radixanthone and mannitol from mycelium of *Aspergillus stellatus*, Cruzi. *J. Sci. Indus. Res.* **1970**, *13*, 251–255.
9. Prompanya, C.; Dethoup, T.; Bessa, L.J.; Pinto, M.M.M.; Gales, L.; Costa, P.M.; Silva, A.M.S.; Kijjoa, A. New isocoumarin derivatives and meroterpenoids from the marine sponge-associated fungus *Aspergillus similanensis* sp. nov. KUFA 0013. *Mar. Drugs* **2014**, *12*, 5160–5173. [CrossRef]
10. Manojlović, I.; Bogdanović-Dusanović, G.; Gritsanapan, W.; Manojlović, N. Isolation and identification of anthraquinones of *Caloplaca cerina* and *Cassia tora*. *Chem. Pap.* **2006**, *60*, 466–468. [CrossRef]
11. Hawas, U.W.; El-Beih, A.A.; El-Halawany, A.M. Bioactive anthraquinones from endophytic fungus *Aspergillus versicolor* isolated from red sea algae. *Arch. Pharm. Res.* **2012**, *35*, 1749–1756. [CrossRef] [PubMed]
12. Noinart, J.; Buttachon, S.; Dethoup, T.; Gales, L.; Pereira, J.A.; Urbatzka, R.; Freitas, S.; Lee, M.; Silva, A.M.S.; Pinto, M.M.M.; et al. A new ergosterol analog, a new bis-anthraquinone and anti-obesity activity of anthraquinones from the marine sponge-associated fungus *Talaromyces stipitatus* KUFA 0207. *Mar. Drugs* **2017**, *15*, 139. [CrossRef] [PubMed]
13. Wen, H.; Chen, C.; Sun, W.; Zang, Y.; Li, Q.; Wang, W.; Zeng, F.; Liu, J.; Zhou, Y.; Zhou, Q.; et al. Phenolic *C*-glycosides and aglycones from marine-derived *Aspergillus* sp. and their anti-inflammatory activities. *J. Nat. Prod.* **2019**, *82*, 1098–1106. [CrossRef]
14. Pornpakakul, S.; Liangsakul, J.; Ngamrojanavanich, N.; Roengsumran, S.; Sihanonth, P.; Piapukiew, J.; Sangvichien, E.; Puthong, S.; Amorn Petsom, A. Cytotoxic activity of four xanthones from *Emericella variecolor,* an endophytic fungus isolated from *Croton oblongifolius*. *Arch. Pharm. Res.* **2006**, *29*, 140–144. [CrossRef]
15. Figueroa, M.; González, M.C.; Rodríguez-Sotres, R.; Sosa-Peinado, A.; González-Andrade, M.; Cerda-Gárcıa-Rojas, C.M.; Mata, R. Calmodulin inhibitors from the fungus *Emericella* sp. *Bioorg. Med. Chem.* **2009**, *17*, 2167–2174. [CrossRef] [PubMed]
16. González, A.M.; Rivera, C.J.; Sosa, P.A.; Figueroa, M.; Rodríguez-Sotres, R.; Mata, R. Development of the fluorescent biosensor h Calmodulin (h CaM) L39C-monobromobimane (mBBr)/V91C-mBBr, a novel tool for discovering new calmodulin inhibitors and detecting calcium. *J. Med. Chem.* **2011**, *54*, 3875–3884. [CrossRef] [PubMed]
17. Takenaka, Y.; Hamada, N.; Tanahashi, T. Aromatic compound from cultured lichen mycobionts of the three *Graphis* species. *Heterocycles* **2011**, *83*, 2157–2164.
18. Damodaran, V.; Ryan, J.L.; Keyzers, R.A. Cyclic 3-alkyl pyridinium alkaloid monomers from a New Zealand *Haliclona* sp. marine sponge. *J. Nat. Prod.* **2013**, *76*, 1997–2001. [CrossRef]
19. Schmidt, G.; Timm, C.; Köck, M.; Haliclocyclin, C. A new monomeric 3-alkyl pyridinium alkaloid from the arctic marine sponge *Haliclona viscosa*. *Z. Naturforsch.* **2011**, *66b*, 745–748. [CrossRef]
20. Maarisit, W.; Abdjul, D.B.; Yamazaki, H.; Kato, H.; Rotinsulu, H.; Wewengkang, D.S.; Sumilat, D.A.; Kapojos, M.M.; Ukai, K.; Namikoshi, M. Anti-mycobacterial alkaloids, cyclic 3-alkyl pyridinium dimers, from the Indonesian marine sponge *Haliclona* sp. *Bioorg. Med. Chem. Lett.* **2017**, *27*, 3503–3506. [CrossRef]
21. Markam, K.R.; Mues, R.; Stoll, M.; Zinsmeister, H.D. NMR spectra of flavone di-C-glycosides from *Apometzgeria pubescens* and the detection of rotational isomerism in 8-C-hexosylflavone. *Z. Naturforsch.* **1987**, *42c*, 1039–1042. [CrossRef]
22. Chexal, K.K.; Fouweather, C.; Holker, J.S.E.; Simpson, T.J.; Young, K. The biosynthesis of fungal metabolites. Part III. Structure of shamixanthone and tajixanthone, metabolites of *Aspergillus variecolor*. *J. Chem. Soc. Perkin Trans.* **1974**, *1*, 1584–1593. [CrossRef]
23. Chexal, K.K.; Holker, J.S.E.; Simpson, T.J. The biosynthesis of fungal metabolites. Part VI. Structure and biosynthesis of some minor metabolites from variant strains of *Aspergillus variecolor*. *J. Chem. Soc. Perkin Trans.* **1975**, *1*, 549–554. [CrossRef]
24. Luís, A.; Cruz, C.; Duarte, A.P.; Domingues, F. An alkenylresorcinol derivative from *Hakea sericea* fruits and their antimicrobial activity. *Nat. Prod. Com.* **2013**, *8*, 1459–1462. [CrossRef]
25. Hafez Ghoran, S.; Fatemeh Taktaz, F.; Ayatollahi, S.A.; Kijjoa, A. Anthraquinones and their analogues from marine-derived fungi: Chemistry and biological activities. *Mar. Drugs* **2022**, *20*, 474. [CrossRef] [PubMed]

26. de Sá, J.D.M.; Pereira, J.A.; Dethoup, T.; Cidade, H.; Sousa, M.E.; Rodrigues, I.C.; Costa, P.M.; Mistry, S.; Silva, A.M.S.; Kijjoa, A. Anthraquinones, diphenyl ethers, and their derivatives from the culture of the marine sponge-associated fungus *Neosartorya spinosa* KUFA 1047. *Mar. Drugs* **2021**, *19*, 457. [CrossRef]
27. Murray, M.G.; Thompson, W.F. Rapid isolation of high molecular weight plant DNA. *Nucleic Acids Res.* **1980**, *8*, 4321–4326. [CrossRef]
28. White, T.J.; Bruns, T.; Lee, S.; Taylor, J. Amplification and direct sequencing of fungal ribosomal RNA genes for phylogenetics. In *PCR Protocols: A Guide to Methods and Applications*; Innis, M.A., Gelfand, D.H., Sninsky, J.J., White, T.J., Eds.; Academic Press: New York, NY, USA, 1990; pp. 315–322.
29. Sanger, F.; Nicklen, S.; Coulson, A.R. DNA sequencing with chain-terminating inhibitors. *Proc. Natl. Acad. Sci. USA* **1977**, *72*, 5463–5467. [CrossRef]
30. Sheldrick, G.M. A short history of SHELX. *Acta Crystallogr. Sect. A* **2008**, *A64*, 112–122. [CrossRef]
31. Flack, H.D. On enantiomorph-polarity estimation. *Acta Crystallogr. Sect. A* **1983**, *39*, 876–881. [CrossRef]
32. Stephens, P.J.; Harada, N. ECD Cotton effect approximated by the Gaussian curve and other methods. *Chirality* **2010**, *22*, 229–233. [CrossRef] [PubMed]
33. Simões, R.R.; Aires-de-Sousa, M.; Conceição, T.; Antunes, F.; da Costa, P.M.; de Lencastre, H. High prevalence of EMRSA-15 in Portuguese public buses: A worrisome finding. *PLoS ONE* **2011**, *6*, e0017630. [CrossRef] [PubMed]
34. Bessa, L.J.; Barbosa-Vasconcelos, A.; Mendes, Â.; Vaz-Pires, P.; Da Costa, P.M. High prevalence of multidrug-resistant *Escherichia coli* and *Enterococcus* spp. in river water, upstream and downstream of a wastewater treatment plant. *J. Water Health* **2014**, *12*, 426–435. [CrossRef]
35. CLSI. *Performance Standards for Antimicrobial Susceptibility Testing*, 28th ed.; CLSI supplement M100; Clinical and Laboratory Standards Institute: Wayne, PA, USA, 2018.
36. CLSI. *Performance Standards for Antimicrobial Disk Susceptibility Tests; Approved Standard*, 11th ed.; CLSI Document M02-A11; Clinical and Laboratory Standards Institute: Wayne, PA, USA, 2012.
37. CLSI. *Methods for Dilution Antimicrobial Susceptibility Tests for Bacteria that Grow Aerobically*, 11th ed.; CLSI Standard M07; Clinical and Laboratory Standards Institute: Wayne, PA, USA, 2018.
38. CLSI. *Methods for Determining Bactericidal Activity of Antimicrobial Agents; Approved Guideline*; CLSI Document M26-A; Clinical and Laboratory Standards Institute: Wayne, PA, USA, 1999.
39. Kumla, D.; Dethoup, T.; Gales, L.; Pereira, J.A.; Freitas-Silva, J.; Costa, P.M.; Silva, A.M.S.; Pinto, M.M.M.; Kijjoa, A. Erubescensoic acid, a new polyketide and a xanthonopyrone SPF-3059-26 from the culture of the marine sponge-associated fungus *Penicillium erubescens* KUFA 0220 and antibacterial activity evaluation of some of its constituents. *Molecules* **2019**, *24*, 208. [CrossRef] [PubMed]
40. Gomes, N.M.; Bessa, L.J.; Buttachon, S.; Costa, P.M.; Buaruang, J.; Dethoup, T.; Silva, A.M.S.; Kijjoa, A. Antibacterial and antibiofilm activities of tryptoquivalines and meroditerpenes isolated from the marine-derived fungi *Neosartorya paulistensis*, *N. laciniosa*, *N. tsunodae*, and the soil *fungi N. fischeri* and *N. siamensis*. *Mar. Drugs* **2014**, *12*, 822–839. [CrossRef]
41. Odds, F.C. Synergy, antagonism, and what the chequer board puts between them. *J. Antimicrob. Chemother.* **2003**, *52*, 1. [CrossRef]
42. Stepanović, S.; Vuković, D.; Hola, V.; Di Bonaventura, G.; Djuki'c, S.; Cirković, I.; Ruzicka, F. Quantification of biofilm in microtiter plates: Overview of testing conditions and practical recommendations for assessment of biofilm production by staphylococci. *Apmis* **2007**, *115*, 891–899. [CrossRef] [PubMed]

marine drugs

MDPI

Article

Noonindoles A–F: Rare Indole Diterpene Amino Acid Conjugates from a Marine-Derived Fungus, *Aspergillus noonimiae* CMB-M0339

Sarani Kankanamge [1], Zeinab G. Khalil [1], Paul V. Bernhardt [2] and Robert J. Capon [1,*]

[1] Institute for Molecular Bioscience, The University of Queensland, St Lucia, QLD 4072, Australia
[2] School of Chemistry and Molecular Bioscience, The University of Queensland, St Lucia, QLD 4072, Australia
* Correspondence: r.capon@uq.edu.au; Tel.: +61-7-3346-2979

Abstract: Analytical scale chemical/cultivation profiling prioritized the Australian marine-derived fungus *Aspergillus noonimiae* CMB-M0339. Subsequent investigation permitted isolation of noonindoles A–F (**5**–**10**) and detection of eight minor analogues (**i**–**viii**) as new examples of a rare class of indole diterpene (IDT) amino acid conjugate, indicative of an acyl amino acid transferase capable of incorporating a diverse range of amino acid residues. Structures for **5**–**10** were assigned by detailed spectroscopic and X-ray crystallographic analysis. The metabolites **5**–**14** exhibited no antibacterial properties against G-ve and G+ve bacteria or the fungus *Candida albicans*, with the exception of **5** which exhibited moderate antifungal activity.

Keywords: indole diterpene; noonindole; marine-derived fungus; *Aspergillus noonimiae*; antifungal; Australia; microbial biodiscovery; molecular network chemical profiling; MATRIX cultivation profiling

Citation: Kankanamge, S.; Khalil, Z.G.; Bernhardt, P.V.; Capon, R.J. Noonindoles A–F: Rare Indole Diterpene Amino Acid Conjugates from a Marine-Derived Fungus, *Aspergillus noonimiae* CMB-M0339. *Mar. Drugs* **2022**, *20*, 698. https://doi.org/10.3390/md20110698

Academic Editor: Hee Jae Shin

Received: 18 October 2022
Accepted: 4 November 2022
Published: 7 November 2022

1. Introduction

Since the indole diterpene (IDT) paxilline (**1**) (Figure 1) was first described in 1975 as a tremorgenic agent of *Penicillium paxilli* [1], a number of fungal natural products sharing this fused hexacyclic skeleton have been reported (i.e., paxillines, paspalines, paspalinines, paspalicine, paspalitrems, penijanthine A, penitrems, aflatrem, penerpenes, sulpinines, and terpendoles) from a wide range of genera, including from terrestrially sourced *Acremonium* [2], *Albophoma* [3–5], *Aspergillus* [6–10], *Chaunopycnis* [11], *Claviceps* [12], *Emericella* [13,14], *Eupenicillium* [15], *Neotyphodium* [16], *Penicillium* [2,17–21], *Phomopsis* [22], and marine-derived *Penicillium* [23–27]. In addition to tremorgenic properties [1,2,6,7,13,14,17,22,28], members of this IDT family have been reported to exhibit anticancer [23,29], anti-insectan [8,9,15] and anti-H1N1 [24] activity, with Merck researchers reporting potent and selective potassium ion channel antagonist properties [28] prompting patent protection for the treatment of neurodegenerative diseases (i.e., Alzheimer's disease) [30] and glaucoma [31]. Paxilline (**1**) has been noted as one of the most potent and selective nonpeptidergic inhibitors of large-conductance, voltage, and Ca^{2+} dependent BK-type potassium channels [32], stimulating interest in chemical synthesis [33–35] and biosynthesis [36–42] across this structure class. For example, a 2022 report [43] described two genes encoding monomodular nonribosomal peptide synthetase (NRPS)-*like* enzymes that catalyse the acylation of 14-hydroxypaspalinine (**2**) (Figure 1) to the only two known natural product examples of amino acid conjugated IDTs: 14-(*N*,*N*-dimethyl-L-valyloxy)paspalinine (**3**) (Figure 1) reported [9] in 1993 from *Aspergillus nominus* NRRL 13,137 and patented in 1993 as an anti-insectan for controlling Coleopteran and Lepidopteran insects [44], and in 2003 for the treatment of glaucoma [31]; and 14-(*N*,*N*-dimethyl-l-leucyloxy)paspalinine (**4**) patented in 2003 for the treatment of glaucoma [31] and subsequently optimised for production from *Aspergillus alliaceus* [10].

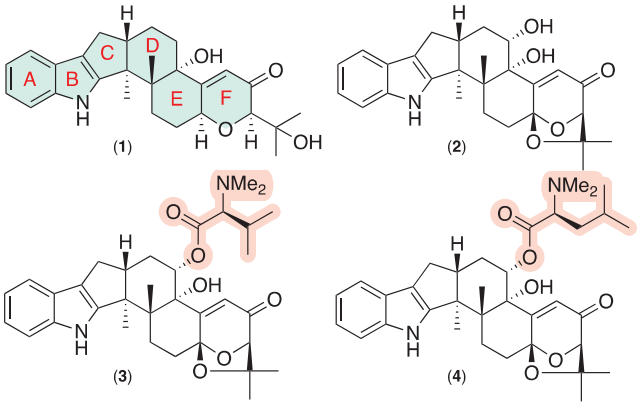

Figure 1. Known fungal IDTs highlighting the paxilline scaffold (blue) and rare amino acid acyl functionality (tan).

This current report describes our discovery of new IDT amino acid conjugates produced by the Australian marine-derived fungus *Aspergillus noonimiae* CMB-M0339. Using an integrated strategy of chemical and cultivation profiling to both prioritize and facilitate production, we successfully detected, isolated, characterised, and identified five new IDT amino acid conjugates and a key hydroxy precursor, noonindoles A–F (**5**–**10**), together with the four known analogues paspaline (**11**) [12], paspaline B (**12**) [18], the carboxylic acid (**13**) [24], and emindole SB (**14**) [13]. Structures for **5**–**14** were assigned by detailed spectroscopic and X-ray analysis as summarised below, along with a plausible biogenetic relationship. We also made use of biosynthetic considerations and diagnostic MS/MS fragmentations to tentatively assign structures to a series of eight minor IDT amino acid co-metabolites (**i**–**viii**).

2. Results

An EtOAc extract was prepared from a 3.3% saline M1 agar plate cultivation of the marine-derived fungus *Aspergillus noonimiae* CMB-M0339. UPLC-DAD (Figure S6) was subjected to a global natural product social (GNPS) [45] molecular network (Figure 2) analysis to reveal peaks/nodes for three prominent and structurally related metabolites: **5** (*m*/*z* 579 (M+H), $C_{34}H_{46}N_2O_6$); **6** (*m*/*z* 565 (M+H), $C_{33}H_{44}N_2O_6$); and **7** (*m*/*z* 593 (M+H), $C_{35}H_{48}N_2O_6$). Online database searching suggested these metabolites were unprecedented in the natural products literature. Subsequent cultivation profiling using a miniaturized 24-well plate microbioreactor methodology (MATRIX) [46] employing ×11 different media under solid agar (2 mL), as well as static and shaken broth (1.5 mL) conditions (Figure S7) supported by UPLC-DAD and GNPS chemical profiling (Figures 3 and S8) confirmed D400 solid phase agar as the optimal culture condition. The EtOAc extract of a ×300 plate D400 solid phase 12 day cultivation was subjected to solvent trituration and reversed-phase HPLC (Figure S9) to yield **5**–**14** (Figure 4). Detailed spectroscopic analysis successfully identified the known natural products paspaline (**11**) [12], paspaline B (**12**) [18], the carboxylic acid **13** [24], and emindole SB (**14**) [13] (Tables S8–S11, Figures S50–S68). Further spectroscopic analysis identified the new noonindoles A–F (**5**–**10**) as summarised below.

HRESIMS analysis of **5** revealed a molecular formula ($C_{34}H_{46}N_2O_6$, Δmmu +2.7) requiring thirteen double bond equivalents (DBE). The NMR (methanol-d_4) data for **5** (Tables 1 and S2, and Figures S10–S15) disclosed resonances for ten sp^2 olefinic carbons and two sp^2 ester/lactone carbonyls, accounting for seven DBE and requiring that **5** be hexacyclic, while diagnostic 2D NMR correlations (Figure 5) established a carbon/hetero skeleton in common with **1** further annotated by an *N*,*N*-dimethyl-valinyloxy ester pendant to C-14. The structure and absolute configuration for noonindole A (**5**) were confirmed by a single crystal X-ray analysis (Figure 6 and Table S13).

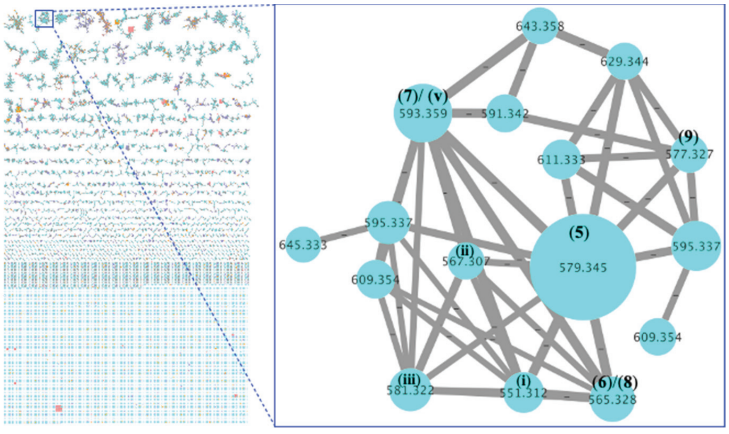

Figure 2. GNPS molecular network of an inhouse fungal extract library, revealing a unique cluster of metabolites (expansion) associated exclusively with strain CMB-M0339.

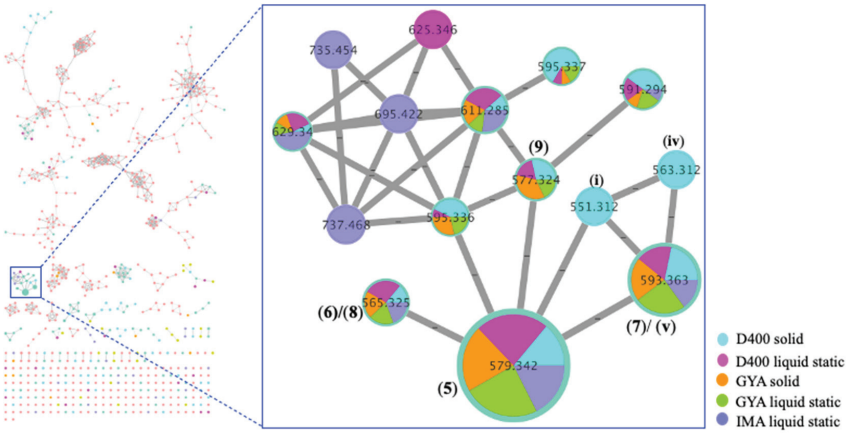

Figure 3. GNPS molecular network of a set of MATRIX extracts of CMB-M0339 showing production of noonindoles A–E (**5**–**9**) and related minor metabolites under selected culture conditions.

HRESIMS analysis of **6**–**8** revealed molecular formulae ($C_{33}H_{44}N_2O_6$, Δmmu +2.0; $C_{35}H_{48}N_2O_6$, Δmmu +2.6; $C_{33}H_{44}N_2O_6$, Δmmu +1.5) consistent with lower/higher homologues of **5**. Comparison of the NMR (methanol-d_4) data for **6** (Tables 1 and S3, Figures S17–S22) with **5** allowed the principle differences to be attributed to replacement of the *N*,*N*-dimethyl-valinyloxy side chain in **5** (δ_H 2.90, s; δ_C 43.1) with an *N*-methyl-valinyloxy side chain in **6** (δ_H 2.72, s, NH(C$\underline{H}_3$); δ_C 33.8, NH($\underline{C}H_3$)). Likewise, comparison of the NMR (methanol-d_4) data for **7** (Tables 1 and S4, and Figures S24–S29) and **8** (Tables 2 and S5, and Figures S31–S35) with **5** allowed the principle differences to be attributed to replacement of the *N*,*N*-dimethyl-valinyloxy moiety in **5** with an *N*,*N*-dimethyl-leucinyloxy moiety in **7** and an *N*,*N*-dimethyl-homoalaninyloxy in **8**. These conclusions were reinforced by diagnostic 2D NMR correlations (Figure 5) which, together with biogenetic considerations, allowed assignment of structures to noonindoles B–D (**6**–**8**).

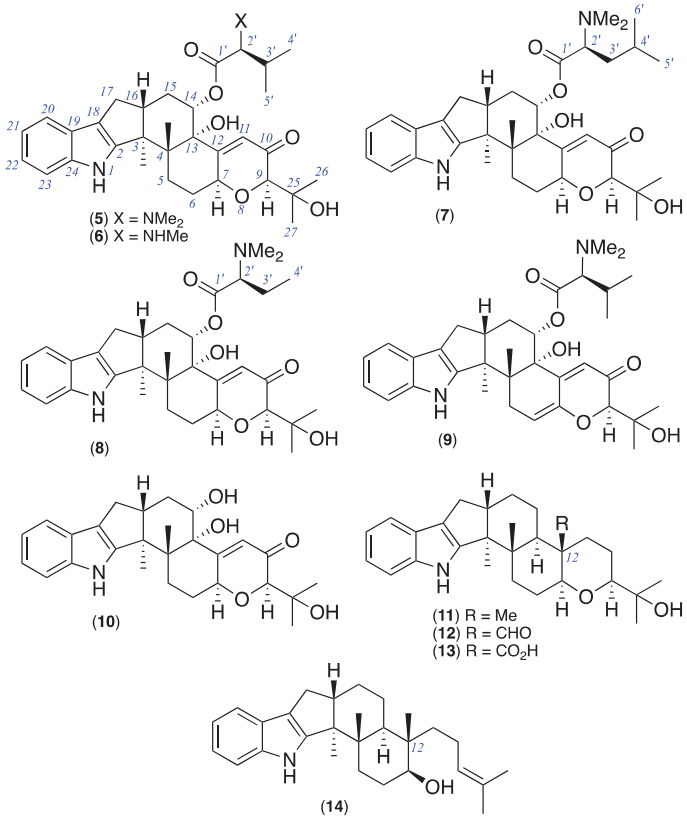

Figure 4. New noonindoles A–F (**5**–**10**) and known **11**–**14**.

Table 1. 1D NMR (methanol-d_4) data for noonindoles A–C (**5**–**7**) [#].

Pos.	(5) δ_H, mult. (*J* in Hz)	δ_C	(6) δ_H, mult. (*J* in Hz)	δ_C	(7) δ_H, mult. (*J* in Hz)	δ_C
2	-	152.4	-	152.3	-	152.2
3	-	52.0	-	51.9	-	51.8
4	-	46.4	-	46.2	-	46.2
5	*a* 2.87, ddd (*13.6*, *13.6*, *5.2*) *b* 1.81, br dd (*13.6*, *5.2*)	28.1	*a* 2.88, ddd (*13.5*, *13.5*, *5.1*) *b* 1.83, br dd (*13.5*, *5.1*)	28.0	*a* 2.87, ddd (*13.8*, *13.8*, *5.4*) *b* 1.84, br dd (*13.8*, *5.4*)	27.9
6	*a* 2.38, m *b* 1.91, m	30.6	*a* 2.39, m *b* 1.93, m	30.5	*a* 2.39, m *b* 1.93, m	30.5
7	4.91, m	74.6	4.90, m	74.8	4.92, br t (*8.5*)	74.8
9	3.68, d (*1.9*)	84.0	3.72, d (*1.5*)	83.9	3.71, br s	84.0
10	-	198.5	-	198.1	-	197.9
11	5.62, d (*1.9*)	122.4	5.57, d (*1.5*)	122.0	5.57, d (*1.9*)	121.8
12	-	165.9	-	165.8	-	165.0
13	-	80.0	-	80.0	-	80.1
14	5.53, dd (*10.2*, *5.3*)	77.9	5.50, dd (*10.4*, *5.0*)	77.3	5.51, dd (*10.4*, *5.1*)	77.5
15	*a* 2.24, dd (*11.1*, *10.2*) *b* 2.21, m	28.5	*a* 2.25, dd (*13.0*, *10.4*) *b* 2.17, m	28.3	*a* 2.25, dd (*13.2*, *10.4*) *b* 2.20, m	28.1
16	2.92, m	47.4	2.98, m	47.5	2.97, m	47.5

Table 1. *Cont.*

Pos.	(5) δ_H, mult. (*J* in Hz)	δ_C	(6) δ_H, mult. (*J* in Hz)	δ_C	(7) δ_H, mult. (*J* in Hz)	δ_C
17	*a* 2.73, dd (*13.0*, *6.2*) *b* 2.47 [a], m	27.6	*a* 2.74, dd (*13.1*, *6.3*) *b* 2.47, dd (*13.1*, *11.1*)	27.6	*a* 2.74, dd (*13.0*, *6.3*) *b* 2.47, dd (*13.0*, *10.8*)	27.6
18	-	117.4	-	117.3	-	117.2
19	-	126.2	-	126.0	-	126.1
20	7.31, d (*7.5*)	119.0	7.30, d (*7.9*)	118.8	7.30, d (*7.8*)	118.9
21	6.94, ddd (*7.5*, *7.5*, *1.1*)	120.1	6.93, br dd (*7.9*, *7.7*)	119.9	6.93, ddd (*7.8*, *7.8*, *1.1*)	119.9
22	6.98, ddd (*7.5*, *7.5*, *1.1*)	121.1	6.97, ddd (*7.9*, *7.9*, *0.9*)	121.1	6.98, ddd (*7.8*, *7.8*, *1.1*)	121.1
23	7.27, d (*7.5*)	112.7	7.28, d (*7.9*)	112.7	7.28, d (*7.8*)	112.7
24	-	141.8	-	141.9	-	141.9
25	-	73.3	-	73.0	-	73.0
26	1.28, s	25.4	1.28, s	25.3	1.30, s	25.5
27	1.26, s	26.2	1.26, s	26.4	1.27, s	25.8
1′	-	167.4	-	168.9	-	168.9
2′	3.86, d (*5.5*)	74.8	3.90, br s	68.7	4.02, m	67.5
3′	2.47 [a], m	28.4	2.31, m	30.7	*a* 1.90, m	37.4
	-	-	-	-	*b* 1.69, m	37.4
4′	1.05 [b]	19.4	1.09, br d (*5.3*)	18.7	1.56, m	26.2
5′	1.03, d (*7.1*)	17.0	0.99, d (*7.0*)	17.7	0.97, d (*6.4*)	23.4
6′	-	-	-	-	0.91, d (*6.4*)	21.4
3-Me	1.37, s	16.7	1.37, s	16.6	1.38, s	16.6
4-Me	1.04 [b]	19.4	1.10, s	19.5	1.09, br s	19.4
NHMe	-	-	2.72, s	33.8	-	-
NMe_2	2.90, s	43.0	-	-	2.93, s	42.1

[#] Data acquired on the TFA salts. [a,b] Resonances with the same superscript overlap and assignments can be interchanged.

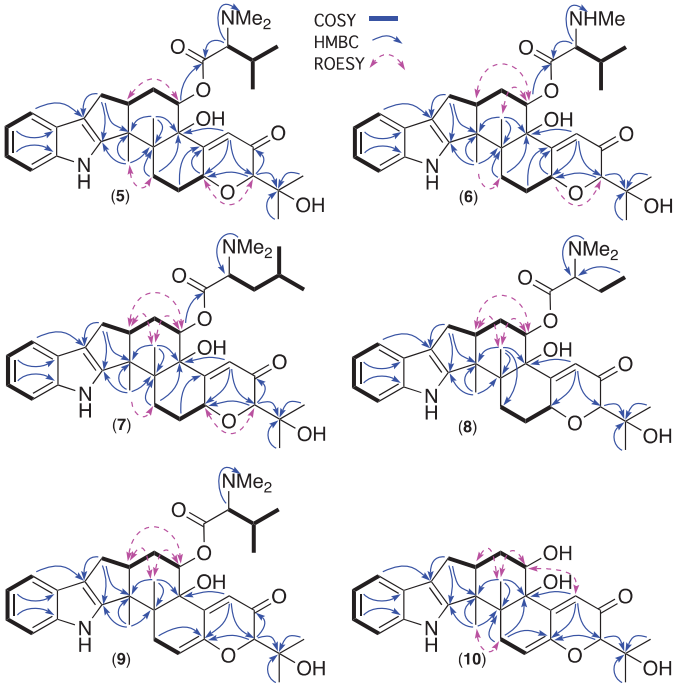

Figure 5. 2D NMR (methanol-d_4) correlations for **5**–**10**.

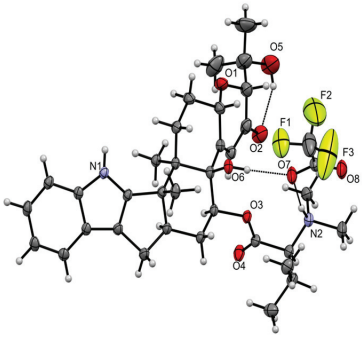

Figure 6. X-ray crystal structure of noonindole A (**5**).

Table 2. 1D NMR (methanol-d_4) data for noonindoles D–F (**8**–**10**).

Pos.	(8) δ_H, mult. (*J* in Hz)	δ_C	(9) δ_H, mult. (*J* in Hz)	δ_C	(10) δ_H, mult. (*J* in Hz)	δ_C
2	-	151.1	-	152.5	-	152.9
3	-	50.5	-	51.9	-	51.8
4	-	44.6	-	46.2	-	44.7
5	*a* 2.87 [a], m	28.0	*a* 3.28 *	33.0	*a* 2.80, ddd (*13.5*, *13.5*, *5.1*)	28.1
	b 1.80, m		*b* 2.36, d (*6.3*)		*b* 1.79, dd (*13.5*, *5.1*)	
6	*a* 2.37, m	30.4	5.74, m	113.5	*a* 2.33, m	30.2
	b 1.91, m				*b* 1.90, m	
7	4.90, m	74.6	-	146.4	4.88, m	74.7
9	3.71, d (*1.9*)	83.7	4.09, s	87.6	3.78, d (*1.5*)	84.0
10	-	nd	-	196.8	-	200.0
11	5.58, d (*1.9*)	121.7	5.71, br s	119.5	6.01, br s	122.9
12	-	nd	-	nd	-	167.5
13	-	78.9	-	77.8	-	80.8
14	5.37, dd (*10.6*, *5.1*)	74.4	5.41, dd (*9.8*, *5.8*)	75.5	4.16, dd (*10.5*, *4.9*)	70.3
15	*a* 2.16, m	28.4	2.18, m	30.0	*a* 2.08, dd (*13.3*, *10.5*)	31.7
	b 2.04, ddd (*7.1*, *5.1*, *2.3*)				*b* 1.93, m	
16	2.95, m	47.0	2.90, m	47.5	2.90, m	48.0
17	*a* 2.72, dd (*13.1*, *6.4*)	27.5	*a* 2.72, dd (*13.0*, *6.5*)	28.0	*a* 2.68, dd (*13.0*, *6.1*)	27.8
	b 2.45, dd (*13.1*, *10.7*)		*b* 2.44, dd (*13.0*, *10.8*)		*b* 2.42, dd (*13.0*, *10.0*)	
18	-	116.8	-	117.4	-	117.4
19	-	124.7	-	126.2	-	126.2
20	7.30, d (*7.7*)	118.6	7.30, d (*7.2*)	119.1	7.29, d (*7.6*)	118.8
21	6.92, ddd (*7.7*, *7.3*, *0.9*)	119.6	6.93, m	120.0	6.92, br dd (*7.6*, *7.2*)	119.8
22	6.97, ddd (*8.1*, *7.3*, *0.9*)	120.7	6.97, m	121.2	6.95, br dd (*7.4*, *7.2*)	120.9
23	7.27, d (*8.1*)	112.4	7.27, d (*7.5*)	112.8	7.26, d (*7.4*)	112.7
24	-	140.4	-	142.1	-	141.8
25	-	71.6	-	75.6	-	73.2
26	1.28, s	25.1	1.33, s	27.1 [a]	1.29, s	25.2
27	1.26, s	25.9	1.26, s	27.1 [a]	1.27, s	26.2
1′	-	nd	-	nd	-	-
2′	2.87 [a], m	72.9	2.86, d (*9.4*)	76.0	-	-
3′	*a* 1.77, m	23.8	2.11, m	28.7	-	-
	b 1.69, m				-	-
4′	0.91, t (*7.4*)	10.1	0.97, t (*7.4*)	19.9	-	-
5′	-	-	0.97, t (*7.4*)	19.9	-	-
3-Me	1.37, s	16.3	1.40, s	16.9	1.32, s	16.5
4-Me	1.08, s	19.4	1.14, s	21.0	1.04, s	19.6
NMe_2	2.26, s	43.4	2.34, s	42.4	-	-

nd: Not detected. [a] Resonances with the same superscript within a column are overlapping. * Obscured by residual solvent resonance. [#] Data for **8**–**9** acquired on the free bases (not TFA salts).

HRESIMS analysis of **9** revealed a molecular formula ($C_{34}H_{44}N_2O_6$, Δmmu +1.2) consistent with an oxidised analogue of **5**. Comparison of the NMR (methanol-d_4) data for **9** (Tables 2 and S6, and Figures S37–S41) with **5** allowed the principle differences to be attributed to replacement of the sp^3 H-7/C- 7 methine in **5** (δ_H 4.91, H-7; δ_C 74.6, C-7) with an sp^2 quaternary C-7 and sp^2 H-6/C-6 methine in **9** (δ_H 5.74, m, H-6; δ_C 113.5, C-6; δ_C

146.4, C-7), consistent with incorporation of a $\Delta^{6,7}$. These conclusions were reinforced by 2D NMR correlations (Figure 5) which, together with biogenetic considerations, allowed assignment of the structure for noonindole E (**9**).

HRESIMS analysis of **10** revealed a molecular formula ($C_{27}H_{33}NO_5$, Δmmu +1.1) consistent with a hydrolysed analogue of **5** lacking the *N*,*N*-dimethyl-valinyloxy ester side chain. This hypothesis was confirmed on comparison of the NMR (methanol-d_4) data for **10** (Tables 2 and S7, and Figures S43–S48) with **5** which revealed the absence of resonances for the *N*,*N*-dimethyl-valinyloxy moiety and a significant shielding of the resonance for H-14 in **10** (δ_H 4.16) compared with **5** (δ_H 5.53). These conclusions were reinforced by 2D NMR correlations (Figure 5) which, together with biogenetic considerations, allowed assignment of a structure for noonindole F (**10**).

Co-isolation of noonindoles A–F (**5**–**10**) and the known IDTs **11**–**14** together with an X-ray crystal analysis of **5** supported a common absolute configuration across the hexacyclic indole terpene core, and established the configuration of the *N*,*N*-dimethyl-L-valinyloxy moiety in **5**. Although low yields combined with *N*-alkylation precluded hydrolysis and independent assignment of the amino acid residue absolute configuration in **6**–**9** (i.e., Marfey's analysis), an amino acid L configuration across **6**–**9** was proposed based on the likelihood of a common NRPS-*like* aminoacyl modifying enzyme in the noonindole biosynthetic gene cluster (BGC) (see below).

The metabolites **5**–**14** did not inhibit the growth of human colon (SW620) or lung (NCI-H460) carcinoma cells (IC_{50} > 30 μM) (Figure S81), or the fungus *Candida albicans* ATCC10231, the Gram-negative bacterium *Escherichia coli* ATCC11775, or the Gram-positive bacteria *Staphylococcus aureus* ATCC25923 or *Bacillus subtilis* ATCC6633 (IC_{50} > 30 μM), with the exception of noonindole A (**5**) which displayed modest antifungal activity (IC_{50}~5 μM) (Figure S80). This lack of cellular toxicity bodes well for future (ongoing) evaluation of noonindole ion channel inhibitory pharmacology.

GNPS analysis of the EtOAc extract of the analytical scale D400 (MATRIX) culture of CMB-M0339 detected **5**–**9** along with associated nodes for a selection of putative minor analogues (Figure 7). The MS/MS spectra for **5**–**9** (Figures S72–S75) revealed three common fragmentations attributed to loss of water (Figure 8A), retro-Aldol loss of acetone (Figure 8B), and loss of the amino acid residue (Figure 8C). While low yields precluded isolation of the minor analogues **i**–**viii**, diagnostic MS/MS fragmentations and high-resolution mass measurements (i.e., molecular formulae) permitted tentative assignments for **i**–**v** (Figures S74, S76–S79, Table S12) and on the basis of GNPS co-clustering and biosynthetic considerations to **vi**–**viii**, albeit with some allowance isomeric alternatives (Tables 3 and S12). The diversity of IDT amino acid conjugates produced by CMB-M0339 is in stark contrast to existing knowledge, which is limited to **3** from *Aspergillus nomius* [9] and **4** from *A. alliaceus* [10]. Unlike these earlier published accounts, it appears CMB-M0339 employs an NRPS-*like* aminoacylation enzyme with an adenylation domain tolerant of different amino acid substrates (i.e., Val, Leu, Ile, Pro, Ser, Thr, and homo-Ala).

A preliminary assessment of the noonindole biosynthetic gene cluster (BGC) suggests a biogenetic relationship linking **5**–**14** and inclusive of the minor co-metabolites **i**–**viii** starting with emindole SB (**14**) undergoing stereospecific epoxidation and ring closure to paspaline (**11**) followed by sequential oxidation to paspaline B (**12**) and the carboxylic acid **13**, followed by decarboxylation and oxidation to paxilline (**1**) (Figure 9). Oxidation of **1** could then yield noonindole F (**10**) with further oxidation and/or amino acid acylation returning noonindoles A–E (**5**–**9**) and co-clustering minor analogues (**i**–**viii**). Consistent with this hypothesis, close examination of the CMB-M0339 D400 extract GNPS and UPLC-DAD-MS data using single ion extraction (SIE) detected an ion with a molecular formula attributable to **1** (Figure S71).

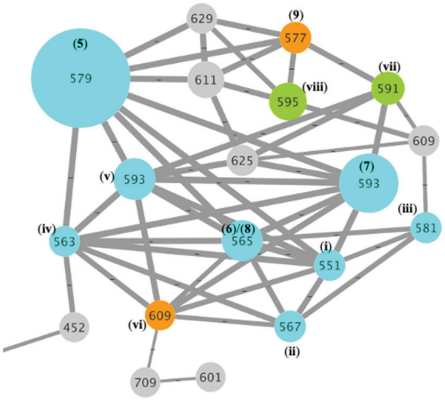

Figure 7. GNPS cluster of the EtOAc extract of a D400 (MATRIX) culture of CMB-M0339 revealing **5**–**9** along with closely associated nodes for the minor analogues **i**–**viii**.

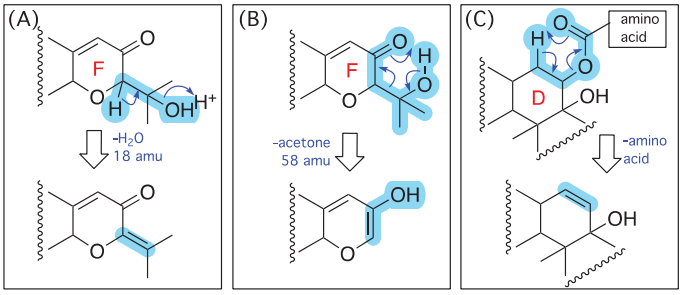

Figure 8. MS/MS fragmentations common to **1**–**5** and minor co-metabolites **i**–**viii**; (**A**) loss of water, (**B**) retro-Aldol loss of acetone and, (**C**) loss of the amino acid residue.

Table 3. Comparison of **5**–**9** and minor co-metabolites **i**–**viii**.

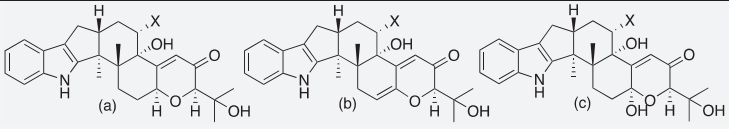

X (ester)	(a)	(b)	(c)
N,*N*-dimethyl-valine	(**5**)	(**9**)	(**viii**)
N-methyl-valine	(**6**)	-	-
N,*N*-dimethyl-leucine	(**7**)	(**vii**)	(**vi**)
N,*N*-dimethyl-homoalanine	(**8**)	-	-
N,*N*-dimethyl-alanine [A]	(**i**)	-	-
N,*N*-dimethyl-serine [B]	(**ii**)	-	-
N,*N*-dimethyl-threonine	(**iii**)	-	-
N-methyl-proline [C]	(**iv**)	-	-
N,*N*-dimethyl-isoleucine [D]	(**v**)	-	-

(a,b,c) Proposed hexacyclic scaffolds. Possible alternate isomers: [A] *N*-methyl-homoalanine, valine; [B] *N*-methyl-threonine; [C] pipecolic acid; [D] *N*,*N*-dimethyl-*allo*-isoleucine.

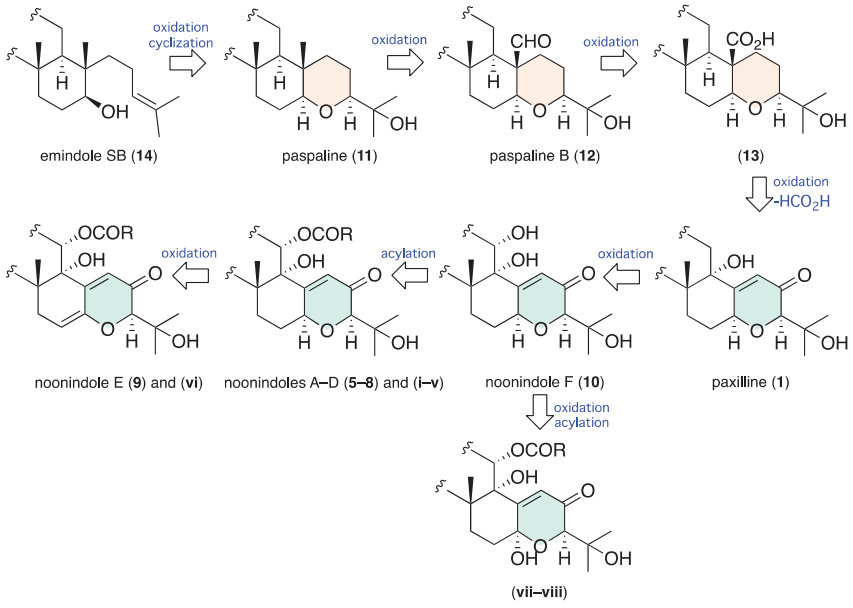

Figure 9. Plausible biogenetic relationship linking **5**–**14** (and **1**) and inclusive of the minor co-metabolites **i**–**viii**.

Our investigation into the marine-derived *Aspergillus noonimiae* CMB-M0339 led to the discovery of noonindoles A–F (**5**–**10**) and related minor analogues (**i**–**viii**) as new examples of a rare class of fungal indole diterpene amino acid conjugate. This discovery highlights the continued capacity of fungi to provide access to new chemical space and validates molecular networking (GNPS) as an effective platform to detect, dereplicate, and prioritize new over known chemistry, and cultivation profiling (MATRIX) as a means to optimise the production. Our discovery of the noonindoles suggests the CMB-M0339 features an NRPS-*like* aminoacyl modifying enzyme in the noonindole biosynthetic gene cluster (BGC) capable of accommodating and incorporating multiple lipophilic amino acids. Further studies into the structure, biosynthesis, and biology of these and other CMB-M0339 indole diterpenes are ongoing, and will be reported elsewhere.

3. Materials and Methods

3.1. General Experimental Procedures

Chemicals were purchased from Sigma-Aldrich or Merck unless otherwise specified. Solvent extractions were performed using analytical-grade solvents, while HPLC, UPLC, and HPLC-MS analyses employed HPLC-grade solvents supplied by Labscan or Sigma-Aldrich and filtered/degassed through 0.45 μm polytetrafluoroethylene (PTFE) membrane prior to use. Deuterated solvents were purchased from Cambridge Isotopes (Tewksbury, MA, USA). Microorganisms were manipulated under sterile conditions in a Laftech class II biological safety cabinet and incubated in either an MMM Friocell incubator (Lomb Scientific, NSW, Australia) or an Innova 42R incubator shaker (John Morris, NSW, Australia) at 26.5 °C. Semi-preparative and preparative HPLCs were performed using Agilent 1100 series HPLC instruments with corresponding detectors, fraction collectors, and software. Analytical UPLC chromatograms were obtained on an Agilent 1290 infinity UPLC instrument equipped with a diode array multiple wavelength detector (Zorbax C_8 RRHD 1.8 μm, 50 × 2.1 mm column, gradient elution at 0.417 mL/min over 2.50 min from 90% H_2O/MeCN to 100% MeCN with isocratic 0.01% TFA/MeCN modifier). UPLC-QTOF analyses were performed on an Agilent 6545 Q-TOF instrument incorporating an Agilent 1290 Infinity II UHPLC (Zorbax C_8 RRHD 1.8 μm, 50 × 2.1 mm column, gradient elution

at 0.417 mL/min over 2.5 min from 90% H_2O/MeCN to 100% MeCN with isocratic 0.1% formic acid/MeCN modifier). Chiroptical measurements ($[\alpha]_D$) were obtained on a JASCO P-1010 polarimeter in a 100 × 2 mm cell at specified temperatures. Nuclear magnetic resonance (NMR) spectra were acquired on a Bruker Avance 600 MHz spectrometer with either a 5 mm PASEL 1H/D-13C Z-Gradient probe or 5 mm CPTCI 1H/19F-13C/15N/DZ-Gradient cryoprobe, controlled by TopSpin 2.1 software, at 25 °C in either methanol-d_4, $CDCl_3$, or DMSO-d_6, with referencing to residual ^1H or ^{13}C solvent resonances (methanol-d_4: δ_H 3.31 and δ_C 49.15; $CDCl_3$: δ_H 7.24 and δ_C 77.23; DMSO-d_6: δ_H 2.50 and δ_C 39.50). High-resolution ESIMS spectra were obtained on a Bruker micrOTOF mass spectrometer by direct injection in MeOH at 3 µL/min using sodium formate clusters as an internal calibrant. Structural assignments were made with additional information from gCOSY, gHSQC, and gHMBC experiments.

3.2. Fungal Isolation and DNA Taxonomic Analysis

A marine sediment collected in 2008 from a location off Perth, Western Australia, was used to inoculate an M1 agar plate (inclusive of 3.3% artificial sea salt) which was incubated at 27 °C for 10–14 days, after which colony selection yielded an array of isolates including fungus CMB-M0339. Genomic DNA was extracted from the mycelia of CMB-M0339 using the DNeasy Plant Mini Kit (Qiagen) as per the manufacturers protocol, and the 18s rRNA genes were amplified by PCR using the universal primers ITS-1 (5′-TCCGTAGGTGAACCTGCGG-3′) and ITS-4 (5′-TCCTCCGCTTATTGATATGC-3′) purchased from Sigma-Aldrich. The PCR mixture (50 µL) containing 1 µL of genomic DNA (20–40 ng), 200 µM of each deoxynucleoside triphosphate (dNTP), 1.5 mM $MgCl_2$, 0.3 µM of each primer, 1 U of *Taq* DNA polymerase (Fisher Biotec), and 5 µL of PCR buffer was amplified using the following conditions: initial denaturation at 95 °C for 3 min, 30 cycles in series of 94 °C for 30 s (denaturation), 55 °C for 60 s (annealing), and 72 °C for 60 s (extension), followed by one cycle at 72 °C for 6 min. PCR products were purified with PCR purification kit (Qiagen, Victoria, Australia) and examined by agarose gel electrophoresis, with DNA sequencing performed by the Australian Genome Research Facility (AGRF) at The University of Queensland. A BLAST analysis (NCBI database) on the resulting CMB-M0339 ITS gene sequence (Figures S1–S3, GenBank accession no. OP132523) revealed 92.5% identity with the fungal strain *Aspergillus noonimiae.*

3.3. Global Natural Product Social (GNPS) Molecular Networking

Aliquots (1 µL) of CMB-M0339 cultivation extract (100 µg/mL in MeOH) were analysed on an Agilent 6545 Q-TOF LC/MS equipped with an Agilent 1290 Infinity II UPLC system (Zorbax C_8, 0.21 µm, 1.8 × 50 mm column, gradient elution at 0.417 mL/min over 2.5 min from 90% H_2O/MeCN to MeCN with an isocratic 0.1% formic acid/MeCN modifier). UPLC-QTOF-(+) MS/MS data acquired for all samples at a collision energy of 35 eV were converted from Agilent MassHunter data files (d) to mzXML file format using MSConvert software, and transferred to the GNPS server (gnps.ucsd.edu). Molecular networking was performed using the GNPS data analysis workflow [45] employing the spectral clustering algorithm with a cosine score of 0.5 and a minimum of 6 matched peaks. The resulting spectral network was imported into Cytoscape version 3.7.1 [47] and visualized using a ball-and-stick layout where nodes represent parent mass and cosine score was reflected by edge thickness. Moreover, group abundances were set as pie charts, which reflected the intensity of MS signals. MS/MS fragmentation analysis was performed on the same machine for ion detected in the full scan range at an intensity above 1000 counts at ten scans/s, with an isolation width of 4~m/z using fixed collision energy and a maximum of 3 selected precursors per cycle. General instrument parameters including gas temperature at 325 °C, drying gas 10 L/min, nebulizer 20 psig, sheath gas temperature 400 °C, fragmentation Volta 180eV, and skimmer 45 eV.

3.4. MATRIX Cultivation Profiling

The fungus CMB-M0339 was cultured in a 24-well plate microbioreactor under ×11 different media for 10–14 days in solid phase (27 °C), as well as in static (30 °C) and shaken broths (30 °C, 190 rpm) [46], with regular monitoring of growth (Figure S7). At this point, wells were individually extracted with EtOAc (2 mL), and the organic phase was centrifuged (13,000 rpm, 3 min) and dried under N_2 at 40 °C to yield ×33 extracts. Individual extracts were redissolved in MeOH (30 µL) containing calibrant (2,4-dinitrophenoldecane ether, 50 µg/mL), and aliquots (1 µL) were subjected to: (i) UPLC-DAD analysis (Zorbax C_8 1.8 µm, 2.1 × 50 mm column, gradient elution at 0.417 mL/min over 2.52 min from 90% H_2O/MeCN to 100% MeCN followed by 0.83 min isocratic elution with MeCN, inclusive of an isocratic 0.01% TFA/MeCN modifier) (Figure S8); and (ii) GNPS analysis (Figure 3). This process identified solid phase D400 as the optimal culture conditions for producing targeted CMB-M0339 natural products.

3.5. Scale Up Cultivation and Fractionation

The fungus CMB-M0339 was cultivated on D400 agar (×300 plates) at 27 °C for 10–14 days after which the agar and fungal mycelia were harvested and extracted with EtOAc (2 × 5 L), and the combined organic phase was filtered and concentrated in vacuo at 40 °C to yield an extract (2.9 g). This extract was sequentially triturated with *n*-hexane (20 mL), CH_2Cl_2 (20 mL), MeOH (20 mL), and concentrated in vacuo to afford *n*-hexane (961.8 mg), CH_2Cl_2 (1783.8 mg), and MeOH (80.3 mg) soluble fractions. A portion of the CH_2Cl_2 soluble fraction (1363 mg) was subjected to preparative reversed-phase HPLC (Phenomenex Luna-C_8 10 µm, 21.2 × 250 mm column, with gradient elution at 20 mL/min over 20 min from 90% H_2O/MeCN to 100% MeCN with constant 0.1% TFA/MeCN modifier) to yield noonindole A (**5**) (R_f 15.7 min, 83.5 mg, 4.3%). The remaining mixed fractions were subjected to semi-preparative reversed-phase HPLC to yield noonindole B (**6**) (R_f 18.3 min, 2.0 mg, 0.1%) (semi-preparative HPLC (Zorbax C_8 5mm column, 9.4 × 250 mm, 3 mL/min isocratic elution of 37% MeCN/H_2O over 20 min with constant 0.1% TFA modifier)); noonindole F (**10**) (R_f 19.9 min, 0.7 mg, 0.03%) (semi-preparative HPLC (Agilent C_8-Ep 5mm column, 9.4 × 250 mm, 3 mL/min isocratic elution of 50% MeCN/H_2O over 25 min with constant 0.1% TFA modifier)); noonindole D (**8**) (R_f 28.6 min, 0.4 mg, 0.02%) (semi-preparative HPLC (Zorbax C_{18} 5mm column, 9.4 × 250 mm, 3 mL/min isocratic elution of 40% MeCN/H_2O over 30 min with constant 0.1% TFA modifier)); noonindole E (**9**) (R_f 20.9 min, 0.8 mg, 0.04%) (semi-preparative HPLC (Zorbax C_{18} 5mm column, 9.4 × 250 mm, 3 mL/min isocratic elution of 40% MeCN/H_2O over 30 min with constant 0.1% TFA modifier)); 12-demethylpaspaline-12-carboxylic acid (**13**) (R_f 9.8 min, 1.6 mg, 0.08%) (semi-preparative HPLC (Zorbax C_{18} 5mm column, 9.4 × 250 mm, 3 mL/min isocratic elution of 85% MeCN/H_2O over 15 min with constant 0.1% TFA modifier)); paspaline B (**12**) (R_f 26.1 min, 0.3 mg, 0.01%) (semi-preparative HPLC (Agilent C_8-Ep 5mm column, 9.4 × 250 mm, 3 mL/min isocratic elution of 60% MeCN/H_2O over 25 min with constant 0.1% TFA modifier)); paspaline (**11**) (R_f 17.8 min, 1.2 mg, 0.06%) (Semi-preparative HPLC (Agilent CN 5mm column, 9.4 × 250 mm, 3 mL/min isocratic elution of 60% MeCN/H_2O over 20 min with constant 0.1% TFA modifier)); emindole SB (**14**) (R_f 19.7 min, 1.2 mg, 0.06%) (semi-preparative HPLC (Agilent CN 5mm column, 9.4 × 250 mm, 3 mL/min isocratic elution of 60% MeCN/H_2O over 20 min with constant 0.1% TFA modifier)); and solid-phase extraction (Sep-Pak (Agilent Bond Elut C_{18} cartridge, 5 g) gradient elution from 90% H_2O/MeCN to 100% MeCN) and semi-preparative reversed-phase HPLC (Zorbax C_8 5mm column, 9.4 × 250 mm, 3 mL/min isocratic elution of 40% MeCN/H_2O over 20 min with constant 0.1% TFA modifier) to yield noonindole C (**7**) (R_f 21.9 min, 2.0 mg, 0.1%) (Figure S9). (Note: All % yields are weight to weight estimates based on unfractionated EtOAc extract).

3.6. Characterization of Metabolites **5**–**14**

noonindole A (**5**); pale yellow solid; $[\alpha]D^{21}$–18 (*c* 0.02, MeOH); NMR (600 MHz, methanol-d_4), see Table S2 and Figures S10–S15; HRMS (ESI) *m*/*z*: $[M+H]^+$ calcd for $C_{34}H_{47}N_2O_6$ 579.3429; found 579.3456.
noonindole B (**6**); white solid; $[\alpha]D^{21}$–13 (*c* 0.08, MeOH); NMR (600 MHz, methanol-d_4), see Table S3 and Figures S17–S22; HRMS (ESI) *m*/*z*: $[M+H]^+$ calcd for $C_{33}H_{45}N_2O_6$, 565.3272; found 565.3292.
noonindole C (**7**); white solid; $[\alpha]D^{21}$–9 (*c* 0.06, MeOH); NMR (600 MHz, methanol-d_4), see Table S4 and Figures S24–S29; HRMS (ESI) *m*/*z* $[M+H]^+$ calcd for $C_{35}H_{49}N_2O_6$, 593.3585; found 593.3611.
noonindole D (**8**); white solid; $[\alpha]D^{23}$–30 (*c* 0.03, MeOH); NMR (600 MHz, methanol-d_4), see Table S5 and Figures S31–S35; HRMS (ESI) *m*/*z* $[M+H]^+$ calcd for $C_{33}H_{45}N_2O_6$, 565.3272; found 565.3287.
noonindole E (**9**); white solid; $[\alpha]D^{23}$–13 (*c* 0.06, MeOH); NMR (600 MHz, methanol-d_4), see Table S6 and Figures S37–S41; HRMS (ESI) *m*/*z* $[M+H]^+$ calcd for $C_{34}H_{45}N_2O_6$, 577.3272; found 577.3284.
noonindole F (**10**); white solid; $[\alpha]D^{21}$–18 (*c* 0.02, MeOH); NMR (600 MHz, methanol-d_4), see Table S7 and Figures S43–S48; HRMS (ESI) *m*/*z* $[M+Na]^+$ calcd for $C_{27}H_{33}NO_5Na$, 474.2251; found 474.2262.
paspaline (**11**); white solid; $[\alpha]D^{22}$–21 (*c* 0.09, $CHCl_3$); [24] NMR (600 MHz, DMSO-d_6), see Table S8 and Figures S50–S53; [24] HRMS (ESI) *m*/*z* $[M+H]^+$ calcd for $C_{28}H_{40}NO_2$, 422.3054; found 422.3071.
paspaline B (**12**) white solid; $[\alpha]D^{22}$–24 (*c* 0.02, $CHCl_3$); [18] NMR (600 MHz, $CDCl_3$), see Table S9 and Figures S55–S58; [18] HRMS (ESI) *m*/*z* $[M+Na]^+$ calcd for $C_{28}H_{37}NO_3Na$, 458.2666; found 458.2680.
12-demethylpaspaline-12-carboxylic acid (**13**); white solid; $[\alpha]D^{22}$ + 37 (*c* 0.01, $CHCl_3$); [24] NMR (600 MHz, DMSO-d_6), see Table S10 and Figures S60–S63; [24] HRMS (ESI) *m*/*z* $[M+H]^+$ calcd for $C_{28}H_{38}NO_4$,452.2795; found 452.2807.
emindole SB (**14**); white solid; $[\alpha]D^{21}$–18 (c 0.05, $CHCl_3$); [24] NMR (600 MHz, DMSO-d_6), see Table S11 and Figures S65–S68; [24] HRMS (ESI) *m*/*z* $[M+H]^+$ calcd for $C_{28}H_{40}NO$, 406.3104; found 406.3126.

3.7. Phylogenetic Comparison of CMB-M0339 with Fungi Reported to Produce Biosynthetically Related Indole Terpenes

Phylogenetic tree obtained by PhyML Maximum Likelihood analysis was constructed using the top similar 18S rRNA sequences displayed after BLAST on Refseq RNA NCBI database using CMB-M0339 18S rRNA as queries (Figure S4). The JC69 model was used to infer phylogeny sequences [48]. Sequence alignments were produced with the MUSCLE program [49]. Phylogenetic tree was constructed using the UGENE program using the aforementioned models and visualized using Ugene's tree view [50].

3.8. UPLC-QTOF-SIE Detection of **5**–**14** *in CMB-M0339 Extract*

The EtOAc extract of a CMB-M0339 D400 agar culture was dissolved in MeOH and subjected to UPLC-QTOF analysis with single ion extraction (SIE) analysis (Figure S70).

3.9. X-ray Crystallography

Crystals of **5** were obtained by slow evaporation from 50% DCM/Hexane in the cold room (−4 °C). Crystallographic data (Cu Kα, $2\theta_{max}$ = 125°) for **5** were collected on an Oxford Diffraction Gemini S Ultra CCD diffractometer with the crystal cooled to 190 K with an Oxford Cryosystems Desktop Cooler. Data reduction and empirical absorption corrections were carried out with the CrysAlisPro program. The structure was solved with SHELXT and refined with SHELXL [51]. The thermal ellipsoid diagrams were generated with Mercury [52]. All calculations were carried out within the WinGX graphical user interface [53]. The disordered water molecules in the structure were modelled with

SQUEEZE implemented in PLATON [54]. The crystal data for **5** in CIF format were deposited in the CCDC database (2206901) (Table S13).

3.10. Antifungal Assay

The fungus *Candida albicans* ATCC 10231 was streaked onto a LB (Luria–Bertani) agar plate and was incubated at 37 °C for 48 h, after which a colony was transferred to fresh LB broth (15 mL) and the cell density was adjusted to 10^4–10^5 CFU/mL. Test compounds were dissolved in DMSO and diluted with H_2O to prepare 600 μM stock solutions (20% DMSO), which were serially diluted with 20% DMSO to provide concentrations from 600 μM to 0.2 μM in 20% DMSO. An aliquot (10 μL) of each dilution was transferred to a 96-well microtiter plate and freshly prepared fungal broth (190 μL) was added to prepare final concentrations of 30–0.01 μM in 1% DMSO. The plates were incubated at 27 °C for 48 h and the optical density of each well was measured spectrophotometrically at 600 nm using POLARstar Omega plate (BMG LABTECH, Offenburg, Germany). Amphotericin B was used as the positive control (40 μg/mL in 10% DMSO). The IC_{50} value was calculated as the concentration of the compound or antibiotic required for 50% inhibition of the bacterial cells using Prism 7.0 (GraphPad Software Inc., La Jolla, CA, USA). See Figure S80.

3.11. Antibacterial Assay

The bacterium to be tested was streaked onto an LB agar plate and was incubated at 37 °C for 24 h, after which a colony was transferred to fresh LB broth (15 mL) and the cell density was adjusted to 10^4–10^5 CFU/mL. Test compounds were dissolved in DMSO and diluted with H_2O to give 600 μM stock solutions (20% DMSO), which were serially diluted with 20% DMSO to prepare concentrations from 600 μM to 0.2 μM in 20% DMSO. An aliquot (10 μL) of each dilution was transferred to a 96-well microtiter plate and freshly prepared microbial broth (190 μL) was added to provide final concentrations of 30–0.01 μM in 1% DMSO. The plates were incubated at 37 °C for 24 h and the optical density of each well was measured spectrophotometrically at 600 nm using POLARstar Omega plate (BMG LABTECH, Offenburg, Germany). Each test compound was screened against the Gram-negative bacterium *Escherichia coli* ATCC 11775 and the Gram-positive bacteria *Staphylococcus aureus* ATCC 25923 and *Bacillus subtilis* ATCC 6633. Rifampicin was used as the positive control (40 μg/mL in 10% DMSO) for Gram-positive bacteria and a mixture of rifampicin and ampicillin was used as the positive control for Gram-negative bacteria. The IC_{50} value was calculated as the concentration of the compound or antibiotic required for 50% inhibition of the bacterial cells using Prism 7.0 (GraphPad Software Inc., La Jolla, CA, USA). See Figure S80.

3.12. Cytotoxicity Assays

Human colorectal (SW620) and lung carcinoma (NCI-H460) cells were seeded evenly in a 96-well micro-plate (2000 cells/well in 180 μL of RPMI 1640 medium (Roswell Park Memorial Institute medium) supplemented with 10% FBS (Fetal Bovine Serum)) and the plate was incubated for 18 h (37 °C; 5% CO_2) to allow cells to attach. Test compounds were dissolved in 5% DMSO (*v*/*v*) and dilutions were generated from 300 μM to 300 nM. Aliquots (20 μL) of each dilution (or 5% aqueous DMSO for negative control and 5% aqueous SDS for positive control) were added to the plate in duplicate. After 68 h of incubation (37 °C; 5% CO_2), a solution of 3-(4,5-dimethylthiazol-2-yl)-2,5-diphenyltetrazolium bromide (MTT; Sigma, USA) in PBS (Phosphate Buffered Saline) was added to each well to a final concentration of 0.4 mg/mL and plates were incubated for a further 4 h (37 °C; 5% CO_2) after which the medium was carefully aspirated and precipitated formazan crystals were dissolved in DMSO (100 μL/well). The absorbance of each well at 580 nm was measured with a PowerWave XS Microplate Reader from Bio-Tek Instruments Inc. (Vinooski, VT) and IC_{50} values were calculated as the concentration of the compound required for 50% inhibition of the cancer cells using Prism 5.0 from GraphPad Software Inc. (La Jolla, CA, USA). See Figure S81.

Supplementary Materials: The following supporting information can be downloaded at: https://www.mdpi.com/article/10.3390/md20110698/s1, Figure S1: ITS gene sequence of CMB-M0339, Figure S2: NCBI-BLAST search of 18S rRNA sequence of CMB-M0339, Figure S3: Blast search for CMB-M0339, Figure S4: Phylogenetic tree, Figure S5: CMB-M0339 cultivated on SD agar, Figure S6: UPLC-DAD chromatograms of crude extract of CMB-M0339, Figure S7: CMB-M0339 cultivated under MATRIX conditions, Figure S8: UPLC-DAD chromatograms of MATRIX extracts, Figure S9: Isolation scheme for **5–14**, Figures S10–S69: Annotated 1D and 2D NMR spectra and HRMS spectra for **5–14**, Figure S70–S71: Single ion extraction of fresh crude extract from CMB-M0339 showing the presence of **5–14** and **1**, Figures S72–S79: MS/MS fragmentation pattern of **5–9** and **i-v**, Figures S80–S81: Antimicrobial and cytotoxic activities of **5–14**. Table S1: Composition of media used for cultivation profiling, Tables S2–S11: 1D and 2D NMR data for **5–14**, Table S12: Predicted molecular formulae generated for **5–9** and **i-viii** observed in GNPS cluster, Table S13: Bond lengths and angles for X-ray crystal structure of **5**. Refs. [18,24] are cited in the Supplementary Materials.

Author Contributions: R.J.C. conceptualized the research; S.K. carried out the isolation, spectroscopic characterization, crystallization, and antibacterial, antifungal and cytotoxicity assays; P.V.B. performed the X-ray analyses; S.K. and Z.G.K. performed the taxonomic identification of the fungal strain; assigned molecular structures, and constructed the supplementary material; R.J.C. reviewed all data and drafted the manuscript, with support from S.K. and Z.G.K. All authors have read and agreed to the published version of the manuscript.

Funding: This research was funded in part by the Institute for Molecular Bioscience, The University of Queensland.

Institutional Review Board Statement: Not applicable.

Data Availability Statement: Raw NMR data is available at https://npmrd-project.org/ (access on 26 September 2022).

Acknowledgments: We thank R. Ritesh for isolation of CMB-M0339. S. K. thanks The University of Queensland for an International Postgraduate Scholarship.

Conflicts of Interest: The authors declare no conflict of interest.

References

1. Springer, J.P.; Clardy, J.; Wells, J.M.; Cole, R.J.; Kirksey, J.W. The structure of paxilline, a tremorgenic metabolite of *Penicillium paxilli* bainier. *Tetrahedron Lett.* **1975**, *16*, 2531–2534. [CrossRef]
2. Mantle, P.G.; Weedon, C.M. Biosynthesis and transformation of tremorgenic indolediterpenoids by *Penicillium paxilli* and *Acremonium lolii*. *Phytochemistry* **1994**, *36*, 1209–1217. [CrossRef]
3. Huang, X.-H.; Tomoda, H.; Nishida, H.; Masuma, R.; Omura, S. Terpendoles, novel ACAT inhibitors produced by *Albophoma yamanashiensis*. I. Production, isolation and biological properties. *J. Antibiot.* **1994**, *48*, 1–4. [CrossRef] [PubMed]
4. Huang, X.H.; Nishida, H.; Tomoda, H.; Tabata, N.; Shiomi, K.; Yang, D.J.; Takayanagi, H.; Omura, S. Terpendoles, novel ACAT inhibitors produced by *Albophoma yamanashiensis*. II. Structure elucidation of terpendoles A, B, C and D. *J. Antibiot.* **1995**, *48*, 5–11. [CrossRef] [PubMed]
5. Tomoda, H.; Tabata, N.; Yang, D.-J.; Takayanagi, H.; Omura, S. Terpendoles, Novel ACAT inhibitors produced by *Albophoma yamanashiensis*. III. Production, isolation and structure eucidation of new components. *J. Antibiot.* **1995**, *48*, 793–804. [CrossRef]
6. Gallagher, R.T.; Clardy, J.; Wilson, B.J. Aflatrem, a tremorgenic toxin from *Aspergillus flavus*. *Tetrahedron Lett.* **1980**, *21*, 239–242. [CrossRef]
7. Gallagher, R.T.; Wilson, B.J. Aflatrem, the tremorgenic mycotoxin from *Aspergillus flavus*. *Mycopathologia* **1979**, *66*, 183–185. [CrossRef]
8. Laakso, J.A.; Gloer, J.B.; Wicklow, D.T.; Dowd, P.F. Sulpinines A–C and secopenitrem B: New antiinsectan metabolites from the sclerotia of *Aspergillus sulphureus*. *J. Org. Chem.* **1992**, *57*, 2066–2071. [CrossRef]
9. Staub, G.M.; Gloer, K.B.; Gloer, J.B.; Wicklow, D.T.; Dowd, P.F. New paspalinine derivatives with antiinsectan activity from the sclerotia of *Aspergillus nomius*. *Tetrahedron Lett.* **1993**, *34*, 2569–2572. [CrossRef]
10. Junker, B.; Walker, A.; Connors, N.; Seeley, A.; Masurekar, P.; Hesse, M. Production of indole diterpenes by *Aspergillus alliaceus*. *Biotechnol. Bioeng.* **2006**, *95*, 919–937. [CrossRef]
11. Bills, G.F.; Polishook, J.D.; Goetz, M.A.; Sullivan, R.F.; White, J.F. *Chaunopycnis pustulata* sp. nov., a new clavicipitalean anamorph producing metabolites that modulate potassium ion channels. *Mycol. Prog.* **2002**, *1*, 3–17. [CrossRef]
12. Springer, J.P.; Clardy, J. Paspaline and paspalicine, two indole-mevalonate metabolites from *Claviceps paspalli*. *Tetrahedron Lett.* **1980**, *21*, 231–234. [CrossRef]

13. Nozawa, K.; Nakajima, S.; Kawai, K.; Udagawa, S. Isolation and structures of indoloditerpenes, possible biosynthetic intermediates to the tremorgenic mycotoxin, paxilline, from *Emericella striata*. *J. Chem. Soc. Perkin Trans. 1* **1988**, 2607–2610. [CrossRef]
14. Nozawa, K.; Horie, Y.; Udagawa, S.; Kawai, K.; Yamazaki, M. Isolation of new tremorgenic indolediterpene, 1′-*O*-acetylpaxilline, from *Emericella striata* and distribution of paxilline in *Emericella* sp. *Chem. Pharm. Bull.* **1989**, *37*, 1387–1389. [CrossRef] [PubMed]
15. Belofsky, G.N.; Gloer, J.B.; Wicklow, D.T.; Dowd, P.F. Antiinsectan alkaloids: Shearinines A–C and a new paxilline derivative from the ascostromata of *Eupenicillium shearii*. *Tetrahedron* **1995**, *51*, 3959–3968. [CrossRef]
16. Gatenby, W.A.; Munday-Finch, S.C.; Wilkins, A.L.; Miles, C.O. Terpendole M, a novel indole-diterpenoid isolated from *Lolium perenne* infected with the endophytic fungus *Neotyphodium lolii*. *J. Agric. Food. Chem.* **1999**, *47*, 1092–1097. [CrossRef]
17. De Jesus, A.E.; Steyn, P.S.; Van Heerden, F.R.; Vleggaar, R.; Wessels, P.L.; Hull, W.E. Structure and biosynthesis of the penitrems A–F, six novel tremorgenic mycotoxins from *Penicillium crustosum*. *J. Chem. Soc. Chem. Commun.* **1981**, *6*, 289–291. [CrossRef]
18. Munday-Finch, S.C.; Wilkins, A.L.; Miles, C.O. Isolation of paspaline B, an indole-diterpenoid from *Penicillium paxilli*. *Phytochemistry* **1996**, *41*, 327–332. [CrossRef]
19. Itabashi, T.; Hosoe, T.; Wakana, D.; Fukushima, K.; Takizawa, K.; Yaguchi, T.; Okada, K.; Takaki, G.M.C.; Kawai, K. A new indoloditerpene derivative, penijanthine A, isolated from *Penicillium janthinellum*. *J. Nat. Med.* **2009**, *63*, 96–99. [CrossRef]
20. Ariantari, N.P.; Ancheeva, E.; Wang, C.; Mandi, A.; Kendel, T.O.; Kurtan, T.; Chaidir, C.; Muller, W.E.G.; Kassack, M.U.; Janiak, C.; et al. Indole diterpenoids from an endophytic *Penicillium* sp. *J. Nat. Prod.* **2019**, *82*, 1412–1423. [CrossRef]
21. Yu, J.; Wang, J.-P.; Liu, S.-F.; Yin, C.-Y.; Tang, D.-Y.; Li, Y.-H.; Zhang, L.-X. 7-Methoxy-13-dehydroxypaxilline: New indole diterpenoid from an endophytic fungus *Penicillium* sp. Nb 19. *Nat. Prod. Res.* **2022**, 1–9. [CrossRef]
22. Bills, G.F.; Giacobbe, R.A.; Lee, S.H.; Pelaez, F.; Tkacz, J.S. Tremorgenic mycotoxins, paspalitrem A and C, from a tropical *Phomopsis*. *Mycol. Res.* **1992**, *96*, 977–983. [CrossRef]
23. Sallam, A.A.; Houssen, W.E.; Gissendanner, C.R.; Orabi, K.Y.; Foudah, A.I.; Sayed, K.A.E. Bioguided discovery and pharmacophore modeling of the mycotoxic indole diterpene alkaloids penitrems as breast cancer proliferation, migration, and invasion inhibitors. *Med. Chem. Comm.* **2013**, *4*, 1360–1369. [CrossRef] [PubMed]
24. Fan, Y.; Wang, Y.; Liu, P.; Fu, P.; Zhu, T.; Wang, W.; Zhu, W. Indole-diterpenoids with anti-H1N1 activity from the aceduric fungus *Penicillium camemberti* OUCMDZ-1492. *J. Nat. Prod.* **2013**, *76*, 1328–1336. [CrossRef] [PubMed]
25. Zhou, L.-M.; Kong, F.-D.; Li, J.-H.; Zheng, H.-Z.; Dai, H.-F.; Luo, D.-Q.; Zhao, Y.-X. Indole-diterpenoids with protein tyrosine phosphatase inhibitory activities from the marine-derived fungus *Penicillium* sp. KFD28. *J. Nat. Prod.* **2019**, *82*, 2638–2644. [CrossRef] [PubMed]
26. Chen, M.Y.; Xie, Q.Y.; Kong, F.D.; Ma, Q.Y.; Zhou, L.M.; Yuan, J.Z.; Dai, H.F.; Wu, Y.G.; Zhao, Y.X. Two new indole-diterpenoids from the marine derived fungus *Penicillium* sp. KFD28. *J. Asian Nat. Prod. Res.* **2020**, *23*, 1030–1036. [CrossRef] [PubMed]
27. Dai, L.-T.; Yang, L.; Kong, F.-D.; Ma, Q.-Y.; Xie, Q.-Y.; Dai, H.-F.; Yu, Z.-F.; Zhao, Y.-X. Cytotoxic indole-diterpenoids from the marine-derived fungus *Penicillium* sp. KFD28. *Mar. Drugs* **2021**, *19*, 613. [CrossRef] [PubMed]
28. Knaus, H.; McManus, O.W.; Lee, S.H.; Schmalhofer, W.A.; Garcia-Calvo, M.; Helms, L.M.H.; Sanchez, M.; Giangiacomo, K.; Reuben, J.P.; Smith, A.B.; et al. Tremorgenic indole alkaloids potently inhibit smooth muscle high-conductance calcium-activated potassium channels. *Biochemistry* **1994**, *33*, 5819–5828. [CrossRef]
29. Sallam, A.A.; Ayoub, N.M.; Foudah, A.I.; Gissendanner, C.R.; Meyer, S.A.; Sayed, K.A.E. Indole diterpene alkaloids as novel inhibitors of the Wnt/β-catenin pathway in breast cancer cells. *Eur. J. Med. Chem.* **2013**, *70*, 594–606. [CrossRef]
30. Garcia, M.L.; Giacobbe, R.A.; Hensens, O.D.; Lee, S.H.; McManus, O.B.; Zink, D.L. Indole diterepene alkaloid compounds. Patent EP 0 804 186 B1, 20 January 1995.
31. Goetz, M.A.; Kaczorowski, G.J.; Monaghan, R.L.; Strohl, W.R.; Tkacz, J.S. Novel Maxi-K Channel Blockers, Methods of Use and Process for Making the Same. Patent WO 03/105868 A1, 24 December 2003.
32. Zhou, Y.; Xia, X.-M.; Lingle, C.J. The functionally relevant site for paxilline inhibition of BK channels. *Proc. Natl. Acad. Sci. USA* **2020**, *117*, 1021–1026. [CrossRef]
33. Mewshaw, R.E.; Taylor, M.D.; Smith, A.B. Indole diterpene synthetic studies. 2. First-generation total synthesis of (−)-paspaline. *J. Org. Chem.* **1989**, *54*, 3449–3462. [CrossRef]
34. Sharpe, R.J.; Johnson, J.S. Asymmetric total synthesis of the indole diterpene alkaloid paspaline. *J. Org. Chem.* **2015**, *80*, 9740–9766. [CrossRef] [PubMed]
35. Schatz, D.J.; Kuenstner, E.J.; George, D.T.; Pronin, S.V. Synthesis of rearranged indole diterpenes of the paxilline type. *Nat. Prod. Rep.* **2021**, *39*, 946–968. [CrossRef] [PubMed]
36. Young, C.; McMillan, L.; Telfer, E.; Scott, B. Molecular cloning and genetic analysis of an indole-diterpene gene cluster from *Penicillium paxilli*. *Mol. Microbiol.* **2001**, *39*, 754–764. [CrossRef] [PubMed]
37. Young, C.A.; Felitti, S.; Shields, K.; Spangenberg, G.; Johnson, R.D.; Bryan, G.T.; Saikia, S.; Scott, B. A complex gene cluster for indole-diterpene biosynthesis in the grass endophyte *Neotyphodium lolii*. *Fungal. Genet. Biol.* **2006**, *43*, 679–693. [CrossRef] [PubMed]
38. Saikia, S.; Parker, E.J.; Koulman, A.; Scott, B. Defining paxilline biosynthesis in *Penicillium paxilli* functional characterization of two cytochrome p450 monooxygenases. *J. Biol. Chem.* **2007**, *282*, 16829–16837. [CrossRef] [PubMed]
39. Nicholson, M.J.; Koulman, A.; Monahan, B.J.; Pritchard, B.L.; Payne, G.A.; Scott, B. Identification of two aflatrem biosynthesis gene loci in *Aspergillus flavus* and metabolic engineering of *Penicillium paxilli* to elucidate their function. *Appl. Environ. Microbiol.* **2009**, *75*, 7469–7481. [CrossRef] [PubMed]

40. Scott, B.; Young, C.A.; Saikia, S.; McMillan, L.K.; Monahan, B.J.; Koulman, A.; Astin, J.; Eaton, C.J.; Bryant, A.; Wrenn, R.E.; et al. Deletion and gene expression analyses define the paxilline biosynthetic gene cluster in *Penicillium paxilli*. *Toxins* **2013**, *5*, 1422–1446. [CrossRef]
41. Tagami, K.; Minami, A.; Fujii, R.; Liu, C.; Tanaka, M.; Gomi, K.; Dairi, T.; Oikawa, H. Rapid reconstitution of biosynthetic machinery for fungal metabolites in *Aspergillus oryzae*: Total biosynthesis of aflatrem. *Chembiochem* **2014**, *15*, 2076–2080. [CrossRef]
42. Liu, C.; Tagami, K.; Minami, A.; Matsumoto, T.; Frisvad, J.C.; Suzuki, H.; Ishikawa, J.; Gomi, K.; Oikawa, H. Reconstitution of biosynthetic machinery for the synthesis of the highly elaborated indole diterpene penitrem. *Angew. Chem. Int. Ed.* **2015**, *54*, 5748–5752. [CrossRef]
43. McLellan, R.M.; Cameron, R.C.; Nicholson, M.J.; Parker, E.J. Aminoacylation of indole diterpenes by cluster-specific monomodular NRPS-like enzymes. *Org. Lett.* **2022**, *24*, 2332–2337. [CrossRef] [PubMed]
44. Laakso, J.A.; Tepaske, M.R.; Dowd, P.F.; Gloer, J.B.; Wicklow, D.T.; Staub, G.M. Indole antiinsectan metabolites. U.S. Patent 5227396, 13 July 1993.
45. Wang, M.; Carver, J.J.; Phelan, V.V.; Sanchez, L.M.; Garg, N.; Peng, Y.; Nguyen, D.D.; Watrous, J.; Kapono, C.A.; Luzzatto-Knaan, T.; et al. Sharing and community curation of mass spectrometry data with Global Natural Products Social Molecular Networking. *Nat. Biotechnol.* **2016**, *34*, 828–837. [CrossRef] [PubMed]
46. Salim, A.A.; Khalil, Z.G.; Elbanna, A.H.; Wu, T.; Capon, R.J. Methods in microbial biodiscovery. *Mar. Drugs* **2021**, *19*, 503. [CrossRef] [PubMed]
47. Shannon, P.; Markiel, A.; Ozier, O.; Baliga, N.S.; Wang, J.T.; Ramage, D.; Amin, N.; Schwikowski, B.; Ideker, T. Cytoscape: A software environment for integrated models of biomolecular interaction networks. *Genome Res.* **2003**, *13*, 2498–2504. [CrossRef] [PubMed]
48. Yang, Z.; Goldman, N.; Friday, A. Comparison of models for nucleotide substitution used in maximum-likelihood phylogenetic estimation. *Mol. Biol. Evol.* **1994**, *11*, 316–324.
49. Edgar, R.C. MUSCLE: A multiple sequence alignment method with reduced time and space complexity. *BMC Bioinformatics* **2004**, *5*, 1–19. [CrossRef]
50. Okonechnikov, K.; Golosova, O.; Fursov, M. Unipro UGENE: A unified bioinformatics toolkit. *Bioinformatics* **2012**, *28*, 1166–1167. [CrossRef]
51. Sheldrick, G.M. A short history of SHELX. *Acta. Crystallogr.* **2008**, *64*, 112–122. [CrossRef]
52. Macrae, C.F.; Edgington, P.R.; McCabe, P.; Pidcock, E.; Shields, G.P.; Taylor, R.; Towler, M.; Streek, J.V.D. Mercury: Visualization and analysis of crystal structures. *J. App. Crystallogr.* **2006**, *39*, 453–457. [CrossRef]
53. Farrugia, L.J. WinGX suite for small-molecule single-crystal crystallography. *J. App. Crystallogr.* **1999**, *32*, 837–838. [CrossRef]
54. Spek, A.L. Single-crystal structure validation with the program PLATON. *J. App. Crystallogr.* **2003**, *36*, 7–13. [CrossRef]

marine drugs

MDPI

Article

Thiolactones and $\Delta^{8,9}$-Pregnene Steroids from the Marine-Derived Fungus *Meira* sp. 1210CH-42 and Their α-Glucosidase Inhibitory Activity

Hee Jae Shin [1,2,*], Min Ah Lee [1,3], Hwa-Sun Lee [1,3] and Chang-Su Heo [1,2]

[1] Marine Natural Products Chemistry Laboratory, Korea Institute of Ocean Science and Technology, 385 Haeyang-ro, Yeongdo-gu, Busan 49111, Republic of Korea; minah@kiost.ac.kr (M.A.L.); hwasunlee@kiost.ac.kr (H.-S.L.); science30@kiost.ac.kr (C.-S.H.)
[2] Department of Marine Biotechnology, University of Science and Technology (UST), 217 Gajungro, Yuseong-gu, Daejeon 34113, Republic of Korea
[3] Department of Chemistry, Pukyong National University, Busan 48513, Republic of Korea
* Correspondence: shinhj@kiost.ac.kr; Tel.: +82-51-664-3341; Fax: +82-51-664-3340

Abstract: The fungal genus *Meira* was first reported in 2003 and has mostly been found on land. This is the first report of second metabolites from the marine-derived yeast-like fungus *Meira* sp. One new thiolactone (**1**), along with one revised thiolactone (**2**), two new $\Delta^{8,9}$-steroids (**4**, **5**), and one known $\Delta^{8,9}$-steroid (**3**), were isolated from the *Meira* sp. 1210CH-42. Their structures were elucidated based on the comprehensive spectroscopic data analysis of 1D, 2D NMR, HR-ESIMS, ECD calculations, and the pyridine-induced deshielding effect. The structure of **5** was confirmed by oxidation of **4** to semisynthetic **5**. In the α-glucosidase inhibition assay, compounds **2**–**4** showed potent in vitro inhibitory activity with IC_{50} values of 148.4, 279.7, and 86.0 μM, respectively. Compounds **2**–**4** exhibited superior activity as compared to acarbose (IC_{50} = 418.9 μM).

Keywords: marine fungus; natural product; *Meira* sp.; thiolactone; pregnene steroid; epimer; stereochemistry; α-glucosidase inhibitor

Citation: Shin, H.J.; Lee, M.A.; Lee, H.-S.; Heo, C.-S. Thiolactones and $\Delta^{8,9}$-Pregnene Steroids from the Marine-Derived Fungus *Meira* sp. 1210CH-42 and Their α-Glucosidase Inhibitory Activity. *Mar. Drugs* **2023**, *21*, 246. https://doi.org/10.3390/md21040246

Academic Editor: Xian-Wen Yang

Received: 5 April 2023
Revised: 13 April 2023
Accepted: 14 April 2023
Published: 16 April 2023

1. Introduction

Fungi constitute one of the largest groups of organisms. Fungal-derived natural products (NPs) are pharmaceutically abundant, with several important biological applications ranging from highly potent toxins to approved drugs [1]. In particular, secondary metabolites obtained from marine fungi have garnered significant interest due to their unique chemical structures and potential biomedical applications [1,2]. While the number of cultivable marine fungi is extremely low (1% or less) compared to their global biodiversity [1,3], more than 1000 molecules have been reported and characterized from marine fungi, including alkaloids, lipids, peptides, polyketides, prenylated polyketides, and terpenoids [4–7]. Most research on secondary metabolites produced by marine fungi has primarily focused on a few genera, including *Penicillium*, *Aspergillus*, *Fusarium*, and *Cladosporium* [8,9]. Research into natural products derived from marine fungi is continually expanding, and as a result, a broader range of genera is now being investigated, with a particular focus on those associated with unique substrates and previously unexplored habitats [10–12].

In 2003, the genus *Meira* was first reported, namely *M. geulakonigii* and *M. argovae*, as a novel basidiomycetous [13]. *M. geulakonigii* was isolated from the citrus rust mite on pummelo (*Citrus grandis*), and *M. argovae* originated from a carmine spider mite on the leaves of castor bean (*Ricinus communis*) [8]. These *Meira* species have a similar morphology to yeast-like fungi. Nonetheless, the phylogenetic analysis of rDNA sequence data has identified *Meira* as a member of the Brachybasidiaceae family within the Exobasidiales, which

is classified under the Ustilaginomycetes (Basidiomycota) in the Exobasidiomycetidae group [14]. *M. geulakonigii* has been used successfully as a biological control agent against citrus and other phytophagous mites, as well as powdery mildew fungi [13,15–17]. A potential biocontrol agent against five mite species has been demonstrated for *M. argovae* [18]. Recently, *M. nicotianae* came from the rhizosphere of tobacco root, and that strain has the capability to promote plant growth possible in similar ways as plant growth-promoting fungi and arbuscular mycorrhizal fungi [19].

In this study, we isolated a yeast-like fungal species from a seawater sample. Phylogenetic analysis of ITS rDNA indicated that strain 1210CH-42 is closely related to other *Meira* species: *Meira* sp. M40, *M. nashicola* CY-1, and *M. miltonrushii* NIOSN-SK46-S121. So far, there are only a few reports on the isolation of *Meira* strains, but natural products from the genus *Meira* have not been investigated. This is the first report on the secondary metabolites from the marine-derived yeast-like fungus *Meira*. Herein, we report the isolation, structure elucidation, α-glucosidase inhibitory activity of **1**–**5**, and the structure revision of **2** isolated from the *Meira* strain 1210CH-42 (Figure 1).

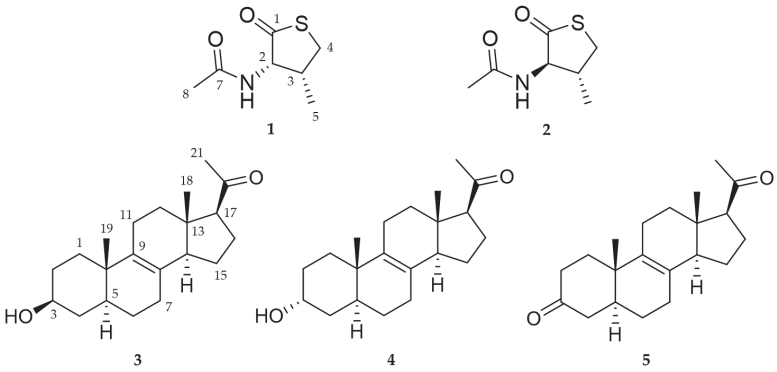

Figure 1. Structures of **1**–**5** from the marine fungus strain *Meira* sp. 1210CH-42.

2. Results and Discussion

2.1. Structure Elucidation of New Compounds

Compound **1** was obtained as a white amorphous powder, and its molecular formula was determined to be $C_7H_{11}NO_2S$ by HR-ESIMS, with three degrees of unsaturation. The ^{1}H and ^{13}C NMR data of **1** are summarized in Table 1. The ^{1}H NMR spectrum of **1** in CD_3OD revealed two methine protons (δ_H 4.79 and 2.86), one methylene proton (δ_H 3.64 and 3.10), and two methyl protons (δ_H 2.03 and 1.04). The ^{13}C NMR and HSQC spectra showed the presence of seven signals, including two carbonyl carbons (δ_C 206.5 and 173.8), two methines (δ_C 63.9 and 36.0), one methylene (δ_C 35.9) and two methyl carbons (δ_C 22.4 and 13.0). The planar structure of **1** was elucidated by analysis of ^{1}H-^{1}H COSY and HMBC correlations (Figure 2). The COSY correlations from H-2 (δ_H 4.79)/H-3 (δ_H 2.86), H-3 (δ_H 2.86)/H-4 (δ_H 3.64), and H-3 (δ_H 2.86)/H-5 (δ_H 1.04) were observed. In addition, the HMBC correlations from H-2 (δ_H 4.79) to C-1 (δ_C 206.5)/C-3 (δ_C 36.0)/C-5 (δ_C 13.0)/C-7 (δ_C 173.8), H-4 (δ_H 3.10 and 3.64) to C-1 (δ_C 206.5)/C-2 (δ_C 63.9)/C-5 (δ_C 13.0) and H-8 (δ_H 2.03) to C-7 (δ_C 206.5) suggested that **1** has a ring system, and confirmed the planar structure of **1**.

Detailed analysis of $^3J_{H,H}$ coupling constants and 1D NOESY data determined the relative configuration of **1**. The relative stereochemistry of C-2 could be established by the observation of strong selective 1D NOESY correlations between H-2 and H-3/H-4b, between H-4b and H-2/H-3, and between H-5 and H-4a (Figure 2). These correlations suggested that the relative configurations of C-2 and C-3 must be *cis* rather than *trans*-configuration in **1**. Thus, the relative configuration of **1** could be assigned as 2*S**, 3*R**. To determine the absolute configuration of **1**, the theoretical electronic circular dichroism (ECD) spectra of **1** and its enantiomer were calculated. The experimental ECD spectrum of **1**

showed a good agreement with the calculated ECD spectrum of the 2*S*, 3*R*-isomer (Figure 3). Therefore, the structure of **1** was elucidated to be a 2*S*-acetamide-3*R*-methyl-thiolactone.

Table 1. ^{1}H and ^{13}C NMR data of **1** and **2** (600 MHz for ^{1}H and 150 MHz for ^{13}C, in CD_3OD).

Position	1		2	
	δ_C, Type	δ_H, Mult. (*J* in Hz)	δ_C, Type	δ_H, Mult. (*J* in Hz)
1	206.5, C		206.5, C	
2	63.9, CH	4.79, d (6.6)	65.7, CH	4.29, d (12.5)
3	36.0, CH	2.86, m	40.2, CH	2.37, m
4a	35.9, CH_2	3.10, dd (11.4, 2.2)	34.7, CH_2	3.08, t (11.2)
4b		3.64, dd (11.4, 5.4)		3.34, d (11.2)
5	13.0, CH_3	1.04, d (6.9)	17.5, CH_3	1.20, d (6.5)
6-NH				
7	173.8, C		174.0, C	
8	22.4, CH_3	2.03, s	22.6, CH_3	2.02, s

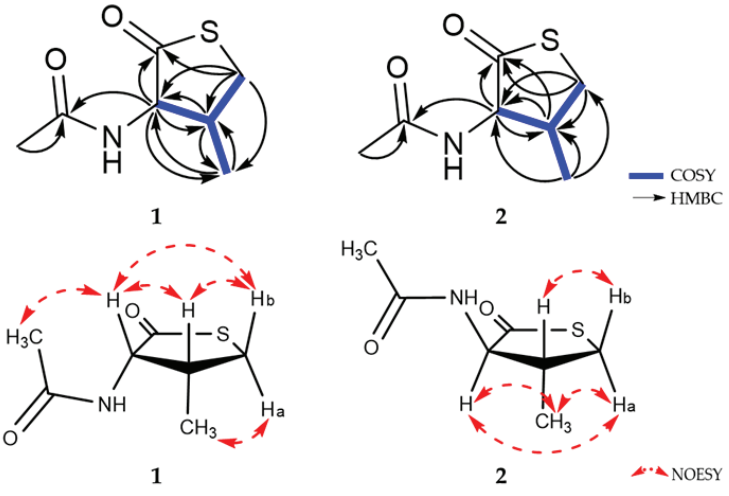

Figure 2. ^{1}H-^{1}H COSY and key 2D NMR correlations of **1** and **2**.

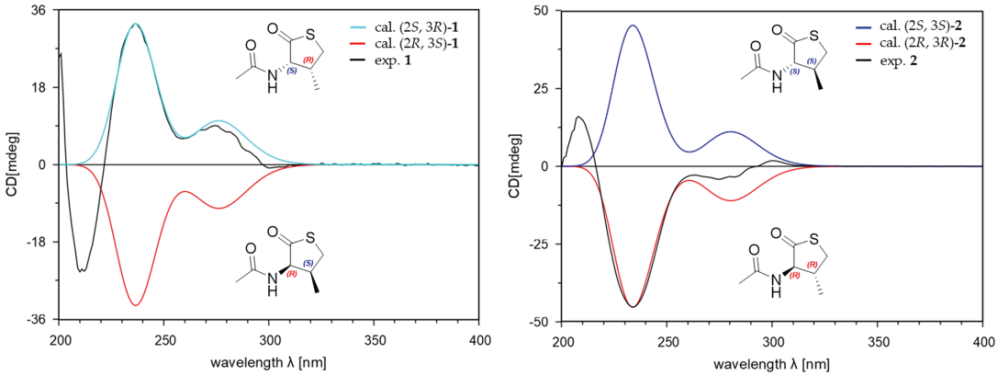

Figure 3. Experimental CD spectra and the calculated ECD spectra of **1** and **2**.

Compound **2** was isolated as a white amorphous powder. The molecular formula of **2** was the same as that of **1** ($C_7H_{11}NO_2S$) based on the HR-ESIMS data. Furthermore,

the 1D NMR data of **2** were also similar but not identical to those of **1** (Table 1). The planar structure of **2** was determined to be the same as **1** by analysis of ^{1}H-^{1}H COSY and HMBC data (Figure 2). However, the ^{1}H and ^{13}C chemical shifts of **2** were different from **1**, especially those for the chiral centers, suggesting that the stereochemistry of **2** might be different from **1**. The relative configuration of **2** was also determined by analysis of $^{3}J_{H,H}$ coupling constants and selective 1D NOESY data. The relative stereochemistry of C-2 could be established through the observation of strong NOESY contacts between H-2 and H-4a/H-5, between H-4a and H-2/H-5, and between H-4b and H-3. A relatively large coupling constant was observed between H-2 and H-3 ($^{3}J_{H,H}$ = 12.5 Hz). Thus, the relative configurations of H-2 and H-3 had a *trans*-configuration in **2** (Figure 2). The *J*-based configurational analysis and NOESY measurements could not discriminate the possible relative configurations for (2*S**, 3*S**) or (2*R**, 3*R**). To solve this issue and to determine the absolute configuration of **2**, the ECD spectra of **2** and its enantiomer were calculated. The experimental ECD spectrum of **2** showed a good agreement with the calculated ECD spectrum of the 2*R*, 3*R*-isomer (Figure 3). Therefore, the structure of **2** was elucidated as an epimer of **1** and to be a 2*R*-acetamide-3*R*-methyl-thiolactone.

Notably, the ^{1}H and ^{13}C NMR data in $CDCl_3$ of **2** were almost the same as those of the previously reported thiolactone with 2*R*, 3*S*-configuration isolated from a *Penicillium chrysogenum* (Table S1 and Figure S15) [20]. The reported compound with 2*R*, 3*S*-configuration possesses the same planar structure as **2** in this study. In the original paper for the compound with 2*R*, 3*S*-configuration, by the NOE correlation between H-3 (δ_H 2.24) and H-2 (δ_H 4.45), the authors insisted that the two protons were oriented on the same side of the ring system. However, its 1D NOE spectrum for the reported compound showed signals from H-3 (δ_H 2.24) to H-2/H-4/H-5/H-6 and NH, making it unclear to determine the orientation of H-3 to the same side of H-2 or not (Figures S15 and S16). Moreover, if the reported configuration is correct, H-2 and H-3 are in *syn* relation, and they should have a small scalar coupling constant, but H-2 in the reported thiolactone had a large coupling constant (12.5 Hz) as in the revised structure (Table S1). In this study, we carefully compared and checked the selective 1D NOESY data of **2** with those for the reported compound. As noted above, **2** exhibited strong NOE correlations from H-2 to H-5/H-4a and from H-4b to H-3 but not from H-4b to H-2, suggesting that H-2 and H-5 are on the same face. Furthermore, the reported compound with 2*R*, 3*S*-configuration and **1** (2*S*, 3*R*-configuration) are enantiomers and should have the same but opposite-in-sign specific rotation values. However, the optical rotation values of the reported thiolactone and **1** were $[\alpha]_D^{25}$ +1.5 (*c* 0.1, MeOH) and $[\alpha]_D^{25}$ +60.0 (*c* 0.1, MeOH), respectively. Considering all these results, the structure of the reported compound (2*R*, 3*S*-configuration) should be revised to 2*R*-acetamide-3*R*-methyl-thiolactone (Figure 4).

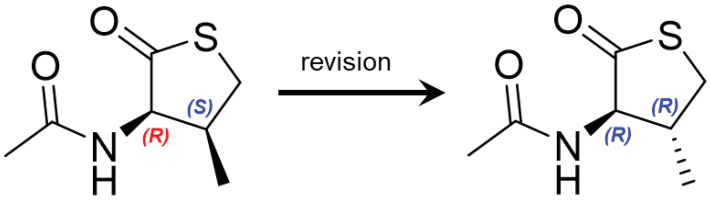

Figure 4. Reported and revised structures of **2**.

Compound **3** was isolated as a white amorphous powder, and its molecular formula was determined to be $C_{21}H_{32}O_2$. By the comparison of the ^{1}H and ^{13}C NMR (Table 2), HR-ESIMS, and optical rotation data of **3** with those reported previously in the literature, **3** was identified as a known compound, (+)-03219A, $\Delta^{8,9}$-3β-hydroxy-5α-17-acetyl steroid [21–23].

Table 2. ^{1}H and ^{13}C NMR data of **3**–**5** (600 MHz for ^{1}H and 150 MHz for ^{13}C, in CD_3OD).

Position	3		4		5	
	δ_C, Type	δ_H, Mult. (*J* in Hz)	δ_C, Type	δ_H, Mult. (*J* in Hz)	δ_C, Type	δ_H, Mult. (*J* in Hz)
1a	36.6, CH_2	1.22, td (16.2, 5.2)	32.0, CH_2	1.55, m	38.0, CH_2	1.55, m
1b		1.80, o.l [1]				
2a	32.4, CH_2	1.42, o.l	37.1, CH_2	1.48, o.l	39.1, CH_2	2.31, o.l
2b		1.80, o.l		1.54, o.l		2.53, m
3	71.8, CH	3.53, m	67.2, CH	3.97, t (2.8)	214.6, C	
4a	39.2, CH_2	1.31, o.l	30.0, CH_2	1.68, m	45.7, CH_2	2.11, o.l
4b		1.61, m				2.40, t (14.6)
5	42.3, CH	1.40, o.l	36.4, CH	1.86, m	44.4, CH	1.80, m
6a	26.8, CH_2	1.39, o.l	26.7, CH_2	1.32, m	26.7, CH_2	1.47, o.l
6b		1.52, m		1.46, o.l		1.60, m
7	28.5, CH_2	2.02, m	28.4, CH_2	2.02, m	28.4, CH_2	2.04, m
8	129.2, C		129.0, C		130.1, C	
9	136.3, C		137.2, C		135.6, C	
10	37.1, CH		37.6, CH		37.3, CH	
11a	24.0, CH_2	2.15, m	23.6, CH_2	2.13, o.l	24.1, CH_2	2.20, m
11b		2.27, o.l		2.28, o.l		2.25, o.l
12a	37.3, CH_2	1.69, m	37.3, CH_2	1.70, o.l	37.2, CH_2	1.70, o.l
12b		2.07, m		2.07, o.l		2.08, o.l
13	45.0, C		45.1, C		45.0, C	
14	53.3, CH	2.27, o.l	53.4, CH	2.30, o.l	53.2, CH	2.29, m
15a	25.3, CH_2	1.42, o.l	25.3, CH_2	1.42, o.l	25.3, CH_2	1.45, o.l
15b		1.72, m		1.72, o.l		
16a	24.3, CH_2	1.72, o.l	24.2, CH_2	1.72, o.l	24.3, CH_2	1.72, o.l
16b		2.21, m		2.21, m		2.21, m
17	63.5, CH	2.69, t (8.7)	63.5, CH	2.70, t (8.6)	63.5, CH	2.70, t (8.7)
18	13.2, CH_3	0.57, s	13.2, CH_3	0.57, s	13.2, CH_3	0.60, s
19	18.3, CH_3	0.97, s	17.3, CH_3	0.94, s	17.3, CH_3	1.18, s
20	212.4, C		212.5, C		212.3, C	
21	31.7, CH_3	2.13, s	31.7, CH_3	2.13, s	31.7, CH_3	2.14, s

[1] Signals were overlapped with other signals.

Compound **4** was purified as a white amorphous powder, and its molecular formula was determined to be $C_{21}H_{32}O_2$ by HR-ESIMS, which is identical to that of **3**, with 6 degrees of unsaturation. The ^{1}H and ^{13}C NMR data of **4** are summarized in Table 2. The ^{1}H NMR data for **4** revealed the signals of three methyl groups (δ_H 0.57, 0.94, and 2.13), one oxymethine (δ_H 3.97), nine methylenes, and three sp^3 methines. The ^{13}C NMR and HSQC data of **4** exhibited 21 carbon signals containing three methyls (δ_C 13.2, 17.3, and 31.7), one oxymethine (δ_C 67.2), nine methylenes, two olefinic quaternary carbons (δ_C 129.0 and 137.2), two sp^3 quarternary carbons (δ_C 37.6 and 45.1), and one ketone carbonyl carbon (δ_C 212.5). The planar structure of **4** was elucidated by ^{1}H-^{1}H COSY and HMBC data (Figure 5). The ^{1}H-^{1}H COSY correlations suggested the presence of four ^{1}H-^{1}H spin systems: from H-1 to H-4, from H-5 to H-7, from H-11 to H-12, and from H-14 to H-17. The HMBC correlations from H-6/H-7/H-11/H-14/H-15 to C-8 (δ_C 129.0) and from H-11/H-12/H-14/H-19 to C-9 (δ_C 137.2) indicated a double bond was located at C-8 and C-9. Additionally, the HMBC correlations from H-21 to C-17 (δ_C 63.5)/C-20 (δ_C 212.5) supported the assignment of an acetyl moiety connected to C-17 of the five-membered ring. The planar structure of **4** was the same as that of **3**, (+)-03219A [23], except for the difference in the chemical shifts around the oxymethine (δ_H 3.97 and δ_C 67.2) at C-3, suggesting that the stereochemistry of C-3 might be different from **3** (Figure 1 and Table 2). The stereochemistry of **4** was determined by analysis of the ROESY spectrum, 1D NOESY data, coupling constants, and the pyridine-induced deshielding effect. The relative configuration of **4** was confirmed by the ROESY correlations from H-3 to H-2a/H-2b/H-4, from H-19 to H-2b/H-4/H-11/H-18, and from H-18 to H-15/H-21 (Figure 5). The selective 1D NOE correlations were observed

from H-3 to H-2a/H-2b/H-4/H-19 (Figure S27). Furthermore, the small coupling constant of H-3 at δ_H 3.97 (t, J = 2.8) was indicative of the C-3 hydroxyl group being axial from an examination of the Dreiding model (Table 2 and Figure 5) [24]. The significant deshielded chemical shifts of H_{eq}-3 ($\Delta\delta_H$ = +0.32) and H_{ax}-5 ($\Delta\delta_H$ = +0.48) in pyridine-d_5 compared with those in CD_3OD indicated that OH-3 and H-5 adopted α-orientation, supporting the identified orientation (Figure 6 and Figure S29) [25–28]. Consequently, the structure of **4** was determined as a new epimer of **3**, $\Delta^{8,9}$-3α-hydroxy-5α-17-acetyl steroid.

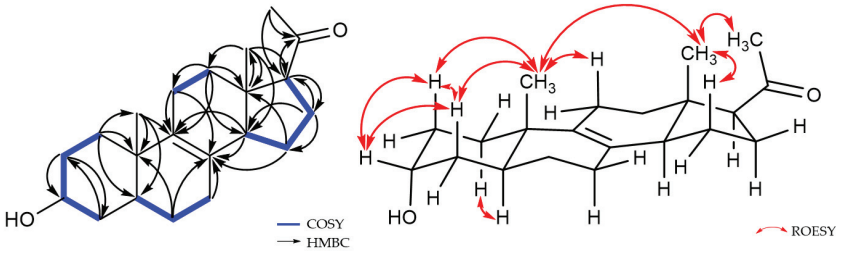

Figure 5. ^{1}H-^{1}H COSY and key 2D NMR correlations of **4**.

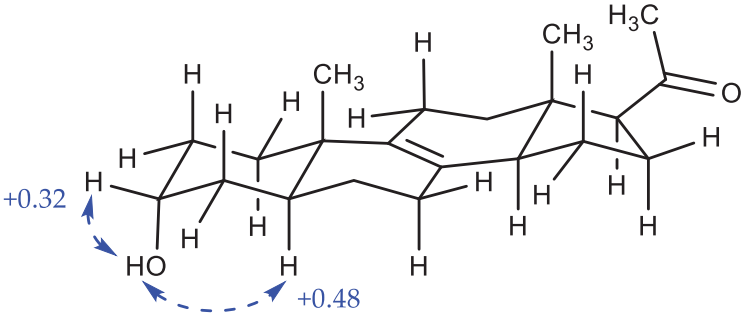

Figure 6. Pyridine-induced deshielding effects of **4** ($\Delta\delta = \delta_H$ in C_5D_5N-δ_H in CD_3OD).

Compound **5** was obtained as a white amorphous powder. The NMR data of **5** were similar to those of **4**, except for the absence of signals for the oxymethine at C-3 (δ_H 3.97 and δ_C 67.2) in **4** and the appearance of a ketone signal at C-3 (δ_C 214.6) in **5** (Table 2), revealing that **5** would be an oxidized form of **4**. The ^{1}H and ^{13}C NMR spectra, compared to those of **3** and **4**, showed the significantly deshielded chemical shifts of C-2 (δ_H 2.31/2.53 and δ_C 39.1) and C-4 (δ_H 2.11/2.40 and δ_C 45.7). Additionally, the HMBC correlations between H-2b (δ_H 2.53)/H-4 (δ_H 2.11/2.40) and C-3 (δ_C 214.6) determined the position of the ketone at C-3 (Figure 7). To clearly confirm the structure of **5**, **4** was oxidized to obtain the semisynthetic **5**. Both **5** and semisynthetic **5** exhibited identical ^{1}H NMR, HSQC, and HMBC spectra (Figures S35, S36 and S37). The molecular formula of semisynthetic **5** was determined to be $C_{21}H_{30}O_2$ by HR-ESIMS (m/z 337.2134 $[M + Na]^+$, calcd. for $C_{21}H_{30}O_2Na$, 337.2138). Based on these results, the structure of **5** was determined as a 3-keto derivative of **4**, with 7 degrees of unsaturation. Therefore, the structures of **5** and semisynthetic **5** were designated as $\Delta^{8,9}$-5α-3,20-dione-17-acetyl steroids.

2.2. α-Glucosidase Inhibitory Activities of Compounds

Compounds **1**–**4** were evaluated for α-glucosidase inhibitory activities (Table 3). Compound **4** exhibited the most significant inhibitory effect with an IC_{50} value of 86.0 μM, while **2** and **3** showed moderate activities with IC_{50} values of 148.4 and 279.7 μM, respectively. Further, **1** exhibited weak inhibitory activity at a concentration of 400 μM. The change in the stereochemistry of the compounds remarkably altered the α-glucosidase inhibitory

activities. Compounds **1** and **2**, as well as **3** and **4**, are stereoisomers of each other. Compounds **2** and **4** showed stronger α-glucosidase inhibitory effects than **1** and **3**. It could be noted herein that the stereochemistry was important for α-glucosidase inhibitory activity.

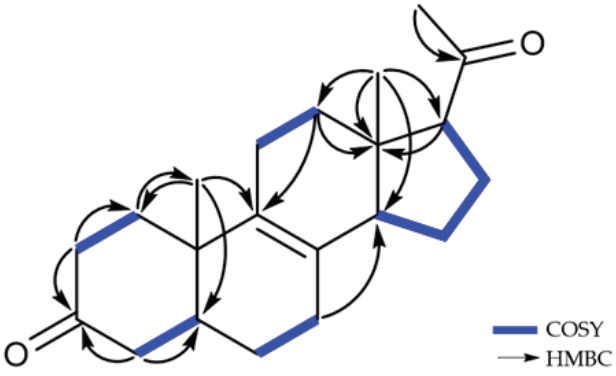

Figure 7. ^{1}H-^{1}H COSY and key HMBC correlations of **5**.

Table 3. α-Glucosidase inhibitory activities of **1**–**4**.

Compounds	IC_{50} (μM) [1]
1	>400
2	148.4
3	279.7
4	86.0
Acarbose [2]	418.9

[1] The 50% inhibitory concentration (μM). [2] Acarbose is used as a positive control.

3. Materials and Methods

3.1. General Experimental Procedures and Reagents

NMR spectra were acquired with a Bruker AVANCE III 600 spectrometer (Bruker BioSpin GmbH, Rheinstetten, Germany) with a 3 mm probe operating at 600 MHz (^{1}H) and 150 MHz (^{13}C). Chemical shifts were expressed in ppm with reference to the solvent peaks (δ_H 3.31 and δ_C 49.15 ppm for CD_3OD, δ_H 7.26 and δ_C 77.26 ppm for $CDCl_3$). UV spectra were recorded with a Shimadzu UV-1650PC spectrophotometer (Shimadzu Corporation, Kyoto, Japan). IR spectra were obtained on a JASCO FT/IR-4100 spectrophotometer (JASCO Corporation, Tokyo, Japan). Optical rotations were measured with a Rudolph analytical Autopol III S2 polarimeter (Rudolph Research Analytical, Hackettstown, NJ, USA). LR-ESIMS data were obtained with an ISQ EM mass spectrometer (Thermo Fisher Scientific Korea Ltd., Seoul, Republic of Korea). HR-ESIMS data were obtained with a Waters SYNPT G2 Q-TOF mass spectrometer (Waters Corporation, Milford, CT, USA) at Korea Basic Science Institute (KBSI) in Cheongju, Republic of Korea and a Sciex X500R Q-TOF spectrometer (Framingham, MA, USA). ECD spectra were recorded with a JASCO J-1500 polarimeter at the Center for Research Facilities, Changwon National University, Changwon, Republic of Korea. HPLC was performed using a BLS-Class pump (Teledyne SSI, Inc., State College, PA 16803, USA) with Shodex RI-201H refractive index detector (Shoko Scientific Co., Ltd., Yokohama, Japan). Columns for HPLC were YMC-ODS-A (250 mm × 10 mm, 5 μm; and 250 mm × 10 mm, 5 μm) and YMC-Triart (250 mm × 10 mm, 5 μm; and 250 mm × 10 mm 5 μm). C_{18}-reversed-phase silica gel (YMC-Gel ODS-A, 12 nm, S-75 μm) was used for open-column chromatography. Organic solvents were purchased as HPLC grade, and ultrapure waters were obtained from the Milipore Mili-Q Direct 8 system (Milipore S.A.S. Molsheim, France). The reagents used in the bioassay were purchased

from Sigma-Aldrich (Merck Korea, Seoul, Republic of Korea) and Tokyo Chemical Industry (TCI Co., Ltd., Tokyo, Japan).

3.2. Fungal Strain and Fermentation

The strain 1210CH-42 was isolated from a seawater sample collected at Chuuk Islands, Federated States of Micronesia, in 2010. The seawater sample was filtered, concentrated, and diluted (10^{-1} and 10^{-2}) with sterile seawater under aseptic conditions. Then the diluted sample was spread on Bennett's agar plates (1% D-glucose, 0.2% tryptone, 0.1% yeast extract, 0.1% beef extract, 0.5% glycerol, 1.7% agar, sea salt 32 g/L, pH 7.0). The plates were incubated for 7 days at 28 °C, and the single colony of the strain 1210CH-42 was collected. The fungus was identified as *Meira* sp. (GenBank accession number OQ693946) by DNA amplification and sequencing of the ITS region of the rRNA gene. The used primers were ITS4 (TCCTCCGCTTATTGATATGC) and ITS5 (GGAAGTAAAAGTCGTAACAAG G). The cultures of the strain 1210CH-42 were performed in modified Bennett's broth medium (1% D-glucose, 0.2% tryptone, 0.1% yeast extract, 0.1% beef extract, 0.5% glycerol, sea salt 10 g/L, pH 7.0). A seed culture was prepared from a spore suspension of the strain 1210CH-42 by inoculating into 1 L flasks and incubating it at 28 °C for 5 days on a rotary shaker at 120 rpm. The seed culture was inoculated aseptically into 2 L flasks (total 32 flasks) containing 1.0 L of medium and a 20 L fermenter containing 18 L of sterilized culture medium (0.1% *v*/*v*), respectively. The large-scale fermentation was done under the same conditions as the seed culture for 8 days and then harvested.

3.3. Extraction and Isolation of Compounds **1**–**5**

The culture broth (total 50 L) of the strain 1210CH-42 was harvested by high-speed centrifugation (60,000 rpm), and then the supernatant was extracted two times with ethyl acetate (100 L). The EtOAc extract was evaporated to afford a crude extract (3.05 g). The crude extract was subjected to ODS open column chromatography (YMC Gel ODS-A, 12 nm, S75 μm) followed by stepwise gradient elution with MeOH/H_2O (*v*/*v*) (20:80, 40:60, 60:40, 80:20, and 100:0) as eluent. The 20% MeOH fraction was purified by a reversed-phase HPLC (YMC ODS-A column, 250 × 10 mm i.d., 5 μm; 10% MeOH in H_2O; flow rate: 1.5 mL/min; detector: RI) to yield **1** (2.9 mg, t_R 44.0 min). Peak 10 from the 20% MeOH fraction was further purified by a reversed-phase HPLC (YMC ODS-A column, 250 × 10 mm i.d., 5 μm; 5% MeOH in H_2O; flow rate: 1.5 mL/min; detector: RI) to yield **2** (0.6 mg, t_R 64.0 min). The 80% MeOH fraction was purified by a reversed-phase HPLC (YMC ODS-A column, 250 × 10 mm i.d., 5 μm; 70% MeOH in H_2O; flow rate: 1.5 mL/min; detector: RI) to yield **3** (0.6 mg, t_R 84.0 min), **4** (2.1 mg, t_R 95.5 min), and **5** (0.3 mg, t_R 79.0 min).

Compound **1**: White amorphous powder; $[\alpha]_D^{25}$ +60.0 (*c* 0.1, MeOH); UV (MeOH) λ_{max} (log ε) 204 (3.64), 235 (3.33) nm; IR (MeOH) ν_{max} 3296, 2940, 1667, 1548, 1448, 1021 cm^{-1}; ^1H and ^{13}C NMR data (CD_3OD), see Table 1; HR-ESIMS *m*/*z* 196.0408 $[M + Na]^+$, calcd. for $C_7H_{11}NO_2NaS$, 196.0408.

Compound **2**: White amorphous powder; $[\alpha]_D^{25}$ +10.0 (*c* 0.1, MeOH); UV (MeOH) λ_{max} (log ε) 206 (3.88), 234 (3.69) nm; IR (MeOH) ν_{max} 3275, 2933, 1700, 1650, 1548, 1448, 1021 cm^{-1}; ^1H and ^{13}C NMR data (CD_3OD), see Table 1; HR-ESIMS *m*/*z* 196.0406 $[M + Na]^+$, calcd. for $C_7H_{11}NO_2NaS$, 196.0408.

Compound **3**: White crystalline needles; $[\alpha]_D^{25}$ +86.0 (*c* 0.1, MeOH); UV (MeOH) λ_{max} (log ε) 202 (4.10) nm; IR (MeOH) ν_{max} 3371, 2925, 2855, 1703, 1452, 1357, 1032 cm^{-1}; ^1H and ^{13}C NMR data (CD_3OD), see Table 2; HR-ESIMS *m*/*z* 339.2297 $[M + Na]^+$, calcd. for $C_{21}H_{32}O_2Na$, 339.2300.

Compound **4**: White crystalline needles; $[\alpha]_D^{25}$ +97.3 (*c* 0.1, MeOH); UV (MeOH) λ_{max} (log ε) 202 (3.96) nm; IR (MeOH) ν_{max} 3286, 2925, 2870, 1703, 1452, 1353, 1025 cm^{-1}; ^1H and ^{13}C NMR data (CD_3OD), see Table 2; HR-ESIMS *m*/*z* 339.2301 $[M + Na]^+$, calcd. for $C_{21}H_{32}O_2Na$, 339.2300.

Compound **5**: White amorphous; $[\alpha]_D^{25}$ +63.3 (*c* 0.1, MeOH); UV (MeOH) λ_{max} (log ε) 204 (3.86) nm; IR (MeOH) ν_{max} 3378, 2933, 2866, 1707, 1456, 1367, 1036 cm^{-1}; ^1H and ^{13}C NMR data (CD_3OD), see Table 2.

Oxidation of **4**. To a compound **4** (2.0 mg, 6.32 μmol) in anhydrous CH_2Cl_2 (0.5 mL) was added Dess-Martin reagent (8.04 mg, 18.96 μmol) at 0 °C. The mixture was stirred at r.t. for 24 h under N_2 gas. The solution was washed with 5% $NaHCO_3$ and brine and concentrated under reduced pressure [29,30]. Then the reactant was partitioned with EtOAc and H_2O. The EtOAc layer was concentrated, and subjected to a reversed-phase HPLC (YMC-Triart C_{18} column, 250 × 10 mm i.d., 5 μm; 70% MeOH in H_2O; flow rate: 2.0 mL/min; detector: RI) to yield semisynthetic **5** (0.5 mg): white amorphous solid; ^1H NMR (600 MHz, CD_3OD, representative signals) δ_H 2.71 (t, *J* = 8.7 Hz, 1H), 2.53–2.31 (m, 2H), 2.40–2.08 (t, *J* = 14.6, o. l, 2H), 2.30 (o. l, H), 2.23 (o. l, 2H), 2.14 (s, 3H), 2.21–1.71 (o. l, 2H), 2.07 (o. l, 2H), 1.81 (m, 2H), 1.70–1.47 (o. l, 2H), 1.56 (o. l, 2H), 1.45 (o. l, 2H), 1.18 (s, 3H), 0.60 (s, 3H); ^{13}C NMR data from HMBC spectrum (CD_3OD, representative signals) δ_C 214.5, 212.3, 135.6, 130.4, 63.5, 53.2, 45.7, 45.0, 44.4, 39.1, 38.1, 37.2, 31.7, 28.4, 26.7, 25.3, 24.3, 24.1, 23.7, 17.5, 13.1; HR-ESIMS *m*/*z* 327.2134 $[M + Na]^+$, calcd. for $C_{21}H_{30}O_2Na$, 327.2138.

3.4. Computational Analysis

The initial geometry optimization and conformational searches were generated using the Conflex 8 (Rev. B, Conflex Corp., Tokyo, Japan). The optimization and calculation for ECD were carried out using the Gaussian 16 program (rev. B.01, Gaussian Corp., Wallingford, C.T., USA). Conformational searches were performed using MMFF94s force field calculations with a 10 kcal/mol search limit. The conformers were optimized using the ground state method at the B3LYP/6-311+G (d, p) level in MeOH with a default model for ECD. The theoretical calculations of ECD spectra were performed using TD-SCF at the B3LYP /6-311+G (d, p) level in the gas phase. The ECD spectra were simulated by SpecDis (v. 1.71) using σ = 0.30–0.50 eV. All calculated curves were shifted to +10 nm to simulate experimental spectra better.

3.5. Measurement of α-Glucosidase Inhibitory Activity

The evaluation of α-glucosidase inhibitory activity was performed with reference to previously reported literature [31,32]. All the assays were carried out under 0.1 M PBS buffer (pH 7.4, Sigma). The samples (10 mM) were dissolved with DMSO (Sigma) and diluted into gradient concentrations with PBS buffer. The pre-reaction mixture consisted of the 130 μL sample with 30 μL α-glucosidase solution (0.2 U/mL, Sigma) and shaken well, then added to a 96-well plate and placed at 37 °C for 10 min in an incubator. Subsequently, 40 μL of 5 mM *p*-nitrophenyl-α-D-glucopyranoside (*p*NPG, TCI) was added and further incubated at 37 °C for 20 min. Finally, the α-glucosidase inhibitory activity was determined by measuring the release of *p*NPG at 405 nm of the microplate reader. The negative control was prepared by adding PBS buffer instead of the sample in the same way as the test. The blank was prepared by adding PBS buffer instead of *p*NPG using the same method. Acarbose was used as the positive control, and experiments were carried out in triplicate.

4. Conclusions

In summary, one new thiolactone (**1**), along with one revised thiolactone (**2**), two new $\Delta^{8,9}$-steroids (**4**, **5**), and one known $\Delta^{8,9}$-steroid (**3**), were isolated from the marine-derived fungus *Meira* sp. 1210CH-42. The absolute configurations of **1** and **2** were determined by analysis of the selective 1D NOESY and ECD data. Compounds **1** and **2** were identified as a pair of acetamide epimers at C-2. While compounds **3** and **4** were identified as epimers for the hydroxyl group at C-3, which was confirmed by analysis of ^1H NMR, ROESY, 1D NOESY, coupling constants, and the pyridine-induced deshielding effect. In addition, the structure of **5** was obtained as the 3-keto derivative of **3**. Compounds **1**–**4** were screened for their α-glucosidase inhibitory activity preliminarily. Compound **4** exhibited intense activity with an IC_{50} value of 86.0 μM. Furthermore, compounds **2** (IC_{50} = 148.4 μM)

and **3** (IC_{50} = 279.7 μM) demonstrated superior activity as compared to acarbose (IC_{50} = 418.9 μM). To the best of our knowledge, this is the first report of new bioactive metabolites with potent α-glucosidase inhibitory activity from the yeast-like fungus *Meira*. These results show that *Meira* sp. 1210CH-42 produces unique and diverse metabolites which have the potential for an anti-diabetic agent. The genus *Meira* is mostly found on land, and secondary metabolites from the marine-derived genus have not yet been reported. Therefore, further research is needed for the marine-derived fungus *Meira* sp. 1210CH-42 to discover novel secondary metabolites and investigate their biological properties.

Supplementary Materials: The following are available online at: https://www.mdpi.com/article/10.3390/md21040246/s1, Figures S1–S14: ^{1}H, ^{13}C NMR, HSQC, COSY, HMBC, selective 1D NOESY, and HR-ESIMS data of **1** and **2**, Table S1 and Figures S15–S16: ^{1}H, ^{13}C NMR data, and 1D NOESY data of the reported compound, Figures S17–S20: ^{1}H, ^{13}C NMR, HSQC, and HR-ESIMS data of **3**, Figures S21–S28: ^{1}H, ^{13}C NMR, HSQC, COSY, HMBC, ROESY, 1D NOESY, and HR-ESIMS data of **4**, Figure S29: Comparison of ^{1}H data of **4** in pyridine-d_5 and in CD_3OD, Figures S30–S34: ^{1}H, ^{13}C NMR, HSQC, COSY, and HMBC data of **5**, Figures S35–S38: ^{1}H MMR, HSQC, HMBC, and HR-ESIMS data of semisynthetic **5.**

Author Contributions: Conceptualization, H.J.S.; investigation, M.A.L., H.-S.L. and C.-S.H.; resources, M.A.L.; writing—original draft preparation, M.A.L.; writing—review and editing, H.J.S.; project administration, H.J.S.; funding acquisition, H.J.S. All authors have read and agreed to the published version of the manuscript.

Funding: This research was supported by the Korea Institute of Marine Science & Technology Promotion (KIMST) grant funded by the Ministry of Oceans and Fisheries, Korea (Grant no. 20220027) and the Korea Institute of Ocean Science and Technology (PEA0121).

Institutional Review Board Statement: Not applicable.

Data Availability Statement: The data presented in the article are available in the Supplementary Materials.

Acknowledgments: The authors express gratitude to Jung Hoon Choi, Korea Basic Science Institute, Ochang, Korea, for providing mass data.

Conflicts of Interest: The authors declare no conflict of interest.

References

1. Schueffler, A.; Anke, T. Fungal natural products in research and development. *Nat. Prod. Rep.* **2014**, *31*, 1425–1448. [CrossRef] [PubMed]
2. Duraes, F.; Szemeredi, N.; Kumla, D.; Pinto, M.; Kijjoa, A.; Spengler, G.; Sousa, E. Metabolites from Marine-Derived Fungi as Potential Antimicrobial Adjuvants. *Mar. Drugs* **2021**, *19*, 475. [CrossRef] [PubMed]
3. Arrieche, D.; Cabrera-Pardo, J.R.; San-Martin, A.; Carrasco, H.; Taborga, L. Natural Products from Chilean and Antarctic Marine Fungi and Their Biomedical Relevance. *Mar. Drugs* **2023**, *21*, 98. [CrossRef] [PubMed]
4. El-Demerdash, A.; Kumla, D.; Kijjoa, A. Chemical Diversity and Biological Activities of Meroterpenoids from Marine Derived-Fungi: A Comprehensive Update. *Mar. Drugs* **2020**, *18*, 317. [CrossRef]
5. Hafez Ghoran, S.; Kijjoa, A. Marine-Derived Compounds with Anti-Alzheimer's Disease Activities. *Mar. Drugs* **2021**, *19*, 410. [CrossRef]
6. Jiang, M.; Wu, Z.; Guo, H.; Liu, L.; Chen, S. A Review of Terpenes from Marine-Derived Fungi: 2015–2019. *Mar. Drugs* **2020**, *18*, 321. [CrossRef] [PubMed]
7. Rateb, M.E.; Ebel, R. Secondary metabolites of fungi from marine habitats. *Nat. Prod. Rep.* **2011**, *28*, 290–344. [CrossRef]
8. Imhoff, J.F. Natural Products from Marine Fungi-Still an Underrepresented Resource. *Mar. Drugs* **2016**, *14*, 19. [CrossRef]
9. Shin, H.J. Natural Products from Marine Fungi. *Mar. Drugs* **2020**, *18*, 230. [CrossRef]
10. El-Bondkly, E.A.M.; El-Bondkly, A.A.M.; El-Bondkly, A.A.M. Marine endophytic fungal metabolites: A whole new world of pharmaceutical therapy exploration. *Heliyon* **2021**, *7*, e06362. [CrossRef] [PubMed]
11. Gonçalves, M.F.M.; Esteves, A.C.; Alves, A. Marine Fungi: Opportunities and Challenges. *Encyclopedia* **2022**, *2*, 559–577. [CrossRef]
12. Julianti, E.; Abrian, I.A.; Wibowo, M.S.; Azhari, M.; Tsurayya, N.; Izzati, F.; Juanssilfero, A.B.; Bayu, A.; Rahmawati, S.I.; Putra, M.Y. Secondary Metabolites from Marine-Derived Fungi and Actinobacteria as Potential Sources of Novel Colorectal Cancer Drugs. *Mar. Drugs* **2022**, *20*, 67. [CrossRef]

13. Boekhout, T.; Theelen, B.; Houbraken, J.; Robert, V.; Scorzetti, G.; Gafni, A.; Gerson, U.; Sztejnberg, A. Novel anamorphic mite-associated fungi belonging to the Ustilaginomycetes: *Meira geulakonigii* gen. nov., sp nov., *Meira argovae* sp nov and *Acaromyces ingoldii* gen. nov., sp nov. *Int. J. Syst. Evol. Micr.* **2003**, *53*, 1655–1664. [CrossRef] [PubMed]
14. Rush, T.A.; Aime, M.C. The genus *Meira*: Phylogenetic placement and description of a new species. *Anton. Leeuw. Int. J. G.* **2013**, *103*, 1097–1106. [CrossRef]
15. Gerson, U.; Gafni, A.; Paz, Z.; Sztejnberg, A. A tale of three acaropathogenic fungi in Israel: *Hirsutella*, *Meira* and *Acaromyces*. *Exp. Appl. Acarol.* **2008**, *46*, 183–194. [CrossRef] [PubMed]
16. Paz, Z.; Burdman, S.; Gerson, U.; Sztejnberg, A. Antagonistic effects of the endophytic fungus *Meira geulakonigii* on the citrus rust mite *Phyllocoptruta oleivora*. *J. Appl. Microbiol.* **2007**, *103*, 2570–2579. [CrossRef]
17. Sztejnberg, A.; Paz, Z.; Boekhout, T.; Gafni, A.; Gerson, U. A new fungus with dual biocontrol capabilities: Reducing the numbers of phytophagous mites and powdery mildew disease damage. *Crop. Prot.* **2004**, *23*, 1125–1129. [CrossRef]
18. Paz, Z.; Gerson, U.; Sztejnberg, A. Assaying three new fungi against citrus mites in the laboratory, and a field trial. *Biocontrol* **2007**, *52*, 855–862. [CrossRef]
19. Cao, Y.; Li, P.-D.; Zhao, J.; Wang, H.-K.; Jeewon, R.; Bhoyroo, V.; Aruna, B.; Lin, F.-C.; Wang, Q. Morph-molecular characterization of *Meira nicotianae* sp. nov., a novel basidiomycetous, anamorphic yeast-like fungus associated with growth improvement in tobacco plant. *Phytotaxa* **2018**, *365*, 169–181. [CrossRef]
20. Han, X.; Li, P.; Luo, X.; Qiao, D.; Tang, X.; Li, G. Two new compounds from the marine sponge derived fungus *Penicillium chrysogenum*. *Nat. Prod. Res.* **2020**, *34*, 2926–2930. [CrossRef]
21. Dos Santos, A.; Rodrigues-Filho, E. New$\Delta^{8,9}$-pregnene steroids isolated from the extremophile fungus *Exophiala oligosperma*. *Nat. Prod. Res.* **2021**, *35*, 2598–2601. [CrossRef]
22. Shalit, Z.A.; Valdes, L.C.; Kim, W.S.; Micalizio, G.C. From an ent-Estrane, through a nat-Androstane, to the Total Synthesis of the Marine-Derived $\Delta^{8,9}$-Pregnene (+)-03219A. *Org. Lett.* **2021**, *23*, 2248–2252. [CrossRef]
23. Zhang, Y.; Zhou, X.; Huang, H.; Tian, X.; Song, Y.; Zhang, S.; Ju, J. 03219A, a new $\Delta^{8,9}$-pregnene isolated from *Streptomyces* sp. SCSIO 03219 obtained from a South China Sea sediment. *J. Antibiot.* **2013**, *66*, 327–331. [CrossRef]
24. Qiu, S.X.; van Hung, N.; Xuan, L.T.; Gu, J.Q.; Lobkovsky, E.; Khanh, T.C.; Soejarto, D.D.; Clardy, J.; Pezzuto, J.M.; Dong, Y.M.; et al. A pregnane steroid from Aglaia lawii and structure confirmation of cabraleadiol monoacetate by X-ray crystallography. *Phytochemistry* **2001**, *56*, 775–780. [CrossRef]
25. Cao, V.A.; Kwon, J.H.; Kang, J.S.; Lee, H.S.; Heo, C.S.; Shin, H.J. Aspersterols A-D, Ergostane-Type Sterols with an Unusual Unsaturated Side Chain from the Deep-Sea-Derived Fungus *Aspergillus unguis*. *J. Nat. Prod.* **2022**, *85*, 2177–2183. [CrossRef] [PubMed]
26. Demarco, P.V.; Farkas, E.; Doddrell, D.; Mylari, B.L.; Wenkert, E. Pyridine-induced solvent shifts in the nuclear magnetic resonance spectra of hydroxylic compounds. *J. Am. Chem. Soc.* **1968**, *90*, 5480–5486. [CrossRef]
27. Luo, X.; Li, F.; Shinde, P.B.; Hong, J.; Lee, C.O.; Im, K.S.; Jung, J.H. 26,27-cyclosterols and other polyoxygenated sterols from a marine sponge *Topsentia* sp. *J. Nat. Prod.* **2006**, *69*, 1760–1768. [CrossRef] [PubMed]
28. Shi, Q.; Huang, Y.; Su, H.; Gao, Y.; Peng, X.; Zhou, L.; Li, X.; Qiu, M. C_{28} steroids from the fruiting bodies of *Ganoderma resinaceum* with potential anti-inflammatory activity. *Phytochemistry* **2019**, *168*, 112109. [CrossRef] [PubMed]
29. Han, Y.; Cheng, Y.; Tian, L.W. Semisynthesis of 22,25-Epoxylanostane Triterpenoids: Structure Revision and Protective Effects against Oxygen-Glucose Deprivation/Reoxygenation Injury in H9c2 Cells. *J. Nat. Prod.* **2023**, *86*, 406–415. [CrossRef] [PubMed]
30. Lee, H.S.; Kang, J.S.; Cho, D.Y.; Choi, D.K.; Shin, H.J. Isolation, Structure Determination, and Semisynthesis of Diphenazine Compounds from a Deep-Sea-Derived Strain of the Fungus *Cystobasidium laryngis* and Their Biological Activities. *J. Nat. Prod.* **2022**, *85*, 857–865. [CrossRef]
31. Li, M.; Li, S.; Hu, J.; Gao, X.; Wang, Y.; Liu, Z.; Zhang, W. Thioester-Containing Benzoate Derivatives with alpha-Glucosidase Inhibitory Activity from the Deep-Sea-Derived Fungus *Talaromyces indigoticus* FS688. *Mar. Drugs* **2021**, *20*, 33. [CrossRef] [PubMed]
32. Zhao, W.; Zeng, Y.; Chang, W.; Chen, H.; Wang, H.; Dai, H.; Lv, F. Potential α-Glucosidase Inhibitors from the Deep-Sea Sediment-Derived Fungus *Aspergillus insulicola*. *Mar. Drugs* **2023**, *21*, 157. [CrossRef] [PubMed]

marine drugs

MDPI

Article

Diketopiperazine Alkaloids and Bisabolene Sesquiterpenoids from *Aspergillus versicolor* AS-212, an Endozoic Fungus Associated with Deep-Sea Coral of Magellan Seamounts

Yu-Liang Dong [1,2,3], Xiao-Ming Li [1,2,4], Xiao-Shan Shi [1], Yi-Ran Wang [1,2,3], Bin-Gui Wang [1,2,3,4,*] and Ling-Hong Meng [1,2,3,4,*]

1 CAS and Shandong Province Key Laboratory of Experimental Marine Biology, Institute of Oceanology, Chinese Academy of Sciences, Nanhai Road 7, Qingdao 266071, China; dongyuliang@qdio.ac.cn (Y.-L.D.); lixmqd@qdio.ac.cn (X.-M.L.); shixs@hbnu.edu.cn (X.-S.S.); wangyiran@qdio.ac.cn (Y.-R.W.)
2 Laboratory of Marine Biology and Biotechnology, Qingdao National Laboratory for Marine Science and Technology, Wenhai Road 1, Qingdao 266237, China
3 University of Chinese Academy of Sciences, Yuquan Road 19A, Beijing 100049, China
4 Center for Ocean Mega-Science, Chinese Academy of Sciences, Nanhai Road 7, Qingdao 266071, China
* Correspondence: wangbg@ms.qdio.ac.cn (B.-G.W.); menglh@ms.qdio.ac.cn (L.-H.M.)

Abstract: Two new quinazolinone diketopiperazine alkaloids, including versicomide E (**2**) and cottoquinazoline H (**4**), together with ten known compounds (**1**, **3**, and **5**–**12**) were isolated and identified from *Aspergillus versicolor* AS-212, an endozoic fungus associated with the deep-sea coral *Hemicorallium* cf. *imperiale*, which was collected from the Magellan Seamounts. Their chemical structures were determined by an extensive interpretation of the spectroscopic and X-ray crystallographic data as well as specific rotation calculation, ECD calculation, and comparison of their ECD spectra. The absolute configurations of (−)-isoversicomide A (**1**) and cottoquinazoline A (**3**) were not assigned in the literature reports and were solved in the present work by single-crystal X-ray diffraction analysis. In the antibacterial assays, compound **3** exhibited antibacterial activity against aquatic pathogenic bacteria *Aeromonas hydrophilia* with an MIC value of 18.6 μM, while compounds **4** and **8** exhibited inhibitory effects against *Vibrio harveyi* and *V. parahaemolyticus* with MIC values ranging from 9.0 to 18.1 μM.

Keywords: diketopiperazine; *Aspergillus versicolor*; deep-sea coral; endophytic fungus; antimicrobial activity

Citation: Dong, Y.-L.; Li, X.-M.; Shi, X.-S.; Wang, Y.-R.; Wang, B.-G.; Meng, L.-H. Diketopiperazine Alkaloids and Bisabolene Sesquiterpenoids from *Aspergillus versicolor* AS-212, an Endozoic Fungus Associated with Deep-Sea Coral of Magellan Seamounts. *Mar. Drugs* **2023**, *21*, 293. https://doi.org/10.3390/md21050293

Academic Editor: Hee Jae Shin

Received: 4 April 2023
Revised: 4 May 2023
Accepted: 8 May 2023
Published: 10 May 2023

1. Introduction

Marine-derived fungi living under extreme survival conditions are considered as abundant sources of structurally diverse and biologically active compounds [1,2]. In the deep-sea habitats, seamounts are regarded locations for a wide variety of current-topography interactions and biophysical coupling which have large biomass and higher biodiversity than their surrounding deep-sea floors [3,4]. Endozoic fungi surviving in deep-sea seamounts are a promising new source to mining bioactive secondary metabolites owing to their unique habitats. To date, only three papers investigating bioactive secondary metabolites of fungi derived from deep-sea seamounts have been published [5–7]. Therefore, a study on the chemical diversity of deep-sea seamount-derived endozoic fungi is warranted.

The species in the fungal genus *Aspergillus*, especially *A. versicolor*, is widely distributed in various habitats (marine, terrestrial, and symbiotic sources) and possesses the ability to produce diversified bioactive secondary metabolites such as diketopiperazine alkaloids [8,9], peptides [10], xanthones [9,11], and sesquiterpenes [12]. Most of these metabolites are described to exhibit a variety of bioactivities, including antifungal [9], antitumor [10,11], and neuroprotective activities [12].

In our continuous efforts to explore bioactive metabolites from deep-sea seamount-derived fungi [5–7], chemical investigation of the endozoic fungus *Aspergillus versicolor* AS-212 associated with the deep-sea coral, *Hemicorallium* cf. *imperiale*, which was collected from the Magellan Seamounts in the Western Pacific Ocean was carried out due to its unique HPLC profiles. As a result, two new quinazolinone diketopiperazine alkaloids, namely, versicomide E (**2**) and cottoquinazoline H (**4**), together with five known related analogs (**1**, **3**, **5**–**7**) as well as four known bisabolene derivatives (**8**–**11**) and a bisabolene dimer (**12**), have been isolated and identified. Herein, we report the isolation and structure elucidation as well as the antimicrobial activities of compounds **1**–**12** (Figure 1).

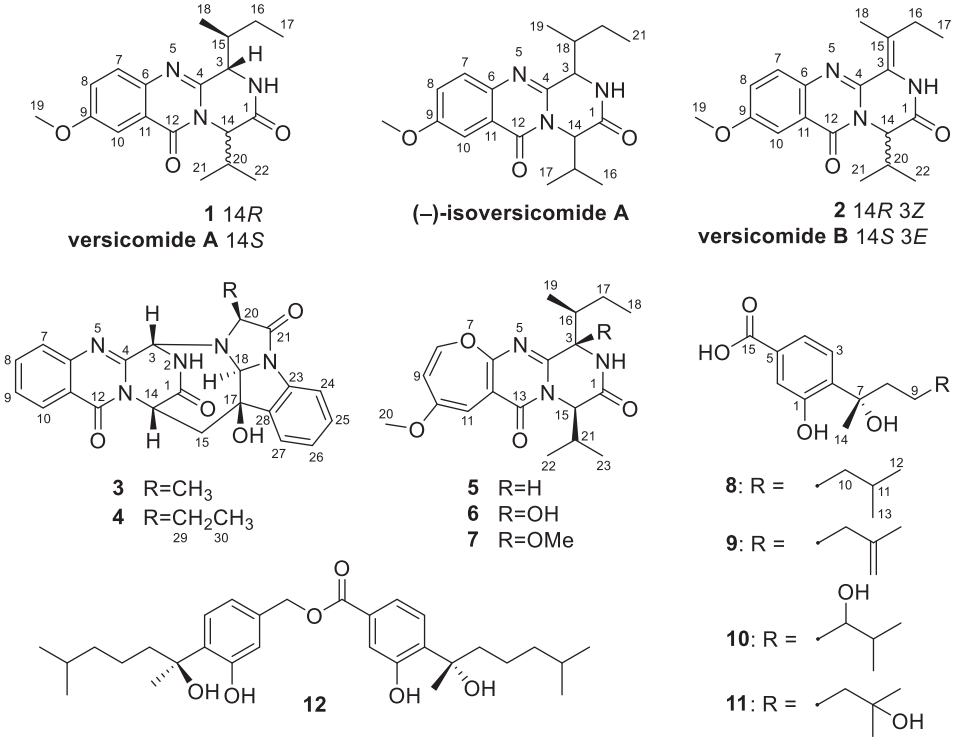

Figure 1. Structures of compounds **1**–**12**, versicomides A and B, and (−)-isoversicomide A.

2. Results and Discussion

2.1. Structure Elucidation of the Isolated Compounds

Compound **1** was isolated as colorless crystals, and the molecular formula was established as $C_{19}H_{25}N_3O_3$ by analysis of the HRESIMS data. The ^1H and ^{13}C NMR of **1** (DMSO-d_6, Table 1) extremely resembled those of versicomide A, a quinazoline-containing compound isolated from the crab-derived fungus *Aspergillus versicolor* XZ-4 which was collected from hydrothermal vent [8]. Further analysis of the 2D NMR spectra (Figure 2) indicated the same planar structure of **1** as that of versicomide A (Figure 1). However, a strong NOE cross-peak of H-3/H-20 was in favor of the structure with the 3*S**- and 14*R**-relative configuration rather than a 3*S** and 14*S** configuration (Figure 3). Single-crystal X-ray diffraction analysis with Cu Kα radiation further demonstrated its structure and absolute configurations (Figure 4). A Flack parameter of 0.0(2) enabled the definition of its absolute configuration as 3*S*, 14*R*, and 15*S*, indicating that **1** was the 14-epimer of versicomide A.

Table 1. ^{1}H (500 MHz) and ^{13}C (125 MHz) NMR Spectroscopic Data for Compounds **1** and **2**.

	Compound 1 [a]			Compound 2 [b]		
No.	**δ_C, Type**	**δ_H (Mult, *J* in Hz)**	**HMBC (From H to C)**	**δ_C, Type**	**δ_H (Mult, *J* in Hz)**	**HMBC (From H to C)**
1	168.0, C			167.1, C		
2		8.40, br s	1, 3, 4, 14		8.02, br s	4
3	58.1, CH	4.70, d (1.7)	4, 15, 16, 18	121.3, C		
4	149.3, C			144.3, C		
6	141.4, C			141.7, C		
7	129.5, CH	7.61, d (8.9)	9, 11	129.3, CH	7.62, d (8.9)	9, 11
8	124.9, CH	7.45, dd (8.9, 2.9)	6, 7, 10	125.1, CH	7.35, dd (8.9, 2.9)	6
9	158.5, C			159.0, C		
10	106.8, CH	7.52, d (2.9)	6, 8, 12	106.4, CH	7.65, d (2.9)	6, 8
11	120.9, C			120.8, C		
12	160.7, C			160.9, C		
14	60.9, CH	4.93, d (8.7)	1, 4, 12, 20	61.2, CH	5.33, dd (8.3, 1.5)	1, 4, 20
15	36.1, CH	2.62, m		135.0, C		
16	23.5, CH_2	1.34, m	15, 17	27.8, CH_2	2.29, m	3, 15
17	12.9, CH_3	0.86, overlap	15, 16	11.6, CH_3	1.15, t (7.6)	15, 16
18	15.5, CH_3	1.13, d (7.2)	3, 15, 16	19.5, CH_3	2.35, s	3, 15, 16
19	56.2, CH_3	3.88, s	9	56.0, CH_3	3.92, s	9
20	30.8, CH	2.26, m		32.2, CH	2.17, m	
21	20.2, CH_3	0.86, overlap	14, 20, 22	19.8, CH_3	1.01, d (6.8)	14, 20, 22
22	19.5, CH_3	1.04, d (6.6)	14, 20, 21	19.0, CH_3	1.09, d (6.8)	14, 20, 21

[a] Recorded in DMSO-d_6. [b] Recorded in $CDCl_3$.

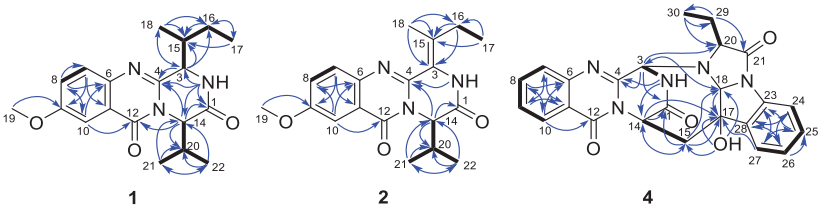

Figure 2. Key COSY (bold lines) and HMBC (blue arrows) correlations for compounds **1**, **2**, and **4**.

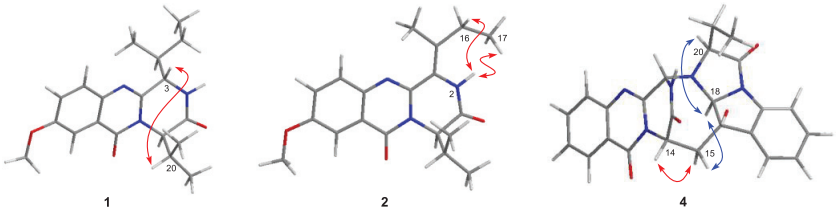

Figure 3. Key NOE correlations for compounds **1**, **2**, and **4** (red lines: β-orientation; blue lines: α-orientation).

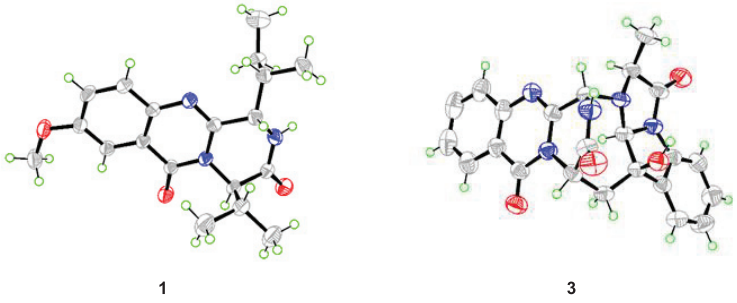

Figure 4. X-ray crystal structures of compounds **1** and **3**.

Compound **1** was initially treated as a new quinazoline alkaloid during the preparation of this manuscript, while Tasdemir and co-workers recently reported a new quinazoline-containing diketopiperazine (−)-isoversicomide A from the deep-sea sediment-derived fungus *Aspergillus versicolor* PS108-62 [13]. Notably, compound **1** shared the same planar structure and virtually similar optical rotation value ($[\alpha]_D^{25}$ −30 vs. $[\alpha]_D^{20}$ −25) as that of (−)-isoversicomide A, in which the stereogenic centers at C-3 and C-14 showed the same relative configurations with that of compound **1**. However, the configuration at C-18 on the short flexible aliphatic chain and the absolute configuration of (−)-isoversicomide A were not assigned due to the limited sample available [13]. Considering their similar rotation values and same relative configuration at C-3 and C-14, we assumed that compound **1** and (−)-isoversicomide A are the same compound. As the reported evidence to determine the absolute configuration of versicomide A does not seem entirely solid and in view of the highly similar NMR data of those isomers with multi-chiral centers, it is necessary to clarify the absolute configuration of **1**. The results from the X-ray diffraction analysis of compound **1** unambiguously determined its absolute configuration as 3*S*, 14*R*, and 15*S*. This is likely the first time the configuration of isoleucine in a quinazoline-containing diketopiperazine skeleton with a Val-Ile cyclic dipeptide moiety was unambiguously defined by X-ray crystallography analysis.

Versicomide E (**2**) was obtained as a colorless amorphous solid with the molecular formula $C_{19}H_{23}N_3O_3$ based on the HRESIMS data. Its NMR data ($CDCl_3$, Table 1) were similar to those of **1**, which indicated that **2** possessed the same quinazoline backbone as **1**. The obvious difference was the absence of signals for two methines at δ_C 58.1/δ_H 4.70 (CH-3) and δ_C 36.1/δ_H 2.62 (CH-15) in the NMR spectra of **1**, whereas additional resonances corresponding to a tetra-substituted double bond at δ_C 121.3 (C-3) and δ_C 135.0 (C-15) were found in that of **2** ($CDCl_3$, Table 1), which were further confirmed by COSY and HMBC correlations (Figure 2). The geometry of the double bond between C-3 and C-15 was determined as *Z*-configuration by key NOE correlations from NH-2 (δ_H 8.02) to H-16 (δ_H 2.29) and H_3-17 (δ_H 1.15) (Figure 3). Compound **2** has the same planar structure as that of versicomide B (Figure 1), which was also isolated from hydrothermal vent crab-derived fungus *Aspergillus versicolor* XZ-4 by Wu and co-workers in 2017 [8], with the exception of the geometry of the double bond at C3(15) (*Z* in **2** vs. *E* in versicomide B) and the absolute configuration of C-14 (*R* in **2** vs. *S* in versicomide B) as well. To clarify the stereochemistry of compound **2**, calculations of specific rotation (SR) were carried out for 14*R*-**2** and 14*S*-**2**, and the calculated SR value for 14*R*-**2** (+59.8) at CAM-B3LYP/TZVP level was compatible with the experimental SR value $[\alpha]_D^{25}$ +112.0 (*c* 0.08, MeOH), contrary to that of versicomide B ($[\alpha]_D^{20}$ −23.4) [8], which allowed the assignment of absolute configuration of C-14 in **2** as 14*R* (Table S2). To further verify the absolute configuration of C-14 in **2**, the time-dependent density functional (TDDFT)-ECD calculation was performed on 14*R*-**2** and 14*S*-**2** at the CAM-B3LYP/TZVP level in Gaussian 09. The experimental curve matched that of the calculated ECD spectrum for 14*R*-**2** and also assigned the absolute configuration of C-14 in **2** as 14*R* (Figure S27).

Compound **3** was obtained as colorless prisms and was identified as cottoquinazoline A by comparing its NMR data (measured in DMSO-d_6, Table S3) with those previously reported in the literature [10]. Cottoquinazoline A is a 16-nor analog of the known fumiquinazoline D and was first isolated from a marine-derived fungal strain of *A. versicolor* (MST-MF495) by Capon and co-workers in 2009, with a partial stereostructure assigned [10]. Considering the complexity of the structure of **3** and the presence of many stereoisomers, it is important to clarify the assignment of the absolute configurations of **3** [10,14]. Fortunately, a suitable crystal of **3** was picked out from DMSO–MeOH (1:1) and subjected to X-ray crystallographic analysis to assign its absolute configurations of the stereogenic centers in **3** as 3*S*, 14*S*, 16*R*, 17*S*, and 19*S* (Figure 4).

Cottoquinazoline H (**4**) was obtained as a colorless amorphous solid. Its molecular formula was established as $C_{24}H_{21}N_5O_4$ by HRESIMS, with one CH_2 unit more than that of **3**. Discreet comparisons of the NMR data (DMSO-d_6, Table 2) and UV absorptions with

3 suggested that they shared the same core scaffold. However, the methyl substitution at C-20 in **3** was replaced by an ethyl group in **4**, as evidenced by the appearance of an additional methylene group resonating at δ_C 21.0 and δ_H 1.90/1.99 (CH_2-29) in the NMR spectra of **4** (DMSO-d_6, Table 2). Additionally, the chemical shift of C-20 was deshielded downfield from δ_C 63.2 in **3** to δ_C 68.1 in **4**. The COSY and HMBC correlations verified the above deduction (Figure 2). The relative configuration of **4** was also deduced from the analysis of NOESY experiments. The NOE cross-peaks from H-20 and H-15α to H-18 revealed the cofacial orientation of these groups (Figure 3). Given that the stereochemistry of co-isolated compound **3** was determined by X-ray diffraction analysis as well as their similar NMR chemical shifts and virtually identical experimental ECD curves (Figure 5), the absolute configurations of all chiral carbons in **4** were established as 3*S*, 14*S*, 17*R*, 18*S*, and 20*S*.

Table 2. ^{1}H (500 MHz) and ^{13}C (125 MHz) NMR data for compound **4** (in DMSO-d_6).

Compound 4			
No.	**δ_C, Type**	**δ_H (Mult, *J* in Hz)**	**HMBC (From H to C)**
1	167.8, C		
2		9.10, d, (5.1)	4, 14
3	65.4, CH	5.22, d, (5.1)	1, 4, 18, 20
4	147.4, C		
6	146.7, C		
7	127.2, CH	7.74, dd, (8.4,1.0)	9, 11
8	134.4, CH	7.84, ddd, (8.4, 7.1, 1.5)	6, 10
9	127.1, CH	7.55, ddd, (8.1, 7.1, 1.0)	7, 11
10	126,1, CH	8.13, dd, (8.0, 1.5)	6, 8, 12
11	120.7, C		
12	159.3, C		
14	53.8, CH	5.27, dd, (5.3, 2.4)	1, 15, 17
15	36.3, CH_2	3.08, dd, (14.9, 5.3) 2.42, dd, (14.9, 2.4)	17, 18 1, 14
17	73.9, C		
18	79.6, CH	4.87, d (1.8)	3, 17
20	68.1, CH	4.06, m	
21	164.6, C		
23	135.9, C		
24	113.6, CH	7.29, overlap	26, 28
25	129.3, CH	7.29, overlap	23, 27
26	124.3, CH	7.09, ddd (7.6, 4.2, 3.4)	24, 25, 28
27	124.4, CH	7.42, d, (7.6)	17, 25
28	139.6, C	-	
29	21.0, CH_2	1.90, m 1.99, m	21, 30
30	8.9, CH_3	1.06, t, (7.4)	20, 29
17-OH		5.35, s	15, 17, 18

In addition to compounds **1**–**4**, three related quinazolinone diketopiperazine alkaloids, namely, versicoloids A and B (**5** and **6**) [9], and chrysopiperazine A (**7**) [15], as well as five known bisabolene derivatives (**8**–**12**) including sydonic acid (**8**) [16], (*S*)-(+)-11-dehydrosydonic acid (**9**) [17], (−)-10-hydroxysydonic acid (**10**) [18], hydroxysydonic acid (**11**) [16], and peniciaculin B (**12**) [18] were also identified and isolated from the fungus *A. versicolor* AS-212, which were determined by the comparison of their NMR data and those previously described in the literature. Structurally, (−)-isoversicomide A (**1**) might be a plausible biosynthetic precursor that undergoes the transformation of the benzene ring to the oxepine ring to generate versicoloid A (**5**) [19], which provides the basis for the biosynthetic origins of versicoloid A.

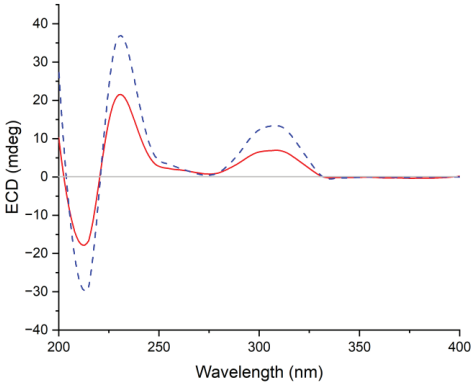

Figure 5. Comparison of the experimental ECD spectra of compounds **3** (in red) and **4** (in blue) in CH_3OH.

2.2. Antimicrobial Assays

The antimicrobial activity evaluation of all the isolated compounds was performed against human pathogenic bacterium (*Escherichia coli*), marine-derived aquatic pathogenetic bacteria (*Aeromonas hydrophila*, *Edwardsiella ictarda*, *Micrococcus luteus*, *Pseudomonas aeruginosa*, *Vibrio harveyi*, *V. parahemolyticus*, *V. vulnificus*), and plant-pathogenic fungi (*Colletotrichum gloeosporioides*, *Curvularia spicifera*, *Epicoccum sorghinum*, *Fusarium oxysporum*, *F. proliferatum*, and *Penicillium digitatum*) (Table 3). In the antimicrobial screening, compounds **4** and **8** exhibited potent inhibitory activity against the aquatic pathogenic bacterium *V. parahaemolyticus* with MIC values of 9.0 and 15.0 μM, while compounds **8** and **9** showed inhibitory activity against the aquatic pathogenic bacterium *V. harveyi* with the MIC values of 15.0 and 15.2 μM. In addition, compounds **3** and **4** displayed a broad spectrum of antimicrobial activity against most of the tested strains, with the MIC values ranging from 9.0 to 74.6 μM. The bisabolene derivatives (**8**–**12**) mainly exhibited activities against *M. luteus*, *V. harveyi*, and *V. parahaemolyticus*, with MIC values ranging from 15.0 to 121.2 μM. However, neither the quinazoline-containing diketopiperazine derivatives (**1** and **2**) nor the oxepine-containing diketopiperazine analogs (**5**–**7**) showed any activity against all the tested pathogenic bacteria. These data suggested that the 16-*nor*-methyl fumiquinazoline alkaloids generally showed higher antimicrobial activity than that of quinazolinone alkaloids (**3** and **4** vs. **1** and **2**) and the oxepine congeners (**5**–**7**). A comparison of the antimicrobial results of **3** and **4** revealed that different substituent groups at C-20 could influence the inhibitory potency against the pathogenic bacteria. Concerning bisabolene derivatives, the antimicrobial results revealed that compound **12**, a dimeric bisabolene analog, showed weaker antimicrobial activities than that of the monomeric bisabolenes (**8**–**11**) against *M. luteus* and *V. harveyi*. In addition, hydroxylation at C-10 or C-11 likely decreased the activity against *V. harveyi*, *V. parahaemolyticus*, and *C. gloeosporioides* (**8** vs. **10** and **11**).

Table 3. The antimicrobial activities of compounds **1**–**12** (MIC, μM) [a].

Strains	1	2	3	4	5	6	7	8	9	10	11	12	Positive Control
A. hydrophila	-	-	18.6	-	-	-	-	-	-	-	-	-	6.2 [b]
E. coli	-	-	-	72.2	-	-	-	-	-	-	-	-	6.2 [b]
M. luteus	-	-	74.6	36.1	-	-	-	-	-	-	-	-	3.1 [b]
V.harveyi	-	-	37.3	18.1	-	-	-	15.0	15.2	28.4	-	-	3.1 [b]
V. parahaemolyticus	-	-	37.3	9.0	-	-	-	15.0	121.2	113.5	113.5	64.0	3.1 [b]
V. vulnificus	-	-	74.6	72.2	-	-	-	-	-	-	-	-	3.1 [b]
C. spicifera	93.3	187.7	74.6	72.2	-	170.1	-	-	-	-	-	-	1.1 [c]
C. gloeosporioides	186.6	-	74.6	72.2	89.1	170.1	164.5	120.3	121.2	-	-	-	2.2 [c]

[a] (-) = MIC > 200 μM; Positive control: [b] Chloromycetin; [c] amphotericin B.

The above results showed that compounds **4**, **8**, and **9** were found to be efficient in suppressing the growth of aquatic pathogenic bacteria *V. parahaemolyticus* and *V. harveyi*. To a great degree, the endozoic fungus *A. versicolor* AS-212 which is associated with the deep-sea coral *Hemicorallium* cf. *imperiale* may provide a chemical defense to help its host to fight off the aquatic pathogenic bacteria by producing an array of antimicrobial secondary metabolites.

3. Experimental Section

3.1. General Experimental Procedures

The general experimental procedures, apparatus, and solvents/reagents used in this work were the same as those described in our previous reports [5–7].

3.2. Fungal Material

The endophytic fungus *Aspergillus versicolor* AS-212 associated with deep-sea coral, *Hemicorallium* cf. *imperial*, was collected from the Magellan Seamounts (depth 1420 m) in May 2018. By comparing its ITS region sequence with that of *A. versicolor* (accession no. MT582751.1) in the GenBank database, the sequence data of strain AS-212 were identical (100%) to those of *A. versicolor* and subsequently uploaded in GenBank with accession no. OP009765.1. The fungus AS-212 has been conserved at the Key Laboratory of Experimental Marine Biology, Institute of Oceanology, Chinese Academy of Sciences (IOCAS).

3.3. Fermentation, Extraction, and Isolation

The fungal strain AS-212 was cultivated on potato dextrose agar (PDA) plates at 28 °C for 7 days to generate spores. The fresh mycelia were transferred into 1 L Erlenmeyer flasks, each containing 300 mL potato-dextrose broth (PDB) medium, which was reported in our previous publication [5], and fermented under static conditions for 30 days at room temperature. After 30 days of incubation, a total of 33 L cultures were filtered and collected to separate the broth and mycelia. The broth was adequately extracted three times with EtOAc, while the mycelia were mechanically crushed and then extracted three times with 80% volume aqueous acetone. Acetone was removed in vacuo to afford an aqueous solution, which was successively extracted with EtOAc. Based on their virtually similar TLC and HPLC profiles (Figure S26), both EtOAc extracts from broth and mycelia were combined and evaporated under a vacuum to render the EtOAc extract (61 g).

The EtOAc extract was subjected to vacuum liquid chromatography (VLC) eluted with petroleum ether (PE)–EtOAc gradient (20:1 to 1:1, *v*/*v*) and then CH_2Cl_2–MeOH (20:1 to 1:1, *v*/*v*) to afford nine fractions (Frs. 1–9). Fr. 4 (2.3 g) was fractionated by reverse-phase column chromatography (CC) with a MeOH–H_2O gradient (from 10:90 to 100:0) to afford nine subfractions (Frs.4.1–4.9). Fr. 4.2 was directly purified by semi-preparative HPLC (Elite ODS-BP, 5μm; 10 × 250 mm; 80% MeOH–H_2O, 2.5 mL/min) to yield compound **6** (3.0 mg, t_R = 17 min). Fr. 4.4 (16 mg) was further purified by prep. TLC (plate: 20 × 20 cm, developing solvents: PE–EtOAc, 2:1) and by Sephadex LH-20 (MeOH) column to afford **7** (3.1 mg). Fr. 4.5 was purified by CC over Sephadex LH-20 chromatography (MeOH) and then by semi-preparative HPLC (85% MeOH–H_2O, 2.5 mL/min) to give compound **1** (6.6 mg, t_R = 14 min). Fr. 4.6 (75 mg) was fractionated by CC on Sephadex LH-20 column (MeOH) to yield five subfractions Frs.4.6.1–4.6.5. Fr. 4.6.5 (20 mg) was further purified by prep. TLC (developing solvents: DCM–MeOH, 20:1) and by Sephadex LH-20 (MeOH) to afford compound **9** (7.7 mg). Fr. 4.7 (36 mg) was directly purified by prep. TLC (developing solvents: CH_2Cl_2–EtOAc, 3:1) and by Sephadex LH-20 (MeOH) to afford compound **8** (4.0 mg). Fr. 4.8 (67 mg) was purified by CC on silica gel eluting with CH_2Cl_2–MeOH gradient (from 200:1 to 50:1) to obtain compound **12** (4.3 mg). Fr. 5 (3.4 g) was separated by reversed-phase CC using step-gradient elution with MeOH–H_2O (from 10:90 to 100:0) to yield seven subfractions (Frs. 5.1–5.7). Fr. 5.2 (241 mg) was fractionated by CC on silica gel eluting with CH_2Cl_2–MeOH gradient (from 150:1 to 20:1) and then purified on Sephadex LH-20 (MeOH) to afford compounds **10** (11.3 mg) and **11** (4.3 mg). Fr. 5.4 (126 mg) was fractionated by CC on Sephadex LH-20 (MeOH) and further purified by

semi-preparative HPLC (70% MeOH–H_2O, 2.5 mL/min) to afford compound **5** (6.3 mg, t_R = 22 min). Fr. 5.6 was chromatographed via a Sephadex LH-20 column (MeOH) and then by semi-preparative HPLC (78% MeOH-H_2O, 2.5 mL/min) to afford compound **2** (6.7 mg, t_R = 20 min). Fr. 7 (5.8 g) was fractionated by reverse-phase CC with a MeOH–H_2O gradient (from 10:90 to 100:0) to yield five subfractions (Frs. 7.1–7.5). Fr. 7.5 (328 mg) was applied to silica gel CC eluted with CH_2Cl_2/MeOH to give nine subfractions (Frs. 7.5.1–7.5.9). Fr.7.5.7 (36 mg) was purified by semi-preparative HPLC (45% MeCN–H_2O, 2.5 mL/min) to provide compounds **3** (4.3 mg, t_R = 9 min) and **4** (3.2 mg, t_R = 12 min).

(−)-Isoversicomide A (**1**): colorless crystals; mp 197−199 °C; $[\alpha]_D^{25}$ −30 (*c* 0.10, MeOH); UV (MeOH) λ_{max} (log ε) 227 (3.47), 277 (3.00), 326 (2.58) nm; ECD (0.52 mM, MeOH) λ_{max} ($\Delta\varepsilon$) 210 (−4.87), 233 (−15.03), 277 (+1.88), 328 (−1.02) nm; for ^{1}H and ^{13}C NMR data, see Table 1; HRESIMS *m/z* 344.1960 $[M + H]^+$ (calcd for $C_{19}H_{26}N_3O_3$, 344.1969).

Versicomide E (**2**): colorless amorphous solid; $[\alpha]_D^{25}$ +112 (*c* 0.08, MeOH); UV (MeOH) λ_{max} (log ε) 221 (3.26), 309 (2.88) nm; ECD (0.59 mM, MeOH) λ_{max} ($\Delta\varepsilon$) 207 (+6.69), 233 (−3.87), 255 (+6.18), 300 (+1.41), 343 (−1.15) nm; for ^{1}H and ^{13}C NMR data, see Table 1; HRESIMS *m/z* 340.1663 $[M - H]^-$ (calcd for $C_{19}H_{22}N_3O_3$, 340.1667).

Cottoquinazoline A (**3**): colorless prisms (MeOH-DMSO 1:1); mp 215−217 °C; $[\alpha]_D^{25}$ +160 (*c* 0.10, MeOH); UV (MeOH) λ_{max} (log ε) 205 (3.39), 227 (3.17), 256 (2.81), 268 (2.74), 280 (2.68), 305 (2.26), 315 (2.14) nm; ECD (0.58 mM, MeOH) λ_{max} ($\Delta\varepsilon$) 211 (−13.16), 230 (+12.22), 308 (+3.60) nm; for ^{1}H and ^{13}C NMR data, see Table S2.

Cottoquinazoline H (**4**): colorless amorphous solid; $[\alpha]_D^{25}$ +150 (*c* 0.10, MeOH); UV (MeOH) λ_{max} (log ε) 205 (3.60), 227 (3.43), 257 (3.11), 270 (3.03), 279 (2.96), 304 (2.52), 317 (2.40) nm; ECD (0.56 mM, MeOH) λ_{max} ($\Delta\varepsilon$) 212 (−22.91), 231 (+21.65), 308 (+7.16) nm; for ^{1}H and ^{13}C NMR data, see Table 2; HRESIMS *m/z* 444.1663 $[M + H]^+$ (calcd for $C_{24}H_{22}N_5O_4$, 444.1666).

3.4. X-ray Crystallographic Analysis of Compounds **1** *and* **3**

Suitable crystals were picked out to obtain crystallographic data using a Bruker Smart-1000 or Bruker D8 VENTURE CCD diffractometer with Cu Kα radiation (λ = 1.54178 Å). Absorption correction was applied using the program SADABS [20]. The structures were solved by direct methods with the SHELXTL software package [21,22]. All non-hydrogen atoms were refined anisotropically. The absolute structures were determined by refinement of the Flack parameter [23]. The structures were optimized by full-matrix least-squares techniques. Crystallographic data have been deposited with the Cambridge Crystallographic Data Centre with deposition numbers CCDCs 2192654 and 2192653 for **1** and **3**, respectively. Crystal data and structure refinements for **1** and **3** are listed in Table S1.

*Crystal data for compound **1**:* $C_{19}H_{25}N_3O_3$, F.W. = 343.2, space group P2(1)2(1)2(1), unit cell dimensions a = 13.2384(3) Å, b = 19.9347(4) Å, c = 6.8103(2) Å, V = 1797.26(8) Å^3, α = β = γ = 90°, Z = 4, d_{calcd} = 1.269 g/cm^3, crystal dimensions 0.350 × 0.330 × 0.300 mm, μ = 0.702 mm^{-1}, F(000) = 736. The 4007 measurements yielded 2826 independent reflections after equivalent data were averaged. The final refinement gave R_1 = 0.0379 and wR_2 = 0.0989 [I > 2σ(I)]. Flack parameter = 0.0(2).

*Crystal data for compound **3**:* $2(C_{23}H_{18}N_5O_4)\cdot C_2OS_2$, F.W. = 960.99, orthorhombic space group $C222_1$, unit cell dimensions a = 9.4022(11) Å, b = 25.878(4) Å, c = 19.112(2) Å, V = 4650.2(11) Å^3, α = β = γ = 90°, Z = 4, d_{calcd} = 1.373 g/cm^3, crystal dimensions 0.200 × 0.180 × 0.150 mm, μ = 1.612 mm^{-1}, F(000) = 1992. The 21,138 measurements yielded 4267 independent reflections after equivalent data were averaged. The final refinement gave R_1 = 0.0951 and wR_2 = 0.2851 [I > 2σ(I)]. Flack parameter = 0.145(12).

3.5. Antimicrobial Assay

A two-fold serial dilution method using 96-well microtiter plates was applied to evaluating the antimicrobial activities against a panel of aquatic pathogenic bacteria (*Aeromonas hydrophilia* QDIO-1, *Edwardsiella ictarda* QDIO-9, *Micrococcus luteus* QDIO-3, *Pseudomonas*

aeruginosa QDIO-4, *Vibrio harveyi* QDIO-7, *V. parahaemolyticus* QDIO-8, and *V. vulnificus* QDIO-10), one human pathogenic bacterium (*Escherichia coli* EMBLC-1), and six plant-pathogenic fungi (*Penicillium digitatum* QDAU-3, *Colletotrichum gloeosporioides* QA-29, *Fusarium oxysporum* QDAU-8, *Curvularia spicifera* QA-26, *Epicoccum sorghinum* QA-20, and *F. proliferatum* QA-28) [24]. The aquatic pathogenic strains and human pathogenic bacterium were provided by IOCAS, while the plant-pathogenic fungi were provided by IOCAS and Qingdao Agricultural University. To assay the antimicrobial activities, DMSO was added to dissolve all isolated compounds and positive control (chloramphenicol and amphotericin B) to prepare a stock solution with a specific concentration.

3.6. Specific Rotation and ECD Calculations

General computational procedures were consistent with our previous reports [5,25].

4. Conclusions

In conclusion, two new quinazolinone derivatives, versicomide E (**2**) and cottoquinazoline H (**4**), along with ten known compounds (**1**, **3**, and **5**–**12**), were isolated and identified from the deep-sea coral-derived *Aspergillus versicolor* AS-212. This marks the first time that the absolute configurations of all the stereogenic centers in (−)-isoversicomide A (**1**) and cottoquinazoline A (**3**), which were not assigned in the previous literature, were accurately solved in the present work by X-ray crystallographic analysis. Compound **3** exhibited activity against aquatic pathogenic bacteria *A. hydrophilia* with an MIC value of 18.6 μM, while compounds **4** and **8**–**10** exhibited inhibitory effects against *V. harveyi* with MIC values ranging from 15.0 to 28.4 μM. In addition, compounds **4** and **8** exhibited potent inhibitory effects against *V. parahaemolyticus* with MIC values of 9.0 and 15.0 μM, which might have the potential to be developed as leading compounds in discovering aquatic antibiotics.

Supplementary Materials: The following supporting information can be downloaded at: https://www.mdpi.com/article/10.3390/md21050293/s1, Figures S1–S27: The analyzed data of MS, 1D and 2D NMR spectra of compounds **1**–**4**, crystal packing of compounds **1** and **3**, HPLC analysis of mycelia extract, broth extract, and compounds **1**–**12** of *Aspergillus versicolor* AS-212, and experimental and calculated ECD spectra of compound **2** at the CAM-B3LYP/TZVP level. Table S1: Crystal data and structure refinement for compounds **1** and **3**. Table S2: Calculated specific rotation values at 589.44 nm for the enantiomers 14*R*-**2** and 14*S*-**2** at the CAM-B3LYP/TZVP level. Table S3: ^{1}H and ^{13}C NMR spectroscopic data for compound **3**.

Author Contributions: Y.-L.D. performed the experiments for the extraction, isolation, structure elucidation, and bioactivity evaluation and prepared the manuscript; X.-M.L. performed the 1D and 2D NMR experiments; X.-S.S. and Y.-R.W. contributed to the isolation, identification, and small-scale screening of the fungus AS-212. L.-H.M. contributed to NMR analysis and structure elucidation; B.-G.W. supervised the research work and revised the manuscript. All authors have read and agreed to the published version of the manuscript.

Funding: This work was financially supported by the National Natural Science Foundation of China (U2006203 and 41976090), the Senior User Project of RV *KEXUE* (KEXUE2020GZ02), and the Shandong Provincial Natural Science Foundation (ZR2021ZD28 and ZR2019ZD18).

Data Availability Statement: Not applicable.

Acknowledgments: B.-G.W. acknowledges the support of the Research Vessel *KEXUE* of the National Major Science and Technology Infrastructure from the Chinese Academy of Sciences (for sampling).

Conflicts of Interest: The authors declare no conflict of interest.

References

1. Newman, D.J.; Cragg, G.M. Natural products as sources of new drugs over the nearly four decades from 01/1981 to 09/2019. *J. Nat. Prod.* **2020**, *83*, 770–803. [CrossRef]
2. Wang, Y.N.; Meng, L.H.; Wang, B.G. Progress in research on bioactive secondary metabolites from deep-sea derived microorganisms. *Mar. Drugs* **2020**, *18*, 614. [CrossRef]

3. Xu, K.D. Exploring seamount ecosystems and biodiversity in the tropical Western Pacific Ocean. *J. Oceanol. Limnol.* **2021**, *39*, 1585–1590. [CrossRef]
4. Clark, M.R.; Rowden, A.A.; Schlacher, T.; Williams, A.; Consalvey, M.; Stocks, K.I.; Rogers, A.D.; O'Hara, T.D.; White, M.; Shank, T.M. The ecology of seamounts: Structure, function, and human impacts. *Annu. Rev. Mar. Sci.* **2010**, *2*, 253–278. [CrossRef] [PubMed]
5. Meng, L.H.; Li, X.M.; Zhang, F.Z.; Wang, Y.N.; Wang, B.G. Talascortenes A–G, highly oxygenated diterpenoid acids from the sea-anemone-derived endozoic fungus *Talaromyces scorteus* AS-242. *J. Nat. Prod.* **2020**, *83*, 2528–2536. [CrossRef] [PubMed]
6. Hu, X.Y.; Li, X.M.; Wang, B.G.; Meng, L.H. Tanzawaic acid derivatives: Fungal polyketides from the deep-sea coral-derived endozoic *Penicillium steckii* AS-324. *J. Nat. Prod.* **2022**, *85*, 1398–1406. [CrossRef]
7. Hu, X.Y.; Li, X.M.; Wang, B.G.; Meng, L.H. Uncommon polyketides from *Penicillium steckii* AS-324, a marine endozoic fungus isolated from deep-sea coral in the Magellan seamount. *Int. J. Mol. Sci.* **2022**, *23*, 6332. [CrossRef]
8. Pan, C.Q.; Shi, Y.T.; Chen, X.G.; Chen, C.A.; Tao, X.Y.; Wu, B. New compounds from a hydrothermal vent crab-associated fungus *Aspergillus versicolor* XZ-4. *Org. Biomol. Chem.* **2017**, *15*, 1155–1163. [CrossRef]
9. Wang, J.F.; He, W.J.; Huang, X.L.; Tian, X.P.; Liao, S.R.; Yang, B.; Wang, F.Z.; Zhou, X.J.; Liu, Y.H. Antifungal new oxepine-containing alkaloids and xanthones from the deep-sea-derived fungus *Aspergillus versicolor* SCSIO 05879. *J. Agric. Food Chem.* **2016**, *64*, 2910–2916. [CrossRef]
10. Fremlin, L.J.; Piggott, A.M.; Lacey, E.; Capon, R.J. Cottoquinazoline A and cotteslosins A and B, metabolites from an Australian marine-derived strain of *Aspergillus versicolor*. *J. Nat. Prod.* **2009**, *72*, 666–670. [CrossRef]
11. Yu, G.H.; Wu, G.W.; Sun, Z.C.; Zhang, X.M.; Che, Q.; Gu, Q.Q.; Zhu, T.J.; Li, D.H.; Zhang, G.J. Cytotoxic tetrahydroxanthone dimers from the mangrove-associated fungus *Aspergillus versicolor* HDN1009. *Mar. Drugs* **2018**, *16*, 335. [CrossRef] [PubMed]
12. Weng, H.Z.; Zhu, J.Y.; Yuan, F.Y.; Tang, Z.Y.; Tian, X.Q.; Chen, Y.; Fan, C.Q.; Tang, G.H.; Yin, S. Homo/Hetero-dimers of aromatic bisabolane sesquiterpenoids with neuroprotective activity from the fungus *Aspergillus versicolor* A18 from South China Sea. *Mar. Drugs* **2022**, *20*, 322. [CrossRef] [PubMed]
13. Magot, F.; Van Soen, G.; Buedenbender, L.; Li, F.J.; Soltwedel, T.; Grauso, L.; Mangoni, A.; Blümel, M.; Tasdemir, D. Bioactivity and metabolome mining of deep-sea sediment-derived microorganisms reveal new hybrid PKS-NRPS macrolactone from *Aspergillus versicolor* PS108-62. *Mar. Drugs* **2023**, *21*, 95. [CrossRef]
14. Lin, S.; Yu, H.M.; Yang, B.Y.; Li, F.L.; Chen, X.; Li, H.Q.; Zhang, S.T.; Wang, J.P.; Hu, Y.C.; Hu, Z.X.; et al. Reisolation and configurational reinvestigation of cottoquinazolines E–G from an arthropod-derived strain of the fungus *Neosartorya fischeri*. *J. Nat. Prod.* **2020**, *83*, 169–173. [CrossRef]
15. Xu, W.F.; Mao, N.; Xue, X.J.; Qi, Y.X.; Wei, M.Y.; Wang, C.Y.; Shao, C.L. Structures and absolute configurations of diketopiperazine alkaloids chrysopiperazines A–C from the gorgonian-derived *Penicillium chrysogenum* fungus. *Mar. Drugs* **2019**, *17*, 250. [CrossRef]
16. Hamasaki, T.; Nagayama, K.; Hatsuda, Y. Two new metabolites, sydonic acid and hydroxysydonic acid, from *Aspergillus sydowi*. *Agric. Biol. Chem.* **1978**, *42*, 37–40. [CrossRef]
17. Lu, Z.Y.; Zhu, H.J.; Fu, P.; Wang, Y.; Zhang, Z.H.; Lin, H.P.; Liu, P.P.; Zhuang, Y.B.; Hong, K.; Zhu, W.M. Cytotoxic polyphenols from the marine-derived fungus *Penicillium expansum*. *J. Nat. Prod.* **2010**, *73*, 911–914. [CrossRef]
18. Li, X.D.; Li, X.M.; Xu, G.M.; Zhang, P.; Wang, B.G. Antimicrobial phenolic bisabolanes and related derivatives from *Penicillium aculeatum* SD-321, a deep sea sediment-derived fungus. *J. Nat. Prod.* **2015**, *78*, 844–849. [CrossRef]
19. Zheng, L.J.; Wang, H.W.; Fan, A.L.; Li, S.M. Oxepinamide F biosynthesis involves enzymatic D-aminoacyl epimerization, 3*H*-oxepin formation, and hydroxylation induced double bond migration. *Nat. Commun.* **2020**, *11*, 4914. [CrossRef]
20. Sheldrick, G.M. *SADABS, Software for Empirical Absorption Correction*; University of Göttingen: Göttingen, Germany, 1996.
21. Sheldrick, G.M. *SHELXTL, Structure Determination Software Programs*; Bruker Analytical X-ray System Inc.: Madison, WI, USA, 1997.
22. Sheldrick, G.M. *SHELXL-97 and SHELXS-97, Program for X-ray Crystal Structure Solution and Refinement*; University of Göttingen: Göttingen, Germany, 1997.
23. Parsons, S.; Flack, H.D.; Wagner, T. Use of intensity quotients and differences in absolute structure refinement. *Acta Crystallogr. Sect. B Struct. Sci. Cryst. Eng. Mater.* **2013**, *B69*, 249–259. [CrossRef]
24. Pierce, C.G.; Uppuluri, P.; Tristan, A.R.; Wormley, F.L.; Mowat, E.; Ramage, G.; Lopez-Ribot, J.L. A simple and reproducible 96-well plate-based method for the formation of fungal biofilms and its application to antifungal susceptibility testing. *Nat. Protoc.* **2008**, *3*, 1494–1500. [CrossRef] [PubMed]
25. Yan, L.H.; Li, P.H.; Li, X.M.; Yang, S.Q.; Liu, K.C.; Wang, B.G.; Li, X. Chevalinulins A and B, proangiogenic alkaloids with a spiro [bicyclo [2.2. 2] octane-diketopiperazine] skeleton from deep-sea cold-seep-derived fungus *Aspergillus chevalieri* CS-122. *Org. Lett.* **2022**, *24*, 2684–2688. [CrossRef] [PubMed]

marine drugs

MDPI

Article

Anthraquinone Derivatives and Other Aromatic Compounds from Marine Fungus *Asteromyces cruciatus* KMM 4696 and Their Effects against *Staphylococcus aureus*

Olesya I. Zhuravleva [1,2,†], Ekaterina A. Chingizova [1,†], Galina K. Oleinikova [1], Sofya S. Starnovskaya [1], Alexandr S. Antonov [1], Natalia N. Kirichuk [1], Alexander S. Menshov [1], Roman S. Popov [1], Natalya Yu. Kim [1], Dmitrii V. Berdyshev [1], Artur R. Chingizov [1], Alexandra S. Kuzmich [1], Irina V. Guzhova [3], Anton N. Yurchenko [1,*] and Ekaterina A. Yurchenko [1,*]

[1] G.B. Elyakov Pacific Institute of Bioorganic Chemistry, Far Eastern Branch of the Russian Academy of Sciences, Prospect 100-Letiya Vladivostoka, 159, Vladivostok 690022, Russia; zhuravleva.oi@dvfu.ru (O.I.Z.); martyyas@mail.ru (E.A.C.)

[2] Institute of High Technologies and Advanced Materials, Far Eastern Federal University, 10 Ajax Bay, Russky Island, Vladivostok 690922, Russia

[3] Institute of Cytology Russian Academy of Sciences, Tikhoretskiy Ave. 4, St. Petersburg 194064, Russia; irina.guzhova@incras.ru

* Correspondence: yurchenkoan@piboc.dvo.ru (A.N.Y.); eyurch@piboc.dvo.ru (E.A.Y.)

† These authors contributed equally to this work.

Abstract: New anthraquinone derivatives acruciquinones A–C (**1**–**3**), together with ten known metabolites, were isolated from the obligate marine fungus *Asteromyces cruciatus* KMM 4696. Acruciquinone C is the first member of anthraquinone derivatives with a 6/6/5 backbone. The structures of isolated compounds were established based on NMR and MS data. The absolute stereoconfigurations of new acruciquinones A–C were determined using ECD and quantum chemical calculations (TDDFT approach). A plausible biosynthetic pathway of the novel acruciquinone C was proposed. Compounds **1**–**4** and **6**–**13** showed a significant antimicrobial effects against *Staphylococcus aureus* growth, and acruciquinone A (**1**), dendryol B (**4**), coniothyrinone B (**7**), and ω-hydroxypachybasin (**9**) reduced the activity of a key staphylococcal enzyme, sortase A. Moreover, the compounds, excluding **4**, inhibited urease activity. We studied the effects of anthraquinones **1**, **4**, **7**, and **9** and coniothyrinone D (**6**) in an in vitro model of skin infection when HaCaT keratinocytes were cocultivated with *S. aureus*. Anthraquinones significantly reduce the negative impact of *S. aureus* on the viability, migration, and proliferation of infected HaCaT keratinocytes, and acruciquinone A (**1**) revealed the most pronounced effect.

Keywords: marine-derived fungus; secondary metabolites; anthraquinones; antibiotics; skin infection; HaCaT; sortase A; urease; migration

Citation: Zhuravleva, O.I.; Chingizova, E.A.; Oleinikova, G.K.; Starnovskaya, S.S.; Antonov, A.S.; Kirichuk, N.N.; Menshov, A.S.; Popov, R.S.; Kim, N.Y.; Berdyshev, D.V.; et al. Anthraquinone Derivatives and Other Aromatic Compounds from Marine Fungus *Asteromyces cruciatus* KMM 4696 and Their Effects against *Staphylococcus aureus*. *Mar. Drugs* **2023**, *21*, 431. https://doi.org/10.3390/md21080431

Academic Editor: Hee Jae Shin

Received: 22 June 2023
Revised: 26 July 2023
Accepted: 26 July 2023
Published: 29 July 2023

1. Introduction

Anthraquinones are usual metabolites for marine fungi. A recent review by Hafez Ghoran and coauthors described 296 specialized metabolites belonging to the anthraquinone class, which were isolated from 28 marine fungal strains from 2000 to 2021 [1]. They are acetate-derivative metabolites originating from a polyketide containing eight C2 units, which generates, in turn, with three aldol condensations, the carbon skeleton of anthraquinones, except for the two carbonyl oxygens of the central ring. The presence in their structure of many different functional groups makes them very active in interaction with various molecular targets and exhibit wide spectrum of biological activities, including anticancer and antibacterial effects [2].

One of the five main causative agents of nosocomial infections, which are united by the abbreviation ESKAPE, is *Staphylococcus aureus* [3]. A decrease in the protective

properties of the skin and the body in hospital patients leads to damage to keratinocytes under the influence of *S. aureus* lytic toxins, the destruction of the protective barrier, and the penetration of *S. aureus* into the bloodstream [4]. The global prevalence of bacterial skin diseases in 2019, according to the Global Burden of Disease project, was 14,684.3 cases per 100,000 population [5]. These diseases have rarely been fatal (0.9 cases per 100,000), but the slightest infection can lead to sepsis if the course is unfavorable. There were an estimated 48.9 million cases of sepsis and 11.0 million sepsis-related deaths worldwide in 2017, accounting for 19.7% of all deaths worldwide [6], and the Gram-positive bacterium *S. aureus* is one of the main reasons for this.

Recently, chlorine-containing compounds acrucipentyns A–F were isolated by us from *Asteromyces cruciatus* KMM4696 fungus associated with brown alga *Sargassum pallidum*, and these compounds showed significant antibacterial activity against *Staphylococcus aureus* [7]. The detailed separation of the non-polar part of this fungal extract resulted in the isolation of a number of new and known anthraquinone derivatives. Thus, in this work, we describe the isolation and determination of the structure of these compounds, as well as the study of their antimicrobial properties, including their effects against *Staphylococcus aureus*-infected human HaCaT keratinocytes.

2. Results

2.1. Isolated Compounds from Asteromyces cruciatus

As a result of chromatographic separation of the ethyl acetate extract of the culture of the fungus *Asteromyces cruciatus* KMM 4696, new acruciquinones A–C (**1**–**3**), as well as known dendryol B (**4**) [8], pleosporone (**5**) [9], coniothyrinone D (**6**) [10], coniothyrinone B (**7**) [10], rubrumol (**8**) [11], ω-hydroxypachybasin (**9**) [12,13], trans-3,4-dihydroxy-3,4-dihydroanofinic acid (**10**) [14], quadricinctapyran A (**11**) [15], 7-hydroxymethyl-1,2-naphthalenediol (**12**) [16], and gliovictin (**13**) [17] (Figure 1), were isolated. The known compounds (**4**–**13**) were characterized by ^{1}H, ^{13}C NMR, and HR ESI MS data and identified by comparison with literature data.

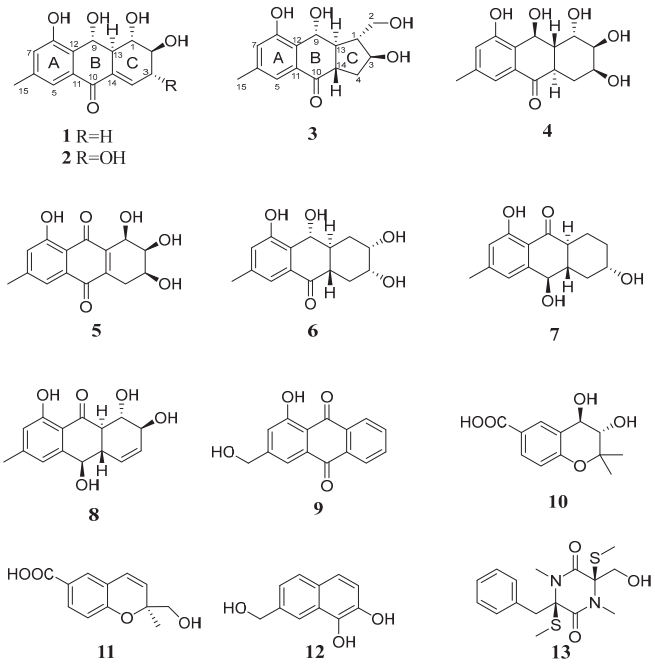

Figure 1. Isolated compounds from *Asteromyces cruciatus*.

2.2. Structural Characterization of New Compounds

The molecular formula of **1** was determined as $C_{15}H_{16}O_5$ based on the analysis of the (+)-HRESIMS spectrum (Figure S87) containing the peak of the cationized molecule [M + Na]+ (*m*/*z* 299.0887) and was confirmed by the ^{13}C NMR data. In the ^{1}H and ^{13}C NMR spectra of compound **1** (Table 1, Figures S7–S12) there were signals of a tetrasubstituted benzene ring; an olefinic proton; a methyl; a methylene, and four methine groups, three of which were oxygenated; five sp^2-hybridized quaternary carbons; and one unsaturated keto group.

Table 1. ^{1}H NMR spectroscopic data (acetone-d_6, δ in ppm, *J* in Hz) for **1** and **2**.

Position	1		2	
	δ_C, mult	δ_H (*J* in Hz) [a]	δ_C, mult	δ_H (*J* in Hz) [b]
1	78.9, CH	3.99, t (9.0)	77.9, CH	4.09, t (9.5)
2	70.1, CH	3.81, m	77.8, CH	3.61, dd (9.6, 8.4)
3	34.7, CH_2	α: 2.76, m β: 2.30, m	72.8, CH	4.30, m
4	137.1, CH	6.98, m	139.6, CH	6.85, t (2.7)
5	120.1, CH	7.35, d (1.3)	120.1, CH	7.36, d (1.2)
6	140.0, C	-	140.1, C	-
7	123.3, CH	6.87, d (1.3)	123.6, CH	6.89, d (1.2)
8	157.4, C		157.6, C	
9	75.0, CH	5.37, d (9.8)	74.9, CH	5.39, d (9.9)
10	184.1, C	-	184.3, C	-
11	132.9, C	-	132.8, C	-
12	125.5, C	-	125.5, C	-
13	48.5, CH	2.96, m	48.6, CH	3.02, m
14	132.2, C	-	130.9, C	-
15	21.0, CH_3	2.30, s	21.0, CH_3	2.31, s

[a] Chemical shifts were measured at 500.13 MHz. [b] Chemical shifts were measured at 700.13 MHz.

The HMBC correlations from H-5 to C-7, C-10, C-12, and C-15; from H-7 to C-5, C-8, and C-12; from H3-15 to C-5, C-6, and C-7; and from H-9 to C-8, C-11, C-12, and C-13 (Figures 2a and S11) established the structure of rings A and B and determined the position of the methyl and hydroxyl groups in the tetrasubstituted benzene ring and the hydroxyl and keto groups in ring B. Observed ^{1}H-^{1}H-COSY interactions (H-9/H-13/H-1/H-2/H2-3/H-4) and HMBC correlations from H-1 to C-2, C-3, C-9, and C-13; from H-3α to C-1, C-2, C-4, and C-14; and from H-4 to C-10 determined the structure of ring C, its fusion with ring B at C-13/C-14, the position of hydroxyl groups at C-1 and C-2, and the Δ4,14 position of the trisubstituted double bond.

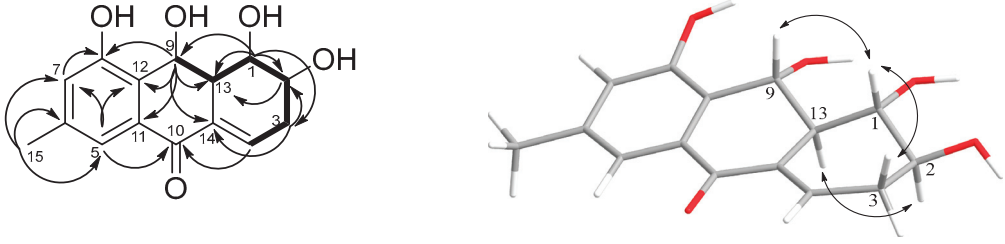

(**a**) (**b**)

Figure 2. Key ^{1}H–^{13}C HMBC and ^{1}H-^{1}H-COSY correlations (**a**) and ROESY correlations (**b**) of **1**.

The vicinal coupling constant values (Table 1), as well as the ROESY correlations (Figures 2b and S12) of the H-1/H-3β, H-9, and H-2/H-13 correlations, show that the first

three protons in **1** are on the same side of the molecule, while H-2 and H-13 are oriented in the opposite direction.

The molecular formula of compound **2** was determined as $C_{15}H_{16}O_6$ based on the analysis of the (+)-HRESIMS spectrum data containing the peak of the cationized molecule $[M + Na]^+$ (*m*/*z* 315.0830) and was confirmed by the ^{13}C NMR data. The ^1H and ^{13}C NMR spectra of compound **2** (Table 1, Figures S14–S18) were very similar to those for **1**, with the exception of proton and carbon signals at C-1, C-2, C-3, C-4, and C-14 of the cyclohexene ring. Downfield chemical shifts at C-3 and the presence of an additional methine group in **2** instead of a methylene group in 1 suggested the structure of **2** as a 3-hydroxy derivative of **1**. Observed ^1H-^1H COSY interactions (H-13/H-1/H-2/H-3/H-4) proved the position of the hydroxyl groups in compound **2** at C-1, C-2, and C-3 (Figure S17).

The coupling constant values (Table 1), as well as the ROESY correlations (Figure 3) between H-1, H-3, and H-9 and between H-2 and H-13 showed that the relative structure of **2** was the same as that of **1**.

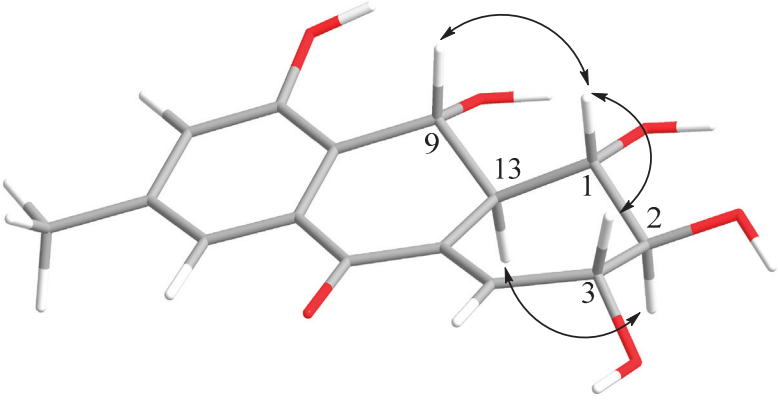

Figure 3. Key ROESY correlations in **2**.

An analysis of the literature data showed that the NMR spectra of compounds **1** and **2** were close to those for the known anthraquinones, dendryols A and D [8]. However, the values of chemical shifts and coupling constants of vicinal protons at C-1 and C-2 in the spectra of **1** and **2** significantly differed from those for known dendryols. Thus, compounds **1** and **2** are new stereoisomers of known dendryols A and D, respectively, and were named acruciquinones A (**1**) and B (**2**), respectively.

The molecular formula of compound **3** was determined as $C_{15}H_{18}O_5$ based on the analysis of the (+)-HRESIMS spectrum data containing the peak of the cationized molecule $[M + Na]^+$ (*m*/*z* 301.1042) and was confirmed by the ^{13}C NMR data. The ^1H and ^{13}C NMR spectra of **3** (Table 2, Figures S19–S24) contain signals of a tetrasubstituted benzene ring; a methyl ring; two methylene groups, one of which is oxygenated; five methine groups, two of which are bonded to oxygen; four quaternary sp^2-carbons; and one unsaturated ketone group.

HMBC correlations from H-5 (δ_H 7.25) to C-6 (δ_C 139.7), C-7 (δ_C 122.7), C-10 (δ_C 197.8), C-12 (δ_C 127.8), and C-15 (δ_C 21.0); from H-7 (δ_H 6.86) to C-5 (δ_C 118.9), C-8 (δ_C 158.3), C-12, and C-15; from H_3-15 (δ_H 2.31) to C-5, C-6, and C-7; and from H-9 (δ_H 5.07) to C-8, C-11 (δ_C 134.7), C-12, C-13 (δ_C 54.7), and C-14 (δ_C 51.4) (Figures 4a and S23) establish that the structure of rings A and B are the same as those for compounds **1** and **2**.

Table 2. ^{1}H and ^{13}C NMR spectroscopic data (δ in ppm, 700.13 /125.75 MHz, acetone-d_6) for **3**.

Pos.	δ_C, Mult	δ_H (J in Hz)
1	54.4, CH	2.14, m
2	62.9, CH_2	3.76, t (10.3) 4.13, dd (10.7, 2.8)
3	73.1, CH	4.47, brs
4	35.0, CH_2	α: 1.98, ddd (14.3, 9.5, 2.9) β: 2.35, m
5	118.9, CH	7.25, s
6	139.7, C	-
7	122.7, CH	6.86, s
8	158.3, C	-
9	74.5, CH	5.07, d (9.4)
10	197.8, C	-
11	134.7, C	-
12	127.8, C	-
13	54.7, CH	2.37, m
14	51.4, CH	2.69, dt (13.6, 9.2)
15	21.0, CH_3	2.31, s
2-OH	-	5.31, brs
3-OH	-	3.82, d (4.7)
8-OH	-	9.36, brs
9-OH	-	7.31, brs

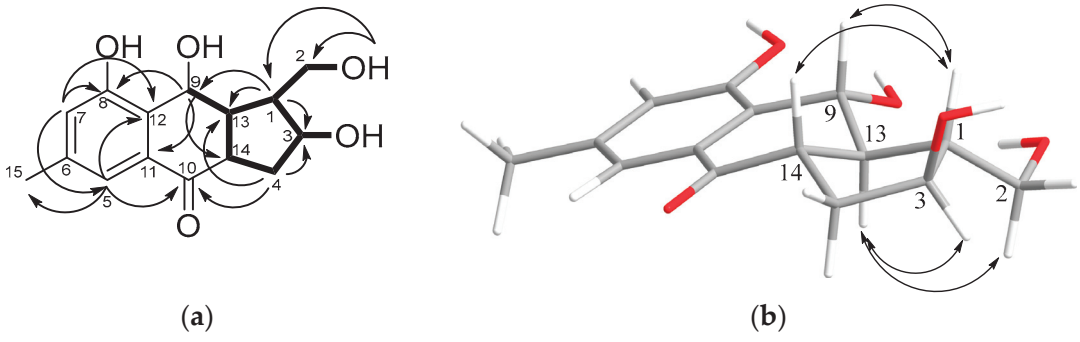

(**a**) (**b**)

Figure 4. Key ^{1}H–^{13}C HMBC and ^{1}H–^{1}H COSY correlations (**a**) and ROESY correlations (**b**) of **3**.

The observed ^{1}H-^{1}H COSY correlations (H-9/H-13/H-1(H_2-2)/H-3/H_2-4/H-14) and HMBC correlations from H-1 (δ_H 2.14) to C-2 (δ_C 62.9), C-3 (δ_C 73.1), C-9 (δ_C 74.5), and C-13; from H-4α (δ_H 1.98) to C-1, C-3, C-10, and C-14; and from H-14 to C-4, C-10, and C-13 revealed the structure of ring C, its fusion with ring B, and the position of hydroxymethyl and hydroxyl groups at C-1 and C-3, respectively (Figure 4a).

The relative configurations of **3** were established based on the ROESY correlations (Figures 4b and S24): H-1/H-9, H-14, and H-13/H-2a, H-3.

Thus, the structure of compound **3** was determined and named acruciquinone C. It should be noted that acruciquinone C is the first and only representative of anthraquinone derivatives with a 6/6/5 framework.

The absolute configurations of **1**–**3** were determined using an approach based on a comparison of the ECD spectra recorded for these compounds (Figures S2, S4, and S6) with the theoretical spectra calculated for them using the B3LYP exchange–correlation functional and cc-pvTz basis set implemented in GAUSSIAN 16 software (Figure 5) [18].

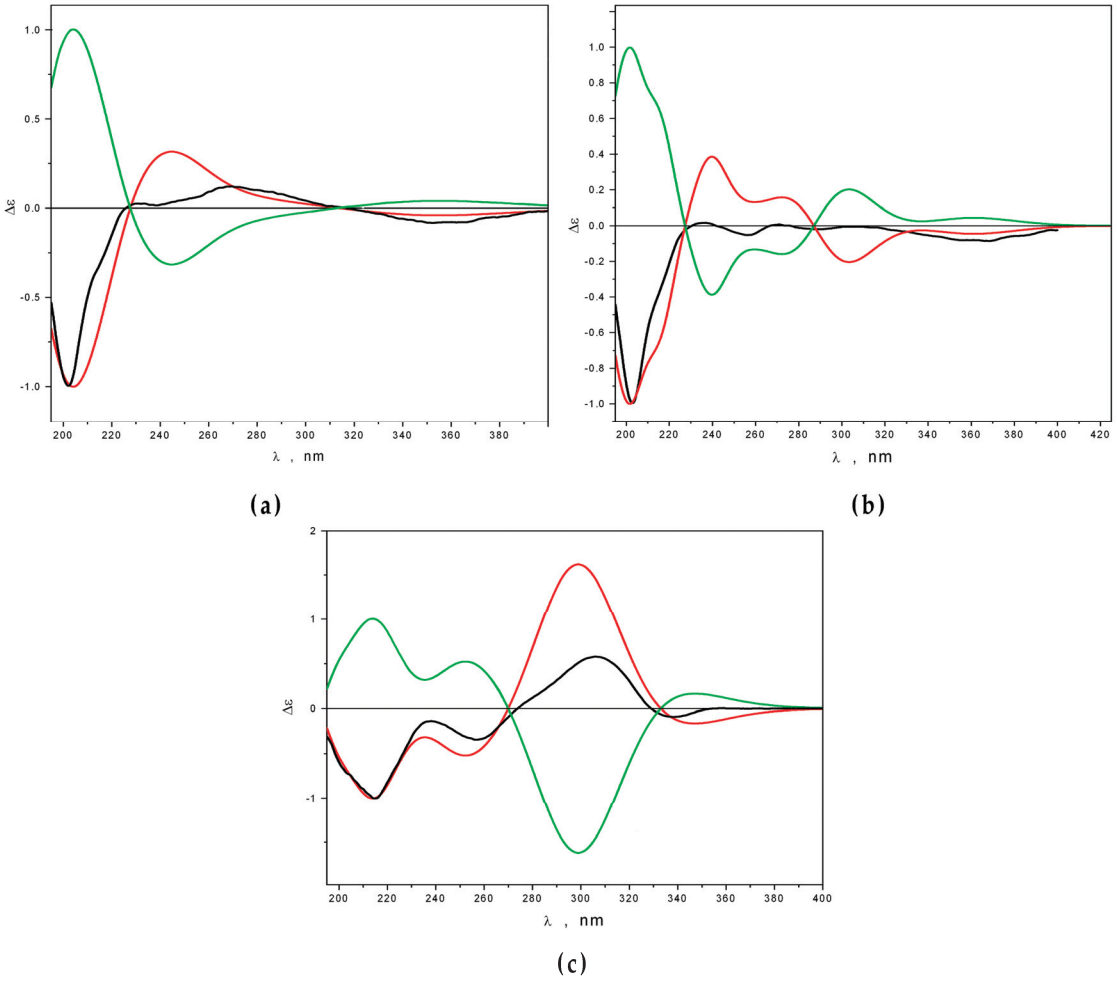

Figure 5. Calculated (red) and experimental (black) CD spectra for compounds **1** (**a**), **2** (**b**), and **3** (**c**). The green color ECD curves were calculated for enantiomers of compounds **1**–**3**.

The best agreement between $\Delta\varepsilon_{exp}$ and $\Delta\varepsilon_{calc}$ is achieved for **1**–**3** in the case of configurations 1*S*,2*S*,9*R*,13*S*, 1*S*,2*S*,3*R*,9*R*,13*S*, and 1*R*,3*S*,9*R*,13*S*,14*S*, respectively.

2.3. Bioactivity of Isolated Compounds

The effects of isolated anthraquinones on *Staphylococcus aureus* growth and the activity of its some enzymes were experimentally investigated. Moreover, the influence of antibacterial compounds on viability, migration, and proliferation of *S. aureus*-treated HaCaT keratinocytes was investigated. Compound **5** was isolated in an insufficient amount (1.0 mg) and was not investigated in any bioactivity tests. Compounds **2**, **3**, and **11** were isolated in very small amounts (0.9 mg, 1.5 mg, and 1.1 mg, respectively), so, only their influence on *S. aureus* growth was investigated.

2.3.1. Antimicrobial Activity

The antimicrobial activity of compounds **1**–**4** and **6**–**13** against *Staphylococcus aureus* is presented in Figure 6.

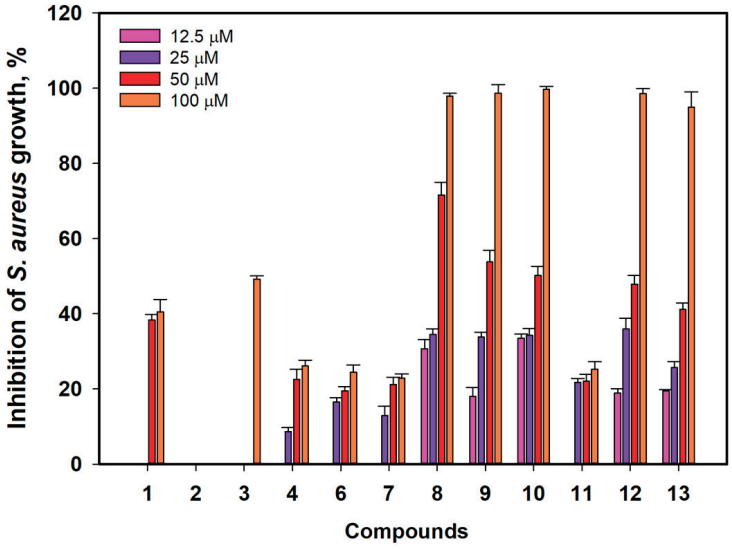

Figure 6. Antimicrobial activity against *Staphylococcus aureus* of compounds **1**–**4** and **6**–**13**. All experiments were carried out in triplicate. The data are presented as a mean ± standard error of mean (SEM).

Acruciquinone B (**2**) did not show any influence on *S. aureus* growth up to a concentration of 100 μM. Acruciquinone A (**1**) inhibited *S. aureus* growth by 38.4 ± 1.5% and 40.5 ± 3.3% at concentrations of 50 and 100 μM, respectively. Compounds **4**, **6**, **7**, and **11** showed inhibition of *S. aureus* growth near 30% at concentrations up to 100 μM.

The half-maximal concentration (IC_{50}) of antistaphylococcal action was calculated for compounds **3**, **8**–**10**, **12**, and **13** (Table 3).

Table 3. The calculated half-maximal (IC_{50}) effect of compounds on *S. aureus* growth.

Compound	3	8	9	10	12	13
IC_{50}, μM	≥100	35.4 ± 1.5	45.3 ± 3.1	49.7 ± 2.4	52.1 ± 1.3	58.2 ± 1.7

Compounds **8**-**10** showed the best effect on *S. aureus* growth, with calculated IC_{50} values of 35.4, 45.3, and 49.7 μM, respectively. Compounds **12** and **13** were less effective, with IC_{50} values of 52.1 and 58.2 μM, respectively. Acruciquinone C (**3**) had an IC_{50} near 100 μM.

Antimicrobial compounds can influence various aspects of bacterial life, including modification of environmental conditions via urease enzymes [19] or sortase A processing of the bacterial cell wall [20].

We investigated the effect of compounds **1**, **4**, **6**–**10**, **12**, and **13** on the activity of urease and sortase A from *S. aureus* in cell-free assays.

2.3.2. Influence of Some Isolated Compounds on Urease Activity

Compounds **1**, **4**, **6**–**10**, **12**, and **13** were investigated as urease inhibitors, and only dendryol B (4) did not inhibit urease activity (Figure 7). The most significant effect was observed for compounds **8**, **10**, and **13**, which, at 100 μM, decreased the urease activity by 39.2%, 38.5%, and 38.3%, respectively, and, at a concentration of 50 μM, inhibited urease activity by 15.3%, 21.9%, and 21.2%, respectively. Compounds **12** and **9**, at 50 μM, decreased the urease activity by 20.3% and 13.5% and, at 100 μM, decreased urease activity by 31.6% and 21.8%, respectively. New acruciquinone A (**1**) decreased the urease activity by 10.7%

and 14.6% at concentrations of 50 μM and 100 μM, respectively, and compounds **6** and **7** showed similar effects.

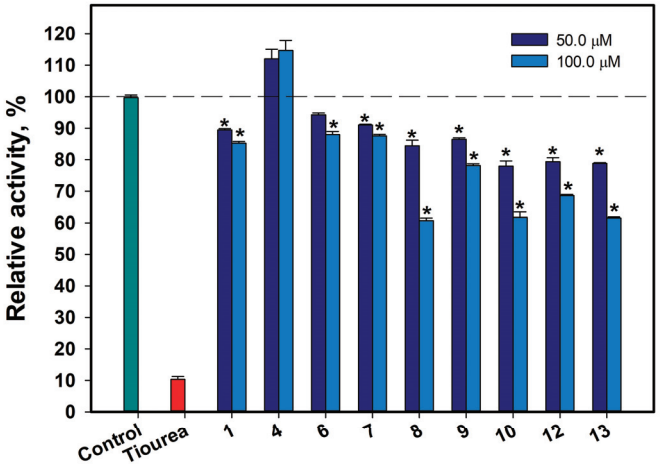

Figure 7. Effects of compounds **1**, **4**, **6**–**10**, and **12**–**13** on urease activity. Thiourea was used as a control. All experiments were carried out in triplicate. The data are presented as a mean ± standard error of mean (SEM). * Indicates significant differences between the control (DMSO) and compounds (p value ≤ 0.05).

2.3.3. Influence of Some Isolated Compounds on Sortase A Activity

The effects of the investigated compounds on sortase A activity are presented in Figure 8a. Dendryol B (**4**) showed the most significant inhibitory effect on sortase A activity. It inhibited sortase A activity at concentrations of 50 μM and 80 μM by 27.6% and 32.1%, respectively, and its effect was stable during all periods of observation (Figure 8b).

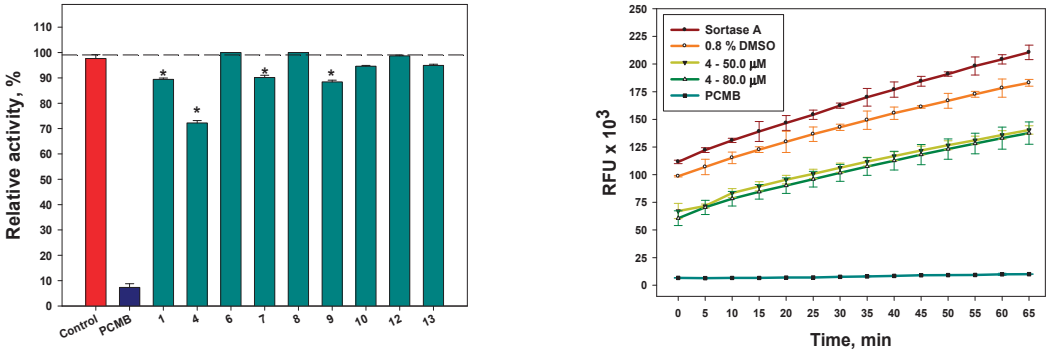

(**a**) (**b**)

Figure 8. The effects of compounds **1**, **4**, **6**–**10**, and **12**–**13** on sortase A activity after 10 min of incubation (**a**) and time-dependent graph of inhibitory effect of dendryol B (**4**) (**b**). 4-(Hydroxymercuri)benzoic acid (PCMB) was used as a control. All experiments were carried out in triplicate. The data are presented as a mean ± standard error of mean (SEM). * Indicates significant differences between the control (DMSO 0.8%) and compounds (p value ≤ 0.05).

Compounds **1**, **7**, and **9** had similar effects on sortase A activity, with significant inhibition of 14.7%, 6.3%, and 14.7%, respectively, at a concentration of 80 μM. The minimal effects of **10** and **13**, as well as those of **6** and **8**, were not statistically significant.

To detect the key structural moieties of anthraquinone derivatives for their inhibitory effect on sortase A, the molecular docking of compounds **1**, **4**, **5**, and **7–9** with sortase A was evaluated using fast online service SwissDock.

In the apo structure of sortase A (PDB ID 1T2P), a V-shaped pocket is formed by the β4, β7, and β8 strands on one side of the β barrel, together with three surrounding loops. The left side of the pocket is a hydrophobic tunnel formed by Ala92, Ala104, Ala118, Val161, Pro163, Val166, Val 168, Ile182, Val193, Trp194, Ile199, and Val201, along with two putative catalytic residues: Cys184 and Arg197 [21]. The right side of the pocket consists of several polar residues: Glu105, Asn114, Ser116, and Thr180. Earlier, the anthraquinone dimer skyrin N1287 was found as a sortase A inhibitor, and its complex with sortase A (PDB ID 1T2P) was investigated by molecular docking features. It was reported that skyrin, similar to curcumin, forms a hydrogen-bonding interaction or salt bridge with the guanidinium moiety of Arg197. N1287 and curcumin form extensive interactions with residues in the hydrophobic tunnel. In particular, the aromatic moiety from N1287 forms a cation-π interaction with Arg197. N1287 also forms hydrogen-bonding interactions with polar residues on the right side of the pocket, such as Asn114 and Ser116 [22].

In our calculations, the most active sortase A inhibitor, dendryol B (**4**), can form a pose (ΔG −6.8640547 kkal/mol) with the hydrogen-bonding interactions between Arg197 and its 9-OH, Glu105 and 3-OH, Asn114 and keto-group C-10, and Gly167 and 8-OH. Moreover, hydrophobic interactions between **4** and Val168, Ile199, and Leu169 were detected. In the other side, the stable pose (ΔG −6.800687) forms the hydrogen-binding interaction between Glu105 and 1-OH and the hydrophobic interactions between Cys184 and Me-15; Ala92 and C-7, H-7, Trp194, and Me-15; Ile182 and keto group C-10; and Ala118 and C-15 of **4**.

Acruciquinone A (**1**) can form complex ΔG −6.5611596 with hydrogen-bonding interactions between Arg197 and 2-OH of **1** and Ala92 and 1-OH, as well as with the hydrophobic interactions with Ala92, Gly192 (C-2, H-2), Ala104 (keto-group C-10), Ile182 (C-7 and H-7), Thr93 (1-OH), and Trp194 (H-1). Another pose was calculated (ΔG −6.747401) with the hydrogen-bonding interactions with Arg197 (keto-group C-10) and the hydrophobic interactions with Cys184 (Me-15), Trp194 (Me-15), Ala104 (C-5 and C-6), and Leu169 (2-OH).

Therefore, we can assume that the main differences in the structures of compounds **4** and **1** that influence their complexes with sortase A are the stereochemistry of the 9-OH group: the β orientation of 9-OH provides the opportunity to form a maximum number of interactions if both 9-OH and C(=O)-10 with sortase A (Figure 9).

Coniothyrinone B (**7**) can form complex ΔG −7.046784 with the hydrogen-bonding interactions with Arg197 and Gly192 and the hydrophobic interactions with Ile182, Trp194, Tyr187, Ala104, Gly192, and Thr93. Another complex (ΔG −6.411958) has hydrogen-bonding interactions with Glu105 and hydrophobic interactions with Cys184, Trp194, Ala92, Leu97, and Ile182.

ω-Hydroxypachybasin (**9**) can form complex ΔG −6.769604 with the hydrogen-bonding interactions with Arg197, Asn114, and Gly167 and the hydrophobic interactions with Val168, Thr180, Ile199, Val166, Val201, and Gly167. The complex consists of hydrophobic interactions with Cys184 (as well as Ala92, Trp194, Thr93, and Ala104), whereas ΔG -6.2245307 does not have hydrogen-bonding interactions.

Rubrumol (**8**), which did not inhibit sortase A activity, can form complex ΔG −6.9308696 with the hydrogen-bonding interactions with Ala92 and the hydrophobic interactions with Cys184, Ala92, Trp194, and Ile182. Another complex (ΔG −6.237157) has hydrogen-bonding interactions with Glu105 and Ala92 and hydrophobic interactions with Cys184, Ala92, and Ile182.

Therefore, compounds **1**, **4**, **7**, and **9**, which inhibited the activity of sortase A in a SensoLyte 520 Sortase A Activity Assay, may form the interactions with Arg197. No poses with the interactions with Arg197 were predicted for compound **8**. This observation confirms the conclusion about the significance of building with Arg197 for inhibition of sortase A′ activity by anthraquinones.

Pleosporone (**5**), which was not investigated in a SensoLyte 520 Sortase A Activity Assay, can form complex ΔG −6.9511595 with the hydrogen-bonding interactions with Arg197 (keto-group C-9), Asn114 (keto-group C-10), and Gly167 (8-OH) and the hydrophobic interactions with Val 166 (H-7), Val168 (aromatic ring A, C-9, C-10), Val201 (Me-15), Ile199 (C-6, C-7), Thr180 (C-5, C-10, C-11), and Gly167 (8-OH). Another calculated complex (ΔG −6.2182164) has hydrogen-bonding interactions with Ala92 (1-OH, 2-OH) and hydrophobic interactions with Cys184 (3-OH), Ile182 (3-OH, H-4b, C-4), Ala92 (1-OH), and Trp194 (2-OH).

A comparison of these poses with complexes of **4** allows us to assume that pleosporone (**5**) may also act as an inhibitor of sortase A activity.

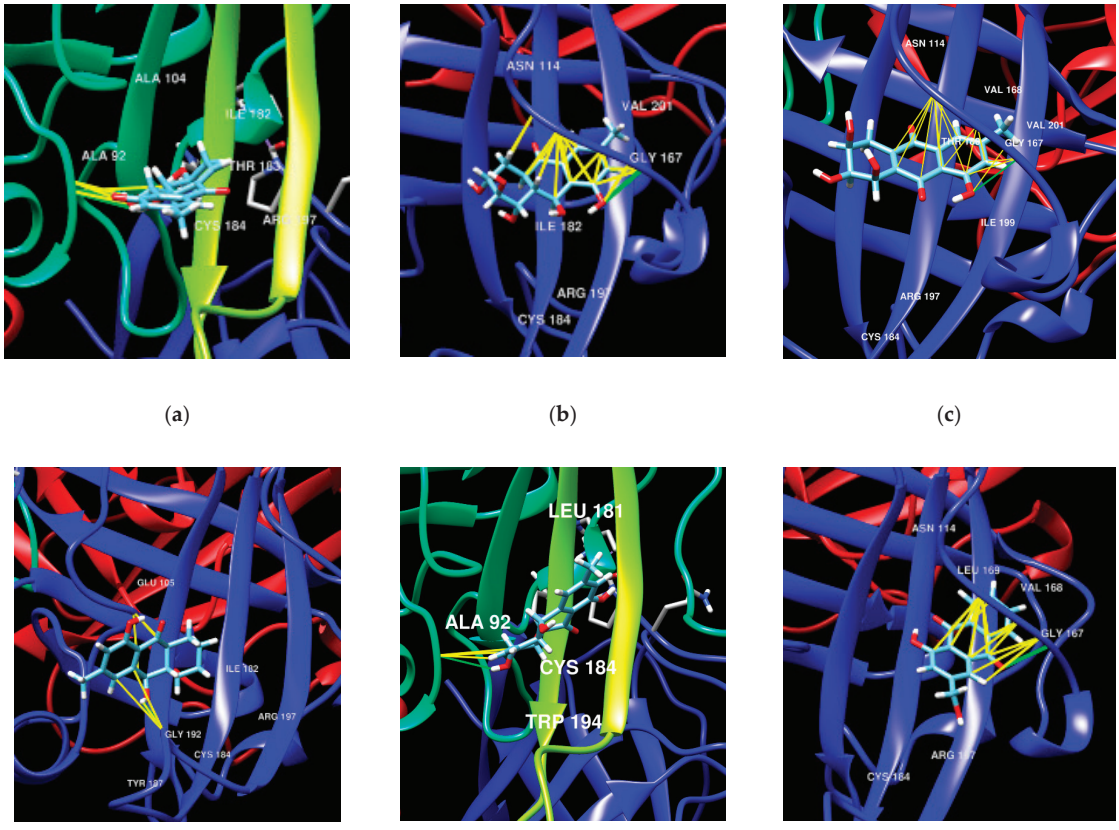

(**a**) (**b**) (**c**)

(**d**) (**e**) (**f**)

Figure 9. Figure 9. The molecular docking poses of some anthraquinones with sortase A (PDB ID 1T2P): **1** (**a**), **4** (**b**), **5** (**c**), **7** (**d**), **8** (**e**), and **9** (**f**).

2.3.4. Effects of Compounds on HaCaT Keratinocytes Infected with *Staphylococcus aureus*

Thus, the investigated secondary metabolites of *Asteromyces cruciatus* KMM4696 fungus can inhibit sortase A, especially urease enzyme activities, and affect *S. aureus* growth. However, it is advisable to study the effects of these anthraquinone derivatives in a co-culture of *S. aureus* with human cells before confidently talking about their real antibacterial potential. Therefore, the protective influence of compounds **1**, **4**, **7**, and **9** at a concentration of 10 μM on human HaCaT keratinocyte cells infected with *S. aureus* was experimentally investigated. Compound **6** did not show a significant effect on sortase A activity and had

a small influence on urease activity and *S. aureus* growth; therefore, it was selected for in vitro investigation for comparison of its effect with that of **7**.

S. aureus produces a number of lysing molecules causing the disruption of mammalian cells, so the release of lactate dehydrogenase (LDH) is used for detection of infected cell viability [23]. The effect of compounds **1**, **4**, **6**–**10**, **12**, and **13** on the LDH release from *S. aureus*-infected HaCaT cells is presented in Figure 10.

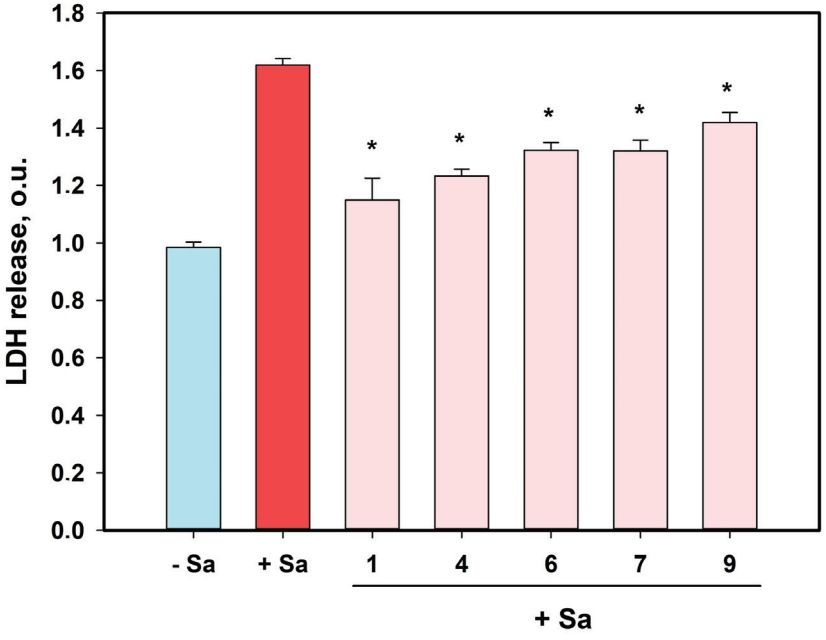

Figure 10. The effects of compounds **1**, **4**, **6**, **7**, and **9** on LDH release from HaCaT cells after infection with *S. aureus* (Sa) for 48 h. All compounds were used at a concentration of 10 μM. The experiments were carried out in triplicate. * Indicates statistically significant differences between S. aureus-infected cells and *S. aureus*-infected cells treated with compounds ($p < 0.05$).

The incubation of HaCaT cells with *S. aureus* induced an increase in LDH release of 64.4%. All compounds investigated at a concentration of 10 μM showed significant effects on LDH release from staphylococci-infected HaCaT cells. After 48 h of coincubation, compounds **1**, **4**, **6**, **7**, and **9** caused statistically significant diminishments in LDH release from these cells of 29.4%, 23.8%, 18.3%, 18.4%, and 12.3%, respectively.

The effects of compounds **1**, **4**, **6**, **7**, and **9** on the proliferation of *S. aureus*-infected HaCaT cells were investigated using CFDA SE vital fluorescent dye and the flow cytometry technique described in [24]. The CFDA SE covalent builds with intracellular cytoplasm components, and its quantity (and intensity of fluorescence, respectively) in the cell decreases equivalent to the number of past divisions.

The analysis of obtained flow cytometry data resulted in the detection of four HaCaT cell subpopulations (Figure 11a), and *S. aureus* infection significantly changed the ratio between them (Figure 11b). The percentage of each subpopulation is presented in Table 4.

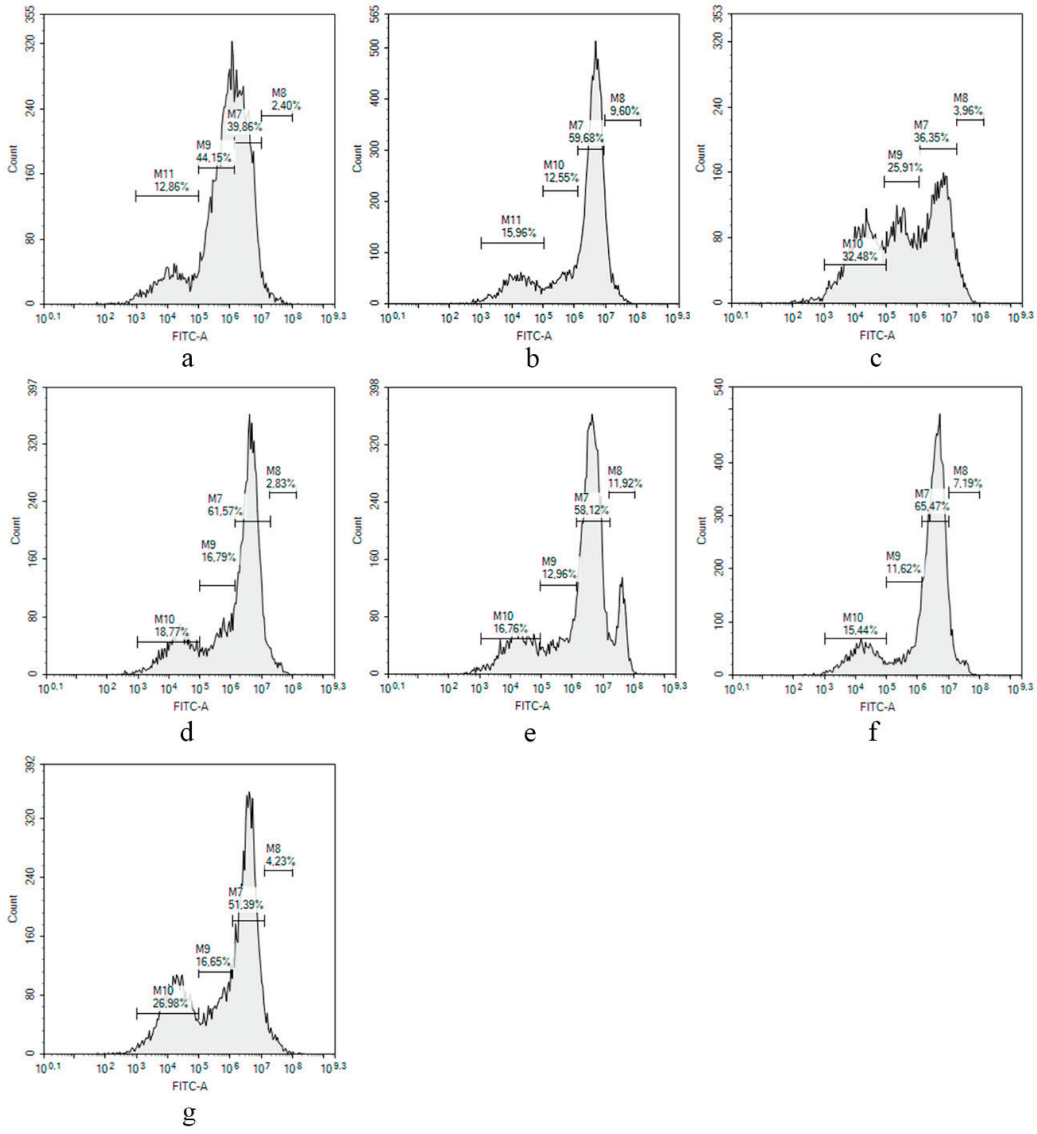

Figure 11. The proliferative profiles of non-treated HaCaT cells (**a**), *S. aureus*-infected HaCaT cells (**b**), and infected cells treated with compounds **1** (**c**), **4** (**d**), **6** (**e**), **7** (**f**), and **9** (**g**). All compounds were used at a concentration of 10 μM. The experiments were carried out in triplicate. The most representative picture for each case is presented.

The most noticeable change as a result of a staphylococcal infection was a change in the ratio between division 1 and division 2, which indicates a slowdown in HaCaT proliferation. Compounds **4**, **6**, and **7** did not show any observed changes in the picture (Figure 11d–f). Compound **9** induced a significant decrease in the amount of the cells in division 1 and an increase in the amount of cells in division 3. The most significant influence on infected HaCaT cells was observed for compound **1** (Figure 11c), which greatly increased the number of the cells in division 3 in comparison with infected and non-infected HaCaT cells.

Table 4. The effects of compounds on proliferation of *S. aureus*-infected HaCaT cells.

Sample [1]	Division 0, % of Total Amount	Division 1, % of Total Amount	Division 2, % of Total Amount	Division 3, % of Total Amount
HaCaT cells	3.0 ± 0.8	37.7 ± 3.0	43.2 ± 1.4	15.5 ± 3.7
S. aureus	8.7 ± 1.2	58.2 ± 2.0	16.8 ± 6.0	14.9 ± 1.5
1	3.6 ± 0.5	34.0 ± 3.3	25.9 ± 0.4	35.5 ± 4.2
4	3.1 ± 0.4	63.2 ± 2.3	15.4 ± 1.9	17.6 ± 1.7
6	8.6 ± 4.7	60.5 ± 3.4	12.1 ± 1.2	18.1 ± 2.0
7	7.2 ± 2.1	65.5 ± 6.4	11.6 ± 1.3	15.4 ± 5.6
9	3.4 ± 1.2	46.3 ± 7.2	18.3 ± 6.5	30.2 ± 4.5

[1] All compounds were used at a concentration of 10 μM. The experiments were carried out in triplicate, and the percentage of each HaCaT cell subpopulation is presented as mean ± standard error of mean.

Finally, the effects of compounds **1**, **4**, **6**, **7**, and **9** on the migration of *S. aureus*-infected HaCaT cells were investigated (Figure 12). Manufacturing devices from Ibidi®were used for the creation of a cell-free zone in a monolayer of HaCaT cells stained with CFDA SE fluorescent dye, after which the *S. aureus* suspension and compounds were added and the cell migration to this cell-free zone was monitored by a fluorescent microscope for 24 h.

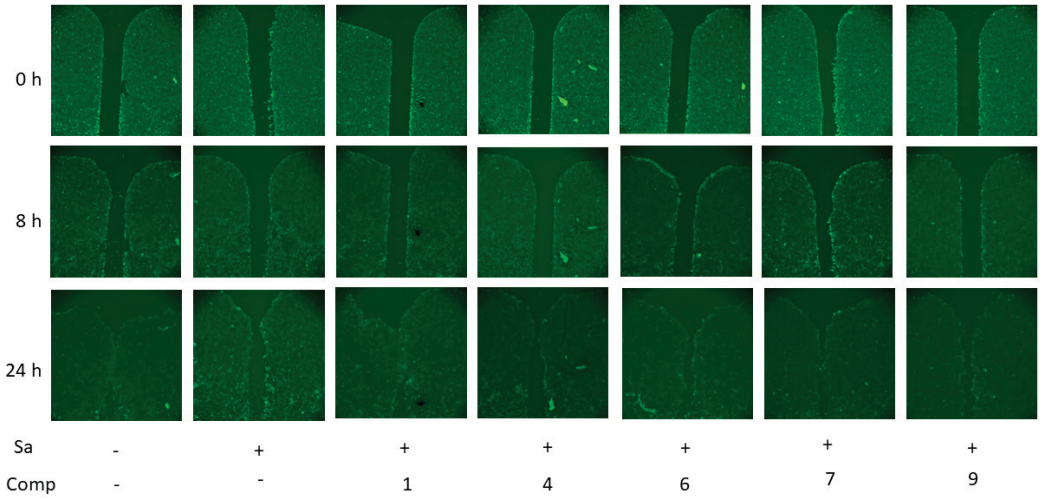

Figure 12. The effects of compounds **1**, **4**, **6**, **7**, and **9** on migration of *S. aureus* (Sa)-infected HaCaT cells. All compounds were used at a concentration of 10 μM. The experiments were carried out in triplicate. The most representative picture for each case is presented.

The first differences in cell position were detected after 8 h of observation, and full fusion of the cell-free zone in the non-infected cell layer was observed after 24 h. *S. aureus* infection inhibits fusion of this cell-free area, which was observed after 24 h. All investigated compounds improved migration of the *S. aureus*-infected cells in a cell-free zone. Complete confluence, similar to control cells, was observed for compound **1**, and compounds **6**, **9**, and especially **7** caused almost complete cell overgrowth of the cell-free zone. Compound **4** surprisingly showed the most incomplete fusion of the cell-free zone, but its positive effect was noticeable.

3. Discussion

3.1. Secondary Metabolites of Asteromyces cruciatus KMM4696

A biogenesis pathway for the framework of the novel acruciquinone C (**3**) has been proposed (Figure 13). It is obvious that the first steps of acruciquinone C biosynthesis are common to most fungal anthraquinones originating from the octaketide precursor [25]. The dehydration and tautomerization of intermediate *i2* result in anthrone *i3*, which is a plausible direct precursor of compounds **4**, **5**, and **7**–**9**. *i3* can also be sequentially oxidized and reduced to *i4*, from which compounds **1**, **2**, and **6** are most likely formed. Moreover, *i4* probably undergoes several reductions and tautomerizations, which, via diketone *i5*, lead to intermediate *i6* with monoene ring C [26]. Further oxidative cleavage of the double bond and tautomerization lead to *i7*, which, as a result of aldol condensation, turns into a direct precursor of acruciquinone C (**3**) with a 6/6/5 skeleton. Compound 3 is formed as a result of the reduction of aldehyde in *i8*.

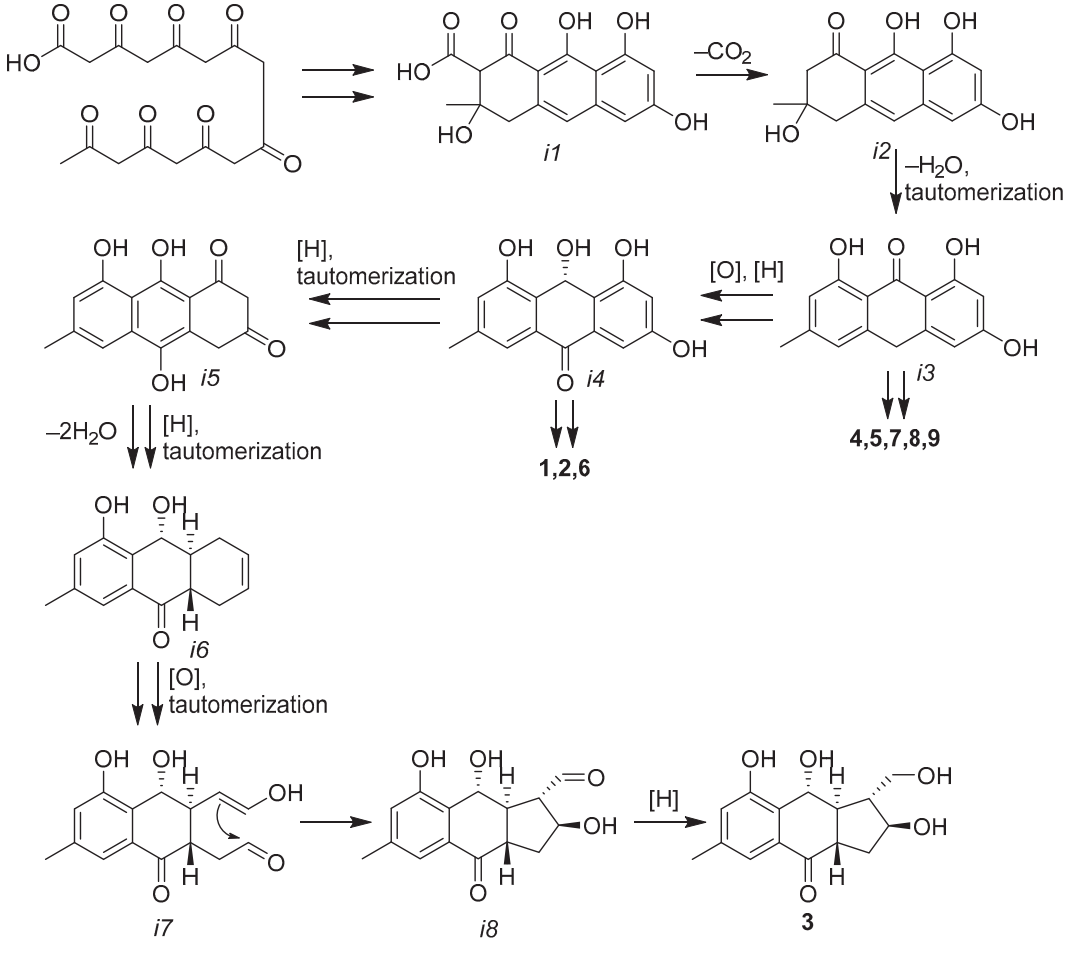

Figure 13. Plausible biogenetic pathway of acruciquinone C (**3**).

Naphthalene derivative 12 was previously reported only as a synthetic compound [16]. This compound is undoubtedly a cyclization product of the linear hexaketide precursor.

Gliovictin (**13**), a diketopiperazine isolated from terrestrial fungi of the genera *Helminthosporium* and *Penicillium*, has been isolated from culture broths of the marine deuteromycete *Asteromyces cruciatus* [17].

It was previously shown that strain *A. cruciatus* KMM 4696 can produce the first chlorine-contained monocyclic cyclohexanols containing a 3-methylbutenynyl unit that obviously originated from a tetraketide precursor [7]. Benzopyranes **10** and **11** obviously originated from the same precursor. Thus, the *A. cruciatus* KMM 4696 fungal strain is a promising producer of structurally unique polyketides.

3.2. Biological Activity of Isolated Anthraquinone Derivatives

In our work, known dendryol B (**4**), rubrumol (**8**), trans-3,4-dihydroxy-3,4-dihydroanofinic acid (**10**), quadricinctapyran A (**11**), and gliovictin (**13**) were found as agents against *S. aureus* for the first time.

Dendryol B (**4**) was previously isolated from a weed pathogenic fungus, *Dendryphiella* sp., and caused necrotic events on barnyardgrass leaves [8]. Rubrumol (**8**) was assessed for cytotoxic activities against A549, MDA-MB-231, PANC-1, and HepG2 human cancer cell lines but displayed no significant cytotoxic activities. However, the authors showed the significant effect of **8** on the relaxation activity of topoisomerase I [11]. *Trans*-3,4-dihydroxy-3,4-dihydroanofinic acid (**10**) exhibited potent acetylcholinesterase-inhibitory activity [27]. The antimicrobial activity for quadricinctapyran A (**11**), which was not previously detected up to a concentration of 256 μg/mL [15], but the inhibition of *S. aureus* bacterial growth in microplates was estimated by visual observation only. The activity of gliovictin (**13**) against *Escherichia coli* and *Bacillus megaterium* was not observed [28], but it was tested in agar diffusion assays, which are subject to some limitations. In the present work, the antistaphylococcal activity of the compounds was tested using liquid broth titration with spectrophotometric detection, which can be crucial for detection of the effects of compounds.

Coniothyrinone D (**6**) and coniothyrinone B (**7**) were previously isolated from the culture of an endophytic fungus. *Coniothyrium* sp. They were studied as antimicrobials by the diffusion agar method and, their effects against Gram-positive *B. megaterium* were greater than their effects against Gram-negative *E. coli* [10]. The hydroxylated derivatives of coniothyrinone B (**7**), 8-hydroxyconiothyrinone B, 8,11-dihydroxyconiothyrinone B, 4R,8-dihydroxyconiothyrinone B, and 4S,8-dihydroxyconiothyrinone B, from marine algicolous fungus *Talaromyces islandicus* EN-501 showed pronounced activity against *S. aureus* EMBLC-2 growth [29]. Antistaphylococcal activity of ω-hydroxypachybasin (**9**) was reported when this compound was isolated from the plant *Ceratotheca triloba* [30].

In our work, we not only studied the influence of coniothyrinones B (**6**) and D (**7**) and ω-hydroxypachybasin (**9**) on *S. aureus* growth in detail but also their effects on sortase A and urease activity, as well as their potential for skin infection treatment for the first time.

3.3. Perspectives of Isolated Anthraquinones for the Treatment of Skin Infections

HaCaT keratinocytes cocultured with *S. aureus* are widely used in vitro models for antibiotic discovery, despite some limitations [23]. Our previously reported results showed that *S. aureus* infection caused HaCaT keratinocyte damage and cell cycle arrest in the G0/G1 phase [31] and resulted in inhibition of cell proliferation and migration, as observed in this work. The studied anthraquinones protect HaCaT cells from *S. aureus*-caused damage because a decrease in the LDH release from treated cells was detected. Moreover, one of the significant anthraquinones changes the proliferation profile and migration of *S. aureus*-infected HaCaT cells.

The various aspects of bacteria's vital activity are the targets for antibiotics. Bactericidal antibiotics were targeted at a diverse set of biomolecules for inhibition to achieve cell death, including DNA topoisomerases (quinolones ciprofloxacin, levofloxacin, and gemifloxacin), RNA polymerase (rifamycin), penicillin-binding proteins, transglycosylases and peptidoglycan building blocks (*β*-lactam penicillins, carbapenems, cephalosporins,

glycopeptides, vancomycin, fosfomycin, and daptomycin), and ribosomes (macrolides, lincosamides, streptogramins, and others) [32]. But these strategies have led to the emergence of resistant bacterial strains, which has become one of the major global public health problems [33].

Therefore, new strategies including inhibition of bacterial sortase A or urease activities have led to the discovery of new drugs to which developing resistance will be less possible. The sortase A enzyme was named an "ideal target" for the development of new anti-infective drugs [34] because it plays a significant role in the pathogenesis of Gram-positive bacteria. Sortase A is a bacterial cell membrane enzyme that anchors crucial virulence factors to the cell wall surface [35], and numerous studies have aimed to find new sortase A inhibitors [22,36]. The urease enzyme is able to do so by virtue of its ability to catalyze the conversion of urea into ammonia, thereby allowing bacterial colonies to live in acidic conditions. To date, according to Hameed and coauthors, only one commercial urease inhibitor, Lithostat (acetohydroxamic acid), is available, but it has a number of limitations [37]. Currently, urease inhibitors are considered mainly as potential leaders in urinary tract infections. However, a number of works indicate the promise of this approach for skin staphylococcal infections [19].

Our data point to the great importance of the structure of anthraquinones for the inhibition of sortase A activity. β-Orientation of the 9-OH group in the structure of dendryol B (**4**) makes its interaction with residues in the binding site the most effective.

In the case of urease inhibition, the differences between the action of all the studied anthraquinones are insignificant, which does not allow us to discuss their structure–activity relationship. The highest activity was found for an alkaloid, i.e., gliovictin (**13**). Recently, a large number of sulfur- and nitrogen-containing compounds have been described as urease inhibitors [38]. Obviously, it is precisely the thiodiketopiperazine moiety of gliovictin that makes it interesting for further study against *Helicobacter pylori* and other urease-producing bacteria.

However, the effect on bacterial growth or enzyme activities does not yet mean that substances will be active in real infections, since an infection model is a more complex and multicomponent system. In this regard, the study of the effects of promising compounds in in vitro infection models can lead to unexpected results, as we see here. In our experiments, dendryol B (**4**) exhibited the greatest inhibition of sortase A activity, with a weak effect on *S. aureus* growth, but its effects in coculture experiments were not so great. In contrast, acruciquinone A (**1**) showed a weak (yet noticeable) inhibition of sortase A and urease activity and a moderate effect on *S. aureus*, but this new metabolite from *Asteromyces cruciatus* was the most effective against *S. aureus*-caused HaCaT cell damage and in a skin wound model. ω-Hydroxypachybasin (**9**) exhibited the most significant effect against *S. aureus* growth and a weak inhibition of urease and sortase A activities but showed the least pronounced protection against HaCaT damage, as well as coniothyrinones D (**6**) and B (**7**).

Thus, the protection of *S. aureus*-infected HaCaT keratinocytes by acruciciquinone A (**1**) is due to both its direct antibacterial action and the effect on the keratinocytes themselves.

4. Materials and Methods

4.1. General Experimental Procedures

Optical rotations were measured on a Perkin-Elmer 343 polarimeter (Perkin Elmer, Waltham, MA, USA). UV spectra were recorded on a Shimadzu UV-1601PC spectrometer (Shimadzu Corporation, Kyoto, Japan) in methanol. CD spectra were measured with a Chirascan-Plus CD spectrometer (Leatherhead, UK) in methanol. NMR spectra were recorded in $CDCl_3$, acetone-d_6, and DMSO-d_6 on a Bruker DPX-300 (Bruker BioSpin GmbH, Rheinstetten, Germany), a Bruker Avance III-500 (Bruker BioSpin GmbH, Rheinstetten, Germany), and a Bruker Avance III-700 (Bruker BioSpin GmbH, Rheinstetten, Germany) spectrometer. A calibration of NMR spectra was carried out using the residual solvent signals (7.26/77.16 for $CDCl_3$ and 2.05/29.84 for acetone-d_6 according to [39]). HRESIMS spectra were measured on a Maxis impact mass spectrometer (Bruker Daltonics GmbH,

Rheinstetten, Germany). Microscopic examination and photography of fungal cultures were performed with an Olympus CX41 microscope equipped with an Olympus SC30 digital camera. Detailed examination of the ornamentation of the fungal conidia was performed using an EVO 40 scanning electron microscope (SEM).

Low-pressure liquid column chromatography was performed using silica gel (50/100 μm, Imid Ltd., Krasnodar, Russia) and Gel ODS-A (12 nm, S—75 um, YMC Co., Ishikawa, Japan). Plates precoated with silica gel (5–17 μm, 4.5 cm × 6.0 cm, Imid Ltd., Russia) and silica gel 60 RP-18 $F_{254}S$ (20 cm × 20 cm, Merck KGaA, Darmstadt, Germany) were used for thin-layer chromatography. Preparative HPLC was carried out on an Agilent 1100 chromatograph (Agilent Technologies, Santa Clara, CA, USA) with an Agilent 1100 refractometer (Agilent Technologies, Santa Clara, CA, USA) and a Shimadzu LC-20 chromatograph (Shimadzu USA Manufacturing, Canby, OR, USA) with a Shimadzu RID-20A refractometer (Shimadzu Corporation, Kyoto, Japan) using YMC ODS-AM (YMC Co., Ishikawa, Japan) (5 μm, 10 mm × 250 mm), YMC ODS-AM (YMC Co., Ishikawa, Japan) (5 μm, 4.6 mm × 250 mm), and Fusion Hydro-RP (Phenomenex, Torrance, CA, USA) (4 μm, 250 mm × 10 mm) columns.

4.2. Fungal Strain

The strain of the obligate marine fungus *Asteromyces cruciatus* KMM 4696 was isolated from the surface of the thallus of the brown alga *Sargassum pallidum* (Sea of Japan) and identified using morphological and molecular genetic features [7]. The fungal strain is stored in the Collection of Marine Microorganisms (KMM) of PIBOC FEB RAS (Vladivostok, Russia).

4.3. Cultivation of Fungus

A. cruciatus fungus was cultured on a rice medium at 22 °C for three weeks in 100 Erlenmeyer flasks (500 mL), each containing 20 g of rice, 20 mg of yeast extract, 10 mg of KH2PO4, and 40 mL of natural seawater from the Marine Experimental Station of PIBOC FEB RAS, Troitsa (Trinity) Bay, Sea of Japan.

4.4. Extraction and Isolation

At the end of the incubation period, the mycelium of the *Asteromyces cruciatus* KMM 4696 fungus, together with the medium, was homogenized and extracted with EtOAc (2 L). The obtained extract was concentrated to dryness. The dry residue (7.9 g) was dissolved in a $H_2O-EtOH$ (4:1) system (200 mL) and extracted successively with *n*-hexane (3 × 0.2 L) and EtOAc (3 × 0.2 L). The ethyl acetate extract was evaporated to dryness (5.3 g) and chromatographed on a silica gel column (3 × 14 cm), which was first eluted with *n*-hexane (200 mL), then with a stepwise gradient of 5% to 50% EtOAc in *n*-hexane (total volume 20 L). Fractions of 250 ml were collected and combined based on TLC data.

The fractions eluted with *n*-hexane-EtOAc (95:5, 80 mg) and *n*-hexane-EtOAc (90:10, 200 mg) were combined and separated on a YMC ODS-A reverse-phase column (1.5 × 5.5 cm), which was eluted with a step gradient from 40% to 80% MeOH in H_2O (total volume: 1 L) to afford subfractions I and II. Subfraction I (40% MeOH, 146 mg) was separated by reverse-phase HPLC on a YMC ODS-A column, eluting first with MeOH–H_2O (90:10) to afford two subfractions: I-1 and I-2. Subfraction I-1 was rechromatographed on a YMC ODS-A column eluting with MeOH–H_2O (55:45) to **13** (4.8 mg). Subfraction I-2 was rechromatographed on an Ultrasfera Si column eluting with *n*-hexane–ethyl acetate (60:40) to **11** (1.1 mg). Subfraction II (60% MeOH, 110 mg) was separated by reverse-phase HPLC on a YMC ODS-AM column eluting with MeOH–H_2O (80:20), then with MeOH–H_2O (55:45) to **9** (4 mg) and **12** (21.6 mg).

The fraction of *n*-hexane-EtOAc (80:20, 470 mg) was separated on a Gel ODS-A column (1.5 × 5.5 cm), which was eluted with a step gradient from 40% to 80% MeOH in H_2O (total volume 1 L) to afford subfraction III. Subfraction III (40% MeOH, 250 mg) was separated by reverse-phase HPLC on a YMC ODS-A column, eluting with MeOH–H_2O (90:10), then

with MeOH–H_2O (60:40) and MeCN–H_2O (60:40) to **1** (4.8 mg), **5** (1.0 mg), **8** (2.2 mg), and **10** (6.4 mg).

The *n*-hexane-EtOAc fraction (70:30, 580 mg) was separated on a column with a reverse-phase sorbent YMC ODS-A (1.5 × 5.5 cm), which was eluted with a step gradient from 40% to 100% MeOH in H_2O (total volume 1 L) to subfractions IV and V. Subfraction IV (40% MeOH, 390 mg) was separated by reverse-phase HPLC on a YMC ODS-A column eluting with MeOH–H_2O (95:5), then with MeOH–H_2O (70:30) to afford compounds **3** (1.5 mg), **6** (4.6 mg), and **7** (3 mg). Subfraction V (100% MeOH, 40 mg) was separated by reverse-phase HPLC on a YMC ODS-A column eluting with MeOH-H_2O (55:45), then with CH_3CN-H_2O (25:75) to **2** (0.9 mg) and **4** (2.7 mg).

4.5. Spectral Data

Acruciquinone A (**1**): amorphous solids; $[\alpha]_D^{20}$ −92.0 (*c* 0.1 MeOH); UV (MeOH) λ_{max} (log ε) 335 (3.14), 285 (3.88), 198 (4.24) nm (see Supplementary Figure S1); CD (*c* 9.6 × 10^{-4}, MeOH), λ_{max} ($\Delta\varepsilon$) 202 (−16.07), 232 (0.35), 269 (1.94), 351 (−1.30) nm (see Supplementary Figure S2); for ^{1}H and ^{13}C NMR data, see Table 1 and Supplementary Figures S7–S12; HRESIMS *m*/*z* 275.0914 $[M - H]^-$ (calcd. for $C_{15}H_{15}O_5$, 275.0925), 299.0887 $[M + Na]^+$ (calcd. for $C_{15}H_{16}O_5Na$, 299.0890) (see Figure S87).

Acruciquinone B (**2**): amorphous solids; $[\alpha]_D^{20}$ −121.4 (*c* 0.07 MeOH); UV (MeOH) λ_{max} (log ε) 334 ( ), 283 (3.76), 198 (4.09) nm (see Supplementary Figure S3); CD (*c* 9.6 × 10^{-4}, MeOH), λ_{max} ($\Delta\varepsilon$) 203 (−10.73), 256 (−0.56), 288 (−0.21), 366 (−0.91) nm (see Supplementary Figure S4); for ^{1}H and ^{13}C NMR data, see Table 1 and Supplementary Figures S13–S18; HRESIMS *m*/*z* 291.0882 $[M - H]^-$ (calcd. for $C_{15}H_{15}O_6$, 291.0874), 315.0830 $[M + Na]^+$ (calcd. for $C_{15}H_{16}O_6Na$, 315.0839) (see Figure S88).

Acruciquinone C (**3**): amorphous solids; $[\alpha]_D^{20}$ −58.0 (*c* 0.10 MeOH); UV (MeOH) λ_{max} (log ε) 315 (3.55), 261 (3.86), 213 (4.96) nm (see Supplementary Figure S5); CD (*c* 9.6 × 10^{-4}, MeOH), λ_{max} ($\Delta\varepsilon$) 215 (−10.42), 257 (−3.62), 306 (6.04), 339 (−0.95) nm (see Supplementary Figure S6); for ^{1}H and ^{13}C NMR data, see Table 2 and Supplementary Figures S19–S24; HRESIMS *m*/*z* 277.1087 $[M - H]^-$ (calcd. for $C_{15}H_{17}O_5$, 277.1081), 301.1042 $[M + Na]^+$ (calcd. for $C_{15}H_{18}O_5Na$, 301.1046) (see Figure S89).

4.6. Quantum Chemical Calculations

The quantum chemical calculations for compounds **1**–**3** in methanol were performed using exchange–correlation functional B3LYP, the polarization continuum model (PCM), and the cc-pvTz basis set implemented in the Gaussian 16 package of programs [18]. Conformations with relative Gibbs free energies in the range of $\Delta G_{im} \leq 5$ kcal/mol were chosen for calculations of the UV and ECD spectra at the B3LYP/cc-pvTz_PCM//B3LYP/cc-pvTz_PCM level of theory. The statistical weights of conformations are:

$$g_{im} = e^{-\frac{\Delta G_{im}}{RT}} \Big/ \sum_i e^{-\frac{\Delta G_{im}}{RT}}$$

where T = 298.15 K, and the subscript "m" denotes conformation, for which G is minimal.

Each individual transition from electronic ground state to the i-th calculated excited electronic state ($1 \leq i \leq 55$) was simulated as a Gauss-type function. The bandwidths taken at 1/e peak heights were chosen to be σ = 0.34 eV for **1** and **3** and 0.24 eV for **2**. The UV shifts taken for simulations of spectra are $\Delta\lambda$ = 0 nm for **1** and **2** and $\Delta\lambda$ = −7 nm for **3**.

The scaled theoretical and experimental ECD spectra were obtained according to the following equation:

$$\Delta\varepsilon_{scaled}(\lambda) = \Delta\varepsilon(\lambda) \Big/ \left|\Delta\varepsilon\left(\lambda_{peak}\right)\right|$$

where the denominator ($|\Delta\varepsilon(\lambda_{peak})|$) is a modulo of the peak value for the chosen characteristic negative band in corresponding ECD spectra ($200 \leq \lambda_{peak} \leq 220$ nm).

4.7. Sortase A Activity Inhibition Assay

The enzymatic activity of sortase A from *Staphylococcus aureus* was determined using a SensoLyte 520 Sortase A Activity Assay Kit * Fluorimetric * (AnaSpec AS-72229, AnaSpec, San Jose, CA, USA) in accordance with the manufacturer's instructions. The compounds were dissolved in DMSO and diluted with reaction buffer to obtain a final concentration of 0.8% DMSO, which did not affect enzyme activity. DMSO at a concentration of 0.8% was used as a control. 4-(Hydroxymercuri)benzoic acid (PCMB) was used as sortase A enzyme activity inhibitor. Fluorescence was measured with a PHERAStar FS plate reader (BMG Labtech, Offenburg, Germany) for 60 min, with a time interval of 5 min. The data were processed with MARS Data Analysis v. 3.01R2 (BMG Labtech, Offenburg, Germany). The results are presented as relative fluorescent units (RFUs) and percentage of the control data and were calculated using STATISTICA 10.0 software.

4.8. Urease Inhibition Assay

A reaction mixture consisting of 25 μL enzyme solution (urease from *Canavalia ensiformis*, Sigma, 1U final concentration) and 5 μL of test compounds dissolved in water (10–300.0 μM final concentration) was preincubated at 37 °C for 60 min in 96-well plates. Then, 55 μL of phosphate buffer solution with 100 μM urea was added to each well and incubated at 37 °C for 10 min. The urease-inhibitory activity was estimated by determining ammonia production using the indophenol method. Briefly, 45 μL of phenol reagent (1% *w*/*v* phenol and 0.005% *w*/*v* sodium nitroprusside) and 70 μL of alkali reagent (0.5% *w*/*v* NaOH and 0.1% active chloride NaClO) were added to each well. The absorbance was measured after 50 min at 630 nm using a MultiskanFS microplate reader (Thermo Scientific Inc., Beverly, MA, USA). All reactions were performed in triplicate in a final volume of 200 μL. The pH was maintained at 7.3–7.5 in all assays. DMSO 5% was used as a positive control.

4.9. Antimicrobial Activity

The bacterial culture of *Staphylococcus aureus* ATCC 21027 (Collection of Marine Microorganisms PIBOC FEBRAS) was cultured in a Petri dish at 37 °C for 24 h on solid Mueller Hinton broth medium with agar (16.0 g/L).

The assays were performed in 96-well microplates in appropriate Mueller Hinton broth. Each well contained 90 μL of bacterial suspension (10^9 CFU/mL). Then, 10 μL of a compound diluted at concentrations from 1.5 μM to 100.0 μM using twofold dilution was added (DMSO concentration < 1%). Culture plates were incubated overnight at 37 °C, and the OD_{620} was measured using a MultiskanFS spectrophotometer (Thermo Scientific Inc., Beverly, MA, USA). Gentamicin was used as a positive control at a concentration of 1 mg/mL, and 1% DMSO solution in PBS was used as a negative control. The results were calculated as a percentage of the control data by SigmaPlot 14.0 software.

4.10. Cell Line and Culture Conditions

The human HaCaT keratinocyte cell line was kindly provided by Prof. N. Fusenig (Cancer Research Centre, Heidelberg, Germany). All cells had a passage number ≤ 30. The cells were incubated in humidified 5% CO_2 at 37 °C in DMEM medium (BioloT, St. Petersburg, Russia) containing 10% FBS and 1% penicillin/streptomycin (BioloT, St. Petersburg, Russia).

4.11. Cocultivation of HaCaT Cells with S. aureus and Lactate Dehydrigenase Release Test

HaCaT cells at a concentration of 1.5×10^4 cells per well were seeded in 96-well plates for 24 h. Then, a culture medium in each well was changed with *S. aureus* suspension (10^2 CFU/mL) in full DMEM medium. Fresh DMEM medium without *S. aureus* suspension was added to other wells as needed. The compounds at a concentration of 10 μM were added to wells after 1 h, and HaCaT cells and *S. aureus* were cultured at 37 °C in a humidified atmosphere with 5% (*v*/*v*) CO_2 for 48 h.

After incubation, the plate was centrifuged at 250× *g* for 10 min, and 50 µL of supernatant from each well was transferred into the corresponding wells of an optically clear 96-well plate. An equal volume of the reaction mixture (50 µL) from an LDH Cytotoxicity Assay Kit (Abcam, Cambridge, UK) was added to each well and incubated for up to 30 min at room temperature. The absorbance of all samples was measured at λ = 450 nm using a Multiskan FC microplate photometer (Thermo Scientific, Waltham, MA, USA) and expressed in optical units (o.u.).

4.12. Migration of HaCaT Cells Cocultivated with S. aureus

The silicon 2-well inserts (Ibidi®, Gräfelfing, Germany) were placed in the center of wells in a 24-well plate, and HaCaT cell suspension was added to each well for 24 h. After adhesion, the inserts were removed, and the cells were labeled with (5,6)-carboxyfluorescein succinimidyl ester (CFDA SE) dye (LumiTrace CFDA SE kit, Lumiprobe, Moscow, Russia). CFDA SE stock solution at 5 mM in DMSO was dissolved in PBS for preparation of a 10 µM solution. The cell culture medium was replaced with this CFDA SE solution for 5 min at 37 °C. Then, the cells were washed twice with PBS, and *S. aureus* suspension (10^2 CFU/mL) in full DMEM medium was added to each well as necessary. The medium without bacteria was added to control wells. The compounds at a concentration of 10 µM were added to wells after 1 h, and HaCaT cells and *S. aureus* were cultured at 37 °C in a humidified atmosphere with 5% (*v*/*v*) CO_2.

The silicon 2-well inserts from Ibidi®formed cell-free zones and migration of HaCaT cells in these zones were observed using an MBF-10 fluorescent microscope (Lomo Microsystems, St.-Peterburg, RF, Russia) during 30 h of incubation.

4.13. Proliferation of HaCaT Cells Cocultivated with S. aureus

The HaCaT cells at a concentration of 1.5×10^4 were seeded in a 12-well plate for 24 h. After adhesion, the cells were strained with (5,6)-carboxyfluorescein succinimidyl ester (CFDA SE) dye (LumiTrace CFDA SE kit, Lumiprobe, Moscow, Russia). CFDA SE stock solution at 5 mM in DMSO was dissolved in PBS for preparation of a 10 µM solution. The cell culture medium was replaced with this CFDA SE solution for 5 min at 37 °C. Then, the cell layer was washed with PBS twice, an *S. aureus* suspension (10^2 CFU/mL) in full DMEM medium was added to each need well, and after 1 h, the compound at a concentration of 10 µM was added to the wells. The medium without bacterial suspension was added to the control well.

After 48 h of incubation, the cells were washed with PBS twice, scrabbed, and collected in 1.5 mL tubes. The intensity of CFDA fluorescence was analyzed with a NovoCyte flow cytometer (Agilent, Austin, TX, USA).

4.14. Molecular Docking

The pdb file of sortase A (PDB ID 1T2P) was obtained from the RCSB Protein Data Bank (https://www.rcsb.org accessed on 25 July 2023) and prepared for docking by the PrepDock package of UCFS Chimera 1.16 software. The chemical structures of ligands were prepared for docking by ChemOffice and checked by the PrepDock package of UCFS Chimera 1.16 software.

Docking was conducted on the SwissDock online server (http://www.swissdock.ch accessed on 25 July 2023) based on EADock DSS docking software [40]. The algorithm implies the generation of many binding modes in the vicinity of all target cavities (blind docking) and estimation of their CHARMM energies via the Chemistry at HARvard Macromolecular Mechanics (CHARMM) algorithm [41] for evaluation of the binding modes with the most favorable energies with FACTS (Fast Analytical Continuum Treatment of Solvation) [42] and, finally, clustering of these binding modes [43].

The predicted building models for each target/ligand pair were visualized and analyzed by UCFS Chimera 1.16 software. Docking parameters such as Gibb's free energy

(ΔG, kcal/mol), FullFitness score (FF, kcal/mol), and hydrogen-bonding (H-bond) and hydrophobic interactions were used for analysis of target/ligand complexes.

4.15. Statistical Data Evaluation

All data were obtained in three independent replicates, and calculated values are expressed as a mean ± standard error mean (SEM). Student's *t*-test was performed using SigmaPlot 14.0 (Systat Software Inc., San Jose, CA, USA) to determine statistical significance. Differences were considered statistically significant at $p < 0.05$.

5. Conclusions

The *Asteromyces cruciatus* KMM4696 fungal strain is a promising producer of structurally unique and antibacterial polyketides. New acruciquinone C (**3**) possessed an unprecedented 6/6/5 anthraquinone-derived skeleton. The effect of new acruciquinone A (**1**) and known dendryol B (**4**) on sortase A activity and their weak antimicrobial effects indicate their potential antivirulence properties, with a reduced risk of antimicrobial resistance, made both these compounds very interesting as antivirulence agents. Their effects against *Staphylococcus aureus* in coculture with human HaCaT keratinocytes conditioned inhibition of sortase A and urease activity but did not limit inhibition, which ensures their positive effect on migration and proliferation of infected keratinocytes.

Supplementary Materials: The following are available online at https://www.mdpi.com/article/10.3390/md21080431/s1, Figures S1–S6: ECD and UV spectra of compounds **1**–**3**; Figures S7–S90: NMR spectra of compounds **1**–**13**; Figures S91–S104: HR ESI MS spectra of compounds **1**–**3** and **6**–**13**.

Author Contributions: Conceptualization, O.I.Z. and E.A.Y.; Data curation, N.N.K. and A.N.Y.; Formal analysis, O.I.Z., E.A.C. and S.S.S.; Funding acquisition, E.A.C.; Investigation, O.I.Z., E.A.C., G.K.O., A.S.A., N.N.K., A.S.M., R.S.P., N.Y.K., D.V.B., A.R.C., A.S.K. and E.A.Y.; Methodology, E.A.C. and I.V.G.; Resources, O.I.Z., I.V.G. and A.N.Y.; Software, D.V.B.; Supervision, I.V.G.; Validation, A.N.Y.; Visualization, E.A.C., S.S.S., D.V.B., A.S.K. and E.A.Y.; Writing—original draft, O.I.Z., E.A.C. and S.S.S.; Writing—review and editing, A.N.Y. and E.A.Y. All authors have read and agreed to the published version of the manuscript.

Funding: This research was funded by the Russian Science Foundation (grant number 23-24-00471).

Institutional Review Board Statement: Not applicable.

Informed Consent Statement: Not applicable.

Data Availability Statement: The original data presented in the study are included in the article/Supplementary Material; further inquiries can be directed to the corresponding author.

Acknowledgments: This study was carried out using the equipment of the Collective Facilities Center "The Far Eastern Center for Structural Molecular Research (NMR/MS) PIBOC FEB RAS" and the Collective Facilities Center "Collection of Marine Microorganisms PIBOC FEB RAS".

Conflicts of Interest: The authors declare no conflict of interest.

References

1. Ghoran, S.H.; Taktaz, F.; Ayatollahi, S.A.; Kijjoa, A. Anthraquinones and Their Analogues from Marine-Derived Fungi: Chemistry and Biological Activities. *Mar. Drugs* **2022**, *20*, 474. [CrossRef] [PubMed]
2. Masi, M.; Evidente, A. Fungal Bioactive Anthraquinones and Analogues. *Toxins* **2020**, *12*, 714. [CrossRef] [PubMed]
3. Santajit, S.; Indrawattana, N. Mechanisms of Antimicrobial Resistance in ESKAPE Pathogens. *Biomed. Res. Int.* **2016**, *2016*, 2475067. [CrossRef] [PubMed]
4. Abril, A.G.; Villa, T.G.; Barros-Velázquez, J.; Cañas, B.; Sánchez-Pérez, A.; Calo-Mata, P.; Carrera, M. *Staphylococcus aureus* Exotoxins and Their Detection in the Dairy Industry and Mastitis. *Toxins* **2020**, *12*, 537. [CrossRef] [PubMed]
5. Abbafati, C.; Machado, D.B.; Cislaghi, B.; Salman, O.M.; Karanikolos, M.; McKee, M.; Abbas, K.M.; Brady, O.J.; Larson, H.J.; Trias-Llimós, S.; et al. Global burden of 369 diseases and injuries in 204 countries and territories, 1990–2019: A systematic analysis for the Global Burden of Disease Study 2019. *Lancet* **2020**, *396*, 1204–1222. [CrossRef]

6. Rudd, K.E.; Johnson, S.C.; Agesa, K.M.; Shackelford, K.A.; Tsoi, D.; Kievlan, D.R.; Colombara, D.V.; Ikuta, K.S.; Kissoon, N.; Finfer, S.; et al. Global, regional, and national sepsis incidence and mortality, 1990-2017: Analysis for the Global Burden of Disease Study. *Lancet* **2020**, *395*, 200–211. [CrossRef] [PubMed]
7. Zhuravleva, O.I.; Oleinikova, G.K.; Antonov, A.S.; Kirichuk, N.N.; Pelageev, D.N.; Rasin, A.B.; Menshov, A.S.; Popov, R.S.; Kim, N.Y.; Chingizova, E.A.; et al. New Antibacterial Chloro-Containing Polyketides from the Alga-Derived Fungus *Asteromyces cruciatus* KMM 4696. *J. Fungi* **2022**, *8*, 454. [CrossRef]
8. Tanaka, M.; Ohra, J.; Tsujtno, Y.; Fujimori, T.; Ago, H.; Tsuge, H. Dendryol A, B, C, and D, Four New Compounds Produced by a Weed Pathogenic Fungus *Dendryphiella* sp. *Z. Naturforschung C* **1995**, *50*, 751–756. [CrossRef]
9. Zhang, C.; Ondeyka, J.G.; Zink, D.L.; Basilio, A.; Vicente, F.; Collado, J.; Platas, G.; Huber, J.; Dorso, K.; Motyl, M.; et al. Isolation, structure and antibacterial activity of pleosporone from a pleosporalean ascomycete discovered by using antisense strategy. *Bioorg. Med. Chem.* **2009**, *17*, 2162–2166. [CrossRef]
10. Sun, P.; Huo, J.; Kurtan, T.; Mandi, A.; Antus, S.; Tang, H.; Draeger, S.; Schulz, B.; Hussain, H.; Krohn, K.; et al. Structural and stereochemical studies of hydroxyanthraquinone derivatives from the endophytic fungus *Coniothyrium* sp. *Chirality* **2013**, *25*, 141–148. [CrossRef]
11. Zhang, Y.; Jia, A.; Chen, H.; Wang, M.; Ding, G.; Sun, L.; Li, L.; Dai, M. Anthraquinones from the saline-alkali plant endophytic fungus *Eurotium rubrum*. *J. Antibiot.* **2017**, *70*, 1138–1141. [CrossRef]
12. Imre, S.; Sar, S.; Thomson, R.H. Anthraquinones in *Digitalis* species. *Phytochemistry* **1976**, *15*, 317. [CrossRef]
13. Arrebola, M.L.; Ringbom, T.; Verpoorte, R. Anthraquinones from *Isoplexis isabelliana* cell suspension cultures. *Phytochemistry* **1999**, *52*, 1283–1286. [CrossRef]
14. Abraham, W.R.; Arfmann, H.A. Hydroxy-(methylbutenynyl)-benzoic acid and derivatives from *Curvularia fallax*. *Phytochemistry* **1990**, *29*, 2641. [CrossRef]
15. Prompanya, C.; Dethoup, T.; Gales, L.; Lee, M.; Pereira, J.A.C.; Silva, A.M.S.; Pinto, M.M.M.; Kijjoa, A. New Polyketides and New Benzoic Acid Derivatives from the Marine Sponge-Associated Fungus *Neosartorya quadricincta* KUFA 0081. *Mar. Drugs* **2016**, *14*, 134. [CrossRef] [PubMed]
16. Golyshin, P.N.; Golyshina, O.V.; Timmis, K.N.; Chernikova, T.; Waliczek, A.; Ferrer, M.; Beloqui, A.; Guazzaroni, M.E.; Vieites, J.M.; Pazos, F.; et al. Preparation of fluorescent probe-based reactome array for detection, immobilization and isolation of enzymes. Patent EP 2230312A1, 22 September 2010.
17. Shin, J.; Fenical, W. Isolation of gliovictin from the marine deuteromycete *Asteromyces cruciatus*. *Phytochemistry* **1987**, *26*, 3347. [CrossRef]
18. Frisch, M.J.; Trucks, G.W.; Schlegel, H.B.; Scuseria, G.E.; Robb, M.A.; Cheeseman, J.R.; Scalmani, G.; Barone, V.; Petersson, G.A.; Nakatsuji, H.; et al. *Gaussian 16 Rev. A.03*; Scientific Research Publishing: Wallingford, CT, USA, 2016.
19. Zhou, C.; Bhinderwala, F.; Lehman, M.K.; Thomas, V.C.; Chaudhari, S.S.; Yamada, K.J.; Foster, K.W.; Powers, R.; Kielian, T.; Fey, P.D. Urease is an essential component of the acid response network of *Staphylococcus aureus* and is required for a persistent murine kidney infection. *PLOS Pathog.* **2019**, *15*, e1007538. [CrossRef]
20. Sapra, R.; Rajora, A.K.; Kumar, P.; Maurya, G.P.; Pant, N.; Haridas, V. Chemical Biology of Sortase A Inhibition: A Gateway to Anti-infective Therapeutic Agents. *J. Med. Chem.* **2021**, *64*, 13097–13130. [CrossRef]
21. Zong, Y.; Bice, T.W.; Ton-That, H.; Schneewind, O.; Narayana, S.V.L. Crystal Structures of *Staphylococcus aureus* Sortase A and Its Substrate Complex. *J. Biol. Chem.* **2004**, *279*, 31383–31389. [CrossRef]
22. Thappeta, K.R.; Zhao, L.N.; Nge, C.E.; Crasta, S.; Leong, C.Y.; Ng, V.; Kanagasundaram, Y.; Fan, H.; Ng, S.B. In-Silico Identified New Natural Sortase A Inhibitors Disrupt *S. aureus* Biofilm Formation. *Int. J. Mol. Sci.* **2020**, *21*, 8601. [CrossRef]
23. Wiegand, C.; Abel, M.; Ruth, P.; Hipler, U.C. HaCaT keratinocytes in co-culture with *Staphylococcus aureus* can be protected from bacterial damage by polihexanide. *Wound Repair Regen.* **2009**, *17*, 730–738. [CrossRef] [PubMed]
24. Girich, E.V.; Trinh, P.T.; Nesterenko, L.E.; Popov, R.S.; Kim, N.Y.; Rasin, A.B.; Menchinskaya, E.S.; Kuzmich, A.S.; Chingizova, E.A.; Minin, A.S.; et al. Absolute Stereochemistry and Cytotoxic Effects of Vismione E from Marine Sponge-Derived Fungus *Aspergillus* sp. 1901NT-1.2.2. *Int. J. Mol. Sci.* **2023**, *24*, 8150. [CrossRef] [PubMed]
25. Sebak, M.; Molham, F.; Greco, C.; Tammam, M.A.; Sobeh, M.; El-Demerdash, A. Chemical diversity, medicinal potentialities, biosynthesis, and pharmacokinetics of anthraquinones and their congeners derived from marine fungi: A comprehensive update. *RSC Adv.* **2022**, *12*, 24887–24921. [CrossRef] [PubMed]
26. Griffiths, S.; Mesarich, C.H.; Saccomanno, B.; Vaisberg, A.; De Wit, P.J.; Cox, R.; Collemare, J. Elucidation of cladofulvin biosynthesis reveals a cytochrome P450 monooxygenase required for anthraquinone dimerization. *Proc. Natl. Acad. Sci. USA* **2016**, *113*, 6851–6856. [CrossRef]
27. Chapla, V.M.; Honório, A.E.; Gubiani, J.R.; Vilela, A.F.L.; Young, M.C.M.; Cardoso, C.L.; Pavan, F.R.; Cicarelli, R.M.; Ferreira, P.M.P.; Bolzani, V.d.S.; et al. Acetylcholinesterase inhibition and antifungal activity of cyclohexanoids from the endophytic fungus *Saccharicola* sp. *Phytochem. Lett.* **2020**, *39*, 116–123. [CrossRef]
28. Gulder, T.A.M.; Hong, H.; Correa, J.; Egereva, E.; Wiese, J.; Imhoff, J.F.; Gross, H. Isolation, Structure Elucidation and Total Synthesis of Lajollamide A from the Marine Fungus *Asteromyces cruciatus*. *Mar. Drugs* **2012**, *10*, 2912–2935. [CrossRef]
29. Li, H.L.; Li, X.M.; Li, X.; Wang, C.Y.; Liu, H.; Kassack, M.U.; Meng, L.H.; Wang, B.G. Antioxidant Hydroanthraquinones from the Marine Algal-Derived Endophytic Fungus *Talaromyces islandicus* EN-501. *J. Nat. Prod.* **2017**, *80*, 162–168. [CrossRef]

30. Mohanlall, V.; Odhav, B. Antibacterial, anti-inflammatory and antioxidant activities of anthraquinones from *Ceratotheca triloba* (Bernh) Hook F. *J. Med. Plant Res.* **2013**, *7*, 877–886.
31. Chingizova, E.A.; Menchinskaya, E.S.; Chingizov, A.R.; Pislyagin, E.A.; Girich, E.V.; Yurchenko, A.N.; Guzhova, I.V.; Mikhailov, V.V.; Aminin, D.L.; Yurchenko, E.A. Marine Fungal Cerebroside Flavuside B Protects HaCaT Keratinocytes against *Staphylococcus aureus* Induced Damage. *Mar. Drugs* **2021**, *19*, 553. [CrossRef]
32. Kohanski, M.A.; Dwyer, D.J.; Collins, J.J. How antibiotics kill bacteria: From targets to networks. *Nat. Rev. Microbiol.* **2010**, *8*, 423–435. [CrossRef]
33. WHO. *Ten Threats to Global Health in 2019*; World Health Organization: Geneva, Switzerland, 2019.
34. Cascioferro, S.; Totsika, M.; Schillaci, D. Sortase A: An ideal target for anti-virulence drug development. *Microb. Pathog.* **2014**, *77*, 105–112. [CrossRef]
35. Nitulescu, G.; Margina, D.; Zanfirescu, A.; Olaru, O.T.; Nitulescu, G.M. Targeting bacterial sortases in search of anti-virulence therapies with low risk of resistance development. *Pharmaceuticals* **2021**, *14*, 415. [CrossRef] [PubMed]
36. Ha, M.W.; Yi, S.W.; Paek, S.-M. Design and Synthesis of Small Molecules as Potent *Staphylococcus aureus* Sortase A Inhibitors. *Antibiotics* **2020**, *9*, 706. [CrossRef]
37. Hameed, A.; Al-Rashida, M.; Uroos, M.; Qazi, S.U.; Naz, S.; Ishtiaq, M.; Khan, K.M. A patent update on therapeutic applications of urease inhibitors (2012–2018). *Expert Opin. Ther. Pat.* **2019**, *29*, 181–189. [CrossRef] [PubMed]
38. Kafarski, P.; Talma, M. Recent advances in design of new urease inhibitors: A review. *J. Adv. Res.* **2018**, *13*, 101–112. [CrossRef]
39. Gottlieb, H.E.; Kotlyar, V.; Nudelman, A. NMR chemical shifts of common laboratory solvents as trace impurities. *J. Org. Chem.* **1997**, *62*, 7512–7515. [CrossRef]
40. Grosdidier, A.; Zoete, V.; Michielin, O. SwissDock, a protein-small molecule docking web service based on EADock DSS. *Nucleic Acids Res.* **2011**, *39*, W270–W277. [CrossRef] [PubMed]
41. Brooks, B.R.; Brooks, C.L., III; Mackerell, A.D., Jr.; Nilsson, L.; Petrella, R.J.; Roux, B.; Won, Y.; Archontis, G.; Bartels, C.; Boresch, S.; et al. CHARMM: The biomolecular simulation program. *J. Comput. Chem.* **2009**, *30*, 1545–1614. [CrossRef] [PubMed]
42. Haberthür, U.; Caflisch, A. FACTS: Fast analytical continuum treatment of solvation. *J. Comput. Chem.* **2008**, *29*, 701–715. [CrossRef]
43. Grosdidier, A.; Zoete, V.; Michielin, O. Fast docking using the CHARMM force field with EADock DSS. *J. Comput. Chem.* **2011**, *32*, 2149–2159. [CrossRef]

MDPI
St. Alban-Anlage 66
4052 Basel
Switzerland
www.mdpi.com

Marine Drugs Editorial Office
E-mail: marinedrugs@mdpi.com
www.mdpi.com/journal/marinedrugs

Academic Open
Access Publishing

mdpi.com

ISBN 978-3-0365-9087-5